2012

Factors Affecting Short-term Oxygen Variability in the Northern Gulf of Mexico Hypoxic Zone

Brenda Leroux Babin
Louisiana State University and Agricultural and Mechanical College

FACTORS AFFECTING SHORT-TERM OXYGEN VARIABILITY IN THE NORTHERN GULF OF MEXICO HYPOXIC ZONE

A Dissertation

Submitted to the Graduate Faculty of the
Louisiana State University and
Agricultural and Mechanical College
in partial fulfillment of the
requirements for the degree of
Doctor of Philosophy

Department of Oceanography and Coastal Sciences

by
Brenda Leroux Babin
B. A., Nicholls State University, 1982
M.Ed., Nicholls State University, 1984
M.P.S., Loyola University, New Orleans, 1996
December 2012

This work is dedicated to my dad, the late John Dale Leroux (1933-1979). My dad also gave me my passion for learning and my love of the Ocean. I often picture him as a young boy sitting on the levee of the Mississippi River daydreaming about where the muddy water had been and where it was going. When I was six years old while sitting in his "bookroom," my dad said, "You will get a PhD someday!" That inspiration has kept me going every step of the way.

ACKNOWLEDGEMENTS

First and foremost, I am grateful for God's grace in creating this work. As God provided everything I needed in order to accomplish this, I pray that this achievement may provide new tools for service to God's will.

I would like to thank my major professor, Dr. Dubravko Justić, who took this English major/Computer Science Instructor on as a student and taught me to be a scientist. I will always remember Dr. Justić's words of wisdom and life lessons that carried me through the entire process. I hope I never stop climbing the steeple and wondering what is in the next village. I am also extremely grateful to my co-chair, Dr. Kenneth Rose, for always asking probing questions and challenging me to think deeper and to be the best that I can be. I appreciate the tireless efforts of both committee chairs as they gave countless hours of assistance in creating this work.

I am grateful to other members of committee: Dr. Haosheng Huang who pointed me toward ancillary datasets and assisted with the time-series analysis, Dr. Bin Li who opened my eyes to data mining, and Dr. William Stickle (Dean's Representative) who taught me about the effects of hypoxia on living organisms.

I am eternally grateful to my family without whom this work would not have been possible. Ernest Babin, Jr., my husband, provided unending support by keeping me fed, clothed and happy. My two children, Billie Elizabeth Babin and Ernest John Babin, III, sacrificed time with their mom and gave endless support. My mom, Yvonne Leroux and brother, David Leroux, also supported me through the entire process.

Many friendships have also carried me through this project by providing loving support and helping hands where needed: Fellow graduate students, Dr. Jennifer Lentz and Dr. Anindita Das were always there to listen and offer advice. Anne Parr and Debbie Bergeron listened as I

rambled on about hypoxia, dissolved oxygen, and diel patterns and pretended to understand every word I was talking about. Dena Babin kept me sane and my house clean.

I thank the taxpayers of the United States for funding the data collection for this project. Public funds supported the acquisition of the time-series data including but not limited to the Louisiana Board of Regents Education Support Fund (1989-1990); U.S. Environmental Protection Agency, Louisiana EPSCoR program (2000-2003); and National Oceanic and Atmospheric Administration, Coastal Ocean Program (NECOP, 1990-1995; Hypoxia Studies 1996-1999; and Center for Sponsored Coastal Ocean Research, NGOMEX00, NGOMEX03 and NGOMEX06). Public funds also supported the acquisition and creation of all other datasets as described herein.

IN THE BEGINNING….

Billions of years ago before life and before oxygen existed on Earth, the Sun beamed her energy onto some chemicals, and those chemicals began to photosynthesize. They captured the Sun's energy becoming the first life forms. A heliobacteria and green sulfur type such as Chorobium transformed the Sun's energy by using iron-sulfur clusters as electron acceptors. Purple photosynthetic type bacteria used phaeophytin and a quinone as electron acceptors to transform the Sun's energy. A third type used carateinoid pigment protein to pump protons out of the cell or chloride ions into the cell to harvest the Sun's energy[*]*. Although these life forms did not produce oxygen, they did use the Sun's energy to sequester carbon and reproduce. As they reproduced, they evolved into photosynthesizing life forms that used the Sun's energy to convert carbon dioxide into stored energy and oxygen. Eventually, this stored energy evolved into life forms that no longer needed the Sun's energy, but could use the oxygen and return carbon dioxide to the atmosphere creating the great circle of life as we know it today.*

This circle has broken down in the northern Gulf of Mexico as well as other places throughout the world. The Sun's energy no longer provides oxygen to the depths of many areas of the sea posing a threat to life in these aquatic ecosystems.

[*]Falkowski, P.G. and Raven, J.A. (2007) Aquatic Photosynthesis. Malden, MA: Blackwell Science.

TABLE OF CONTENTS

ABSTRACT

Open-water continuous monitoring of DO concentrations at a single station (C6) in the Gulf of Mexico from 1989 to 2008 afforded an excellent opportunity to characterize short-term oxygen variability and to estimate the relative importance of key physical and biological factors controlling the development, persistence, and dissipation of hypoxia. I investigated temporal trends in three aspects of short-term DO variability: respiration rates (i.e., how quickly bottom waters become hypoxic), persistence of hypoxia, and the dissipation of hypoxia (i.e., re-aeration events). I identified the range of respiration rates present at the study site, and showed how these rates vary throughout the year and from year to year. Although a strong relationship between the persistence of hypoxia at station C6 and the areal extent of hypoxia in the NGOM was not present, both were statistically related to the monthly Mississippi River nitrogen flux. Using time-series analysis, I found no consistent periodicities in DO across the three depths (near-surface, mid-water-column, and near-bottom) or related to water levels (tides). I did find a diel signal in the DO that could be related to the diel pattern in available light for photosynthesis reaching the near-bottom. Percent of days exhibiting a diel pattern was 20 at the surface, 12 at the mid-water column, and 7 for the near-bottom measurements. Using regression trees and matching of the timing of events, I found that the density gradient was a good predictor of severe hypoxia (DO <=1.0 mg l^{-1}) and that 65% of the re-aeration events could be associated with wind stress events, cold fronts or tropical cyclones. These results suggest that continuous DO monitoring at a single location provides valuable information on short-term variability that will help in assessing the exposure and the resulting biological responses to hypoxia, in interpreting the possible variability around the annual hypoxia maps generated from the single, shelf-wide cruises, and as a basis for improving predictive models of hypoxia.

CHAPTER 1

INTRODUCTION

BACKGROUND

Northern Gulf of Mexico Hypoxic Zone

The Northern Gulf of Mexico off the Louisiana-Texas coast, USA, is one of the most productive areas of the world's oceans. The Mississippi River drains 40% of the conterminous United States (Milliman and Meade, 1983) and empties into the Gulf of Mexico through the Mississippi River bird foot delta and the Atchafalaya River delta and Wax Lake outlet. Ekman dynamics and southeasterly winds push the plume of the Mississippi River primarily to the western shelf off the Louisiana-Texas coast. These waters have long been known as the fertile fisheries crescent (Gunter, 1963). The northwestern Gulf of Mexico supports some of the nation's most important commercial and recreational fisheries, which annually generate over $2 billion. Texas and Louisiana are national leaders in US commercial shrimp landings, and in 2004, these states landed 64% of the nation's shrimp tails (Chesney et al., 2000).

While the nutrients from the Mississippi River play an important role in supporting the fertile fisheries crescent, the nutrient-enhanced productivity creates the undesirable effects of eutrophication. A large area of hypoxia, or low oxygen, has been recurring every summer in the bottom waters of the Northern Gulf of Mexico (NGOM) off the Louisiana-Texas coast (Dale et al., 2010). The operational definition of hypoxia for the NGOM is dissolved oxygen (DO) concentration ≤ 2 mg l^{-1}, based on a lack of fish catch in bottom trawls below this level (Renaud, 1986). Hypoxia is a result of numerous physical, biological, and chemical processes operating in unison to reduce DO in bottom waters. The two primary requirements for bottom hypoxia to occur are a decomposing carbon source and a stratified water column (Justić et al., 1996;

Wiseman et al., 1997). In the summer, the water column stratifies in response to lighter fresher water from the Mississippi River located atop the saltier heavier water. Although the plume from the Mississippi River creates a freshwater density gradient, summer stratification is also enhanced by the seasonal warming of the upper water column creating a distinct thermal gradient (Wiseman et al., 1997). Reduced mixing and reduced vertical turbulent diffusion facilitate stratification, which results in diminished oxygen flux between layers isolating the lower layer from the more oxygen rich upper layers of the water column. In the lower layer of the water column, oxygen consumption by bacteria and other heterotrophic organisms that decompose organic matter deplete the bottom DO pool faster than photosynthesis can replace it. This sustained oxygen consumption via respiration, without replenishment of oxygen, creates hypoxic conditions in the water column below the pycnocline. Stronger winds associated with cold fronts and tropical storms weaken the pycnocline mixing oxygen saturated water through the entire water column (Wiseman and Garvin, 1995). The mixed water column usually persists throughout the winter with the increased frequency of cold fronts until the following spring when the frequency of cold fronts decreases and the water column again stratifies (Rabalais et al., 2002).

Historical Perspective

Hypoxia was first documented in the northern Gulf of Mexico in 1972 by Wilma Subra, working with a team of scientists from the Gulf Coast Research Institute that was studying the effects of oil and gas exploration on the aquatic ecosystems (Subra, 2010). Since then, much work has been done to monitor DO concentrations in the NGOM, and to document the annual occurrence of low oxygen across the shelf. From 1978 through 1995, the Louisiana Department of Wildlife and Fisheries (LDWF) collected water quality samples as part of the LDWF

Louisiana Offshore Oil Port (LOOP) monitoring program consisting of monthly DO concentration samples from several stations located near the mouth of the Mississippi River (Turner et al., 2005).

Every summer since 1985, a team of scientists from Louisiana Universities Marine Consortium (LUMCON) has been mapping the areal extent of hypoxia in the NGOM (Rabalais et al., 2007). The LUMCON team has also been sampling monthly along a north-south transect south of Terrebonne Bay to explore the seasonal variability of DO concentrations. In 1989, Rabalais et al. (1994) began continuous monitoring of DO concentrations near the bottom of the water column at a site 20 km south of Terrebonne Bay (Figure 1.1). This monitoring effort continues today, and can be viewed in real-time at http:www.wavcis.lsu.edu. Several other research groups have been monitoring DO concentrations in the NGOM to better understand the dynamics of hypoxia and the effects of hypoxia on aquatic organisms (Forrest et al., 2011).

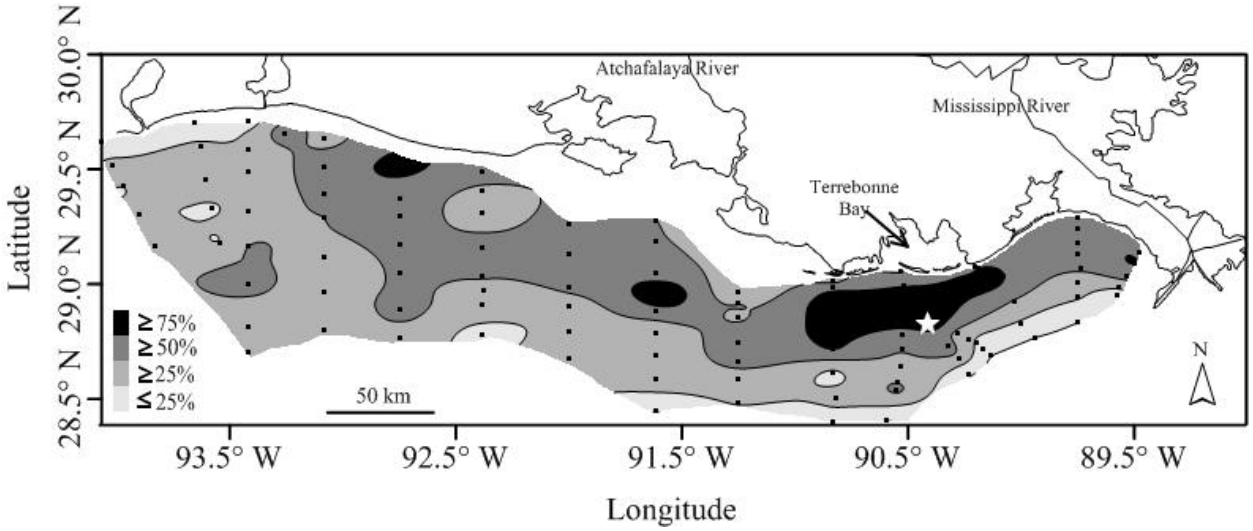

Figure 1.1. Frequency of occurrence of midsummer hypoxia between 1985 and 2008 based on a 60-90 station grid. Continuous monitoring data collection site (Station C6) is indicated by the white star. Dots represent stations sampled during the annual areal extent mapping cruise. (Babin and Rabalais, 2009)

Although hindcast models indicate that the annual occurrence of hypoxia was not present prior to the 1970s (Justić et al., 2007; Scavia et al., 2004; Turner et al., 2006), sediment cores

show evidence of hypoxia prior to 1900 suggesting that hypoxia has been a common feature in the NGOM, but has increased in frequency and severity since the 1950s (Osterman et al., 2008).

Scales of Oxygen Variability

Factors affecting oxygen variability in the northern Gulf of Mexico operate on a variety of spatial and temporal scales. One example of an interaction on large spatial and temporal scales is the effect of climate change on oxygen variability in the NGOM. Justić et al. (1996) showed that climate change would likely increase the discharge of the Mississippi River leading to an increased potential for hypoxia in the NGOM. These changes are expected to occur on decadal to century scales.

Variations in the flux of nitrogen and other nutrients from the Mississippi River watershed impact NGOM hypoxia on annual to decadal scales. As mentioned before, the Mississippi River drains 40% of the conterminous United States. Nutrients from the watershed flow down the Mississippi River into the Gulf of Mexico causing eutrophication. Studies have shown that it can take a decade or more for a eutrophied coastal ecosystem to return to a more pristine state after the supply of nutrients has decreased. For example, the hypoxic conditions on the northwestern shelf of the Black Sea improved over the decade from 1990 to 2000 (Mee, 2001). During that time period, nutrient loads from the Danube River decreased substantially due to a sharp decline in intensive farming following the breakdown of the Soviet Union. By 1995, nutrient loads significantly decreased and the extent of bottom water hypoxia decreased. By 2000, hypoxia was essentially absent from the northwestern shelf of the Black Sea (Mee, 2001; 2006; Mee et al., 2005). Variation in annual Mississippi River discharge affects the location of hypoxia formation on the NGOM shelf. Rowe et al. (2002) divided the area of the Gulf that experiences frequent hypoxia into three regions defined primarily by distance from the

mouth of the Mississippi River and sea surface salinity. The first region, or the near-field region, is closest to the Mississippi River delta site. The salinity range in this region is 0-18 psu. Although nutrients are abundant, phytoplankton growth is light limited and geochemical processes are driven primarily by allocthonous organic matter supplied by the river (Elridge and Roelke, 2010). In the second region, or mid-field region, salinity ranges between 18-27 psu. Phytoplankton growth rates are at their maximum. Autochthonous processes (i.e., production of organic matter and respiration) dominate in the mid-field region (Elridge and Roelke, 2010). This region has high chlorophyll *a* and is dominated by large celled phytoplankton mostly diatoms. In the third region, or far-field region, the salinity range is 27-32 psu. Phytoplankton is nutrient-limited and grazing is heavier. In these fringes bottom water low DO concentrations are controlled by physical stratification preventing atmospheric oxygen from mixing to the bottom (Elridge and Roelke, 2010). The northern Gulf of Mexico beyond the region that experiences hypoxia has a salinity range between 32 and 36 psu. Station C6 (see Figure 1.1), the site of data collection used in this study, has a near-surface salinity range from 9 to 37 psu with an average salinity of 29 psu. Therefore, this location can fit any of the three regions described above.

Much of the variability in DO concentrations from geochemical and physical processes occurs over short temporal and small spatial scales within one of these regions. These processes exert a strong control over the timing and location of the development of hypoxia (Elridge and Morse, 2008). Although a correlation exists between the magnitude of the Mississippi River annual nutrient freshwater fluxes and the area of the mid-summer areal extent of hypoxia (Forrest et al., 2011), the factors that influence DO concentrations and play a role in hypoxia dynamics on short temporal (hours to days) and spatial scales have not been clearly identified.

On scales of hours to days, DO concentrations vary in response to factors such as light, temperature, tide, and episodic events. Biologically, the diel cycle of photosynthesis and respiration in the aquatic environment is primarily controlled by the daily cycle of photosynthetically active radiation (Odum, 1956). Temperature also plays a role in this diel cycle. Another periodic factor that has been shown to have a physical impact on short-term DO variability is tide. Water column stratification and frontal activity are also factors that drive the development and dissipation of hypoxia in the NGOM (Elridge and Morse, 2008).

RATIONALE

Understanding changes in short-term oxygen variability and the dynamics of hypoxia in particular is important because hypoxia is often a symptom of a stressed aquatic ecosystem. Odum (1985) reviewed eighteen trends that can be expected in a stressed ecosystem. The first five of these trends labeled "Energetics", for example, concern changes in primary production, or changes in the production of oxygen. These five trends include: 1) community respiration increases, 2) P/R (production/respiration) becomes unbalanced (< 1 or > 1), 3) P/B and R/B (maintenance: biomass structure) ratios increase, 4) importance of auxiliary energy increases, and 5) exported or unused primary production increases. Because a disturbance to the ecosystem requires diverting energy from growth and production to maintenance, one of the first indicators of stress to an ecosystem is an increase in community respiration and a subsequent disruption in the production to respiration (P/R) ratio.

Another reason why understanding short-term variability in DO concentrations is important is because neglecting short-term variability may lead to errors in measurements of long-term variability (Sanford et al., 1990). For example, the areal extent of hypoxia in the Gulf of Mexico is mapped every summer. The annual areal extent, that is compared to the river

discharge and nutrient flux and is used for management purposes, is measured on a scale of 100 kilometers distributed across the Louisiana shelf west of the mouth of the Mississippi River to the Texas coast extending from near-shore to as far as 125 km offshore at about the 60 m isobath. The average areal size measured from 1985 to 2007 is 13,500 km^2. In 2002, the largest areal extent measured to date was 22,000 km^2, and extended from the mouth of the Mississippi River to the Louisiana-Texas border (Rabalais et al., 2007). Figure 1.1 shows the frequency of occurrence of midsummer hypoxia between 1985 and 2008 and the location of these occurrences. The short-term variability in DO may represent changes that occur between the beginning and the end of the cruise and may be a source of error in the final measure.

OBJECTIVES

This dissertation takes a data mining and analysis approach to elucidate the dynamics of hypoxia through a better understanding of the factors that affect the variability in DO on short temporal and spatial scales. Although NGOM hypoxic zone often encompasses the northern Gulf of Mexico from west of the mouth of the Mississippi River to just beyond the Texas border, this project focuses on a single site in the northern Gulf of Mexico that experiences frequent mid-summer hypoxia and has been continuously monitored for over 20 years. The primary data collection site (station C6) is located about 26 km south of Terrebonne Bay (Figure 1.1). The purpose of this dissertation is to characterize short-term oxygen variability at a single site in the NGOM and to quantify the relative importance of the factors that affect that variability. The objectives are:

1) to characterize the short-term variability in DO concentrations between 1989 and 2008 at a single NGOM location that experiences frequent summer hypoxia,

2) to identify trends in short-term oxygen variability and compare those trends to the trends in the Mississippi River nutrient and fresh water fluxes,

3) to identify periodicities in the short-term DO variability and quantify the relative importance of periodic factors (solar radiation, temperature, and tide), and

4) to quantify the effects of episodic factors (fronts and tropical storms) on short-term DO variability.

I use a 20 year time-series of DO concentrations collected at a station C6 that experiences frequent hypoxia, augmented with other relevant environmental time-series data, and I analyze these data using a variety of graphical and statistical methods.

DATA SET

The primary data set consists of 20 years, 1989-2008, of DO concentrations along with other parameters collected with electronic sensors at 15 minute intervals (Figure 1.2). Although portions of this DO time-series have been published in various research projects, this data set has never before been analyzed in its entirety. Rabalais et al. (1994) have performed a limited analysis of the 1989 and 1990 data, and Rabalais and Harper (1992) published continuously monitored data from 1990 and 1991. Also, data were published from the year 1993 showing how physical factors like frontal passages, hurricanes, and upwelling events re-aerate the bottom waters dissipating hypoxia (Rabalais et al. 2001, 2007; Rabalais and Turner, 2006). Justić et al. (1997, 2002, 2003) used data between 1989 and 1993 to formulate and validate a two box model exploring the impact of variations in climate and anthropogenic nutrient loading on the severity of hypoxia. Rabalais et al. (2009) published 2003 data indicating storm events and the subsequent re-aerating effect on hypoxia. Rabalais et al. (2002) published graphs from 1990 showing mid-June through mid-September bottom oxygen values, while describing the general

pattern of variability within a year as indicated by the continuously recording sensors at this site from 1990-2000. More recently, Baustian and Rabalais (2009) and Baustian et al. (2009) published data from March 2003 to October 2004 looking at the effects of oxygen variability, especially the occurrences of severe hypoxia, on benthic macroinfauna. In this dissertation, I analyze the entire 20-year time series and expand and extend these earlier analyses.

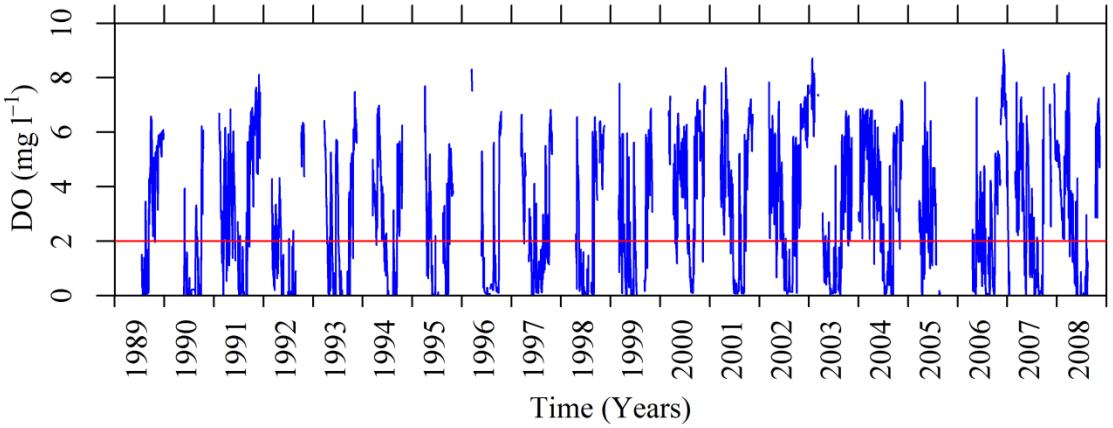

Figure 1.2. Daily averages of DO concentrations station C6, a single site in the northern Gulf of Mexico located about 26 km south of Terrebonne Bay that experiences frequent mid-summer hypoxia and has been continuously monitored for over 20 years (1989-2008).

SUMMARY

In Chapter 2, I characterize the data set and explore trends in the three aspects of variability in the time-series of DO concentrations, and compare these trends to trends in the Mississippi River nutrient and freshwater fluxes. I quantify the seasonal patterns in DO concentrations based on daily averages over the 20 year period, as well as the inter-annual variations in this seasonal pattern. I also determine the three aspects of short-term variability: 1) rate at which DO concentrations decrease to hypoxic conditions, 2) the persistence of hypoxic events (duration of hypoxia), the possible use of hypoxia persistence as a metric of severity of hypoxia, and 3) the frequency at which hypoxic conditions return to normoxic conditions (mixing events). Other studies (e.g. Turner et al., 2006; 2012; Forrest et al. 2011) have used

regression analysis to relate trends in the severity of hypoxia to trends in nutrient fluxes from the Mississippi River. I repeat some of these analyses using the short-term DO measurements to assess whether the relationships also apply to variability in high-frequency temporal resolution observations measured at a single location.

Chapter 3 explores the periodicities in the 20 year DO dataset and analyzes the dataset along with other periodic factors using time-series analysis methods. The analysis identifies and quantifies the effects of periodic factors on short-term (hours to days) DO variability. The three periodic factors analyzed were: a component of short-wave radiation flux known as photosynthetically active radiation (PAR), water temperature, and tidal conditions. I also identify individual days with cyclical diurnal pattern and compared these days to PAR measurements.

Chapter 4 explores the episodic factors that impact short-term oxygen variability. Some of the variation in DO values in the dataset is controlled by episodic events in the environment like cold fronts and tropical cyclones. The strength of stratification of the water column and the forces that influence stratification causing episodic mixing are the primary factors that have a rapid impact on the increase in DO concentrations. Frontal activity and tropical cyclones mix the water column causing re-aeration of near-bottom waters. I explored how these and other possible episodic events influence the short-term variability of DO concentrations. First, I looked at the relationship between daily delta sigma-t as an index for the strength of stratification and the daily DO threshold category in the bottom waters. Then, I characterized the re-aeration events using a trigger algorithm. Finally, I quantified the coincidence of these re-aeration events with the episodic events of wind stress, cold fronts, and tropical cyclones.

Chapter 5 summarizes the conclusions of the entire study. I discuss the implications of the results from this study and how it might apply to other studies. I also discuss how determining the severity of hypoxia in the single NGOM site could be used for management purposes extrapolated to the entire NGOM hypoxic zone.

REFERENCES

Babin, B.L. and Rabalais, N.N., 2009. Trends in oxygen variability in the northern Gulf of Mexico hypoxic zone. Proceedings of OCEANS '09 MTS/IEEE Biloxi.

Baustian, M.M., Craig, J.K. and Rabalais N.N. 2009. Effects of summer 2003 hypoxia on macrobenthos and Atlantic croaker foraging selectivity in the northern Gulf of Mexico. Journal of Experimental Marine Biology and Ecology 381, S31-S37.

Baustian, M.M. and Rabalais N.N. 2009. Seasonal composition of benthic macroinfauna exposed to hypoxia in the northern Gulf of Mexico. Estuaries and Coasts 32(5), 975-983.

Chesney, E.J., Baltz, D.M., and Glenn, T. R. 2000. Louisiana Estuarine and Coastal Fisheries and Habitats: Perspectives from a Fish's Eye View. Ecological Applications, 10(2), 350-366.

Dale, V.H., et al. (Eds.) 2010, Hypoxia in the northern Gulf of Mexico, Springer, New York.

Eldridge, P.M., and Morse, J.W. 2008. Origins and temporal scales of hypoxia on the Louisiana shelf: Importance of benthic and sub-pycnocline water metabolism. Marine Chemistry, 108(3-4), 159-171.

Eldridge, P.M., and Roelke, D.L. 2010. Origins and scales of hypoxia on the Louisiana shelf: Importance of seasonal plankton dynamics and river nutrients and discharge. Ecological Modelling, 221(7), 1028-1042.

Forrest, D.R., Hetland, R.D., and DiMarco, S.F. 2011. Multivariable statistical regression models of the areal extent of hypoxia over the Texas–Louisiana continental shelf. Environmental Research Letters 6, 045002.

Gunter, G. 1963. The fertile fisheries crescent. Journal of Mississippi Academy of Science 9, 286-290.

Justić, D., Bierman, V.J., Scavia, D., and Hetland, R.D. 2007. Forecasting Gulf's hypoxia: The next 50 years? Estuaries and Coasts 30, 791-801.

Justić, D., Rabalais N.N., and Turner, R.E. 1996. Effects of climate change on hypoxia in coastal waters: A doubled CO2 scenario for the northern Gulf of Mexico. Limnology and Oceanography 41, 992-1003.

Justić, D., Rabalais, N.N., and Turner, R.E. 1997. Impacts of climate change on net productivity of coastal waters: implications for carbon budgets and hypoxia. Climate Research, 8(3), 225-237.

Justić, D., Rabalais, N.N., and Turner, R.E. 2003. Simulated responses of the Gulf of Mexico hypoxia to variations in climate and anthropogenic nutrient loading. Journal of Marine Systems 42(3-4), 115-126.

Justić, D, Rabalais, N.N., and Turner, R.E. 2002. Modeling the impacts of decadal changes in riverine nutrient fluxes on coastal eutrophication near the Mississippi River delta. Ecological Modelling 152(1), 33-46.

Mee, L.D. 2001. Eutrophication in the Black Sea and a basin-wide approach to its control, in: Science and Integrated Coastal Management, edited by: von Bodungen, B. and Turner, R. K., Berlin: Dahlem University Press, 71–91.

Mee, L.D., Friedrich, J., and Gomoiu, M.T. 2005. Restoring the Black Sea in times of uncertainty, Oceanography 18, 100–111.

Mee, L.D. 2006. Reviving dead zones. Scientific American, November 2006, 80–85.

Milliman, J.D. and Meade, R.H. 1983. World-wide delivery of river sediment to the Oceans. The Journal of Geology 91(1), 1-21.

Odum, E.P. 1985. Trends expected in stressed ecosystems. Bioscience 35(7), 419-422.

Odum, H.T. 1956. Primary production in plowing waters. Limnology and Oceanography 1(2), 102-117.

Osterman, L.E., Poore, R.Z., and Swarzenski, P.W. 2008. The last 1000 years of natural and anthropogenic low-oxygen bottom-water on the Louisiana shelf, Gulf of Mexico. Marine Micropaleontology 66(3-4), 291-303.

Rabalais, N.N., and Harper, D.E., Jr., 1992. Studies of benthic biota in area affected by moderate and severe hypoxia. In: National Oceanic and Atmospheric Administration, Coastal Ocean Program Office, Nutrient Enhanced Coastal Ocean Productivity, Proceedings of a Workshop. Louisiana Universities Marine Consortium, October 1991. Sea Grant Program, Texas A & M University, Galveston, TX, TAMU-SG-92–109. pp. 150–153.

Rabalais, N.N, Turner, R.E., Sen Gupta, B.K, Boesch, D.F., Chapman, P., and Murrell, M.C. 2007, Hypoxia in the northern Gulf of Mexico: does the science support the plan to reduce, mitigate, and control hypoxia? Estuaries Coasts 30, 753–72.

Rabalais, N.N., Wiseman, W.J. Jr, and Turner, R.E. 1994. Comparison of continuous records of near-bottom dissolve oxygen from the hypoxia zone along the Louisiana coast. Estuaries 17 (4), 850-861.

Rabalais, N.N. and Turner, R.E. 2006. Oxygen depletion in the Gulf of Mexico adjacent to the Mississippi River. In Lev N. Neretin (Ed.), Past and Present Water Column Anoxia, Netherlands: Springer 64, 225-245.

Rabalais, N.N., Turner, R.E., Diaz, R.J., and Justić, D., 2009. Global change and eutrophication of coastal waters. ICES Journal of Marine Science, fsp047.

Rabalais, N.N., Turner, R.E., and Wiseman, W.J. Jr,. 2002. Gulf of Mexico Hypoxia, a.k.a. "The Dead Zone". Annual Review of Ecology and Systematics 33, 235-263.

Rabalais, N.N., Smith, L.E., Harper, D.E. Jr., and Justić, D. 2001. Effects of seasonal hypoxia on continental shelf benthos. In Coastal hypoxia: Consequences for living resources and ecosystems, Coastal and Estuarine Studies 58, ed. N.N. Rabalais and R. E. Turner Washington, DC: American Geophysical Union 211–240.

Renaud, M.L. 1986. Hypoxia in Louisiana coastal waters during 1983: Implications for fisheries. Fishery Bulletin 84, 19-26.

Rowe, G.T., Kaegi, M.E.C., Morse, J.W., Boland, G.S., and Briones, E.G.E. 2002. Sediment community metabolism associated with continental shelf hypoxia, Northern Gulf of Mexico. Estuaries 25(6A), 1097-1106.

Sanford, L.P., Sellner, K.G., and Breitburg, D.L. 1990. Covariability of dissolved oxygen with physical processes in the summertime Chesapeake Bay. Journal of Marine Research 48, 567-590.

Scavia, D., Justić, D. and Bierman, V.J. 2004. Reducing hypoxia in the Gulf of Mexico: Advice from three models. Estuaries 27(3), 419-425.

Subra, W. 2010. Reasons to worry about the dead zone. In Oceans: The threats to our seas and what you can do to turn the tide, ed. Jon Bowermaster. New York: Public Affairs, 131-136.

Turner, R.E., Rabalais, N.N., and Justić, D. 2006. Predicting summer hypoxia in the northern Gulf of Mexico: Riverine N, P, and Si loading. Marine Pollution Bulletin 52(2), 139-148.

Turner, R.E., Rabalais, N.N., and Justić, D. 2012. Predicting summer hypoxia in the northern Gulf of Mexico: Redux. Marine Pollution Bulletin, 64(2), 319-324.

Turner, R.E., Rabalais, N.N., Swenson, E.M., Kasprzak, M., and Romaire, T. 2005. Summer hypoxia in the northern Gulf of Mexico and its prediction from 1978 to 1995. Marine Environmental Research 59(1), 65-77.

Wiseman, Jr., W.J. and Garvine R.W. 1995. Plumes and coastal currents near large river mouths. Estuaries 18(3), 509-517.

Wiseman, W.J., Rabalais, N.N., Turner, R.E., Dinnel, S.P., and MacNaughton, A., 1997. Seasonal and interannual variability within the Louisiana coastal current: stratification and hypoxia. Journal of Marine Systems 12(1-4): 237-248.

CHAPTER 2

PATTERNS IN SHORT-TERM OXYGEN VARIABILITY IN THE NORTHERN GULF OF MEXICO HYPOXIC ZONE

INTRODUCTION

Monitoring dissolved oxygen (DO) concentrations in the bottom waters of the northern Gulf of Mexico (NGOM) is important to better understand the distribution and dynamics of the hypoxic waters (DO $\leq$ 2.0 mg l^{-1}) off the Louisiana-Texas coast (Rabalais et al., 2007). Hypoxia is a phenomenon caused by two synergistic factors. First, a decomposing carbon source must be present in the bottom waters to consume oxygen faster than it is produced, and second, the water column must be sufficiently stratified to prevent oxygen-rich water in the surface from replenishing the bottom waters (Justić et al., 1996; Wiseman et al., 1997). In the NGOM, hypoxia recurs each spring when organic matter generated during spring phytoplankton blooms settles to the bottom providing fuel for oxygen consumption, and the water column concurrently stratifies due to the flux of freshwater from the Mississippi River and Atchafalaya River and due to the seasonal warming of the surface waters. Hypoxia persists throughout the summer months, only dissipating occasionally due to mixing. In the fall, as the surface waters cool and cold fronts mix the water column, oxygen is supplied to the bottom and hypoxia dissipates (Rabalais et al., 2002).

Hypoxia poses threats to ecosystems with varying consequences for marine life, including mortality and reduced biodiversity (Vaquer-Sunyer and Duarte, 2008). Although no one single low dissolved oxygen threshold applies to all organisms, hypoxic conditions (DO $\leq$ 2 mg l^{-1}) generally induce responses in marine life including avoidance behavior, slowed growth, reduced reproduction, and lowered survival in comparison to normoxic (6 to 8 mg O_2 l^{-1}) conditions (Levin et al., 2009). In the NGOM, DO concentrations equal to or less than 2.0 mg l^{-1}

is used as the operational definition of hypoxia because of the many effects on biota observed at this threshold (Renaud, 1986). The NGOM's shallow continental shelf that experiences annual hypoxia shows signs of stress, including low abundance of fish and shrimp and distinctly altered benthic communities (Baustian et al., 2009). While ecological effects of hypoxia are not well understood, potential impacts may include a decline in ecologically and commercially important fish and shellfish species (Renaud, 1986). The extent and duration of hypoxic events affect conditions in the spawning grounds, migratory pathways, and feeding habitats, possibly leading to declines in productivity of higher trophic levels (CENR, 2000).

Because the exposure of biota to hypoxia occurs in a dynamic environment and mobile organisms move within this dynamic environment, it is important to understand the short-term (i.e., hours to days) variability in DO concentrations. The DO concentration in marine waters is dependent on both physical and biogeochemical processes. Physical processes include advection, mixing, and air-sea exchange. Several biogeochemical sources and sinks of oxygen contribute to the patterns of dissolved oxygen concentrations in bottom waters, and influence the variability observed on sub-daily scales and among years. Photosynthesis is the only biogeochemical source of oxygen in the marine environment, while the oxidation of organic matter, both through oxic respiration and the oxidation of metabolites (Mn(II), Fe(II), S(-II)) by chemolithic bacteria, consumes dissolved oxygen (Sell and Morse, 2006; Elridge and Morse, 2008). Respiration, defined here as the decrease of DO in the water measured in mg $O_2\, l^{-1}\, h^{-1}$, is the most important oxygen sink. The rate of decrease in DO concentrations determines the length of time it takes for water with normal oxygen levels (~6 to 8 mg $O_2\, l^{-1}$) to progress to hypoxic conditions.

Oxygen variability occurs at various temporal scales (seconds to decades) and over a range of spatial scales (cm to km); therefore, adequate characterization of the oxygen variability with regard to hypoxia requires measurements on multiple temporal and spatial scales. Our knowledge of oxygen dynamics in the NGOM has come from a variety of monitoring efforts that have used different metrics to determine the intensity and severity of hypoxia.

Perhaps the most well-known metric in the NGOM is the areal extent of summertime hypoxia that has been measured by Louisiana Universities Marine Consortium (LUMCON) researchers since 1985. Areal extent is determined by a quasi-synoptic survey over a consistent grid (Rabalais et al., 2010). This metric is estimated by interpolation of DO conditions based on a sampling grid of approximately 90 stations (Figure 2.1). The bottom DO is measured at each station with a dissolved oxygen sensor mounted on a Conductivity-Temperature-Depth (CTD) rosette, with an independently lowered oxygen sensor, and from a water sample using Winkler titrations. The lowest DO concentration value of the three measurements becomes the "station" value. These DO concentration station values are then interpolated to the entire NGOM hypoxia region, and the areal extent of the gridded data is computed using a hand contouring method. This method produces a spatial quasi-snapshot of bottom DO concentration values across the NGOM region where hypoxia frequently occurs. Trends in the annual areal extent have been compared to trends in nutrient flux from the Mississippi River (Turner et al., 2006). The annual areal extent measurements are then compared to previous years and are used for management purposes in creating the action plan goal, which is to reduce the 5-year running average of the areal extent to < 5000 km^2 (Figure 2.2).

Although decadal and seasonal variability of coastal hypoxia is relatively well understood, shorter term dissolved oxygen variability (minutes to days) has yet to be explored

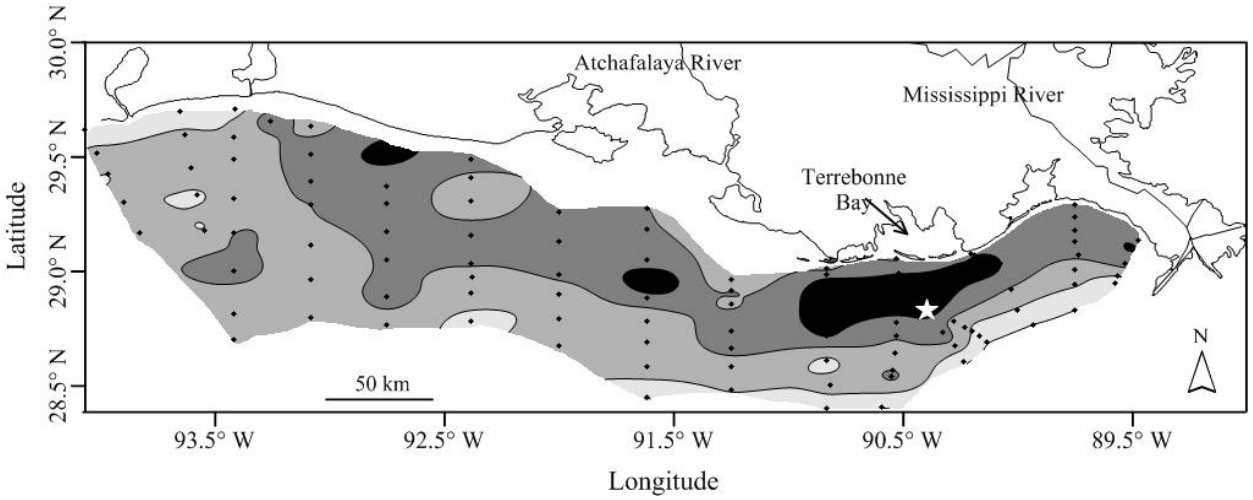

Figure 2.1. Frequency of occurrence of midsummer hypoxia between 1985 and 2008 based on a 60-90 station grid. Continuous data collection site (Station C6) is indicated by the white star. Dots represent stations sampled during the annual areal extent mapping cruise (Figure from Babin and Rabalais, 2009).

over a long-term time-series. Continuous monitoring with electronic sensors allows the study of both long-term and short-term variation in dissolved oxygen and the comparison of this variation to changes in other environmental variables. Cloern and Jassby (2010) discussed three patterns of temporal variability that can be explored using a long-term time-series: (1) climate variability, usually defined with respect to a 30 year average for atmospheric parameters; (2) seasonal variability that involves changes within a given year allowing us to look at changes that may be related to astronomical forcings, such as the annual cycles of temperature, solar radiation, and river flow; and (3) event-scale variability, where perturbations in the time-series are the direct result of episodic forcings. In the case of dissolved oxygen, these episodic forcings include mixing events such as frontal activity, hurricanes, and other physical processes that mix the water column. One approach to understanding long-term time-series is to decompose the time-series into its three components: trend, periodicities and episodic events. In time series analysis, "trend" determines whether or not a value or some aspect of the variability of that value increases or decreases with time.

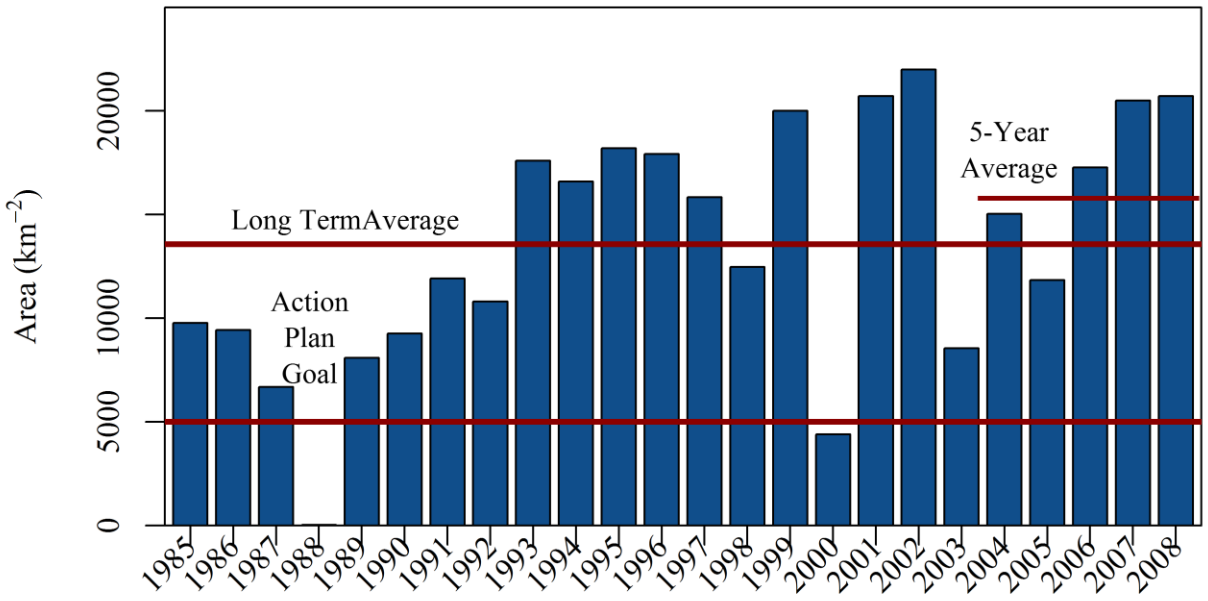

Figure 2.2. The areal extent of mid-summer hypoxia (bottom water dissolved oxygen concentrations ≤ 2.0 mg l^{-1}) measured during the Louisiana Universities Marine Consortium's annual shelf-wide cruises from 1985 to 2008. Red horizontal lines represent values of interest to management. The action plan goal, to reduce the 5-year running average of the areal extent to <5000 km^2, is represented by the bottom red line. The middle red line represents the long-term average and the top shorter red line represents the 5 year running average from 2004-2008 (data source: http:www.gulfhypoxia.net).

This chapter explores the patterns and trends in seasonal and short-term (hours to days) oxygen variability over a 20-year period (1989-2008) by analyzing a dissolved oxygen time-series collected at a station (C6) located in the core of the Gulf of Mexico hypoxic zone (Figure 2.1). First, I characterize the magnitudes of short-term oxygen variability. Then, I determine the trends in the short-term variability and how these trends relate to trends in other environmental variables like Mississippi River Flow and nutrient flux. The specific objectives of this chapter are to: (1) determine the seasonal pattern in DO concentrations based on daily averages over the 20-year period and characterize inter-annual variation within this seasonal pattern, (2) to determine the three aspects of short-term DO variability the rate at which DO concentrations decrease to hypoxic conditions (respiration rates), the persistence of hypoxic events (duration

events) and the relationship of these duration events to river flow and riverine nutrient fluxes, and the frequency at which hypoxic conditions return to normoxic conditions (re-aeration events), and (3) to compare the trends in persistence to Mississippi River fresh water and nutrient flux. An earlier work by Babin and Rabalais (2009) began the characterization of the magnitudes of short-term oxygen variability of these data.

METHODS

Study Area

The study area encompasses the northern Gulf of Mexico from the mouth of the Mississippi River to just beyond the Louisiana-Texas border. The primary data collection site (station C6) is located about 26 km south of Terrebonne Bay, and experiences frequent mid-summer hypoxia (Figure 2.1). Freshwater discharge from the Mississippi River and the prevailing westward coastal current maintain a strong vertical stratification throughout most of the summer season. Stratification breaks down as a result of frontal passages in the winter or tropical storm events during the late summer and early fall (Wiseman et al., 1997). An acoustic Doppler current profiler (ADCP) deployed at this site from mid-March to mid-November 2002 demonstrated a predominantly alongshore flow rather than cross-shelf flow (Wiseman et al., 2004). The mean bottom currents for 1990 were not statistically distinguishable from zero (Rabalais et al., 1994). Winds are predominantly from the southeast (Walker et al., 2005), causing the Louisiana coastal current to flow mainly westward. The plumes from the Mississippi and Atchafalaya Rivers create regions of strong freshwater influence. Mean winds are generally downwelling favorable; however, from late spring to mid or late summer, upwelling favorable flows and a return flow occurs pushing low salinity waters back up the coast (Cochrane et al., 1986).

Data Sources

I used the dissolved oxygen time-series measured at station C6 (Figure 2.1) from 1989 through 2008. The data were obtained using a multi-parameter water quality instrument located at approximately 20 m depth. Bottom dissolved oxygen concentrations, water temperature, and salinity were recorded at 15 minute intervals. The exact location of the sampling station has changed over time, but remained within 500m of the original site and in the core of an area that experiences frequent hypoxia. In 1989, a team of scientists from Louisiana Universities Consortium (LUMCON) first deployed a moored instrument array near an oil platform located at 28° 50.41'N, 90° 26.03'W. In June of 1991, the site moved to a new mooring west of the original platform at 28° 52.18'N, 90° 28.04'W. Between 1989 and 1995, an Endeco type 1184 pulsed dissolved oxygen and temperature recorder, located approximately one meter from the bottom, collected data at 15-minute intervals. In 1996, the sensors were replaced with Yellow Springs Instruments (YSI) sensors and two additional sensors, one at mid-depth and one near the surface, were added to the array. The YSI sonde measured DO with a 6562 Rapid Pulse Dissolved Oxygen Clark Cell type sensor (Table 2.1). In 2004, the site moved to its current location at 28° 52.12'N and 90° 29.42'W. In August of 2005, Hurricane Katrina damaged the array of sensors creating a gap in the data until the site's reconstruction in May 2006 (See mooring diagrams in Figure 2.3.). All of the YSI model 6600 EDS sensors were upgraded to the V2 system in 2007. At this time, the Clark cell oxygen sensors were replaced with the YSI 6150 ROX Optical Dissolved Oxygen sensor (Table 2.1). Rotating instruments on a four to six week cycle for maintenance, pre- and post-calibration to Winkler dissolved oxygen titrations, and monthly comparisons with an independent water quality sonde further insured data quality. I used these 15 minute sampled data as reported with no further corrections as the starting point for all

analysis. These data were imported into a Microsoft Structured Query Language (MS SQL) database (Microsoft Corporation, 2010) for analysis.

Table 2.1. Different sensors used to measure the dissolved oxygen concentrations throughout the 20 year period (1989-2008).

Sensor	Range	Resolution	Accuracy
Endeco Type 1184		0.08 mg l^{-1}	±0.0256 mg l^{-1}
6562 Rapid Pulse Dissolved Oxygen Sensor (Clark Cell)	0 to 50 mg l^{-1}	0.01 mg l^{-1}	0 to 20 mg l^{-1}: ±2% of reading or 0.2 mg l^{-1}, whichever is greater 20 to 50 mg/L: ±6% of reading
YSI 6150 ROX Optical Dissolved Oxygen	0 to 50 mg l^{-1}	0.01 mg l^{-1}	0 to 20 mg l^{-1}: ± 0.1 mg l^{-1} or 1% of reading, whichever is greater; 20 to 50 mg l^{-1}: ±15% of reading, relative to calibration gases

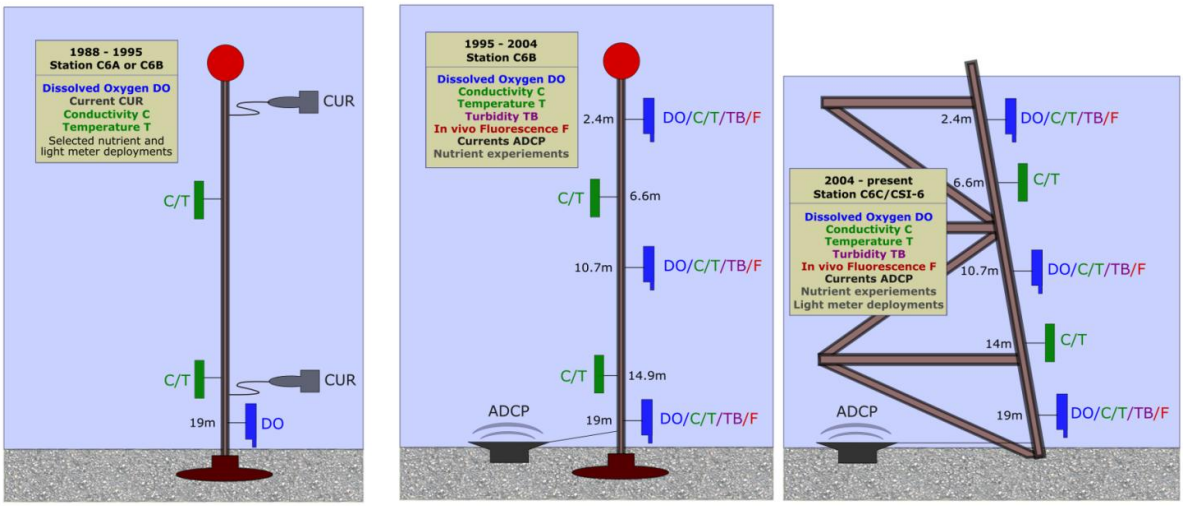

Figure 2.3. Mooring diagrams depict the position of the instruments in the sampling array at site C6. The bottom DO sensor collected the data for this study (figure by K. Sinclair).

Data Analysis

A variety of methods were used to explore the patterns and trends in seasonal and short-term (hours to days) oxygen variability over a 20-year period (1989-2008). Table 2.2 outlines the methods that were used in this study. First, I calculated various summary statistics from the

Table 2.2 Outline of methods used to explore the patterns and trends in seasonal and short-term (hours to days) oxygen variability over a 20-year period (1989-2008)

Analysis	Methods	Data Used	Question	Presentation
Descriptive	Summary statistics (average, minimum, maximum) Graphical Analysis (entire time-series & by years	15 minute samples of DO Concentrations	Does a trend exist in DO concentrations over 20 years (1989-2008)?	Plot of daily averages, daily maximums, and daily minimums Plots for each year
Respiration Rate	Calculated - ΔDO Averaged daily, monthly, annually	Hourly averaged DO Concentrations	Is there an annual trend or seasonal trend in the respiration rates?	Box and Whiskers plot by month
Persistence Events	Moving Window Trigger Algorithm (MWT)	15 minute samples of DO Concentrations	Is there an annual trend in the duration events?	Plot showing duration events by year Table summarizing events
	Regression Analysis	Results from MWT and Areal Extent as published on www.gulfhypoxia.net River Flow from USACE Mississippi River Nutrient Loads from USGS	Are duration events correlated with areal extent and/or river flow?	Regression plots Table of data
Mixing Events	Calculated +ΔDO	Hourly averaged DO Concentrations	Is there an annual trend or seasonal trend in mixing events?	Bar plot of mixing events by year and by month

15 minute samples of near-bottom DO concentrations and created time-series plots from the 15-minute samples. Then, I explored three aspects of oxygen variability: respiration rates, persistence events, or periods of continuous low oxygen, and DO mixing events, or rapid increases in DO

Descriptive Analysis

First, I characterized the near-bottom DO concentrations at station C6 over the 20 year period from 1989 to 2008 by determining an average year and then compared other years to this average year. Daily averages, minima, and maxima were computed from the 15 minute samples of dissolved oxygen concentrations using a Microsoft Transact-SQL query (Spetic and Gennick, 2002). I plotted the entire time-series of daily averages of DO concentrations to determine if a trend exists. Further, I plotted the 15 minute samples of DO concentrations each year separately to look at patterns among the years. Finally, I averaged the DO concentrations daily over the 20 years and plotted these daily values to determine a seasonal trend. All plots for this descriptive analysis were created in R statistical programming software (R Development Core Team, 2011).

Respiration Rate Analysis

I computed respiration rates from the hourly averaged near-bottom DO concentrations from the raw data measured in 15 minute intervals at station C6 from 1989 to 2008. Hourly rates of change in DO were calculated by a backward-in-time differencing method where ΔDO $(mg\ l^{-1}\ h) = DO^{n} - DO^{n-1}$, using R statistical programming software (R Development Core Team, 2011). The calculated rates of change were then divided into positive and negative values, representing increases and decreases in dissolved oxygen concentrations. The positive rates of change in DO concentrations indicated that re-aeration and oxygen production are stronger than respiration. The negative rates indicated the prevalence of respiration. I partitioned the rates of

change into daylight (6:00 am to 6:00 pm CST) and night (6:00 pm to 6:00 am CST) hours to determine if there was a significant difference between nighttime ΔDO and daytime ΔDO values. I found a high correlation (adjusted $R^2 = 0.8157$; p-value < 0.001) between the nighttime and daytime rates in DO, so the entire dataset was used in the analysis.

I then compared these annually and monthly averaged respiration rates to determine if a trend existed among years and within years over the 20 years I plotted box-and-whisker plots for averaged rates by both year and month to determine the annual and seasonal variability of the respiration rates using R Statistical Computing Software (R Development Core Team, 2011).

Persistence Event Analysis (MWT)

The persistence event analysis involved three parts. First, I identified all of the persistence events where the 15-minute sampled DO concentrations stayed below a threshold of low oxygen for an extended amount of time. I used the moving window trigger (MWT) algorithm on the 15-minute near-bottom DO concentration samples taken at station C6 over 20 years, 1989 to 2008, to determine the number and duration of persistence events. I then used these events to determine a "season" for hypoxia for each year. I compared season and number of days below the low oxygen thresholds to the areal extent and Mississippi River flow and nutrient flux.

I first identified and characterized persistence, or low DO, events using a moving window trigger (MWT) algorithm programmed in Matlab (Mathworks, 2009). Codiga et al., (2009) developed this algorithm to provide a general method to find discrete "hypoxic events" within a time-series record and to quantify the severity of these events. The MWT algorithm uses threshold, minimum event duration, and trigger duration as input parameters. The MWT fills in

gaps in the data shorter than the trigger duration using linear interpolation. Gaps longer than the trigger duration are identified in the graphic representation of the results.

The MWT quantified the event characteristics with three output metrics: duration, event-mean deficit, and deficit duration. The duration is the length of the event in days, and the event-mean deficit is the average DO value less the threshold value. Thus, a higher event-mean deficit means more intense hypoxia. The deficit duration is the integrated deficit during an event computed as the product of the duration and the event mean deficit (Codiga et al., 2009).

Codiga et al. (2009) used the water quality thresholds suboxic at 4.8 mg O_2 l^{-1}, hypoxic at 2.9 mg O_2 l^{-1}, and severely hypoxic at 1.4 mg O_2 l^{-1} from the regulations adopted by the state of Rhode Island (RIDEM, 2006). These regulations were based on the Environmental Protection Agency (USEPA 2000) criteria and took into account larval fish recruitment effects.

I developed a similar set of thresholds for use with the MWT because well-established management thresholds for severity of hypoxia, as used by Codiga et al., (2009) are not universal in the NGOM. I defined three categories of DO concentrations—suboxic, hypoxic, and severely hypoxic. I defined suboxic events as a period of DO concentrations with a threshold of 4.59 mg l^{-1} using the threshold from Vaquer-Sunyer and Duarte (2008). I defined hypoxic events as a period of persistent DO concentrations $\leq$ 2 mg l^{-1}, the operational definition of hypoxia used in the NGOM due to a marked decline in fish and shrimp density that occurs below 2.0 mg l^{-1} (Renaud, 1986). I used the Baustian and Rabalais, (2009) definition for severely hypoxic events as a period of persistent DO concentrations $\leq$ 1 mg l^{-1}.

I ran the MWT three separate times for each of the three hypoxic event categories on the original 15-minute DO concentration data for each of the twenty years (1989-2008) using these

threshold values along with a minimum event duration of 1 day and a trigger duration of 1 hour. The only output value from the MWT algorithm I used in further analysis was duration.

I graphically compared the persistence events identified by the MWT. I plotted all duration events by year delineating the suboxic, hypoxic, and severely hypoxic. I quantified the number of days sampled for each year at each of these thresholds—suboxic ($DO \leq 4.59$ mg l^{-1}), hypoxic ($DO \leq 2$ mg l^{-1}), and severely hypoxic ($DO \leq 1$ mg l^{-1}), to explore the relationship among the duration events at these thresholds by years. I then computed the percentage of the days sampled that the DO concentrations fell below each threshold. Finally, I compared the ratios of these percentages among the three thresholds for all years.

Persistence Event Analysis (Regression)

I compared the persistence measures of length of hypoxic season and the number of days below each threshold, to the areal extent of hypoxia, Mississippi River flow and nutrient flux in the same year to determine if these persistence metrics indicated the same trends in severity as the Gulf-wide areal extent. The hypoxia "season" begins with the first day of the first hypoxic event persistence event and ends with the last day of the last event for that year. Although mixing may occur between persistence events, I used these initial and final days to determine the season of hypoxia. I qualified the length of the hypoxia season for each year by subtracting the last day from the first day. I then compared the length of the hypoxia season and the number of days at each of the thresholds to the annual areal extent. I also compared these annual metrics, areal extent, length of season, number of suboxic days, number of hypoxic days, and number of severely hypoxic days, to the Mississippi River flow rates using data from the Mississippi River at Tarbert Landing, MS. The flow data were obtained from the United States Army Corps of Engineers (USACE) website http://toxics.usgs.gov/hypoxia/mississippi/flux_ests/delivery/. I

also subtracted the date of the maximum Mississippi River flow from the date of the onset of the hypoxia season to determine if a relationship exists with the lag to onset.

I used linear regression to compare the annual metrics, areal extent, season, the number of days suboxic, the number of days hypoxic, and the number of days severely hypoxic, to Mississippi River nutrient fluxes and flow. I used linear regression to compare these annual metrics to year to determine if an annual trend was present over the 20 years. Others have shown that the areal extent correlates with Mississippi River nutrient flux and flow (Forrest et al., 2011), so I ran linear regression comparing the annual metrics from this study to areal extent and to various nutrient and flow variables repeating the regression performed by others. Table 2.3 shows the explanatory variables and the response variables for the linear regressions. The areal extents were obtained from Louisiana Universities Marine Consortium (LUMCON) data (www.gulfhypoxia.net). I compared all five annual metrics, season, the number of days suboxic, the number of days hypoxic, and the number of days severely hypoxic, to the total annual Mississippi River flow, maximum Mississippi River flow, May integrated, or the summed total for the month, Mississippi River flow, June integrated Mississippi River flow, combined May and June integrated Mississippi River flow, and the total combined annual flow from the Mississippi and Atchafalaya Rivers from the USACE data as described above. I also used the May and annual total estimates for the nutrients, nitrate and nitrite combined (NO3+NO2), Total Kjeldahl nitrogen (TKN), anydrous ammonia (NH3), total phosphorus (TP), orthophosphate (OrthoP), silica (SiO2) as published by the United States Geological Survey (USGS) website http://toxics.usgs.gov/hypoxia/mississippi /flux_ests/delivery/index.html (Aulenbach et al., 2007). All of the total annual nutrient fluxes and river flows were summed over the water year (from October the previous year through September).

Table 2.3 Variables used in the regression analysis between annual metrics and Mississippi River flow and nutrient flux.	
Y-variable	X-variable
Areal Extent Season Days Suboxic Days Hypoxic Days Severely Hypoxic	Year
Season Days Suboxic Days Hypoxic Days Severely Hypoxic	Areal Extent
Areal Extent Season Days Suboxic Days Hypoxic Days Severely Hypoxic	Average, Total, Maximum, May integrated, June Integrated, May & June Mississippi River Flow
Areal Extent Season Days Suboxic Days Hypoxic Days Severely Hypoxic	Total MS & AR Flow
Areal Extent Season Days Suboxic Days Hypoxic Days Severely Hypoxic	May NO3+NO2, TKN, NH3, TP, OrthoP, SiO2
Areal Extent Season Days Suboxic Days Hypoxic Days Severely Hypoxic	Total NO3+NO2, TKN, NH3, TP, OrthoP, SiO2

Mixing Event Analysis

I analyzed the frequency and trends of mixing events using the positive ΔDO values from the respiration rate analysis. Mixing events were defined as rapid increases in DO concentrations ($\Delta DO \geq 2$ mg l^{-1} h^{-1}). These events re-aerate the bottom waters dissipating hypoxia often within hours of occurrence. I quantified the number of events by year and by month for $\Delta DO \geq 1.5$ mg l^{-1} h^{-1} and for $\Delta DO \geq 2$ mg l^{-1} h^{-1}. The first counts were inclusive of

the second. I then created a bar graph showing the frequency of occurrences for each of the two definitions of mixing events by year and by month.

RESULTS

Descriptive Analysis

No clear temporal trend was evident from the plot of the entire 1989-2008 time-series of daily averaged DO concentrations. This indicated no overall temporal decrease in DO concentrations over the 20 year period (Figure 1.2). DO concentrations ranged from 0.0 to 8.0 mg O_2 l^{-1}. The mean DO concentration for the entire data set was 2.91 mg l^{-1}, just slightly above the threshold for hypoxia ($\leq$ 2.0 mg O_2 l^{-1}). The plot indicated a consistent hypoxia season each year, whereby DO concentrations dropped below the hypoxia threshold every summer and returned to normal conditions for the remainder of the year.

The averaged daily DO concentrations for the entire data set showed a typical sinusoidal pattern with a maximum of about 7 mg O_2 l^{-1} in December and a minimum of about 0.1 mg O_2 l^{-1} during August (Figure 2.4). During the winter months (January through March), the daily average DO concentrations were between 2.9 and 7.8 mg O_2 l^{-1}. In March, the DO concentrations began to decline. Although the DO concentrations occasionally fell below 2.0 mg O_2 l^{-1} during April and May, a typical range for springtime DO concentrations was between 2.3 and 4.8 mg O_2 l^{-1}. Between June and September, DO concentrations generally stayed below 2.0 mg O_2 l^{-1}. During September and October, DO concentrations rose from 2.0 mg O_2 l^{-1} to 7.1 mg O_2 l^{-1}, and remained at these concentrations throughout the late fall and winter.

It should be noted that because the data were not evenly distributed throughout the entire time-series, some days were sampled with greater frequency than others, causing spikes in the plot of daily averages (Figure 2.4). Winter months (December, January, and February) were the

least sampled, while summer months (June, July, August) had the highest sampling frequency. The maximum daily DO averages showed that of all the years sampled the daily DO average for August 2 was always below the hypoxia threshold. The minimum daily averages indicated that daily DO averages below the hypoxia threshold occurred at all times of the year with the exception of December.

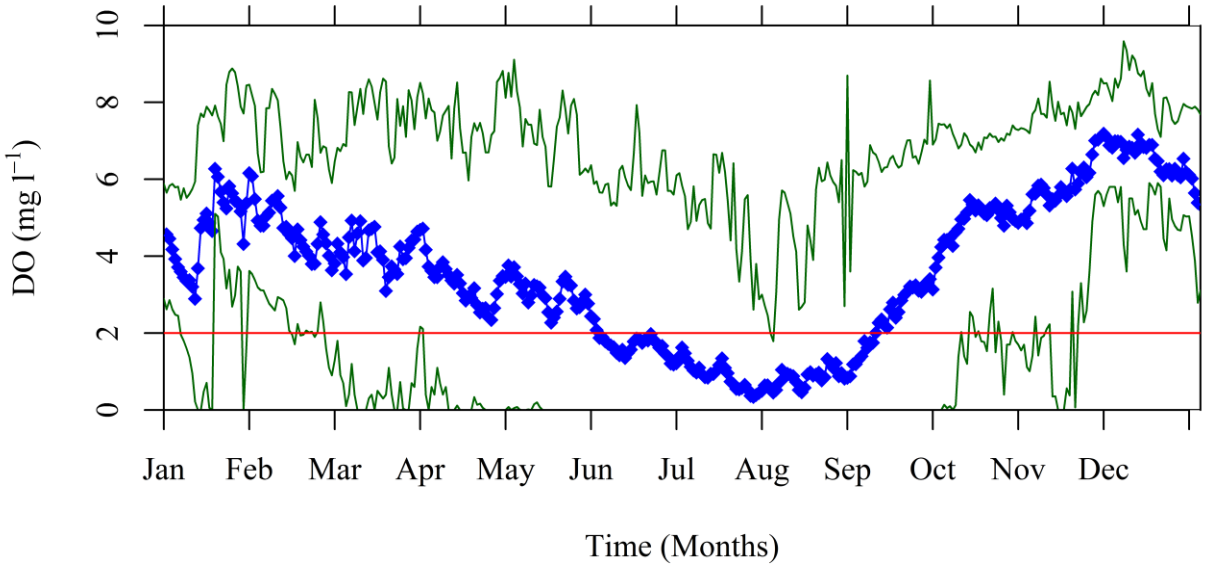

Figure 2.4. Daily averages of dissolved oxygen concentrations for the entire time-series 1989-2008 (blue line and symbols). Green lines indicate the maximum and minimum daily values from all years. The red line indicates the hypoxia threshold (DO $\leq$ 2 mg l^{-1}).

Although the daily averages indicated a seasonal pattern, plots of the 15 minute values showed that the onset, duration, and dissipation of the hypoxia season varied among years (Figure 2.5). This suggests that multiple periodic and episodic factors must be used to explain the short-term variability in the DO concentrations. The earliest onset of the hypoxia season was in January of 2007. In 1993, the hypoxia season began as early as April. In contrast, in 1994, the hypoxia season did not begin to setup until June, and in 2004 hypoxia did not set up until late July. In some years (e.g., 2005 and 2006), mixing fragmented the hypoxia season. Hurricane Cindy mixed the water column in July of 2005. In 2005, the record was cut short due to damage to the platform and equipment from Hurricane Katrina. The hypoxia season for 2006 was

Figure 2.5. Time-series of 15-minute DO concentrations for 1989-2008 at a station (C6) within the core of the NGOM hypoxic zone. Gaps in the data are mostly from the winter months when the conditions were too severe for divers to deploy the sensors. Horizontal shaded red bar marks the hypoxia threshold. Brown vertical bars mark the date of the maximum river flow. Red vertical bars mark the beginning of the hypoxia season and blue vertical bars mark the end of the hypoxia season for that year. (Figure on next page)

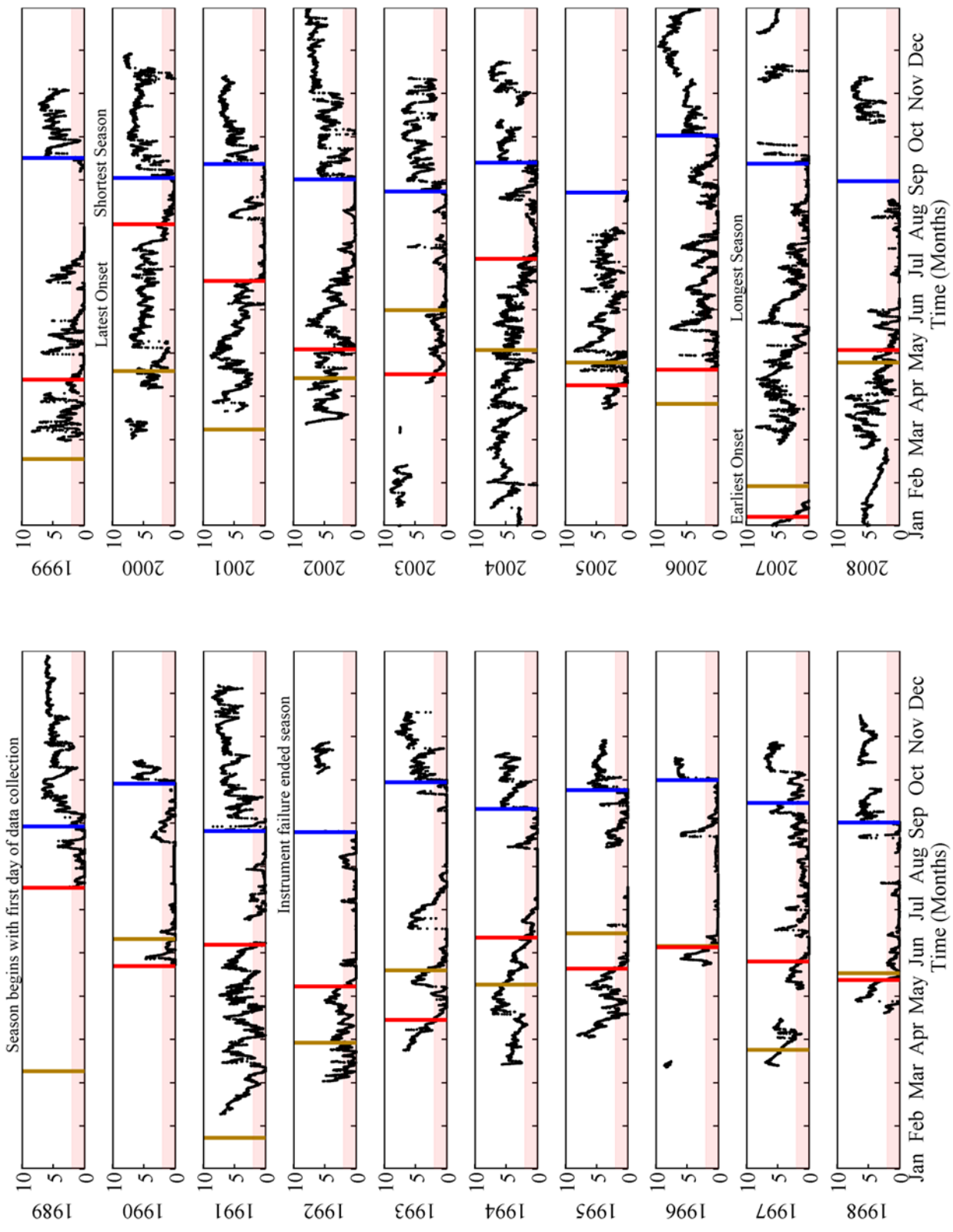
Season begins with first day of data collection
Instrument failure ended season
Latest Onset
Shortest Season
Earliest Onset
Longest Season
1989
1990
1991
1992
1993
1994
1995
1996
1997
1998
1999
2000
2001
2002
2003
2004
2005
2006
2007
2008
Jan Feb Mar Apr May Jun Jul Aug Sep Oct Nov Dec
Time (Months)

interrupted often by episodic wind events even though hypoxia was present 157 days of the year and the season went from late April through October.

Respiration Rate Analysis

Respiration rates varied within the year with a seasonal pattern and among years with a slight upward trend. Hourly respiration rates varied between 0 and 3.69 mg l^{-1} h^{-1}, with an average value of 0.08 mg l^{-1} h^{-1}. Monthly averages of hourly respiration rates ($\Delta DO \leq 0$) averaged over the entire 1989-2008 period varied from 0 to 0.28 mg l^{-1} h^{-1} (Figure 2.6 upper panel). The rates varied more in the spring months (March-June) due to the variability of the onset of hypoxia and the episodic wind events. Average respiration rates were the lowest during June and July, coinciding with the lowest DO concentrations and were the highest during spring and fall. As shown in the lower panel of figure 2.6, the median of the annually averaged hourly respiration rates increased slightly over the 20 year period (1989-2008). The range of hourly respiration rates also increased from 1989 to 2008 this is evident in the increase in the box length in the Box-and-Whiskers plot (lower panel of figure 2.6).

The time for normoxic waters to become hypoxic during the spring months can vary from as short as one day to up to 25 days. The upper panel of figure 2.6 showed that the June and July rates were the lowest. This was possibly due to lower DO concentrations during those months. This was also the time of year when hypoxic conditions were already present and little mixing occurred. The upper panel of figure 2.6 also showed that the rates varied the least in January and February possibly due to lack of samples from these months.

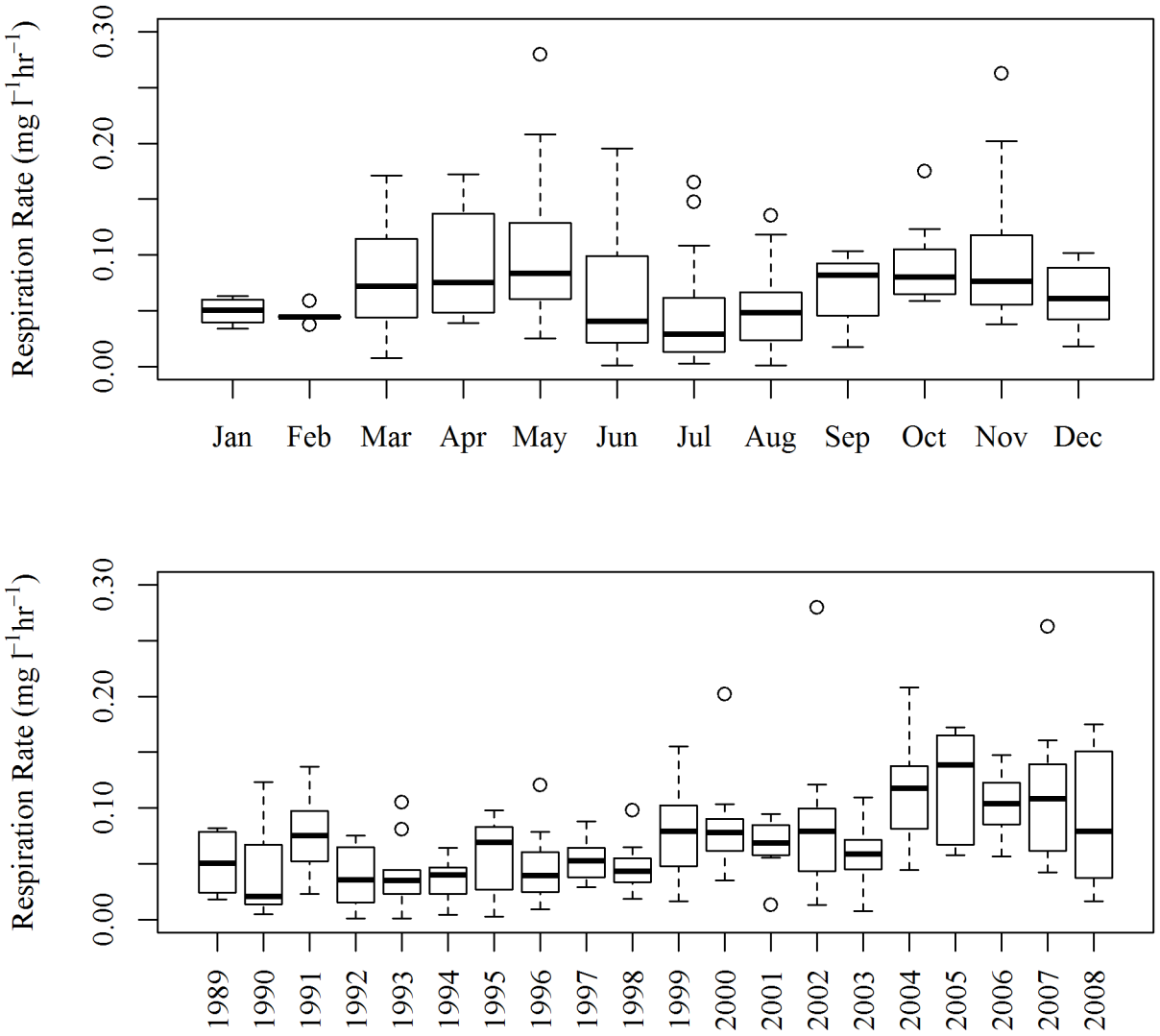

Figure 2.6. Box-and-Whiskers plot of hourly respiration rates ($\Delta DO \leq 0$) over 20 years (1989-2008) averaged by month (top panel) and year (bottom panel). The horizontal lines inside the boxes represent the median, the box bottom and top show the lower and upper quartiles respectively, and the whiskers show the 5th and 95th percentiles. (Upper Panel from Babin and Rabalais, 2009)

Persistence Event Analysis (MWT)

The persistence event analysis using the MWT showed large inter-annual variations in the persistence of hypoxia and no clear trend of increasing intensity of events was present although the longest events occurred in 2002 and 2008 (Figure 2.7). For example, during 1993

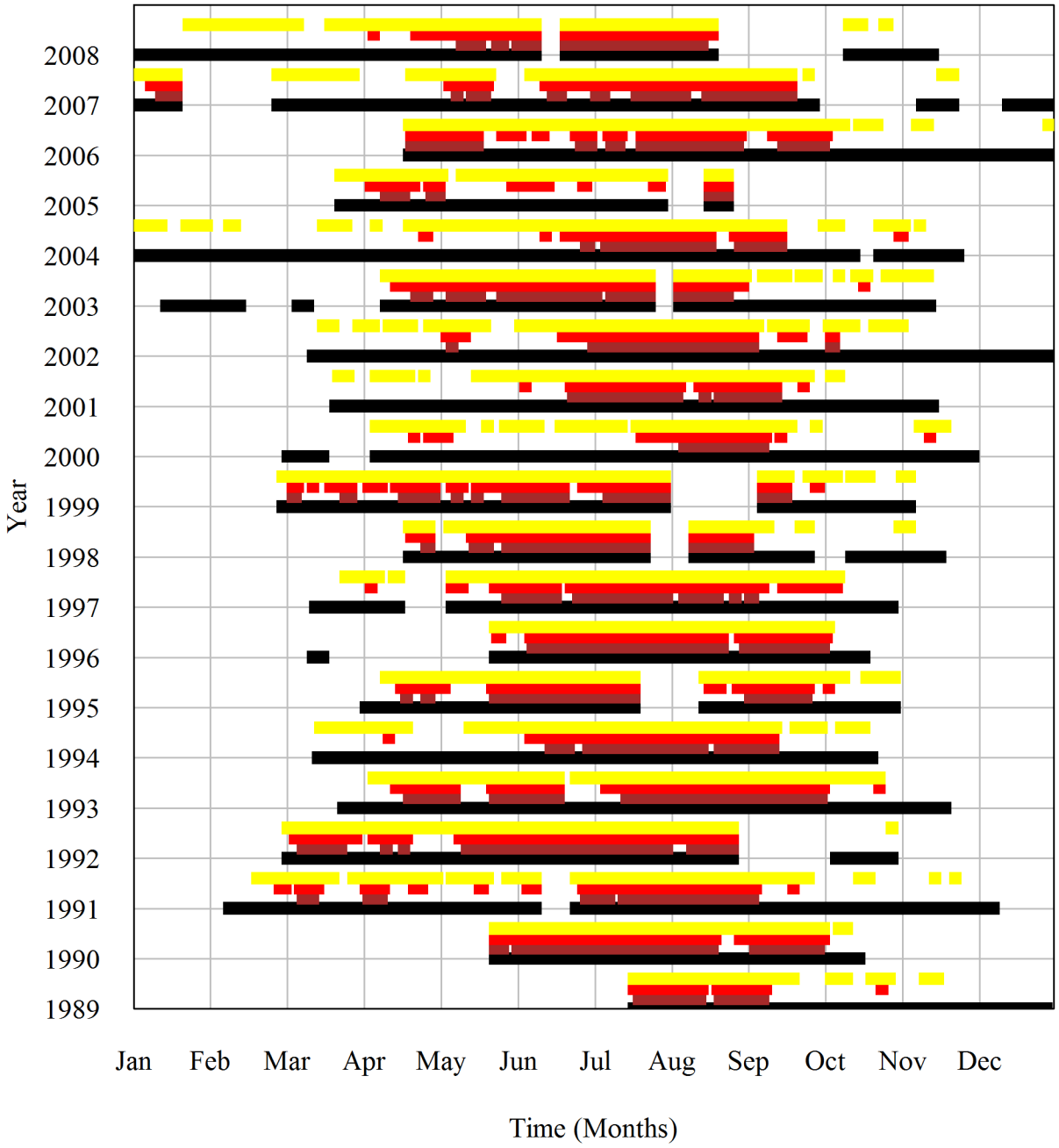

Figure 2.7. Plot showing duration of persistence events by year determined from a near-bottom DO time-series measured in 15-minute intervals at station C6. A persistence event is the period of time that the DO concentrations drop below a threshold. The black lines indicate days sampled. Brown lines indicate severely hypoxic events (≤ 1.0 mg l^{-1}). Red lines indicate hypoxic events (≤ 2.0 mg l^{-1}). Yellow lines indicate suboxic events (≤ 4.59 mg l^{-1}).

there were ten hypoxic events, the longest of which persisted for 46 days. In 2008, there were seven hypoxic events, including the longest hypoxic event in the 1989-2008 record (65 days). The longest severely hypoxic (DO $\leq$ 1 mg l^{-1}) event between 1989 and 2008 was recorded during 1996 (44 days). This event may have been longer than estimated here, but the data collection was interrupted by instrument failure. During 2002, there were three severely hypoxic events lasting 23, 11, and 22 days. The longest suboxic (DO $\leq$ 4.9 mg l^{-1}) event that lasted 132 days was recorded in 2008. The year 2002 had the largest number (22) of recorded suboxic events. These longer events may simply be due to longer sampling periods in later years. Table 2.4 summarizes the duration events identified by the MWT algorithm.

Over the 20 years from 1989 to 2008 the near-bottom DO concentrations at station C6 were below the hypoxic threshold almost half of the time although there was a great deal of variation among years (Figure 2.8). Of the 4516 days sampled, the daily average DO concentration was below the suboxic threshold (4.59 mg l^{-1}) 69% of the time, below the hypoxic threshold (2.0 mg l^{-1}) 42% of the time and below the severely hypoxic threshold (1.0 mg l^{-1}) 31% of the time (Table 2.5). DO values stayed below the suboxic threshold for over 100 days every year except 1989. The year 1989 showed only 76 days below the suboxic threshold, but the sample record consisted of only 163 days that year. In 1996, 100% of the days sampled were below the suboxic threshold. This same year the ratios of hypoxic to suboxic days were 73% and the ratio of hypoxic to severely hypoxic to suboxic days were 67%.

The extreme years (high and low river flow) and the average years appear to correlate well with both length of season and the areal extent based on the snapshot survey reported by others , although there is quite a bit of variation among other years (Table 2.6). For example, the year 2000 was a low flow year, with the lowest average flow of 11,883 $m^3 s^{-1}$ and the lowest

Table 2.4. Results from the Moving Window Trigger Algorithm summarizing the low oxygen events by year and by threshold. Count is the number of events for the indicated year. Mean is the mean duration in days of all events from the year. Min is the duration in days of the shortest event and Max is the duration in days of the longest event.

	Suboxic ($DO \leq 4.59$ mg l^{-1})				Hypoxic ($DO \leq 2.0$ mg l^{-1})				Severely Hypoxic ($DO \leq 1.0$ mg l^{-1})			
Year	Count	Mean	Min	Max	Count	Mean	Min	Max	Count	Mean	Min	Max
1989	7	11	1	28	4	11	3	27	9	4	1	7
1990	8	17	1	33	9	13	1	33	8	12	2	33
1991	17	9	1	49	15	6	1	17	11	5	1	14
1992	4	44	1	119	15	9	1	42	12	9	1	41
1993	13	13	1	46	10	13	1	46	15	7	2	40
1994	12	14	1	65	6	15	1	26	8	9	1	24
1995	10	15	1	66	10	10	0	29	12	6	0	26
1996	6	25	11	45	6	18	1	45	7	14	2	44
1997	10	18	1	63	17	6	1	44	13	4	1	15
1998	11	10	1	38	8	12	1	36	11	7	1	23
1999	17	9	1	34	14	7	1	27	9	8	1	23
2000	19	5	1	52	8	7	1	33	3	9	1	23
2001	15	9	1	48	4	17	1	43	3	22	2	42
2002	27	6	0	79	17	5	0	50	6	10	0	22
2003	13	14	1	105	10	12	1	37	11	8	1	30
2004	22	8	1	67	8	9	1	40	9	5	1	23
2005	18	7	1	30	10	5	1	25	4	6	1	13
2006	9	19	1	77	13	7	1	22	12	6	1	18
2007	16	13	1	80	14	8	1	30	14	6	1	28
2008	10	23	1	132	7	16	2	65	9	9	2	25

Table 2.5. The number of days sampled by year and the number of days at each of the dissolved oxygen concentration thresholds (in mg l^{-1}).

Year	Days Sampled	Days ≤4.59	Days >4.59	% ≤4.59	Days ≤2.0	Days >2.0	% ≤2.0	Days ≤1.0	Days >1.0	% ≤1.0
1989	163	76	87	46	46	117	28	34	129	21
1990	145	134	11	93	115	30	79	95	50	65
1991	303	161	142	53	85	218	28	58	245	19
1992	213	175	38	82	134	79	63	104	109	49
1993	238	171	67	72	131	107	55	111	127	47
1994	220	171	49	78	91	129	41	73	147	33
1995	183	148	35	81	96	87	53	74	109	41
1996	151	150	1	100	110	41	73	101	50	67
1997	208	182	26	87	110	98	53	54	154	26
1998	195	113	82	58	95	100	49	76	119	39
1999	249	158	91	63	104	145	42	73	176	29
2000	257	101	156	39	55	202	21	26	231	10
2001	237	139	98	59	70	167	30	67	170	28
2002	294	152	142	52	82	212	28	59	235	20
2003	241	183	58	76	122	119	51	84	157	35
2004	318	170	148	53	69	249	22	46	272	14
2005	137	126	11	92	49	88	36	24	113	18
2006	254	168	86	66	97	157	38	67	187	27
2007	256	215	41	84	113	143	44	79	177	31
2008	254	235	19	92	114	140	45	79	175	31
Total	4516	3128	1388	69	1888	2628	42	1383	3133	31
Average	225.8	156	69	69	94	131	42	69	157	31

Table 2.6. Compares various annual metrics of Mississippi River flow and hypoxia ($DO \leq 2.0$ mg l^{-1}). Mississippi River flow was measured daily at Tarbert Landing, MS. Lag to onset is the number of days between the maximum daily flow and the beginning of the hypoxia season. The hypoxia season is defined as the time between the first day of the first hypoxia even and the last day of the last hypoxia event in a given year. The areal extent is from the annual mid-summer mapping cruise (Data from www.gulfhypoxia.net).

Year	Average Daily Flow ($m^3 s^{-1}$)	Maximum Daily Flow ($m^3 s^{-1}$)	Max Flow Date	Lag to Onset (days)	Begin Hypoxic Events	End Hypoxic Events	Length of Season (days)	Areal Extent (km^2)
1989	20,214	40,171	3/11	130	7/19	8/31	43	nil
1990	21,687	43,419	6/12	-18	5/24	9/30	129	9,260
1991	22,841	45,996	1/23	137	6/8	8/28	80	11,920
1992	16,589	27,181	3/30	41	5/9	8/26	109	10,804
1993	27,282	42,431	5/21	-34	4/17	10/1	168	17,600
1994	19,626	41,089	5/11	34	6/14	9/12	91	16,600
1995	18,094	41,195	6/16	-24	5/23	9/26	126	18,200
1996	19,838	36,218	6/6	0	6/6	10/1	118	17,920
1997	21,172	52,244	3/26	63	5/28	9/16	112	15,840
1998	21,310	38,124	5/19	-4	5/15	9/3	111	12,480
1999	17,499	41,619	2/17	57	4/15	9/18	156	20,000
2000	11,883	24,145	4/19	105	8/1	9/3	33	4,400
2001	17,632	39,536	3/10	106	6/23	9/13	82	20,720
2002	18,770	35,865	4/15	21	5/6	9/3	120	22,000
2003	17,373	25,946	6/2	-44	4/18	8/25	129	8,560
2004	20,523	43,384	5/4	65	7/8	9/13	68	15,040
2005	15,483	24,145	4/26	-15	4/10	8/24	136	11,840
2006	12,189	25,946	3/28	25	4/22	10/3	165	17,280
2007	16,047	32,829	1/29	-21	1/8	9/14	249	20,500
2008	22,664	51,397	4/25	10	5/4	8/31	119	20,720
Average	18,936	37,644		32			117	15,352
Median	19,198	39,854		23.23			118.34	16600
Max	27,282	52,244		136.92			248.81	22000
Min	11,883	24,145		-44.15			32.54	4400
Low								
Mid								
High								

maximum river flow of 24,145 $m^3 s^{-1}$. This was also the shortest hypoxia season (33 days) beginning August 1 and lasting until September 3 and the lowest areal extent (4400 km^2) of this 20-year period (1989-2008). The lag of the onset of the hypoxia season from the maximum river flow was 105 days. This implied that in low flow years the onset of the hypoxia season was delayed.

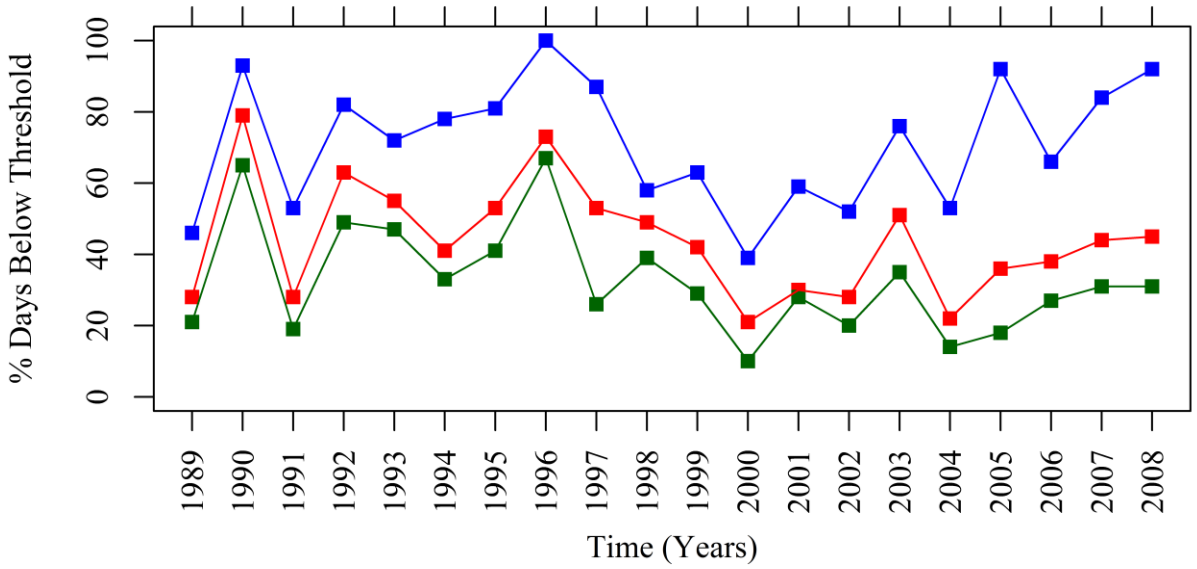

Figure 2.8. Plot showing proportion of days at each threshold to the days sampled for each year. The blue line represents percentage of days sampled where DO $\leq$ 4.59 mg l^{-1}, the red line represents the percentage of days sampled where DO $\leq$ 2.0 mg l^{-1}, and the green line represents the percentage of days where DO $\leq$ 1.0 mg l^{-1}.

In contrast to low flow years, high flow years generally had long hypoxia seasons and large areal extent, but with only loose adherence to the pattern. For example, the year 1993 was a high river flow year with the highest maximum flow (52,244 $m^3 s^{-1}$) and the second to longest hypoxia season (169 days). The onset in 1993 also preceded the maximum river flow by 34 days. However, the areal extent (17,600 km^2) for 1993 was the eighth largest and did not adhere to the pattern because one would have expected it to have the largest areal extent. Another extreme year (2008) had the highest average river flow (22,644 $m^3 s^{-1}$), but the hypoxia season

only lasted 119 days, 2 days more than the overall average. The areal extent in 2008 was tied as the second largest (20,720 km^2). The lag between the maximum river flow and the onset of hypoxia in 2008 was only 10 days. The lags for both years (1993 and 2008) used as examples of high flow years were closer to the maximum river flow, implying an earlier onset of the hypoxia season in high flow years.

All values for 1994 were close to the averages over the entire record. The average flow for 1994 was 19,626 $m^3 s^{-1}$, only 438 more than the average flow over the 20 years and the areal extent was 16,600 km^2, equal to the average areal extent over the 20 years. The length of the season was 91 days, only 26 days less than the average length of the season over the 20 years.

One notable exception to the general patterns seen in the extremes is the year 2007. The year 2007 had the longest hypoxia season (249 days) and one of the largest areal extents on record (20,500 km^2); however the average flow (16,047 $m^3 s^{-1}$) and maximum flow (32,829 $m^3 s^{-1}$) in 2007 were slightly below the average for the 20 years. The onset of the hypoxia season preceded the maximum river flow by 21 days which is earlier than the average onset by 53 days.

Although the average onset of hypoxia for the 20-year period (1989-2008) was 32 days after the peak river flow, the standard deviation was very high (55.5 days). The earliest onset of hypoxia was in January of 2007 preceding the peak river flow by 21 days, and the latest onset was August 1, 2000, with a lag from peak flow of 105 days (Figure 2.5).

Persistence Event Analysis (Regression)

Although none of the annual metrics of season, number of days of suboxic, hypoxic, or severely hypoxic conditions correlated with areal extent of hypoxia, there were combinations that were correlated to the estimated nutrient fluxes from the Mississippi River (Table 2.7). No

relationship existed between any of the annual metrics and year, indicating no consistent trend over time. Thus, these metrics have not shown consistent increase or decrease over the 20 years (1989-2008). None of the annual metric significantly correlated with measures of river. The only annual metrics that showed a correlation to the areal extent was the length of the season (adj $R^2 = 0.27$, p-value = 0.01) and the number of days suboxic (adj $R^2 = 0.31$, p-value = 0.01). None of the other annual metrics, the number of days hypoxic or the number of days severely hypoxic, showed a significant relationship to areal extent. Interestingly, although there was very little correlation between the annual metrics from the time-series measured at station C6 over the 20 years 1989 to 2008 and the annual areal extents measured in the late summer from 1989 to 2008, all five of these annual metrics, areal extent, season, the number of days suboxic, the number of days hypoxic, and the number of days severely hypoxic, correlated with the average May NO_3 + NO_2 flux (Figure 2.9). The number of days below the severely hypoxic threshold had the highest correlation (adj $R^2 = 0.32$, p-value = 0.01), followed by the number of days hypoxic (adj R_2 = 0.31, p-value = 0.01). The correlation between the average May NO_3 + NO_2 flux and the areal extent had an adj $R^2 = 0.27$ (p-value = 0.01).

Another interesting correlation was found between the annual metrics measured at C6 and other nutrients suggesting that other nutrients may play a role as well as the nitrogen in the severity of hypoxia. The areal extent, days hypoxic, and days severely hypoxic, correlated with the average May orthoP: areal extent (adj R^2= 0.25, p-value = 0.02); days hypoxic (adj R^2 = 0.24, p-value = 0.02); days severely hypoxic (adj $R^2 = 0.28$, p-value = 0.01). Days hypoxic and days severely hypoxic also showed some relationship to the total NO_3 + NO_2 (adj R^2= 0.24, p-value = 0.02; adj $R^2 = 0.22$, p-value = 0.02) and the total orthoP (adj $R^2 = 0.21$, p-value = 0.03; adj R^2= 0.21, p-value = 0.03).

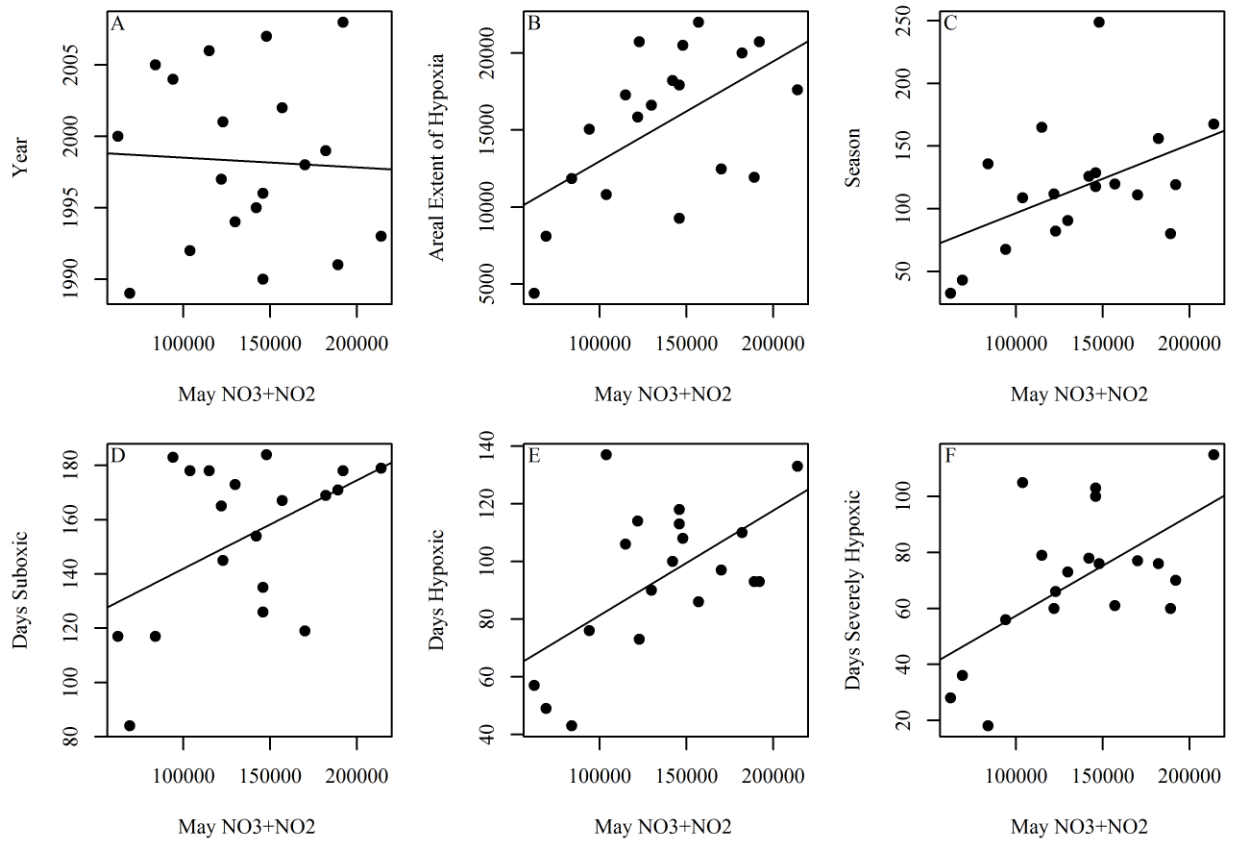

Figure 2.9. Plots of May $NO_3 + NO_2$ flux (in mt) and annual measures of hypoxia severity. Panel A: Year. Panel B: The areal extent of mid-summer hypoxia as measured by the Louisiana Universities Marine Consortium. Panel C: the hypoxia season or the length of time between the first day of the onset of the first hypoxia event in a given year to the last day of the last event. Panel D: Then number of days below the suboxic threshold. Panel E: The number of days below the hypoxic threshold. Panel F: The number of days below the severely hypoxic threshold.

Mixing Event Analysis

Most of the mixing events associated with rapid increase in DO concentrations ($\Delta DO \geq 2.0$ mg l^{-1}) occurred during the spring (March-April) and fall (September-October) (Figure 2.10). Although June and July both had seven mixing events over the 20 year period, July had no intense mixing events. April had a total of 20 mixing events, the most of any month. March had the most intense mixing events of any month. Fifty-nine percent (78/131) of the mixing events

in April increased the DO concentrations above the suboxic threshold (DO $\leq$ 4.9 mg l^{-1}), and all but 3 increased the DO concentrations above the hypoxia threshold (DO $\leq$ 2.0 mg l^{-1}).

Table 2.7. Regression results of comparisons between areal extent of bottom hypoxia as measured by Louisiana Universities Marine Consortium's annual mid-summer cruise over 20 years (1989-2008) and various variables of interest related to river flow and nutrients. Hypoxia season and the number of days at the three thresholds--suboxic, hypoxic, and severely hypoxic--were determined from a C6, a site in the core of the hypoxic zone. Area extent data is from www.hypoxia.net. River flow data is from http://www.mvn.usace.army.mil/cgi-bin/wcmanual.pl?01100. Nutrient data is from http://co.water.usgs.gov/hypoxia/html/nutrients_new.html. Shaded areas indicate significant relationships between variables ($p < 0.05$).

	Areal Extent		Season		Days Suboxic		Days Hypoxic		Days Severely Hypoxic	
	adj. R^2	p-value	adj. R^2	p-value	adj. R^2	p-value	adj. R^2	p-value	adj. R^2	p-value
Year	0.17	0.04	0.08	0.12	0.04	0.21	0.01	0.30	0.04	0.20
Areal Extent	1.00	0.00	0.27	0.01	0.31	0.01	0.05	0.19	0.06	0.15
Average Flow	-0.03	0.52	-0.06	0.93	-0.04	0.57	0.06	0.16	0.11	0.09
Total Flow	-0.03	0.53	-0.06	0.92	-0.04	0.57	0.06	0.16	0.11	0.09
Maximum Flow	0.04	0.19	-0.05	0.69	0.00	0.31	0.00	0.33	-0.01	0.40
May Int. Flow	0.02	0.25	-0.06	0.98	-0.05	0.65	0.08	0.13	0.15	0.06
June Int. Flow	-0.03	0.51	-0.04	0.59	-0.05	0.71	-0.01	0.38	0.05	0.17
May & June Int. Flow	0.02	0.25	-0.06	0.98	-0.05	0.65	0.08	0.13	0.15	0.06
May NO3+NO2	0.27	0.01	0.18	0.04	0.18	0.04	0.31	0.01	0.32	0.01
May TKN	0.00	0.32	-0.05	0.80	0.06	0.16	0.02	0.24	0.03	0.24
May NH3	-0.05	0.76	-0.04	0.60	-0.04	0.63	0.06	0.15	0.16	0.05
May TP	0.32	0.01	0.07	0.14	0.15	0.06	0.04	0.21	0.01	0.28
May OrthoP	0.25	0.02	0.09	0.12	0.14	0.06	0.24	0.02	0.28	0.01
May SiO2	0.12	0.08	0.03	0.24	0.05	0.18	0.25	0.02	0.29	0.01
Total MS & AR Flow	-0.03	0.48	-0.05	0.79	-0.04	0.55	0.01	0.30	-0.01	0.36
Total NO3+NO2	0.04	0.19	0.06	0.16	0.12	0.08	0.24	0.02	0.22	0.02
Total TKN	-0.06	0.97	-0.06	0.82	-0.01	0.39	-0.04	0.56	-0.04	0.58
Total NH3	-0.02	0.43	0.01	0.29	-0.02	0.45	0.01	0.30	0.08	0.13
Total TP	0.11	0.09	-0.02	0.45	0.00	0.35	-0.06	0.99	-0.06	0.99
Total OrthoP	0.14	0.06	0.08	0.13	0.16	0.05	0.21	0.03	0.21	0.03
Total SiO2	-0.01	0.36	0.01	0.30	0.00	0.33	0.10	0.10	0.09	0.11

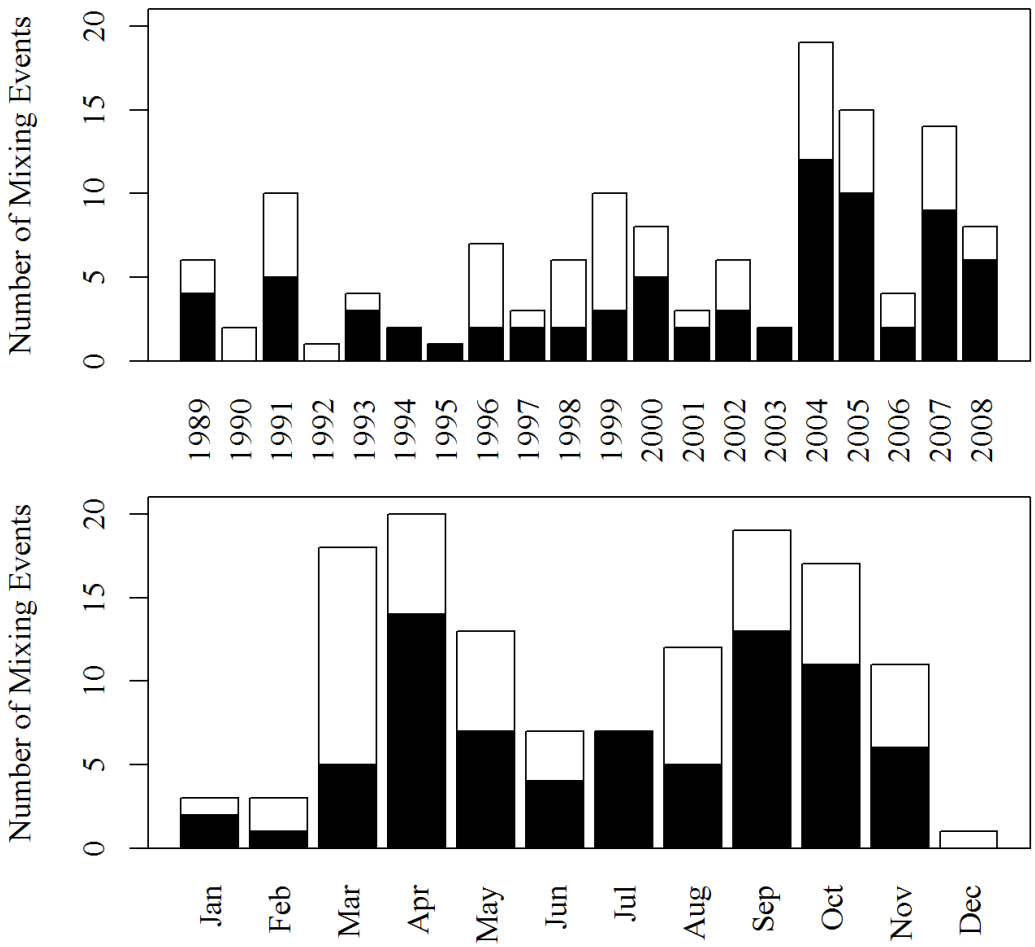

Figure 2.10. The number of mixing events by year (top panel) and by month (bottom panel) for the entire time-series (1989-2008). Bar height represents the total number of mixing events while the shadings indicate the numbers at two intensities. The dark section represents the count of mixing events where $\Delta DO \geq 1.5$ mg l^{-1} but not $\Delta DO \geq 2.0$ mg l^{-1} and light section represents more intense mixing events $\Delta DO \geq 2.0$ mg l^{-1}.

DISCUSSION

Short-term Variability

Prior to this study, our knowledge of the short-term (hours to days) variability of dissolved oxygen concentrations that influenced the dynamics of hypoxia was limited to short (~ 24 hour period) studies with little knowledge of temporal components of this variability. My analyses quantified the short-term variability over 20 years, and also showed that these dynamics

varied seasonally and among the years. Our understanding of hypoxia dynamics depends on how much we know about specific processes affecting short-term variability in DO concentrations, namely respiration rates, duration of hypoxia, and frequency of mixing events. Respiration rates determine how quickly ambient DO concentrations change from normoxia to hypoxia. Respiration rates estimated here varied from within a given year and from year to year, indicating that the respiration rates may change in response to environmental variables and may explain some of the inter-annual variability in the areal extent and the length of the hypoxia season. For example, the highest respiration rate measured in May of 2002 that coincided with the year that the largest areal extent of hypoxia was measured.

Quantifying duration of persistence events explains how persistent hypoxia is throughout a year, and how these conditions might impact living organisms. Although an event may last as long as 65 days, the length and frequency of these events vary in response to other variables. Mixing events determine how frequently hypoxia dissipates and DO conditions return to normal. The frequency of mixing events varied more seasonally than among years indicating a possible relationship to seasonal factors.

Continuous monitoring of dissolved oxygen concentrations over the 20 year period allowed quantification of short-term variability in DO concentrations not available from other monitoring methods. Historically, studying short-term (minutes to days) oxygen variability has been challenging. A common measurement technique includes 24-hour *in situ* sampling and closed dark and light bottle incubations. Although this method may quantify the change in the production and respiration rates of DO concentrations over a twenty-four hour period, it cannot be used to assess changes in DO on time scales ranging from minutes to hours or daily variability. More recently, other techniques of measuring productivity and respiration have been

introduced, including continuously-recording oxygen sensors, laboratory microcosm experiments, the Electron Transport System (ETS) activity (Dortch et al., 1994), and isotope analysis (Quinones-Rivera et al., 2007). The open water continuous monitoring method used in this study allowed me to analyze DO measurements taken at 15 minute intervals and study how DO varies on scales relevant to the manner in which hypoxia impacts the biota and the ecosystem.

In order for hypoxia to occur or re-establish after re-aeration events two conditions must be met. First, the rate at which oxygen is consumed must be greater than the rate at which oxygen is replenished creating the potential for hypoxia, and second, stable water column must be present to prevent resupply of atmospheric oxygen to the bottom water. Variability in both of these processes occurs on short time scales (Hetland and DiMarco, 2008). Oxygen consumption rates are important for hypoxia development because they determine the time it takes for hypoxia to establish or to re-establish after mixing events replenish the DO in the lower water column. Because DO production by photosynthesis is often negligible in the lower water column of the NGOM, the ratio of DO consumption to production is primarily determined by the respiration rate (Quinones-Rivera et al., 2007).

Respiration rates in the NGOM reported by other studies using various methods ranged from 0 to 42 mg l^{-1} h^{-1} (Table 2.8). For example, Turner and Allen (1982) found that respiration rates in the bottom waters of the Louisiana Bight ranged from 0.12 to 8 mg l^{-1} h^{-1}. The average of these rates would reduce the ambient DO concentrations to 0 in less than four weeks. Dortch et al. (1994) studied respiration rates within the Gulf's hypoxic zone and found rates ranging from 0.017 to 13.25 mg l^{-1} h^{-1}. They calculated the time required to deplete the layer below the oxycline by dividing the integrated normoxic concentration by the integrated respiration rate.

Table 2.8. Published respiration rates for the coastal northern Gulf of Mexico

Study	Dates	Rate ($mg\ l^{-1}\ h^{-1}$)	Method	Time to Hypoxia
Turner and Allen, 1982	1976 Nov & July, bottom	0.12-8	light-dark filtered chambers	<100 d to >1,000 d
Chin-Leo and Benner, 1991	1990 July & Aug, surface	1.917-41.167	24-hour light-dark filtered chambers	13 d to 84 d
Chin-Leo and Benner, 1992	1991 Feb, surface	1.958-26.25	24-hour light-dark filtered chambers	
Dortch et al,. 1994	1991 May-Oct, all depths	0.017-13.25	enzymatic measurements of respiratory electron-transport-system (ETS) activity	
Amon and Benner, 1998	May-92	0.011	determined from DO utilization of bacteria assuming a respiratory quotient (RQ) of 1 and multiplying the respiration rate by the incubation time.	
	Jul-93	0.016		
Turner et al., 1998	July, Aug 1992, July 1993, July 1994, April 1994 and Mach 1998	0.0011-0.2	light-dark chambers	< 4 weeks
Rowe et al., 2002	July 1991, April 1992, August 1994	0.6125	SOC-light-dark chambers	
Quinones-Rivera et al., 2007		0.07	stable oxygen isotopes	4 to 5 days
Murrell and Lehrter, 2010		0.02-0.16 (mean 0.085)	SOC-light-dark chambers	~ 4 days
This study	1989-2008	0-3.693 (mean 0.08)	open water continuously monitoring method	~ 4 days

Based on respiration alone, their calculated days-to-oxygen-depletion values ranged from 6 to 1356 days. Murrell and Lehrter (2010) reported respiration rates of 0.02-0.16 mg l^{-1} h^{-1}, with a mean of 0.085 mg l^{-1} h^{-1}, similar to those calculated in this study (0 to 3.693 mg l^{-1} h^{-1}). These rates would reduce normoxic (8 mg l^{-1}) waters to hypoxic in about 4 days. I found that not only did the respiration rates vary seasonally but the variability among the rates also changed from month to month (Figure 2.6). The highest monthly average respiration rate was 0.27 mg l^{-1} h^{-1} in May of 2002, following a high flow year of the Mississippi River and preceding the largest areal extent on record. By consuming DO at a rate of 0.27 mg l^{-1} h^{-1}, it would take only one day to bring the DO concentrations down from normoxia (8 mg l^{-1}) to severe hypoxia (1 mg l^{-1}). The mean respiration rate 0.064 mg l^{-1} h^{-1} calculated for the entire time-series would, in the absence of mixing, create hypoxic conditions in about 4 days. However, the respiration rates were significantly lower during summer months when less DO was present in the bottom waters. Rabalais et al. (1994) showed that it takes 18, 11, or 9 days, in April, May, and June respectively to lower DO concentrations from about 6 mg l^{-1} to less than 2 mg l^{-1}. This study showed that the time it takes to lower DO concentrations from normoxic to hypoxic may have decreased.

The open water continuous monitoring method used to generate the data for this study assumes that the rates of DO consumption are uniform from the pycnocline to the bottom and represents the integrated water column respiration. The open water method does not differentiate between water-column consumption and sediment oxygen consumption (SOC), both of which are important for the development of hypoxia. For example, a mixing model developed by Quinones-Rivera et al. (2007) indicated that benthic respiration was the dominant sink for DO, with SOC accounting for 75% and 42% of the total respiration during the summer and winter periods. Murrell and Lehrter (2010) tested the assumption of a uniform rate below the

pycnocline and found little difference between integrated water column respiration and single bottom water rate measurements. Thus, the single-point method can produce accurate integrated water column estimates in cases where the water below the pycnocline has uniform metabolic characteristics.

The threshold value for defining hypoxia and the duration of hypoxia are both metrics that are important in characterizing the dynamics of hypoxia on scales as it affects aquatic organisms. Organisms experience effects from low DO concentrations at different thresholds. The severity or period of exposure to DO concentrations below 1.0 or 2.0 mg l^{-1} is important to benthic macro-infauna (Rabalais et al., 2010). The most widely accepted DO threshold is 2.0 mg l^{-1} due to a marked decline in fish and shrimp sampling that occurs below 2.0 mg l^{-1} (Renaud, 1986). Baustian and Rabalais (2009) used 1.0 mg l^{-1} as a threshold to describe severely hypoxic waters. Many organisms have the ability to swim and move into more oxygen rich waters to reduce exposure to low DO (Rabalais et al., 2010). This also complicates the selection of a threshold value. In examining the variability of hypoxia thresholds across organisms, Vaquer-Sunyer and Duarte (2008) found ample experimental evidence to show that a single threshold is not adequate to describe how the onset of hypoxia affects many organisms. Ninety percent of experimental studies showed LC_{50} values below concentrations of 4.59 mg l^{-1} (Vaquer-Sunyer and Duarte, 2008). I found that of all of the days sampled, 69% were below this 4.59 mg l^{-1} threshold.

In coastal habitats like the NGOM, benthic organisms are especially susceptible to hypoxia due to their distance from oxygen replenishment from the atmosphere and the fact that sediments tend to be more depleted in oxygen than the water above the bottom (Vaquer-Sunyer and Duarte, 2008). Vaquer-Sunyer and Duarte also found that, based on a review of 206 species

spanning the full taxonomic range of benthic metazoans, the mean lethal time (LT_{50}) to exposure to severe hypoxia (1.0 mg l^{-1}) was 22 days and the median was only 10 days. Ten percent of the species tested showed LT_{50} after only 6.8 h of exposure to acute hypoxia (1.0 mg l^{-1}). The duration analysis showed that an average of 2 severely hypoxic duration events occurred each year and all were severely hypoxic for at least 6.8 h.

Although some severe mixing events ($\Delta DO \geq 2.0$ mg l^{-1} h^{-1}) may have been missed in my analysis due to gaps in the data, the mixing event analysis supported a general seasonal pattern. Most mixing events occurred in the spring and the fall, no strong mixing events occurred in July of any year over the 20 year period. This is probably due to the strength of stratification in the summer requiring more energy to mix the water column, but also due to the absence of tropical storms this early in the season.

Intra-annual Variability

Although every year varies, a seasonal pattern in DO concentrations is indicated by the daily averages over the 20 years. Rabalais et al. (2002) described the general pattern of variability within a year as: (a) a gradual decline in DO concentrations through the spring and summer with episodic increases in DO concentrations from re-aeration by wind-mixing events, (b) extended periods of persistent hypoxia from May through September, (c) episodic increases in DO due to upwelling of deeper water, and (d) persistent wind-mixing events maintaining a mixed water column preventing extended periods of hypoxia.

This conceptual seasonal pattern described by Rabalais et al. (2002) was confirmed by the daily averages over the 20 year-period (1999-2008). As figure 2.4 showed, DO concentrations generally declined in the spring, March, April and May. Hypoxia persisted throughout the summer months, June, July and August. During the fall, September, October, and

November, DO concentrations increased episodically until they stayed completely mixed and normoxic throughout the winter months, December, January, and February.

Inter-annual Variability

Although I described a "typical" seasonal cycle using the data (Figure 2.4), it is evident from the time-series plots (Figure 2.5) that this seasonal pattern varied from year to year in response to annual weather patterns and inter-annual variation in flow and nutrient loads from the Mississippi and the Atchafalaya Rivers. At the extremes (drought and flood years), it seems that Mississippi River flow would easily explain the variability in hypoxia, but the other years exhibit much variability indicating that other factors are needed to obtain a complete picture.

On the lower extreme, a low Mississippi River Flow coincided with smaller areal extent and a shorter hypoxia season. An example of an extreme year was 2000. In the spring of 2000, drought conditions throughout the watershed resulted in a reduced Mississippi River discharge (Rabalais and Turner, 2006). A mean river flow of 11,883 $m^3 s^{-1}$ and a maximum flow of 24,145 $m^3 s^{-1}$ were both the lowest recorded over the 20-year study period. Lower productivity as well as windy spring weather preventing the usual stratification of the water column resulted in an areal extent of only 4,400 km^2 (Rabalais and Turner, 2006), the lowest recorded during the study period. Interestingly, the areal extent of hypoxia during 2000 was smaller than the Action Plan (2008) goal of 5,000 km^2. The onset of hypoxia lagged the peak river flow by 105 days and persisted for only 33 days.

The year 2006 is another example of an extremely low flow year that did not follow the expected pattern. The annual mean flow in 2006 was 12,189 $m^3 s^{-1}$, only slightly greater than that of 2000. However, the areal extent for 2006 measured 17,280 km^2, well above the long-term average. Hypoxia persisted for 165 days, which was also well above the average for persistent

hypoxia (Table 2.6). Although the hypoxia season persisted for 165 days in 2006, an above average number of mixing events that year continually re-aerated the bottom throughout this period.

Viewing the pattern from the other direction, one would expect the year 2002 that had the largest areal extent on record of 22,000 km^2 would also have high river flow. Yet, the daily average river flow for 2002 (18,770 $m^3 s^{-1}$) was only slightly below the daily mean river flow for 1989-2008 (18,936 $m^3 s^{-1}$). The hourly averaged bottom DO concentrations stayed close to the average seasonal curve and the 120 days of persistent hypoxia was only slightly greater than the overall average of 117 days (Table 2.6). Long periods of eastward flow of water on the shelf, contrary to the expected westward flow regime, were observed from May through July 2002. It is common during the summer months for the winds to become southerly along the south Texas coast and force a near shore return flow towards the north and east, thereby causing the low salinity waters to separate from the coast somewhere near the Louisiana-Texas border (Wiseman et al., 2004). Interestingly, the 2002 hurricane season was one of the most active seasons on the Louisiana Coast for more than 100 years with four storms. Hurricane Bertha, Hurricane Hanna, Hurricane Isadore, and Hurricane Lili all made landfall on the Louisiana coast (Stone et al., 2003). Of the four, Hurricane Isadore and Hurricane Lili had the most significant impact on DO concentrations at station C6. These two storms both passed directly over the site shortly after the summertime shelf-wide cruise, so they had no impact on the measured areal extent of hypoxia.

Other partial adherence to the general pattern is provided by years 1993 and 2008. These two years had the longest hypoxic events on record although neither had the longest hypoxia season. The year 1993 is well documented as a flood year, often referred to as the "Great Flood of 1993", where the Mississippi River flow stayed above average during most of the year and the

river had a 62-year maximum discharge for August and September (Justić et al., 1996; Rabalais et al., 1998). In May of 1993, the Mississippi River reached a peak flow of 42,431 $m^3 s^{-1}$, which was a 50-year maximum discharge. The areal extent of hypoxia in the NGOM in 1993 measured 17,600 km^2, exceeding the areal extent of 15,000 km^2 for the first time since the monitoring started in 1985. According to Rabalais et al. (1998), the physical factors of reduced surface water salinities increasing the strength of the pycnocline and biochemical reactions related to 2-4 times higher nutrient concentrations and an order of magnitude greater abundance of phytoplankton contributed to the increased severity and areal extent of hypoxia in 1993.

Again in April 2008, the Mississippi River topped the previous 50 years with a peak flow of 51,397 $m^3 s^{-1}$. The DO concentrations began dropping below the seasonal average as early as April as the Mississippi River flows reached record highs in April and May. The areal extent for 2008 was 20,720 km^2, equal to the areal extent from 2001 as the second largest measurement on record, although Tropical Storm Eduard began re-aerating the bottom waters during the mapping cruise. However, the duration of the hypoxia season was not as record breaking. Hypoxia persisted at the study site for only 119 days, only two more days than the average over the 20-years of this study. Thus, the general seasonal pattern appears stronger at extreme flows years, but my analysis showed that weak adherence and deviations from the pattern occurred among years.

Implications for Management

The areal extent, as measured by the annual mid-summer cruises, is the accepted metric used in the Action Plan to achieve a desired reduction in the areal extent of hypoxia via various nutrient control strategies in the Mississippi River Basin. The current Action Plan goal is targeted at reducing the areal extent of hypoxia to 5000 km^2 by 2015 (Mississippi River/Gulf of

Mexico Watershed Nutrient Task Force, 2008, 2010). In order to determine whether or not this plan is met, the areal extent of hypoxia must be measured on an annual basis. The long term average areal extent of hypoxia is 15,351 km^2, which is over 10,000 km^2 above the goal for the Action Plan (2008). The five year running average over the last five years of my analysis was 17,076 km^2, which is even higher than the long term average (Rabalais et al., 2007). The temporal extent of the survey is 5-6 days and the variability in DO that occurs within that time-period can have a significant impact on the estimation of the areal extent.

Although the current method of assessing the mid-summer extent of hypoxia may be sufficient and consistent enough to support the Action Plan (2008, 2010) of a five-year running average of the hypoxic areal extent less than 5,000 km^2, it may not be the best metric to explain the impact of hypoxia on the ecosystem. The advantages of the areal extent metric include its relative ease of computation, its use as a long-term indicator, and the fact that it is a measure that is readily grasped by the public (Rabalais et al., 2007). However, the short-term oxygen variability is neglected in this metric. The measurements used to derive the areal extent metric are taken during an annual cruise survey in late July-early August. The length of the survey from the sampling of first station to the sampling of the last station may range from 4 to 8 days. During this time, a localized mixing event may affect DO concentrations at any individual station or a subset of stations. Also, the respiration rates reported in this study and in Murrell and Lehrter (2010) are sufficient to reduce the DO concentrations from normoxic to hypoxic levels in less than 4 days. Thus, a station that may not have been hypoxic when the cruise began may become hypoxic by the time it is occupied, and vice-versa.

The Mississippi River controls the amount of freshwater and nutrients delivered to the NGOM, which has an effect on both nutrient loads and the strength of the water column

stratification. Therefore, variability in inflow and associated nutrient fluxes has a large influence on the extent and severity of the areal extent of hypoxia (Rabalais et al., 2010). The river flow affects both the biological processes and the physical processes. The river brings nutrients into the NGOM, promoting increased primary production and chlorophyll. The turbidity of the river plume also prevents light from reaching the lower depths of the water column making primary production less likely. The fresh cold water of the river plume also contributes to the density gradient increasing the stability of the water column.

Several modeling efforts have shown a relationship between river flow as well as the concentration of nutrients from the river and the occurrence of hypoxia. All of these efforts have explored how these factors affect oxygen variability on long temporal scales. After nine summers of mapping the areal extent of hypoxia, Wiseman et al. (1997) found that the best correlation between areal extent and Mississippi River discharge was with the mean discharge from the 11 months of August through June preceding the mid-summer cruise ($R^2 = 0.934$, "but the correlation peak was broad and flat"). Wiseman noted that carbon flux from a major flood may fuel hypoxia for more than the current year. Bianchi et al. (2010) showed the areal extent of summertime hypoxia was significantly correlated with averaged May-June Mississippi River flow in the given year ($R^2 \approx 0.41$, at 95% confidence level). Bianchi et al. (2010) also pointed out the high correlation between May-June flow and May-June nutrient load ($R^2 \approx 0.95$, at 95% confidence level). Turner et al. (2006, 2012) found that the best predictor for the variance of the areal extent of hypoxia is the monthly May load of $NO_3 + NO_2$ prior to the annual July measurement cruise along with a Year term ($R^2 = 0.53$).

This study showed that a similar relationship exists between the duration of the annual hypoxia season at station C6 and both Mississippi River flow and nutrient flux. There is a

significant relationship between the May $NO_3 + NO_2$ flux and the duration of all three thresholds (suboxic, hypoxic, and severely hypoxic) of low oxygen events. This suggests that open water continuous monitoring at a fixed site within the core of the hypoxic zone throughout the year could provide an additional metric for the overall assessment and management of hypoxia in the NGOM. Intensive sampling at a single station is relatively cheap and would include short-term temporal variability that would complement the areal extent metric. Further, the areal extent metric could be improved by the information provided by intensive sampling at single stations and from ongoing modeling efforts (e.g., Hetland and Di Marco, 2008; Wang and Justić 2009) aimed at elucidating short-term variability in DO.

A non-linear relationship including other predictor variables (eg. wind stress) might be a better fit to the data; however, I used simple linear regression in this analysis in order to compare my results to previous analyses that have been used in the management plan designed to mitigate and control hypoxia in the NGOM. A more inclusive model or more complicated model might result in a higher R^2 and be better predictor of hypoxia.

Some of the differences among regression the various analyses can be explained by which years were included in the regressions. I included all 20 years (1989-2008) while other analysis excluded some years due to the occurrence of hurricanes during the summer of the areal extent measurement (Turner et al., 2012). Wiseman et al. (1997) used only years 1985-1994 in their regression analysis. Turner et al. (2006) used years 1985-2005. Turner et al. (2012), used years 1985 to 2011 excluding years of tropical cyclones (1997,2003, 2005, 2008, 2010, 2011) and the year of unusual climatic conditions (2009).

Conclusions

This study characterized the short-term (hours to days) dynamics of DO concentrations in the NGOM hypoxic zone over a 20 year (1989-2008). The three investigated aspects of short-term DO variability included respiration rates (i.e., how quickly bottom waters become hypoxic), duration of hypoxia, and the dissipation of hypoxia (i.e., re-aeration events).

Open-water continuous monitoring of DO concentrations at a single station over a period of 20 years allowed for a better characterization of respiration rates than was done in previous studies. I was able to identify the range of respiration rates present at the study site and show how these rates vary throughout the year and from year to year. The study showed that bottom DO concentrations often change very quickly and that the system can transition from normoxia to hypoxia and vice versa in less than four days. This calls into question the accuracy of the current method of measuring the areal extent of hypoxia in the NGOM whereby different stations are occupied at different times over a ~ week long shelf-wide cruise.

Open-water continuous monitoring of DO concentrations at a single station clearly provides information on DO dynamics that are supplementary to those collected during the annual shelf-wide cruise. Although, no relationship exists between the severity of hypoxia at station C6 and the areal extent of hypoxia in the NGOM, there are significant relationships between the Mississippi River nitrogen flux and severity of hypoxia at station C6. In the absence of an annual cruise to measure the areal extent of hypoxia, managers could benefit from using the metrics of season and/or duration as measured by open-water continuous monitoring to estimate how the severity of hypoxia changes in response to nutrient control actions in the Mississippi Watershed. Although determining the severity of hypoxia at a single station does not capture the DO dynamics over the entire NGOM shelf, it does provide another measure of the

severity hypoxia that is related to riverine nitrogen flux and so it could be used to determine the effectiveness of management practices in reducing nutrient loads from Mississippi Watershed to reduce the severity of hypoxia in the northern Gulf of Mexico.

REFERENCES

Amon, R.M.W. and Benner, R. 1998. Seasonal patterns of bacterial abundance and production in the Mississippi River plume and their Importance for the fate of enhanced primary production. Microbial Ecology 35(3), 289-300.

Aulenbach, B.T., Buxton, H.T., Battaglin, W.A., and Coupe, R.H., 2007, Streamflow and nutrient fluxes of the Mississippi-Atchafalaya River Basin and subbasins for the period of record through 2005: U.S. Geological Survey Open-File Report 2007-1080, http://toxics.usgs.gov/pubs/of-2007-1080/index.html.

Babin, B.L. and Rabalais, N.N., 2009. Trends in oxygen variability in the northern Gulf of Mexico hypoxic zone. Proceedings of OCEANS '09 MTS/IEEE Biloxi.

Baustian, M. and Rabalais, N.N. 2009. Seasonal Composition of Benthic Macroinfauna Exposed to Hypoxia in the Northern Gulf of Mexico. Estuaries and Coasts 32(5), 975-983.

Bianchi, T.S., DiMarco, S.F., Cowan Jr, J.H., Hetland, R. D., Chapman, P., Day, J. W., and Allison, M. A. 2010. The science of hypoxia in the Northern Gulf of Mexico: A review. Science of the Total Environment, 408(7), 1471-1484.

Chin-Leo, G., and Benner, R. 1991. Dynamics of bacterio-plankton abundance and production in seagrass communities of a hypcrsaline lagoon. Marine Ecology Progress Series 73:219-230.

Chin-Leo, G., and Benner, R. 1992. Enhanced bacterio-plankton production and respiration at intermediate salinities in the Mississippi River plume. Marine Ecology Progress Series 87: 87-103.

Cloern, J. and Jassby, A. 2010 Patterns and scales of phytoplankton variability in estuarine–coastal ecosystems. Estuaries and Coasts.

Codiga, D.,H. Stoffel, et al. 2009 Narragansett Bay hypoxic event characteristics based on fixed-site monitoring network time series: Intermittency, geographic distribution, spatial synchronicity, and interannual variability. Estuaries and Coasts 32(4): 621-641.

Dortch, Q., Rabalais, N.N., Turner, R.E., and Rowe, G. 1994 Respiration rates and hypoxia on the Louisiana shelf. Estuaries and Coasts 17(4), 862-872.

Forrest, D.R., Hetland, R. D., and DiMarco, S.F. 2011. Multivariable statistical regression models of the areal extent of hypoxia over the Texas–Louisiana continental shelf, Environmental Research Letters 6, 045002.

Hetland R.D. and DiMarco S.F. 2008. How does the character of oxygen demand control the structure of hypoxia on the Texas-Louisiana continental shelf? Journal of Marine Systems 70, 49-62.

Justić D, Rabalais N.N., and Turner R.E. 1996. Effects of Climate Change on Hypoxia in Coastal Waters: A Doubled CO2 Scenario for the Northern Gulf of Mexico. Limnology and Oceanography, 41: 992-1003.

Levin, L.A. , Ekau, W., Gooday, A.J., Jorissen, F. , Middelburg, J.J. , Naqvi, S.W A., Neira, C., Rabalais, N.N., and Zhang, J. 2009. Effects of natural and human-induced hypoxia on coastal benthos. Biogeosciences 6, 2063-2098.

Mississippi River/Gulf Mexico Watershed Nutrient Task Force.2001, Action plan for reducing, mitigating and controlling hypoxia in the northern Gulf of Mexico, Washington, DC.

Mississippi River/Gulf of Mexico Watershed Nutrient Task Force. 2008. Gulf Hypoxia Action Plan 2008 for Reducing, Mitigating, and Controlling Hypoxia in the Northern Gulf of Mexico and Improving Water Quality in the Mississippi River Basin. Washington, DC.

Murrell, M. and Lehrter, J. 2010. Sediment and lower water column oxygen consumption in the seasonally hypoxic region of the Louisiana continental shelf. Estuaries and Coasts, 1-13.

Quinones-Rivera, Z.J., Wissel, B., Justić D., and Fry B. 2007. Partitioning oxygen sources and sinks in a stratified, eutrophic coastal ecosystem using stable oxygen isotopes. Marine Ecology-Progress Series 342, 69-83.

R Development Core Team. 2011. R: A language and environment for statistical computing. R Foundation for Statistical Computing, Vienna, Austria.

Rabalais N.N., Turner, R.E., Wiseman, W.J., and Dortch, Q. 1998. Consequences of the 1993 Mississippi river flood in the Gulf of Mexico. Regulated Rivers-Research & Management 14, 161-177.

Rabalais, N.N., Díaz, R.J., Levin, L.A., Turner, R.E., Gilbert, D., and Zhang, J. 2010. Dynamics and distribution of natural and human-caused hypoxia. Biogeosciences 7(2), 585-619.

Rabalais, N.N., Turner, R.E., Sen Gupta, B., Boesch, D., Chapman, P., and Murrell, M. 2007. Hypoxia in the northern Gulf of Mexico: Does the science support the Plan to Reduce, Mitigate, and Control Hypoxia? Estuaries and Coasts 30, 753-772.

Rabalais, N.N. and Turner, R.E., 2006. Oxygen depletion in the Gulf of Mexico adjacent to the Mississippi River, Past and Present Water Column Anoxia, pp. 225-245.

Rabalais, N.N., Wiseman, W., and Turner R. 1994. Comparison of continuous records of near-bottom dissolved oxygen from the hypoxia zone along the Louisiana coast. Estuaries and Coasts 17(4), 850-861.

Rabalais, N.N., Turner, R.E., and Wiseman, W.J. 2002. Gulf of Mexico hypoxia, a.k.a. "The dead zone." Annual Review of Ecology and Systematics 33, 235-263.

Renaud, M.L. 1986. Hypoxia in Louisiana coastal waters during 1983: Implications for fisheries. Fishery Bulletin 84, 19-26.

RIDEM. 2006. Water quality regulations. Office of Water Resources, Department of Environmental Management, State of Rhode Island and Providence Plantations. http://www.dem.ri.gov/programs/benviron/water/quality/surfwq/index.htm.

Rowe, G.T., Kaegi, M.E.C., Morse, J.W., Boland, G.S., Briones, E.G.E. 2002. Sediment community metabolism associated with continental shelf hypoxia, northern Gulf of Mexico. Estuaries 25, 1097-1106.

Sell, K. and Morse, J. 2006. Dissolved Fe^{2+} and $\sum H^2S$ Behavior in Sediments Seasonally Overlain by Hypoxic-to-anoxic Waters as Determined by CSV Microelectrodes. Aquatic Geochemistry 12, 179-198.

Spetic, A. and Gennick, J. 2002 Transact-SQL cookbook. Beijing; Sebastopol, Calif., O'Reilly.

Stone, G.W., Zhang, X., Li, J., and Sheremet, A. 2003. Coastal observing systems: key to the future of coastal dynamics investigation. GCAGS/GCSSEPM Transactions 53, 783-799.

The MathWorks™ Inc. 2009. MATLAB® Version 7.8.0.346(R2009a): Natick, MA.

Turner, R.E. and Allen, R.L. 1982. Plankton respiration rates in the bottom waters of the Mississippi River Delta Bight. Contributions in Marine Science 25, 173-179.

Turner, R.E., Qureshi, N., Rabalais, N.N., Dortch, Q., Justić, D., Shaw, R.F., and Cope, J. 1998. Fluctuating silicate:nitrate ratios and coastal plankton food webs. Proc Natl Acad Sci USA, 95,13048-13051.

Turner, R.E., Rabalais, N.N., and Justić, D. 2006. Predicting summer hypoxia in the northern Gulf of Mexico: Riverine N, P, and Si loading. Marine Pollution Bulletin, 52(2), 139-148.

Turner, R.E., Rabalais, N.N., and Justić, D. 2012. Predicting summer hypoxia in the northern Gulf of Mexico: Redux. Marine Pollution Bulletin, 64(2), 319-324.

USEPA. 2000. Ambient aquatic life water quality criteria for dissolved oxygen (saltwater): Cape Cod to Cape Hatteras. United States Environmental Protection Agency, Office of Water. Report EPA-822-R-00-012. 49 pp.

Vaquer-Sunyer, R. and Duarte C.M. 2008. Thresholds of hypoxia for marine biodiversity. Proceedings of the National Academy of Sciences 105(40), 15452-15457.

Walker, N.D., Wiseman, W.J., Rouse, L.J., and Babin, A. 2005. Effects of river discharge, wind stress, and slope eddies on circulation and the satellite-observed structure of the Mississippi River plume. Journal of Coastal Research 21, 1228-1244.

Wang, L., and Justić, D., 2009. A modeling study of the physical processes affecting the development of seasonal hypoxia over the inner Louisiana-Texas shelf: Circulation and stratification. Continental Shelf Research 29, 1464-1476.

Wiseman, W.J., Rabalais, N.N., Turner, R.E., and Justić, D. 2004. Hypoxia and the physics of the Louisiana coastal current. Dying and Dead Seas NATO Advanced Research Workshop Liège, Belgium, NATO ASI Series, Netherlands, Kluwer Academic Publishers.

Wiseman, W.J., Rabalais, N.N., Turner, R.E., Dinnel, S.P., and MacNaughton, A. 1997. Seasonal and interannual variability within the Louisiana coastal current: stratification and hypoxia. Journal of Marine Systems 12(1-4), 237-248.

CHAPTER 3

PERIODIC FACTORS AFFECTING SHORT-TERM OXYGEN VARIABILITY IN THE NORTHERN GULF OF MEXICO HYPOXIC ZONE

INTRODUCTION

Hypoxic bottom waters (≤ 2 mg O_2 l^{-1}) have been documented in the northern Gulf of Mexico (NGOM) off the Louisiana-Texas coast since the early 1970s (Rabalais et al., 2002). Hypoxia occurs when an excess of decomposing carbon on or near the sea floor causes respiration to exceed primary production reducing the dissolved oxygen in the water to levels that can no longer sustain life, and when the water column sufficiently stratifies to prevent mixing of oxygen enriched water from the surface to re-aerate the lower water column. Hypoxia recurs every summer in the NGOM at varying frequencies and for varying lengths of time (Chapter 2). In order to better understand the dynamics of hypoxia, it is important to understand how dissolved oxygen (DO) concentrations vary and what factors affect that variability. While the factors affecting seasonal variability in DO concentrations are generally well understood, we still do not have a clear understanding of factors affecting the short-term (hours to days) variability of DO in the NGOM.

Understanding the factors that affect short-term variability in DO is important for several reasons. First, the biological effects of low oxygen depend on the sub-daily (e.g., hourly) pattern of exposures (Rose et al., 2009). Second, the understanding of short term variability in DO is necessary in order to more accurately predict the occurrence of hypoxia in the NGOM. Current hypoxia models generally focus on longer time scales. For example, a statistical model developed by Turner et al. (2006, 2012) predicts the annual summertime areal extent of hypoxia based on the Mississippi River nutrient flux from the preceding May of the same year. Simulation models have been used to hind-cast and forecast monthly DO concentrations in order

to study the dynamics of hypoxia (Scavia et al., 2004; Justić et al., 2007). Proper interpretation and further refining these models would be informed by a better understanding of factors affecting short-term variability in DO concentrations (Justić et al., 2007). Third, information on short-term variability will help to determine the accuracy of the areal extent of hypoxia that is determined in any given year by the summertime hypoxia shelf-wide mapping cruise. These maps, which are based on a single cruise, are then used to inform management decisions, and so it is important that the uncertainty in these maps that arises from short-term oxygen variability be adequately assessed. For example, the Gulf Hypoxia Action Plan 2008's goal "to reduce or make significant progress toward reducing the five-year running average areal extent of the Gulf of Mexico hypoxic zone to less than 5,000 square kilometers by the year 2015" is dependent on the interpretation of these maps. Better understanding of the short-term variability in DO will enable improved modeling, better assessment of upper trophic level effects and snapshot spatial maps, and ultimately more informed management decisions.

One aspect of short-term variability that is often exhibited in DO concentration time-series is the periodicity in the form of a diel curve. DO concentrations typically vary over a 24-hour period. DO rises during daylight hours due to primary production in response to increasing light levels (photosynthetically active radiation or PAR), and declines at night as respiration overtakes production. According to Odum and Hoskin (1956), respiration, photosynthetic production, and diffusion interact to produce this diel DO curve. Conversely, the observed diel DO patterns can be used to calculate the component rates of production, respiration, and diffusion. If respiration is greater than production, then a downward trend would be present over a 24-hour period.

Water temperature, tides, and PAR are periodic factors that also vary over short-term scales and have been shown to influence the DO concentrations. Temperature is a factor in the

solubility of oxygen in water; therefore, short-term variability in temperature affects how much oxygen is dissolved in the seawater. Also, temperature affects the metabolic rates and therefore the rates of photosynthesis and respiration (Berges, et al. 2002). Tides may also influence the variability in DO concentrations at a fixed site because of the on-shore and off-shore displacement of water parcels due to tidal excursions. For example, such variation in DO concentrations due to tidal excursions have been found in estuaries (Sanford et al, 1990), lakes (Hansen et al, 2006), and in streams (personal observation).

PAR varies periodically over a 24-hour period and affects DO concentrations through its controlling influence on photosynthesis. PAR values are zero during the night time hours and increase beginning at dawn, reaching a maximum as the sun reaches a zenith in the sky, declining as the sun sets, and returning to zero during the night. This creates a modified sinusoidal PAR pattern. Although it is well understood that light promotes primary production at the sea surface, whether or not enough light penetrates the water column to the sea floor and whether or not primary production occurs depends on a number of factors. These factors include the concentrations of phytoplankton, total suspended solids, and colored dissolved organic matter (CDOM), as well as the abundance of benthic algae.

Because of the high respiration rates, the near-bottom waters in the NGOM should become anoxic (0 mg O_2 l^{-1}) in less than four days when no mixing occurs (Chapter 2). However, near-bottom waters rarely become anoxic, suggesting that DO is perhaps continuously replenished by benthic or epi-benthic photosynthesis. Nevertheless, studies have shown that benthic photosynthesis is low in the NGOM hypoxic zone in spite of the fact that benthic diatoms are present (Baustian et al., 2011). Several limiting factors (i.e., carbon dioxide, nutrients and PAR) must be simultaneously present in sufficient quantities for photosynthesis to occur. Carbon dioxide is abundant in the ocean and the primary nutrients required for algal

growth (i.e., nitrogen, phosphorus and silicon) are generally present in sufficient quantities in sediments on the NGOM continental shelf. However, the amount of light that reaches the bottom varies in response to a number of environmental factors. One percent of surface PAR penetrating the water column is sufficient for photosynthesis to occur (Kirk, 2003), and so the layer between the surface and the depth where PAR diminishes to 1% is known as the euphotic zone. If a diel cycle of production and respiration causes a diel periodicity in the near-surface DO concentrations (Tijggen, 1979) and the euphotic zone reaches the seafloor, then the same diel periodicity should be present in DO concentrations from the entire water column.

Currently, there is limited understanding of how DO concentrations near the sea floor vary in time and how periodic factors affect the short-term oxygen variability in bottom waters of the NGOM hypoxic zone. High-resolution DO time-series are required to characterize and explain these processes. I used a 20 year (1989-2008) record of continuously monitored field measurements at a fixed station (C6) to examine how the key periodic factors (i.e., temperature, tides, and PAR), affect the short-time periodicity in near-bottom DO. The primary objectives of this chapter are: 1) to identify the dominant frequency spectra in DO concentrations and examine their relationship with the frequencies present in temperature, tidal amplitude and phase, and PAR, and 2) to examine if the diel production/respiration pattern is present in the DO time-series at different depths within the water column, and whether this diel pattern is related to bottom PAR levels. The extent to which PAR and temperature influence the DO concentrations will help elucidate the role that benthic and epi-benthic photosynthesis plays in hypoxia dynamics. The degree to which tides influence bottom DO concentrations will provide information on the scales of horizontal advection and information on the degree of "DO patchiness" within the hypoxic zone.

METHODS

Study Area

The study area encompasses the northern Gulf of Mexico hypoxic zone. The data collection site for this project, Station C6, is located 20 miles south of Terrebonne Bay (Figure 1.1). Water depth is about 20 m at Station C6 and this location experiences frequent annual summer-time hypoxia. Tides in the NGOM are diurnal and small; the range of tropic tides is 60 cm (Marmer, 1954).

Data Sources

The primary data source is a 20 year dataset collected from a single site in the NGOM. Chapter 2 describes these data in more detail. From 1989 through 1995, a single sonde deployed at the depth of 19.5 m (~0.5 m above the bottom) collected DO concentrations and temperature at 15-minute intervals. Beginning in 1996, two additional sondes were added to the instrument array at this site, including a mid-water column sonde at the depth of 10.7 m, and a near-surface sonde at 2 m below mean sea level. Salinity sensors were also added to the array along with the DO, temperature, and other sensors. I stored the data in a Microsoft SQL database (Microsoft Corporation, 2010).

I identified all of the months from the 20 year dataset where DO concentrations were continuously recorded over the entire month. Of the 240 possible month-long time-series over the 20 years, 110 complete month-long time-series were identified for the near-bottom, 60 for the mid-water column, and 60 for the near-surface. I identified a total of 35 months that had complete information for all three layers. All those 35 month-long time-series were collected between 1997 and 2008, because sampling in the mid-water column and near the surface did not begin until 1997. Every month except December was represented at least once. The year 2004 had the most complete data with 9 complete consecutive months of observations at all three

depths. I calculated hourly average DO concentrations and temperature from the 15 minute samples for each of the 35 month-long data sets using Microsoft Transact-SQL query (Spetic and Gennick, 2002). I interpolated 3 hour shortwave radiation flux data onto a one hour time grid space to obtain a proxy for PAR. I assumed that approximately 50% of the energy in the solar spectrum is PAR from the visible spectrum between 400 and 700 nm (Jones et al., 2003). I downloaded heat flux data from NCEP's North American Regional Reanalysis (NARR) from the NOMADS website (http://nomads.ncdc.noaa.gov/). This dataset includes 3-hour estimates of downward shortwave radiation flux for station C6. I prepared 35 month-long time-series of PAR data by interpolating the 3-hour data onto an evenly spaced hourly time grid using the Matlab "interp1" algorithm with a "linear" method (The Mathworks, 2009) to match the available 35 month-long DO concentration time-series.

I used hourly water level data collected at station C6 compiled into month-long time-series to analyze the tidal constituents. I downloaded water level data from Louisiana State University's Coastal Studies Institute WavCIS program's website (www.wavcis.lsu.edu). Water level data collection at station C6 began in 2002, so the data do not span the entire DO time-series. Nevertheless, tidal forcing remains fairly consistent over the years, so the few years for which the data were available were sufficient to determine the dominant frequencies of the tidal signal at this location. I prepared month-long water level time-series, corresponding to the 35 month-long DO time-series, by interpolating the hourly water level data onto the same time-space grid as the DO data and simultaneously interpolating minor gaps in these data.

The DO concentrations at three depths (near-surface, mid-water column, and near-bottom), the near-bottom temperature, PAR, and water level were combined into 35 month-long time-series with each record representing an hourly value.

I used the Secchi disk depths for station C6, obtained from the National Oceanographic Data Center (NODC) website (www.nodc.noaa.gov), to estimate the underwater light attenuation (Table 3.1). These Secchi depths were used as a proxy for underwater PAR levels because water column PAR measurements were not available for the study site. The Secchi depth measurements were collected during monthly cruises over a 12 year period (1997-2008), as part of the Louisiana Universities Marine Consortium's (LUMCON) hypoxia monitoring program. The measurements were taken by lowering a black and white disk, 25 cm in diameter, over the side of the ship during the period from 6 hours before to 6 hours after apparent noon (Cole and Sapp, 2003).

Table 3.1. Data sources used in the analysis.

Variables Measured	Field Technique	Sampling frequency and duration	Binning/ Interpolation	Reference
Dissolved oxygen Temperature	DO and temperature sensors	Sampled at 15-min. intervals between 1989 and 2008	Averaged hourly	LUMCON
PAR	NARR-A model reanalysis	Sampled every 3 hours	Interpolated hourly	NCEP
Water level	ADCP	Once every hour	Interpolated hourly	WAVCIS-LSU
Secchi depth	Secchi depth readings obtained using a black and white disc (25 cm in diameter)	Monthly	Day measurement taken	NODC-LUMCON

Data Analysis

The data analysis consisted of a spectral analysis component and an analysis of the correspondence of sufficient light and diel patterns in DO (Table 3.2). First, I performed spectral

Table 3.2. Outline of methods used to explore the short-term (hours to days) oxygen variability over a 20-year period (1989-2008)

Analysis	Methods	Data Used	Question	Presentation
Time-series Analysis	Auto- and cross-correlation analysis	Complete month-long samples of hourly averaged DO concentrations, NARR 3 hour data interpolated to match DO concentrations, and WAVCIS hourly water level data	Is there a lagged correlation between DO concentrations and water temperature, water level and PAR?	Auto and cross correlation plots
	Spectral analysis (shortwave radiation, wind, water temperature, water depth, DO concentrations)	Complete month-long samples of Hourly averaged DO Concentrations, NARR 3 hour data interpolated to match DO concentrations, and WAVCIS hourly water level data	To what extent do periodic factors affect DO concentrations?	Time-series plots and periodograms of PAR, wind, water temperature, water depth, and DO concentrations
Diel pattern analysis	Identify days with diel pattern (near-surface, mid-water column, near bottom) Determine proportions of days with diel pattern for three depths	Hourly averaged DO concentrations	To what extent does light affect DO concentrations near-surface, mid-water column, near bottom?	Table of results and plot showing proportions by depth
	Estimate the depth of the euphotic zone for periods with available Secchi disk data	Results from diel pattern analysis, Secchi depth data from monthly cruises	Does photosynthesis occur at or near the bottom?	Table of results

analysis on the 35 month-long time-series to determine what periodicities were present in the data. I compared the spectra of temperature, PAR, and tide to the spectra of the DO concentrations. Second, I returned back to the original 15-minute data from all three depths and identified days that exhibited a diel pattern in DO. I then compared those days to my estimation of whether enough light had penetrated the water column in order to be the likely cause of the diel pattern.

Time-series Analysis

First, I performed cross-correlation analysis ("ccf" command in R) for each of the 35 month-long time-series to determine if a lagged correlation existed within the DO concentrations collected at different depths. I also examined if a lagged correlation existed between the DO concentrations and temperature, water level, and PAR values collected at the same depth. Cross-correlation analysis for water level data was performed only for the periods for which water level data were available (2002 through 2008). In cross-correlation analysis, I used a maximum lag of 72 hours because the primary emphasis of this study is on short temporal variability. Both the "acf" command and the "ccf" command use the Box and Jenkins (Box et al., 1994) method for computing the cross correlation function. Table 3.3 list all of the auto-correlation and cross-correlation analyses performed.

Second, I constructed periodograms of DO, temperature, and water level using a discrete Fourier transform (Cooley and Tukey, 1965) for all 35 months for which data were available. The data were de-meaned by subtracting the mean value from the time-series prior to constructing the periodogram. I plotted the periodograms noting the frequencies of interest on the plots (Table 3.4). The O_1 tidal constituent refers to the lunar declination cycles and the K_1 tidal constituent refers to lunar-solar declinational cycles. The diel (24-hour) and semi-diel (12-hour) refer to solar periods of day and night.

Table 3.3. Listing of the auto- and cross correlations variables used in the analysis.

Analysis	Time-series 1	Time-series 2
ACF	Near-surface DO	
ACF	Mid-water column DO	
ACF	Near-bottom DO	
CCF	Near-surface DO	Near-bottom DO
CCF	Near-surface DO	Mid-water column DO
CCF	Mid-water column DO	Near-bottom DO
CCF	Near-bottom DO	Water temperature
CCF	Near-bottom DO	Water level
CCF	Near-bottom DO	PAR

Table 3.4. Frequencies of interest used in the periodograms. The "Type" denotes common tidal constituents. CPH denotes cycles per hour.

Type	CPH	Period (hours)	Description
O1	0.0388	25.8	Lunar declinational
K1	0.0418	23.9	Lunar-solar declinational
Diel	0.0417	24.0	Solar declinational
Semi-diel	0.0833	12.0	Solar (day/night)

Diel DO Curve Pattern Analysis

I created daily plots from the original 15-minute measurements for every day in the dataset for the near-surface, mid water-column, and bottom DO concentrations. I then identified days that exhibited diel oxygen variation using a "segmented differencing" algorithm. I first calculated the 15-minute differences in DO by a backward-in-time differencing method where

ΔDO (mg l^{-1} 15-minutes) = DO^n - DO^{n-1}, using R (R Development Core Team, 2011). The algorithm divided the day into 4 segments: midnight to 6am (CST), 6am (CST) to noon, noon to 6pm (CST), and 6pm (CST) to midnight. Then, the algorithm determined if the DO concentrations were increasing or decreasing during each segment by summing the differences (ΔDO). A pattern with an increase in DO concentrations during the hours between 6 am and noon (CST), an increase or no change between noon and 6 pm (CST), and no change or decrease between 6 pm and 6 am (CST) the following day was identified as a diel pattern. Figure 3.1 illustrates the detected diel curves. The top two panels illustrate two days, May 22, 1993 and May 22, 1998, for which the 15-minute DO concentrations exhibited a diel curve and the bottom two panels illustrate two days, May 22, 1999 and May 22, 2006, without the diel DO pattern.

I then determined the proportion of the days sampled that were identified as "exhibiting a diel pattern" and tested the proportion using the "prop.test" algorithm in R (R Development Core Team, 2011). The null model probability was 0.5. I also calculated monthly averages of the number of diel days to explore a possible seasonal dependence and plotted these results in a bar plot. The existence of a diel curve indicated that oxygen production was occurring and that sufficient light levels were present in bottom waters for photosynthesis to occur.

I then compared the diel days to the monthly Secchi depths (z_{sd}) to test for whether diel patterns occurred on the same days when sufficient light penetrated the water column to influence DO dynamics near the bottom. I first plotted the monthly Secchi depths to determine if the penetration of light was sufficient to support primary production at 19.5 meters, the depth of the near-bottom sensor where the DO concentrations were measured. I compared these Secchi depths to a theoretical compensation depth (z_c) to determine if the light penetrating the water column was sufficient to support photosynthesis. Two alternative definitions of z_c were used to bracket the possibilities. Wetzel (2001) asserted that depths exceeding two times the Secchi

depth are usually considered to be below z_c for phytoplankton production; therefore, a Secchi depths of ~10 meters at station C6 would suggest that photosynthesis is possible at the depth of 19.5 meters. The Holmes-based method combines the Holmes's (1970) formula, $K_d=1.44/z_{sd}$, where z_{sd} is the Secchi depth, and Kirk's (1994) formulation which states that z_c is approximately equal to $4.6/K_d$, assuming that the attenuation coefficient (K_d) is constant throughout the water column. Combining these two assertions, it follows that the $z_c=z_{sd}$ x 3.16, and so a z_{sd}=6.3 is required to obtain a z_c of ~20 m.

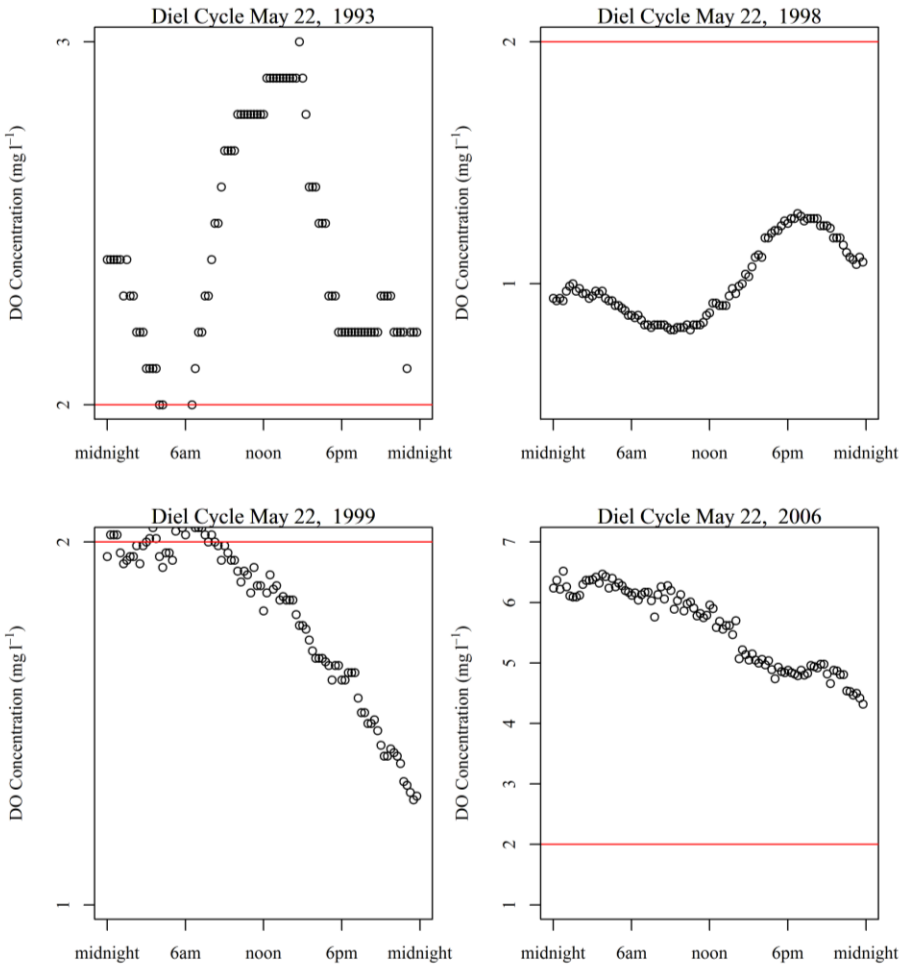

Figure 3.1. Plots of near-bottom dissolved oxygen concentrations at station C6 for May 22 in 1993, 1998, 1999, and 2006. The top two panels, 1993 and 1998, exhibit a diel curve where dissolved oxygen concentrations increase during daylight hours and decrease during nighttime hours. The bottom two panels, 1999 and 2006, are examples of days that do not exhibit a diel curve but rather show continuous respiration throughout the day and night hours.

Finally, I determined whether or not a diel curve existed in the near-bottom DO time-series for the days when Secchi disk data were available. I calculated the proportion of diel days to the Secchi depths to determine if a relationship existed between the diel pattern and the amount of PAR reaching the near-bottom sensor.

RESULTS

Time-series Analysis

I found no lagged auto-correlation in the DO time-series collected at near-surface, mid-water column, and near-bottom depths. A statistically significant correlation with a lag of 24 hours would indicate a persistent diel pattern. However, such a correlation was not detected suggesting that any diel pattern that may be present is not maintained throughout the month-long times-series. Some plots did show some correlation with a 24-hour or a 48-hour lag indicating the presences of a diel periodicity; however, these were not statistically different from neighboring lags at the 95% significance level. One such sample was July 2002. Both the near-surface and mid-water column showed a correlation at the 24-hour and 48-hour lags (Figure 3.2). The plot of the dissolved oxygen concentration shows some possible periodicity during July 2002 in the near-surface DO and the mid-water column indicating that enough light may have been reaching the mid-water column sensor for production to occur. Interestingly, these lag correlations were not present in the near-bottom DO time-series (Figure 3.2). Plots for all months for which the data were available are included in Appendix B.

Cross-correlation analysis showed no statistically significant correlation between DO concentrations at different depths (Figure 3.3). Cross-correlation functions (CCF's) for some months (e.g., July 2002), exhibited similar patterns at different depths, while in other months (e.g., July 2008) they were quite different. While most plots showed no lagged correlation

between near-surface DO concentrations and near-bottom DO concentrations, the DO time-series for July 2008 showed a fairly strong lag of 48-hours (Figure 3.3 top right panel). It is unclear what this correlation might represent from the plot of DO concentrations as the near-bottom DO concentrations stays close to 0 mg l^{-1} most of the month. Three month-long samples of the CCF plots are illustrated in Figure 3.3 and all of the plots are included in Appendix B.

The cross correlations analysis for the near-bottom DO concentrations and the three periodic factors (temperature, water level, and PAR) showed no significant relationships (Figure 3.4). Temperature showed a strong correlation with no lag to near-bottom DO concentrations in only 9 of the 35 month-long time-series. Cross correlation between the water level (a proxy for tides) and near-bottom DO concentrations showed no significant lagged relationships at the 95% level in any of the 14 month-long time-series for which water level data were available. Similarly, PAR, and near-bottom DO concentrations showed no significant lagged correlations suggesting that any relationship that may exists between PAR and near-bottom DO concentrations is not consistent throughout the samples. Figure 3.4 illustrates three examples of these CCFs. All month-long CCF's from this analysis are included in Appendix B.

Although some of the plots of the DO time-series appear to show periodicity in the data (Figure 3.5), the periodograms showed no significant periodicity in the frequencies of interest. An example from July 2004 showing the DO time-series at the three depths, near-surface, mid-water-column, and near-bottom, and the corresponding periodograms for each depth are illustrated in Figure 3.5. Table 3.5 shows the power densities of DO concentrations at each of the three depths of the 0.417 cycles h^{-1} (24-hour) frequency for all 35 samples. None of these time-series showed a significant periodicity at 0.417 cycles h^{-1} (24-hour). Thus, it appears that the 24-hr periodicity that is evident in some time-series is not a consistent feature and is often interrupted by non-periodic factors.

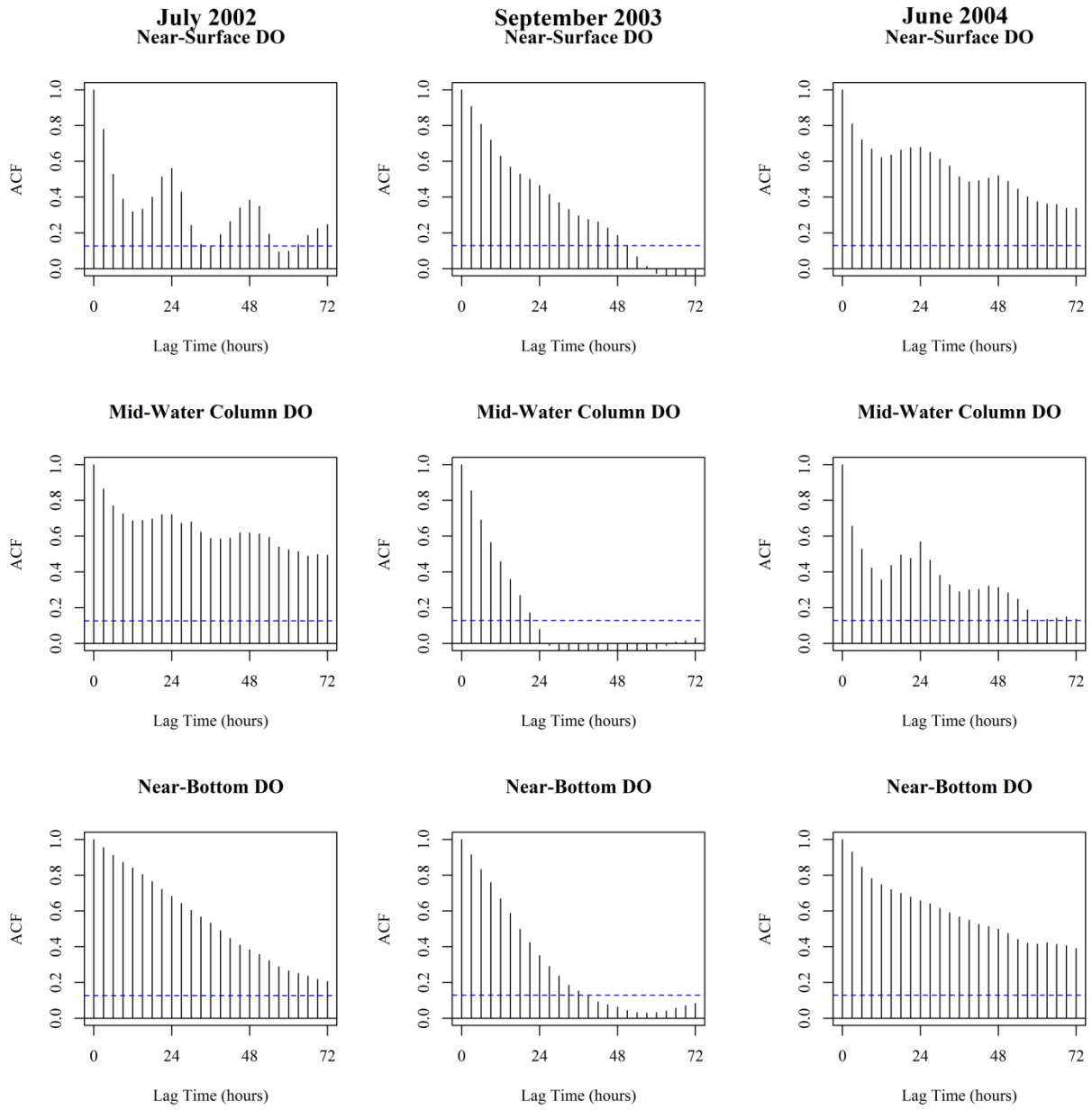

Figure 3.2. Autocorrelation function plots (ACF) of DO concentrations from three depths, near surface, mid-water column, and near-bottom, for 3 of the 35 month-long samples, July 2002 (left column), September 2003 (middle column), and June 2004 (right column). The July 2002 panel shows a 24-hour lagged autocorrelation in the near-surface while the June 2004 panel shows a similar 24-hour lagged autocorrelation in the mid-water column. However, none of these correlations were significantly different from adjacent lags at the 95% significance level. The September 2003 is representative for some 20 of the 35 month-long time-series that showed no lagged autocorrelation at any of the three depths. ACF plots for all 35 month-long samples are included in Appendix B.

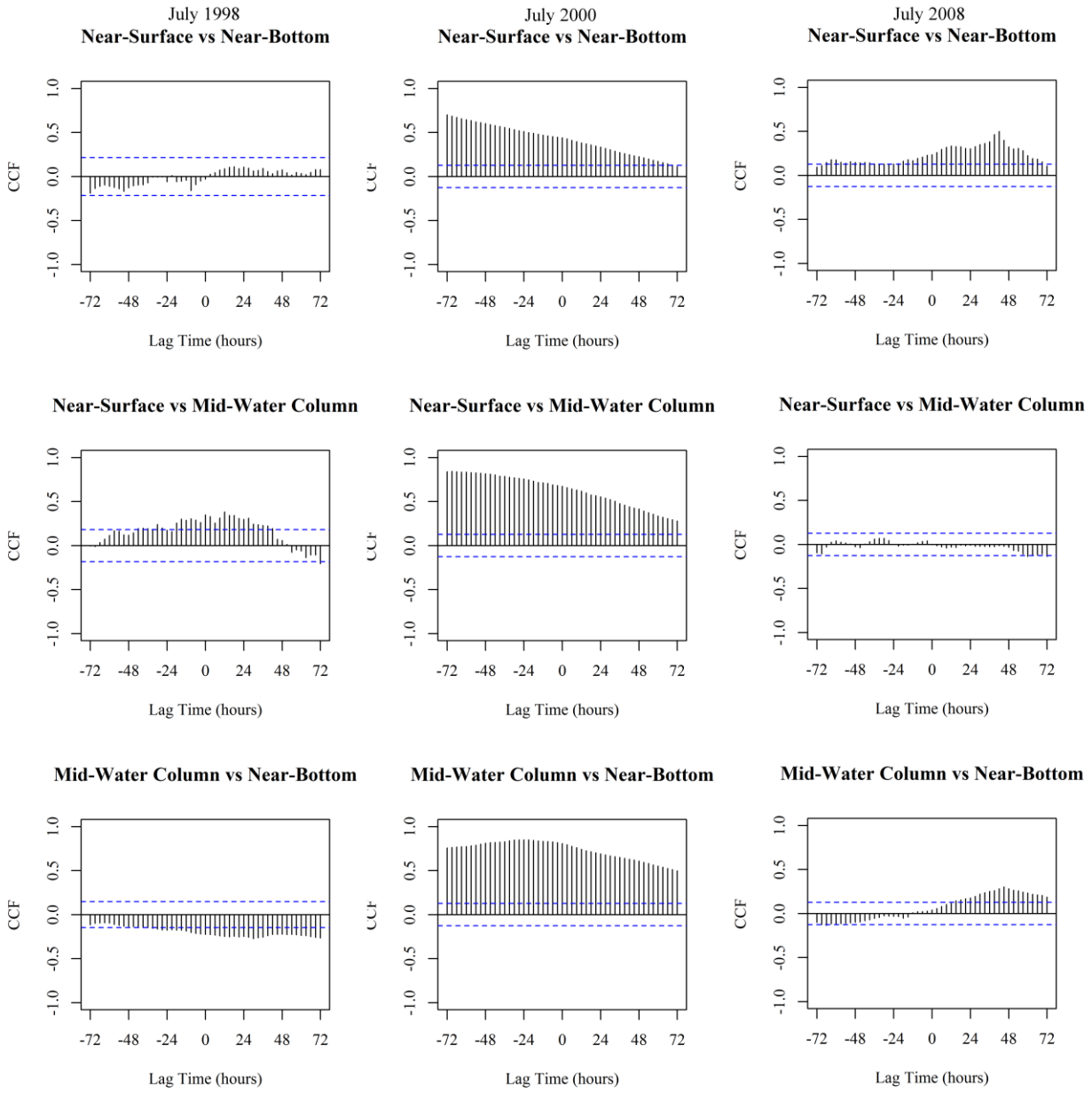

Figure 3.3. Cross-correlation function plots (CCF) of DO concentrations between depths, for 3 of the 35 month-long samples, July 1998 (left column), July 2000 (middle column), and July 2008 (right column). However, none of these correlations were significantly different from adjacent lags at the 95% significance level. The dashed blue lines indicate the 95% significance levels. CCF plots for all 35 month-long time-series are included in Appendix B.

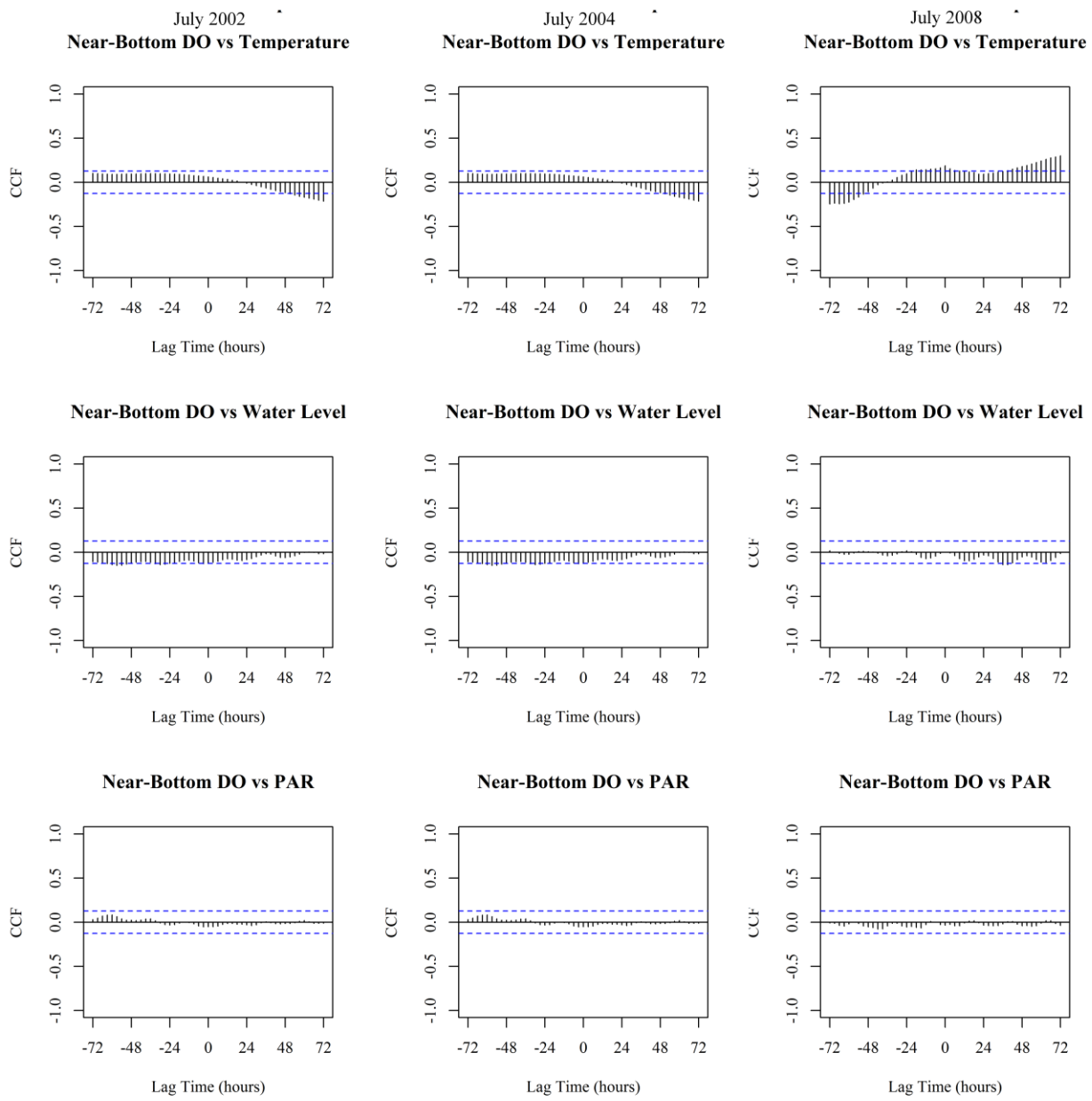

Figure 3.4. Cross-correlation function (CCF) plots of the relationship between DO concentrations and temperature, water level, and PAR values at different depths, for 3 of the 35 month-long time-series that were analyzed in this study, July 2002 (left column), July 2004 (middle column), and July 2008 (right column). Note that none of these correlations were significantly different from adjacent lags at the 95% significance level. The dashed blue lines indicate the 95% significance levels. CCF plots for other months are presented in Appendix B.

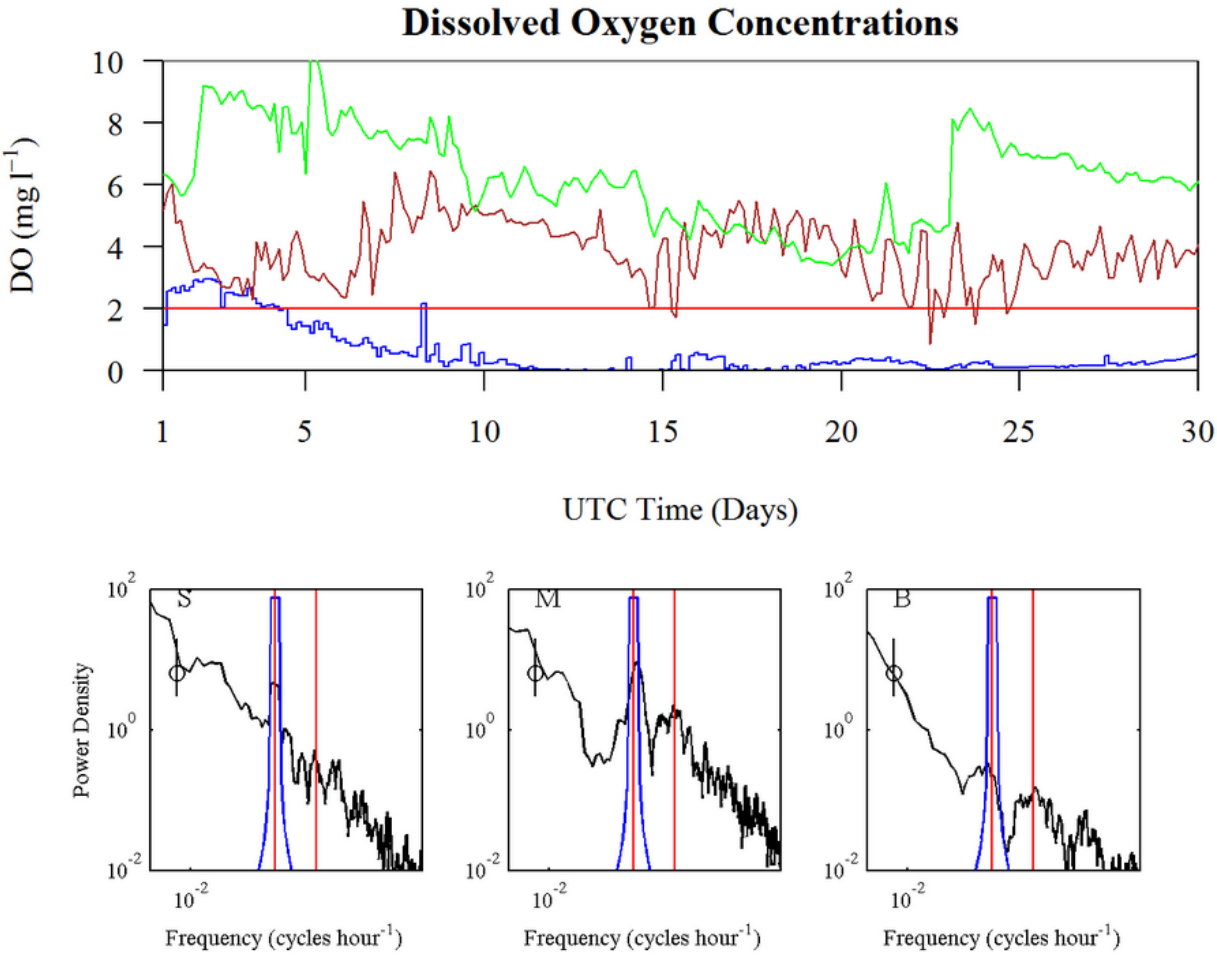

Figure 3.5. DO time-series and periodograms for July 2004. Upper panel: Hourly averages of DO concentrations in mg l^{-1} measured at 15 minute intervals at station C6: green line - near-surface sensor (2 meters below the surface), brown line - mid-water column sensor (10.7 meters below the surface), blue line - near-bottom sensor (19.5 meters below the surface). Red line represents hypoxic threshold (2.0 mg l^{-1}). Lower panel: DO periodograms for near-surface (S), mid water-column (M), near-bottom (B) layers. Vertical red lines in each plot represent frequencies of interest from left to right Diel (24 hours) and semi-diurnal (12 hours). The blue line represents the null hypothesis for a 24-hour periodic signal. Vertical black line with a circle indicates the 95% confidence interval. Plots and periodograms for all 35 month-long time-series are presented in Appendix B.

None of the power densities for the DO time-series exhibited peaks at the K1 (lunar-solar declinational cycles) or O1(lunar declination cycles). This indicated that the DO time-series did not have a periodicity related to these tidal constituents.

Contrary to DO and temperature, water level and PAR variation exhibited continuous short-term periodicity. A diurnal tide with a range of 0.1-0.5 m was clearly evident in the time-series of WAVCIS water levels from station C6 (Figure 3.6). The water level plots also showed the 14 day tropic tidal cycle; however, this signal was not evident in the periodograms because the time-series I used was not long enough for the cycle to be characterized (Figure 3.6). While the K1 tidal signal is prominent in the water level periodograms, both 24-hour and 12-hour cycles are present in the PAR periodograms. As stated previously, in spite of the periodicity in water levels and PAR, the DO periodograms showed no significant periodicities. Temperature time-series plots and periodograms also showed no periodicity. Again, the time-series plots and periodograms for near-bottom temperature, water level (when available) and PAR for all 35 month-long time-series are included in Appendix B.

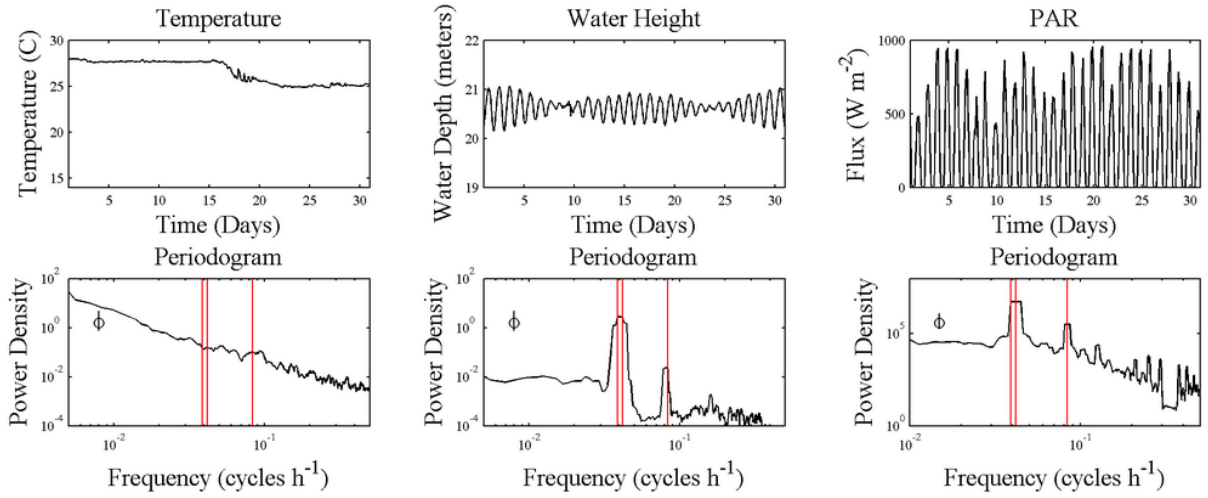

Figure 3.6. Time-series and periodograms for temperature, PAR and water level (tides) at station C6 for July 2004. The upper left panel shows hourly averages of near-bottom temperature. The lower left panel shows the periodogram for near-bottom temperature. The upper-mid panel shows hourly water level (labeled water height here) measurements from WAVCIS data taken at the study site. The lower-mid panel shows the periodogram for the water level measurements. The upper-right panel shows short-wave radiation from NARR data at 3 hour intervals for this site. The lower-right panel shows the periodogram for PAR. Vertical red lines represent frequencies of interest from left to right O1 (25.8 hours), K1 (23.9 hours), and semi-diurnal (12 hours) tidal constituents. Plots and periodograms from all 35 month-long samples are included in Appendix B.

Diel DO Curve Pattern Analysis

The near-surface layer had the greatest proportion of days with a diel DO pattern, followed by the mid-water column and the near-bottom layer (Table 3.5). Nevertheless, the near-surface layer exhibited a diel DO pattern only 20% of the time (χ-squared = 991; 95% significance level), suggesting that the diel signal is interrupted by other non-periodic forcings most of the time (Figure 3.7). The mid-water column showed a diel DO pattern 12% of the time (χ -squared = 1374; 95% significance level), while the near-bottom exhibited this pattern only 7% of the time (χ -squared = 3209; 95% significance level).

Table 3.5. A summary of results for diel DO curve analysis. Depth indicates the depth at which the DO sensor was deployed. Days sampled is the total number of days that DO concentrations were sampled during the study period. Days Diel denotes the total number of days sampled that the "segmented differencing" algorithm identified as exhibiting a diel pattern. The proportion (P) is calculated by dividing the number of diel days with the number of total days sampled. X –squared is the statistic provided by the proportion test. The p-value gives the significance at 95% significance level. CI LL is the lower limit of the confidence interval and CI UP is the upper limit of the confidence interval.

Sonde (Sensor) Position in Water Column	Depth (meters)	Days Sampled	Days Diel	P	χ - squared	p-value	95% CI LL	95% CI UP
Near-Surface	2	2712	536	0.20	991	0	0.18	0.21
Mid-Water	10.7	2368	282	0.12	1374	0	0.11	0.13
Near-Bottom	19.5	4434	331	0.07	3209	0	0.07	0.08

The proportion of days that exhibited a diel pattern (Figure 3.8) was somewhat higher in the spring (May and June) and fall (September and October) compared to the winter months (January and February), suggesting a possible seasonal cycle.

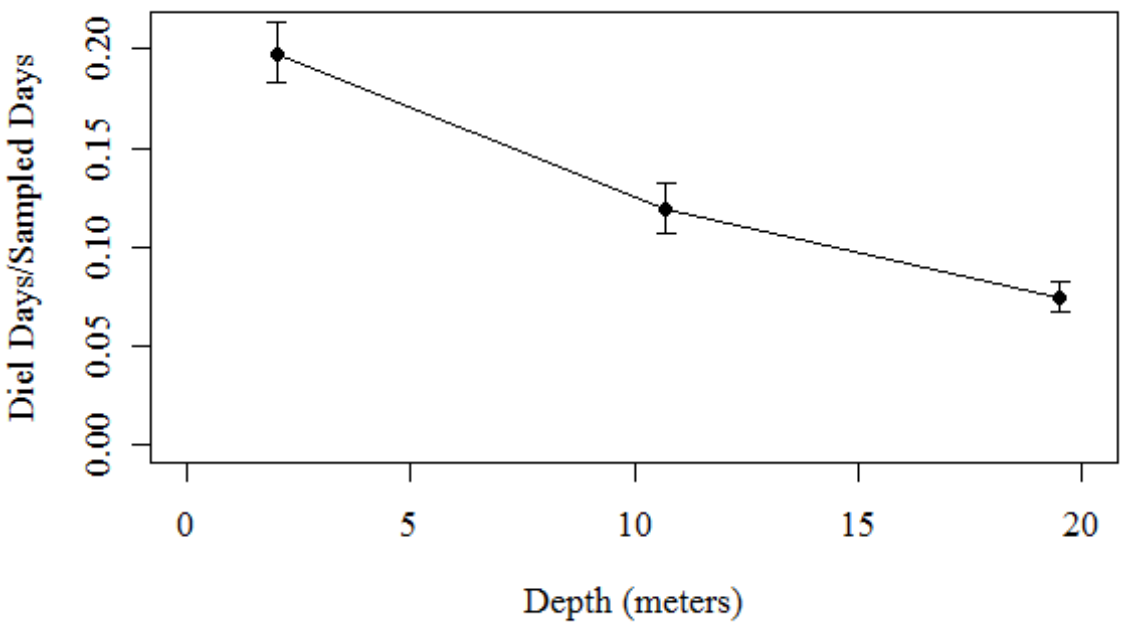

Figure 3.7. The ratio of the number of days showing diel DO pattern to the number of days sampled plotted versus water depth. Error bars indicate the 95% confidence limits.

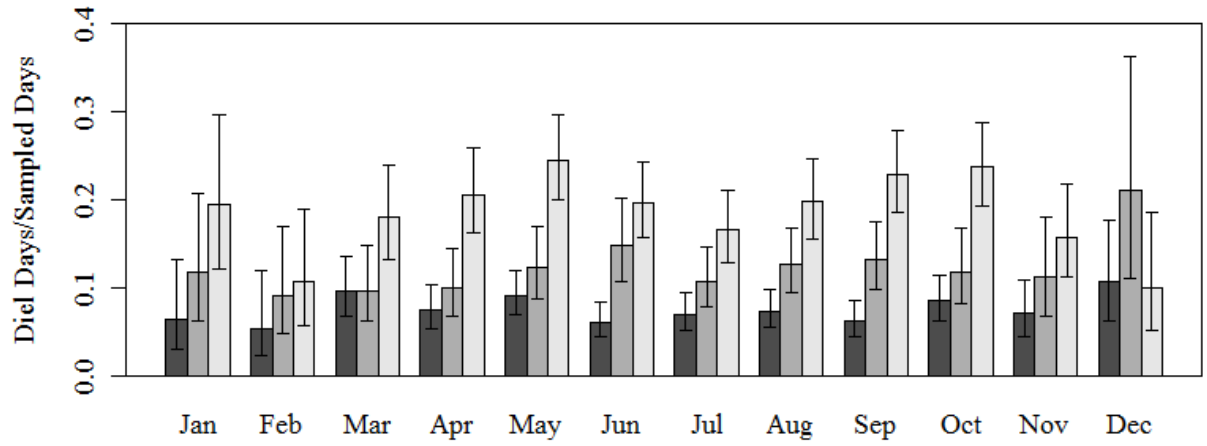

Figure 3.8. Proportion of the number of days that exhibited a diel DO pattern to the number of days sampled for individual months. Dark-grey bars represent the near-bottom samples, gray bars represent the mid-water column samples, and light-grey bars represent the near-surface samples.

The results presented in Figure 3.9 suggest that, depending on season and the depths within the water column, underwater PAR levels at the study site are sufficiently high to support photosynthesis between 9 and 25% of the time. The Secchi disks readings taken at this site during monthly transect cruises ranged between 0.8 and 16 m. Although the average Secchi

depth was about 5 m, the standard deviation of 2.9 indicated that Secchi depths varied substantially. Based on the Wetzel-based estimate of a z_c of 10 m, the Secchi depths exceeded 10 m about 8% of the time (Figure 3.9). According to the Holmes-based estimate of a z_c, of 6.3 m, Secchi depths would be sufficient to allow photosynthesis near the bottom about 25% of the time. Although these percentages compare well to the proportion of days that exhibited diel DO pattern at different depths, Secchi disk readings were not correlated with the ratio of diel days.

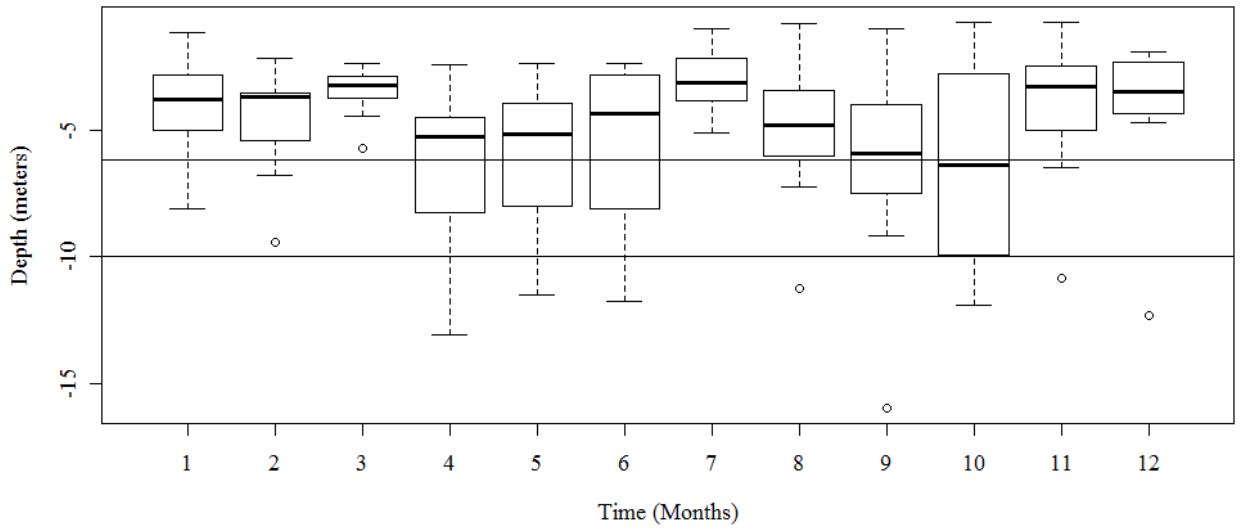

Figure 3.9. Box-and-Whiskers plot of Secchi depth measurements at station C6 taken during monthly cruises along transect C between 1998 and 2008. The horizontal lines inside the boxes represent the median, bottom and top indicate the lower and upper quartiles respectively, and the whiskers show the 5th and 95th percentiles. The horizontal line at -6.2 meters represents the minimum Secchi depth for the compensation depth to reach the near-bottom sensor at 19.5 m, as calculated by Holmes (1970). The horizontal line at -10 m is the compensation depth calculated using Wetzel's (2001) formulation.

Both Wetzel's (2001) and Holmes's (1970) methods produced similar results when comparing the compensation depth to the number of days exhibiting a diel DO pattern (Table 3.6). According to the Wetzel-based method, if the Secchi Depth is greater than 10 m, the compensation depth would be 20 m. The Secchi Depth reached this depth for 29 of the 92 (32%) days sampled and only four of the 29 (14%) days exhibited a diel pattern. Using the Holmes method, the Secchi depth exceeded the compensation depth of 6.3 m for 9 of the 92 (10%) days

sampled. Only 2 of these 9 (22%) days exhibited a diel pattern. However, in neither case did the corrected X^2 (using Yates' correction for continuity) exceed the ideal χ^2, indicating the lack of significant association between the calculated compensation depths reaching the depth of the near-bottom sensor (19.5 m) and the presence of a diel pattern in the DO concentrations (95% significance level, corrected $X^2 = 0.78$ and 1.16, df = 1, $P>0.05$).

Table 3.6. Results of comparing the number of days exhibiting a diel DO pattern (Diel) to the number of days that do not exhibit this pattern (Random) using two theoretical computations of the compensation depth (z_c). Method 1 uses Wetzel (2001) and method 2 uses Holmes (1970).

	Sensor Above z_c Days (%)	Sensor Below z_c Days (%)	Total Days
Method 1: Secchi Depth ≥10 meters, Compensation Depth ~20 meters			
Diel	4 (14)	4 (6)	8
Random	25 (86)	59 (94)	84
Total	29 (100)	63 (100)	92
Method 2: Secchi Depth ≤ 6.3 meters, Compensation Depth ~20 meters			
Diel	2 (22)	6 (7)	8
Random	7 (78)	77 (93)	84
Total	9 (100)	83 (100)	92

DISCUSSION

The DO concentrations showed no or very weak diurnal (24-hour) or semi-diurnal (12-hour) periodicity. PAR and water level variation both showed diurnal periodicity, while temperature did not. Temperature and tide did not significantly influence the variability of DO

concentrations over periods of hours to days. In contrast, a diel DO pattern that was found in 7% (bottom) to 20% (surface) of the data suggests that PAR does play an important role in the short-term DO variability by promoting the biological process of photosynthesis. The importance of light is reinforced by the observed decrease in the percentage of days showing a diel DO cycle with depth, which is consistent with the exponential light attenuation pattern within the water column. However, this pattern was not apparent all the time and was distributed irregularly throughout the dataset.

Temperature

It is known that seasonal variability in the near-bottom temperature affects the seasonal variability in DO concentrations. For example, Rowe et al. (2002) reported higher sediment respiration rates during summer than during winter across the Louisiana continental shelf that was attributed to a temperature effect (Q10 of about 2). However, no short-term periodicity in temperature was present in the dataset that I examined. Near-bottom temperature at the study site varied very little over periods ranging from hours to days, and for that reason, it is not likely that temperature plays an important role in the short-term variability of DO concentrations.

Tides

The water level time-series indicated that a tidal signal existed at station C6; however, no corresponding signal was evident in the DO time-series. Rabalais et al. (1994) estimated that in the bottom waters of NGOM, a diurnal 12-hour on-shore flow at 1 cm s^{-1} could displace a water parcel approximately 0.4 km. A semi-diurnal flow of 1 cm s^{-1} over a 6-hour period would add another 0.2 km. During extreme events, such as hurricanes, the maximum displacement of roughly 3 km might be expected due to the diurnal and semi-diurnal tidal currents (Rabalais et al, 1994). Although the water level data indicated that a tidal signal was present at the study site, the time-series of DO concentrations did not show tidal influence. This conclusion is supported

by the findings of Rabalais et al. (1994) who also noted the lack of tidal signal at the study site. The lack of tidal signal in time-series of DO concentrations collected at station C6 suggests that the surrounding waters had similar DO concentrations as the study site. Obviously, the maximum horizontal displacement of only 3 km due to diurnal and semi-diurnal currents (Rabalais et al., 1994) is not likely to affect DO concentrations at the study site located in the core of a 60-km wide hypoxic area. However, the O_1 and K_1 signals were evident in DO time-series collected at a site closer to the mouth of the Mississippi River and closer to the edge of the hypoxic zone (Rabalais et al., 1994).

Photosynthetically Active Radiation

A diel curve was exhibited in the time-series of near-bottom DO concentrations at station C6 approximately 7% of the time although the periodograms showed no true day-night signal. This indicates that either photosynthesis occurs only 7% of the time, or, more likely, primary production occurs more often but the diel signal is interrupted by episodic events. Mixing events at station C6 occur on average about once a month (Chapter 4). Quinones-Rivera (2007, 2010) found that photosynthesis was small in the near-bottom waters of the northern Gulf of Mexico; at depths greater than 2-3 times the Secchi depth benthic primary production was not likely to occur. Significant phytoplankton photosynthesis only occurs down to the depth z_{eu} at which PAR falls below 1% of surface PAR value (Kirk, 2003). The Secchi depths reached compensation depth ~25% of the time. Thus, assuming K_d to be constant throughout the water column, enough light for primary production to occur is available at the bottom ~25% of the time. Yet, a diel pattern in near-bottom DO concentrations was detected in only 22% of cases where the Secchi disk depths were equal or greater than the compensation depth.

The results discussed above suggest that the observed diel periodicity in DO concentrations at station C6 is primarily controlled by the variation in PAR at the surface.

Baustian et al. (2011) showed that benthic diatoms were present in bottom sediments at the study site suggesting that benthic photosynthesis is likely a source of oxygen for the near-bottom layer. Nevertheless, the attenuation of PAR through the water column is highly variable in the NGOM, and underwater PAR levels are very different compared to those at the surface. Light absorption can be attributed to four components (Branco and Kremer, 2005) absorption by pure water, colored dissolved organic matter (CDOM), the concentration of phytoplankton or chlorophyll-*a*, total suspended solids.

The decrease in the proportions of diel days as a function of depth is consistent with the exponential decrease in light intensity with depth due to the absorption by pure water. The attenuation by pure water is constant for all water bodies and increases exponentially with the depth of the water column (Kirk, 2003). This may explain why the proportion of days with diel DO variability decreased as a function of water depth. On the other hand, variation in CDOM and chlorophyll *a* levels in the water column were likely responsible for variation in the bottom diel DO pattern. For example, excess CDOM in bottom waters of NGOM was associated with low oxygen conditions (D'Sa, 2008). Water high in CDOM absorbs in the blue portion of the visible spectrum preferentially removing light that is critical for photosynthesis (Branco and Kremer, 2005). Also, in highly productive waters, such as NGOM, algal cells intercept a substantial amount of light in the water column (Kirk, 1975). Chlorophyll *a* absorbs light in the 400nm and 680nm spectrum (Lorenzen, 1972), and thus these critical wavelengths are diminished and can no longer support photosynthesis at the bottom.

Conclusion

Continuous diel periodicity was not detected in the time-series of DO concentrations measured in the near-surface, mid-water-column, and near-bottom layers at station C6. Nevertheless, a diel DO pattern was present intermittently throughout the dataset at all three

depths. The proportion of days characterized by the diel periodicity in DO concentrations decreased with depth, from 20% near the surface, 12% in the mid-water-column, to 7% near the bottom. The lack of characteristic tidal signals in the DO periodograms for station C6 suggest that surrounding waters within a tidal excursion length (~ 3 km) from the study site have similar DO levels. Further, the lack of a 24-hour signal in the periodograms of the DO concentrations indicated that the diel cycle of photosynthesis and respiration was largely interrupted by episodic events. The short-term variation in underwater PAR levels were in part responsible for these interruptions in the diel DO pattern.

REFERENCES

Baustian, M.M, Rabalais, N.N., Morrison, W.L., and Turner, R. E. 2011. Seasonal microphytobenthos on the hypoxic northern Gulf of Mexico continental shelf. Marine Ecology Progress Series, 436, 51-66.

Berges, J.A., Varela, D.E., and Harrison, P.J., 2002. Effects of temperature on growth rate, cell composition and nitrogen metabolism in the marine diatom *Thalassiosira pseudonana* (Bacillariophyceae). Marine Ecology Progress Series 225, 139-146.

Box, G.E.P., Jenkins, G.M., and Reinsel G.C. 1994. Time-series analysis: Forecasting and control, 3rd Edition, Holden-Day.

Branco, A.B. and Kremer, J.N. 2005. The relative importance of chlorophyll and colored dissolved organic matter (CDOM) to the prediction of the diffuse attenuation coefficient in shallow estuaries. Estuaries 28(5), 643-652.

Cole, B. and Sapp, S. 2003. http://www.nodc.noaa.gov/archive/arc0014/0002033/1.1/data/0-data/LA_Hypoxia_Surveys_1998.xml.

Cooley, J.W. and Tukey, J.W. 1965. An algorithm for the machine computation of complex. Fourier series: Mathematical Computing 19, 297-301.

D'Sa, E. 2008. Colored dissolved organic matter in coastal waters influenced by the Atchafalaya River, USA: effects of an algal signal. Journal of Applied Remote Sensing 2(023502).

Hanson, P.C., Carpenter, S.R., Armstrong, D.E., Stanley, E.H., and Kratz, T.K. 2006. Lake dissolved inorganic carbon and dissolved oxygen: changing drivers from days to decades. Ecological Monographs 76(3), 343-363.

Holmes, R.W. 1970. The Secchi disk in turbid coastal zones. Limnology and Oceanography 15, 688-694.

Jones, H.G., Archer, N., Rotenberg, E., and Casa, R. 2003. Radiation measurement for plant ecophysiology. Journal of Experimental Botany 54(384), 879-889.

Justić, D., Bierman, V.J., Scavia, D., and Hetland, R.D. 2007. Forecasting Gulf's hypoxia: The next 50 years? Estuaries and Coasts 30, 791-801.

Kirk, J.T.O. 1975. A theoretical analysis of the contribution of algal cells to the attenuation of light within natural waters. I. General treatment of suspensions of pigmented cells. New Phytologist 75(1), 11-20.

Kirk, J.T.O. 1994. Light and photosynthesis in aquatic ecosystems. New York: Cambridge University Press.

Kirk, J.T.O. 2003. The vertical attenuation of irradiance as a function of the optical properties of the water. Limnology and Oceanography 48(1), 9-17.

Lorenzen, C.J. 1972. Extinction of light in the ocean by phytoplankton. Journal du Conseil 34(2), 262-267.

Marmer, H.A. 1954. Tides and sea level in the Gulf of Mexico. Fishery Bulletin 89:101–118.

Microsoft Corporation. 2010. Microsoft SQL Server Express Edition with Advanced Services. Redmond, WA: Microsoft Corporation.

Odum, H.T. and Hoskin, C.M. 1956. Primary production in flowing waters. Limnology and Oceanography 1(2):102-117.

Quinones-Rivera, Z.J., Wissel, B., Justić, D., and Fry, B. 2007. Partitioning oxygen sources and sinks in a stratified, eutrophic coastal ecosystem using stable oxygen isotopes. Marine Ecology-Progress Series 342, 69-83.

Quinones-Rivera, Z.J., Wissel, B., Rabalais, N.N., and Justić, D. 2010. Effects of biological and physical factors on seasonal oxygen dynamics in a stratified, eutrophic coastal ecosystem. Limnology and Oceanography 55: 289-304.

R Development Core Team. 2011. R: A language and environment for statistical computing. R Foundation for Statistical Computing, Vienna, Austria.

Rabalais, N.N., Turner, R.E., and Scavia, D. 2002. Beyond science into policy: Gulf of Mexico hypoxia and the Mississippi River. Bioscience 52(2), 129-142.

Rabalais, N.N., Wiseman, W., and Turner, E.R. 1994. Comparison of continuous records of near-bottom dissolved oxygen from the hypoxia zone along the Louisiana coast. Estuaries and Coasts 17(4): 850-861.

Rose, K.A., Adamack, A.T., Murphy, C.A., Sable, S.E., Kolesar, S.E., Craig, J.K., Breitburg, D.L., Thomas, P., Brouwer, M.H., Cerco, C.F., Diamond, S., 2009. Does hypoxia have population-level effects on coastal fish? Musings from the virtual world. Journal of Experimental Marine Biology and Ecology 381, S188-S203.

Rowe, G.T, Kaegi, M. E. C., Morse, J. W., Boland, G. S., Briones, E. G. E. 2002. Sediment community metabolism associated with continental shelf hypoxia, Northern Gulf of Mexico. Estuaries 25: 1097-1106.

Sanford, L.P., Sellner, K.G., and Breitburg, D.L. 1990. Covariability of dissolved oxygen with physical processes in the summertime Chesapeake Bay. Journal of Marine Research 48(3), 567-590.

Scavia, D., Justic, D., and Bierman, V.J., 2004. Reducing hypoxia in the Gulf of Mexico: Advice from three models. Estuaries 27, 419-425.

Spetic, A. and Gennick, J. 2002 Transact-SQL cookbook. Beijing: Sebastopol, Calif., O'Reilly.

CHAPTER 4

EPISODIC FACTORS AFFECTING SHORT-TERM OXYGEN VARIABILITY IN THE NORTHERN GULF OF MEXICO HYPOXIC ZONE

INTRODUCTION

Scientists have been studying oxygen variability in the Northern Gulf of Mexico (NGOM) since the 1970s to better understand the dynamics of hypoxia (Rabalais et al., 2002). Hypoxia in the NGOM is operationally defined as dissolved oxygen concentrations ≤ 2.0 mg l^{-1}, based on a lack of fish catch in bottom trawls below 2.0 mg l^{-1} (Renaud, 1986). Hypoxia occurs when bacteria decomposing excess carbon use more oxygen than is being produced, and the water column is sufficiently stratified to prevent dissolved oxygen from the atmosphere and upper layers of the water column from re-aerating the bottom waters (Justić et al., 2007).

While much is understood about oxygen variability on large spatial and temporal scales (Rabalais et al., 2010), an understanding of the short-term dynamics of oxygen variability is still lacking. In order to more fully understand the short-term variability of DO in the lower water column in the northern Gulf of Mexico (NGOM) hypoxic zone, it is important to understand the factors that might influence that variability. Short-term DO variability showed a seasonal pattern and the trends in short term oxygen variability among years was correlated with nutrient flux from the Mississippi River (Chapter 2). What little periodicity can be extracted from short-term oxygen variability observed in a time series at a sampling station is often interrupted by other forces, resulting in periodic factors only accounting for a small degree of the variability (Chapter 3). Several types of episodic or irregularly occurring events, like cold fronts and tropical cyclones, affect short-term oxygen variability by mixing the water column, thereby bringing oxygen rich water from the upper layers to the bottom layers of the water column (Wiseman et al., 1997).

The degree of stratification is another source of variability that is a factor in short-term DO related to the episodic events. The key control that governs the persistence of seasonal hypoxia is the stability, or strength of stratification, of the water column (Kemp et al., 2009). The two primary controls on stability are the density gradient of the water column and the energy transferred to the water column by the wind and other forces (Lund-Hansen et al., 1996). The density gradient is controlled by temperature and salinity, factors that vary seasonally. Variation in flow from the Mississippi River could affect DO by lowering sea surface salinity through fresh water flux and by strengthening the stratification of the water column (Wiseman et al., 1997). Seasonal variations in temperature are another source of variability on the density gradient. Stronger stratification reduces the ability of other episodic events to mix the water column (Lund-Hansen et al. 1996).

Although several forces act to weaken stratification and mix the water column, wind stress is the primary force that disturbs a stratified water column and re-aerates the bottom waters with oxygen. Increased wind stress can cause mixing. Wind stress is often associated with events like cold fronts and tropical cyclones.

About 30 to 40 cold fronts per year pass through the Louisiana Coast into the Gulf of Mexico between the months of October and April (Moeller et al., 1993). A cold front is a spatially and temporally ordered system of changes in surface winds, temperature, and humidity (Roberts et al., 1987). A cold front has three phases: a pre-frontal phase, a frontal passage, and a post-frontal or cold air outbreak phase. Cold fronts can be divided into two categories based on the orientation to the coastline. Oblique cold fronts pass at a 45 degree angle to the Gulf coast; whereas parallel cold fronts pass parallel to the Gulf coast. The duration of most cold fronts is between 12 to 24 hours. The fate of cold fronts is either to return as a warm front or to push through the Gulf to the tropics. Two end-member types of fronts are arctic surges and migrating cyclones. Arctic surges

have very weak pre-frontal phases and fairly strong post-frontal phases with dominant northeast winds. Migrating cyclones have strong low pressure cells and strong pre-frontal south winds followed by strong northwest winds in the post-frontal phase (Roberts et al., 1987).

Tropical cyclones also occur over the northern Gulf of Mexico with some frequency. Tropical cyclones are categorized according to the Saffir–Simpson Hurricane Scale. Tropical cyclones can vary from a category of a tropical storm with wind speeds of 18-32 m s^{-1} to a category 5 hurricane with winds in excess of 70 m s^{-1} (Williams and Sheets, 2001). Hurricane strength tropical cyclones strike the Louisiana coast on average once every three years (Stone et al., 1997).

In this chapter, I explore how episodic events like short-term increased wind stress, cold fronts, and tropical cyclones influence the short-term variability of dissolved oxygen concentrations in the NGOM hypoxic zone. The two goals of this chapter are: 1) to explore the relationship between temperature and salinity-based indicators of the strength of stratification and the associated daily average bottom DO concentrations, and 2) to characterize re-aeration events identified from DO concentrations and to explore the coincidence of the timing of these re-aeration events to the timing of cold fronts and tropical cyclones. My analyses in this chapter will further our understanding of the role played by short-term, espisodic factors in mixing that dissipate hypoxia.

METHODS

Study Area

The study area encompasses the northern Gulf of Mexico from the mouth of the Mississippi River west to the Texas border. The data collection site, station C6, was located 20 miles south of Terrebonne Bay in 20 meters of water at a location that experiences annual summer-

time hypoxia (Figure 2.1). Freshwater discharges from the Mississippi and Atchafalaya Rivers, and the prevailing westward-flowing coastal current, maintain a strong vertical stratification in this region throughout most of the summer. Stratification breaks down as a result of frontal passages in the winter or tropical storm events during the late summer and early fall (Wiseman et al., 1997). An acoustic Doppler current profiler (ADCP) deployed at this site from mid-March to mid-November 2002 demonstrated a predominantly alongshore flow rather than cross-shelf flow (Wiseman et al., 2004). The mean bottom currents for 1990 were not statistically distinguishable from zero (Rabalais et al., 1994). Winds are predominantly from the southeast (Walker et al., 2005), causing the Louisiana coastal current to flow mainly westward. The plumes from the Mississippi and Atchafalaya Rivers create regions of strong freshwater influence. Mean winds are generally down-welling favorable; however, from late spring to mid- or late-summer upwelling favorable and a return flow occurs pushing low salinity waters back up the coast (Cochrane and Kelly, 1986).

Data Sources

I used three different data sources in my analysis (Table 4.1). The primary data source was a water quality data set that provided the DO concentrations and other water quality variables collected at station C6, and was used for both the stratification analysis and the re-aeration event analysis. I also used atmospheric variables reported for station C6 and tropical cyclone advisories within a 200 nautical mile radius of station C6 in the identification of wind stress events, cold fronts, and tropical cyclones to compare to the timing of re-aeration events.

First, I used water quality data from a 20 year data set (1989-2009) measured with electronic sensors every 15 minutes at station C6. From 1989 through 1995, a single bottom mounted sonde collected data on DO concentration and temperature. Beginning in 1996, a mid-water column sonde, located at 10.7 m below mean sea level and a near-surface sonde, 2 m below

mean sea level, were added to the instrument array at the site. In 1996, a salinity sensor was also added to the array along with various other instruments. The data set is described in detail in Chapter 2. For periods when salinity measurements were available, I calculated sigma-t (water density minus 1000) from the 15-minute records of temperature and salinity using the International Equation of State of Seawater (UNESCO, 1983).

Table 4.1. Brief description of data sources used in the analysis presented in this chapter.

Component	Variables Measured	Field Technique	Sampling frequency and duration	Reference
Water quality variables	Dissolved oxygen Temperature Salinity sigma-t (derived)	Standard oceanographic analytic techniques measured by electronic sensors	Sampled 4times/hour, Between 1989-2008	LUMCON
Atmospheric variables	Maximum Pressure Temperature U wind component V wind component Wind stress (derived)	NARR-A Model reanalysis	Reported every 3 hours	NCEP
Cyclone Data	Season (year) Name ISO date time Nature (Category) Location	National Hurricane Center Advisories and Tracks	Sampled every 6 hours	NCDC

Second, I used atmospheric data from NOAA National Centers for Environmental Prediction (NCEP) to characterize wind stress events and identify cold front events. NCEP provides both climate and weather model data through the National Operational Model Archive and Distribution System (NOMADS) (Mesinger et al., 2004). I downloaded 3-hour air temperature, barometric pressure, and the u and v wind components from NCEP's North American

Regional Reanalysis (NARR) database from the NOMADS website (http://nomads.ncdc.noaa.gov/). NARR-A assimilates observational data with the model data through reanalysis. The wind data are calculated for 10 m above the sea surface. The downloaded data set consisted of 3-hour single point observations reported for the location of station C6 from 1989 to 2008.

Third, I downloaded the Atlantic Hurricane track data from the NOAA's National Climatic Data Center (http://www.ncdc.noaa.gov/oa/ibtracs/index.php?name=wmo-data) to identify tropical cyclone events. International Best Track Archive for Climate Stewardship (IBTrACS-WMO) data consisted of tropical cyclone advisories issued every 6 hours by the National Hurricane Center from 1951 to 2010 on storms in the Atlantic Basin (Knapp et al., 2010).

Data Analysis

The analysis consisted of stratification analysis using regression trees and a re-aeration event analysis that included both identifying and characterizing the re-aeration events and the correspondence of these events with the timing of wind stress events, cold fronts, and tropical cyclones. The stratification analysis used the delta (Δ) values of temperature, salinity, and sigma-t) as explanatory variables and the categories of DO concentrations as the response variable for the entire time-series in regression trees. The identification and characterization classified re-aeration events and compared them by season. The re-aeration event comparative analysis used predictor events identified by various methods as explanatory variables and the re-aeration event as the response variable.

Stratification Analysis with Regression Trees

I used conditional inference trees (Hothorn et al., 2006) to estimate a regression relationship between a categorical variable based on the categorized daily averaged DO

concentrations and the daily averaged vertical density difference (Δ sigma-t), vertical temperature difference (ΔT) and vertical salinity difference (ΔS) from station C6. First, I computed Δsigma-t by subtracting the near-surface sigma-t from the near-bottom sigma-t using the 15-minute samples from the water quality data described above. I also computed ΔT and ΔS in the same manner. I then computed daily averages for Δsigma-t, ΔT, and ΔS to use in the analysis. I also calculated daily averages for DO concentrations from the 15 minute samples of the water quality dataset and I assigned a category to each DO value: A) normoxic (DO>4.59 mg l^{-1}), B) suboxic (DO≤4.59 and DO>2.0 mg l^{-1}), C) hypoxic (DO≤2.0 mg l^{-1} and DO>1.0 mg l^{-1}), and D) severely hypoxic (DO≤1.0 mg l^{-1}). Then, I modeled this categorical variable by Δsigma-t, ΔT, and ΔS separately creating three conditional inference trees using the ctree command from the party library in R statistical programming software (R Development Core Team, 2011). The flow chart in figure 4.1 outlines this analysis.

Conditional inference trees estimate a regression relationship by recursive calculating a binary partition using a conditional reference framework. The conditional inference trees algorithm involves two steps repeated recursively. First, the global null hypothesis of independence between input variables is tested. If this null hypothesis cannot be rejected, the algorithm stops. If the null hypothesis can be rejected, then the algorithm selects the variable with the strongest association to the response variable. A P-value is assign for the test of a partial null hypothesis of the single input variable against the response variable. Second, a binary split is implemented with the selected input variable. These steps are repeated until all null hypotheses at terminal nodes cannot be rejected (Hothorn et al., 2006).

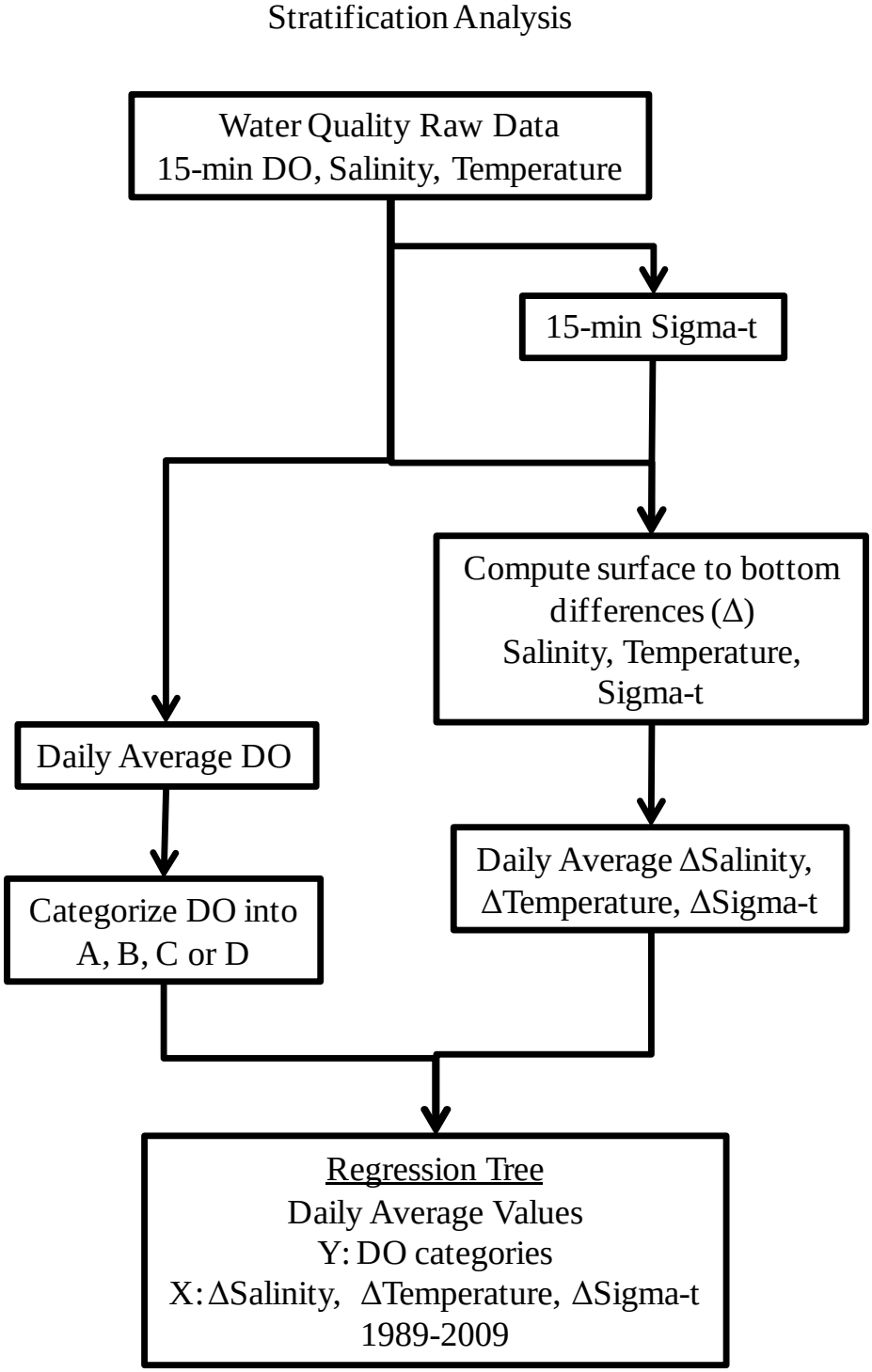

Figure 4.1. Flowchart of the stratification analysis. The letters represent the categories of DO concentrations as A) normoxic (DO > 4.59 mg l^{-1}), B) suboxic (DO between 4.59 and 2.0 mg l^{-1}), C) hypoxic (DO between 2.0 and 1.0 mg l^{-1}), and D) severely-hypoxic (DO ≤ 1.0 mg l^{-1}).

Re-Aeration Event Analysis

The re-aeration event analysis consisted of three steps (Figure 4.2). First, I prepared the data for analysis by identifying three predictor events (wind stress events, cold fronts, and tropical cyclones) and one response event (re-aeration events). The predictor variables were identified using a variety of methods and only the day identification variable (ID) was used in the re-aeration event analysis (Table 4.2). Re-aeration events were identified using a re-aeration event detection algorithm (RED) based on average hourly DO concentrations. Second, I identified and characterized the re-aeration events by type and compared these events by season: spring (March, April, and May), summer (June, July, and August), fall (September, October, and November), and winter (December, January, and February). Third, I compared the timing of the re-aeration events to the timings of the three predictor events. Figure 4.2 outlines this analysis.

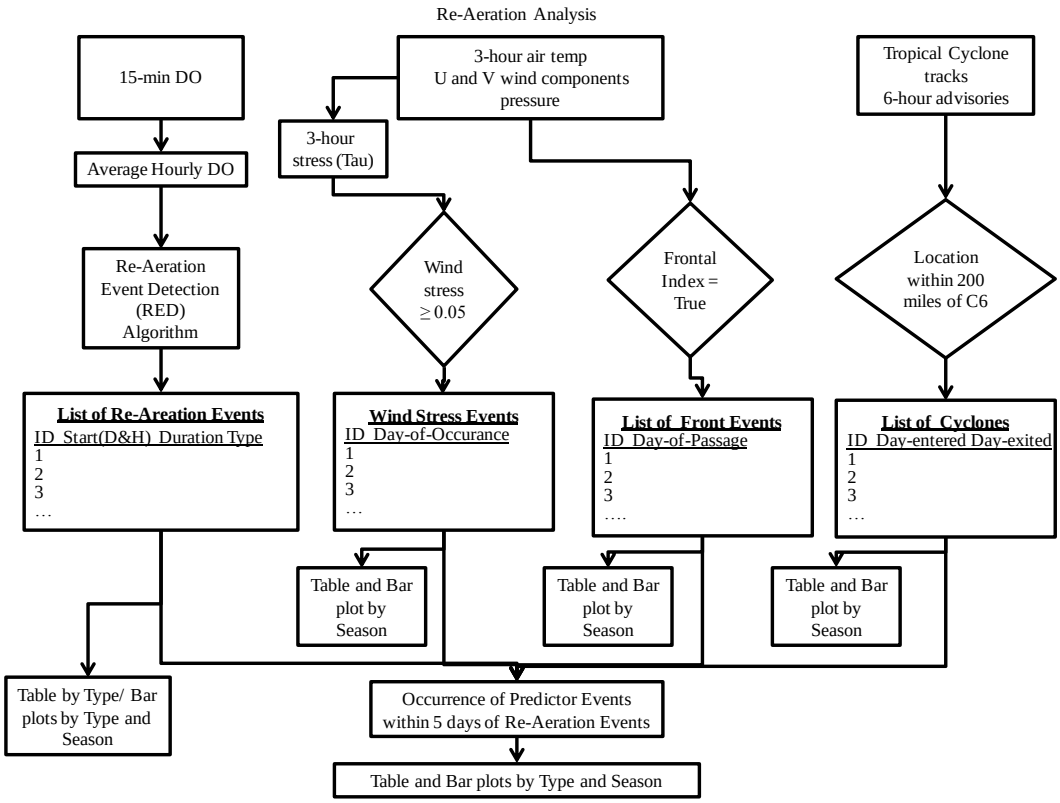

Figure 4.2. Flow chart of re-aeration event analysis

Table 4.2. Predictor and response variables used in the re-aeration event analysis

Event Type	Variables Used in Identification	Method of Identification	Resulting Variable
Wind Stress Events	Tau_{wind} (derived using $\tau_{wind} = \rho_{air} C_D U_h^2$) from 3-hour NARR data)	Minimum daily $Tau_{wind} \geq 0.05$ (the upper quartile of the 20 years from 1989 to 2008)	Day of occurrence of the wind stress event
Cold Front Events	3-hour air temperature, U and V wind components, and barometric pressure from NARR database	Δbarometric pressure ≥ 0 mbar, Δair temperature ≤ -2.1°C. and shift in wind direction (Day 1 V-component > Day 1 U-component and Day 2 U-component > Day 2 V-component) over a 24-hour period midnight to midnight coordinated universal time (UTC)	Day of passage of a cold front
Tropical Cyclone Events	6 hour advisories of Date, latitude, longitude from the cyclone data	Advisory (location) within a 200 nautical mile radius of station C6.	Day of the first advisory within test radius, day of last advisory within test radius
Response Variable: Re-aeration Events	Hourly averages of near-bottom DO concentrations from the 15 minute raw water quality data	Re-aeration event detection algorithm (RED)	Day and hour of the onset of the event, duration in hours, type of event (hour used in plotting)

Wind Stress Events– I defined a wind stress event as a day when the minimum three-hour tau (τ) value was in the upper quartile of the wind stress over the 20 years (1989-2008), or was greater than 0.05 dyn cm^{-2}. Using the three-hour atmospheric data from the NARR database, I calculated wind stress (τ_{wind}) in dyn cm^{-2} using the equation of Hsu (1988): $\tau_{wind} = \rho_{air} C_D U_h^2$,

where ρ_{air} is air density in kg m^{-3}, C_D is a dimensionless quantity representing the drag coefficient, and U_h is wind speed in m s^{-1} as measured at h meters above sea level. Wind was reported for 10 meters above sea level, so no further calculations were needed. I then listed all of the days that the minimum value of τ surpassed 0.05 for 1989 to 2008 at station C6 using a day identification variable.

Cold Fronts—I used the air temperature, wind direction (the u and v components of the wind), and barometric pressure for every three hours for 1989 to 2008 at station C6 from the NARR database to identify cold front events. I defined a cold front event by the day during which a cold front passed over station C6.

I modified the index developed by Perez et al. (2000) to identify cold front events. Their cold front index consisted of testing for an increase in the maximum barometric pressure (Δbarometric pressure $\geq$ 7.2 mbar), a drop in air temperature (Δair temperature $\leq$ 4°C), and a shift in wind direction over a 24-hour period from 8am to 8am central standard time. I used these same metrics in developing my index for frontal passages at station C6; however, the thresholds were lower due to cold fronts weakening as they leave the land mass and pass over the Gulf of Mexico. Thus, my index consisted of testing for an increase in the maximum barometric pressure (Δbarometric pressure $\geq$ 0 mbar), a drop in the average air temperature (Δair temperature $\leq$ -2.1°C), and shift in wind direction (Day 1 V-component > Day 1 U-component and Day 2 U-component > Day 2 V-component) over a 24-hour period midnight to midnight coordinated universal time (UTC) in the NARR database. The difference in time only differed from the Perez et al. (2000) index by two hours due to the data being recorded in different time zones.

I confirmed the accuracy of my index by comparing identified fronts to those identified in 1994 by Perez et al. (2000). I compared my index to the fronts from 1994 identified by Perez et al.

(2000) and the two indices were in 100% agreement. I then applied the index to the three hour data for 1989 to 2008 at station C6 from the NARR database and created a list of cold front events identifying each day where the data exhibited my index conditions for a cold front. I used only the day identifier variable in the analysis with re-aeration events.

Tropical Cyclones— A tropical cyclone event was defined by the first date a tropical cyclone's track entered a radius of 200 nautical miles of station C6 between 1989 and 2008 using the cyclone data described above. The maximum wind radius for a tropical cyclone can exceed 27 nautical (Hsu and Yan, 1998), and the average radius for lesser winds is 100 nautical miles (Knaff et al., 2007); however, wind fields and their associated effect on waves and the water column have been reported to exceed 200 nautical miles (Il-Ju et al., 2003). A 200 nautical mile radius encompassed the entire northern Gulf of Mexico shelf and took into account these wind field radii (Figure 4.3). As identifiers for tropical cyclone events, I used the day identifier of the first advisory and the day of last advisory within test radius.

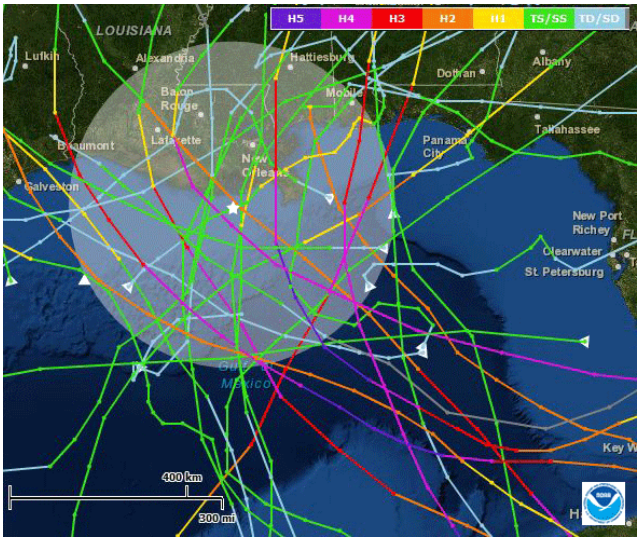

Figure 4.3. Map showing the radius of 200 nautical miles (shaded area) around the station C6 (white star) that was used for tropical cyclone event analysis in this study. If a tropical cyclone track entered the designated area, the event was included in the study. Color bar indicates the intensity of the storm based on the Saffir-Simpson Scale. The map was created using the web service available at http://www.csc.noaa.gov/hurricanes/.

Re-aeration Events—I developed a re-aeration event detection (RED) algorithm to identify and classify re-aeration events occurring at station C6 between 1989 and 2008 based on hourly average DO concentrations. In the RED algorithm, an event is triggered when an hourly value of DO increases above the "trigger threshold." Once an event is triggered, a "test window" is established to determine the completion of the event by assigning the hourly DO values from the next DO value through the window length parameter to the test window. If all of the values in the test window are above or below the threshold, then the algorithm marks the end of the event and classifies the event type. The algorithm increments D, the sliding duration marker, and repeats the window test until the end of the event is marked. If all of the DO values in the test window are above the threshold, then the event is classified as "complete" mixing. If all of the DO values are below the threshold, the event is classified as a "hugger" or a "spike." From these two, the fourth event type, "decreasing" is identified if the DO concentrations prior to the event are above the threshold. Table 4.3 illustrates the different classifications of events. The algorithm outputs the date identifier for each re-aeration event, the duration of the event in hours, and the event type.

Identification and Characterization of Re-aeration Events—I ran the RED algorithm on the hourly averaged near-bottom DO concentrations from the raw water quality data collected from 1989 to 2008 at station C6. I used 2.0 mg l^{-1} as the "trigger threshold" because that is the operational definition of hypoxia in the NGOM. I also used a 48 hour "test window" to determine the end of an event and a four-hour spike duration. The RED algorithm determined the day and hour the event began, the duration of each event, and the classification of the event.

I summarized the identified re-aeration events by year and by season, creating bar charts of the results. The seasons were identified by month as follows: spring (March, April, and May), summer (June, July, and August), fall (September, October, and November), and winter

Table 4.3. The classifications of the re-aeration events identified by the re-aeration event detection algorithm. The identified timing of the re-aeration events are shown with arrows.

Identifier	Sample	Definition	Test
Hugger	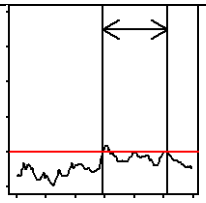	hugs hypoxic threshold	Test window below hypoxic threshold and duration > 4
Spike	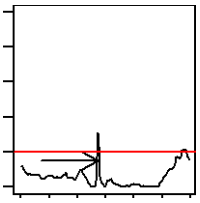	Increases above hypoxic threshold for a short duration and then returns to hypoxic conditions	Test window below hypoxic threshold and duration ≤ 4
Complete	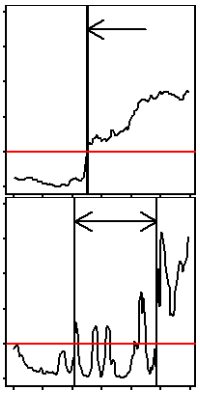	Event ends with DO concentrations consistently above hypoxic threshold (may spike or hug prior to complete mixing)	Test window above hypoxic threshold
Decreasing	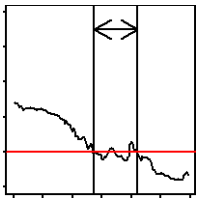	While DO concentrations are decreasing, DO rises above hypoxic threshold for a brief interval but then continues decreasing below the hypoxic threshold.	Pre-DO concentrations above hypoxic threshold and test window below hypoxic threshold
Pre-Mixed	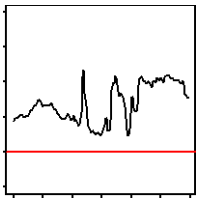	A sudden increase in DO concentrations >=1.5 where the DO never falls below the hypoxic threshold	Currently not detected by the re-aeration event detection algorithm

(December, January, and February). I used the prop.table test in R (R Development Core Team, 2011) to determine the proportions by type and by season using the chi-squared statistic to test for

independence. I confirmed the robustness of the results by repeating the RED algorithm with the other thresholds of low oxygen defined in the stratification analysis suboxic ($\leq$ 4.59 mg l^{-1}) and severely hypoxic ($\leq$ 1.0 mg l^{-1}).

Correspondence of Re-aeration Events with Wind, Cyclones, and Fronts.—I compared the timing of the re-aeration events identified by the RED algorithm to the timing of the predictor events of wind stress, cold fronts, and tropical cyclones. I quantified the number of wind stress events that occurred within 5 days before each re-aeration event. I also quantified the number of cold fronts and the tropical cyclones that occurred within a 10-day window, 5 days before or 5 days after, each re-aeration event. I created stacked plots of DO concentrations at three depths, sigma-t at three depths and Δsigma-t, the u and v wind components, wind stress, and wind vectors for 5 days prior and 5 days after the onset of each re-aeration event identified by the RED algorithm and for each cold front and tropical cyclone event. I compared these by re-aeration event type, month, season, and year testing whether or not the groups have the same proportions in R and bar plots.

Confirmation of Re-Aeration Event using Regression Trees

I compared the Δsigma-t values from seven days surrounding each re-aeration event as input to the regression tree and compared whether the tree would have predicted mixing and compared the tree-predicted DO category expected to the observed daily DO concentration in the event. The estimation of the conditional inference tree used all of the daily averages of DO concentrations and Δsigma-t data, and this was not an independent test of the tree. So, it was important to examine if the events identified by the RED based on DO concentrations on an hourly scale were consistent with the full dataset on a daily scale that was used to estimate the tree. The seven days included three days before the event, the day of the onset of the event, the last day of

the event, and two days after the event. If the duration of the event was less than twenty-four hours, the last day was the same as the day of as the onset of the event.

I created bar charts of the counts of the predicted nodes for the seven days for each type of re-aeration event. I also compared the predicted DO categories from the conditional inference tree to the actual DO categories for the seven days surround each complete mixing re-aeration event. I created a confusion matrix comparing the actual DO category to the predicted DO category, and calculated the accuracy of the predictions from the confusion matrix for each of the seven days.

RESULTS

Stratification Analysis

The conditional inference tree showed that the hypoxic DO category was not clearly correlated with any value of Δsigma-t, while the severely-hypoxic and the normoxic DO categories showed more definite correlations (Figure 4.4). The Δsigma-t tree predicted the normoxic DO category with 63% accuracy and the severely-hypoxic DO category with 48% accuracy. Delta sigma-t greater than 3.52 kg m^{-3} correlated with severely-hypoxic DO conditions. Nodes five and six showed the highest correlation, both with Δsigma-t less than 0.28 kg m^{-3} and greater than 0.56 kg m^{-3}. Node 10 showed no high correlation to any DO category, indicating that the water column is unstable and mixing is occurring at these sigma-t values. Node four showed that Δsigma-t was less than -0.56 kg m^{-3} for only seven days of the 20 years (i.e., n=7), and correlated with the normoxic DO category indicating that the near-surface density was greater than the near-bottom density and an extremely unstable water column was present. The overall accuracy of the predicted DO categories with the actual categories was 48%.

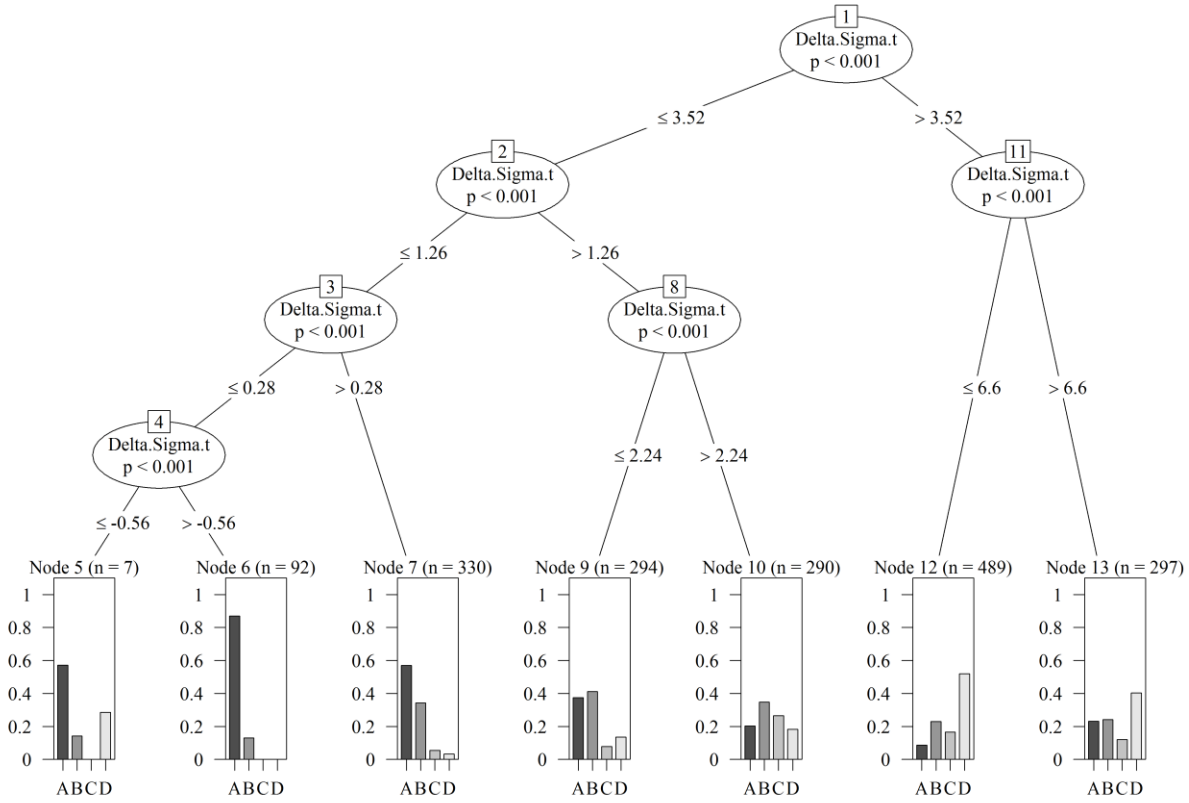

Figure 4.4. Results from conditional inference tree analysis of Δsigma-t by threshold of dissolved oxygen concentrations. Delta sigma-t was calculated by subtracting the near-bottom sigma-t values from the near-surface sigma-t values, where sigma T is density -1000. Sigma-t was computed from temperature and salinity using the International Equation of State of Seawater (UNESCO, 1983) then subtracting 1000. The categories of dissolved oxygen concentrations are identified as A) normoxic (DO>4.59 mg l^{-1}), B) suboxic (DO≤ mg l^{-1} and DO> mg l^{-1}), C) hypoxic (DO≤2.0 mg l^{-1} and DO>1.0 mg l^{-1}), and D) severely-hypoxic (DO≤1.0 mg l^{-1}). Note that for node 4 n=7 indicating that this represents only 7 days of the 20 year dataset where the near-bottom density was less than the surface density.

The conditional inference tree based on temperature more accurately predicted the DO categories than sigma-t (Figure 4.5). The overall accuracy of the temperature-based tree at predicting DO categories accurately was 54%. The temperature tree also did better on the extremes of the normoxic DO category (55% accuracy) and the severely hypoxic category (60% accuracy). A temperature difference of less than -1.79° C correlated with severely-hypoxic category; whereas, hypoxic conditions were not predicted in any of the nodes

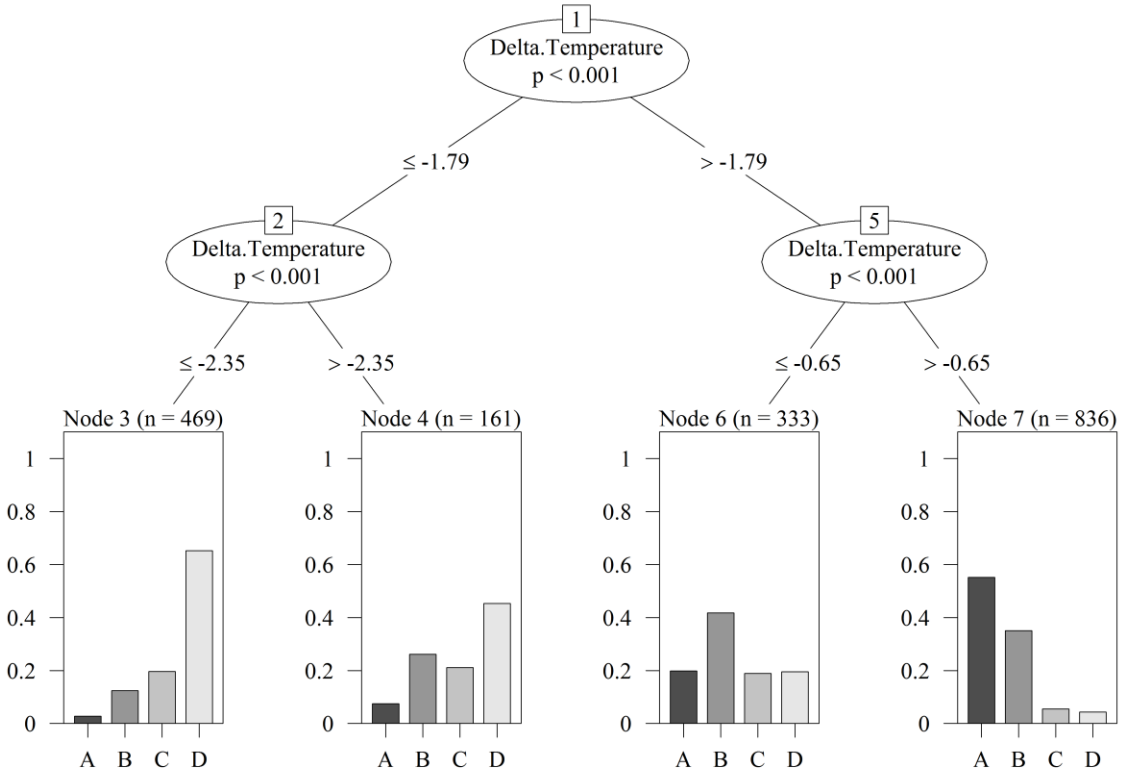

Figure 4.5. Results from conditional inference tree analysis Δtemperature by threshold of dissolved oxygen concentrations. Delta temperature was calculated by subtracting the near-bottom temperature from the near-surface temperature. The categories of dissolved oxygen concentrations are identified as A) normoxic (DO>4.59 mg l^{-1}), B) suboxic (DO≤ mg l^{-1} and DO> mg l^{-1}), C) hypoxic (DO≤2.0 mg l^{-1} and DO>1.0 mg l^{-1}), and D) severely hypoxic (DO≤1.0 mg l^{-1}. Note Δtemperature values are negative because the near-bottom waters are cooler than the near-surface waters; thus the tree appears in reverse order.

The conditional inference tree based on Δsalinity was the least accurate at predicting DO categories; however, it was the only tree for which predicted values correlated with the DO category of hypoxic. The salinity-based tree predicted DO categories with 45% accuracy and predicted the hypoxic DO category with 47% accuracy. The tree predicted lower Δsalinity values for the DO category of severely-hypoxic that for the DO category of hypoxic (Figure 4.6). A difference in salinity of 3.53 psu split the tree between hypoxic and not-hypoxic conditions. The difference in salinity showed a greater correlation to the hypoxic category at greater than 21 psu. Between 9.41 and 21 psu hypoxic conditions decrease considerably. Severely-hypoxic category

was correlated with a salinity difference between 3.53 and 9.41 psu. Interestingly, neither the temperature nor salinity trees split on a negative value, while the Δsigma-t tree did.

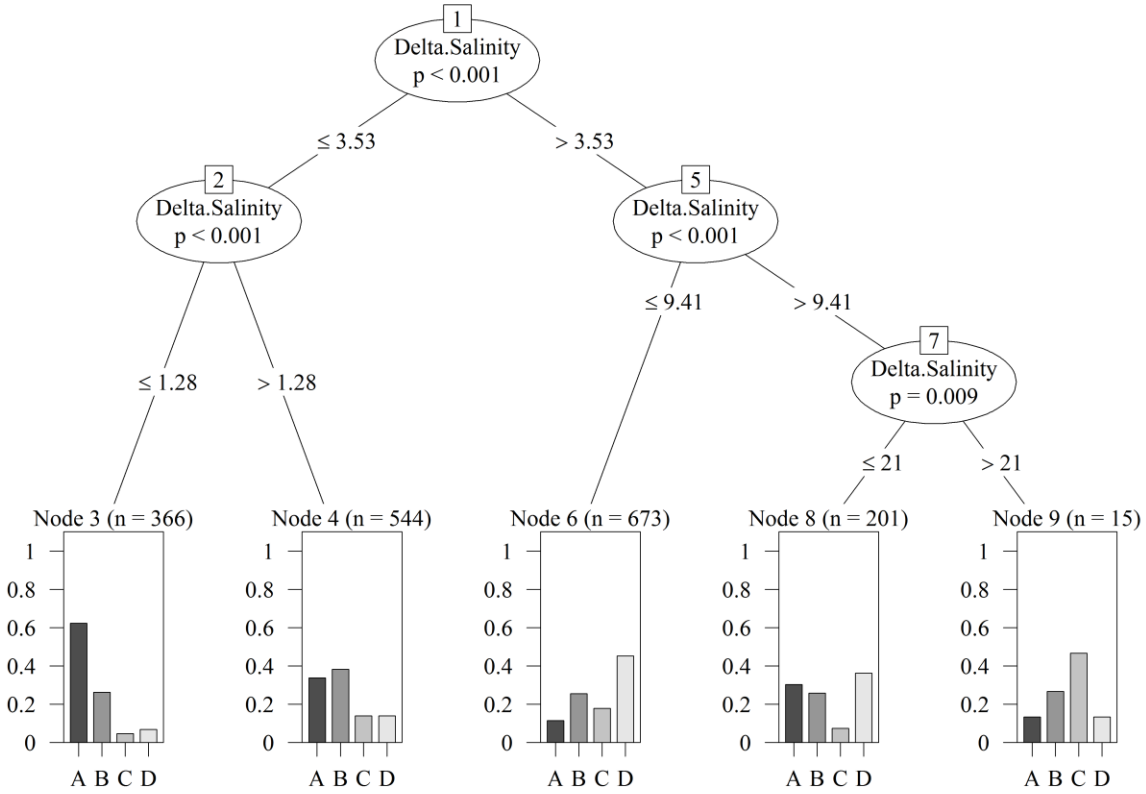

Figure 4.6. Results from conditional inference tree analysis Δsalinity by threshold of dissolved oxygen concentrations. Delta salinity was calculated by subtracting the near-bottom salinity from the near-surface salinity. The categories of dissolved oxygen concentrations are identified as A) normoxic (DO>4.59 mg l^{-1}), B) suboxic (DO≤ mg l^{-1} and DO> mg l^{-1}), C) hypoxic (DO≤2.0 mg l^{-1} and DO>1.0 mg l^{-1}), and D) severely hypoxic (DO≤1.0 mg l^{-1}).

Re-aeration Event Analysis

Characterization of Re-aeration Events

The re-aeration event detection (RED) algorithm captured re-aeration events where the DO concentrations increased from below the hypoxic threshold (DO ≤ 2.0 mg l^{-1}) to above the threshold (Table 4.4 – middle row). The identification of events was robust to other threshold values, as many of the same events were identified with thresholds of 1.0 and 4.59 mg l^{-1} (Table

4.4). One difference was the number of hugger events, with many more identified with higher thresholds. I used the 2.0 mg l^{-1} threshold because that is the value used as the operational definition for hypoxia in the northern Gulf of Mexico and my focus on the complete events, which were almost identical across thresholds.

Table 4.4. The results of varying the threshold in the re-aeration detection (RED) algorithm.

Threshold	Complete	Decreasing	Hugger	Spike	Total
Severely Hypoxic (DO $\leq$ 1.0 mg l^{-1})	118	27	61	15	221
Hypoxic (DO $\leq$ 2.0 mg l^{-1})	116	28	82	12	238
Suboxic (DO $\leq$ 4.59 mg l^{-1})	117	34	107	13	271

The RED algorithm was robust enough to withstand some variation in other parameters beside the threshold. The two other parameters that can be adjusted in the RED algorithm are the length of the test window and the duration that identifies a spike type of event. I tested the algorithm with test window of both 24 and 72 hours with similar results as the 48 hour window. The other parameter was the use of duration to determine spikes. During testing I noticed that some of the events that the RED classified as spikes had DO values decreasing from normoxic conditions prior to the event. So I added a test for decreasing to the algorithm to separate these events from spikes.

The re-aeration events where the DO concentrations increased from below the hypoxia threshold to above the threshold at C6 were episodic and occurred infrequently over the 20 year period from 1989 to 2008. Near-bottom DO concentrations were collected for 4427 days and the

RED algorithm identified 283 re-aeration events over that time period. A re-aeration event occurred on only 5% (χ^2=3524, p<0) of the days sampled. An average of twelve re-aeration events occurred each year from 1989 to 2008. Both years 1999 and 2006 had the most re-aeration events with eighteen, and the year 1996 had the fewest events with only four. Figure 4.7 clearly showed that the spring and summer had the most re-aeration events followed by fall and winter. In spring and summer, the DO concentrations returned to hypoxic conditions rather quickly following re-aeration events, rather than staying mixed making subsequent re-aeration events possible. Winter had the fewest because the water column stayed primarily mixed throughout the winter and because DO was sampled less frequently in winter than in the other seasons. This pattern was only slightly different when comparing the types of re-aeration events by season.

The most common type of re-aeration event where the DO concentrations went from below the hypoxic threshold to above the threshold at station C6 was complete mixing, and most of the complete mixing re-aeration events occurred in the spring. Both fall and summer had about the same number of complete mixing events. Winter had only one complete mixing event because the water column stayed mixed during the winter.

The hugger type of re-aeration event was most prevalent in the spring and summer. This follows the pattern of decreasing DO concentrations and increasing stratification. When a re-aeration event occurred, high respiration quickly lowered the DO concentrations below the hypoxic threshold. Increasing stratification due to the warming of the sea surface prevented wind events from completely mixing the water column.

The RED algorithm identified twelve re-aeration events as spikes. Only two of these occurred within five days of cold fronts, and both occurred before the cold front passed possibly due to prefrontal south winds moving water masses from offshore across the site where the sensor

was deployed. Two of these spikes occurred within five days of hurricanes. The six spikes remaining are attributed to unknown factors possibly due to offshore processes.

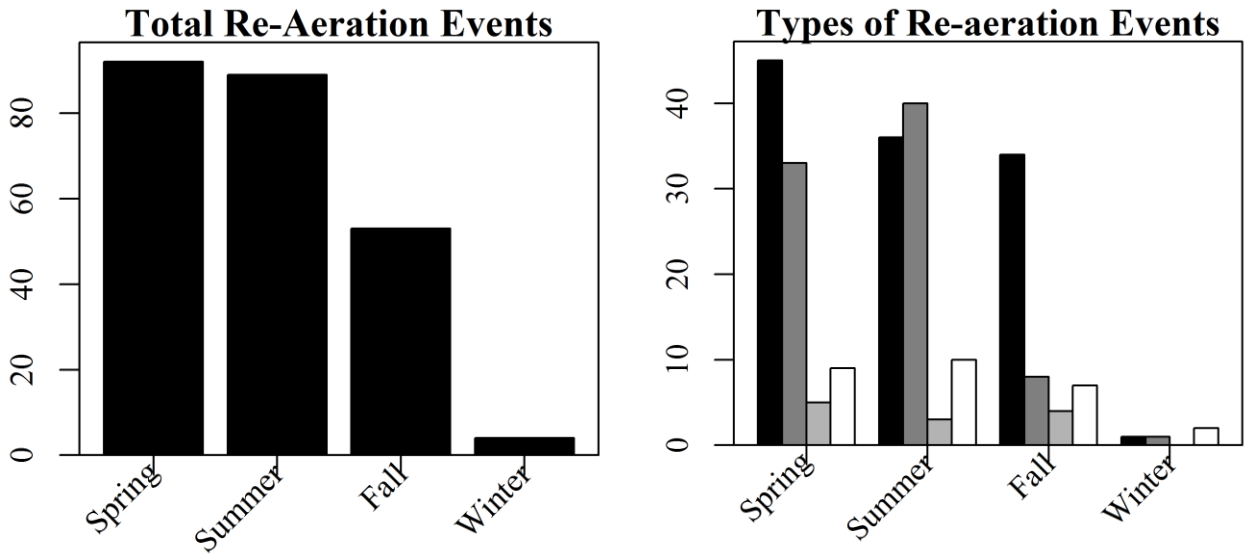

Figure 4.7. Bar plots representing the number of re-aeration events by season. The left panel represents the total number of re-aeration identified by the re-aeration event detection algorithm. The right panel represents the number of re-aeration events of each classified type by season. In the right panel the bar color indicates the type as follows: black—complete mixing, dark gray—hugger, light gray—spike, and white—decreasing.

Wind Stress Events

The greatest number of wind stress events that preceded re-aeration events occurred in the spring even though the fall had the most wind stress events over the 20-year period. A wind stress event occurred prior to a re-aeration event 40% ($X^2 = 6$, $P \leq 00.1$) of all 238 re-aeration events. In the spring, 55 of the 92, or 60%, of the re-aeration events occurred within five days following wind stress events. In the fall, 19 of 53 (36%) of the re-aeration events followed wind stress events. This indicated that the wind stress events had smaller effects in the fall compared to the spring probably because the water column was already mixed in the fall due to the surface waters cooling in response to decreasing solar radiation.

Only 23 of the 89 (26%) of the re-aeration events that occurred in the summer followed wind stress events, even though 239 wind stress events occurred during summer months over the 20-year period (Figure 4.8). Two possible explanations for this low coincidence include a stable water column preventing the force of the wind from mixing the water column to the depth at which the DO sensor was deployed, or the entire water column was below the hypoxia threshold prior to mixing.

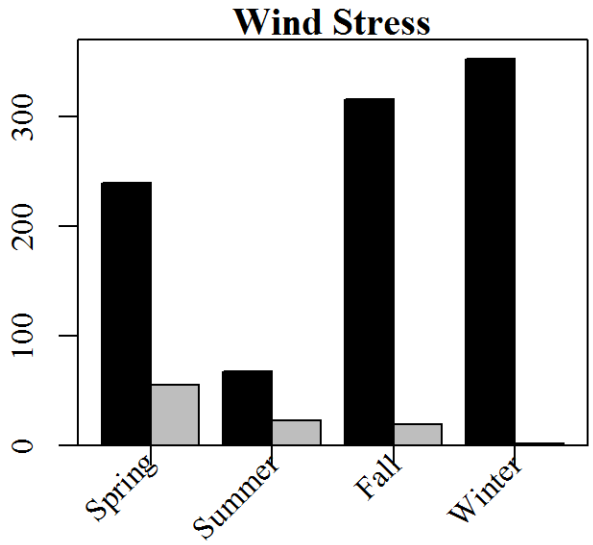

Figure 4.8. Bar plots representing the number of wind stress events by season. A wind stress event is identified when the max wind stress is within the upper quartile of wind stress over the 20-year period 1989-2008. The black bars represent the total number of wind stress events identified at station C6. The grey bars represent the number of wind stress events that occurred within 5 days prior to a re-aeration event.

Cold Fronts

While fewer cold fronts were coincident with re-aeration events than wind stress events, 34% (X-squared = 34.9, $p \leq 0$) of all 238 re-aeration events occurred within 5 days of a cold front. As mentioned above, 44 of the 80 cold fronts that were coincident with re-aeration events were also associated with wind stress events. Forty-seven re-aeration events occurred prior to a front and 33 re-aeration events occurred after a front. Cold fronts have strong winds from the south

preceding the frontal passage and this was just as likely to cause a re-aeration event as the stronger north winds following the frontal passage.

More cold fronts occurred in the fall than any other season; however, more cold fronts were coincident with re-aeration events in the spring than in the fall (Figure 4.9). About one half of the re-aerations events that occurred in the spring and fall occurred within 5 days of a cold front and twice as many of these occurred in the spring than in the fall. As figure 4.9 shows, most of the fronts that affected re-aeration events occurred in the spring. Cold fronts occurred within 5 days of 52 of the 92 (57%) re-aeration events that occurred in the spring and in 23 of 53 events (43%) of the events that occurred in the fall.

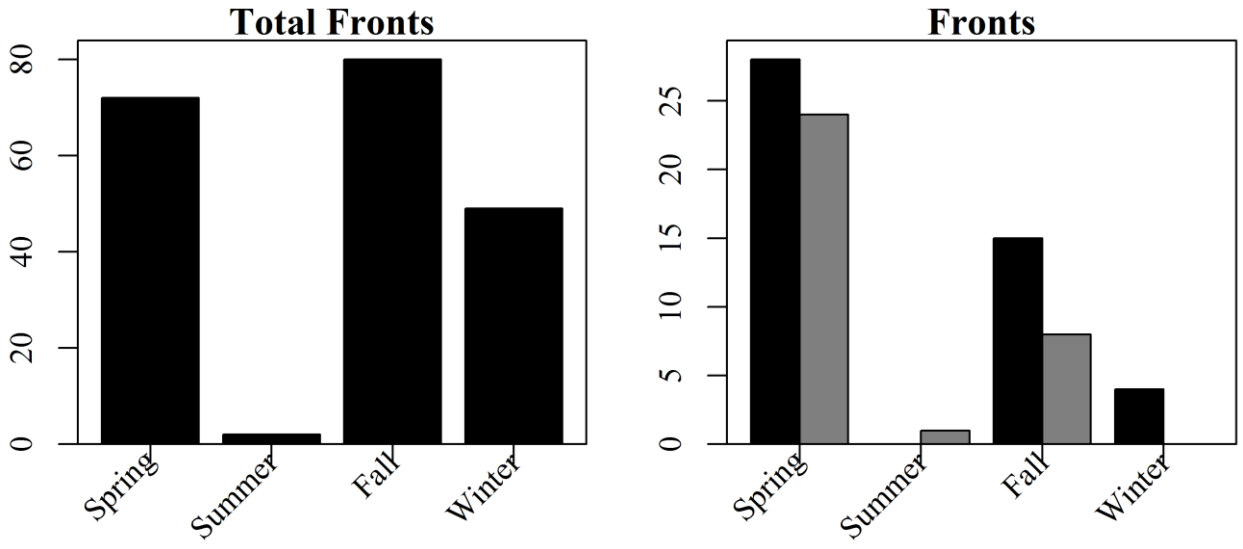

Figure 4.9. Bar plots representing the number of cold fronts identified by the frontal index by season. The left panel represents the total number of cold fronts that passed station C6. The right panel represents the number of cold fronts that that occurred within 5 days prior to (black bars) or within 5 days after (grey bars) a re-aeration event.

Example events show the time evolution of the mixing. Figure 4.10 illustrates an example of a spring re-aeration event that followed two cold fronts that have occurred within a five-day period. The re-aeration event occurred after strong south winds and when the wind shifted back to

the north. Figure 4.11 shows a spring re-aeration event that preceded a cold front by one day. The re-aeration event occurred after persistent strong south winds that preceded the frontal passage. Both of these events were classified as complete mixing because the DO concentrations stayed above the hypoxic threshold for the duration of the test window. However, they both appear to be huggers because the DO concentrations never increase to normoxic levels (> 4.59 mg l^{-1}). In Figure 4.13, the fall re-aeration event followed a front and achieved complete mixing to normoxic levels in response to strong north winds following the front. In Figure 4.14 the re-aeration event followed the front and achieved complete mixing; however, the re-aeration did not occur until the wind shifted back to the south.

The only cold front that occurred in the summer was coincident with a re-aeration event. The one re-aeration event that occurred in the summer within 5 days of a front occurred August 17, 2004, four days after a front passed the site. The stacked plot (Figure 4.12) showed that the front mixed the water column around the mid-water sensor for the first four days following the front. The re-aeration event occurred when the wind direction first shifted to the east and then to the south, causing the complete mixing of the water column.

All four re-aeration events that happened in the winter occurred following a cold front, and all four were classified as decreasing events. This indicated that DO concentrations were continuing to decrease in the winter even though the water column was not sufficiently stratified to maintain hypoxic conditions.

Tropical Cyclones

A total of 31 tropical cyclones, or an average of 1.5 a year, passed within 200 nautical miles of station C6 over the 20 years from 1989 to 2008. Yet, tropical cyclones were coincident in

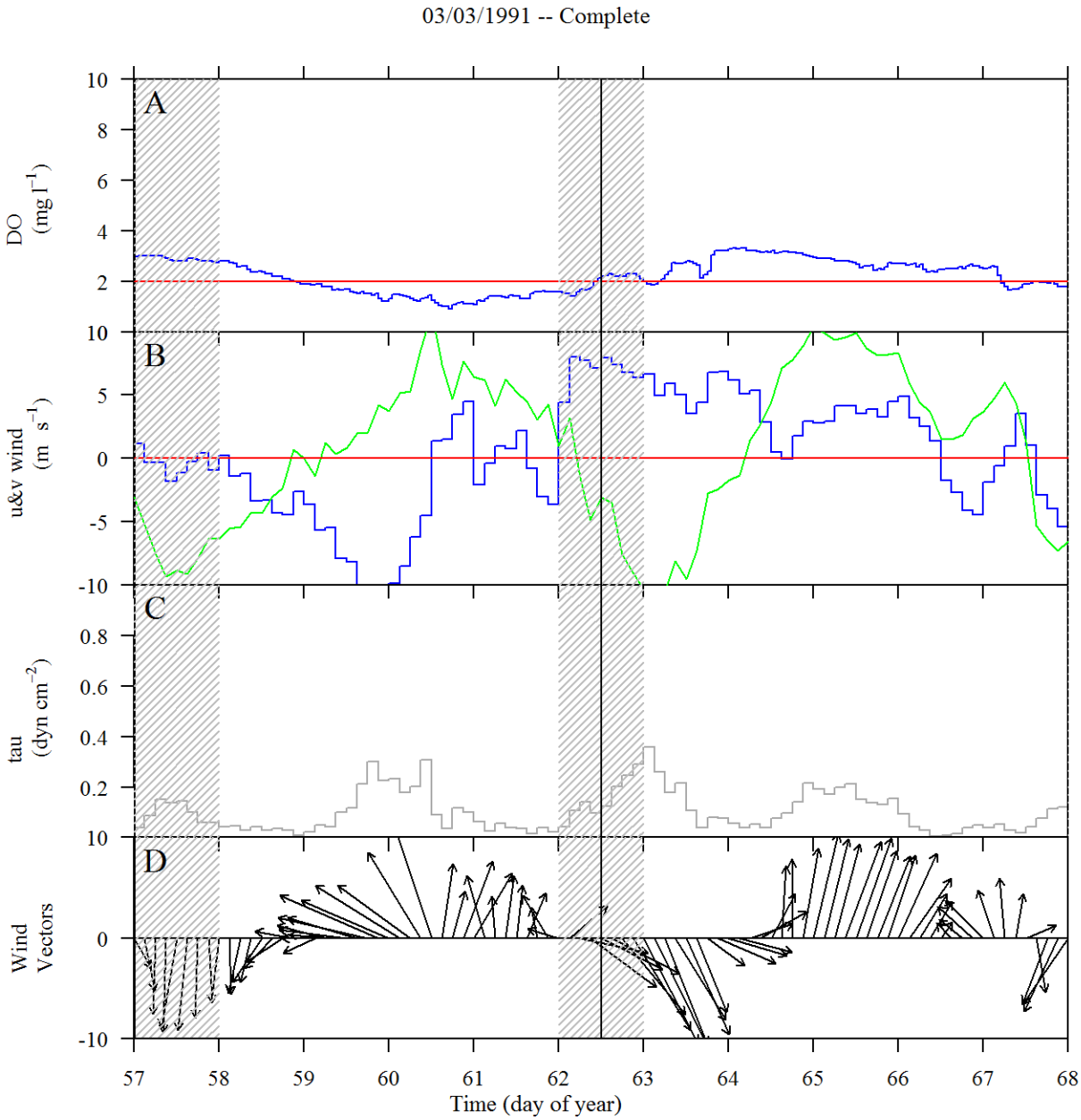

Figure 4.10. Stacked plot of a spring re-aeration event that occurred following two cold fronts within five days. The re-aeration event occurred after strong south winds when the wind shifted back to the north. The solid black vertical line represents the beginning of the re-aeration event. The grey vertical band represents a cold front event. A: near-bottom DO concentrations in mg l^{-1} (blue line), B: blue line represents the u-wind component, or east-west winds, and green line represents the v-wind component, or north-south winds, in m s^{-1}, C: tau, or wind stress, D: wind vectors where the direction of the arrow represents wind direction and the length of the arrow represents wind speed.

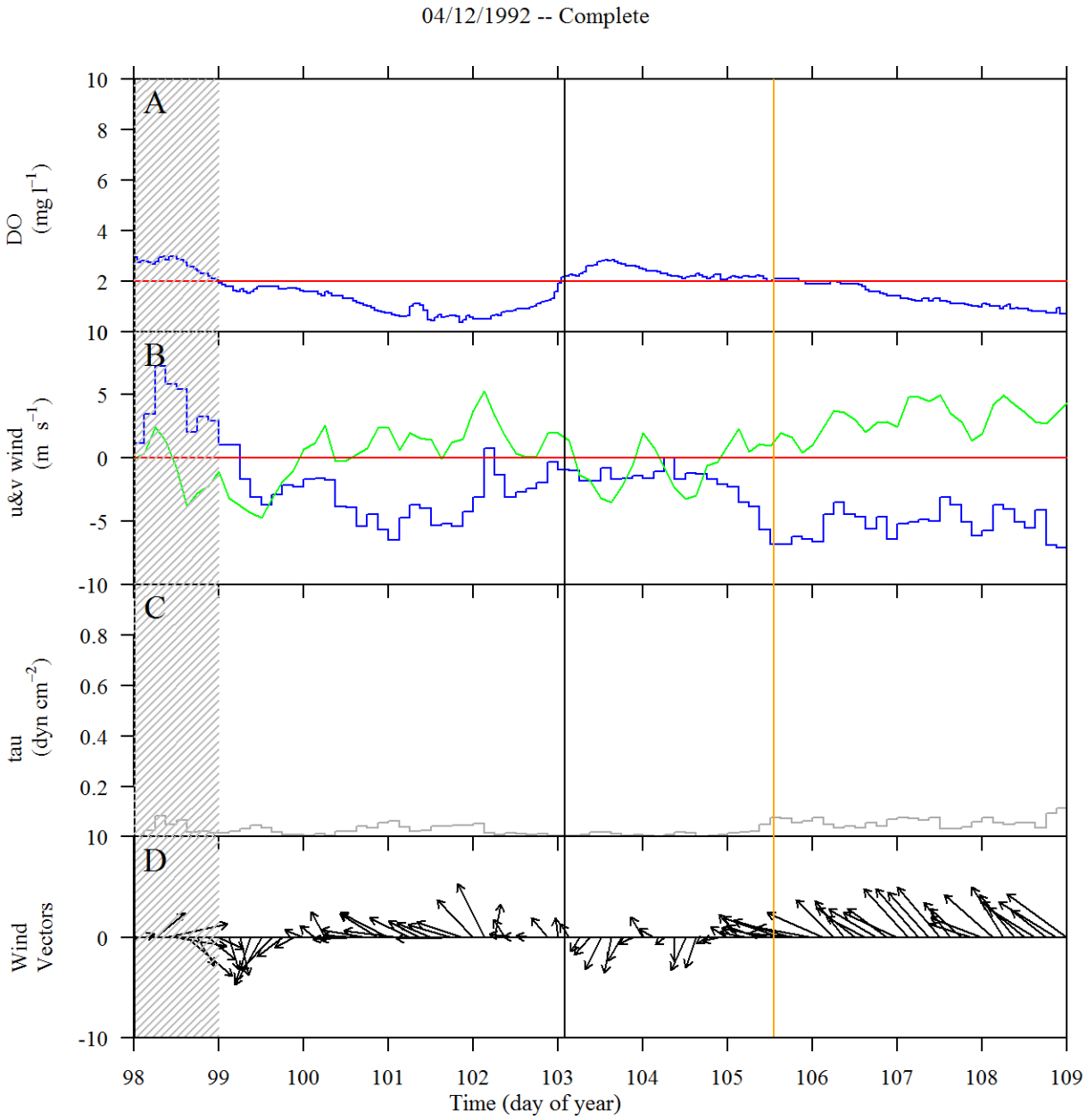

Figure 4.11. Stacked plot of a spring re-aeration event following a cold front. The re-aeration event occurred after persistent strong south winds that preceded the frontal passage. The solid black vertical line represents the beginning of the re-aeration event. The grey vertical band represents a cold front event. A: near-bottom DO concentrations in mg l^{-1} (blue line), B: blue line represents the u-wind component, or east-west winds, and green line represents the v-wind component, or north-south winds, in m s^{-1}, C: tau, or wind stress, D: wind vectors where the direction of the arrow represents wind direction and the length of the arrow represents wind speed. Orange vertical line depicts a subsequent decreasing re-aeration event.

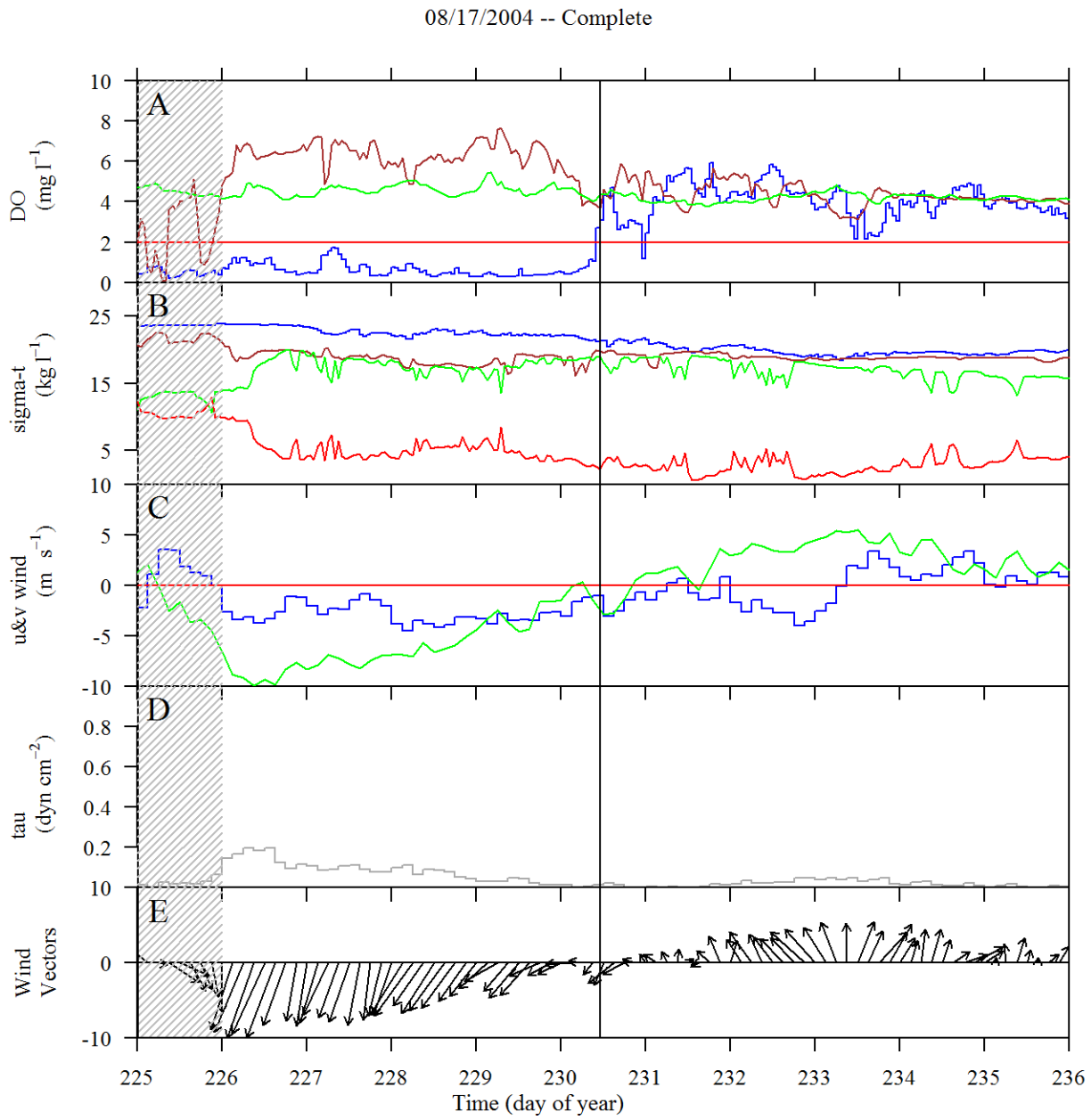

Figure 4.12. Stacked plot of a complete mixing event from August 17, 2004. This is the only re-aeration event that occurred within five days of a cold front during the summer months. The grey line shows represents when the front passed the site. The orange vertical line represents when the re-aeration event occurred. The solid black vertical line represents the beginning of the re-aeration event. A: DO concentrations in mg l-1, blue line—near-bottom, brown line—mid-water column, green line—near-surface, red horizontal line represents the hypoxic threshold (2.0 mg l-1), B: sigma-t, blue line—near-bottom, brown line—mid-water column, green line—near-surface, red line represents delta sigma-t or the difference between near-surface sigma-t and near-bottom sigma-t, C: blue line represents the u-wind component, or east-west winds, and green line represents the v-wind component, or north-south winds, in m s-1, D: tau, or wind stress, E: wind vectors where the direction of the arrow represents wind direction and the length of the arrow represents wind speed.

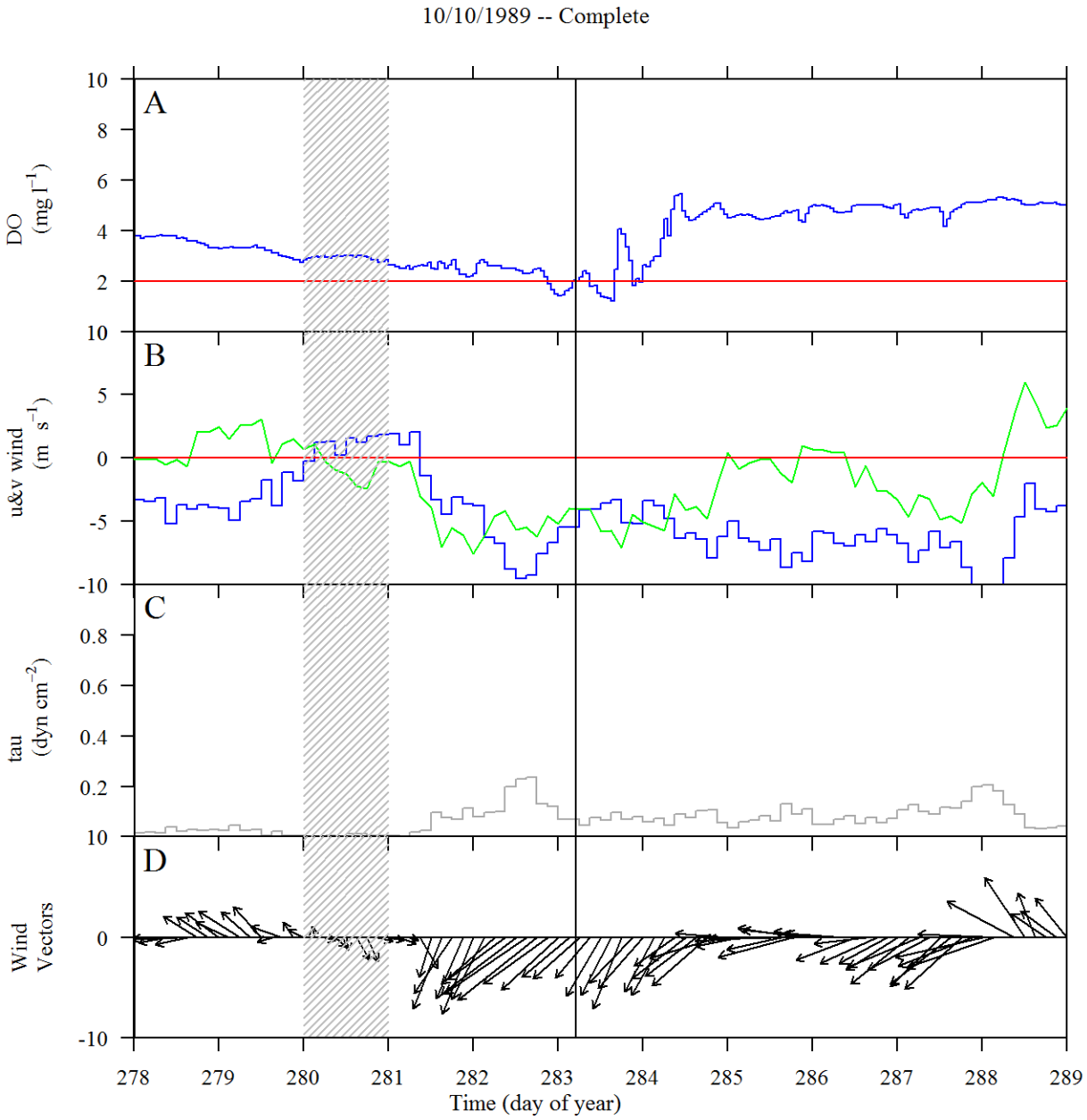

Figure 4.13. Stacked plot of a complete mixing event that occurred three days following a cold front while winds were from the north. The solid black vertical line represents the beginning of the re-aeration event. The grey vertical band represents a cold front event. A: near-bottom DO concentrations in mg l^{-1} (blue line), B: blue line represents the u-wind component, or east-west winds, and green line represents the v-wind component, or north-south winds, in m s^{-1}, C: tau, or wind stress, D: wind vectors where the direction of the arrow represents wind direction and the length of the arrow represents wind speed.

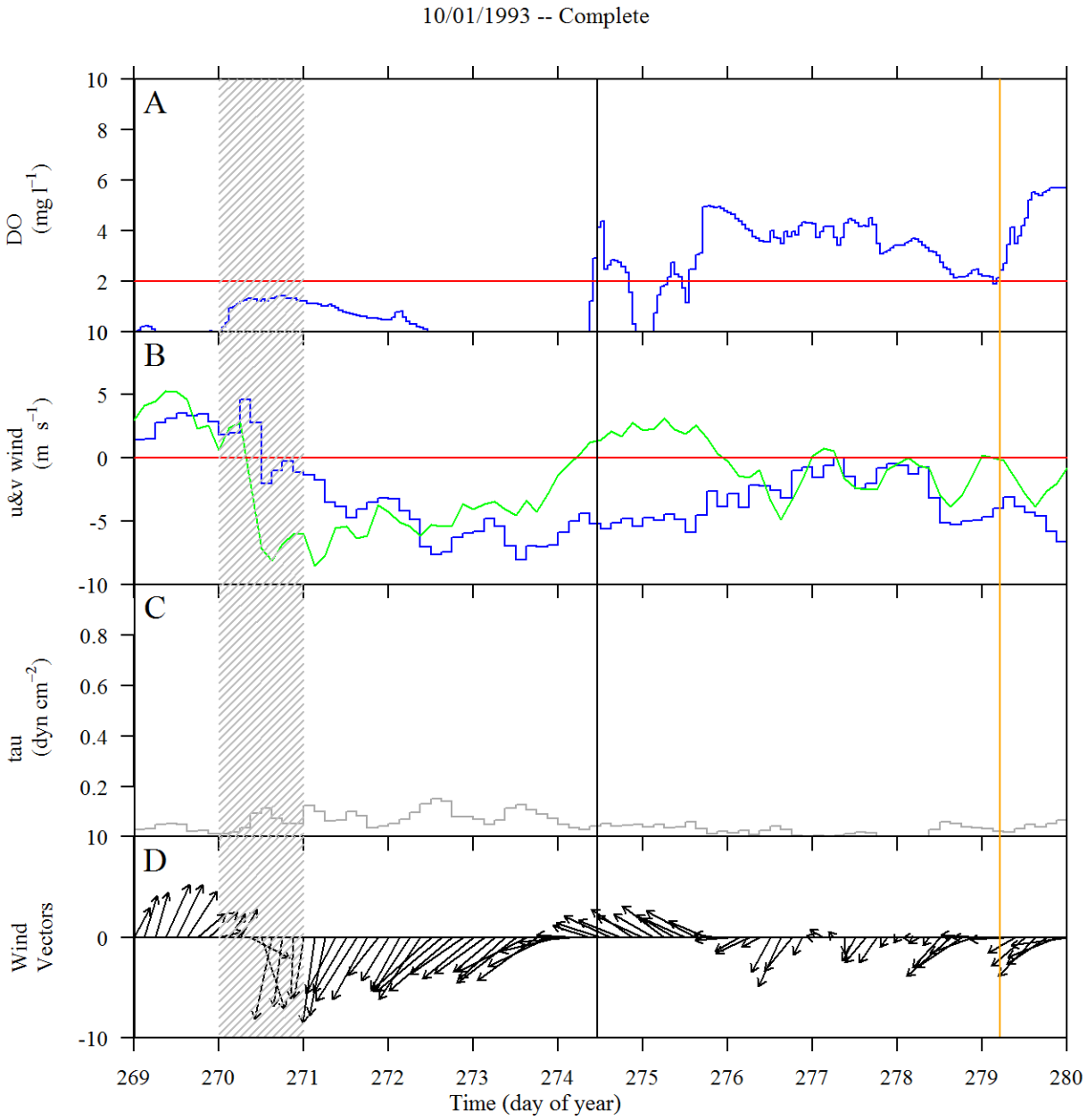

Figure 4.14. Stacked plot a re-aeration event that occurred in the fall when the winds turned to the south following the passage of the cold front. The orange vertical line represents a second re-aeration event occurring within the 11 days. The solid black vertical line represents the beginning of the re-aeration event. The grey vertical band represents a cold front event. A: near-bottom DO concentrations in mg l^{-1} (blue line), B: blue line represents the u-wind component, or east-west winds, and green line represents the v-wind component, or north-south winds, in m s^{-1}, C: tau, or wind stress, D: wind vectors where the direction of the arrow represents wind direction and the length of the arrow represents wind speed. Orange vertical line depicts a subsequent re-aeration event.

28 (12%) ($p<0.01$) of the 238 re-aeration events. All tropical cyclones that were coincident with re-aeration events occurred in the summer (18) and in the fall (13) (Figure 4.15).

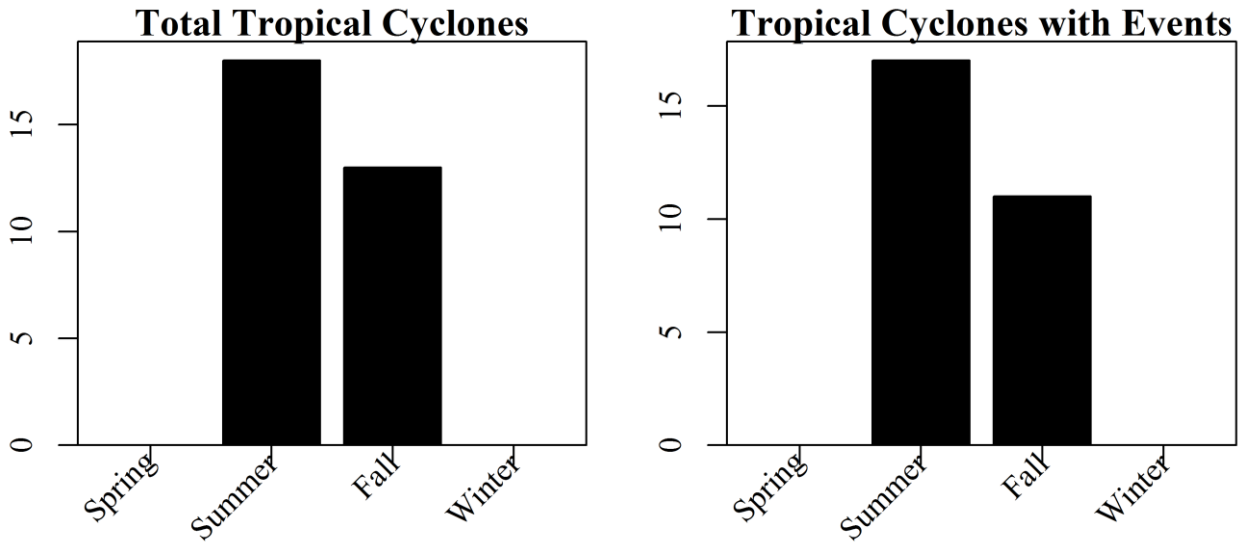

Figure 4.15. Bar plots representing the number of tropical events (hurricanes and tropical storms) by season. The left panel represents the total number of tropical events whose track passed within 200 nautical miles of station C6. The right panel represents the number times a re-aeration events occurred within 5 days before or after a tropical event.

The strength of water column stratification seemed to be a greater factor in determining the variability in DO during tropical cyclones rather than the wind speed; however, not enough data were available to be conclusive. Thirty-one storms passed within 200 nautical miles of the study site between 1989 and 2008 (Table 4.5). Dissolved oxygen concentrations were only sampled before and after 25 of these events. One event that was not a named storm is included because an advisory was issued for the tropical cyclone while it was within 200 nautical miles of station C6, but the low pressure system never developed into a tropical storm. DO concentrations remained mixed and unaffected. Eighteen tropical cyclone events passed through the 200 nautical mile radius of the study site in the summer and thirteen passed through in the fall over the 20-year period. Seventeen re-aeration events are associated with tropical cyclone events in the summer

Table 4.5. Tropical Cyclones that passed with 200 nautical miles of station C6 between the years 1989 and 2008.

Year	Names	CAT	Begin	End	Duration	Season	Pre DO Conc	Post DO Conc	Pre Delta Sigma-t	Post Delta Sigma-t	Pre DO Threshold	Post DO Threshold
1989	CHANTAL	H1	30-Jul	3-Aug	4	Summer	0.09	0.06	NA	NA	SH	SH
1992	ANDREW	H5	16-Aug	28-Aug	12	Summer	0.06	0.14	NA	NA	SH	SH
1994	BERYL	TS	14-Aug	28-Aug	14	Summer	0.00	2.20	NA	NA	SH	SO
1995	DEAN	TS	28-Jul	2-Aug	5	Summer	NA	NA	NA	NA	NA	NA
1995	OPAL	H4	27-Sep	6-Oct	9	Fall	1.21	4.94	NA	NA	H	N
1997	DANNY	H1	16-Jul	27-Jul	11	Summer	0.37	0.37	NA	NA	SH	SH
1998	EARL	H2	31-Aug	8-Sep	8	Summer	0.09	2.61	NA	NA	SH	SO
1998	GEORGES	H5	15-Sep	1-Oct	16	Fall	5.76	5.60	NA	NA	N	N
1998	HERMINE	TS	17-Sep	20-Sep	3	Fall	5.75	5.25	NA	NA	N	N
2000	NOT NAMED	NA	8-Sep	9-Sep	1	Fall	4.87	4.50	3.09	2.63	N	SO
2000	HELENE	TS	15-Sep	25-Sep	10	Fall	3.80	4.95	1.78	0.93	SO	N
2001	ALLISON	TS	5-Jun	19-Jun	14	Summer	3.53	3.45	1.82	1.52	SO	SO
2002	BERTHA	TS	4-Aug	9-Aug	5	Summer	0.14	0.41	4.01	5.48	SH	SH
2002	HANNA	TS	12-Sep	15-Sep	3	Fall	5.44	3.16	NA	NA	N	SO
2002	ISIDORE	H3	14-Sep	27-Sep	13	Fall	5.02	2.62	NA	NA	N	SO

(Table 4.5 continued)

Year	Names	CAT	Begin	End	Duration	Season	Pre DO Conc	Post DO Conc	Pre Delta Sigma-t	Post Delta Sigma-t	Pre DO Threshold	Post DO Threshold
2002	LILI	H4	21-Sep	4-Oct	13	Fall	2.41	3.10	NA	1.30	SO	SO
2003	BILL	TS	28-Jun	3-Jul	5	Summer	0.08	0.17	6.29	8.43	SH	SH
2003	CLAUDETTE	H1	7-Jul	17-Jul	10	Summer	0.94	0.76	6.39	4.67	SH	SH
2003	ERIKA	H1	14-Aug	17-Aug	3	Summer	1.08	0.14	2.61	5.24	H	SH
2003	HENRI	TS	3-Sep	8-Sep	5	Fall	3.18	4.87	2.96	1.30	SO	N
2004	BONNIE	TS	3-Aug	14-Aug	11	Summer	0.73	1.31	10.74	12.38	SH	H
2004	IVAN	H5	2-Sep	24-Sep	22	Fall	0.40	0.26	NA	7.06	SH	SH
2004	MATTHEW	TS	8-Oct	11-Oct	3	Fall	3.95	6.02	0.65	NA	SO	N
2005	ARLENE	TS	8-Jun	14-Jun	6	Summer	2.33	1.62	8.21	8.30	SO	H
2005	CINDY	H1	3-Jul	11-Jul	8	Summer	2.80	3.94	3.47	6.20	SO	SO
2005	KATRINA	H5	23-Aug	31-Aug	8	Summer	0.02	NA	NA	NA	SH	NA
2005	RITA	H5	18-Sep	26-Sep	8	Fall	NA	NA	NA	NA	NA	NA
2008	EDOUARD	TS	3-Aug	6-Aug	3	Summer	0.00	0.78	NA	NA	SH	SH
2008	FAY	TS	15-Aug	28-Aug	13	Summer	0.79	NA	NA	NA	SH	NA
2008	GUSTAV	H4	25-Aug	5-Sep	11	Summer	NA	NA	NA	NA	NA	NA
2008	IKE	H4	1-Sep	15-Sep	14	Fall	NA	NA	NA	NA	NA	NA

and eleven in the fall. Not all tropical events that passed through the study area are associated with re-aeration events and some tropical events had more than one re-aeration event associated with it due to the duration of the track within 200 nautical miles of station C6.

Covariance among Predictor Variables

Over half of the wind stress events (53%) coincided with other episodic events like cold fronts and tropical cyclones (Table 4.6). For example, 44 of the 99 wind stress events were coincident with cold fronts and 9 of the 99 wind stress events were coincident with tropical cyclones. In the winter, two of the four re-aeration events followed wind stress events and since all of the re-aeration events in the winter were coincident with cold fronts, these two wind stress events were also coincident with cold fronts.

Table 4.6. Coincidence of wind stress events with fronts and tropical cyclones by re-aeration event type. Percentages are within the columns.

	Complete (%)	Decreasing (%)	Hugger (%)	Spike (%)	Total (%)
Wind Stress & Front	22 (47)	8 (67)	14 (38)	0 (0)	44 (44)
Wind Stress & Tropical Cyclone	5 (11)	2 (17)	2 (5)	0 (0)	9 (9)
Wind Stress Alone	20 (43)	2 (17)	21 (57)	3 (100)	46 (46)
Total Wind Stress	47 (100)	12 (100)	37 (100)	3 (100)	99 (100)

Comparing Re-aeration Event Type to Episodic Event Type

The type of predictor event was not related to the type of re-aeration event. Figure 4.16 showed that the proportions of types of re-aeration events were similar whether the re-aeration event was before or after a cold front, a tropical cyclone, or a wind stress event. This indicated that all three predictor events affected DO concentrations in a similar manner.

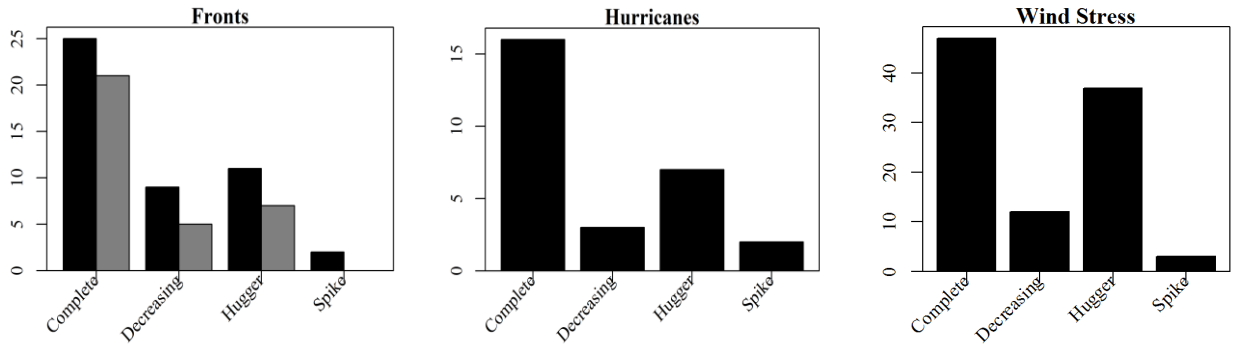

Figure 4.16. Bar plots showing the types of re-aeration events associated with types of episodic events. Left panel is the number of cold fronts by type. The right panel represents the number of cold fronts that that occurred within 5 days prior to (black bars) or within 5 days after (grey bars) a re-aeration event. Middle panel the number of tropical cyclones by type. Right panel the number of wind stress events by type.

Although complete mixing was the most common for all predictor events accounting for 49% of the re-aeration events, there was still variation in predictor events associated with the complete mixing events. Of the 116 complete mixing events, 47 events or 41% were coincident with wind stress events, 40% with fronts, and 14% with tropical cyclones. 44% of the 99 wind stress events that were coincident with re-aeration events were also coincident with cold fronts, and 32% of the 28 tropical cyclone events were also coincident with wind stress events. Of the complete mixing events, 21 occurred after frontal passages and 25 occurred before frontal passages. Still, 34 of 116 (29%) complete mixing events were not coincident with any of the three predictor events.

The complete mixing, the only re-aeration event that resulted in the dissipation of hypoxia, varied substantially in duration. The average duration of a complete mixing event was 34 hours, or about a day and a half; however, the duration spanned from one hour to 251 hours, or approximately ten and half days. While 64%, or 34 of 53, of all re-aeration events in the fall could be classified as complete mixing events, only 29%, or 34 of 116, of all complete mixing events occurred in the fall. Most of the complete mixing events occurred in the spring (38%) and summer (31%).

Some Unexplained Events

Most of the re-aeration events that remained unexplained by cold fronts and tropical cyclones occurred in the summer. Of the 238 re-aeration events identified by the RED algorithm, 24% (X-squared = 61.52, $p \leq 0$) were not explained by the episodic events in this study. Forty of the 58 unexplained events occurred in the summer.

The graphical analysis indicated other possible factors that might play a role in the unexplained re-aeration events. For example, several of the stacked plots showed evidence of a sea breeze (Figure 4.17). In the plots the north-south component of the wind oscillated up and down for several days before the mixing occurred.

Confirmation of Complete Re-Aeration Events using Regression Tree

The confirmation of the complete events using regression tress showed that the hourly events behaved as expected with the changes in stratification indicating that mixing was captured fairly well by the daily averaged sigma-t. Complete mixing events showed the expected shift from the stratified side of the tree (nodes 12 and 13, Figure 4.4) to the mixed side of the tree (nodes 5, 6, 7, and 9) as would be expected (Figure 4.8). The other types of events showed little movement from right to left in the tree as their events progressed from 3 days before to 2 days after (not shown).

The predicted DO categories from the tree showed only moderate agreement with the observed DO (Table 4.8). The most accurate predictions (53%) were made on the day after an event and the least accurate (30%) on the day of the event. During the lead up to the event, many predicted and observed values (10 to 12) were in the severely-hypoxic category (D), and few were in the normoxic (A) category. This is expected as a mixing event starts from a situation of DO below the threshold (i.e., likely low DO for a few days prior to the event). After the events, there was a shift in both predicted and observed categories towards higher DO (categories A and B).

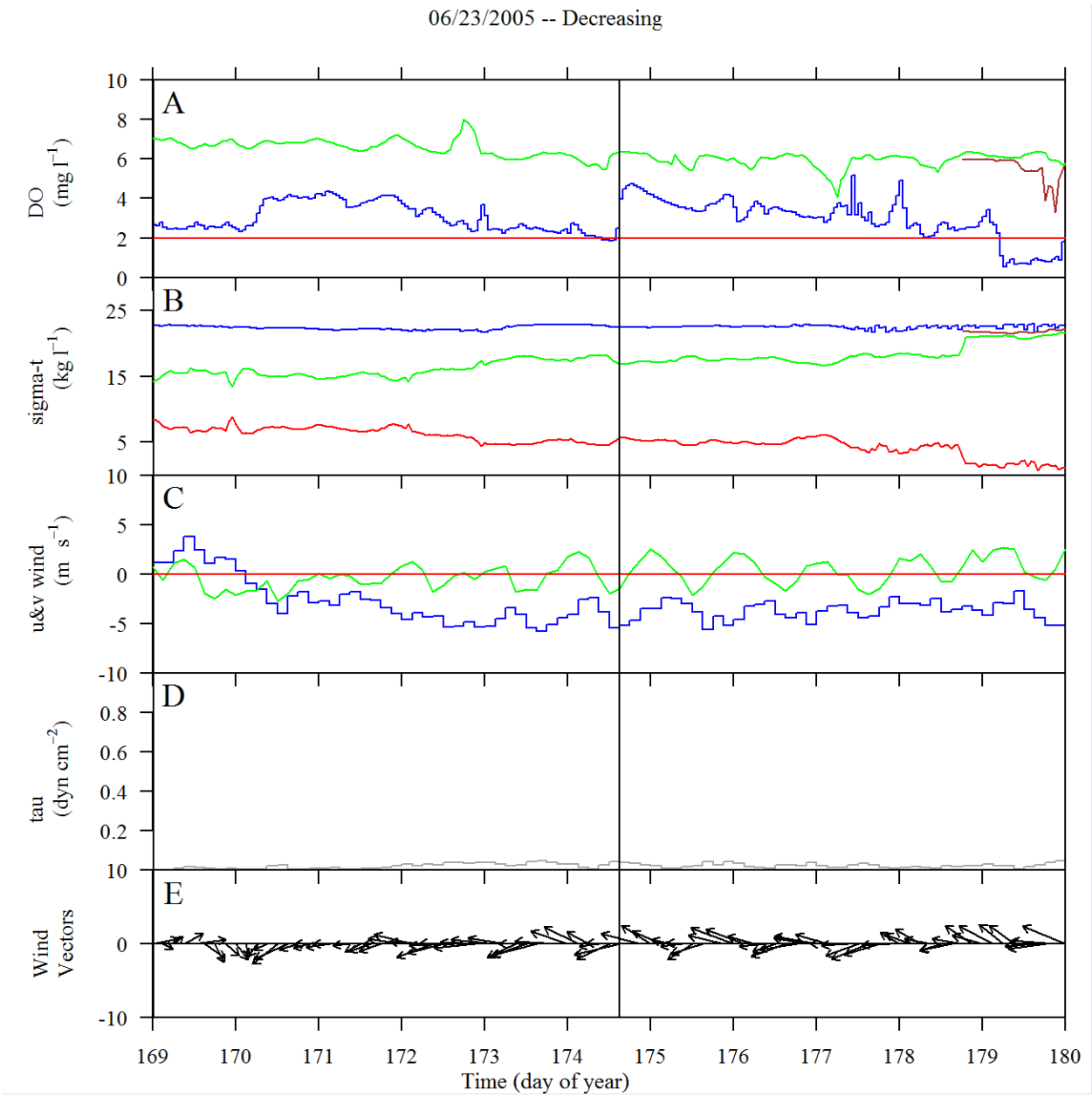

Figure 4.17. Stacked plot illustrating a sea breeze affect. Note the daily oscillation in the wind especially the v-wind component. The solid black vertical line represents the beginning of the re-aeration event. The grey vertical band represents a cold front event. Upper Panel: DO concentrations in mg l^{-1}, blue line—near-bottom, brown line—mid-water column, green line—near-surface, red horizontal line represents the hypoxic threshold (2.0 mg l^{-1}), second panel sigma-t, blue line—near-bottom, brown line—mid-water column, green line—near-surface, red line represents delta sigma-t or the difference between near-surface sigma-t and near-bottom sigma-t, third panel: blue line represents the u-wind component, or east-west winds, and green line represents the v-wind component, or north-south winds, in m s^{-1}, panel four: tau, or wind stress, panel five: wind vectors where the direction of the arrow represents wind direction and the length of the arrow represents wind speed.

However, there remained much disagreement between predicted and observed categories. For example, on the last day of the event, the tree falsely predicted that the 11 severely-hypoxic events (category D) should be high DO (categories A and B). Also, predicted and observed normoxic and suboxic categories were often misclassified (A with B; B with A).

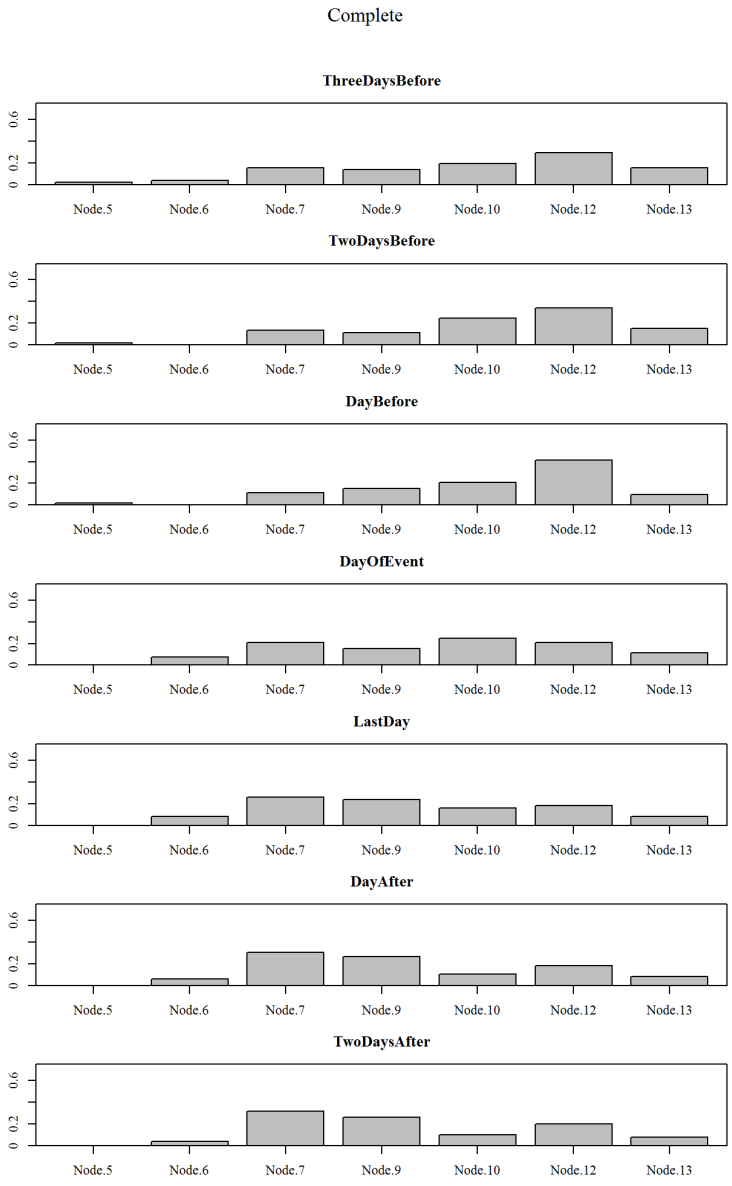

Figure 4.18. Counts of the predictions by nodes from comparing the re-aeration events to the conditional inference tree for the complete mixing type event. The delta sigma-t values seven days, 3 days before the onset of events, 2 days, 1 day, first day of event, last day of event, 1 day after day, 2 days after last day, surrounding a re-aeration event were used to predict the DO category from the conditional inference tree.

Table 4.7. Confusion matrices comparing the actual DO category from the seven days surrounding each re-aeration event to the predicted DO category from the delta sigma-t conditional inference tree for the complete mixing type re-aeration event. The columns in each matrix indicate the predicted values and the rows represent the actual DO categories. The DO categories are represented by the letters: A) normoxic (DO>4.59 mg l^{-1}), B) suboxic (DO≤4.59 and DO>2.0 mg l^{-1}), C) hypoxic (DO≤2.0 mg l^{-1} and DO>1.0 mg l^{-1}), and D) severely hypoxic (DO≤1.0 mg l^{-1}). Note the DO category hypoxic was not predicted by any notes in the tree.

Day in relation to the re-aeration event	Confusion Matrix columns=predicted rows=actual	Overall Accuarcy
Three Days Before	A 5 3 0 1 B 5 6 0 5 C 1 6 0 5 D 0 4 0 10	0.41
Two Days Before	A 1 2 0 0 B 4 10 0 6 C 2 7 0 4 D 1 4 0 12	0.43
Day Before	A 1 1 0 0 B 1 6 0 8 C 4 10 0 7 D 1 3 0 11	0.34
Day of Event	A 2 2 0 0 B 13 15 0 6 C 2 4 0 6 D 0 0 0 0	0.30
Last Day of Event	A 13 7 0 4 B 4 13 0 7 C 1 0 0 0 D 0 0 0 0	0.34
Day After	A 13 7 0 4 B 4 13 0 7 C 1 0 0 0 D 0 0 0 0	0.53
Two Days After	A 9 9 0 3 B 9 9 0 9 C 0 0 0 1 D 0 0 0 0	0.39

DISCUSSION

The episodic events of increased wind stress, cold fronts, and tropical cyclones influence the short-term variability of DO concentrations by mixing water column and re-aerating bottom waters. One or more of the predictor events (wind stress, cold fronts, and tropical cyclones) were coincident with 65% of all re-aeration events and 71% of complete re-aeration events (Table 4.8). The 71% coincidence of predictor events with complete re-aeration events was comprised of 40% cold fronts (18% before and 22% after), 14% cyclones, and 41% wind stress events. However, there was overlap among the predictor events, such that 19% of the wind stress events coincident with complete events were also cold front events and 4% were also cyclone events. When this overlap is removed, 17% of the complete re-aeration events were coincidence with wind stress events that did not occur with cold fronts or cyclones.

Table 4.8. Coincidence of re-aeration events and predictor events as counts of type of predictor event by type of re-aeration event. Numbers in parentheses indicate percentages. Note that percentages in each column refer to the total number of re-aeration events shown in the last row.

	Complete	Decreasing	Hugger	Spike	Total
Re-aeration Event occurred after Cold Front	21 (18)	5 (18)	7 (9)	0 (0)	33 (14)
Re-aeration Event occurred before Cold Front	25 (22)	9 (32)	11 (13)	2 (17)	47 (20)
Tropical Cyclones	16 (14)	3 (11)	7 (9)	2 (17)	28 (12)
All Wind Stress	47 (41)	12 (43)	37 (45)	3 (25)	99 (42)
Wind Stress and Cold Front	22 (19)	8 (28)	14 (17)	0 (0)	44 (19)
Wind Stress and Tropical Cyclones	5 (4)	2 (7)	2 (2)	0 (0)	9 (4)
Wind Stress Alone	20 (17)	2 (7)	21 (26)	3 (25)	46 (19)
Unexplained	34 (29)	9 (32)	36 (44)	5 (42)	84 (35)
All Re-aeration Events	116 (100)	28 (100)	82 (100)	12 (100)	238 (100)

Stratification

The conditional inference tree model used in this study showed that when Δsigma-t is greater than 3.52 kg m^{-3} severely hypoxic conditions are likely. Thus, the strength of stratification is only moderately accurate as a predictor of hypoxia on small temporal scales although several measures of the strength of stratification have been used to predict hypoxia on larger temporal and spatial scales. On a shelf-wide spatial scale, hypoxia in bottom waters are greatest with the vertical density gradient, using the difference in sigma-t, is greatest (Rabalais et al., 1991). Justić et al. (1997) showed that bottom hypoxia in the NGOM was most pronounced when the Δsigma-t was greater than 6 kg m^{-3}. This was based on data obtained from monitoring cruises conducted from 1985 through 1991 across the width of the Louisiana shelf, primarily in mid-summer and along the C-transect running north-south bisecting the southeastern shelf biweekly to monthly. Belabbassi (2006) showed that low-oxygen waters ($\leq$3.4 mg·l^{-1}) was present only when the maximum Brunt-Väisälä frequency was above 40 cycles h^{-1} and hypoxic waters (oxygen concentrations $\leq$2.0 mg·l^{-1}) occurred when the maximum Brunt-Väisälä frequency was less than 100 cycles h^{-1}.

The strength of stratification and the factors that modulate the stability of the water column (i.e., temperature and salinity) vary throughout the year and may have been responsible for the seasonal variability of the effects of wind events on re-aeration events. Stability is the most important physical factor affecting hypoxia in the NGOM during the summer (June through August) (Justić et al., 1996, 2002); therefore the relaxing of stability would also be important in the fall (September through November) when hypoxia is dissipating. According to Wiseman et al. (1997), salinity controls a near surface pycnocline and is a necessary condition for hypoxia; whereas, temperature controls and weaken the pycnocline which determines the spatial distribution of hypoxia. Salinity controls stratification more in the spring because the Mississippi River flow is

highest in April and May and fresh water flux from the river reduces the density of the surface waters. In the fall, a reduction in long-wave radiation flux causes cooling of the surface layers of the water column causing the surface waters to become less dense. This is enhanced by the shoaling of the pycnocline as discharge decreases from the Mississippi River (Wiseman et al. 1997). Stow et al. (2005) estimated a salinity threshold of approximately 4.1 psu for the years 1982 through 2002 from surveys conducted across the Louisiana shelf in July and July. Interestingly, the conditional inference tree I developed for Δsalinity split at 3.54 psu and predicted severely hypoxic conditions at that node. When Δsalinity increased to 21 psu, the hypoxic category was predicted.

Wind Stress

Wind stress events accounted for 40% of the re-aeration events of all types of events, the most of any predictor event. Wind is the primary force that interrupts this seasonal pattern of stratification when kinetic energy transferred from the wind to the surface water reduces the stratification and mixes the water column (Lund-Hansen, 1996) and variability in wind stress is a key factor in short-term near-bottom oxygen variability especially as it affects re-aeration of bottom waters. Strong winds reduce stratification mixing the water column and increase the supply of oxygen to bottom waters. On the other hand, the absence of wind stress reduces the energy supplied to the water column increasing the strength of stratification. Walker and Rabalais (2006) showed a relationship between wind stress and DO concentrations in the northern Gulf of Mexico. When comparing monthly DO concentrations at C6 to environmental factors such as river discharge, nitrate load, chlorophyll-*a*, and wind stress, they found that the only significant positive relationship was between wind stress and DO concentrations ($r^2 = 0.32$, 95% significance).

This analysis used coincidence of events but did not account for the strength of stratification during these events or directly account for the strength of wind, cold fonts, and cyclone mixing power. Seasonal differences in the strength of stratification may be responsible for variations in the coincidence of wind stress events with re-aeration events. When the density difference between the upper layers and the lower layers is greater, more energy is required to mix the water column and re-aerate the bottom waters. Therefore wind stress would have to be greater to re-aerate the bottom waters during the summer when the water column is strongly stratified due to sea surface warming and fresh water flux from the river.

Cold Fronts

Although 34% of the re-aeration events of all types of events were coincident with cold fronts, the frontal activity in the fall had less of an effect on re-aeration events than in the spring. It is widely accepted that cold fronts in the fall (August through October) mix the water column and breakdown hypoxia by re-aerating the near-bottom water (Rabalais, 2002); however, sea-surface cooling may be more responsible for the breakdown of hypoxia in the fall than cold fronts. The sea surface is cooled in the fall as by a decrease in long-wave radiation flux (Huh, 1978). Stratification begins weakening in early fall when fresh water flux from the Mississippi River decreases (Rabalais et al., 1991) and long-wave radiation flux from the atmosphere decreases. When the strength of stratification is weakened, the amount of energy needed to mix the water column is also reduced (Lund-Hansen, et al., 1996). The Δtemperature tree indicated that only a difference of 1.79° C will predict DO concentrations above the hypoxic threshold suggesting that it only takes a little cooling to re-aerate the bottom waters. In the fall due to cooling, the water column was already mixed prior to the cold front passages. In the spring, the DO concentrations are decreasing steadily and fresh water from the Mississippi River is beginning to strengthen the stratification of the water column and cold fronts disrupt this process remixing the water column.

More re-aeration events of all types occurred prior to a cold front (47) than did afterward (33) indicating that the processes that cause re-aeration have more to do with the wind stress than with the actual passing of the cold front. Wind stress is a factor prior to the passage of a cold front as well as during and afterwards. Most of the re-aeration events occurring after the passage of a cold front occurred when the north winds relaxed and strong south winds took over again. Cold fronts have three phases: the prefrontal, frontal passage, and postfrontal (Roberts, et al., 1987). The prefrontal phrase is usually characterized by a decrease in barometric pressure and an increase in winds from the south (Moeller et al., 1993). When the cold front was a migrating cyclone, the winds from the south were strong prior to the passage of the front. When these winds were strong enough to mix the water column, the re-aeration events occurred prior to the front passing in response to strong winds from the south mixing the water column. Winds from the south often exerted more wind stress at station C6 because there is greater fetch south of the station than north of the station. During the frontal phase, the cold arctic air mass from the continent overruns the tropical maritime air mass creating a convergence of the two air masses where the winds rapidly rotate to the opposite direction (Huh et al., 1984). An increase in energy is transferred to the water column with this rapid shift in wind direction (Stone et al., 2007). This increase in energy and wave action will induce mixing and mix oxygen rich water to the bottom waters causing a re-aeration event during the frontal passage. Finally, in the postfrontal phase, winds increase from the north and/or west and the air temperature and humidity decrease while the barometric pressure increases (Moeller et al., 1993).

Tropical Cyclone Events

Numerous factors affect the manner in which tropical cyclones cause variability in short-term DO concentrations, for example like maximum wind radius, forward speed, wind velocity, duration, and the directional approach near site. High winds from tropical cyclones have the

potential to weaken the stratification causing mixing and re-aerate the water column. The data from this study showed that the strength of stratification of the water column prior to a tropical cyclone determined whether or not the tropical cyclone would have an effect on the DO concentrations; however, not enough data were available to make a significant conclusion. For five of tropical cyclones that passed near station C6 and a sigma-t exceeded 3.52 kg m^{-3}, the DO concentrations, remained below the 2.0 mg l^{-1}, the hypoxic threshold. Data to calculate sigma-t were not available for all of the tropical cyclone events. Tropical cyclones are highly variable in size and intensity as determined by wind speeds, barometric pressure, size of the wind field, and the duration of the storm in an area. Rabalais et al. (2007) illustrated the variability in the changes of DO concentrations at station C6 caused by tropical cyclones in 2003 citing four storms, Tropical Storm Bill, Hurricane Claudette, Tropical Storm Erika, and Tropical Storm Grace. Only the first three of these storms passed within 200 nautical miles of station C6. For both Tropical Storm Bill and Hurricane Claudette delta sigma-t was above 3.52 kg m^{-3} before and after the storm; however, for Hurricane Erika, delta sigma-t increased from about 3 to 5 kg m^{-3} indicating an increase in stratification after the storm and also a decrease in DO concentrations possibly due to the hurricane pushing hypoxic water from offshore over the site. Tropical Storm Grace passed too far to the west of the site to have been included in this study and the increase in DO concentrations evident during the time of Tropical Storm Grace may be due to the prefrontal stages of a cold front that merged with Tropical Storm Grace a few days later. Later that same fall, Tropical Storm Henri also passed within 200 nautical miles of station C6; however, the water column was well mixed prior to this storm and no change in DO concentrations was evident.

Unexplained Events

A percentage (24%) of the re-aeration events of all types still remains unexplained. The physics of the system is complicated and many episodic events may occur that may cause these

rapid increases in DO concentrations. One such example is the possible effect of sea-breezes. Several of the re-aeration event stack plots showed evidence of a sea-breeze effect in a daily oscillation of the wind. A sea breeze is caused by the heating of the land surface during the day creating a thermal gradient from offshore to onshore. The wind reverses at night as the land cools. The day and night oscillation of the wind causes a similar oscillation in the currents and creates internal waves along the pycnocline (Zhang et al., 2009, 2010). As this oscillation progresses it weakens the stratification and can mix the water column. This oscillation can also be seen in the mid-water DO concentrations when the sea breeze is present.

Tidal excursions normally do not explain short-term variation in DO concentrations as long as the water surrounding the meter has uniform properties; however, when hypoxia develops patchily, it is possible for the tidal excursion to explain short-term changes in DO concentrations. This may be the case in the re-aeration event that occurred on July 8, 2004, when the DO concentrations are steadily decreasing prior to the event and then a spike occurs with little wind stress evident in the graph. Dynamic offshore processes including, for example, the changing shape of the quasi-permanent anticyclonic gyre from the Mississippi River (Wang and Justić, 2009) and internal waves moving throughout the Gulf of Mexico may explain some of these events.

Implications

The short-term variability in DO concentrations caused by the re-aeration events may be a source of inconsistencies in the measurement of the areal extent of hypoxia as mapped by the annual summertime cruise. Of the 4427 days that DO concentrations were sampled at station C6 over a 20 year period from 1989 to 2008, only 238 (5%) were associated with re-aeration events, suggesting that these events are indeed rare and episodic. Re-aeration events were just as common in the summer as other times of the year and are likely to occur during hypoxia shelf-wide

mapping cruises. For example, Figure 4.19 shows the DO concentrations measured at station C6 during the duration of five annual shelf-wide cruises. Each time station C6 was occupied during these 5 cruises, the near-bottom DO value was reported as hypoxic (≤ 2.0 mg l^{-1}). During the cruise, the DO concentrations are measured by three different instruments (the CTD oxygen sensor, an independent electronic profiler and a Winkler titration from water sampled from about 1 meter off the bottom) and then the lowest value is recorded. If the same station were occupied a day earlier, a day later or within hours, the DO concentrations may have been above the hypoxic threshold due to re-aeration events. The examples in Figure 4.19 also illustrate the different classifications of re-aeration events that may occur during the duration of the hypoxia mapping cruise. In 1998, a spike preceded the cruise sampling by one day. In 2000 and 2006, a hugger event persisted through the sampling. In 2005, there was a decreasing event. I also included 2002 to illustrate an example of a shelf-wide cruise that had no re-aeration events occurring.

Conclusions

In this study, I investigated the impact of episodic events (i.e., wind stress, cold fronts, and tropical cyclones) on short-term DO variability at a single site in the northern Gulf of Mexico (station C6) that experiences frequent hypoxia. I investigated the two controls on the stability of the water column, the density gradient and forces that transfer energy to the water column. I found that the daily density gradient, as exhibited in Δsigma-t, daily Δtemperature, and Δsalinity, was a fairly good predictor of the categorized DO concentration, especially in the extremes of the high normoxic category and the low severely-hypoxic category. I developed a re-aeration event detection (RED) algorithm that was able to identify and characterize re-aeration events from the fine-scale DO time-series. The RED algorithm identified 238 events of the 4427 days that DO concentrations were sampled over a 20 year period from 1989 to 2008. Even though this only

accounted for 5% of the days sampled, many (76%) of the re-aeration events were related to wind stress events like cold fronts and tropical cyclones.

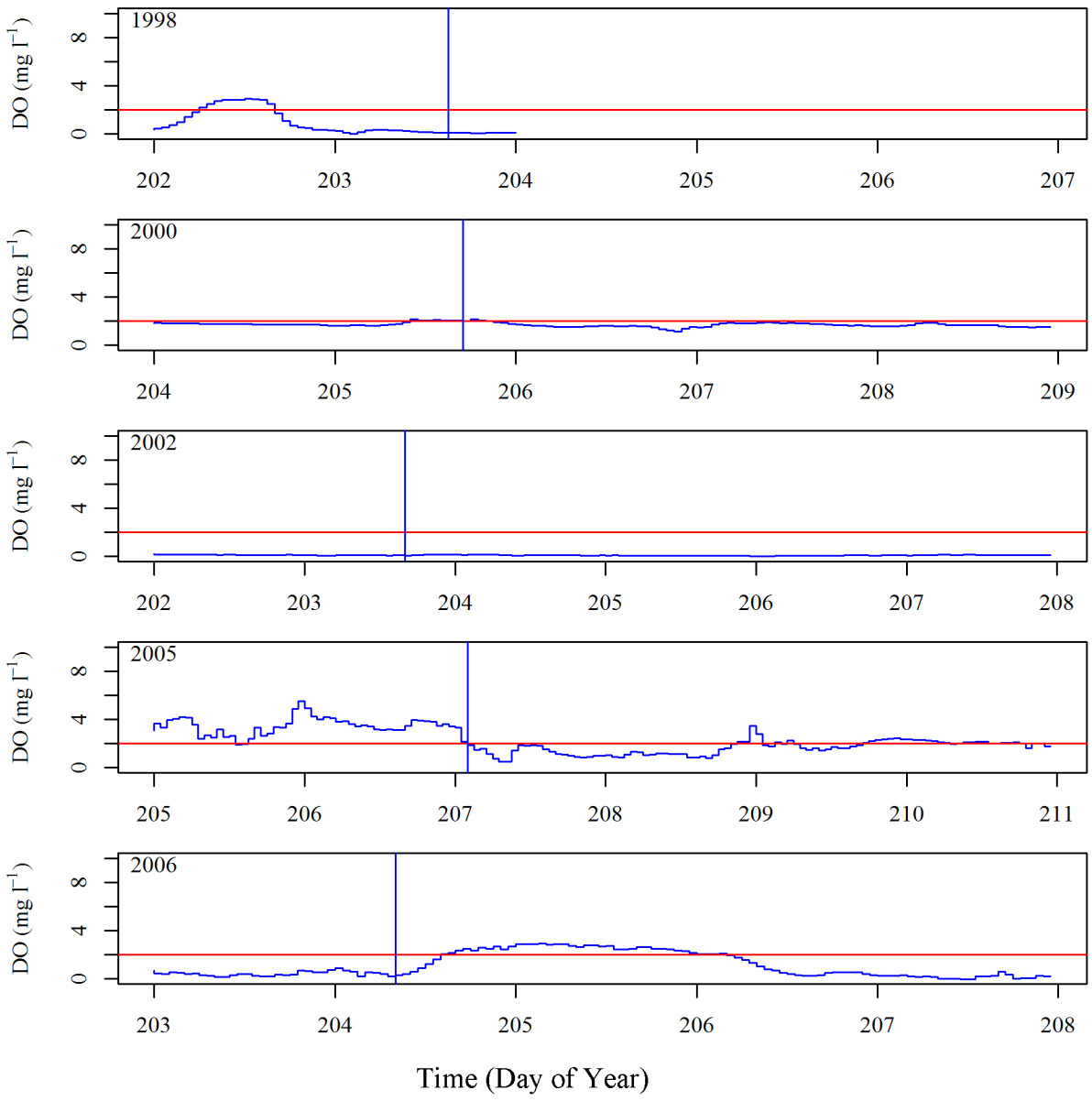

Figure 4.19. Plots of near-bottom dissolved oxygen (DO) concentrations in mg l^{-1} measured at station C6 during the time of the annual summertime shelf-wide cruise to map the areal extent of the hypoxic zone. These examples illustrate the different classifications of re-aeration events that may occur during the duration of the cruise. Labels indicate the year of the cruise. The vertical blue line indicates the time that the station C6 was occupied (sampled) during the cruise. The red horizontal line represents the hypoxic threshold (2 mg l^{-1}). Note: The DO values for this station during each of these cruises were reported hypoxic (≤2 mg l^{-1}).

Short-term variability due to episodic mixing events provides some information on the variability associated with the broad-scale cruises that generate the annual summertime spatial maps of hypoxia. Further analyses can examine retrospectively whether episodic events occurred in the days surrounding the annual shelf-wide cruises.

While this study advances our understanding of how these wind events affect short-term DO concentrations, more research is needed to explain other physical processes that might cause re-aeration events and the dissipation of hypoxia and the end of the hypoxia season in the fall. For example, a better understanding of the role that sea-surface cooling in the fall has on weakening the stability of the water column may better explain the seasonal variability in the effects of cold fronts, or why more cold fronts were coincident with re-aeration events in the spring than in the fall

REFERENCES

Belabbassi, L. 2006. Examination of the relationship of river water to occurrences of bottom water with reduced oxygen concentrations in the northern Gulf of Mexico. Ph.D. Dissertation, Texas A&M University.

Cochrane, J.D. and Kelly F.J. 1986. Low-frequency circulation on the Texas–Louisiana continental shelf. Journal of Geophysical Research 91, 10645–59

Hothorn, T., Hornik, K., and Zeileis, A. 2006. Unbiased Recursive Partitioning: A Conditional Inference Framework. Journal of Computational and Graphical Statistics 15(3), 651–674.

Hsu, S.A., 1988. Coastal meteorology. Academic Press, San Diego, viii, 260.

Hsu, S.A. and Yan, Z., 1998. A note on the radius of maximum wind for hurricanes. Journal of Coastal Research 14, 667-668.

Huh, O.K., and Rouse, L.J., Jr., 1984. Cold air outbreaks over the northwest Florida continental shelf: heat flux processes and hydrographic changes. Journal of Geophysical Research, 89(C1), 717-726.

Huh, O.K., Wiseman, W.J., Rouse, L.J., Jr.1978. Winter cycle of sea surface thermal patterns, northeastern Gulf of Mexico. Journal of Geophysical Research 83(C), 4523-4529.

Il-Ju, M., Ginis, I., Tetsu, H., Tolman, H.L., Wright, C.W., and Walsh, E.J., 2003. Numerical simulation of sea surface directional wave spectra under hurricane wind forcing. Journal of Physical Oceanography 33, 1680.

Justić, D., Bierman, V., Scavia, D. and Hetland, R. 2007. Forecasting gulf's hypoxia: the next 50 years. Estuaries Coasts 30, 791–801.

Justić, D., Rabalais, N.N., Turner, R.E. 1997. Impacts of climate change on net productivity of coastal waters: implications for carbon budgets and hypoxia. Climate Research 8, 225-237.

Justić, D., Rabalais, N.N., Turner, R.E. 2002. Modeling the impacts of decadal changes in riverine nutrient fluxes on coastal eutrophication near the Mississippi River Delta. Ecological Modelling 152, 33-46.

Justić, D., Rabalais, N.N., Turner, R.E., 1996. Effects of Climate Change on Hypoxia in Coastal Waters: A Doubled CO2 Scenario for the Northern Gulf of Mexico. Limnology and Oceanography 41, 992-1003.

Kemp, W. M., Testa, J. M., Conley, D. J., Gilbert, D., and Hagy, J. D. 2009, Temporal responses of coastal hypoxia to nutrient loading and physical controls. Biogeosciences, 6, 2985-3008.

Knaff, J.A., Sampson, C.R., DeMaria, M., Marchok, T.P., Gross, J.M., McAdie, C.J., 2007. Statistical tropical cyclone wind radii prediction using climatology and persistence. Weather and Forecasting 22, 781-791.

Knapp, K. R., M. C. Kruk, D. H. Levinson, H. J. Diamond, and C. J. Neumann, 2010: The International Best Track Archive for Climate Stewardship (IBTrACS): Unifying tropical cyclone best track data. Bulletin of the American Meteorology. Society, 91, 363-376.

Lund-Hansen, L., Chresten, S., P.I., and Christiansen, C. 1996. Modes of stratification in a semi-enclosed bay at the North Sea-Baltic Sea transition. Estuarine, Coastal and Shelf Science, 42(1), 45-54.

Mesinger, F., et al, 2004: NCEP North American Regional Reanalysis, 15th Symposium. On Global Change and Climate Variations, Seattle, WA, 11-15 Jan 2004.

Moeller, C.C., Huh, O.K., Roberts, H.H., Gumley, L.E., and Menzel W.P. 1993. Response of Louisiana coastal environments to a cold front passage. Journal of Coastal Research, 9 (2), 434-447.

Perez, B. C., Day, Jr,, J. W., Rouse, L. J., Shaw, R. F., and Wang, M. 2000. Influence of Atchafalaya River discharge and winter frontal passage on suspended sediment concentration and flux in Fourleague Bay, Louisiana. Estuarine, Coastal and Shelf Science, 50(2), 271-290.

R Development Core Team. 2011. R: A language and environment for statistical computing. R Foundation for Statistical Computing, Vienna, Austria.

Rabalais, N. N., Turner, R. E., and Scavia, D. 2002. Beyond science into policy: Gulf of Mexico hypoxia and the Mississippi River. Bioscience 52(2), 129-142.

Rabalais, N. N., Wiseman, W., and Turner E. R. 1994. Comparison of continuous records of near-bottom dissolved oxygen from the hypoxia zone along the Louisiana coast. Estuaries and Coasts 17(4), 850-861.

Rabalais, N.N., Díaz, R.J., Levin, L.A., Turner, R.E., Gilbert, D., and Zhang, J. 2010. Dynamics and distribution of natural and human-caused hypoxia. Biogeosciences 7(2), 585-619.

Rabalais, N.N., Turner, R.E., Sen Gupta, B., Boesch, D., Chapman, P., and Murrell, M., 2007. Hypoxia in the northern Gulf of Mexico: Does the science support the Plan to Reduce, Mitigate, and Control Hypoxia? Estuaries and Coasts 30, 753-772.

Rabalais, N.N., Turner, R.E., Wiseman, W.J., Jr., Boesch, D.F., 1991. A brief summary of hypoxia on the northern Gulf of Mexico continental shelf: 1985-1988. Geological Society, London, Special Publications 58, 35-47.

Renaud, M.L. 1986. Hypoxia in Louisiana coastal waters during 1983: Implications for fisheries. Fishery Bulletin 84, 19-26.

Roberts, H. H., Huh, O. K., Hsu, S. A., Rouse, L. J., Jr., and Rickman, D., 1987. Impact of cold front passages on geomorphic evolution and sediment dynamics of the complex Louisiana coast. Coastal Sediments '87, Proceedings of a Specialty Conference (May 12-14, 1987, New Orleans, Louisiana). New York: American Society of Civil Engineers, 1950-1963.

Stone, G.W., Grymes, J.M., III., Dinger, J.R., and Pepper, D.A., 1997. Overview and significance of hurricanes on the Louisiana coast, U.S.A.. Journal of Coastal Research, 13 (3), 656-669.

Stone, G.W., Liu, B., and Jose, F., 2007. Winter storm and tropical cyclone impacts on the short-term evolution of beaches and barriers along the northeastern Gulf of Mexico. Coastal Sediments '07 Volume 2, 935-950.

Stow, C.A., Qian, S. S., and Craig, J.K. 2005. Declining threshold for hypoxia in the Gulf of Mexico. Environmental Science & Technology 39(3), 716-723.

UNESCO 1983. Algorithms for computation of fundamental properties of seawater, 1983. UNESCO Technical Papers in Marine Science, No. 44, 53 pp.

Walker, N.D., Wiseman, W.J., Rouse, L.J., Babin, A., 2005. Effects of River Discharge, Wind Stress, and Slope Eddies on Circulation and the Satellite-Observed Structure of the Mississippi River Plume. Journal of Coastal Research 21, 1228-1244.

Walker, N.D. and Rabalais, N.N. 2006. Relationships among satellite chlorophyll a, river inputs and hypoxia on the Louisiana Continental Shelf, Gulf of Mexico. Estuaries and Coasts 29(6B), 1081-1093.

Wang, L. and Justić, D. 2009. A modeling study of the physical processes affecting the development of seasonal hypoxia over the inner Louisiana–Texas shelf: circulation and stratification. Continental. Shelf Research 29, 1464–76.

Williams, J. and Sheets, B. 2001. Hurricane watch: Forecasting the deadliest storms on Earth Knopf Doubleday Publishing Group: New York.

Wiseman, Jr., W. J., Rabalais, N. N., Turner, R. E., and Justić, D. 2004. Hypoxia and the physics of the Louisiana Coastal current. Pp 359-372 in J.C.J. Nihoul et al., "Dying and Dead Seas," NATO Advanced Research Workshop, Liège, Belgium, NATA ASI Series, Kluwer Academic Publishers, Netherlands.

Wiseman, W.J., Rabalais, N.N., Turner, R.E., Dinnel, S.P. and MacNaughton, A. 1997. Seasonal and interannual variability within the Louisiana coastal current: stratification and hypoxia. Journal of Marine Systems 12(1-4), 237-248.

Zhang, X, DiMarco S.F., Smith, D.C. IV, Howard, M.K., Jochens, A.E. and Hetland, R.D. 2009. Near-resonant ocean response to sea breeze on a stratified continental shelf. Journal of Physical Oceanography 39, 2137–55.

Zhang, X., Smith, D.C. IV, DiMarco, S.F., and Hetland, R.D. 2010. Sea breeze driven ocean Poincare wave propagation and mixing near the critical latitude with application to the Gulf of Mexico. Journal of Physical Oceanography 40, 48–56.

CHAPTER 5

CONCLUSION

Oxygen variability in the northern Gulf of Mexico (NGOM) has been studied for the past 30 years to better understand the dynamics of dissolved oxygen (DO) and development of hypoxia (DO < 2.0 mg l^{-1}) in bottom waters. In spite of this long-term research effort, short-term (i.e., hours to days) DO variability in the NGOM is still poorly characterized. Understanding short-term variability in DO is important for three reasons. First, changes in DO are among the first signs of stress in an aquatic ecosystem and it is important to understand variability in DO measurements in order to properly interpret trends. Second, short-term variations in DO determine exposures that result in changes in growth, mortality, and reproduction of important biota. Third, short-term variability can be a source of uncertainty for metrics and indicators (e.g., areal extent of hypoxia) that are based on single cruises and resulting snap-shot pictures of the DO. Open-water continuous monitoring of DO concentrations at a single station over a period of 20 years afforded an excellent opportunity to characterize short-term oxygen variability and to estimate the relative importance of biological and physical processes as controlling factors of hypoxia in the NGOM's hypoxic zone.

I analyzed a 20 year (1989-2008) time-series of dissolved oxygen (DO) concentrations measured at a single NGOM site that experiences frequent summer-time hypoxia (station C6). I augmented this time-series with other relevant environmental time-series data. I used a data mining and analysis approach to elucidate the dynamics of hypoxia through a better understanding of the factors that affect the variability in DO at a location over short temporal scales (hours to days). The overarching goal of this study was to characterize the short-term variability from these time-series and to quantify the relative importance of factors controlling the variability in DO. The objectives were:

1) to characterize the short-term variability in DO concentrations between 1989 and 2008 at a single NGOM location that experiences frequent summer hypoxia,
2) to identify trends in short-term DO variability and compare those trends to the trends in the Mississippi River nutrient and fresh water fluxes,
3) to identify periodicities in the short-term DO variability and quantify the relative importance of periodic factors (solar radiation, temperature, and tide), and
4) to quantify the effects of episodic factors (fronts and tropical storms) on short-term DO variability.

In Chapter 2, I explored the trends in the time series by first characterizing the short-term dynamics in DO concentrations. Although no clear temporal trend was evident in the DO concentrations over the 20 years, I investigated three aspects of short-term DO variability: respiration rates (i.e., how quickly bottom waters become hypoxic), duration of hypoxia, and the dissipation of hypoxia (i.e., re-aeration events). Open-water continuous monitoring of DO concentrations at a single station over a period of 20 years allowed for a better characterization of respiration rates than was done in previous studies. I was able to identify the range of respiration rates present at the study site and show how these rates vary throughout the year and from year to year.

In terms of persistence of hypoxia, this study showed that bottom DO concentrations often change very quickly, and that the system can transition from normoxia to hypoxia and vice versa in less than four days. This information suggests that caution should be used in interpreting the current method of measuring the areal extent of hypoxia in the NGOM whereby different stations are occupied at different times over about a one week long shelf-wide cruise. Open-water continuous monitoring of DO concentrations at a single station also provided

information on DO dynamics that are supplementary to those collected during the annual shelf-wide cruise. Although, no relationship existed between the severity of hypoxia at station C6 and the areal extent of hypoxia in the NGOM, there was a significant relationship between the Mississippi River nitrogen flux and the duration measure of hypoxia at the single station. Managers could benefit from using the metric of duration of hypoxia as measured by open-water continuous monitoring at a single station to estimate how the severity of hypoxia changes in response to nutrient control actions in the Mississippi Watershed. Determining the severity of hypoxia at a single station does not capture the DO dynamics over the entire NGOM shelf; however, it does provide another measure of hypoxia that also responds to changes in riverine nitrogen flux. Thus, fine-scale temporal monitoring of DO at a few stations could be used to augment the shelf-wide spatial maps. A combined approach would likely allow for better determination of the effectiveness of management practices in controlling nutrient loads from Mississippi River watershed designed to reduce the severity of hypoxia in the northern Gulf of Mexico. The third aspect of short-term DO that I studied in Chapter 2 was rapid increases in DO that dissipate hypoxia. These rapid increases in DO occur rather infrequently and more occur in the spring and fall.

In Chapter 3, I analyzed the time-series DO concentrations for periodicity and compared periodicities in DO to the periodicities in temperature, photosynthetically active radiation (PAR), and water levels (tidal forcing). Using auto-correlations and cross correlations, I explored the periodic relationship among the three depths of the DO time-series and between the DO time series and other periodic variables (temperature, water level, and photosynthetically active radiation). Using time-series analysis, I determined that no continuous periodicity was present in the DO time-series at the three depths: near-surface, mid-water-column, and near-bottom.

Although a 24-hour tidal signal was present in the water level data at station C6, this signal was not apparent in the DO concentrations, suggesting that the waters surrounding this site had similar DO concentrations. A diel DO pattern associated with PAR was present irregularly throughout the dataset at all three depths and the percentage of days sampled that exhibited a diel pattern decreased with depth: 20% near the surface, 12% in the mid-water-column, and 7% near the bottom. Although the flux of PAR at the sea surface is a periodic factor, the attenuation of light in the water column often change in a stochastic manner leading to decreased PAR periodicity with depth and ultimately interruptions in the diel DO pattern. In order to more fully understand these processes, more research is needed in the short-term variations of light attenuation and other episodic events that disrupt the diel curve.

In Chapter 4, I investigated the impact of episodic events (i.e., wind stress, cold fronts, and tropical cyclones) on short-term DO variability, using the same fine-scale temporal data at station C6 as used in chapters 2 and 3. The two controls on the stability of the water column are the density gradient and forces that transfer energy to the water column. I used conditional inference trees to determine the relationship between DO category, normoxic (DO>4.59 mg l^{-1}), suboxic (DO≤4.59 and DO>2.0 mg l^{-1}), hypoxic (DO≤2.0 mg l^{-1} and DO>1.0 mg l^{-1}), or severely hypoxic (DO≤1.0 mg l^{-1}), and the daily density gradient, as exhibited in Δsigma-t, daily Δtemperature, and Δsalinity. I found that the daily density gradient was a fairly good predictor of DO category especially in the two extremes of the normoxic category and the severely hypoxic category. I then developed a re-aeration event detection (RED) algorithm that was able to identify and characterize re-aeration events from the fine-scale DO time-series. I characterized four types of re-aeration events (complete mixing, huggers, decreasing, and spikes) based on the variability of the DO concentrations during and after the event. The RED algorithm

identified 238 events of the 4427 days that DO concentrations were sampled over a 20 year period from 1989 to 2008. Even though this only accounted for 5% of the days sampled, many (76%) of the re-aeration events were related to wind stress events like cold fronts and tropical cyclones.

These conclusions have significant implications for management of hypoxia in the NGOM. The Gulf Hypoxia Action Plan 2008's goal for the NGOM is:

> *Subject to the availability of additional resources*, we strive to reduce or make significant progress toward reducing the five-year running average areal extent of the Gulf of Mexico hypoxic zone to less than 5,000 square kilometers by the year 2015 through implementation of specific, practical, and cost-effective voluntary actions by all Federal agencies, States, and Tribes, and address all categories of sources and removals within the Mississippi/Atchafalaya River Basin to reduce the annual discharge of nitrogen and phosphorus into the Gulf (CENR 2008).

This goal is dependent on the annual measurement of the areal extent of NGOM hypoxia. The EPA Science Advisory Board (2008) recognized that mapping of the areal extent is not sufficient to understand the processes and linkages that regulate the onset, duration, and extent of hypoxia. The results of this study suggest that continuous DO monitoring at a single location provides valuable information on short-term variability that will help in assessing the exposure and the resulting biological responses to hypoxia and in interpreting the possible variability around the annual hypoxia maps generated from the single, shelf-wide cruises. Better understanding short-term variability can also help improve the predictive power of numerical models as they explore and dissect the various synergistic factors affecting the development of NGOM hypoxia.

REFERENCES

EPA Science Advisory Board. 2008. Hypoxia in the Northern Gulf of Mexico: An Update by the EPA Science Advisory Board Washington, D.C.

Mississippi River/Gulf of Mexico Watershed Nutrient Task Force. 2008. Gulf Hypoxia Action Plan 2008 for Reducing, Mitigating, and Controlling Hypoxia in the Northern Gulf of Mexico and Improving Water Quality in the Mississippi River Basin. Washington, DC.

APPENDIX A

PLOTS OF DATA BY YEARS

Appendix A is a series of plots generated from the database in support of ecological research (SupER) created for this dissertation. The annual plots illustrate how the database can be used to combine a variety of datasets for scientific study. More information on the data sources included in the database can be found in Appendix D.

Each page represents a plate of 4 plots from various data sets for a single year from 1989 through 2008. The upper panel is a time-series of near-bottom dissolved oxygen (DO) concentrations measured at station C6 (19.5 m depth). The 15 minute DO samples were averaged hourly (blue dotted line). The grey line indicates the daily averages over 20 years 1989 to 2008. The brown line indicates the severely hypoxic threshold (≤ 1.0 mg l^{-1}). The red line indicates the hypoxic threshold (≤ 2.0 mg l^{-1}). The yellow line indicates suboxic threshold (≤ 4.59 mg l^{-1}). The middle panel depicts the daily Mississippi River flow (blue dotted line) as measured at Tarbert Landing, MS. The brown line represents the daily averages over 20 years 1989 to 2008. The green lines show the maximum and minimum for the each day over the 20 years. The bottom left panel represents the bottom water DO concentrations as measured on the annual summertime shelf-wide cruise. DO concentration thresholds are represented as brown: severely hypoxic (≤ 1.0 mg l^{-1}), red: hypoxic (≤ 2.0 mg l^{-1}), and yellow: (≤ 4.59 mg l^{-1}). The white star on the map indicates the location of station C6. The bottom right panel is a wind rose created from the NARR-A data set depicting the wind conditions at station C6 for the year.

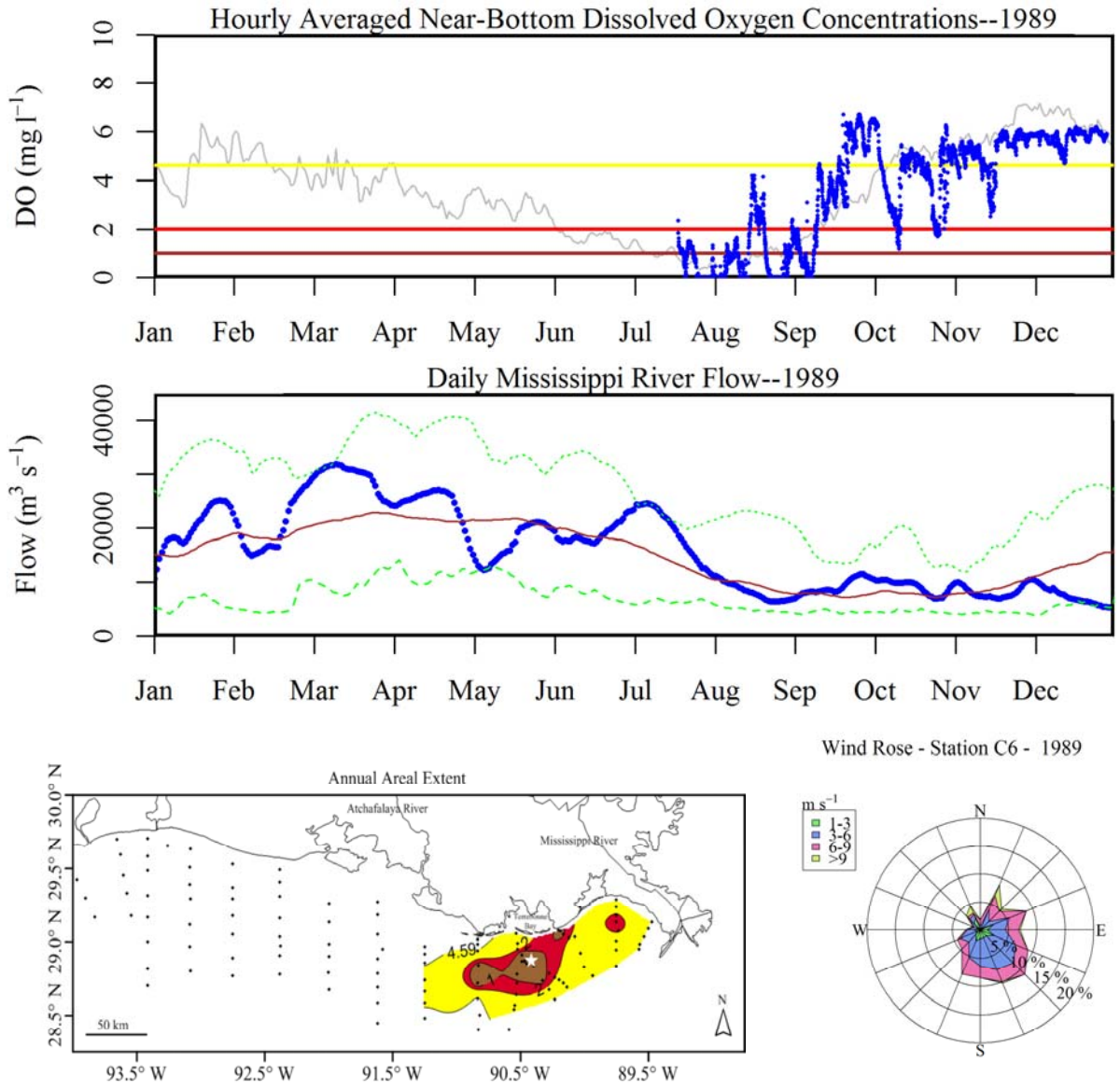

Figure A.1. Plots of various environmental parameters related to hypoxia at station C6 from 1989, upper panel: near-bottom dissolved oxygen (DO) time-series measured at C6 (19.5 m depth), middle panel: daily Mississippi River flow time-series measured at Tarbert Landing, MS., bottom left panel: bottom water DO concentrations as measured on the annual mid-summer shelf-wide cruise by LUMCON, bottom right panel: wind rose created from the NARR-A data set depicting the wind conditions at station C6. Further details are located on the first page of Appendix A.

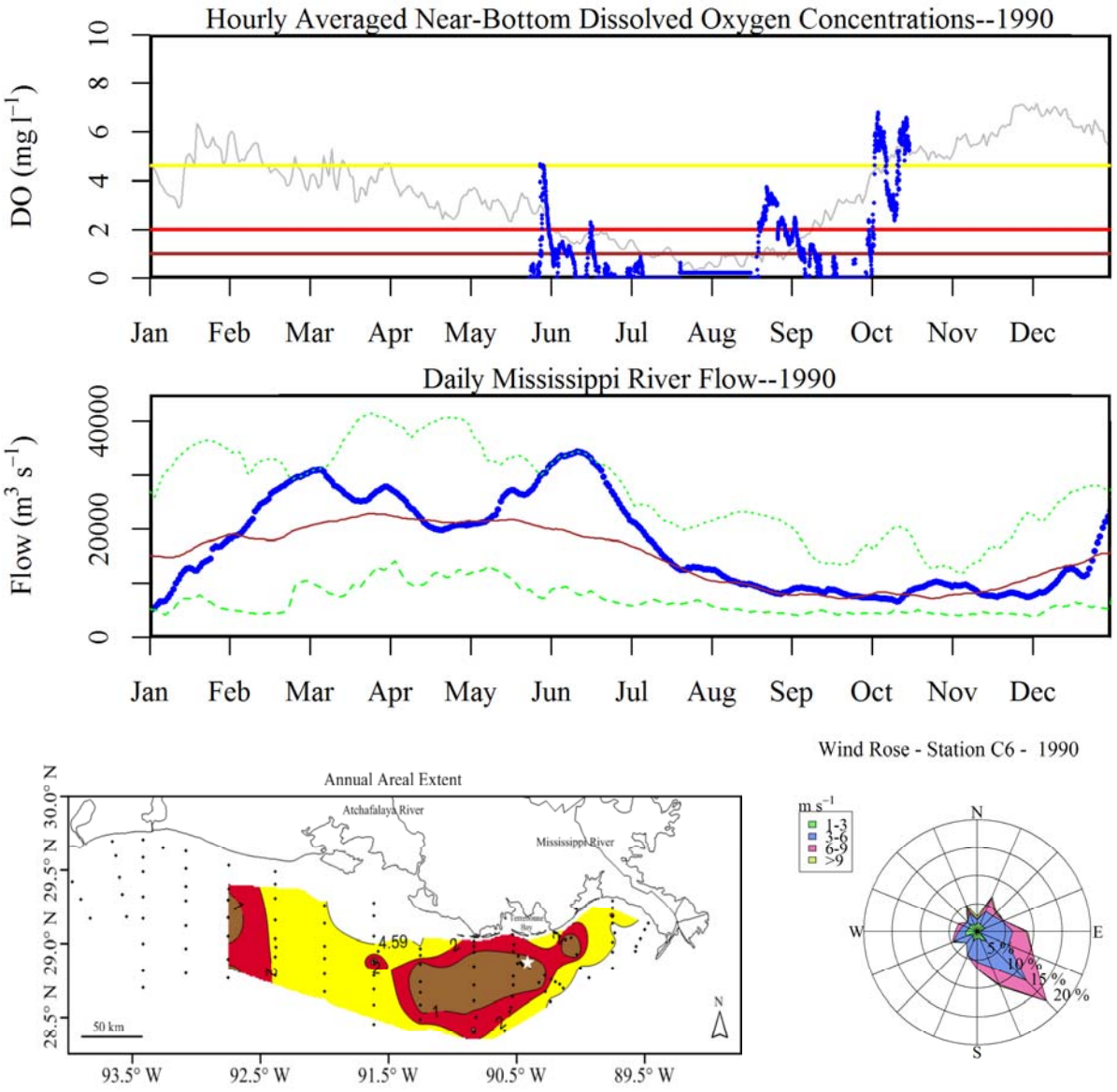

Figure A.2. Plots of various environmental parameters related to hypoxia at station C6 from 1990, upper panel: near-bottom dissolved oxygen (DO) time-series measured at C6 (19.5 m depth), middle panel: daily Mississippi River flow time-series measured at Tarbert Landing, MS., bottom left panel: bottom water DO concentrations as measured on the annual mid-summer shelf-wide cruise by LUMCON, bottom right panel: wind rose created from the NARR-A data set depicting the wind conditions at station C6. Further details are located on the first page of Appendix A.

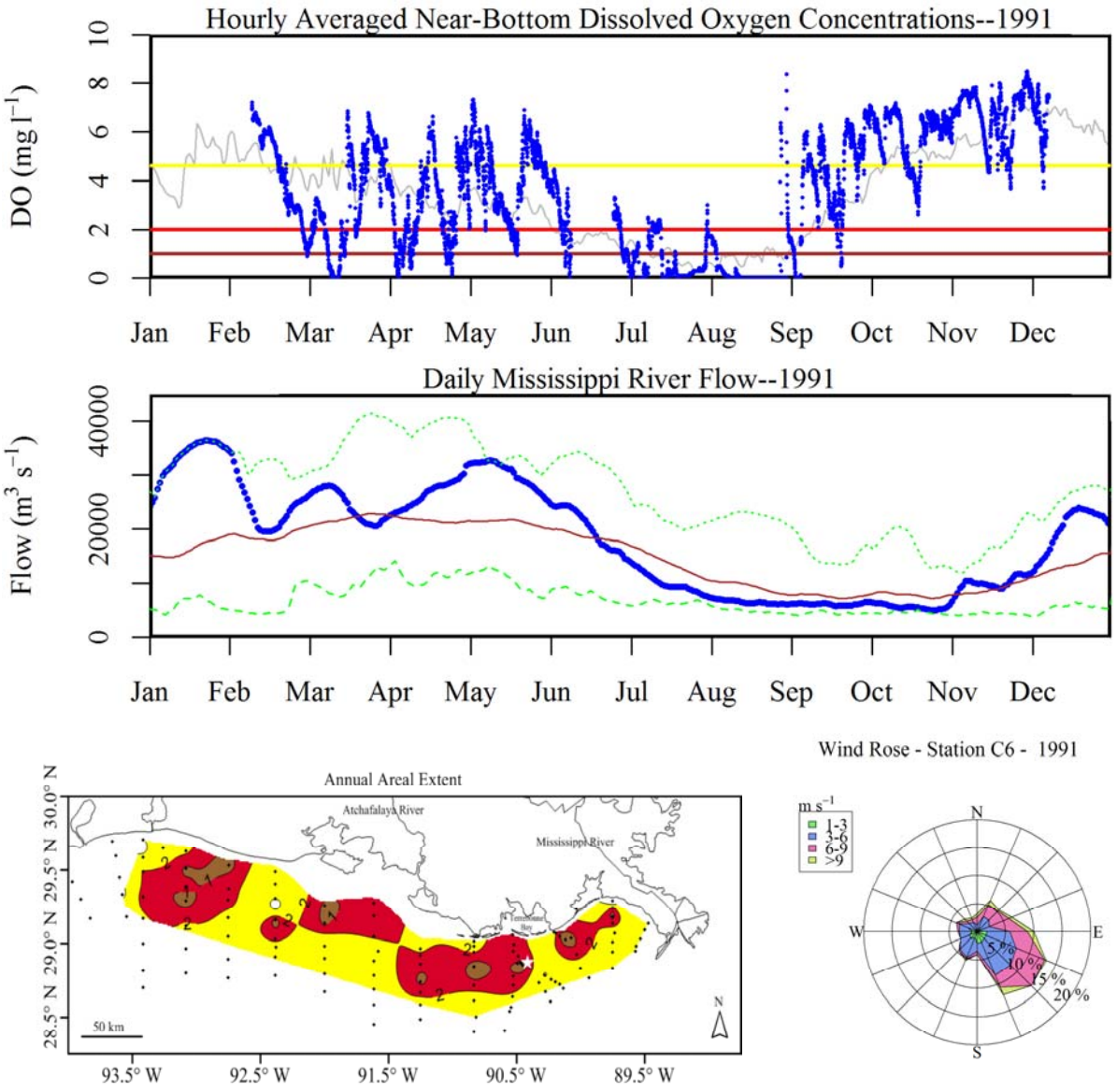

Figure A.3. Plots of various environmental parameters related to hypoxia at station C6 from 1991, upper panel: near-bottom dissolved oxygen (DO) time-series measured at C6 (19.5 m depth), middle panel: daily Mississippi River flow time-series measured at Tarbert Landing, MS., bottom left panel: bottom water DO concentrations as measured on the annual mid-summer shelf-wide cruise by LUMCON, bottom right panel: wind rose created from the NARR-A data set depicting the wind conditions at station C6. Further details are located on the first page of Appendix A.

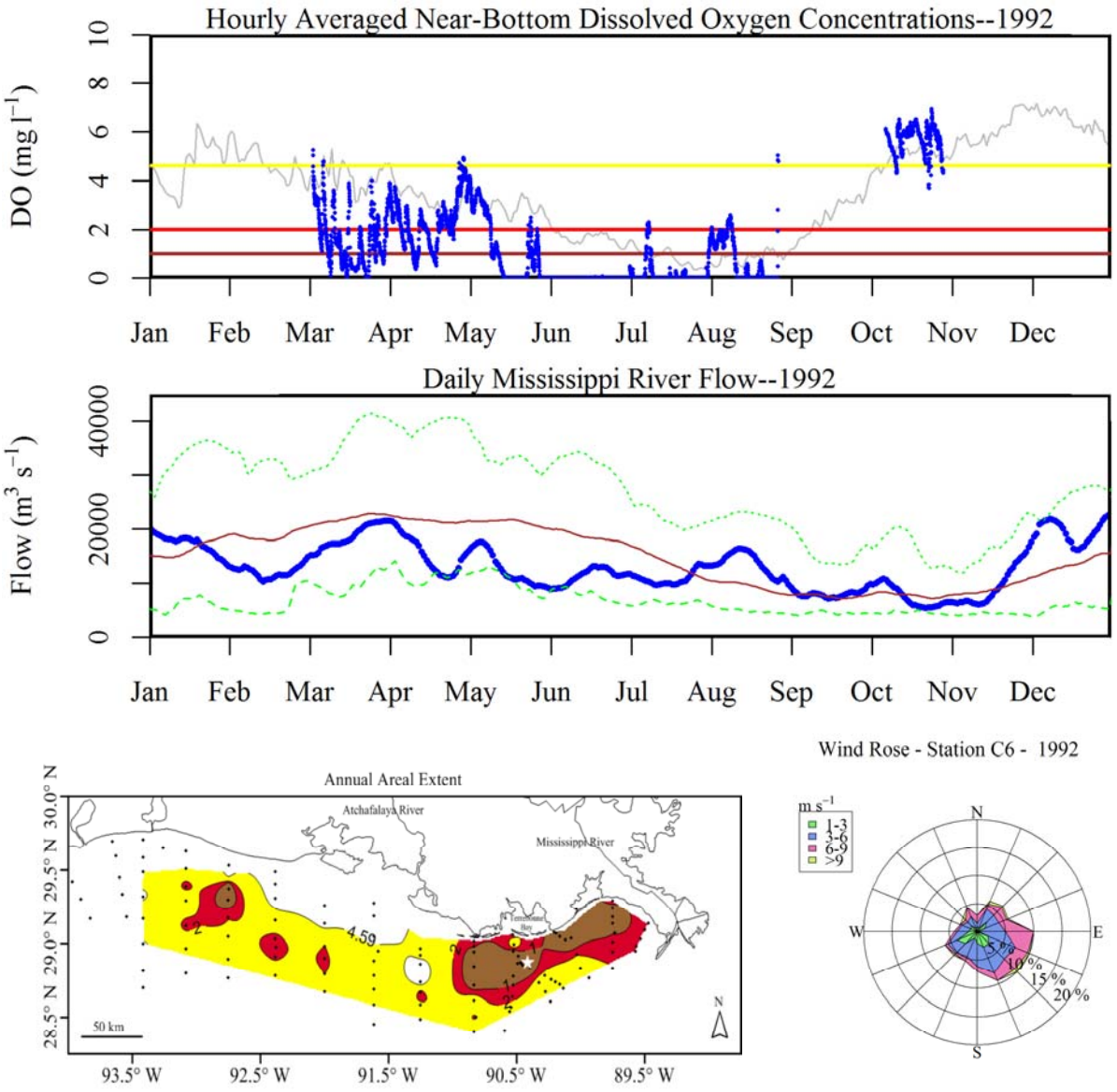

Figure A.4. Plots of various environmental parameters related to hypoxia at station C6 from 1992, upper panel: near-bottom dissolved oxygen (DO) time-series measured at C6 (19.5 m depth), middle panel: daily Mississippi River flow time-series measured at Tarbert Landing, MS., bottom left panel: bottom water DO concentrations as measured on the annual mid-summer shelf-wide cruise by LUMCON, bottom right panel: wind rose created from the NARR-A data set depicting the wind conditions at station C6. Further details are located on the first page of Appendix A.

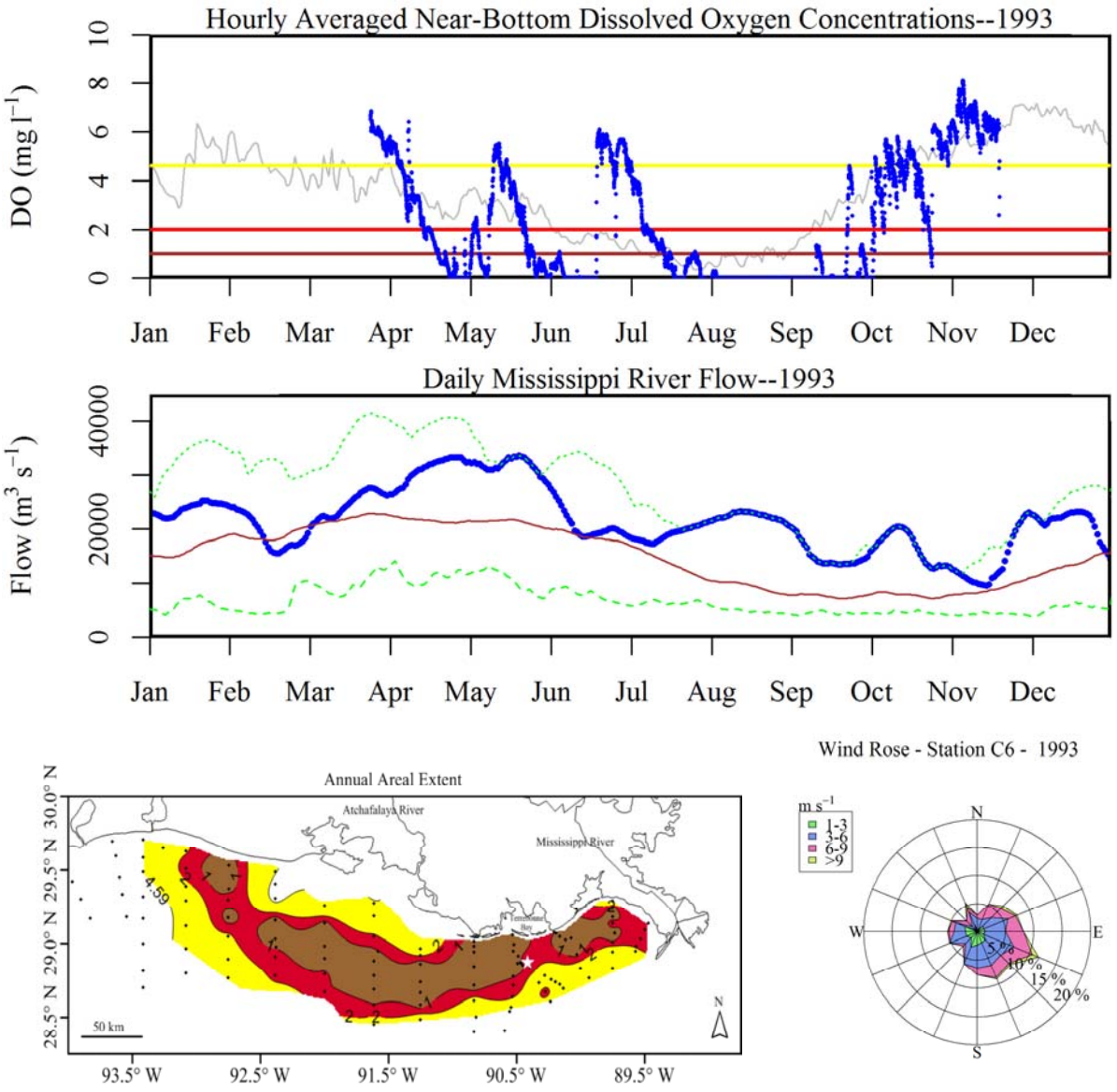

Figure A.5. Plots of various environmental parameters related to hypoxia at station C6 from 1993, upper panel: near-bottom dissolved oxygen (DO) time-series measured at C6 (19.5 m depth), middle panel: daily Mississippi River flow time-series measured at Tarbert Landing, MS., bottom left panel: bottom water DO concentrations as measured on the annual mid-summer shelf-wide cruise by LUMCON, bottom right panel: wind rose created from the NARR-A data set depicting the wind conditions at station C6. Further details are located on the first page of Appendix A.

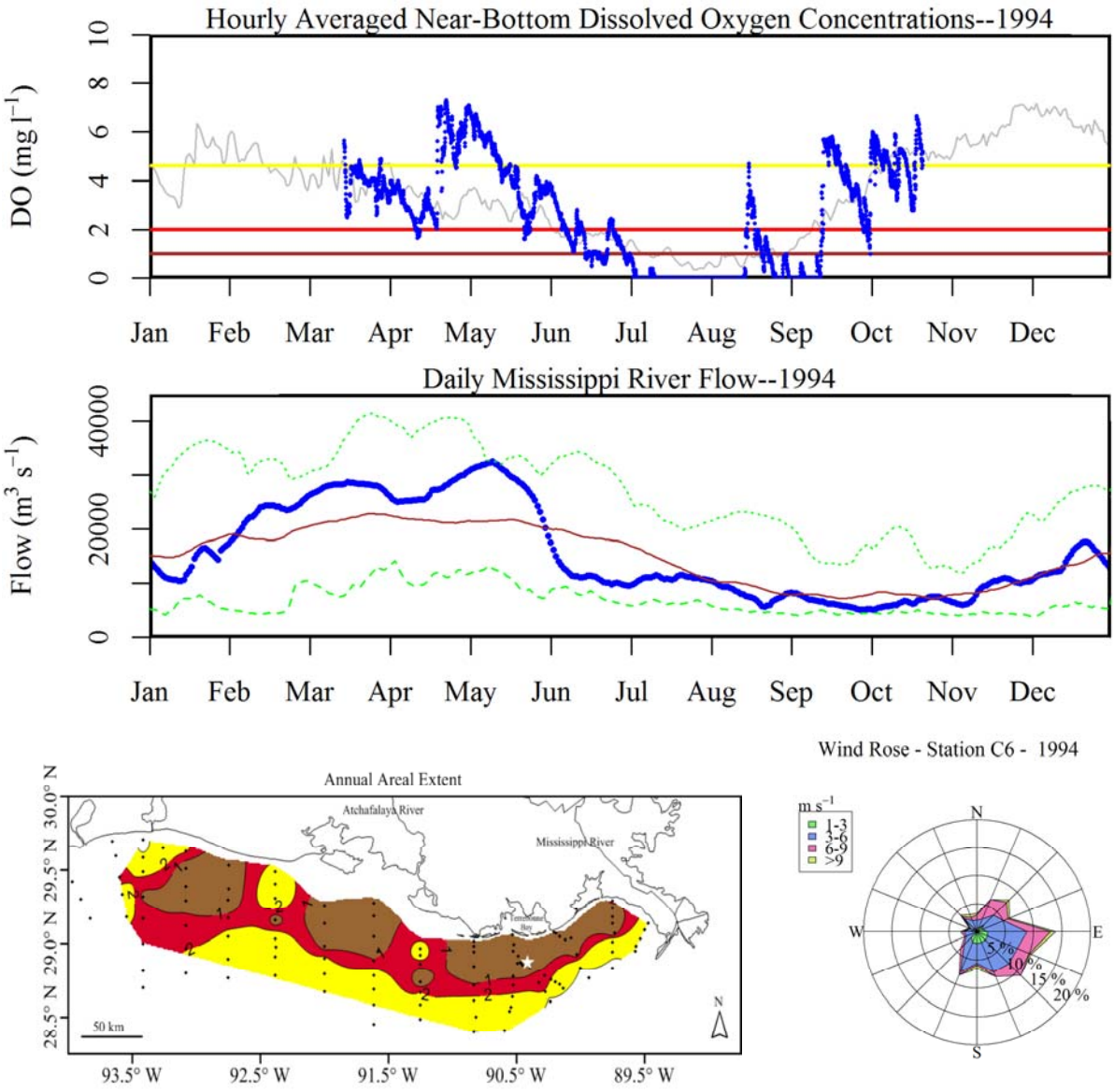

Figure A.6. Plots of various environmental parameters related to hypoxia at station C6 from 1994, upper panel: near-bottom dissolved oxygen (DO) time-series measured at C6 (19.5 m depth), middle panel: daily Mississippi River flow time-series measured at Tarbert Landing, MS., bottom left panel: bottom water DO concentrations as measured on the annual mid-summer shelf-wide cruise by LUMCON, bottom right panel: wind rose created from the NARR-A data set depicting the wind conditions at station C6. Further details are located on the first page of Appendix A.

1995

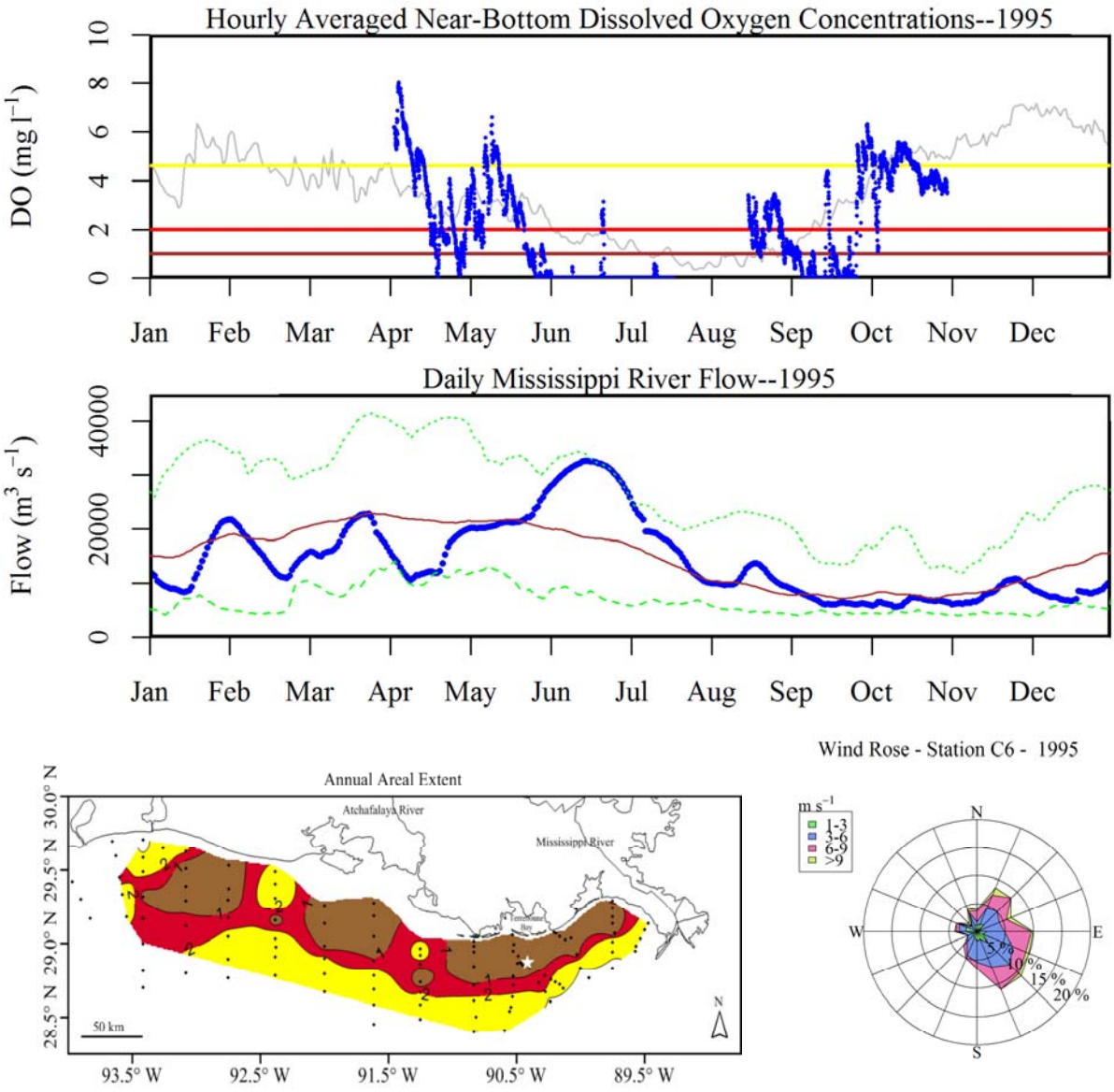

Figure A.7. Plots of various environmental parameters related to hypoxia at station C6 from 1995, upper panel: near-bottom dissolved oxygen (DO) time-series measured at C6 (19.5 m depth), middle panel: daily Mississippi River flow time-series measured at Tarbert Landing, MS., bottom left panel: bottom water DO concentrations as measured on the annual mid-summer shelf-wide cruise by LUMCON, bottom right panel: wind rose created from the NARR-A data set depicting the wind conditions at station C6. Further details are located on the first page of Appendix A.

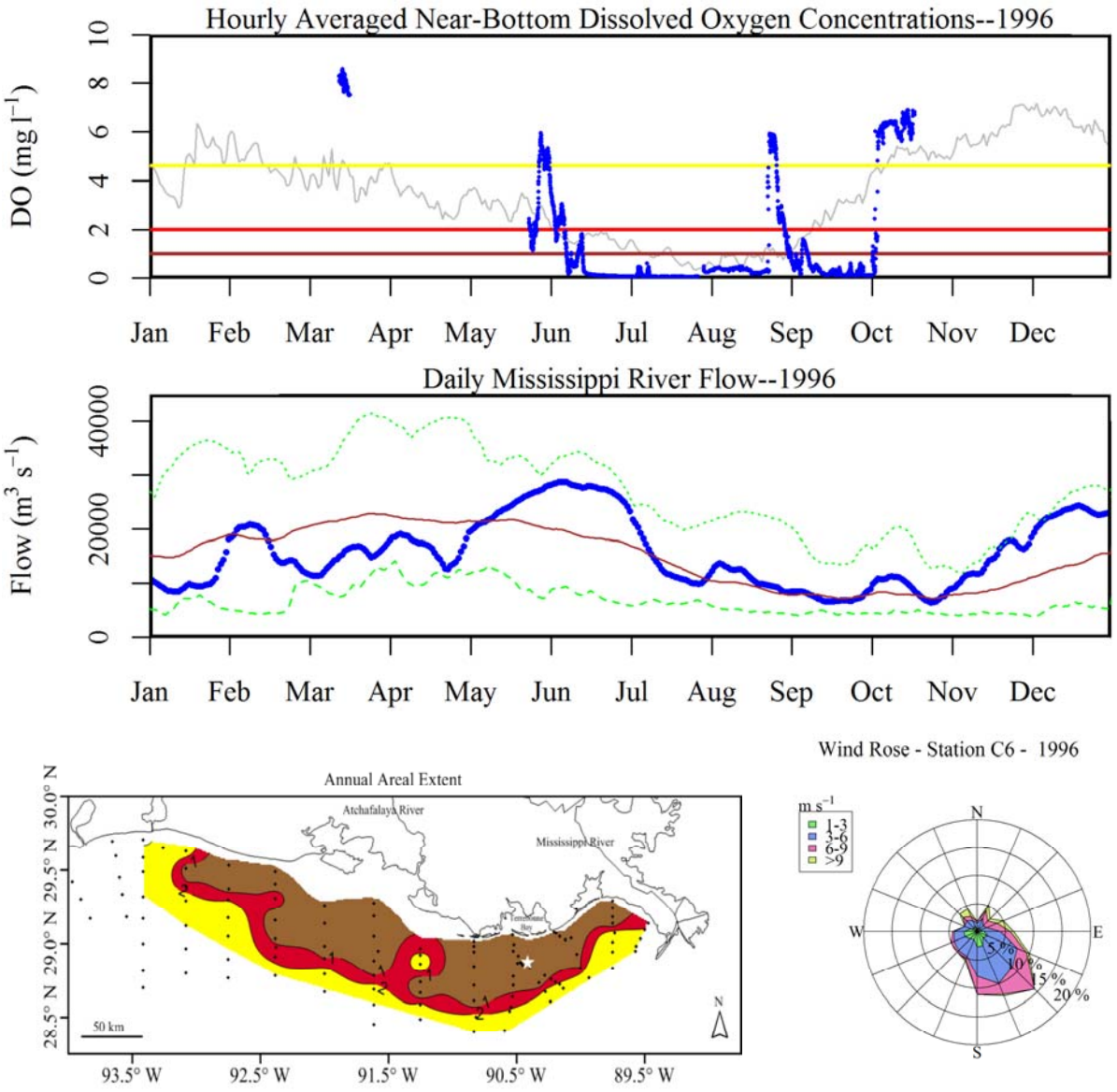

Figure A.8. Plots of various environmental parameters related to hypoxia at station C6 from 1996, upper panel: near-bottom dissolved oxygen (DO) time-series measured at C6 (19.5 m depth), middle panel: daily Mississippi River flow time-series measured at Tarbert Landing, MS., bottom left panel: bottom water DO concentrations as measured on the annual mid-summer shelf-wide cruise by LUMCON, bottom right panel: wind rose created from the NARR-A data set depicting the wind conditions at station C6. Further details are located on the first page of Appendix A.

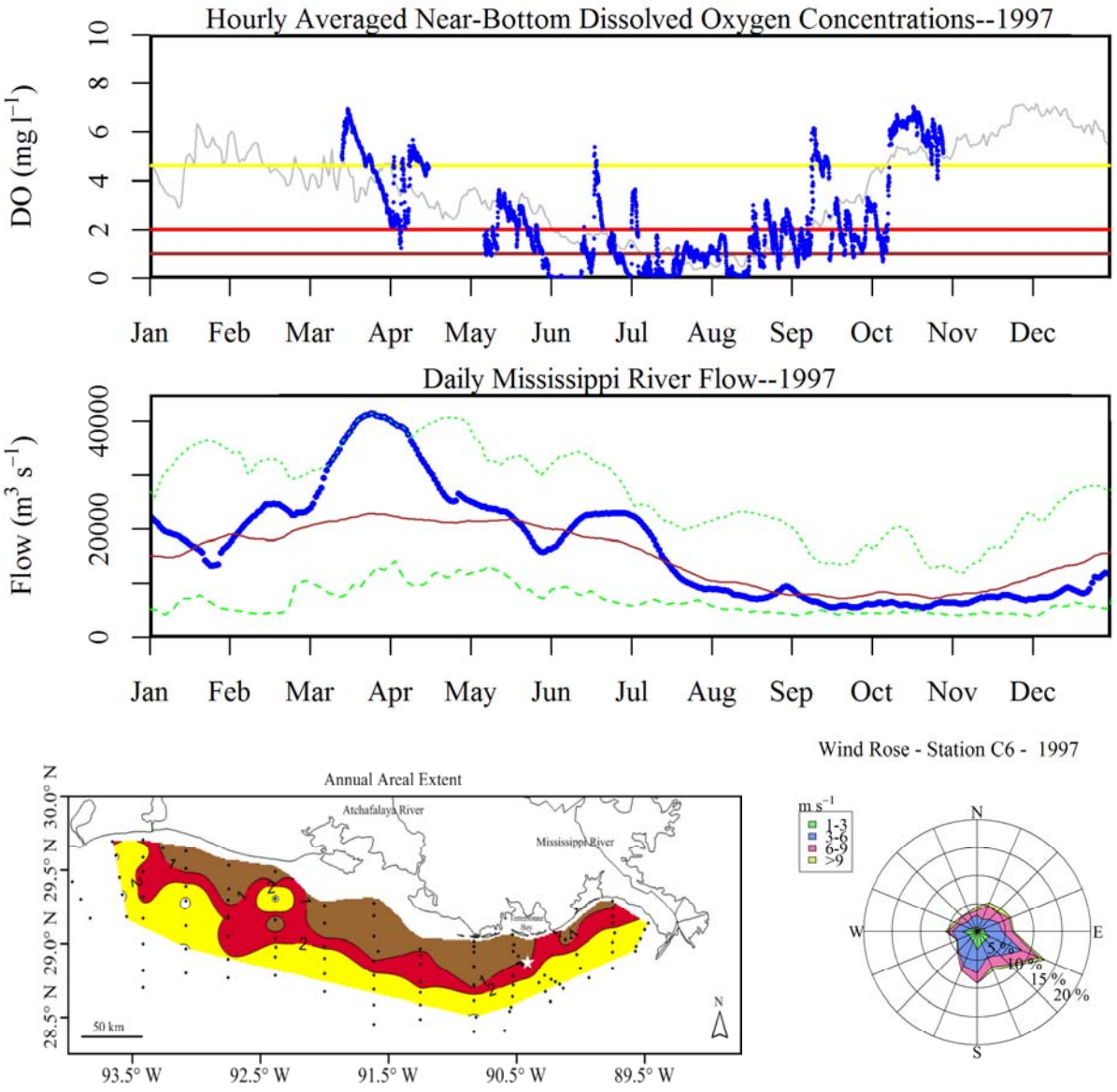

Figure A.9. Plots of various environmental parameters related to hypoxia at station C6 from 1997, upper panel: near-bottom dissolved oxygen (DO) time-series measured at C6 (19.5 m depth), middle panel: daily Mississippi River flow time-series measured at Tarbert Landing, MS., bottom left panel: bottom water DO concentrations as measured on the annual mid-summer shelf-wide cruise by LUMCON, bottom right panel: wind rose created from the NARR-A data set depicting the wind conditions at station C6. Further details are located on the first page of Appendix A.

1998

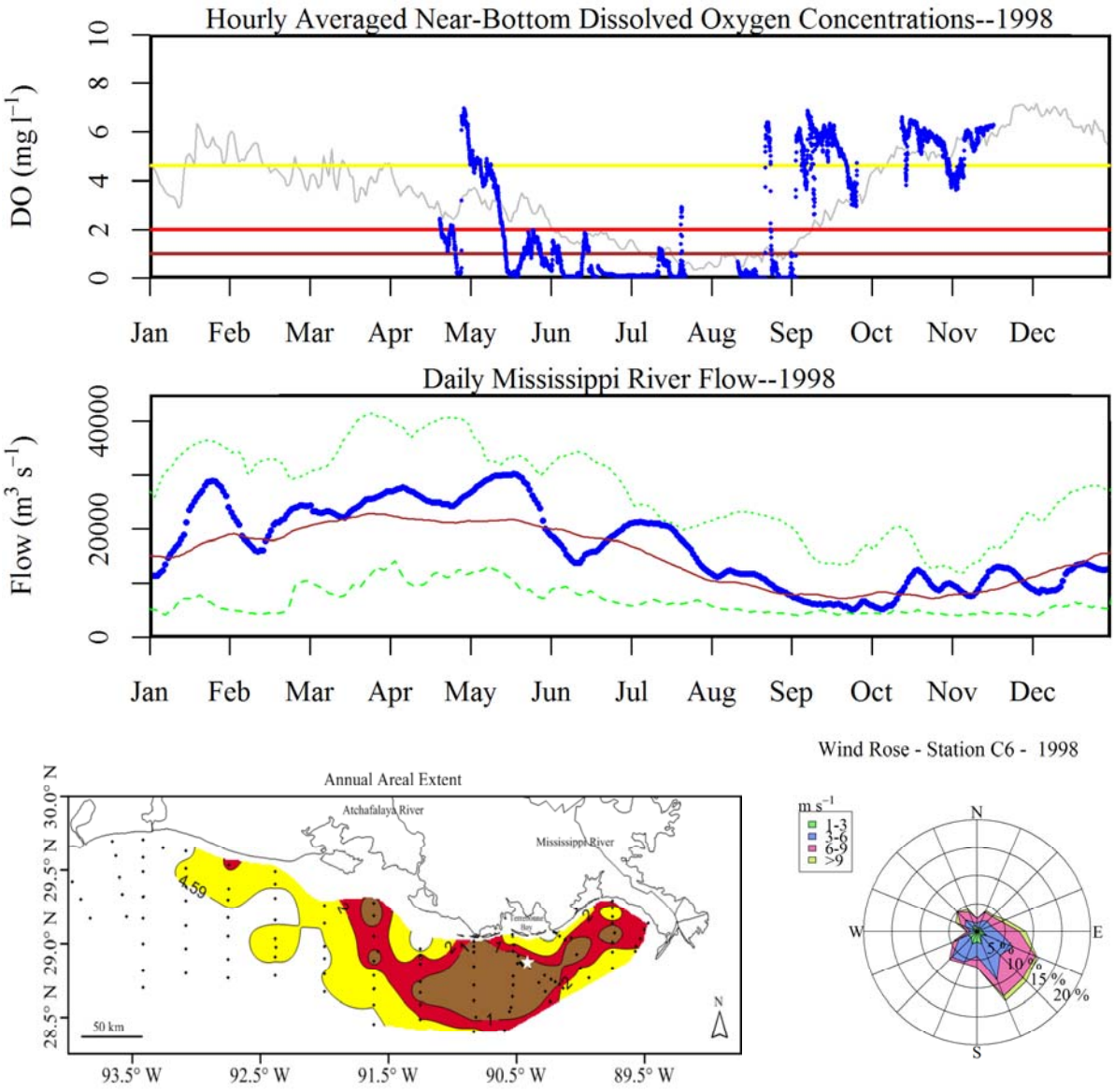

Figure A.10. Plots of various environmental parameters related to hypoxia at station C6 from 1998, upper panel: near-bottom dissolved oxygen (DO) time-series measured at C6 (19.5 m depth), middle panel: daily Mississippi River flow time-series measured at Tarbert Landing, MS., bottom left panel: bottom water DO concentrations as measured on the annual mid-summer shelf-wide cruise by LUMCON, bottom right panel: wind rose created from the NARR-A data set depicting the wind conditions at station C6. Further details are located on the first page of Appendix A.

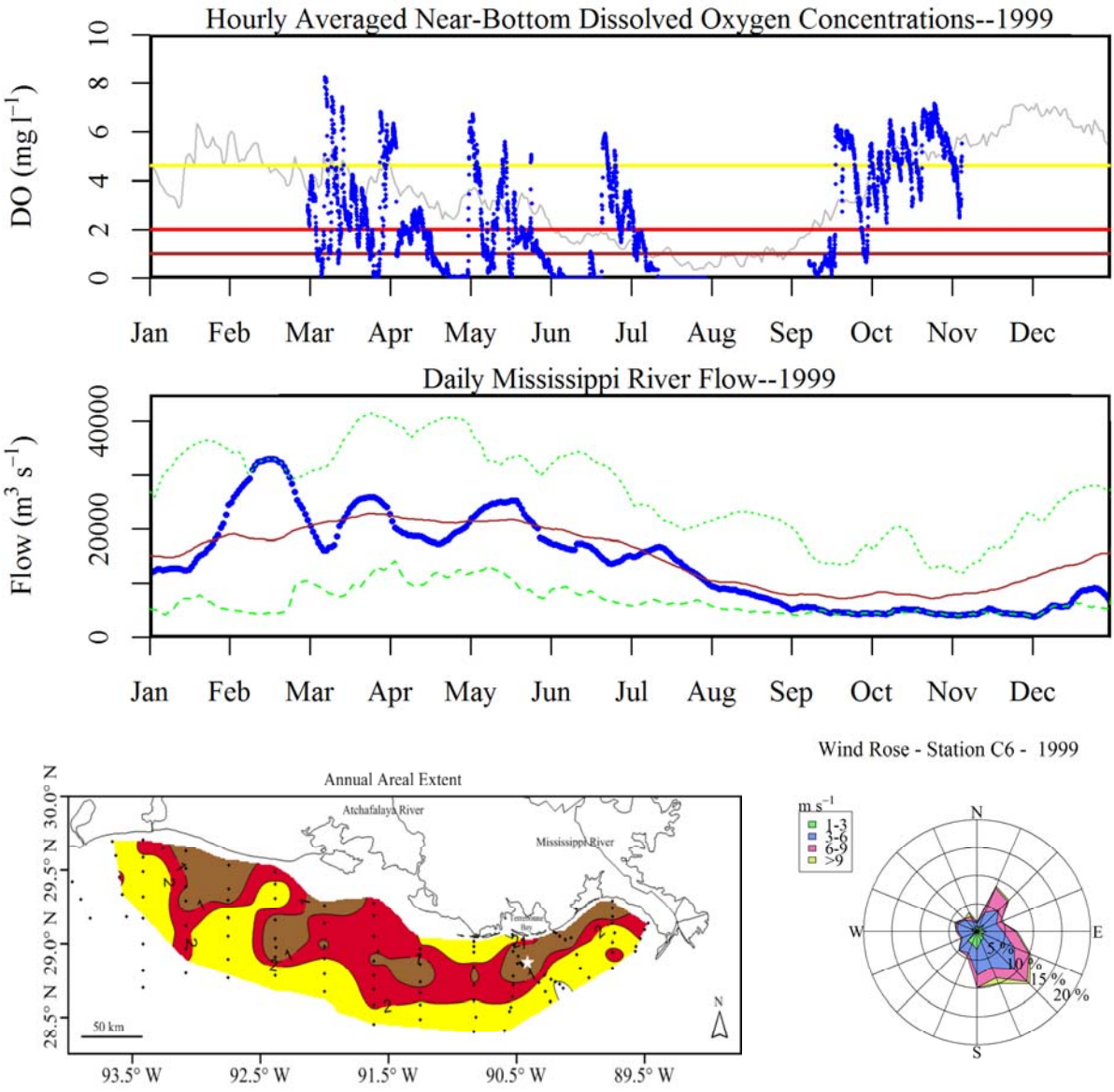

Figure A.11. Plots of various environmental parameters related to hypoxia at station C6 from 1999, upper panel: near-bottom dissolved oxygen (DO) time-series measured at C6 (19.5 m depth), middle panel: daily Mississippi River flow time-series measured at Tarbert Landing, MS., bottom left panel: bottom water DO concentrations as measured on the annual mid-summer shelf-wide cruise by LUMCON, bottom right panel: wind rose created from the NARR-A data set depicting the wind conditions at station C6. Further details are located on the first page of Appendix A.

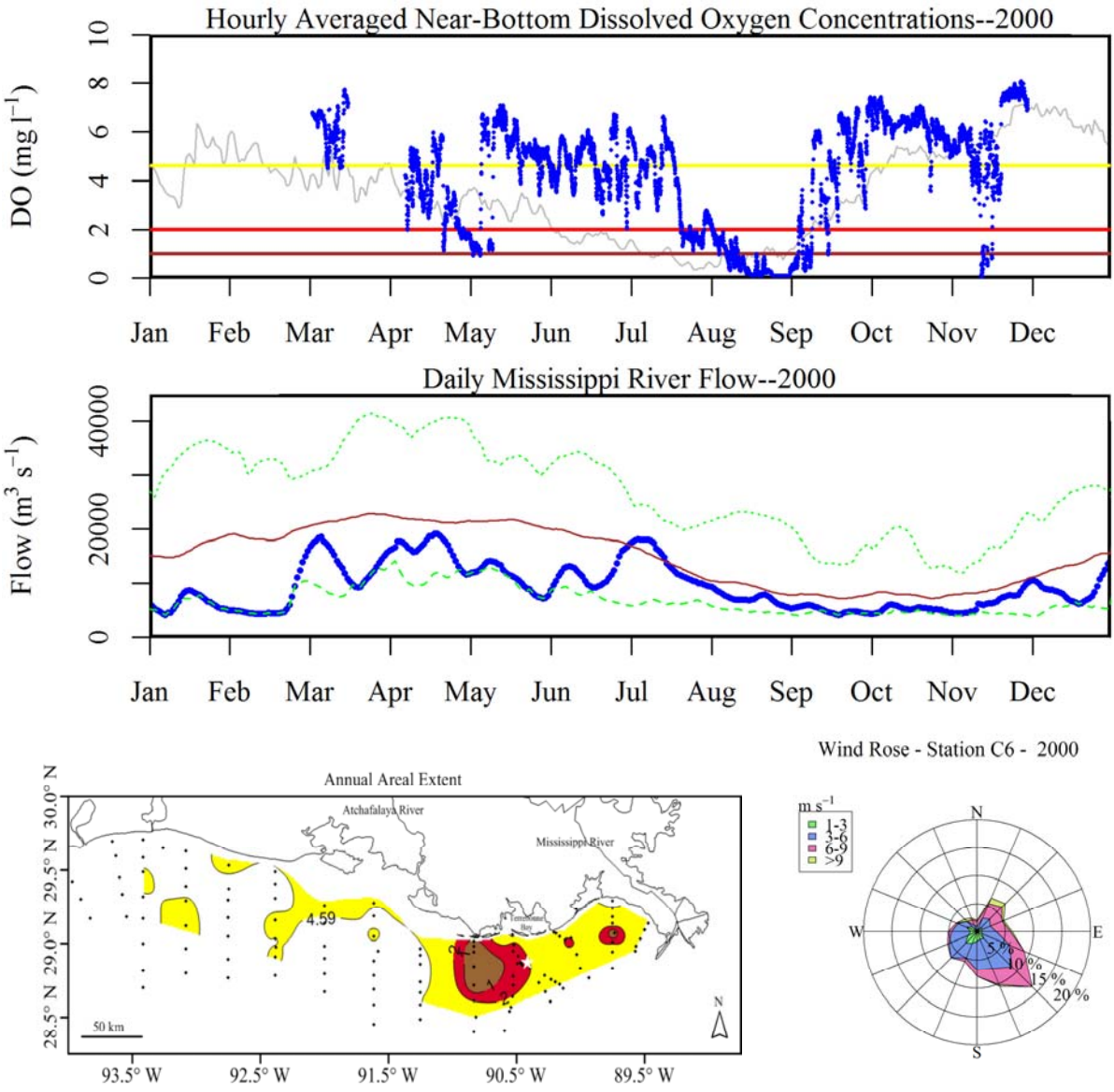

Figure A.12. Plots of various environmental parameters related to hypoxia at station C6 from 2000, upper panel: near-bottom dissolved oxygen (DO) time-series measured at C6 (19.5 m depth), middle panel: daily Mississippi River flow time-series measured at Tarbert Landing, MS., bottom left panel: bottom water DO concentrations as measured on the annual mid-summer shelf-wide cruise by LUMCON, bottom right panel: wind rose created from the NARR-A data set depicting the wind conditions at station C6. Further details are located on the first page of Appendix A.

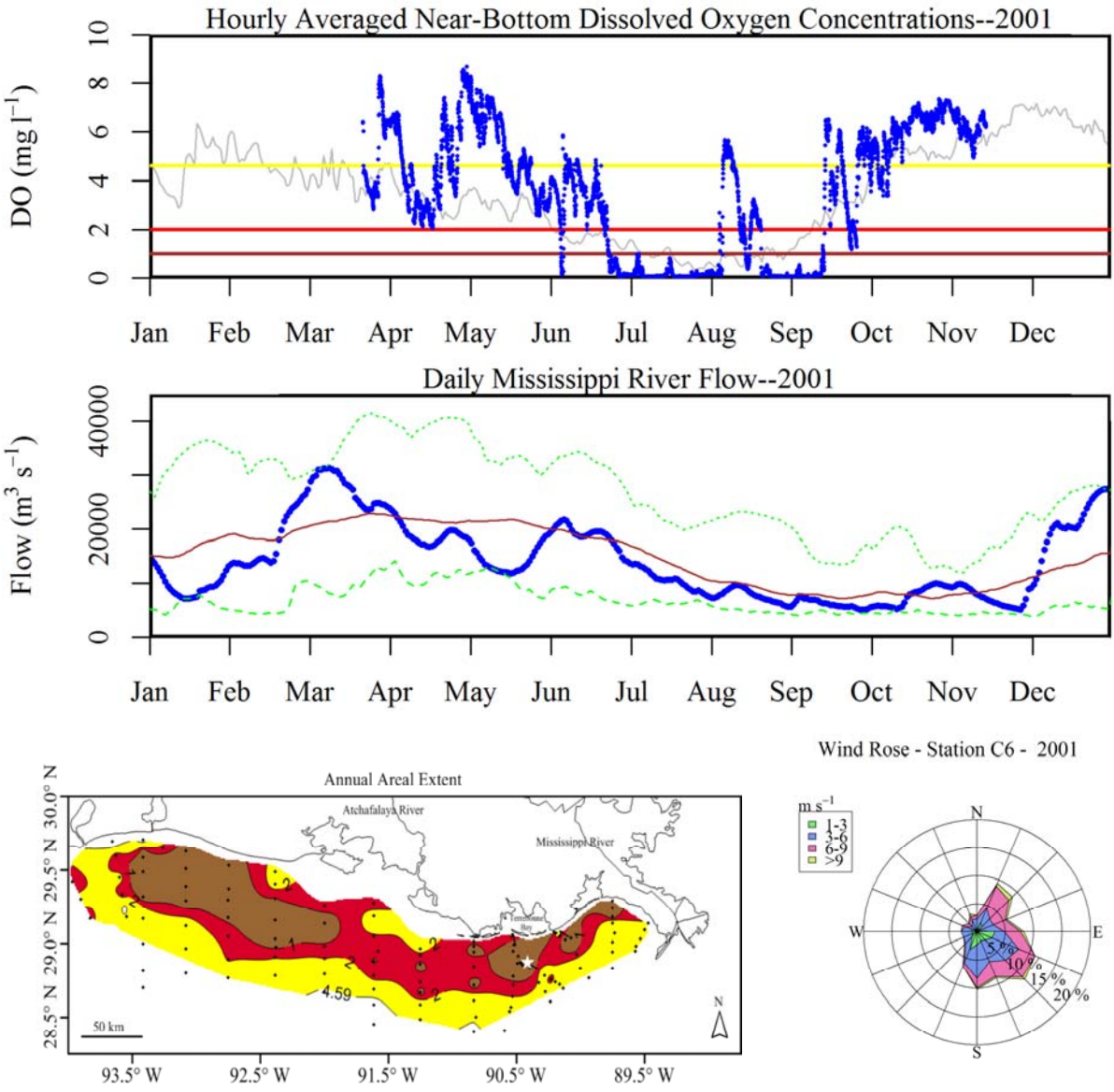

Figure A.13. Plots of various environmental parameters related to hypoxia at station C6 from 2001, upper panel: near-bottom dissolved oxygen (DO) time-series measured at C6 (19.5 m depth), middle panel: daily Mississippi River flow time-series measured at Tarbert Landing, MS., bottom left panel: bottom water DO concentrations as measured on the annual mid-summer shelf-wide cruise by LUMCON, bottom right panel: wind rose created from the NARR-A data set depicting the wind conditions at station C6. Further details are located on the first page of Appendix A.

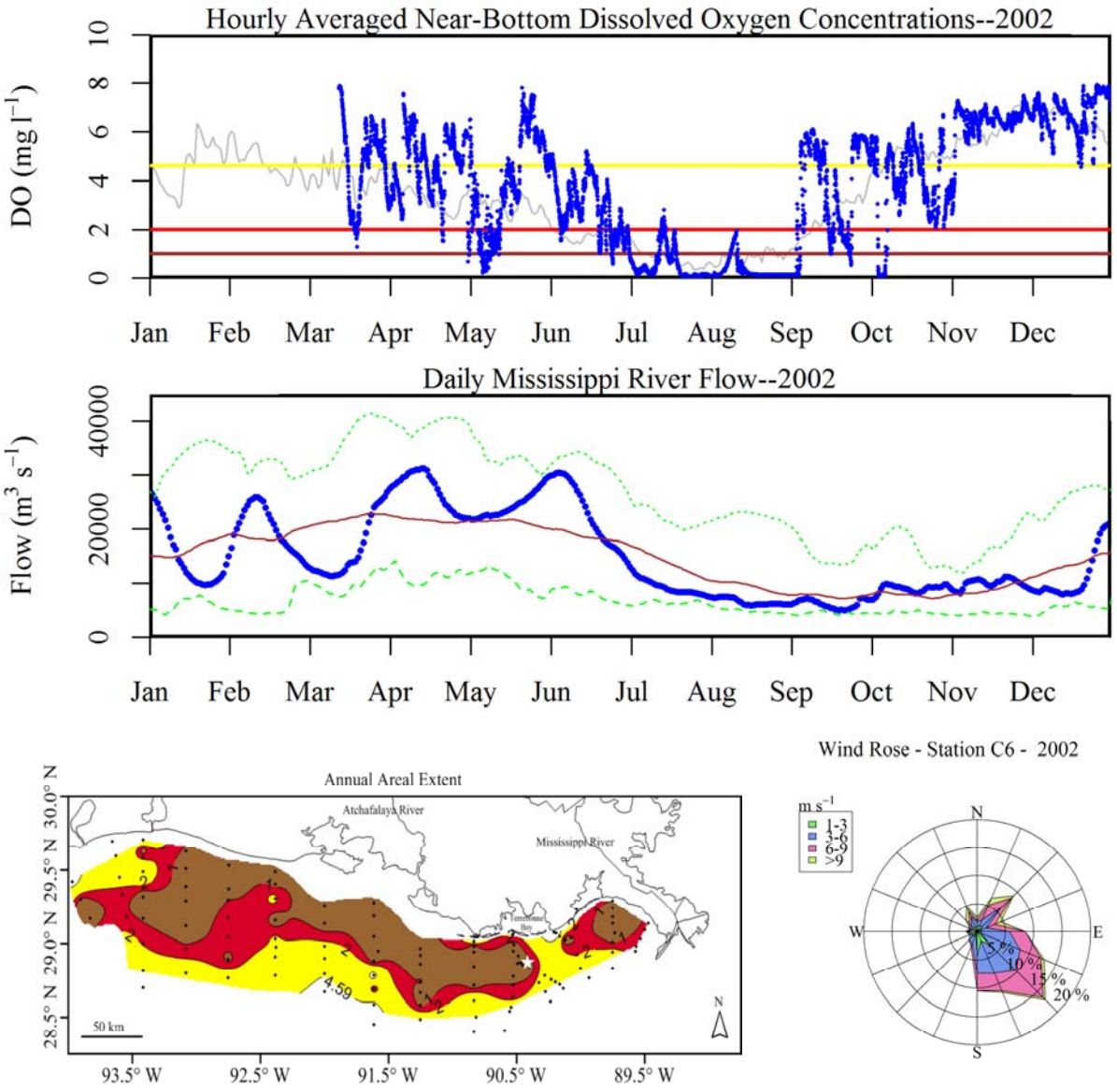

Figure A.14. Plots of various environmental parameters related to hypoxia at station C6 from 2002, upper panel: near-bottom dissolved oxygen (DO) time-series measured at C6 (19.5 m depth), middle panel: daily Mississippi River flow time-series measured at Tarbert Landing, MS., bottom left panel: bottom water DO concentrations as measured on the annual mid-summer shelf-wide cruise by LUMCON, bottom right panel: wind rose created from the NARR-A data set depicting the wind conditions at station C6. Further details are located on the first page of Appendix A.

2003

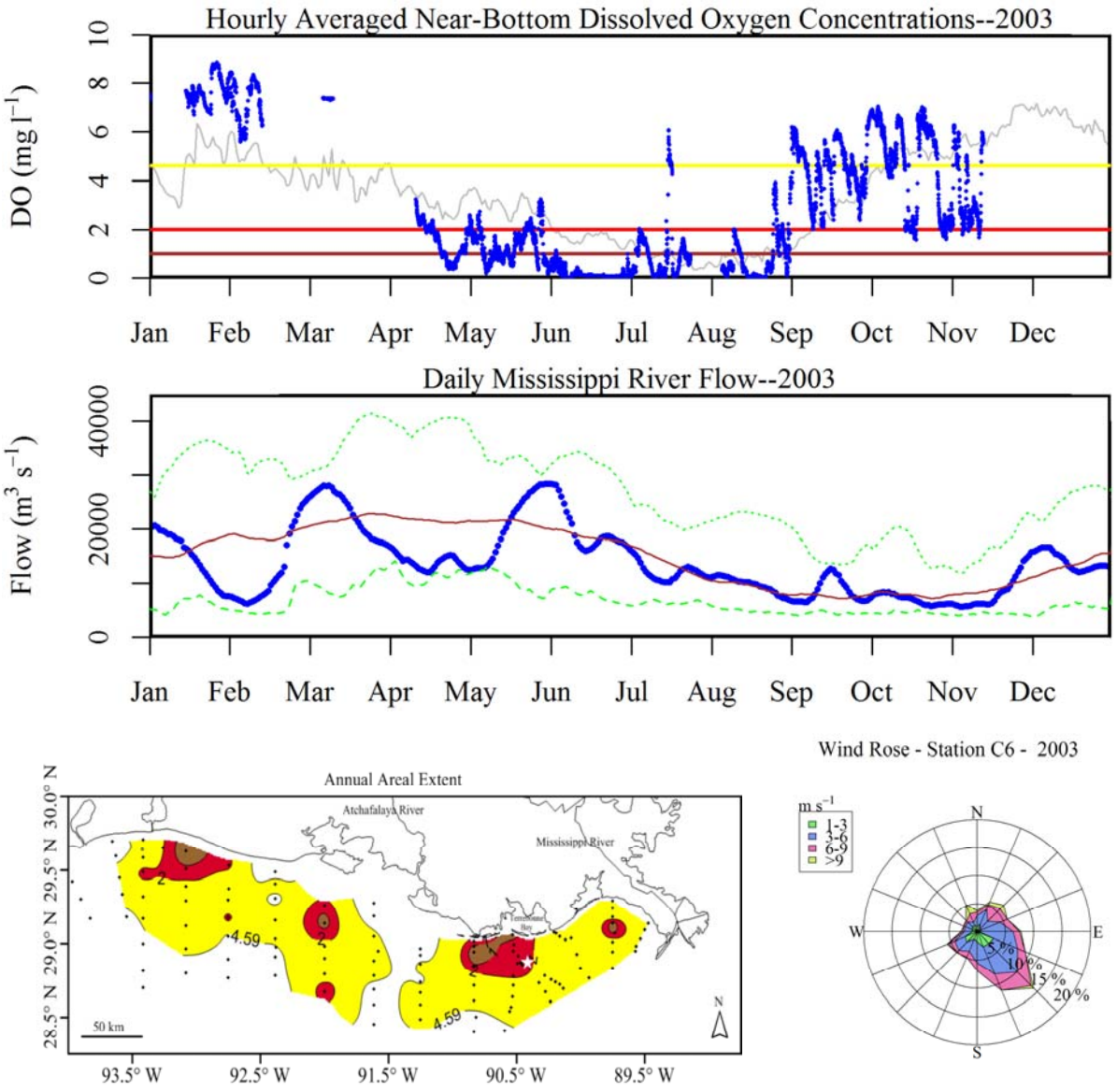

Figure A.15. Plots of various environmental parameters related to hypoxia at station C6 from 2003, upper panel: near-bottom dissolved oxygen (DO) time-series measured at C6 (19.5 m depth), middle panel: daily Mississippi River flow time-series measured at Tarbert Landing, MS., bottom left panel: bottom water DO concentrations as measured on the annual mid-summer shelf-wide cruise by LUMCON, bottom right panel: wind rose created from the NARR-A data set depicting the wind conditions at station C6. Further details are located on the first page of Appendix A.

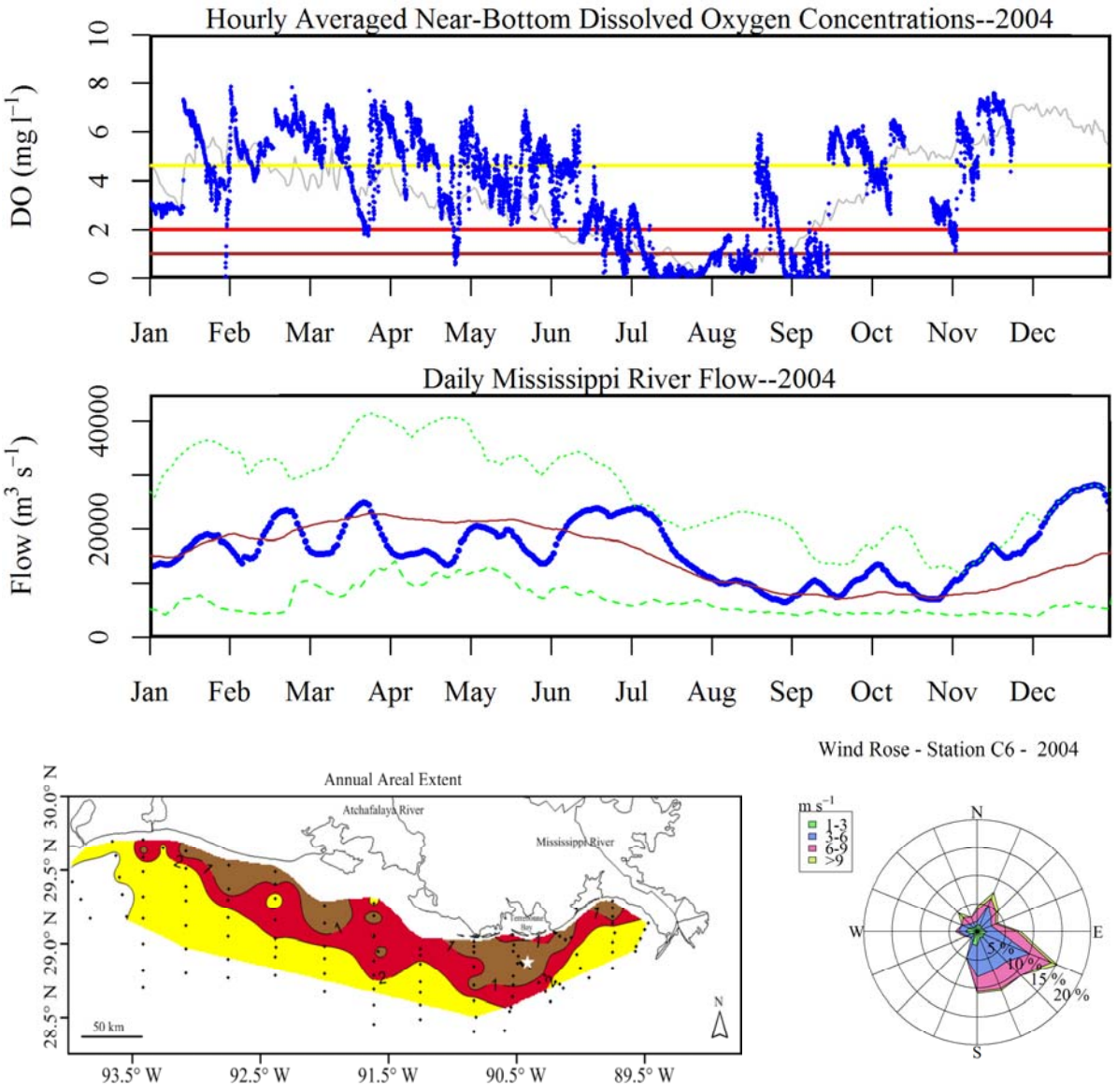

Figure A.16. Plots of various environmental parameters related to hypoxia at station C6 from 2004, upper panel: near-bottom dissolved oxygen (DO) time-series measured at C6 (19.5 m depth), middle panel: daily Mississippi River flow time-series measured at Tarbert Landing, MS., bottom left panel: bottom water DO concentrations as measured on the annual mid-summer shelf-wide cruise by LUMCON, bottom right panel: wind rose created from the NARR-A data set depicting the wind conditions at station C6. Further details are located on the first page of Appendix A.

2005

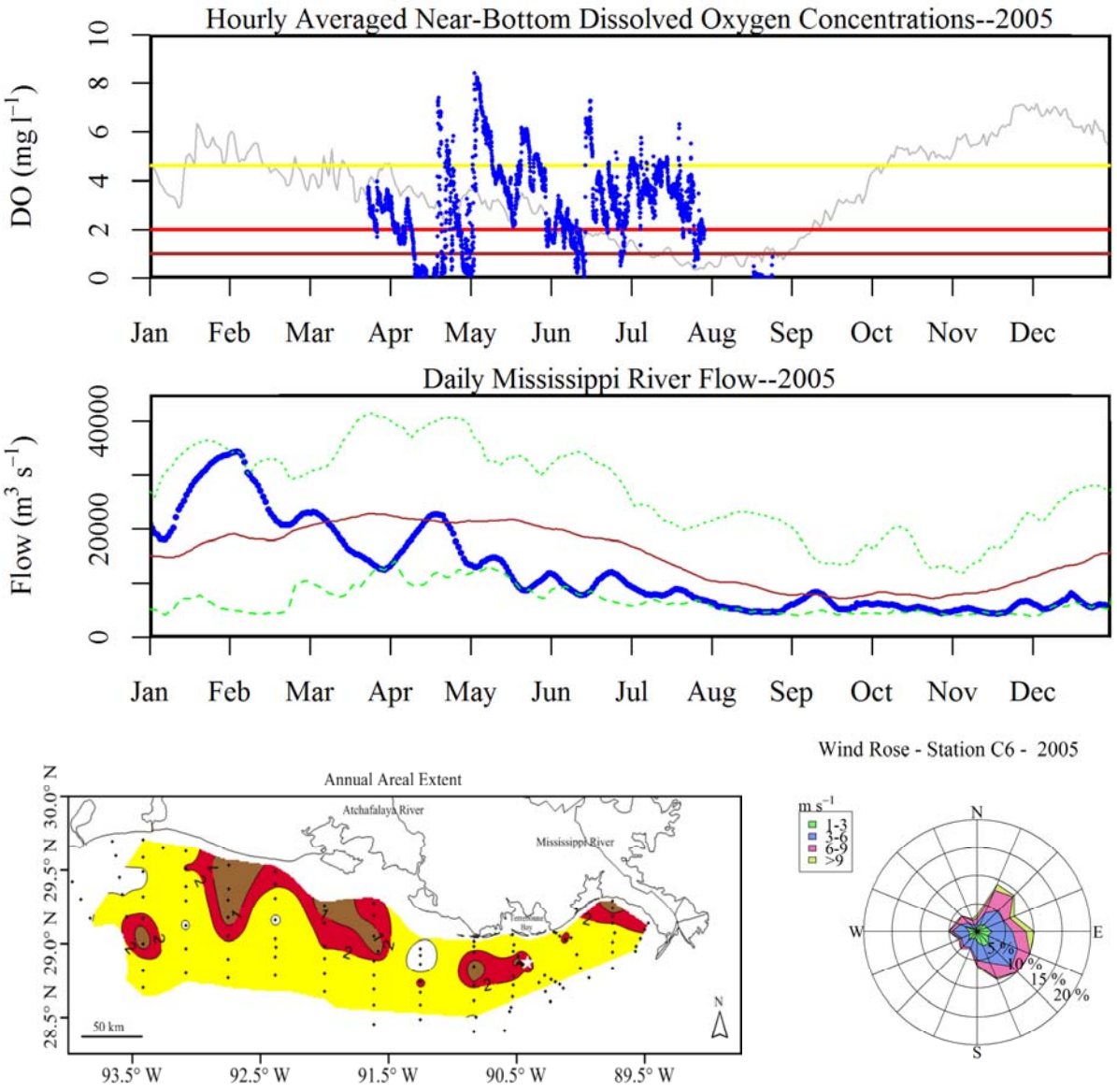

Figure A.17. Plots of various environmental parameters related to hypoxia at station C6 from 2005, upper panel: near-bottom dissolved oxygen (DO) time-series measured at C6 (19.5 m depth), middle panel: daily Mississippi River flow time-series measured at Tarbert Landing, MS., bottom left panel: bottom water DO concentrations as measured on the annual mid-summer shelf-wide cruise by LUMCON, bottom right panel: wind rose created from the NARR-A data set depicting the wind conditions at station C6. Further details are located on the first page of Appendix A.

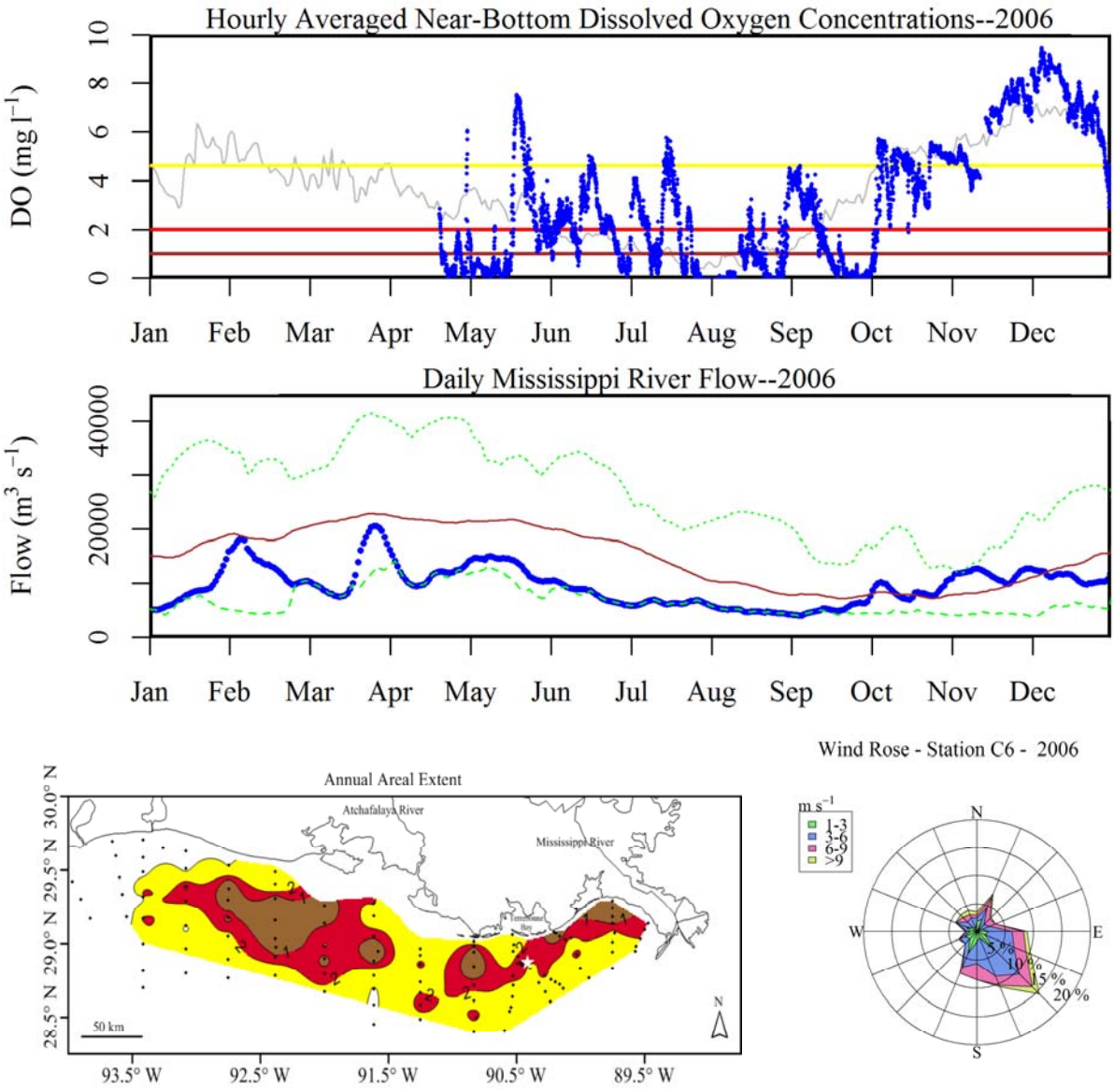

Figure A.18. Plots of various environmental parameters related to hypoxia at station C6 from 2006, upper panel: near-bottom dissolved oxygen (DO) time-series measured at C6 (19.5 m depth), middle panel: daily Mississippi River flow time-series measured at Tarbert Landing, MS., bottom left panel: bottom water DO concentrations as measured on the annual mid-summer shelf-wide cruise by LUMCON, bottom right panel: wind rose created from the NARR-A data set depicting the wind conditions at station C6. Further details are located on the first page of Appendix A.

2007

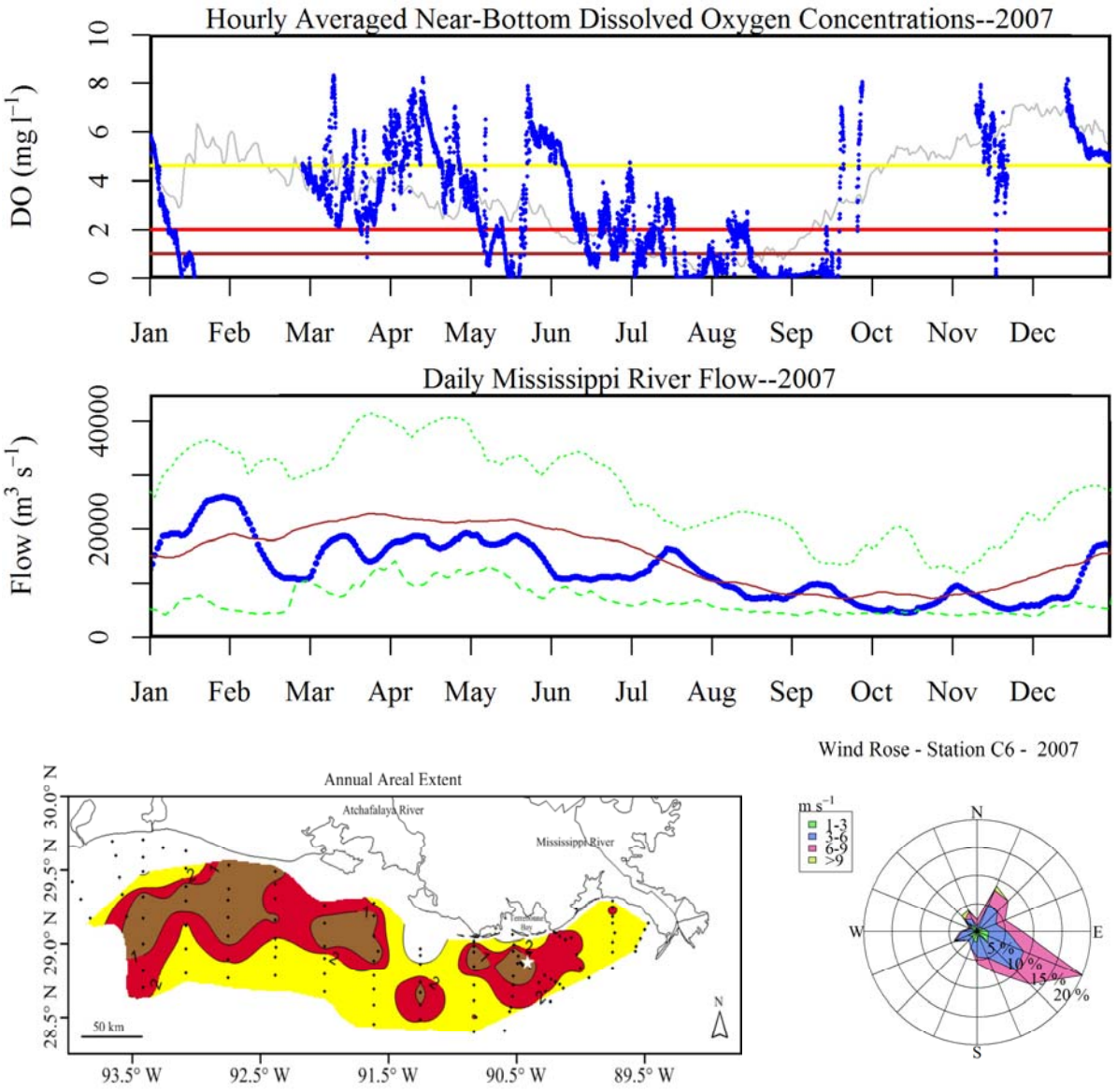

Figure A.19. Plots of various environmental parameters related to hypoxia at station C6 from 2007, upper panel: near-bottom dissolved oxygen (DO) time-series measured at C6 (19.5 m depth), middle panel: daily Mississippi River flow time-series measured at Tarbert Landing, MS., bottom left panel: bottom water DO concentrations as measured on the annual mid-summer shelf-wide cruise by LUMCON, bottom right panel: wind rose created from the NARR-A data set depicting the wind conditions at station C6. Further details are located on the first page of Appendix A.

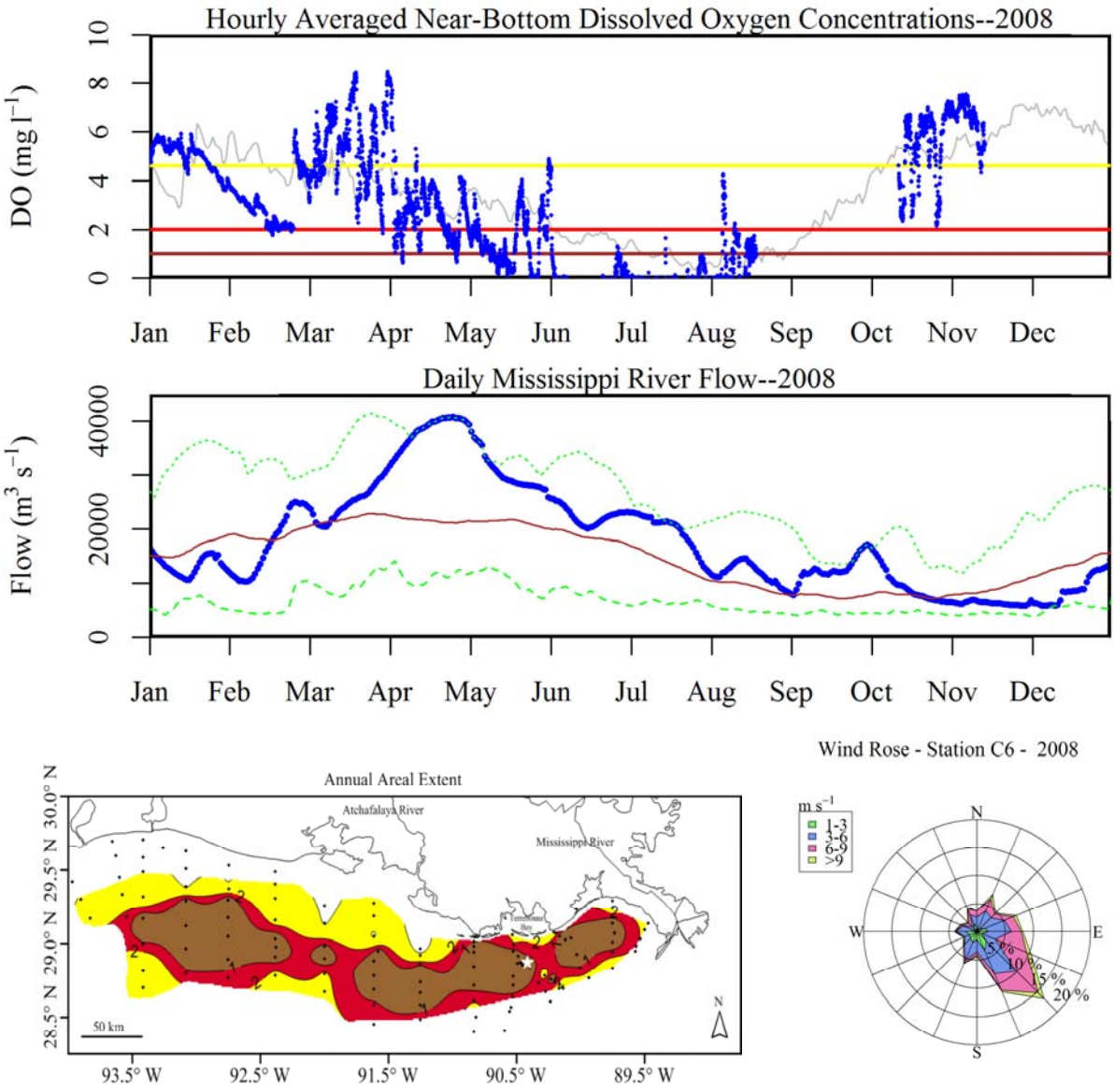

Figure A.20. Plots of various environmental parameters related to hypoxia at station C6 from 2008, upper panel: near-bottom dissolved oxygen (DO) time-series measured at C6 (19.5 m depth), middle panel: daily Mississippi River flow time-series measured at Tarbert Landing, MS., bottom left panel: bottom water DO concentrations as measured on the annual mid-summer shelf-wide cruise by LUMCON, bottom right panel: wind rose created from the NARR-A data set depicting the wind conditions at station C6. Further details are located on the first page of Appendix A.

APPENDIX B

PLOTS OF THE RESULTS FROM THE 35 MONTH-LONG TIME-SERIES

The plots in appendix B are the results of the time-series analysis from Chapter 3. Each group of plots represents the analysis for one of the 35 month-long time-series. All of the time-series were measured at station C6. The methods are described in Chapter 3.

The first plot group in each set represents the DO time-series and periodograms. Upper Panel: Hourly averages of dissolved oxygen concentrations in mg l^{-1} measured at 15 minute intervals. The green line represents the near-surface sensor (2 meters below the surface), the brown line represents mid-water column sensor (10.7 meters below the surface), and the blue line represents near-bottom sensor (19.5 meters below the surface). The red line represents hypoxic threshold (2.0 mg l-1). Lower panel: DO periodograms for near-surface (S), mid water-column (M), near-bottom (B) layers. Vertical red lines represent frequencies of interest from left to right O1 (25.8 hours), K1 (23.9 hours), and semi-diurnal (12 hours) tidal constituents. The blue line represents the null hypothesis for a 24-hour periodic signal. Vertical black line with a circle indicates the 95% confidence interval. The primary data source is a 20 year dataset collected from a single site in the NGOM. Chapter 2 describes these data in more detail. From 1998 through 1995, a single near-bottom-mounted sonde at 19.5 m below mean sea level collected DO concentrations and temperature at 15-minute intervals.

The second plot group of each set is time-series and periodograms for temperature, short-wave radiation, and water level (tides). The upper left panel shows hourly averages of near-bottom temperature. The lower left panel shows the periodogram for near-bottom temperature. The upper mid-panel shows short-wave radiation from NARR data at 3 hour intervals for this site. The lower mid-panel shows the periodogram for the short-wave radiation. The upper right panel shows hourly water level (labeled water height here) measurements from WAVCIS data

taken at the study site. The lower right panel shows the periodogram for the water level measurements. Vertical red lines represent frequencies of interest from left to right O1 (25.8 hours), K1 (23.9 hours), and semi-diurnal (12 hours) tidal constituents.

The next group of plots for each set is auto-correlation and cross-correlation plots. Left Panel: autocorrelation function (ACF) plots of DO concentrations from three depths, near surface (top), mid-water column (middle), and near-bottom (bottom) for Middle Panel: cross-correlation function (CCF) plots of DO concentrations between depths. Right Panel: cross-correlation function (CCF) plots between near-bottom DO concentrations and the factors, temperature, water level, and PAR.

August 1997 (199708)

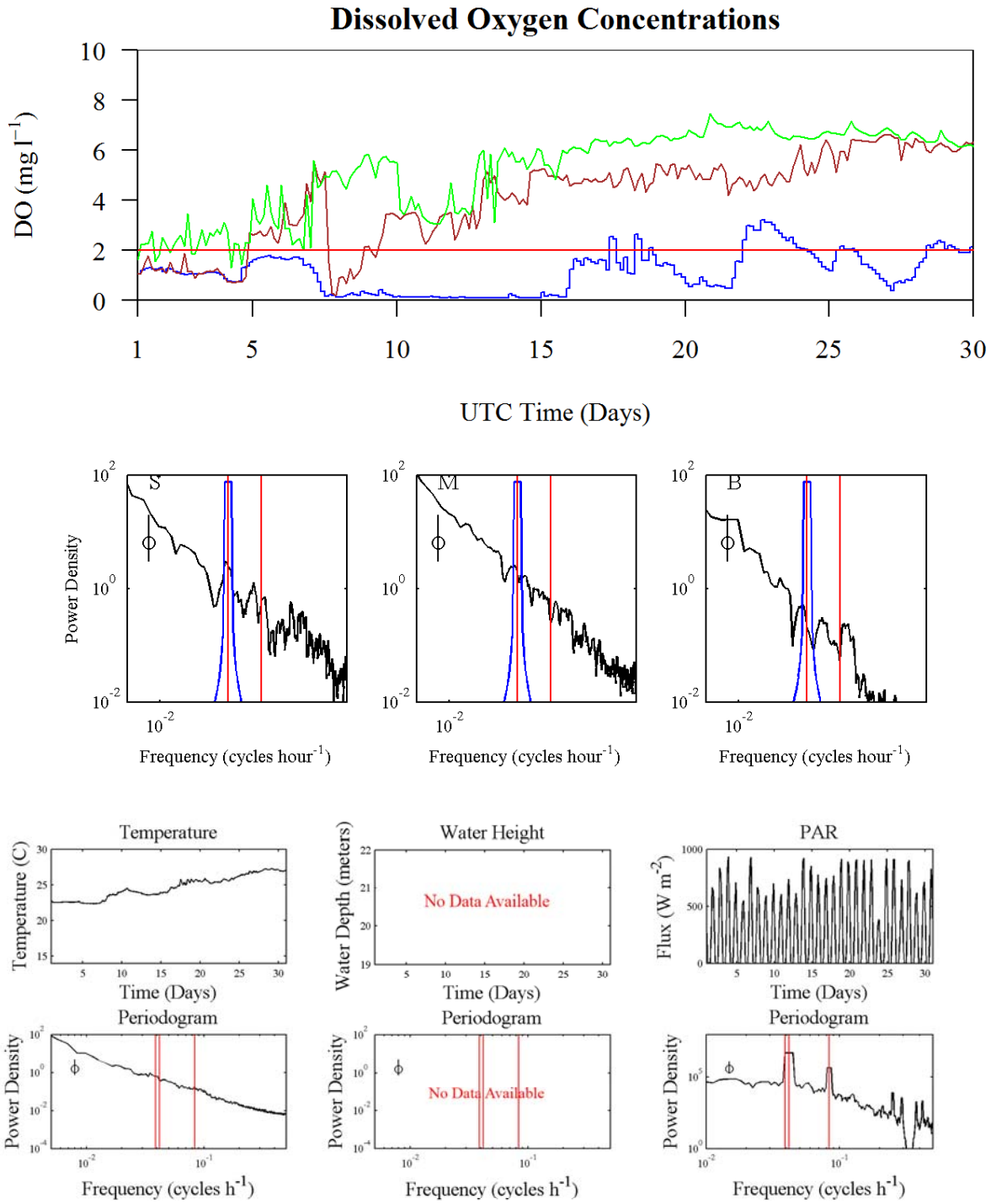

Figure B.1. Time-series plots and periodograms of dissolved oxygen (DO) concentrations and factors affecting DO concentrations for the month August 1997. Further details are located on the first page of Appendix B.

August 1997 (199708)

Autocorrelations and Cross Correlations

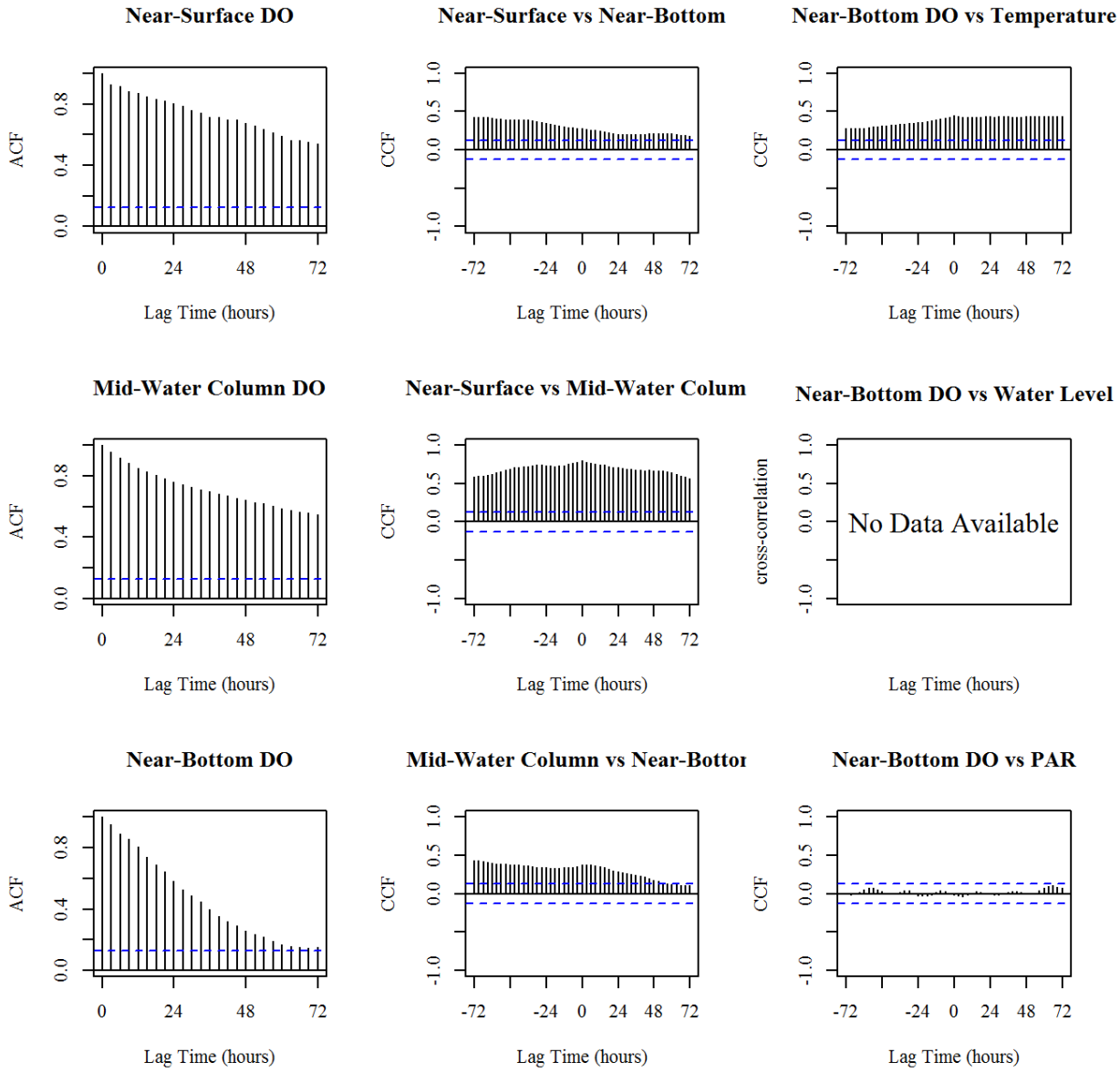

Figure B.2. Results for the month August 1997 (199708). Left Panel: Autocorrelation function (ACF) plots of DO concentrations from three depths, near surface (top), mid-water column (middle), and near-bottom (bottom); Middle Panel: Cross-correlation function (CCF) plots of DO concentrations between depths; Right Panel: Cross-correlation function (CCF) plots between near-bottom DO concentrations and the factors, temperature, water level, and PAR. Blue dotted lines represent 95% confidence limits. Further details are located on the first page of Appendix B.

September 1997 (199709)

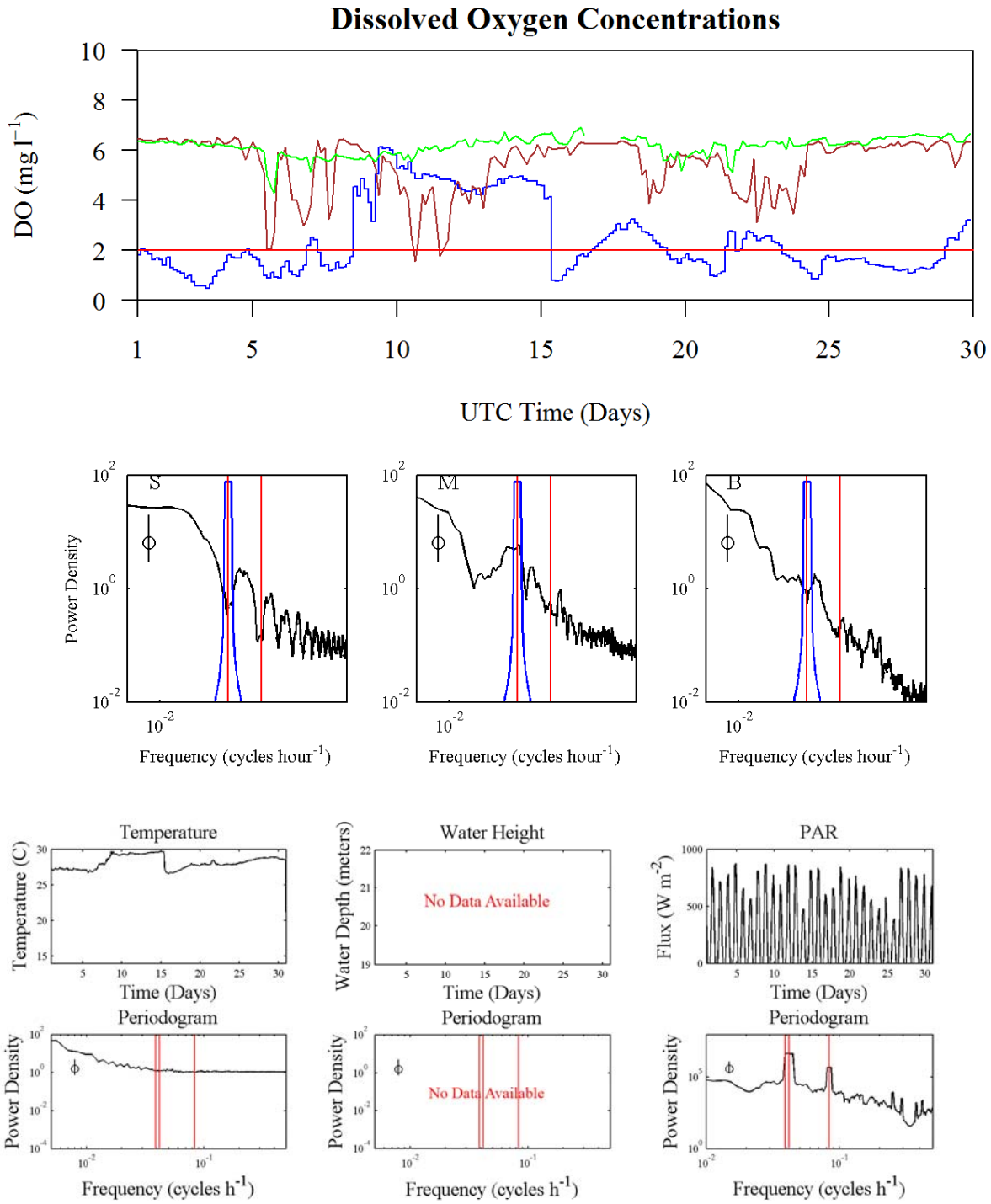

Figure B.2. Time-series plots and periodograms of dissolved oxygen (DO) concentrations and factors affecting DO concentrations for the month September 1997. Further details are located on the first page of Appendix B.

September 1997 (199709)

Autocorrelations and Cross Correlations

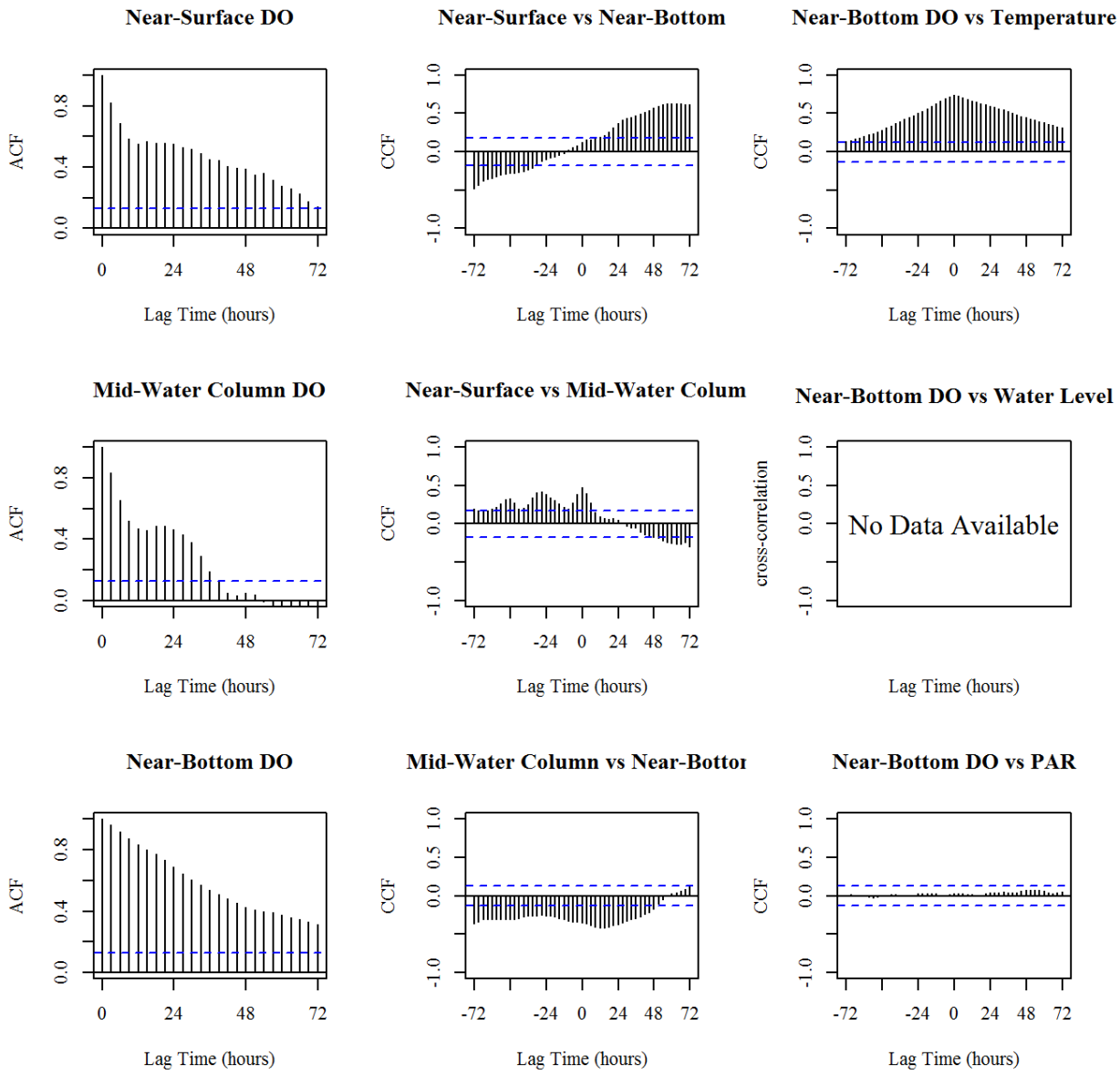

Figure B.3. Results for the month September 1997 (199709). Left Panel: Autocorrelation function (ACF) plots of DO concentrations from three depths, near surface (top), mid-water column (middle), and near-bottom (bottom); Middle Panel: Cross-correlation function (CCF) plots of DO concentrations between depths; Right Panel: Cross-correlation function (CCF) plots between near-bottom DO concentrations and the factors, temperature, water level, and PAR. Blue dotted lines represent 95% confidence limits. Further details are located on the first page of Appendix B.

May 1998 (199805)

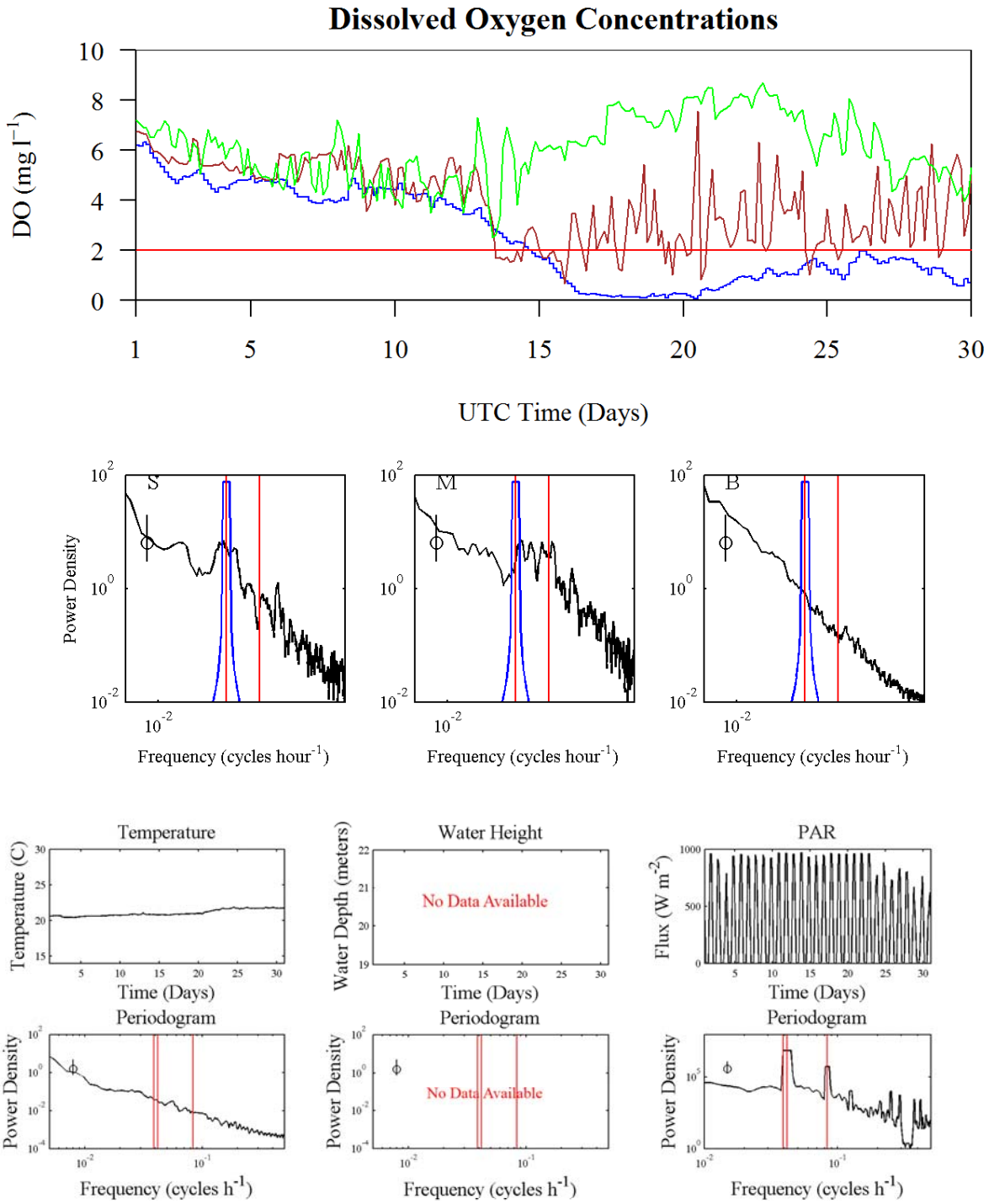

Figure B.3. Time-series plots and periodograms of dissolved oxygen (DO) concentrations and factors affecting DO concentrations for the month May 1998. Further details are located on the first page of Appendix B.

May 1998 (199805)

Autocorrelations and Cross Correlations

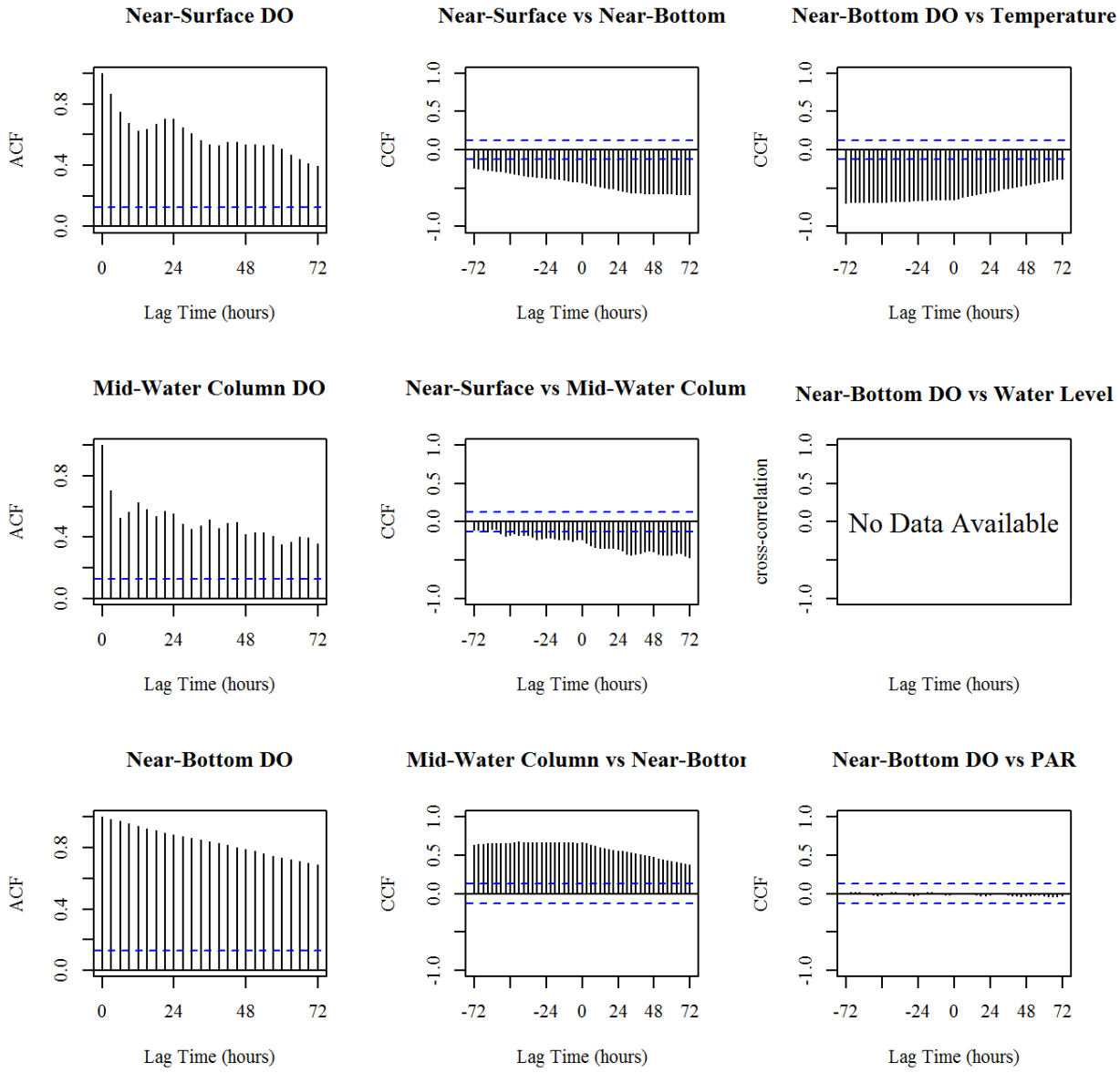

Figure B.4. Results for the month May 1998 (199805). Left Panel: Autocorrelation function (ACF) plots of DO concentrations from three depths, near surface (top), mid-water column (middle), and near-bottom (bottom); Middle Panel: Cross-correlation function (CCF) plots of DO concentrations between depths; Right Panel: Cross-correlation function (CCF) plots between near-bottom DO concentrations and the factors, temperature, water level, and PAR. Blue dotted lines represent 95% confidence limits. Further details are located on the first page of Appendix B.

June 1998 (199806)

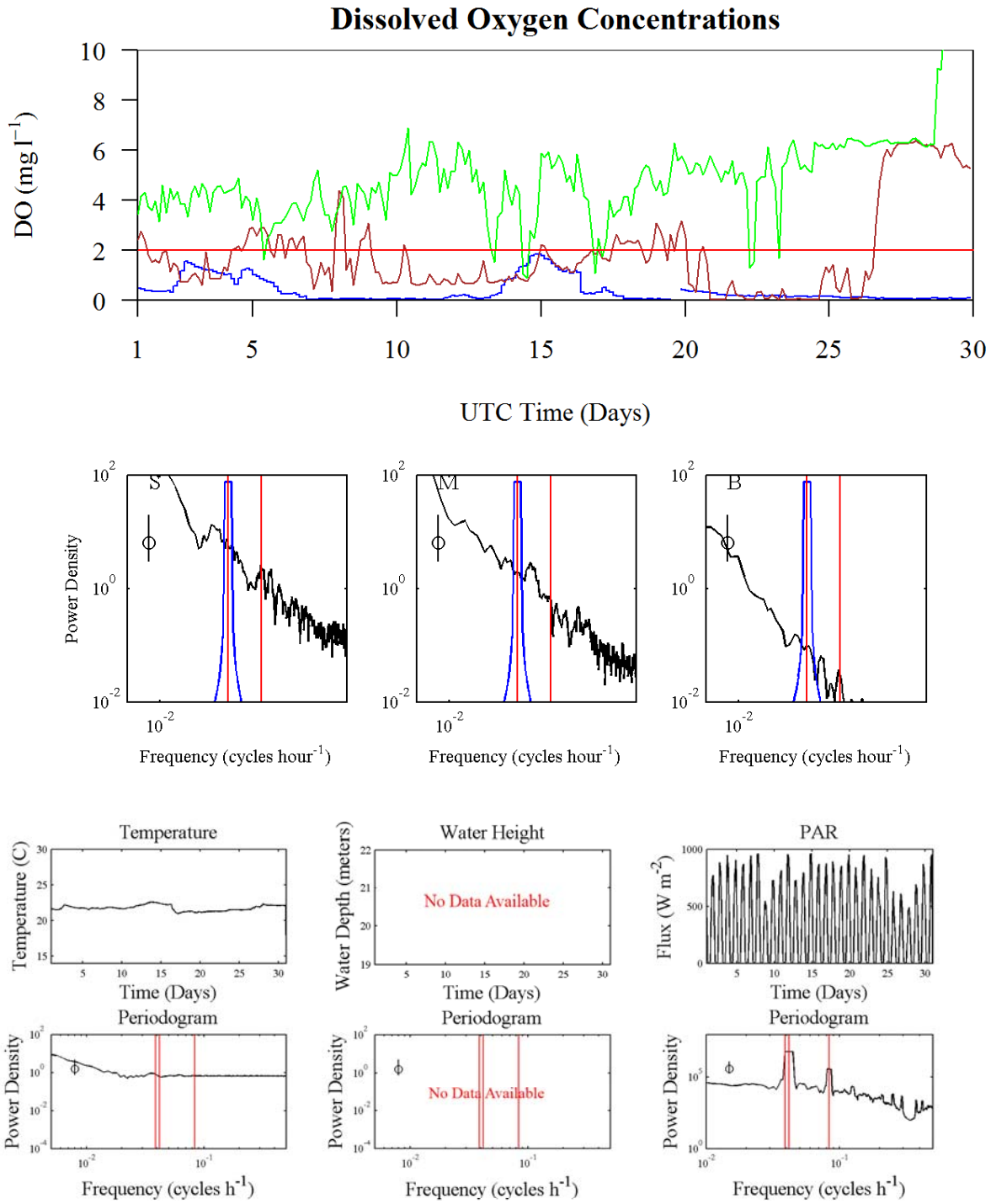

Figure B.4. Time-series plots and periodograms of dissolved oxygen (DO) concentrations and factors affecting DO concentrations for the month June 1998. Further details are located on the first page of Appendix B.

June 1998 (199806)

Autocorrelations and Cross Correlations

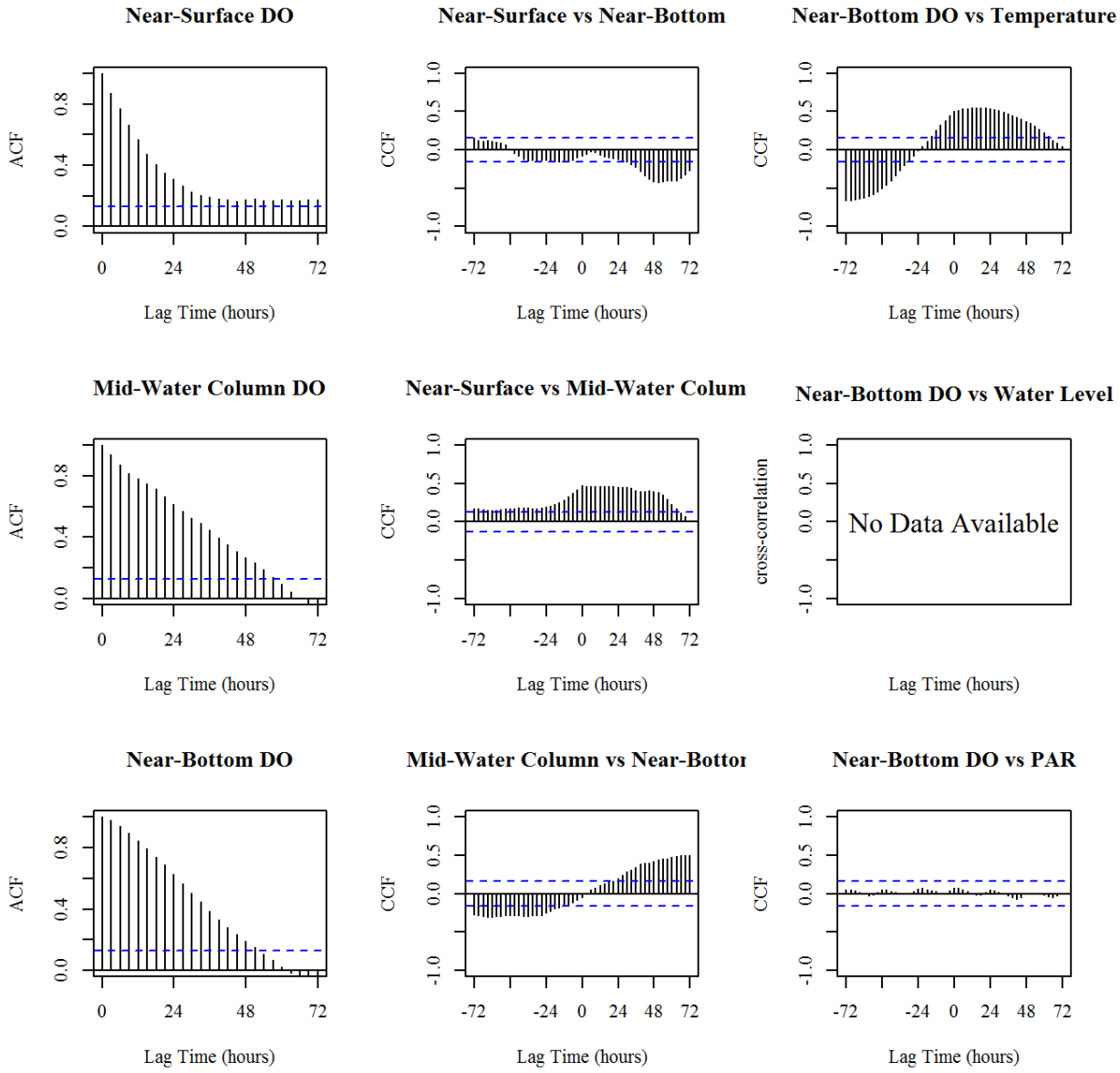

Figure B.5. Results for the month June 1998 (199806). Left Panel: Autocorrelation function (ACF) plots of DO concentrations from three depths, near surface (top), mid-water column (middle), and near-bottom (bottom); Middle Panel: Cross-correlation function (CCF) plots of DO concentrations between depths; Right Panel: Cross-correlation function (CCF) plots between near-bottom DO concentrations and the factors, temperature, water level, and PAR. Blue dotted lines represent 95% confidence limits. Further details are located on the first page of Appendix B.

July 1998 (199807)

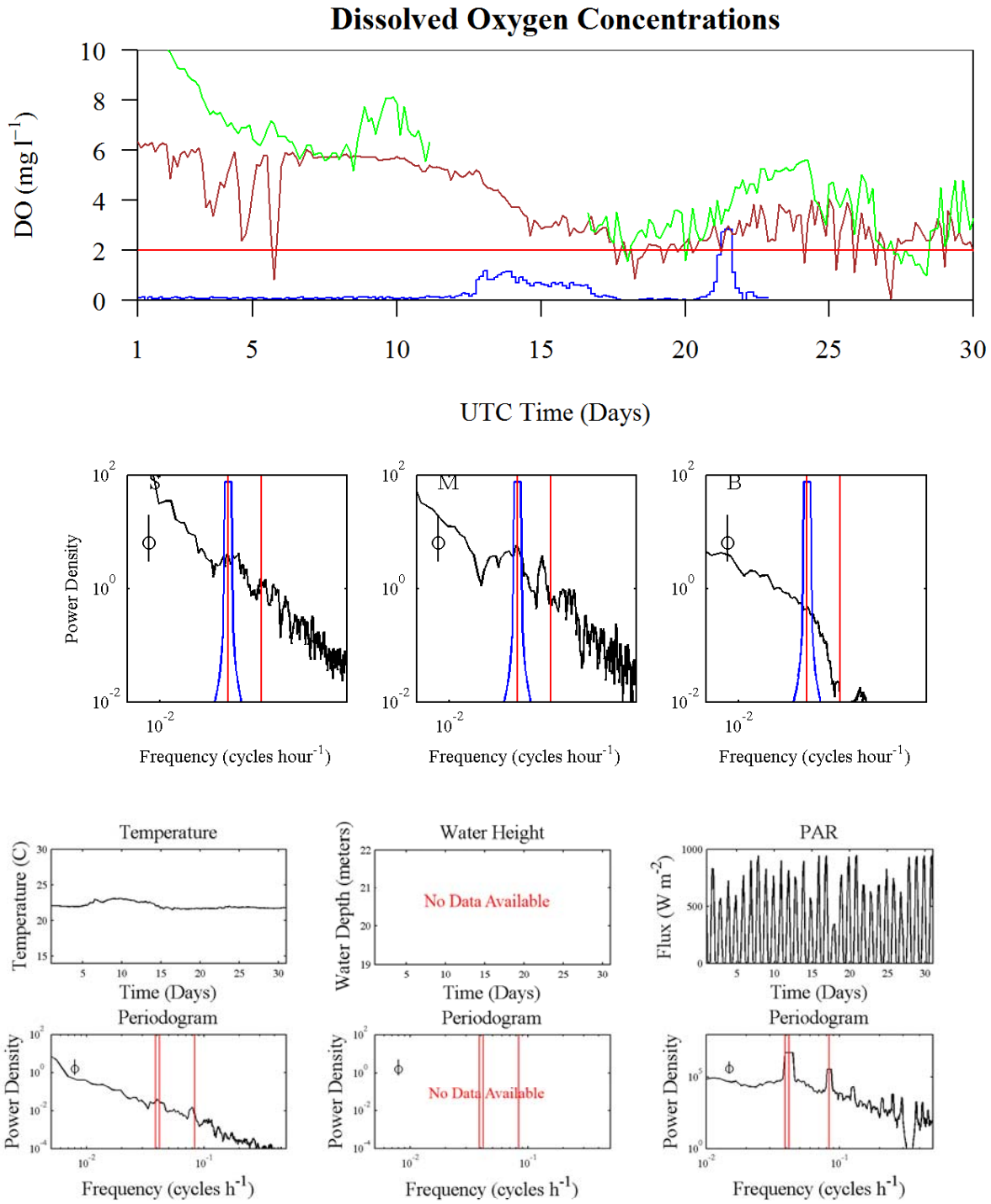

Figure B.5. Time-series plots and periodograms of dissolved oxygen (DO) concentrations and factors affecting DO concentrations for the month July 1998. Further details are located on the first page of Appendix B.

July 1998 (199807)

Autocorrelations and Cross Correlations

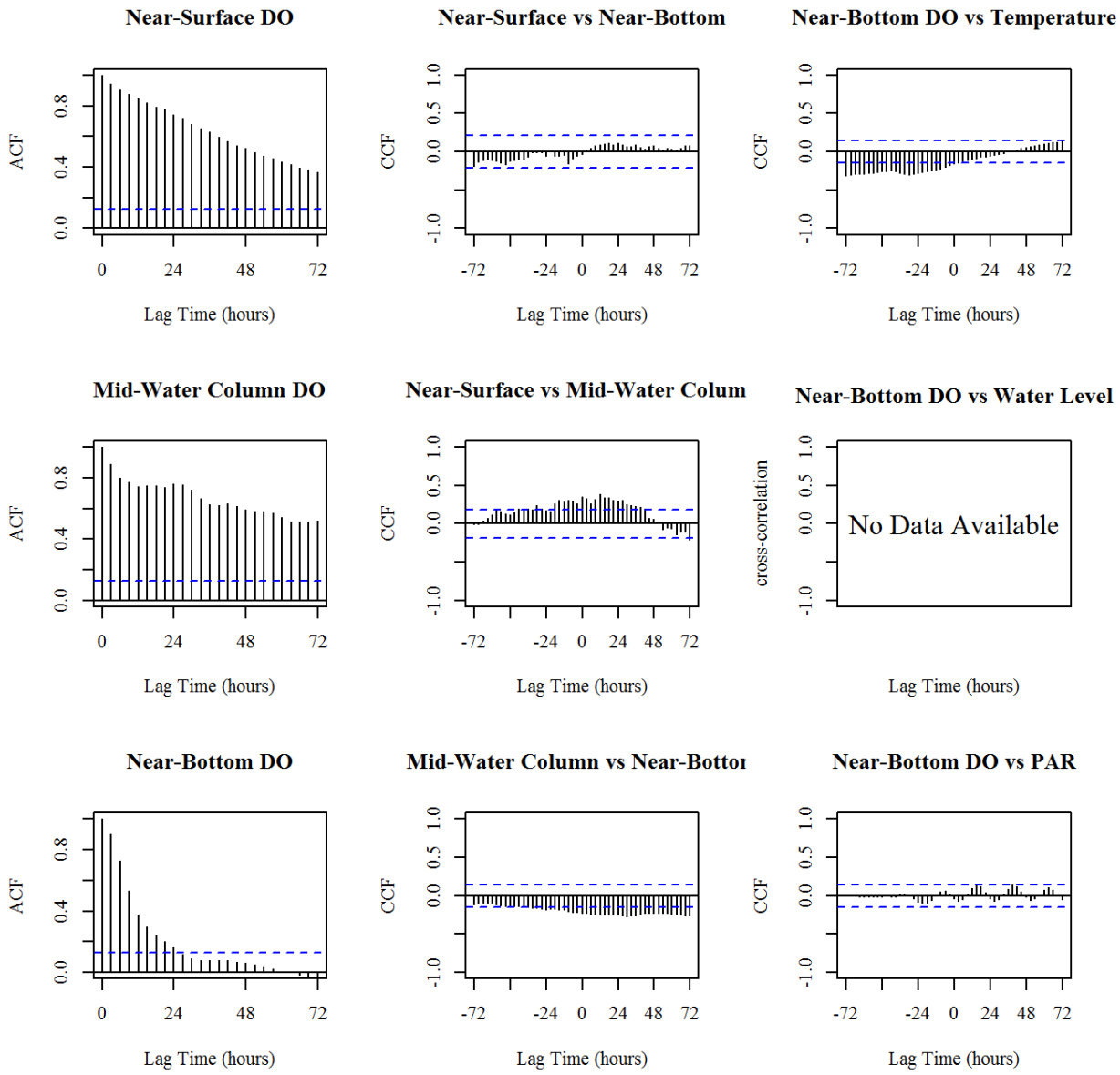

Figure B.6. Results for the month July 1998 (199807). Left Panel: Autocorrelation function (ACF) plots of DO concentrations from three depths, near surface (top), mid-water column (middle), and near-bottom (bottom); Middle Panel: Cross-correlation function (CCF) plots of DO concentrations between depths; Right Panel: Cross-correlation function (CCF) plots between near-bottom DO concentrations and the factors, temperature, water level, and PAR. Blue dotted lines represent 95% confidence limits. Further details are located on the first page of Appendix B.

March 1999 (199903)

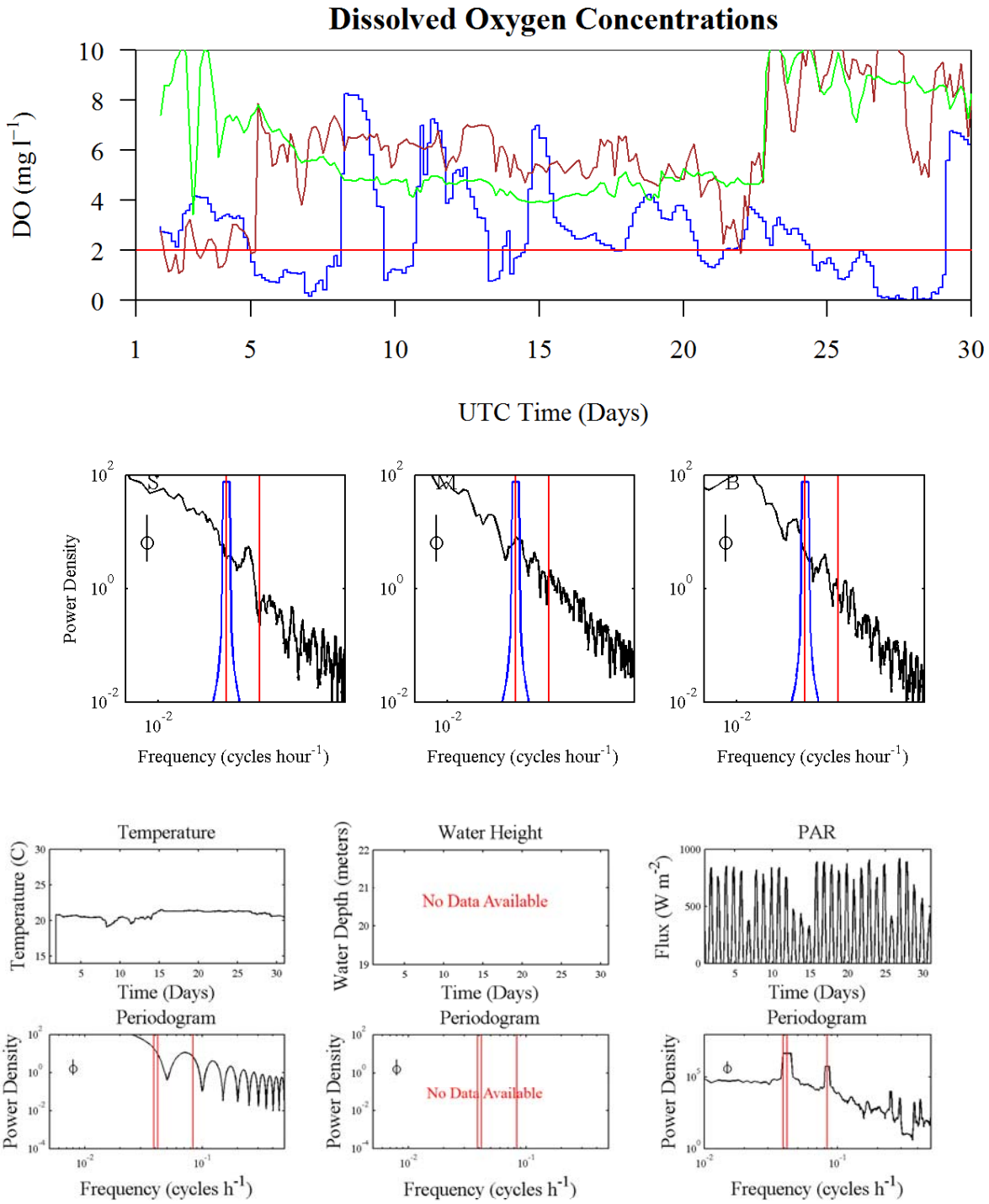

Figure B.6. Time-series plots and periodograms of dissolved oxygen (DO) concentrations and factors affecting DO concentrations for the month March 1999. Further details are located on the first page of Appendix B.

March 1999 (199903)

Autocorrelations and Cross Correlations

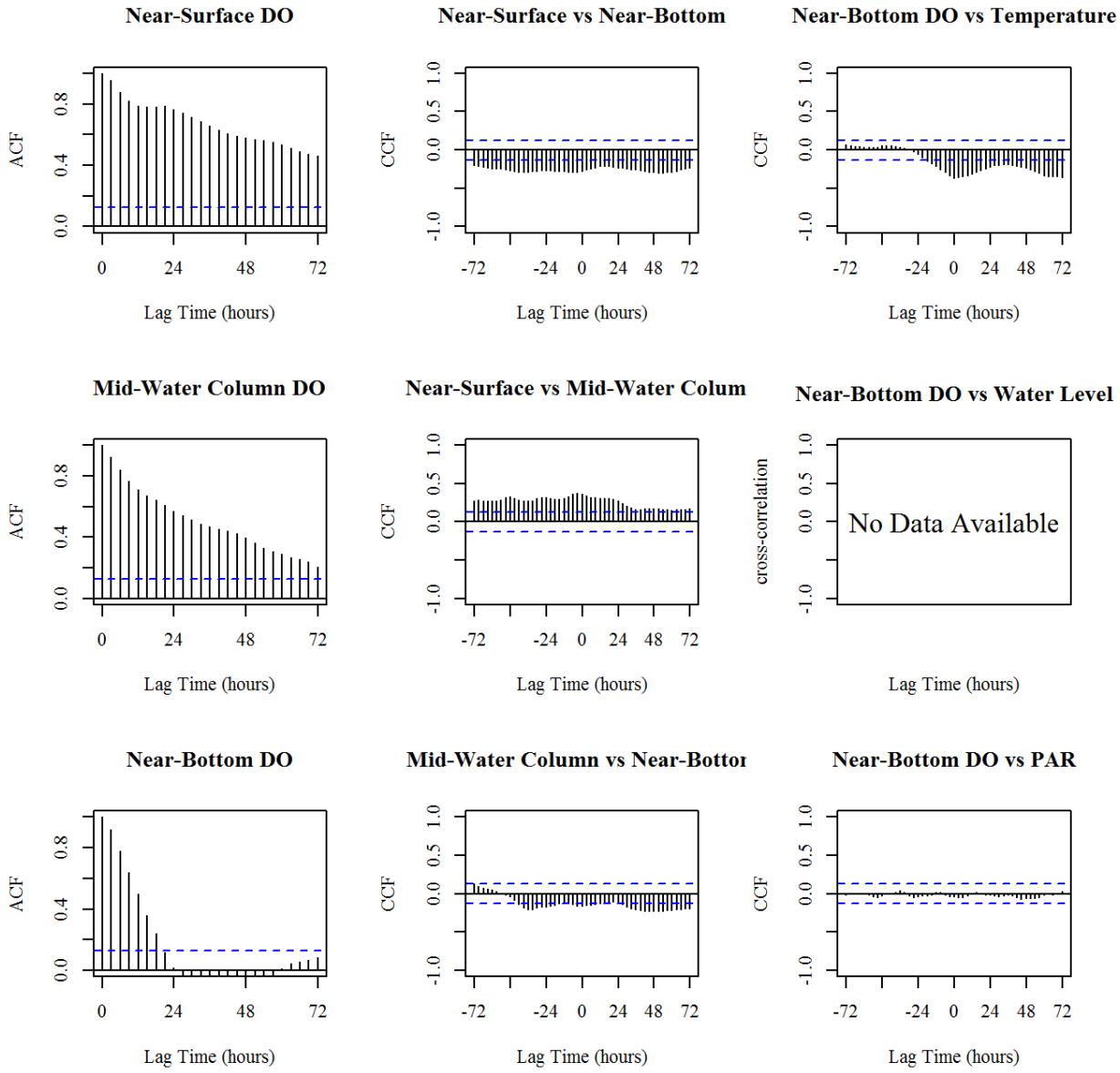

Figure B.7. Results for the month March 1999 (199903). Left Panel: Autocorrelation function (ACF) plots of DO concentrations from three depths, near surface (top), mid-water column (middle), and near-bottom (bottom); Middle Panel: Cross-correlation function (CCF) plots of DO concentrations between depths; Right Panel: Cross-correlation function (CCF) plots between near-bottom DO concentrations and the factors, temperature, water level, and PAR. Blue dotted lines represent 95% confidence limits. Further details are located on the first page of Appendix B.

April 1999 (199904)

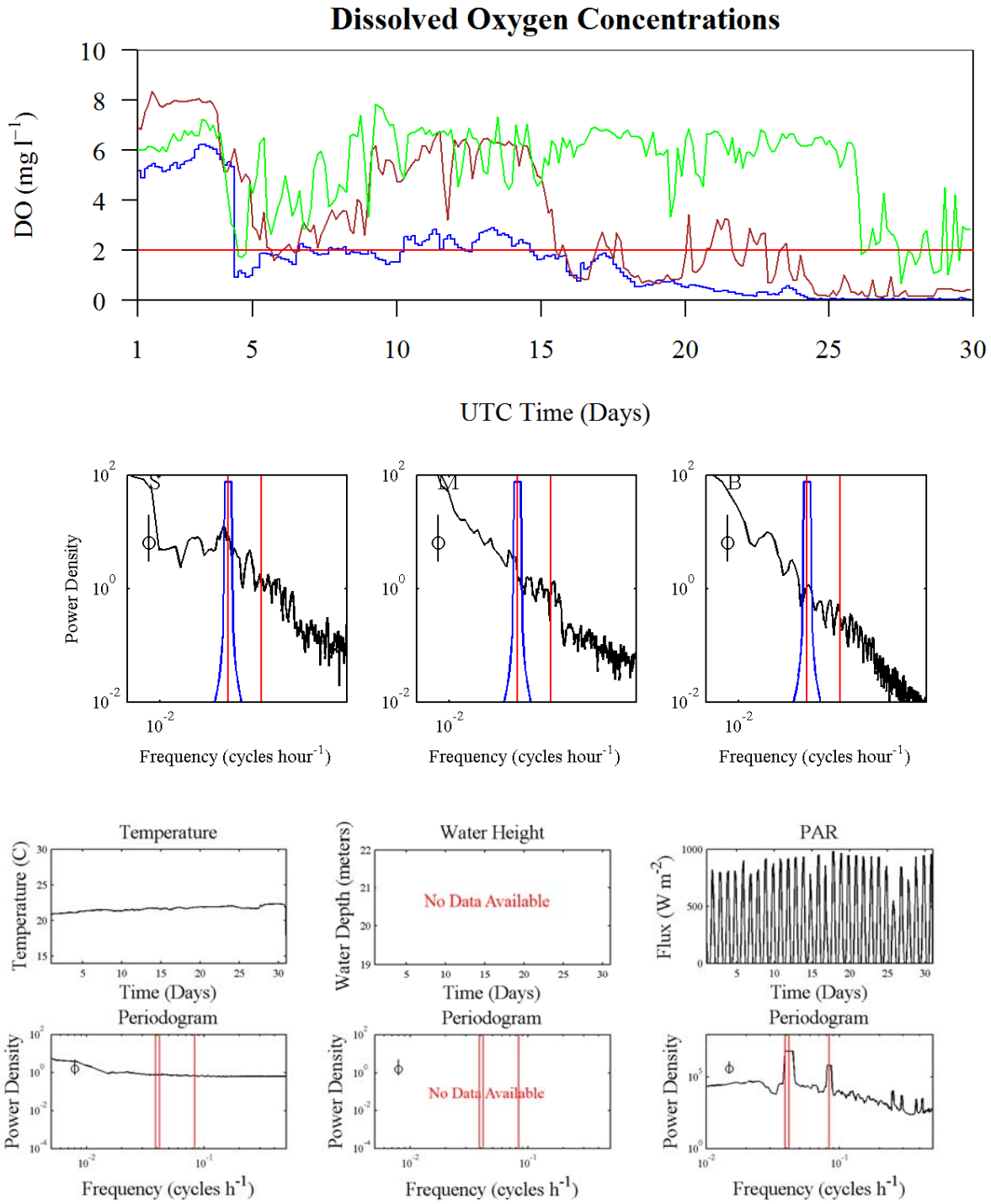

Figure B.7. Time-series plots and periodograms of dissolved oxygen (DO) concentrations and factors affecting DO concentrations for the month April 1999. Further details are located on the first page of Appendix B.

April 1999 (199904)

Autocorrelations and Cross Correlations

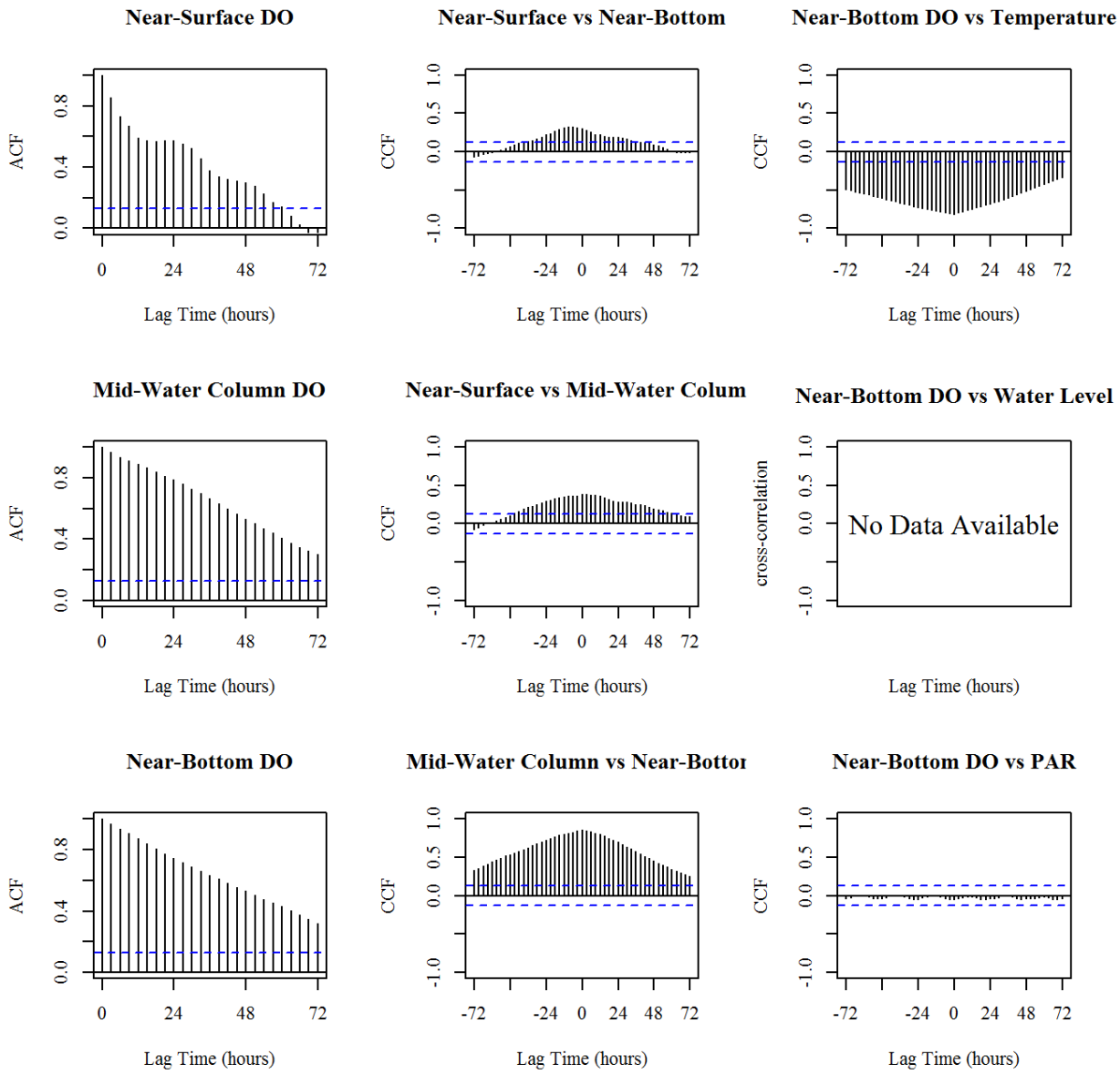

Figure B.8. Results for the month April 1999 (199904). Left Panel: Autocorrelation function (ACF) plots of DO concentrations from three depths, near surface (top), mid-water column (middle), and near-bottom (bottom); Middle Panel: Cross-correlation function (CCF) plots of DO concentrations between depths; Right Panel: Cross-correlation function (CCF) plots between near-bottom DO concentrations and the factors, temperature, water level, and PAR. Blue dotted lines represent 95% confidence limits. Further details are located on the first page of Appendix B.

May 1999 (199905)

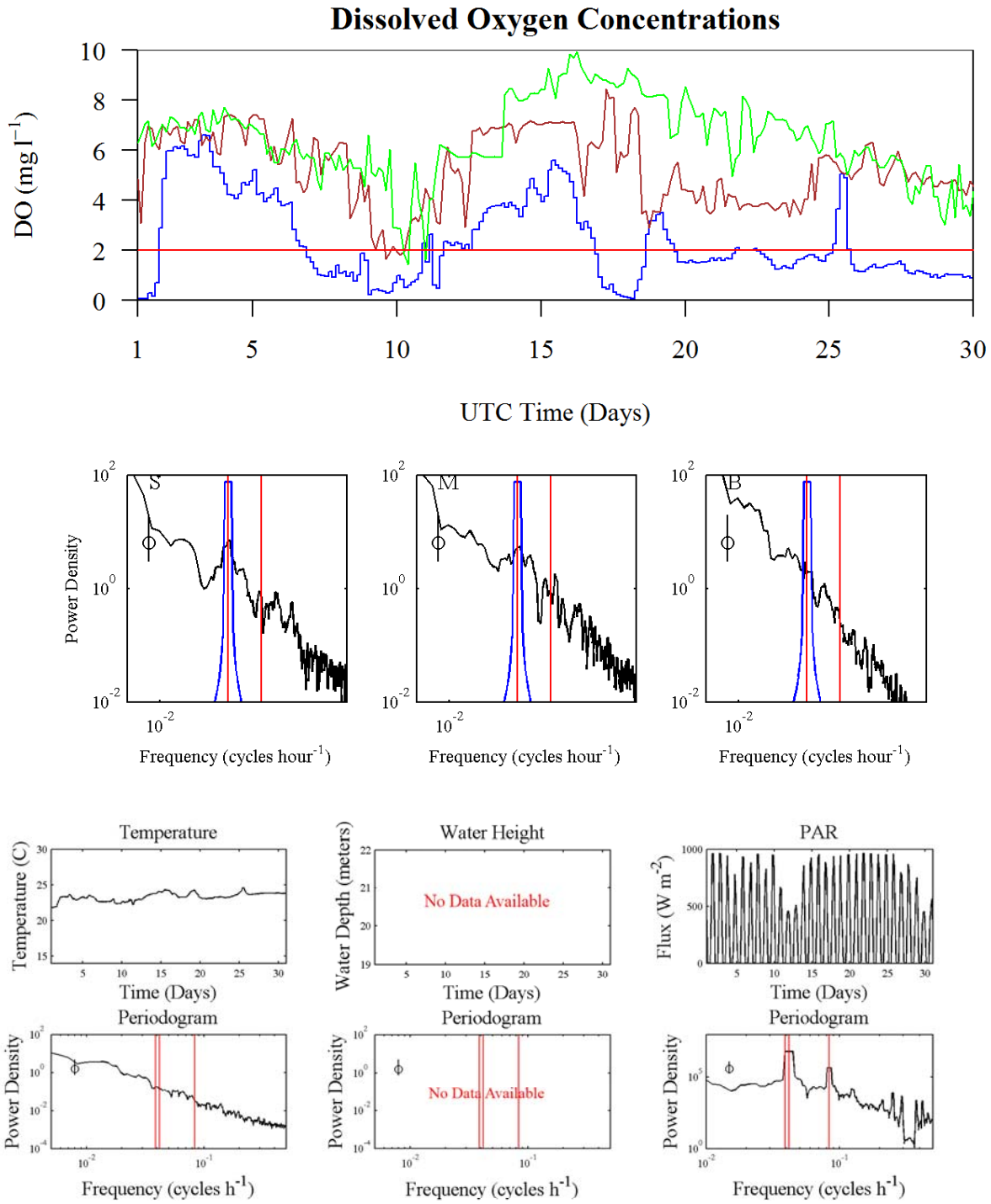

Figure B.8. Time-series plots and periodograms of dissolved oxygen (DO) concentrations and factors affecting DO concentrations for the month May 1999. Further details are located on the first page of Appendix B.

May 1999 (199905)

Autocorrelations and Cross Correlations

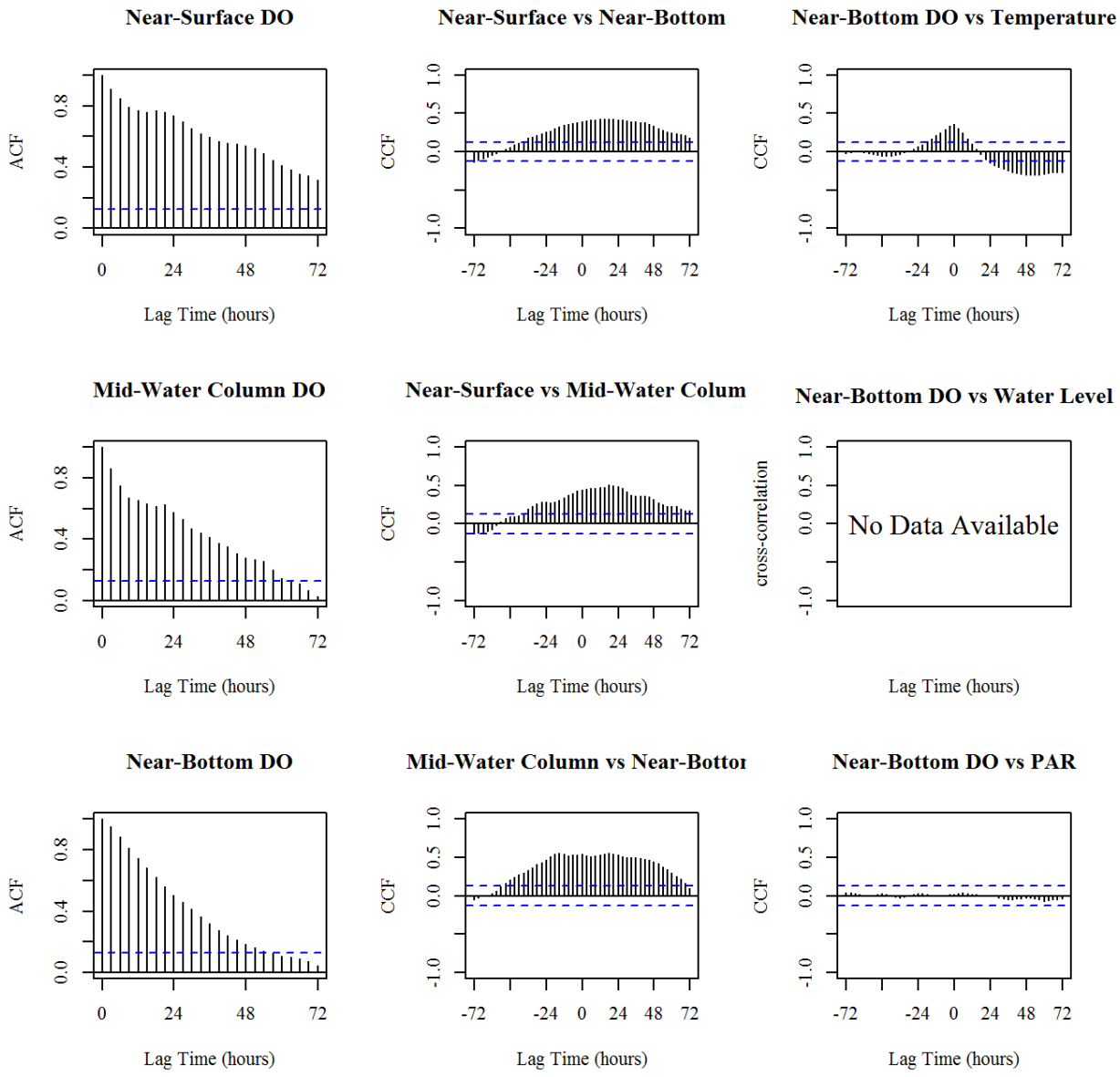

Figure B.9. Results for the month May 1999 (199905). Left Panel: Autocorrelation function (ACF) plots of DO concentrations from three depths, near surface (top), mid-water column (middle), and near-bottom (bottom); Middle Panel: Cross-correlation function (CCF) plots of DO concentrations between depths; Right Panel: Cross-correlation function (CCF) plots between near-bottom DO concentrations and the factors, temperature, water level, and PAR. Blue dotted lines represent 95% confidence limits. Further details are located on the first page of Appendix B.

June 1999 (199906)

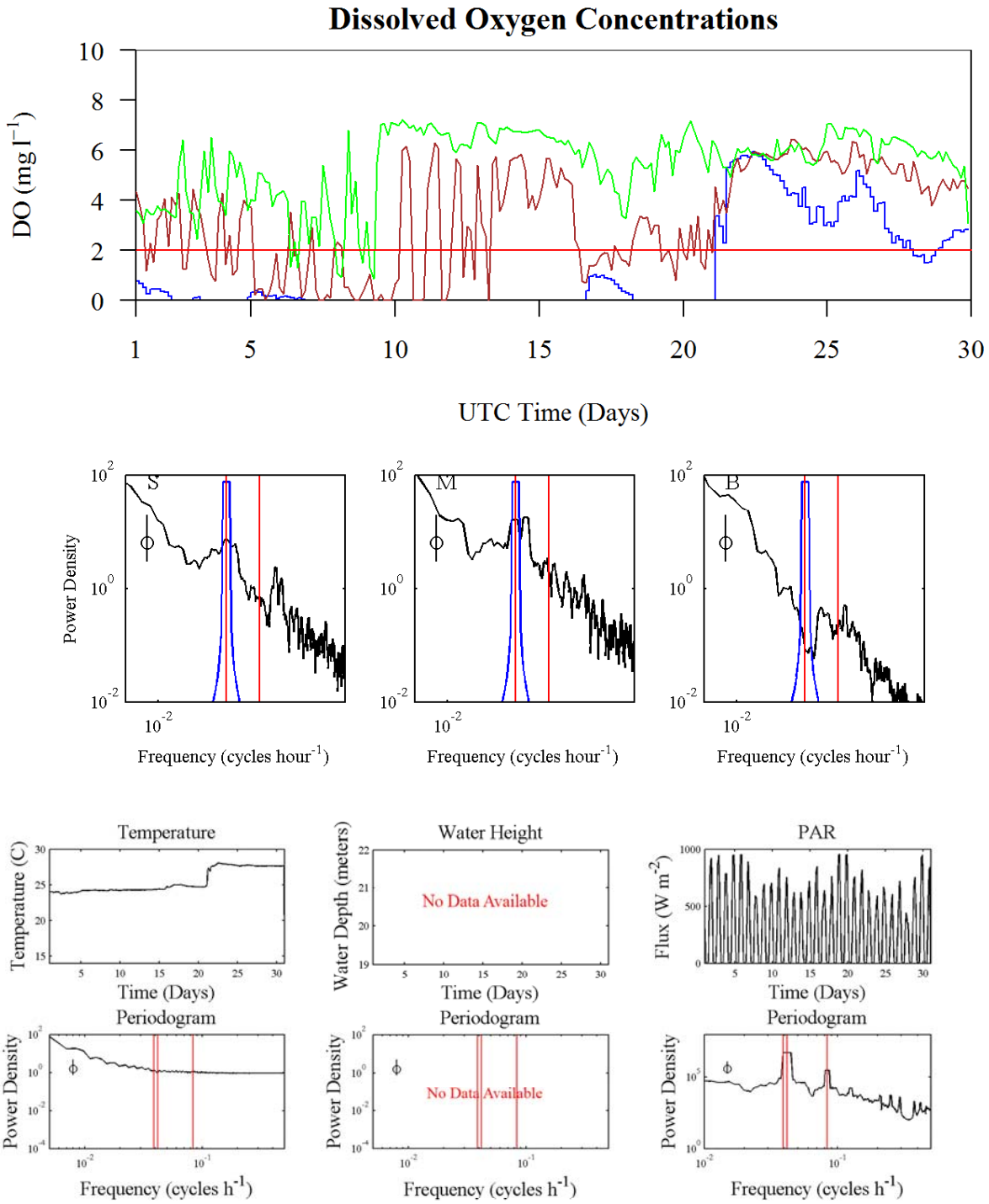

Figure B.9. Time-series plots and periodograms of dissolved oxygen (DO) concentrations and factors affecting DO concentrations for the month June 1999. Further details are located on the first page of Appendix B.

June 1999 (199906)

Autocorrelations and Cross Correlations

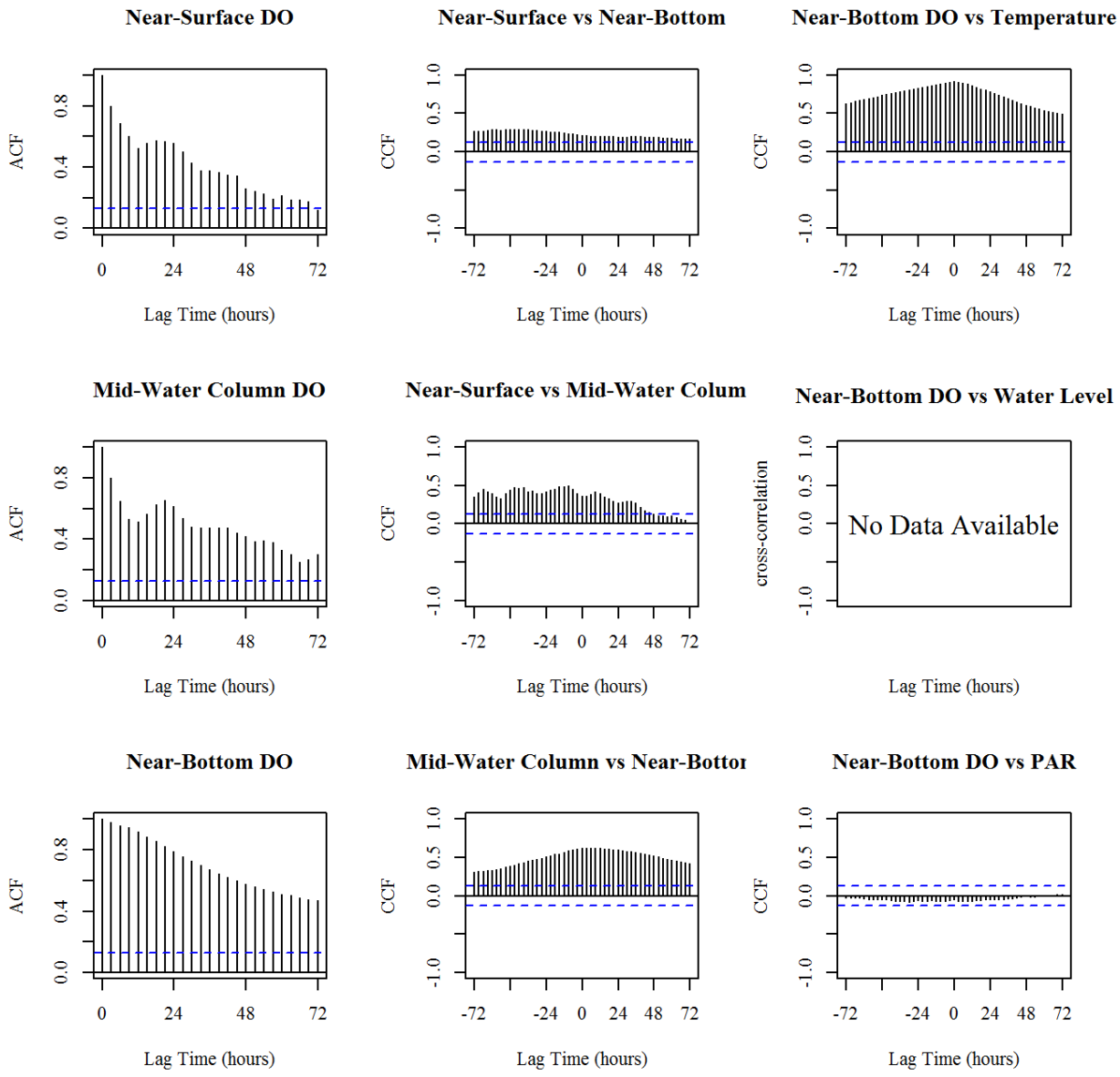

Figure B.10. Results for the month June 1999 (199906). Left Panel: Autocorrelation function (ACF) plots of DO concentrations from three depths, near surface (top), mid-water column (middle), and near-bottom (bottom); Middle Panel: Cross-correlation function (CCF) plots of DO concentrations between depths; Right Panel: Cross-correlation function (CCF) plots between near-bottom DO concentrations and the factors, temperature, water level, and PAR. Blue dotted lines represent 95% confidence limits. Further details are located on the first page of Appendix B.

July 1999 (199907)

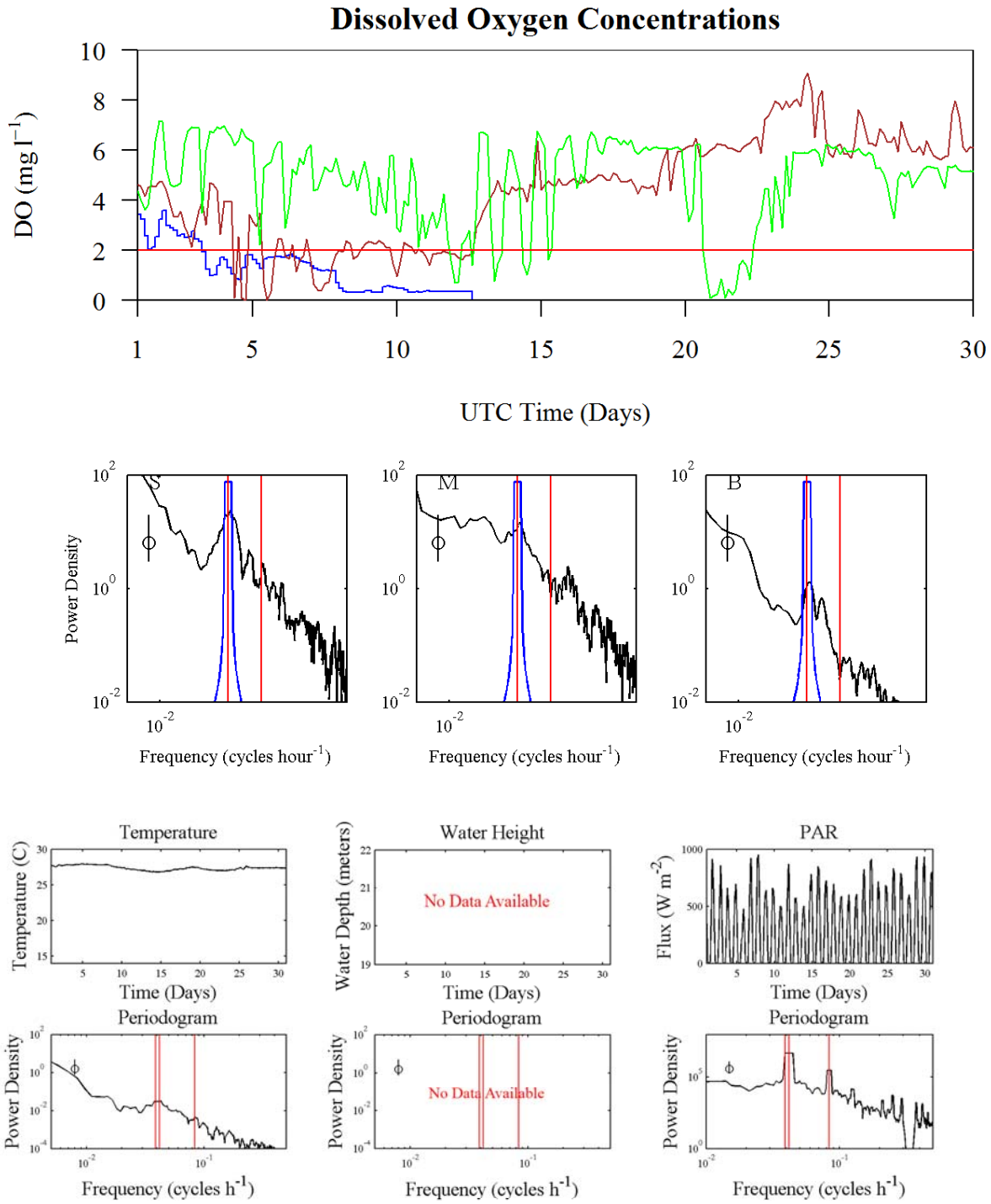

Figure B.10. Time-series plots and periodograms of dissolved oxygen (DO) concentrations and factors affecting DO concentrations for the month July 1999. Further details are located on the first page of Appendix B.

July 1999 (199907)

Autocorrelations and Cross Correlations

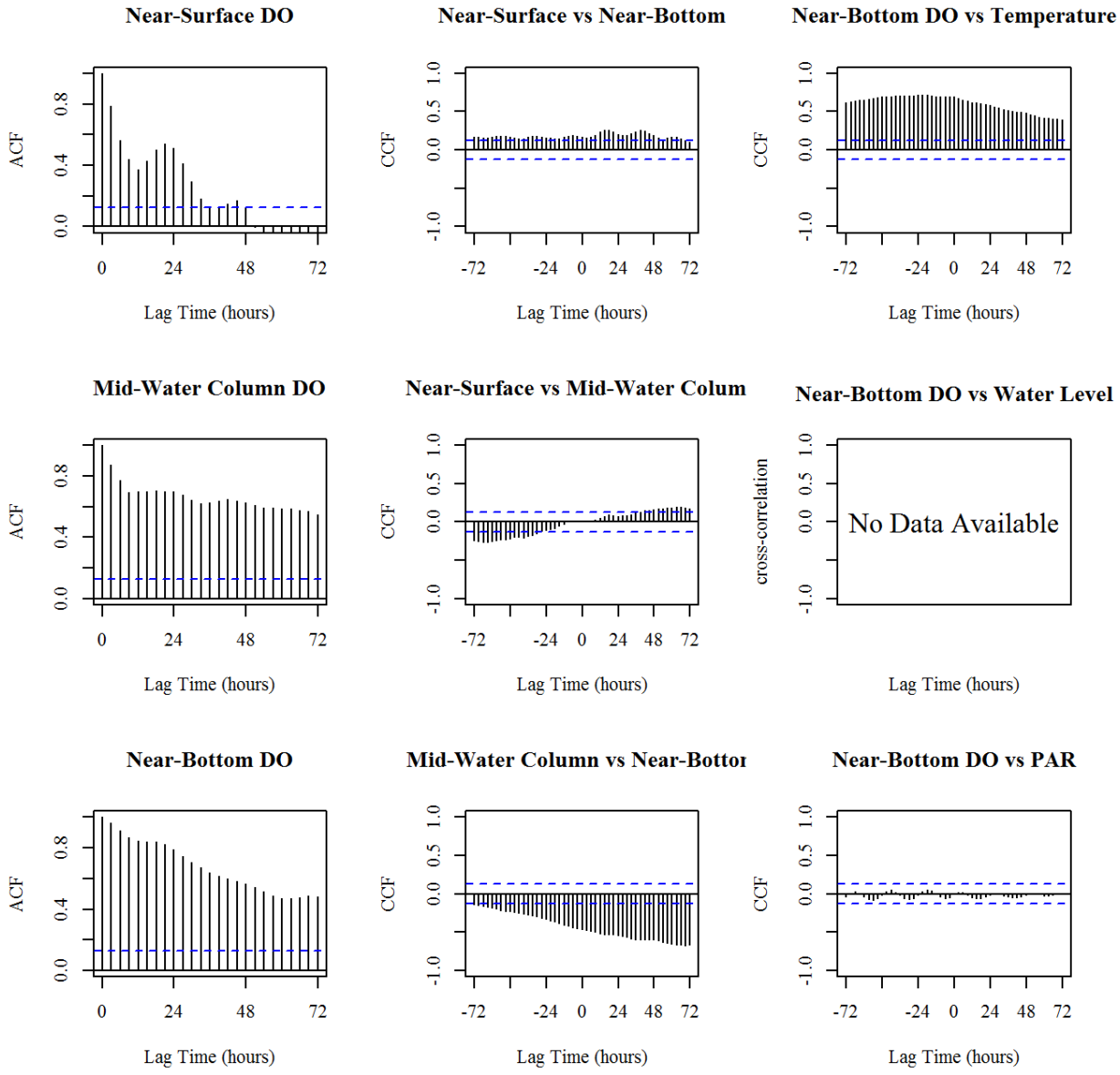

Figure B.11. Results for the month July 1999 (199907). Left Panel: Autocorrelation function (ACF) plots of DO concentrations from three depths, near surface (top), mid-water column (middle), and near-bottom (bottom); Middle Panel: Cross-correlation function (CCF) plots of DO concentrations between depths; Right Panel: Cross-correlation function (CCF) plots between near-bottom DO concentrations and the factors, temperature, water level, and PAR. Blue dotted lines represent 95% confidence limits. Further details are located on the first page of Appendix B.

September 1999 (199909)

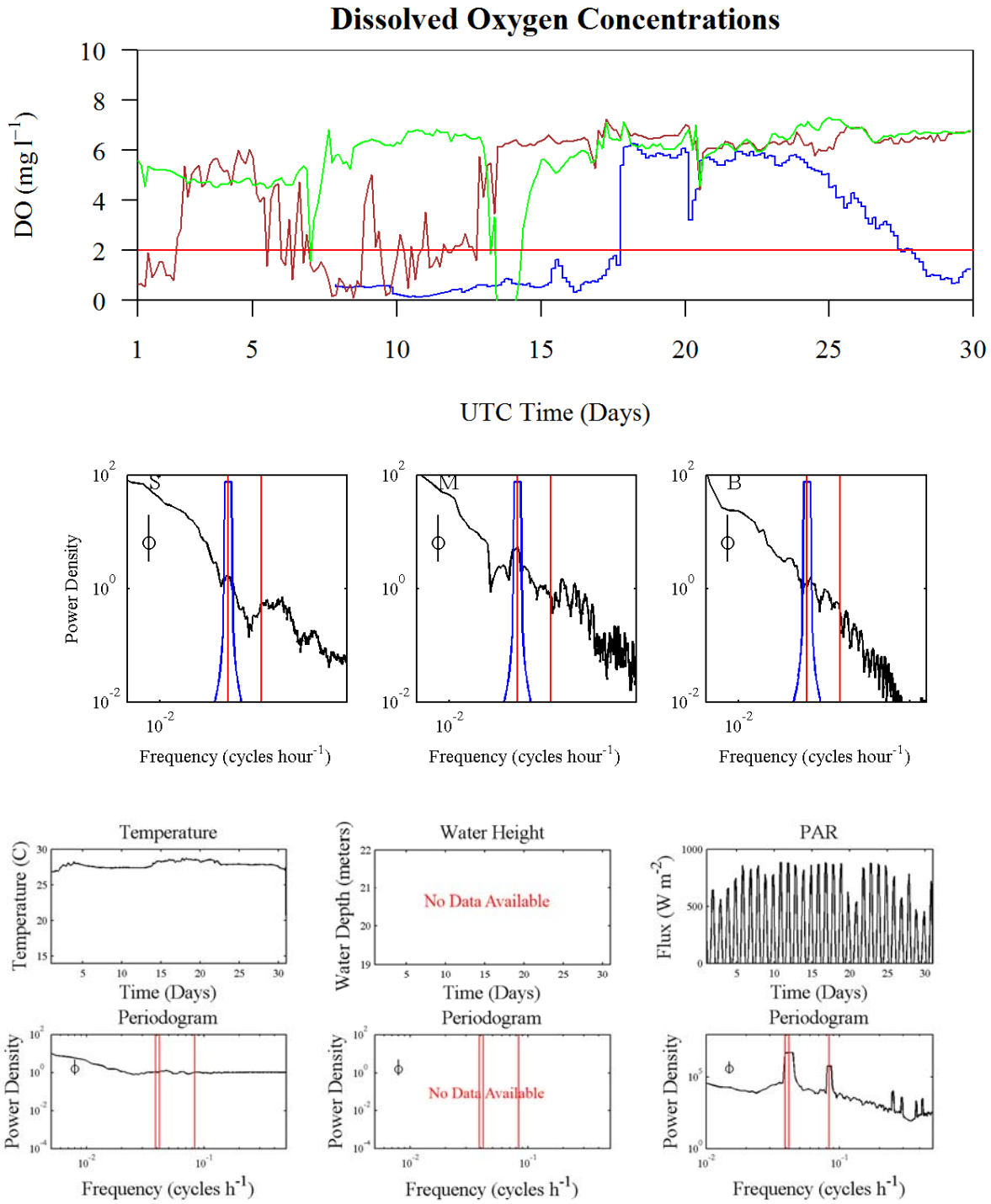

Figure B.11. Time-series plots and periodograms of dissolved oxygen (DO) concentrations and factors affecting DO concentrations for the month September 1999. Further details are located on the first page of Appendix B.

September 1999 (199909)

Autocorrelations and Cross Correlations

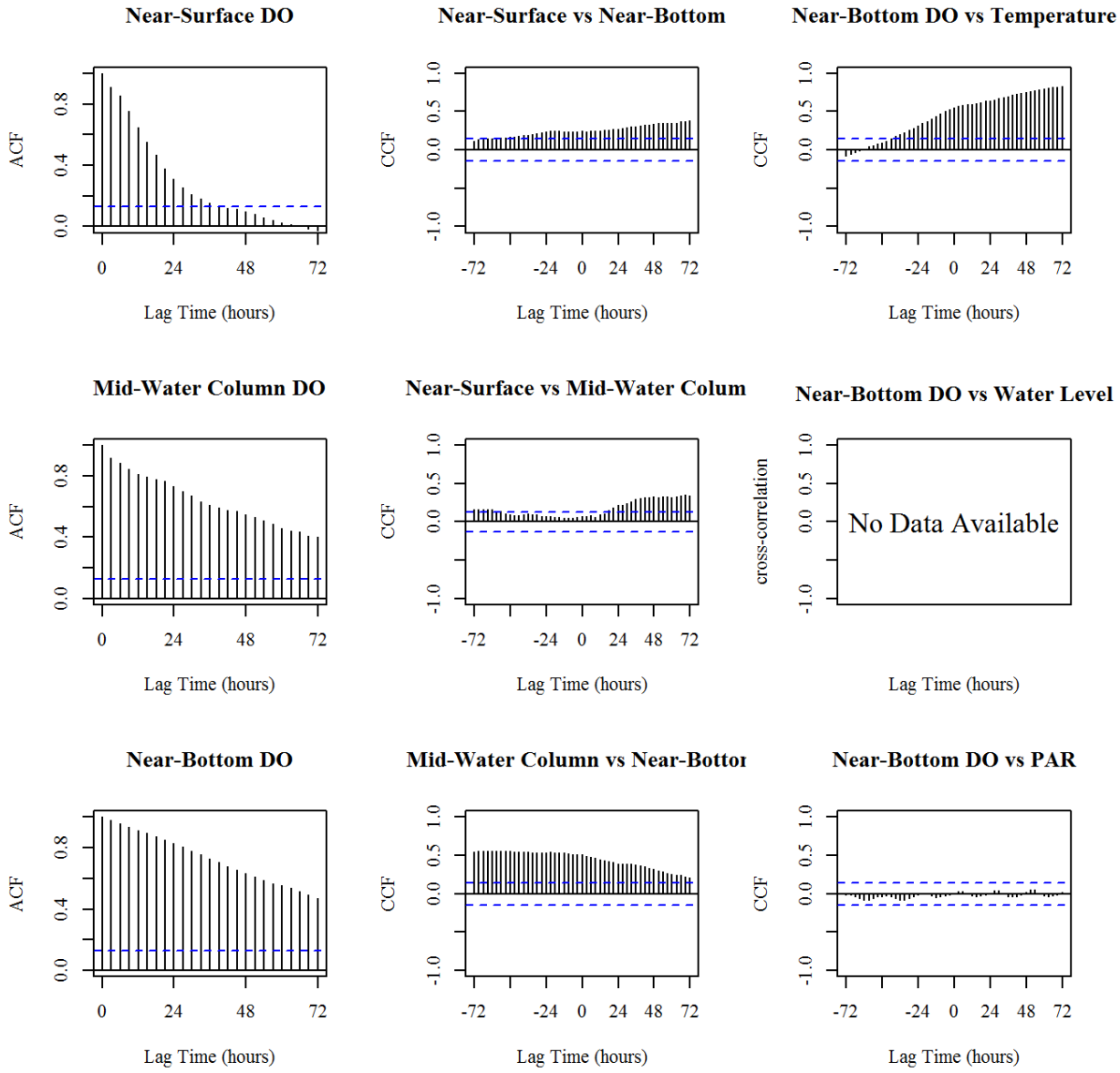

Figure B.12. Results for the month September 1999 (199909). Left Panel: Autocorrelation function (ACF) plots of DO concentrations from three depths, near surface (top), mid-water column (middle), and near-bottom (bottom); Middle Panel: Cross-correlation function (CCF) plots of DO concentrations between depths; Right Panel: Cross-correlation function (CCF) plots between near-bottom DO concentrations and the factors, temperature, water level, and PAR. Blue dotted lines represent 95% confidence limits. Further details are located on the first page of Appendix B.

May 2000 (200005)

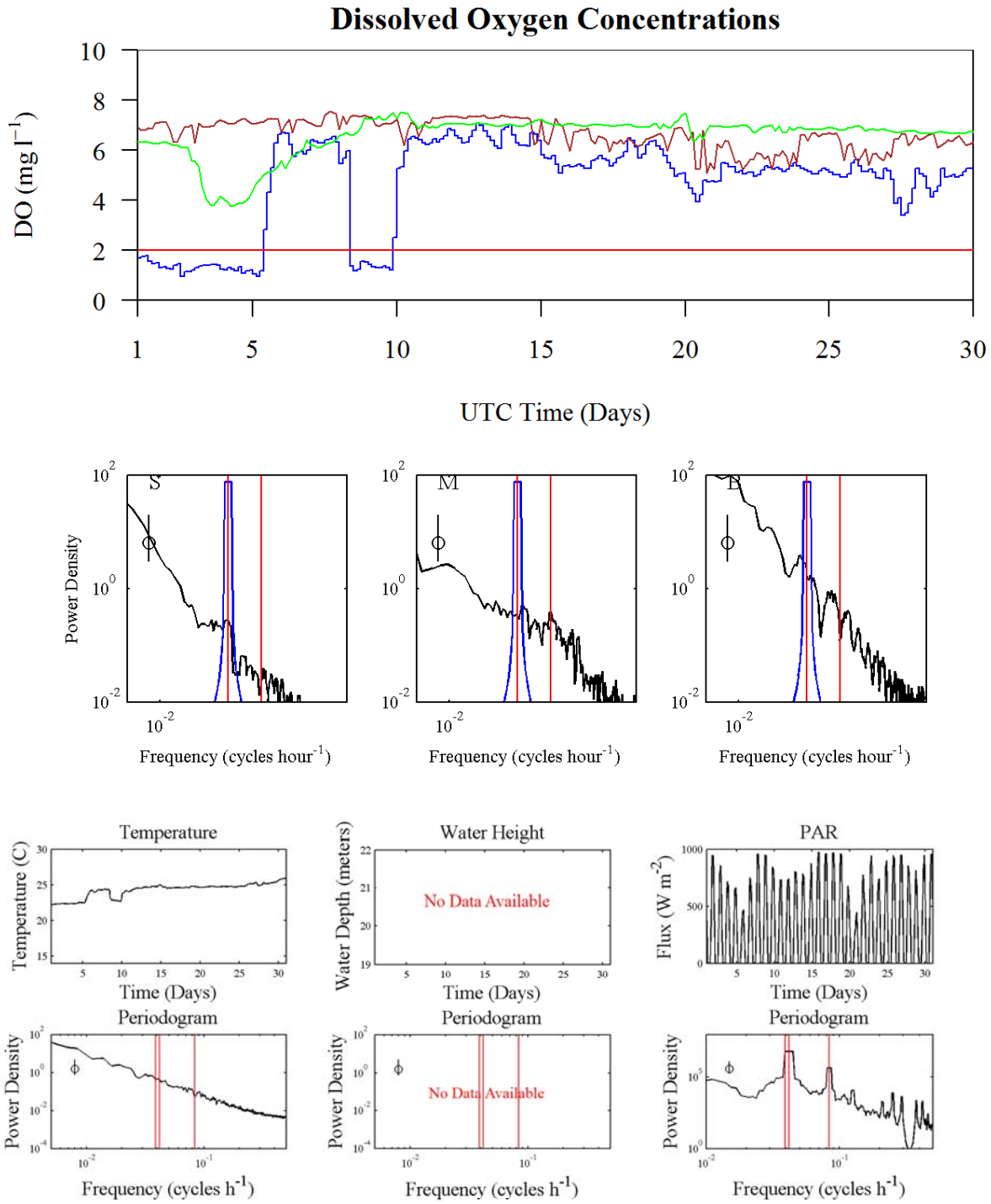

Figure B.12. Time-series plots and periodograms of dissolved oxygen (DO) concentrations and factors affecting DO concentrations for the month May 2000. Further details are located on the first page of Appendix B.

May 2000 (200005)

Autocorrelations and Cross Correlations

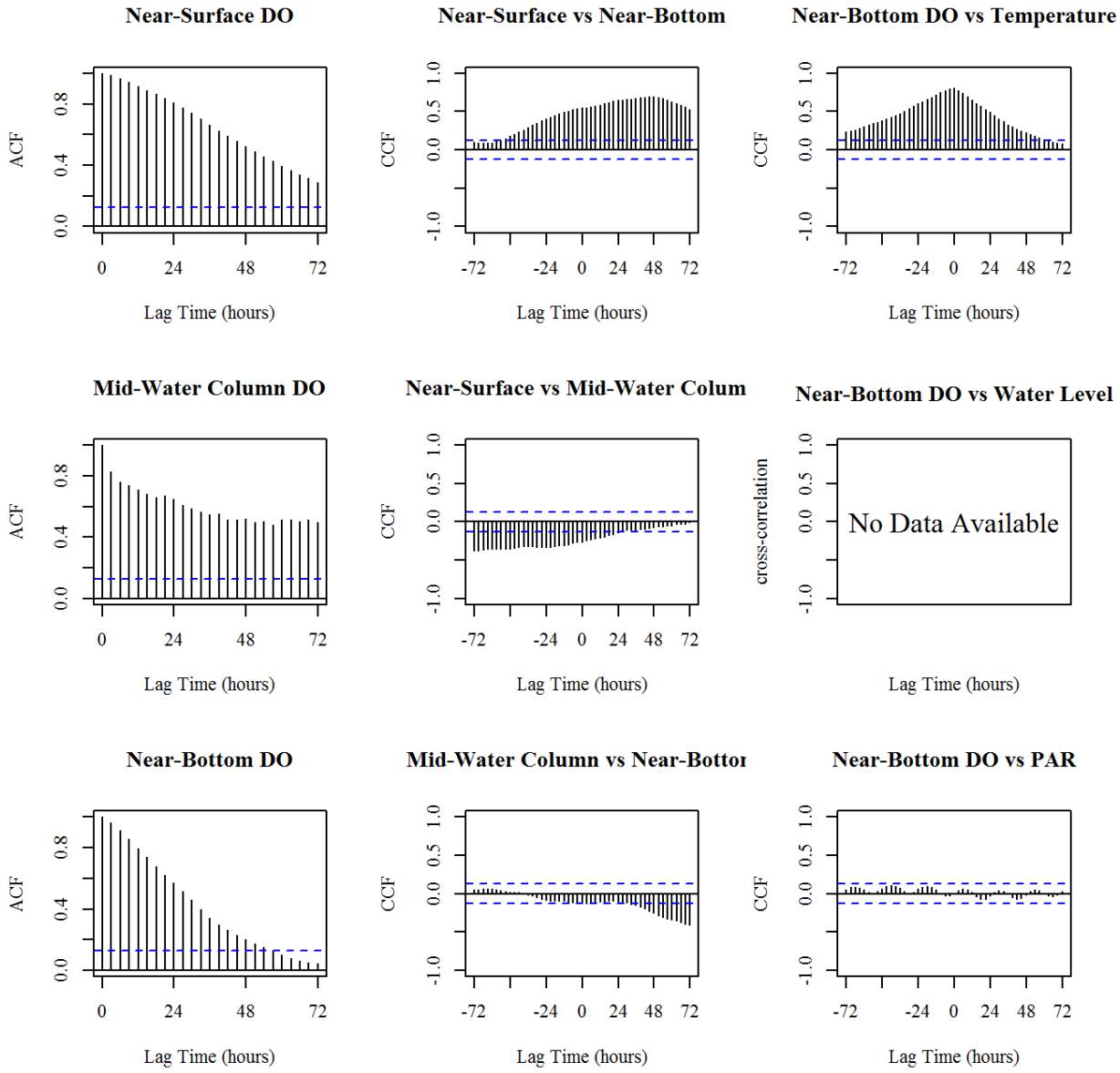

Figure B.13. Results for the month May 2000 (200005). Left Panel: Autocorrelation function (ACF) plots of DO concentrations from three depths, near surface (top), mid-water column (middle), and near-bottom (bottom); Middle Panel: Cross-correlation function (CCF) plots of DO concentrations between depths; Right Panel: Cross-correlation function (CCF) plots between near-bottom DO concentrations and the factors, temperature, water level, and PAR. Blue dotted lines represent 95% confidence limits. Further details are located on the first page of Appendix B.

June 2000 (200006)

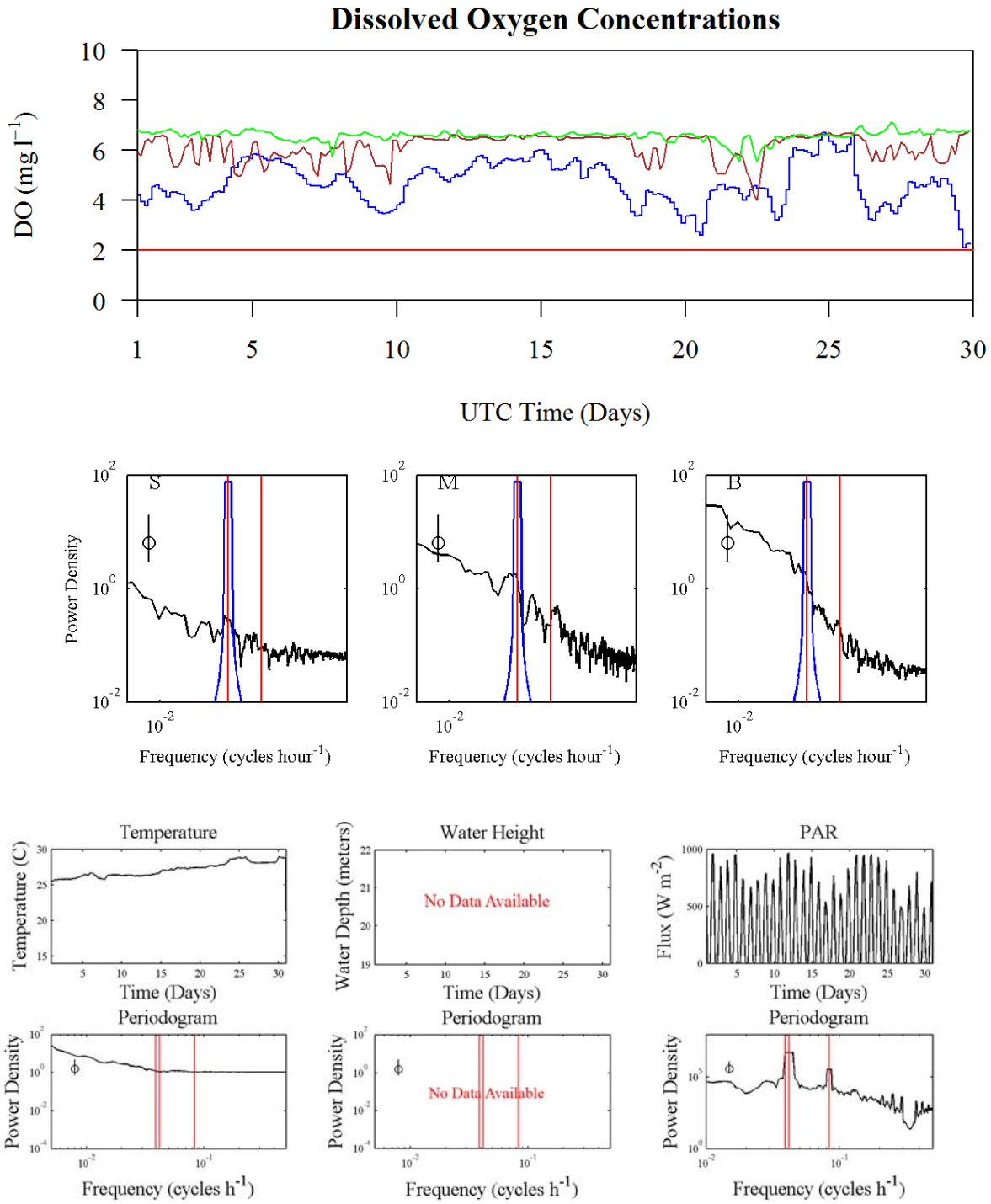

Figure B.13. Time-series plots and periodograms of dissolved oxygen (DO) concentrations and factors affecting DO concentrations for the month June 2000. Further details are located on the first page of Appendix B.

June 2000 (200006)

Autocorrelations and Cross Correlations

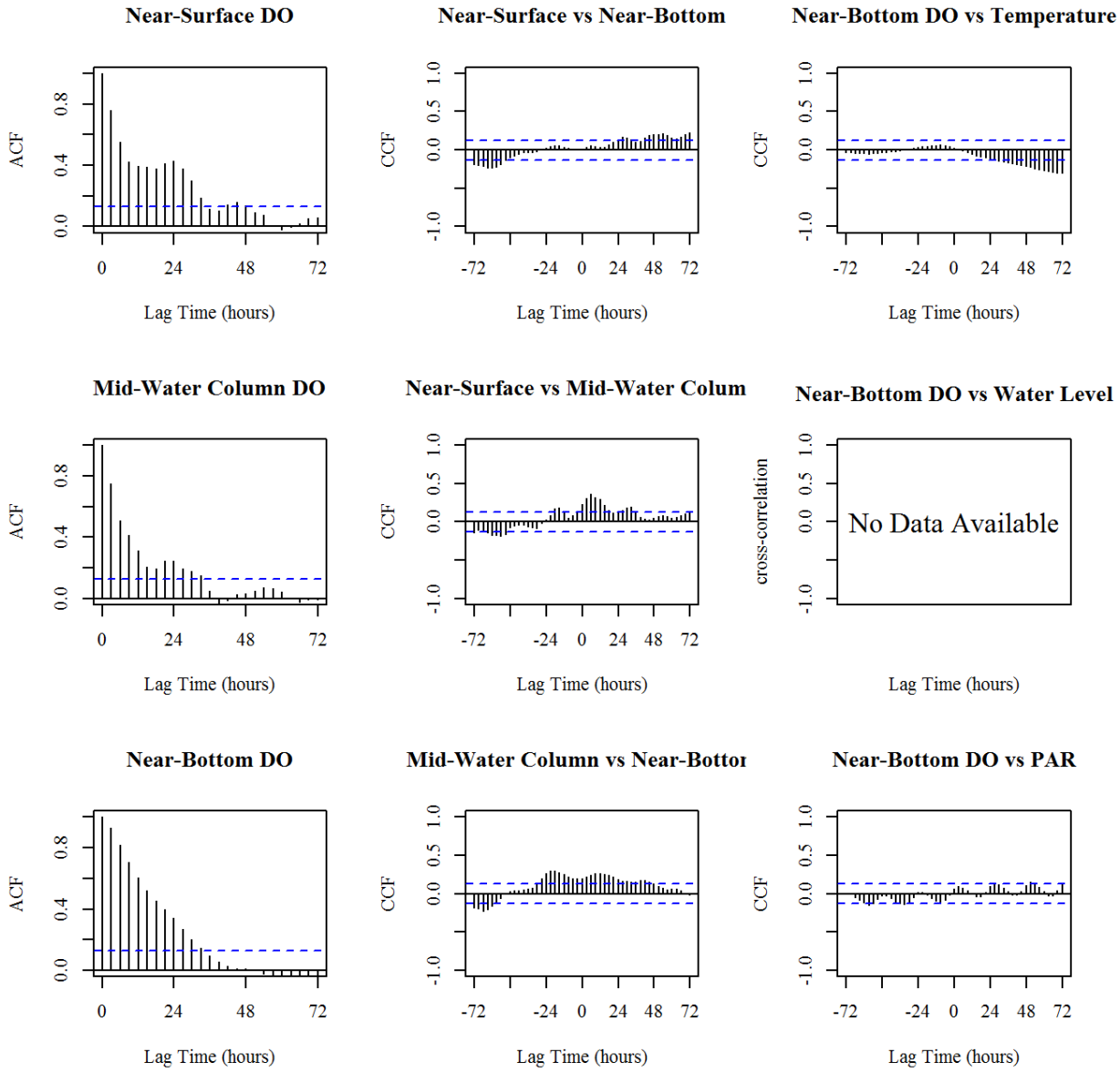

Figure B.14. Results for the month June 2000 (200006). Left Panel: Autocorrelation function (ACF) plots of DO concentrations from three depths, near surface (top), mid-water column (middle), and near-bottom (bottom); Middle Panel: Cross-correlation function (CCF) plots of DO concentrations between depths; Right Panel: Cross-correlation function (CCF) plots between near-bottom DO concentrations and the factors, temperature, water level, and PAR. Blue dotted lines represent 95% confidence limits. Further details are located on the first page of Appendix B.

July 2000 (200007)

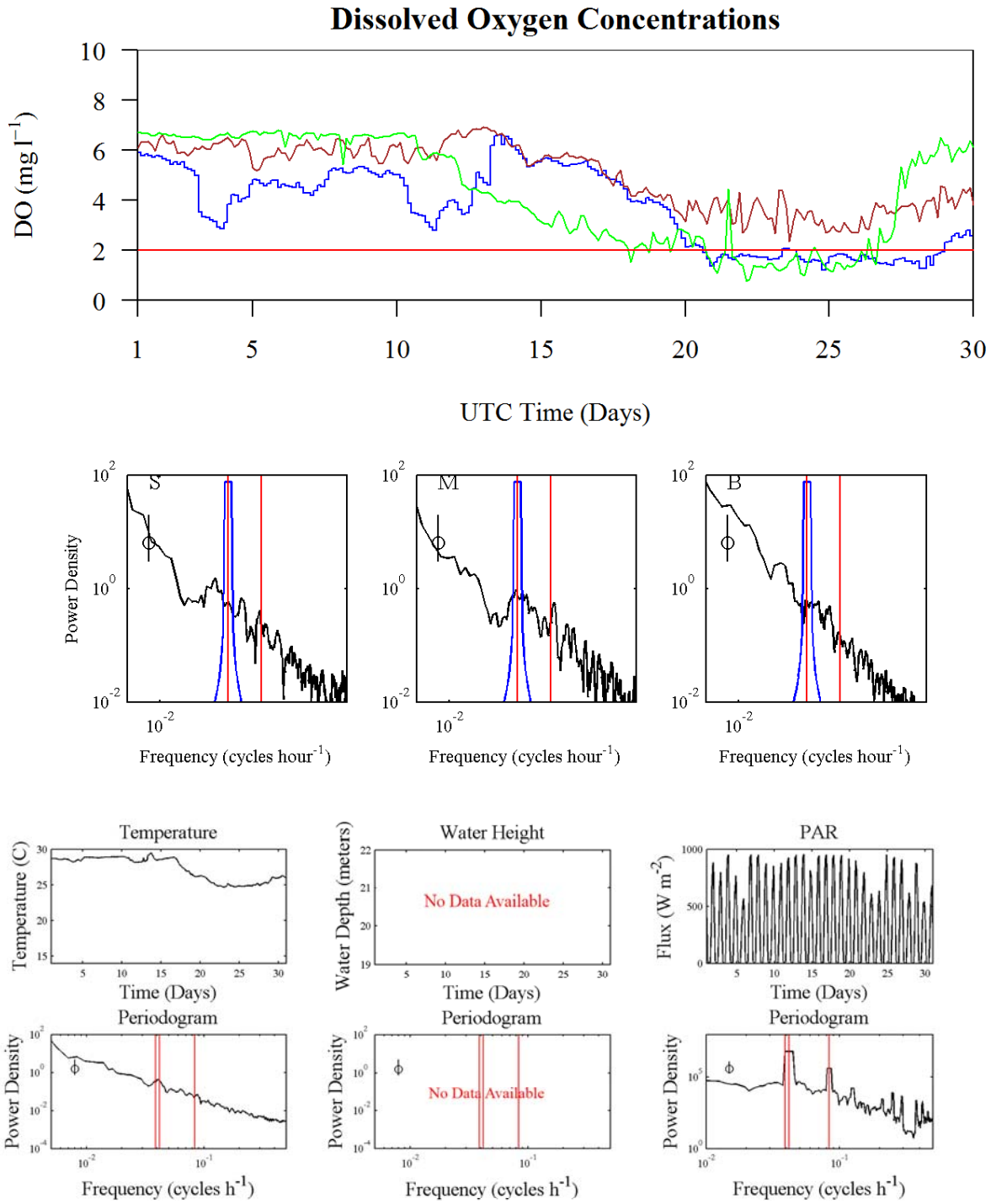

Figure B.14. Time-series plots and periodograms of dissolved oxygen (DO) concentrations and factors affecting DO concentrations for the month July 2000. Further details are located on the first page of Appendix B.

July 2000 (200007)

Autocorrelations and Cross Correlations

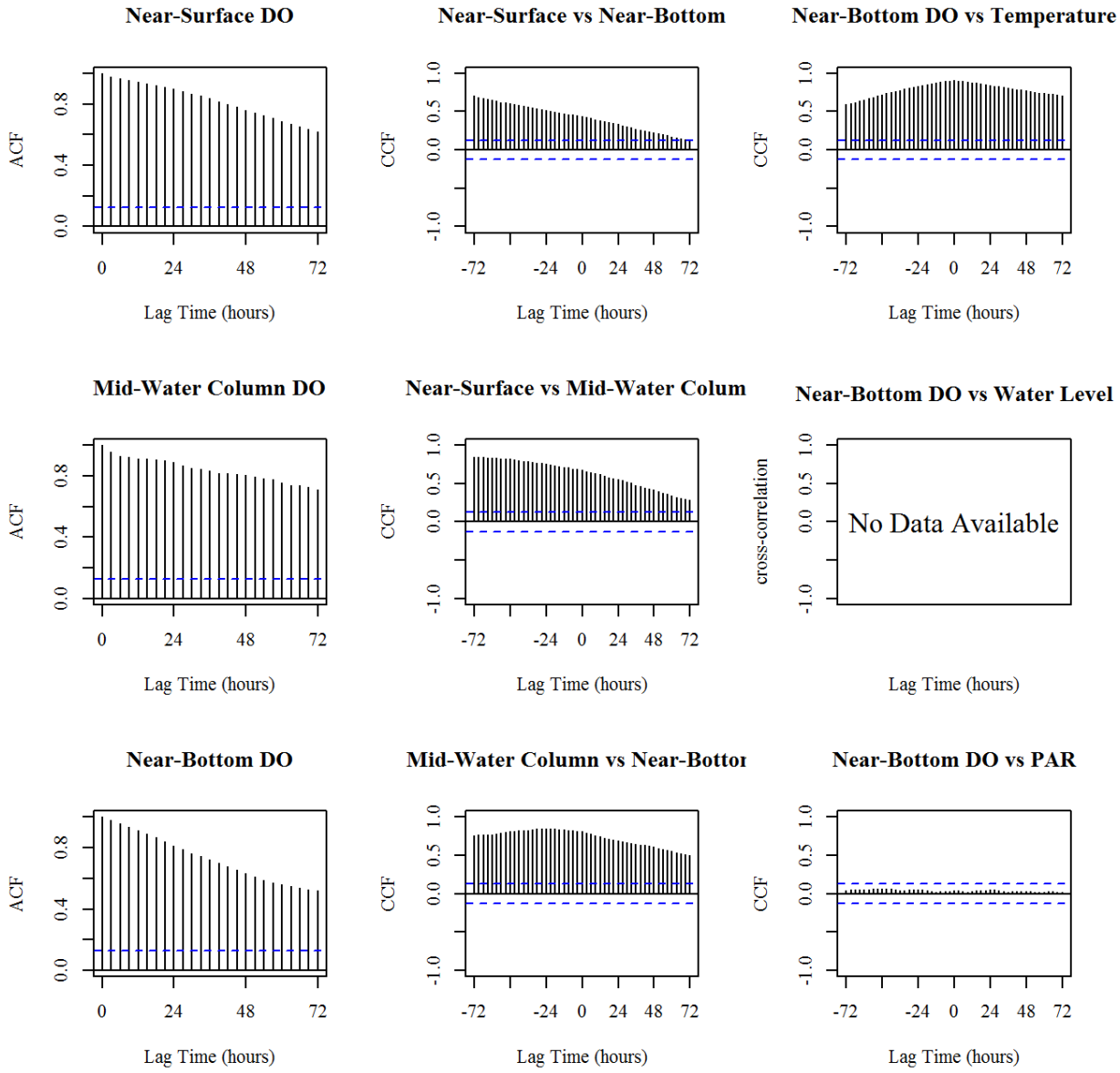

Figure B.15. Results for the month July 2000 (200007). Left Panel: Autocorrelation function (ACF) plots of DO concentrations from three depths, near surface (top), mid-water column (middle), and near-bottom (bottom); Middle Panel: Cross-correlation function (CCF) plots of DO concentrations between depths; Right Panel: Cross-correlation function (CCF) plots between near-bottom DO concentrations and the factors, temperature, water level, and PAR. Blue dotted lines represent 95% confidence limits. Further details are located on the first page of Appendix B.

August 2000 (200008)

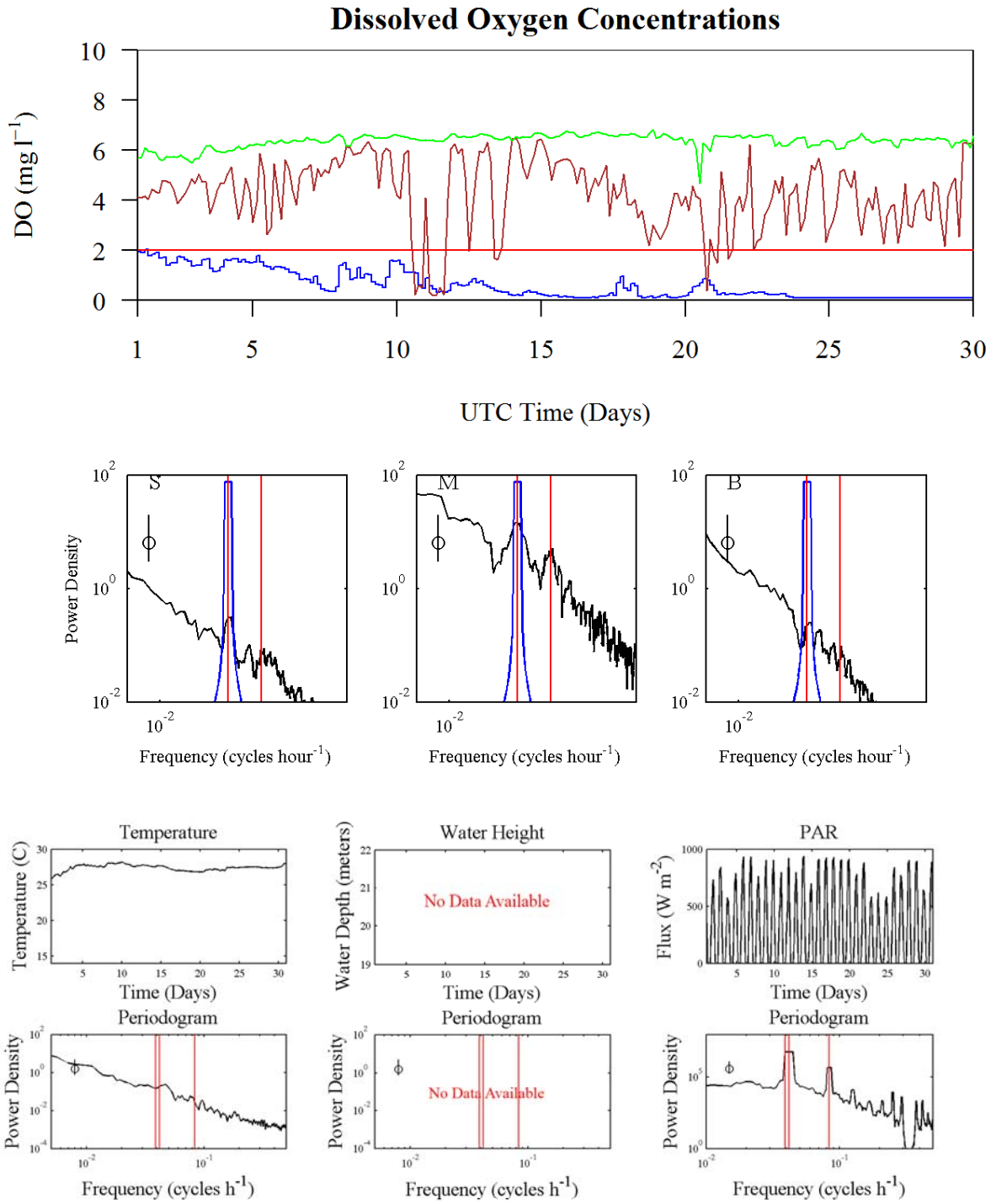

Figure B.15. Time-series plots and periodograms of dissolved oxygen (DO) concentrations and factors affecting DO concentrations for the month August 2000. Further details are located on the first page of Appendix B.

August 2000 (200008)

Autocorrelations and Cross Correlations

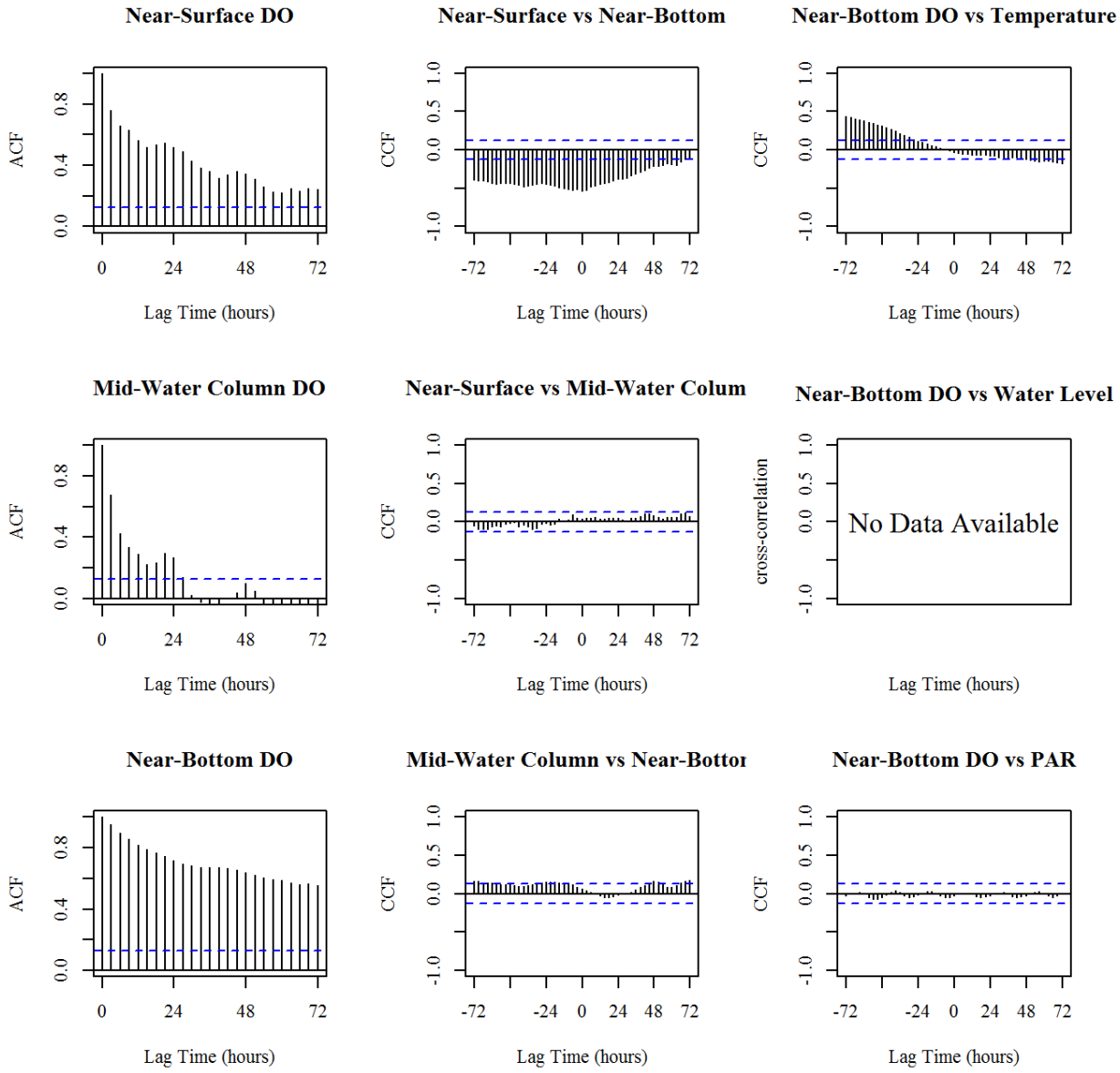

Figure B.16. Results for the month August 2000 (200008). Left Panel: Autocorrelation function (ACF) plots of DO concentrations from three depths, near surface (top), mid-water column (middle), and near-bottom (bottom); Middle Panel: Cross-correlation function (CCF) plots of DO concentrations between depths; Right Panel: Cross-correlation function (CCF) plots between near-bottom DO concentrations and the factors, temperature, water level, and PAR. Blue dotted lines represent 95% confidence limits. Further details are located on the first page of Appendix B.

September 2000 (200009)

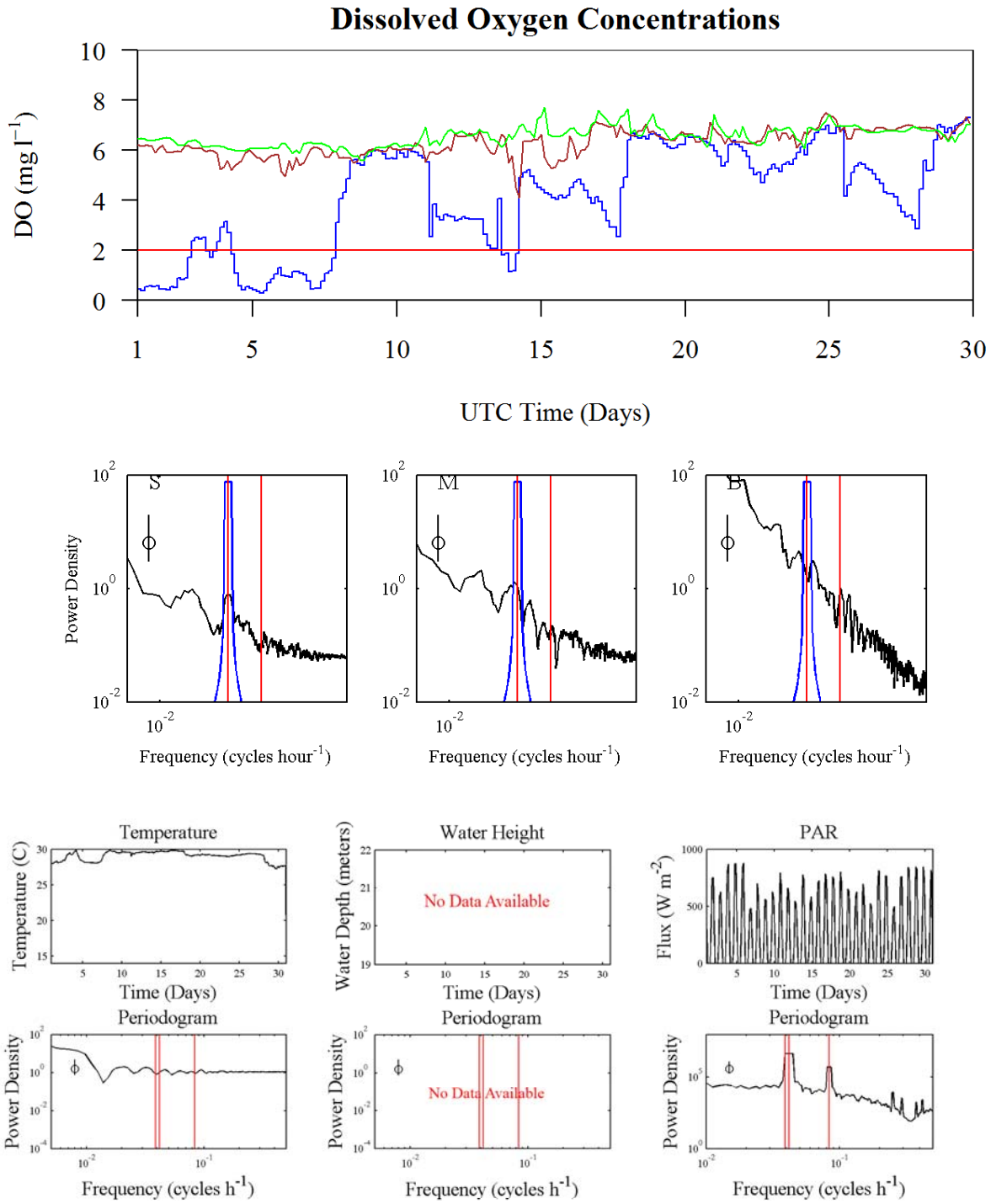

Figure B.16. Time-series plots and periodograms of dissolved oxygen (DO) concentrations and factors affecting DO concentrations for the month September 2000. Further details are located on the first page of Appendix B.

September 2000 (200009)

Autocorrelations and Cross Correlations

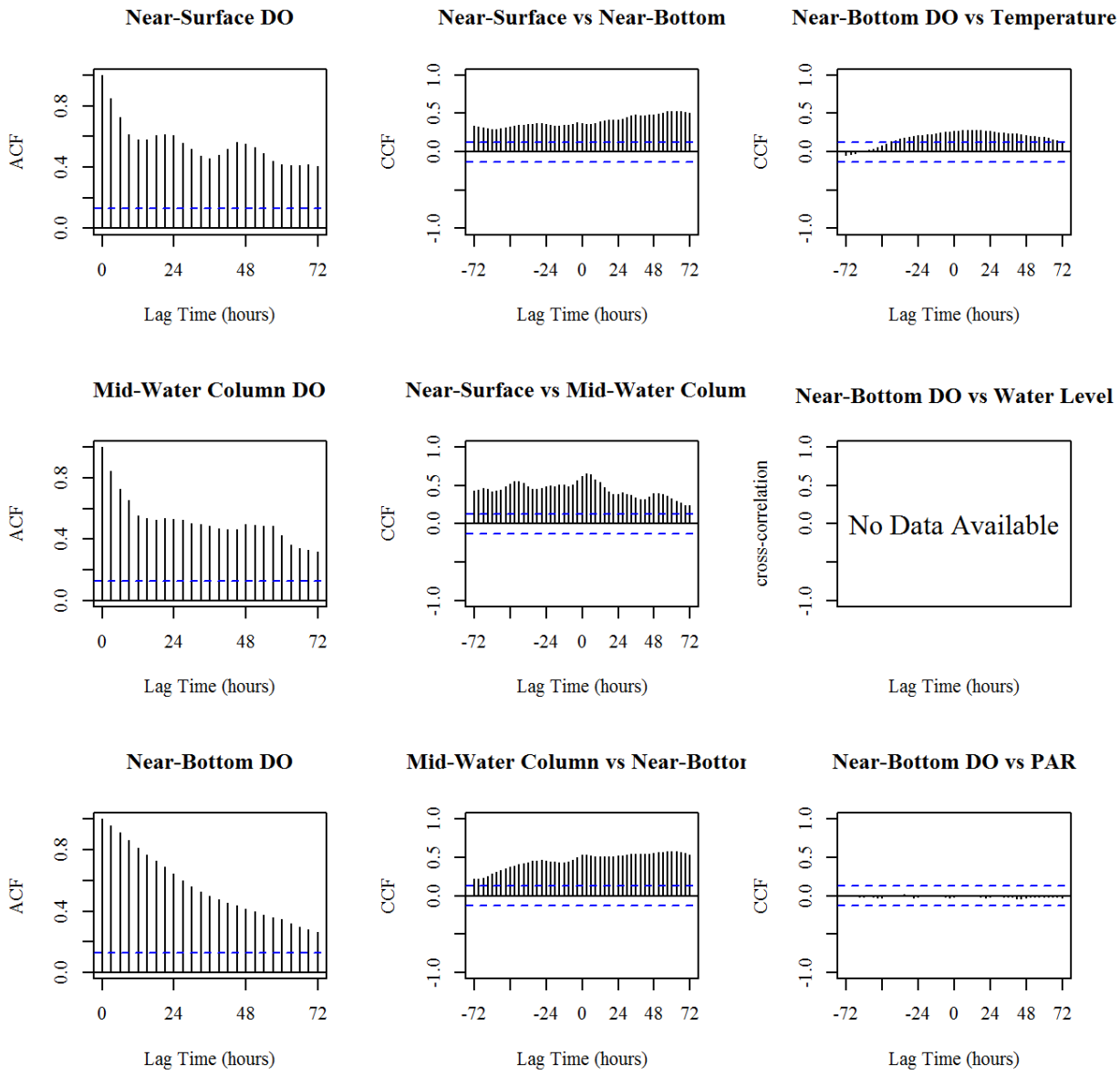

Figure B.17. Results for the month September 2000 (200009). Left Panel: Autocorrelation function (ACF) plots of DO concentrations from three depths, near surface (top), mid-water column (middle), and near-bottom (bottom); Middle Panel: Cross-correlation function (CCF) plots of DO concentrations between depths; Right Panel: Cross-correlation function (CCF) plots between near-bottom DO concentrations and the factors, temperature, water level, and PAR. Blue dotted lines represent 95% confidence limits. Further details are located on the first page of Appendix B.

October 2000 (200010)

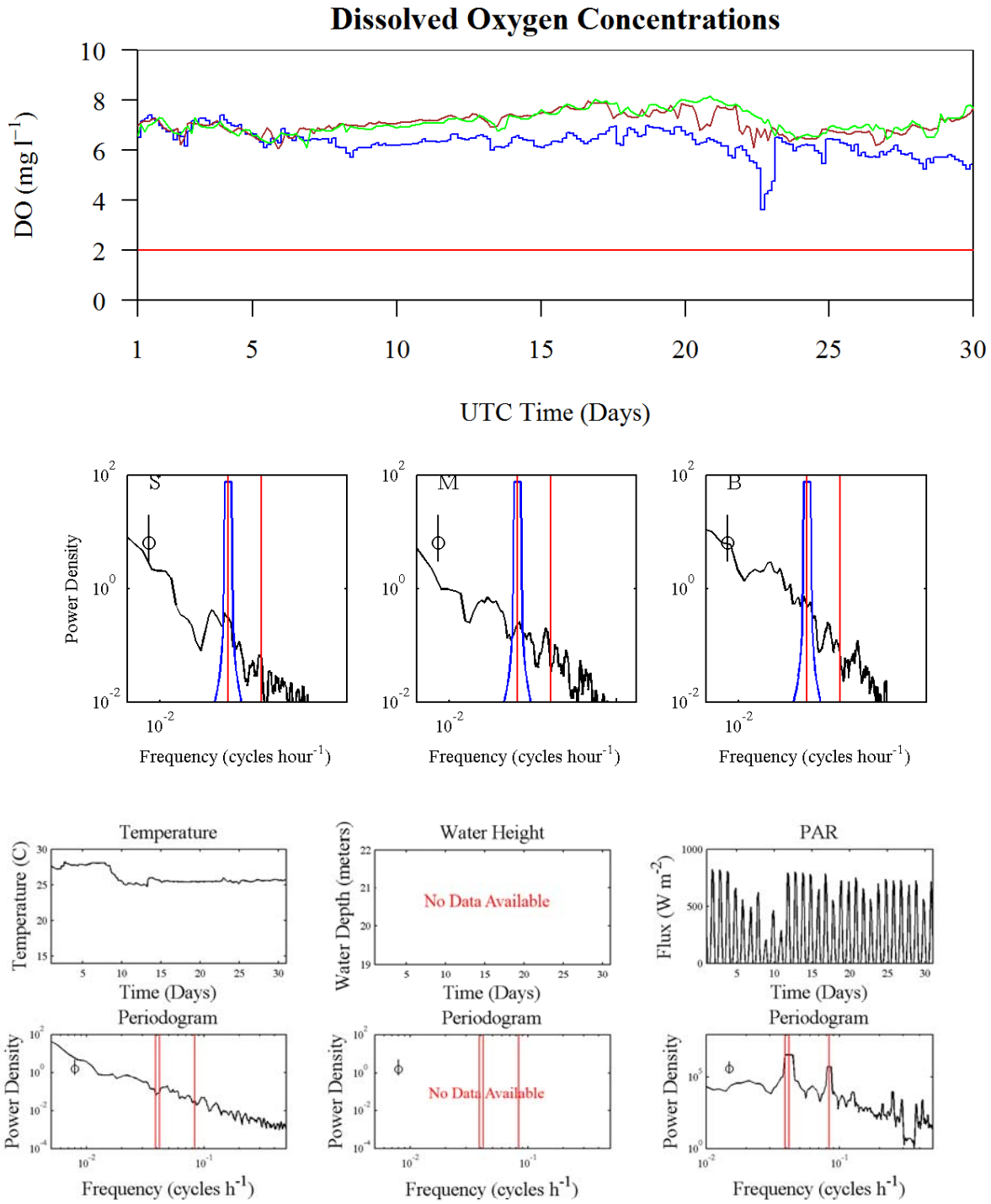

Figure B.17. Time-series plots and periodograms of dissolved oxygen (DO) concentrations and factors affecting DO concentrations for the month October 2000. Further details are located on the first page of Appendix B.

October 2000 (200010)

Autocorrelations and Cross Correlations

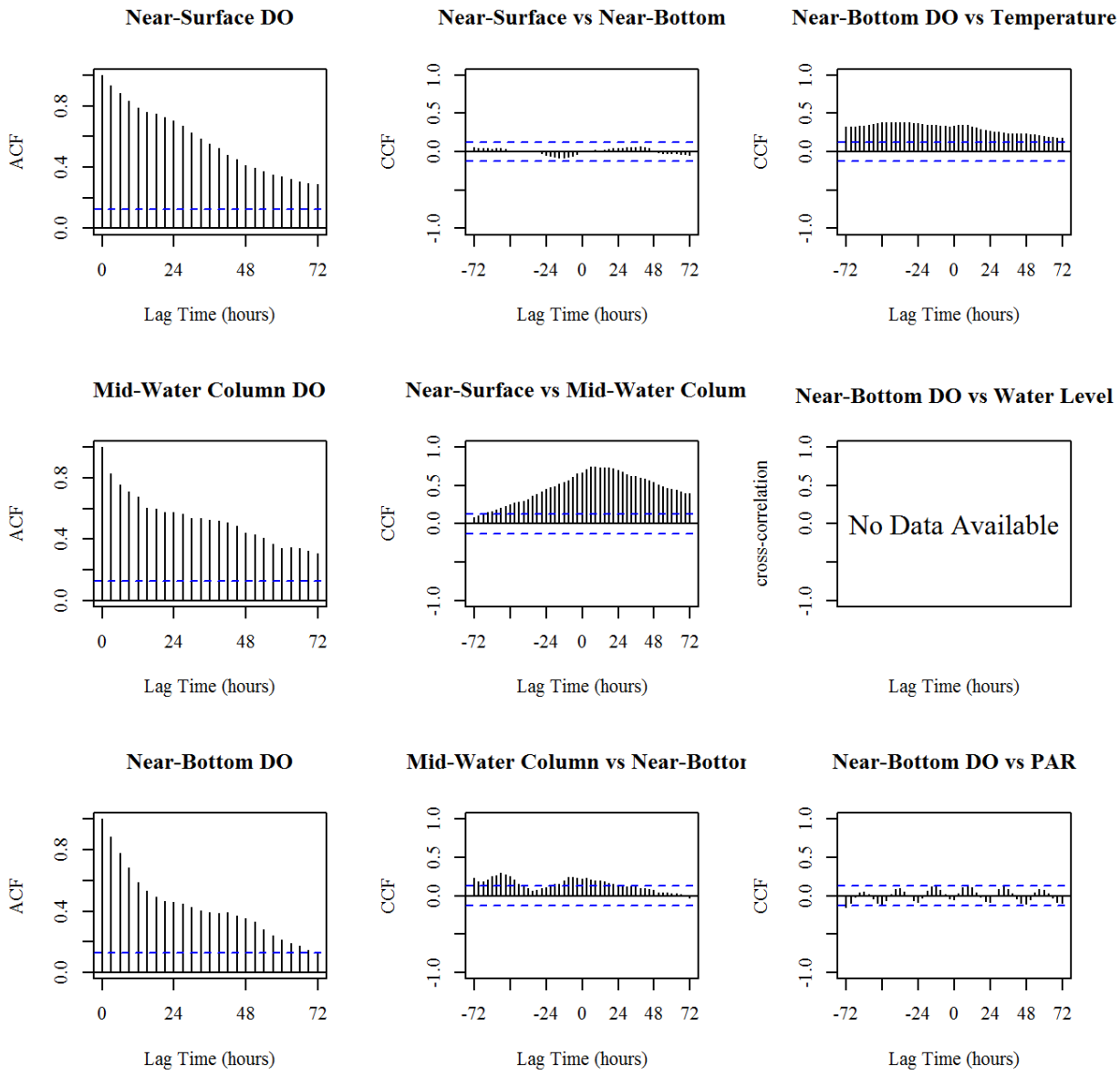

Figure B.18. Results for the month October 2000 (200010). Left Panel: Autocorrelation function (ACF) plots of DO concentrations from three depths, near surface (top), mid-water column (middle), and near-bottom (bottom); Middle Panel: Cross-correlation function (CCF) plots of DO concentrations between depths; Right Panel: Cross-correlation function (CCF) plots between near-bottom DO concentrations and the factors, temperature, water level, and PAR. Blue dotted lines represent 95% confidence limits. Further details are located on the first page of Appendix B.

April 2002 (200204)

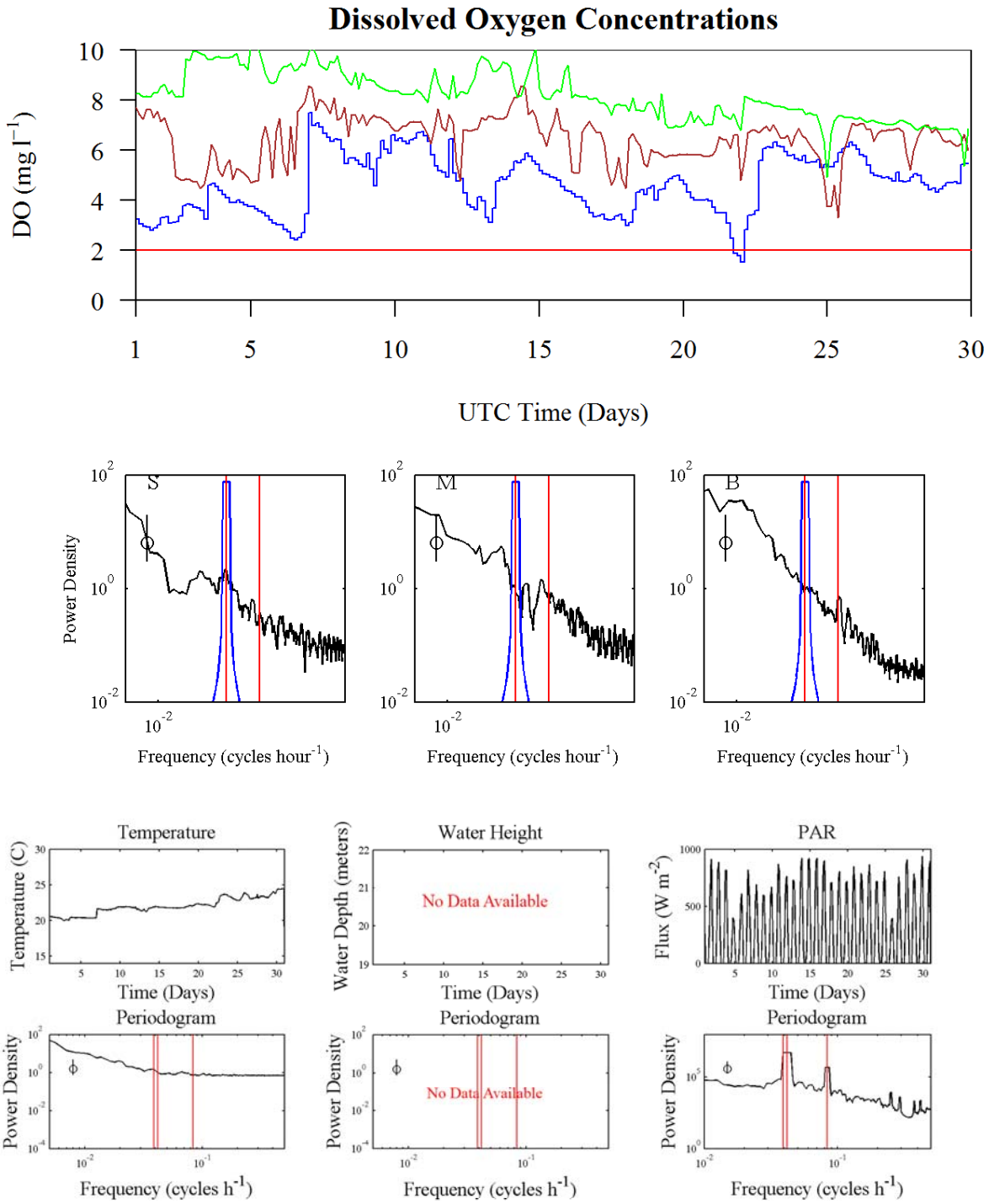

Figure B.18. Time-series plots and periodograms of dissolved oxygen (DO) concentrations and factors affecting DO concentrations for the month April 2002. Further details are located on the first page of Appendix B.

April 2002 (200204)

Autocorrelations and Cross Correlations

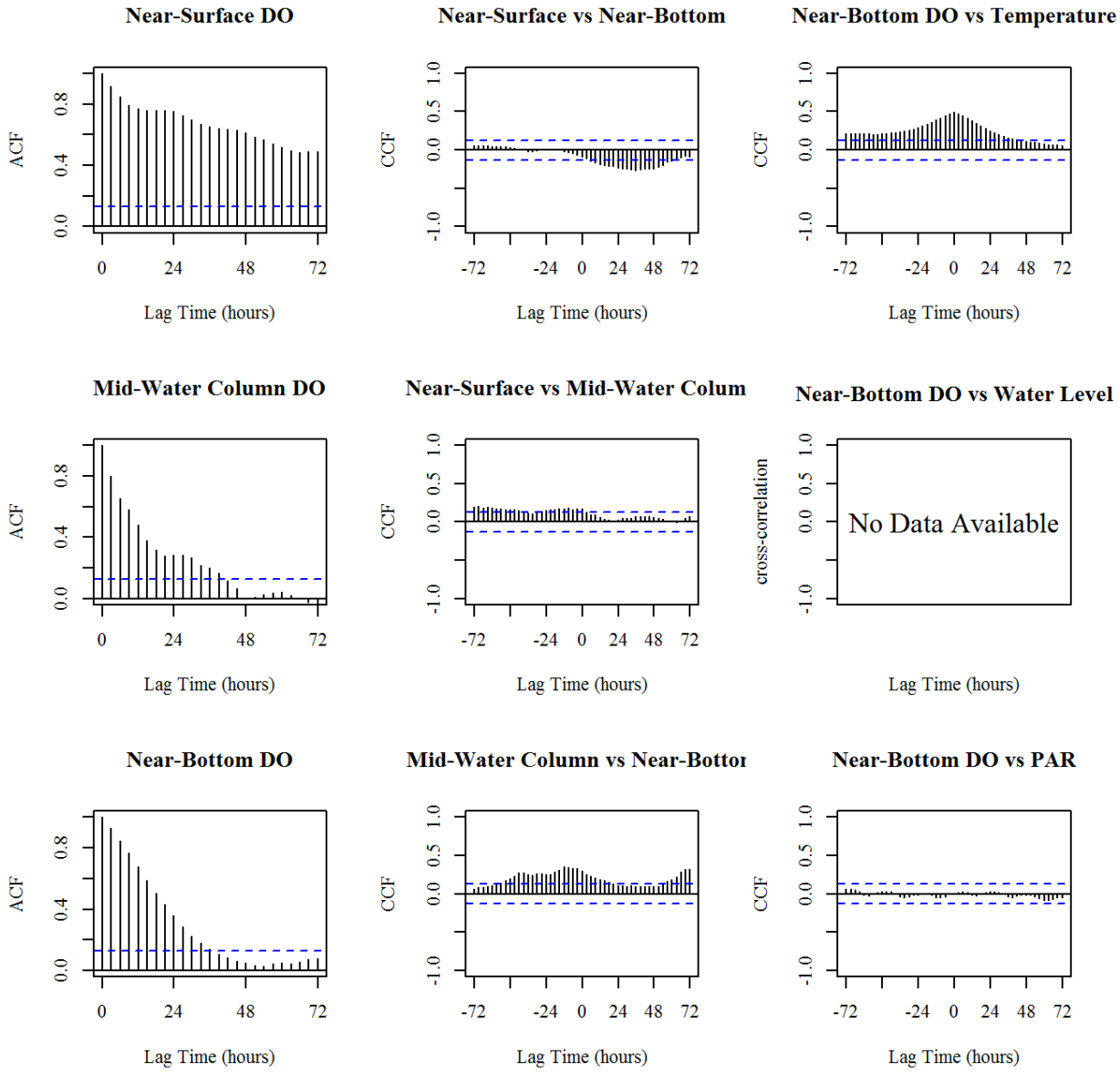

Figure B.19. Results for the month April 2002 (200204). Left Panel: Autocorrelation function (ACF) plots of DO concentrations from three depths, near surface (top), mid-water column (middle), and near-bottom (bottom); Middle Panel: Cross-correlation function (CCF) plots of DO concentrations between depths; Right Panel: Cross-correlation function (CCF) plots between near-bottom DO concentrations and the factors, temperature, water level, and PAR. Blue dotted lines represent 95% confidence limits. Further details are located on the first page of Appendix B.

May 2002 (200205)

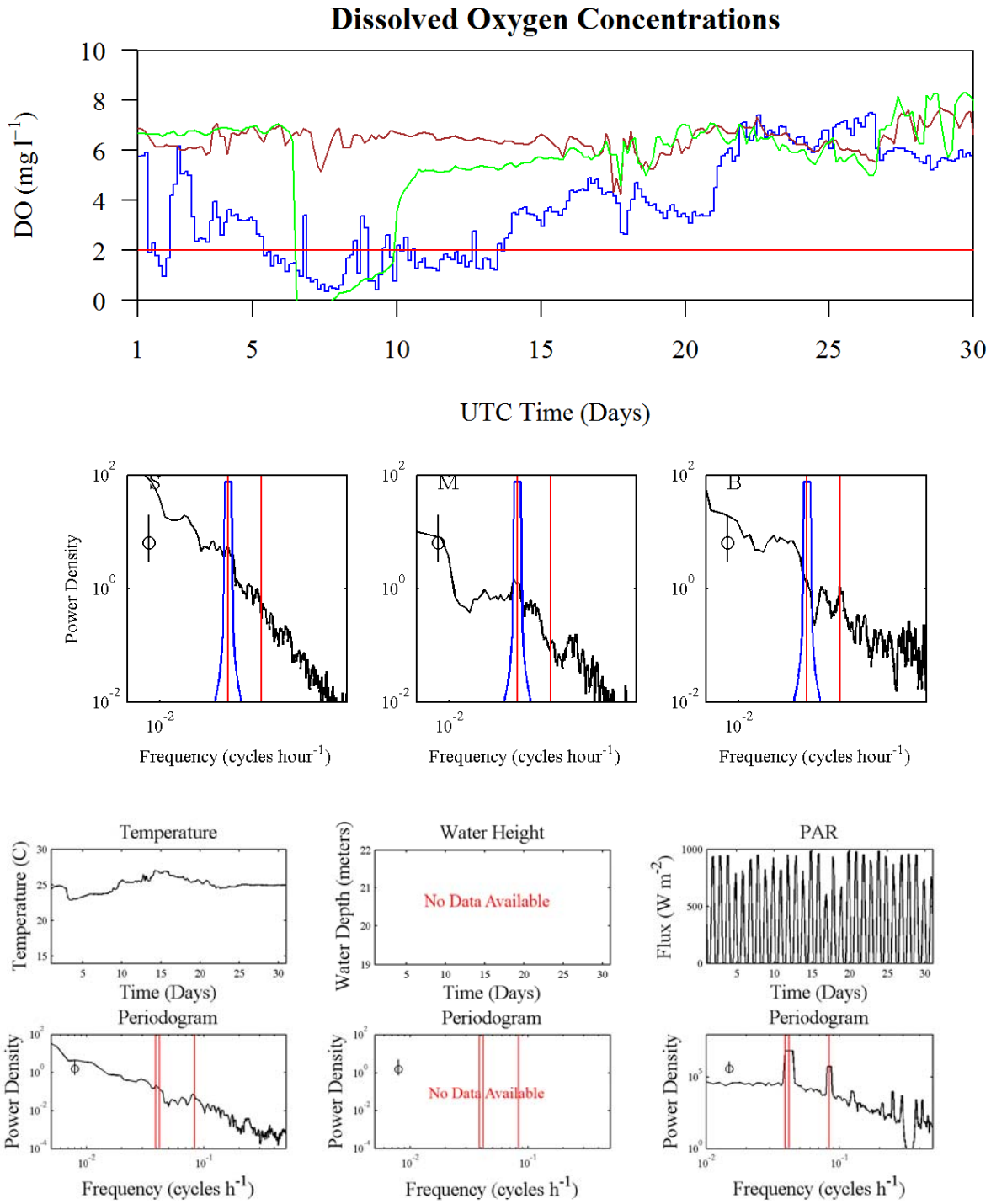

Figure B.19. Time-series plots and periodograms of dissolved oxygen (DO) concentrations and factors affecting DO concentrations for the month May 2002. Further details are located on the first page of Appendix B.

May 2002 (200205)

Autocorrelations and Cross Correlations

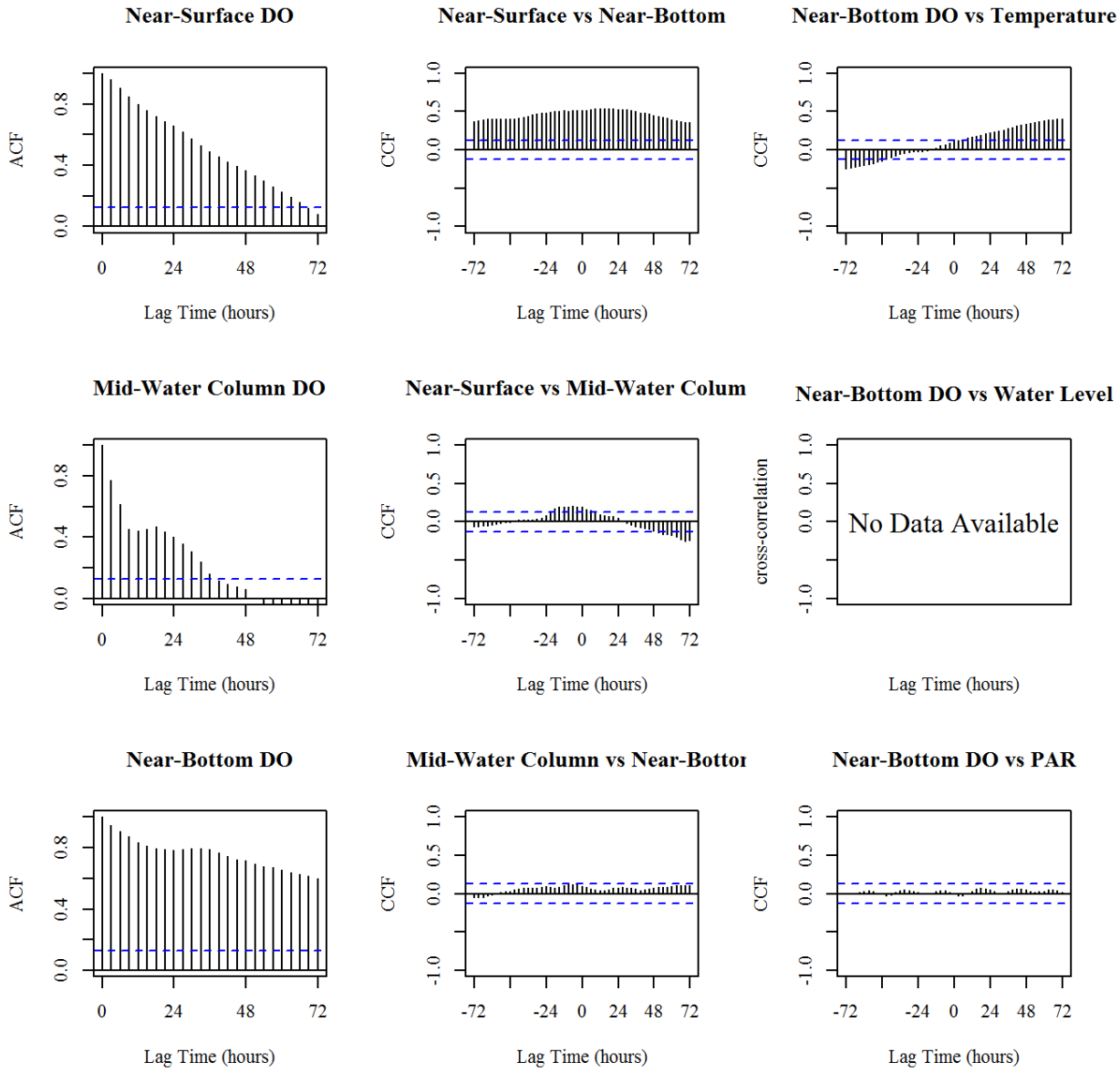

Figure B.20. Results for the month May 2002 (200205). Left Panel: Autocorrelation function (ACF) plots of DO concentrations from three depths, near surface (top), mid-water column (middle), and near-bottom (bottom); Middle Panel: Cross-correlation function (CCF) plots of DO concentrations between depths; Right Panel: Cross-correlation function (CCF) plots between near-bottom DO concentrations and the factors, temperature, water level, and PAR. Blue dotted lines represent 95% confidence limits. Further details are located on the first page of Appendix B.

June 2002 (200206)

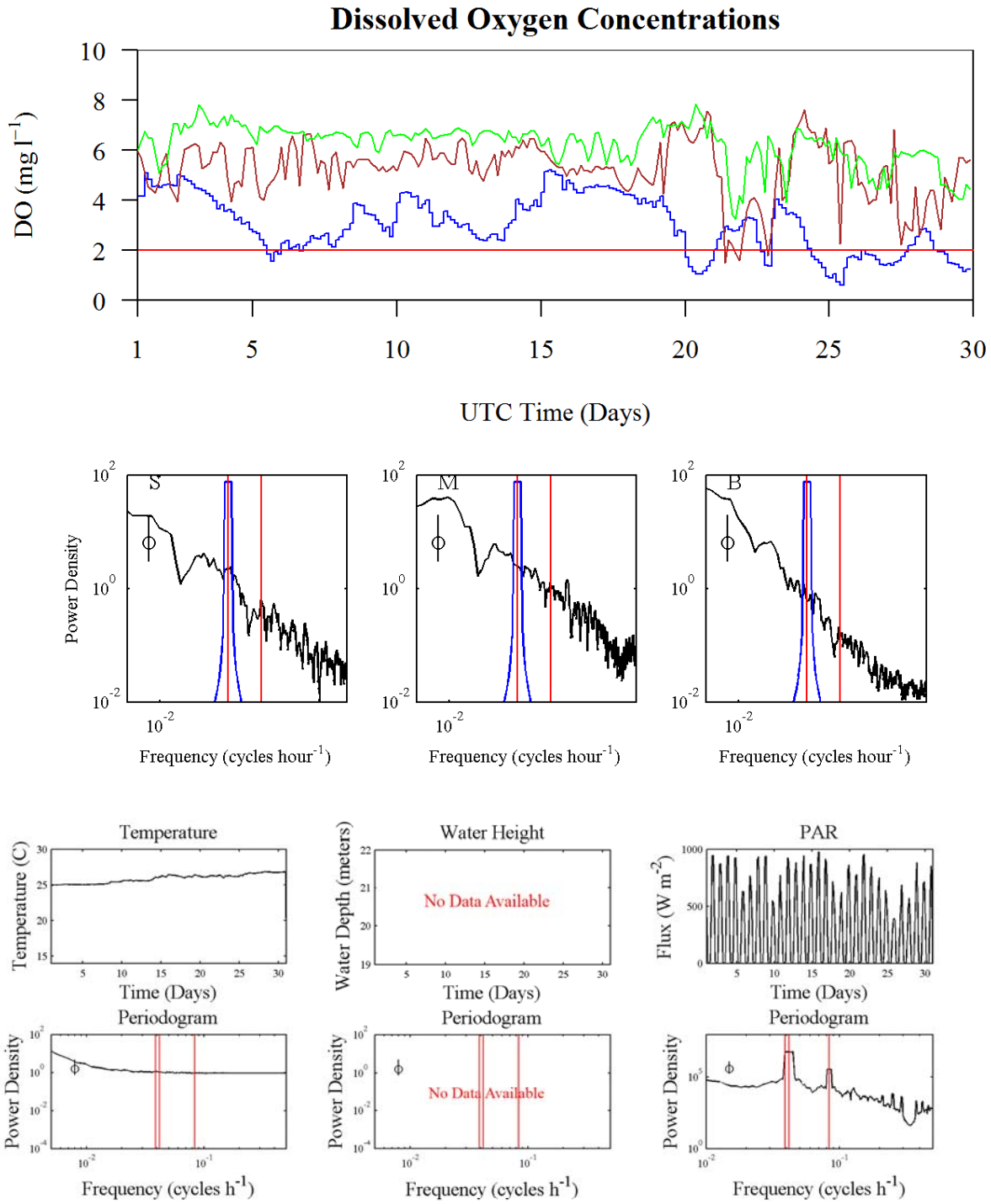

Figure B.20. Time-series plots and periodograms of dissolved oxygen (DO) concentrations and factors affecting DO concentrations for the month June 2002. Further details are located on the first page of Appendix B.

June 2002 (200206)

Autocorrelations and Cross Correlations

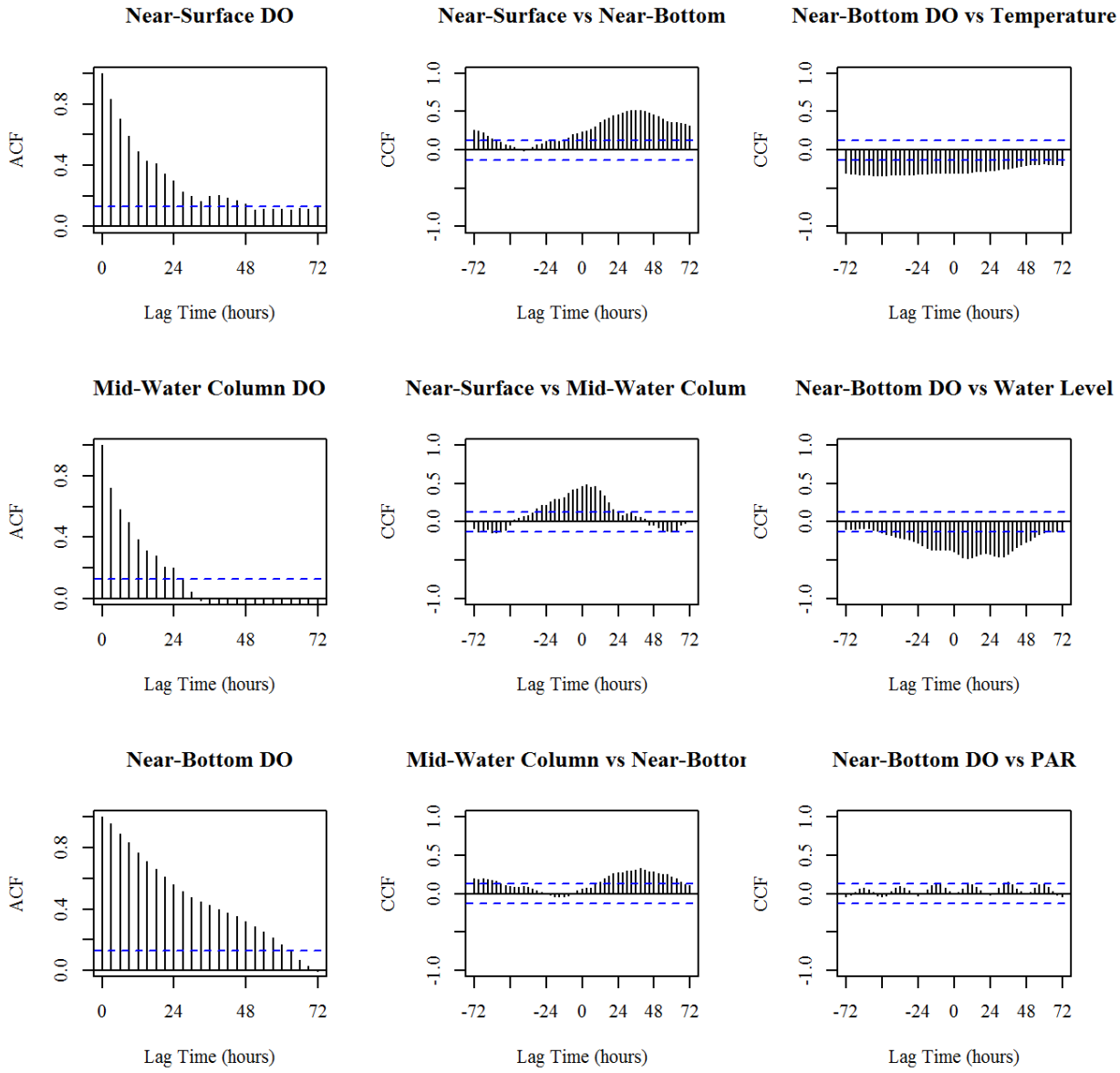

Figure B.21. Results for the month June 2002 (200206). Left Panel: Autocorrelation function (ACF) plots of DO concentrations from three depths, near surface (top), mid-water column (middle), and near-bottom (bottom); Middle Panel: Cross-correlation function (CCF) plots of DO concentrations between depths; Right Panel: Cross-correlation function (CCF) plots between near-bottom DO concentrations and the factors, temperature, water level, and PAR. Blue dotted lines represent 95% confidence limits. Further details are located on the first page of Appendix B.

July 2002 (200207)

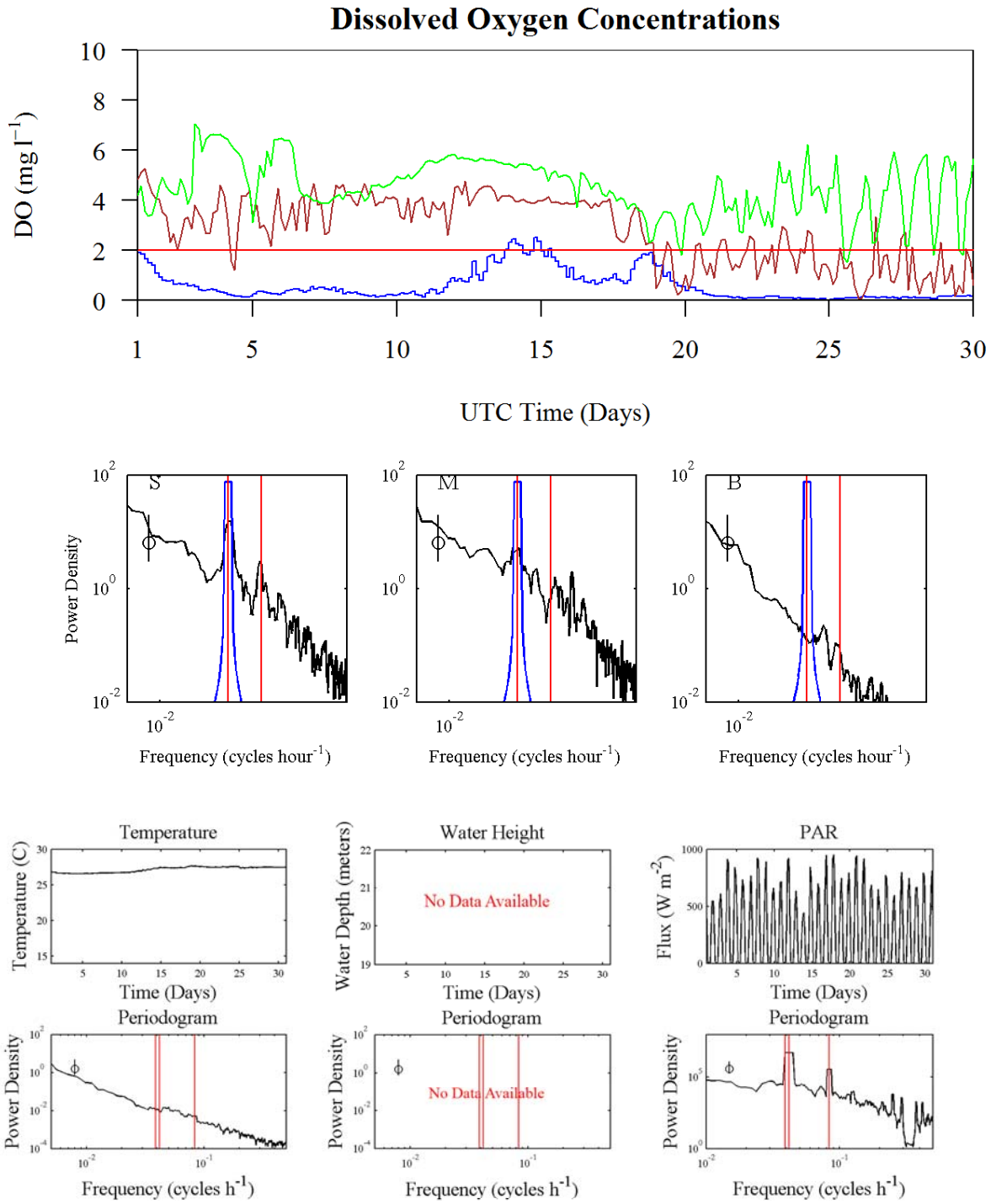

Figure B.21. Time-series plots and periodograms of dissolved oxygen (DO) concentrations and factors affecting DO concentrations for the month July 2002. Further details are located on the first page of Appendix B.

July 2002 (200207)

Autocorrelations and Cross Correlations

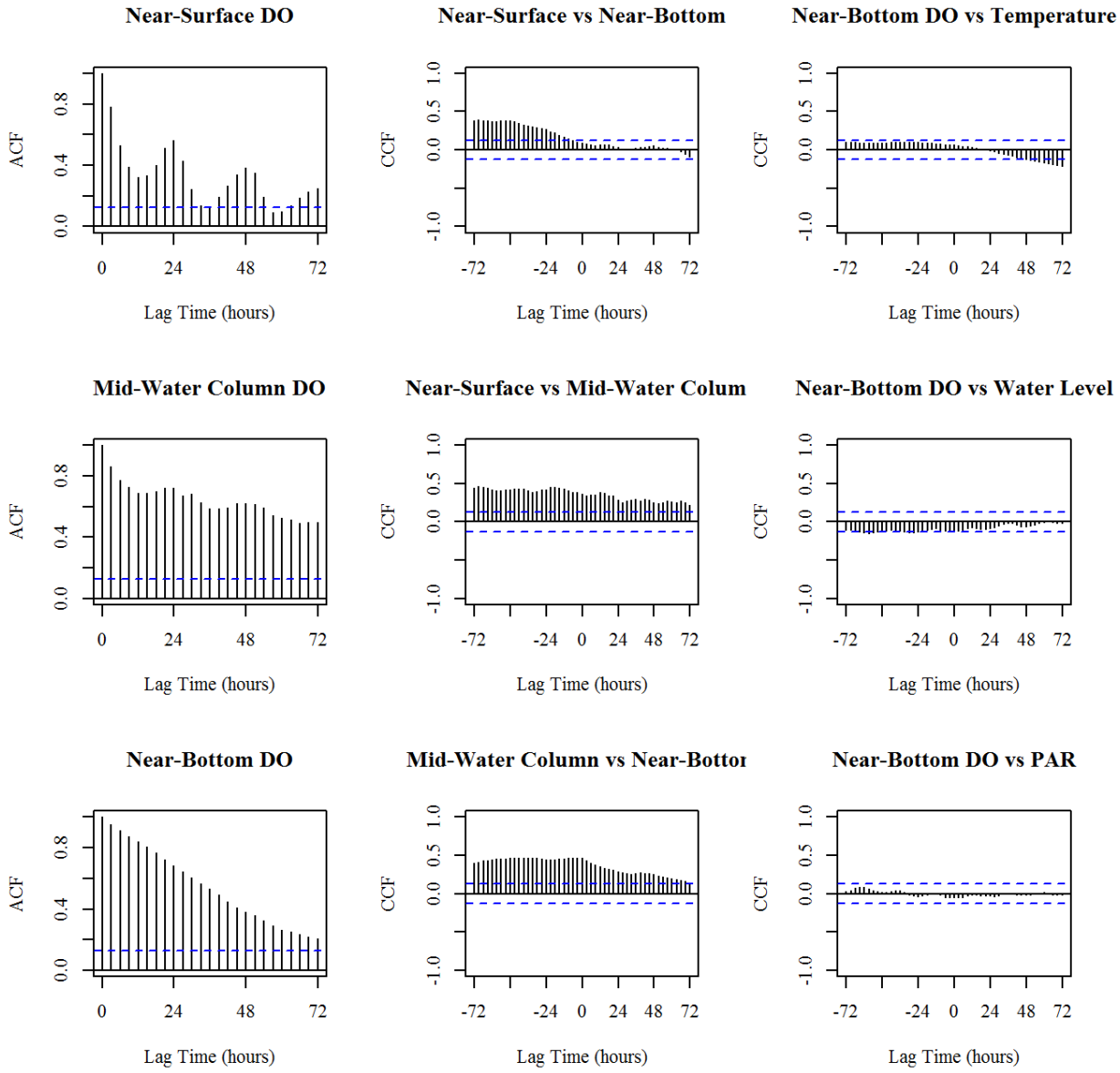

Figure B.22. Results for the month July 2002 (200207). Left Panel: Autocorrelation function (ACF) plots of DO concentrations from three depths, near surface (top), mid-water column (middle), and near-bottom (bottom); Middle Panel: Cross-correlation function (CCF) plots of DO concentrations between depths; Right Panel: Cross-correlation function (CCF) plots between near-bottom DO concentrations and the factors, temperature, water level, and PAR. Blue dotted lines represent 95% confidence limits. Further details are located on the first page of Appendix B.

May 2003 (200305)

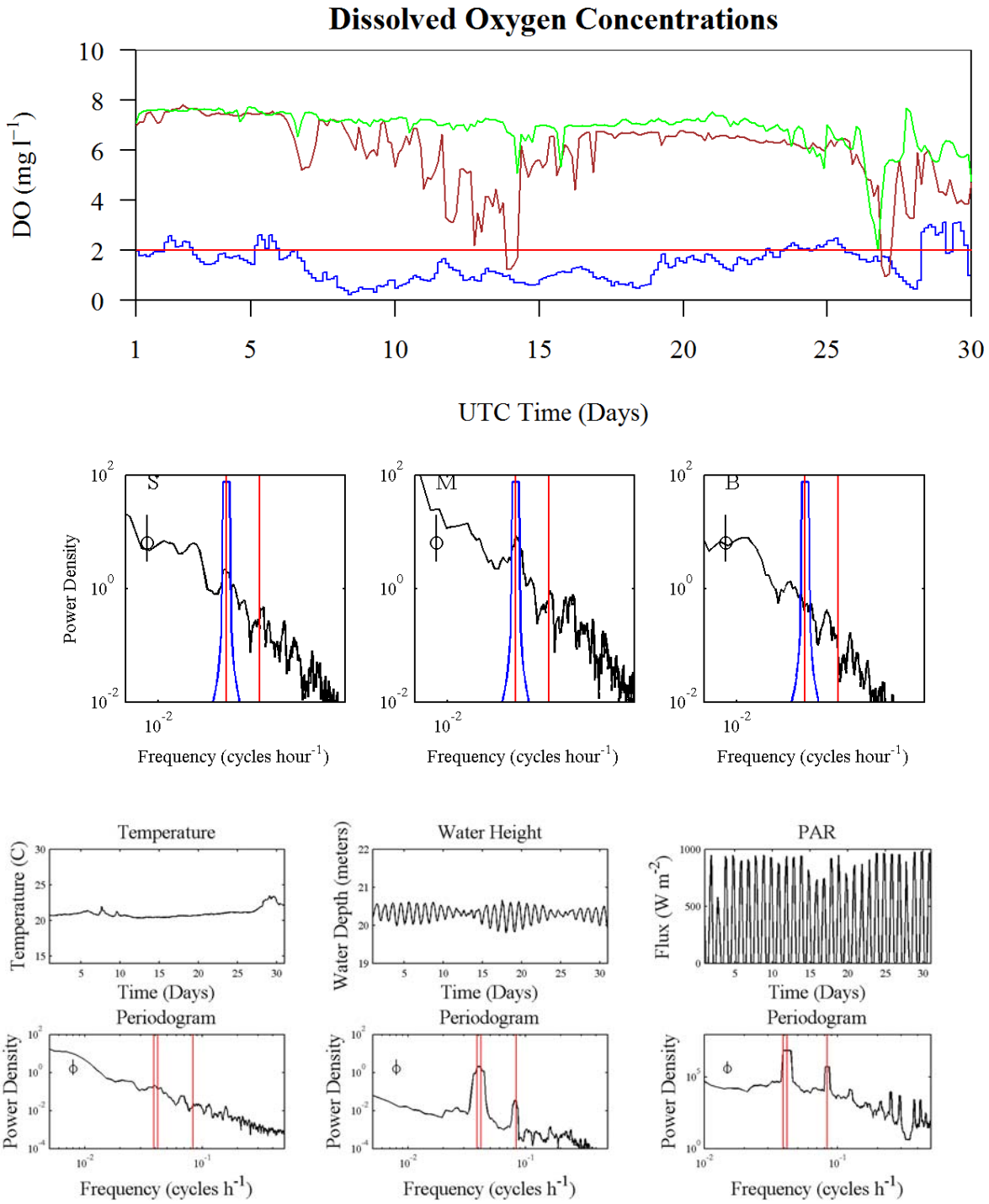

Figure B.22. Time-series plots and periodograms of dissolved oxygen (DO) concentrations and factors affecting DO concentrations for the month May 2003. Further details are located on the first page of Appendix B.

May 2003 (200305)

Autocorrelations and Cross Correlations

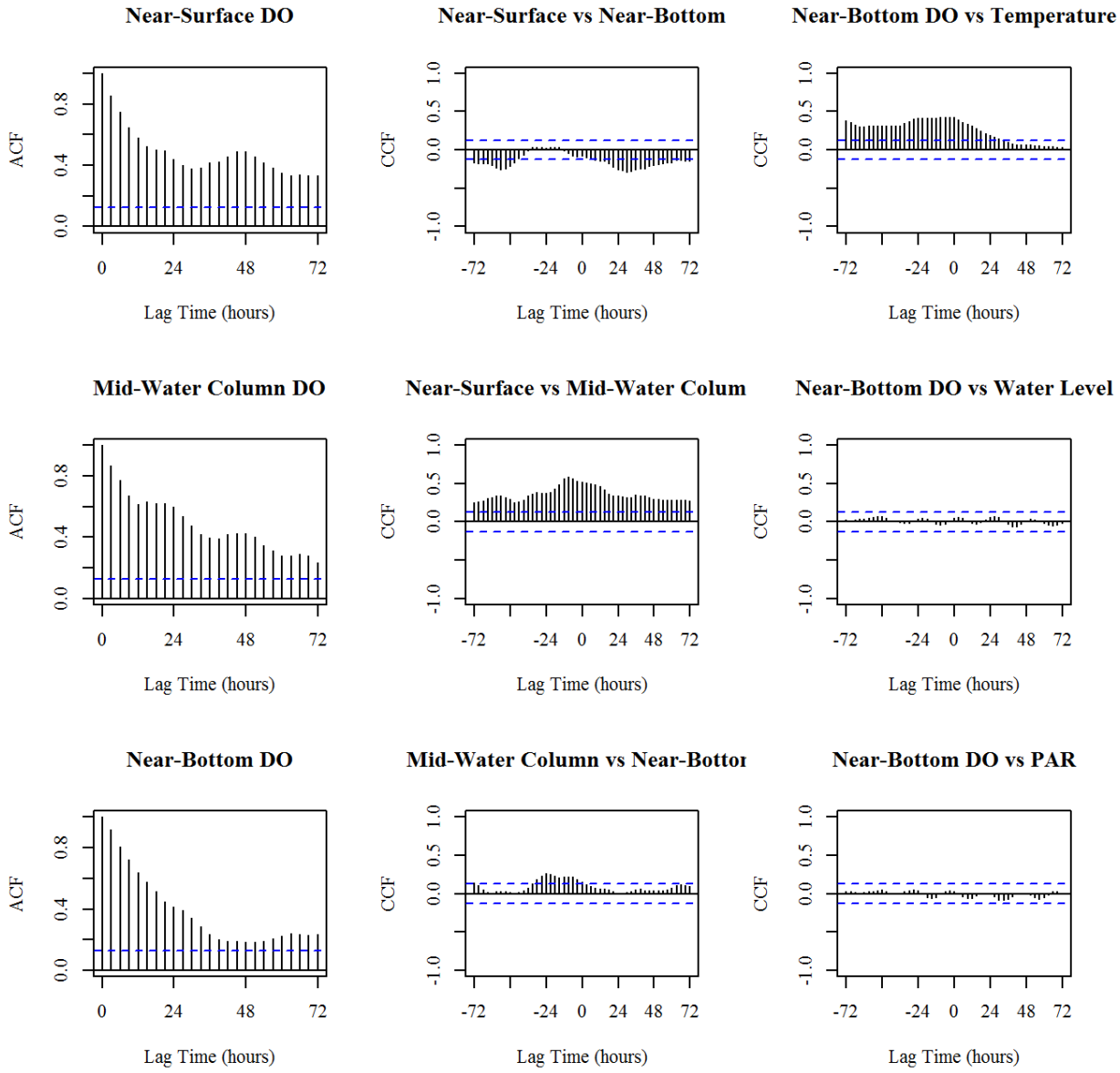

Figure B.23. Results for the month May 2003 (200305). Left Panel: Autocorrelation function (ACF) plots of DO concentrations from three depths, near surface (top), mid-water column (middle), and near-bottom (bottom); Middle Panel: Cross-correlation function (CCF) plots of DO concentrations between depths; Right Panel: Cross-correlation function (CCF) plots between near-bottom DO concentrations and the factors, temperature, water level, and PAR. Blue dotted lines represent 95% confidence limits. Further details are located on the first page of Appendix B.

September 2003 (200309)

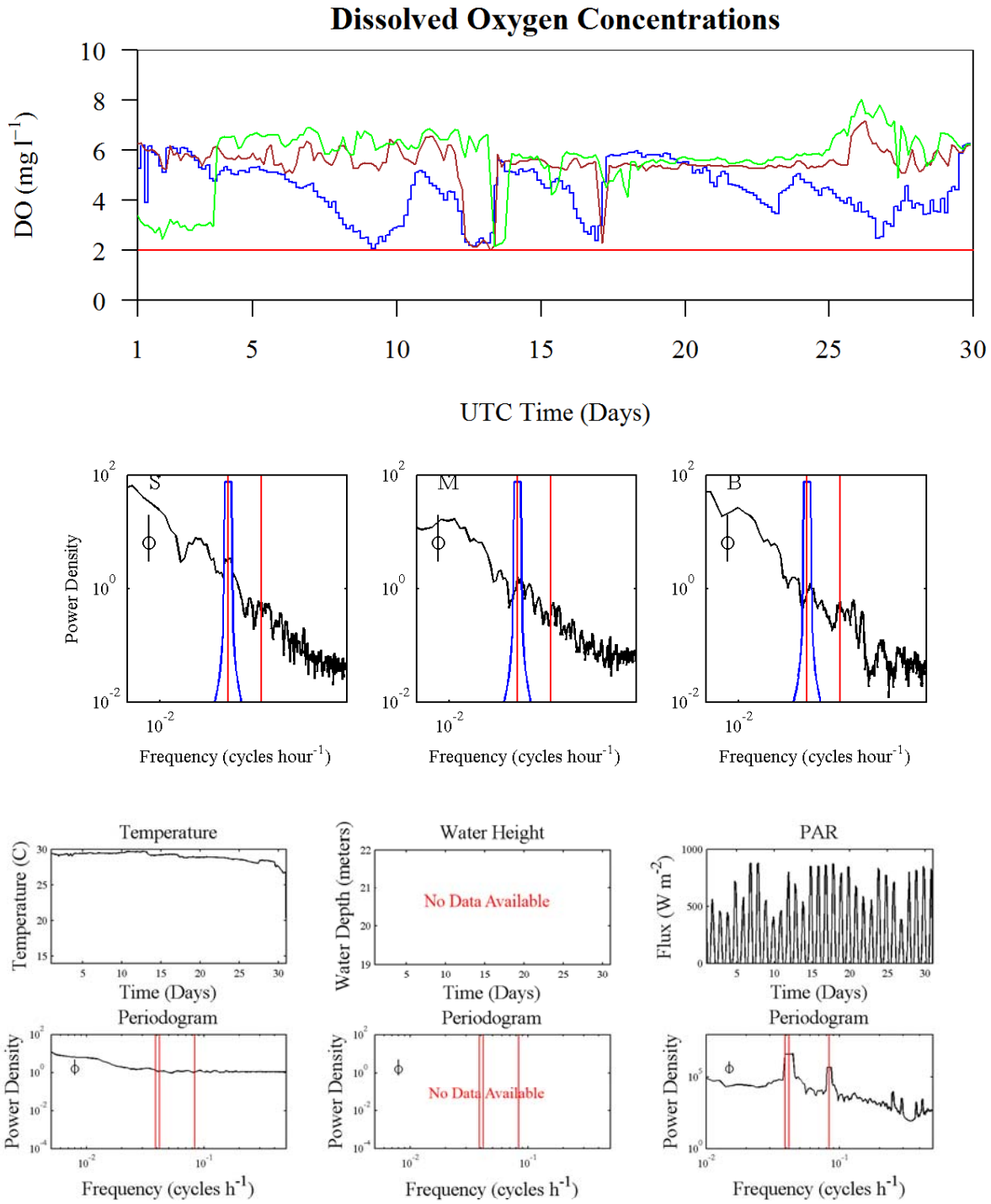

Figure B.23. Time-series plots and periodograms of dissolved oxygen (DO) concentrations and factors affecting DO concentrations for the month September 2003. Further details are located on the first page of Appendix B.

September 2003 (200309)

Autocorrelations and Cross Correlations

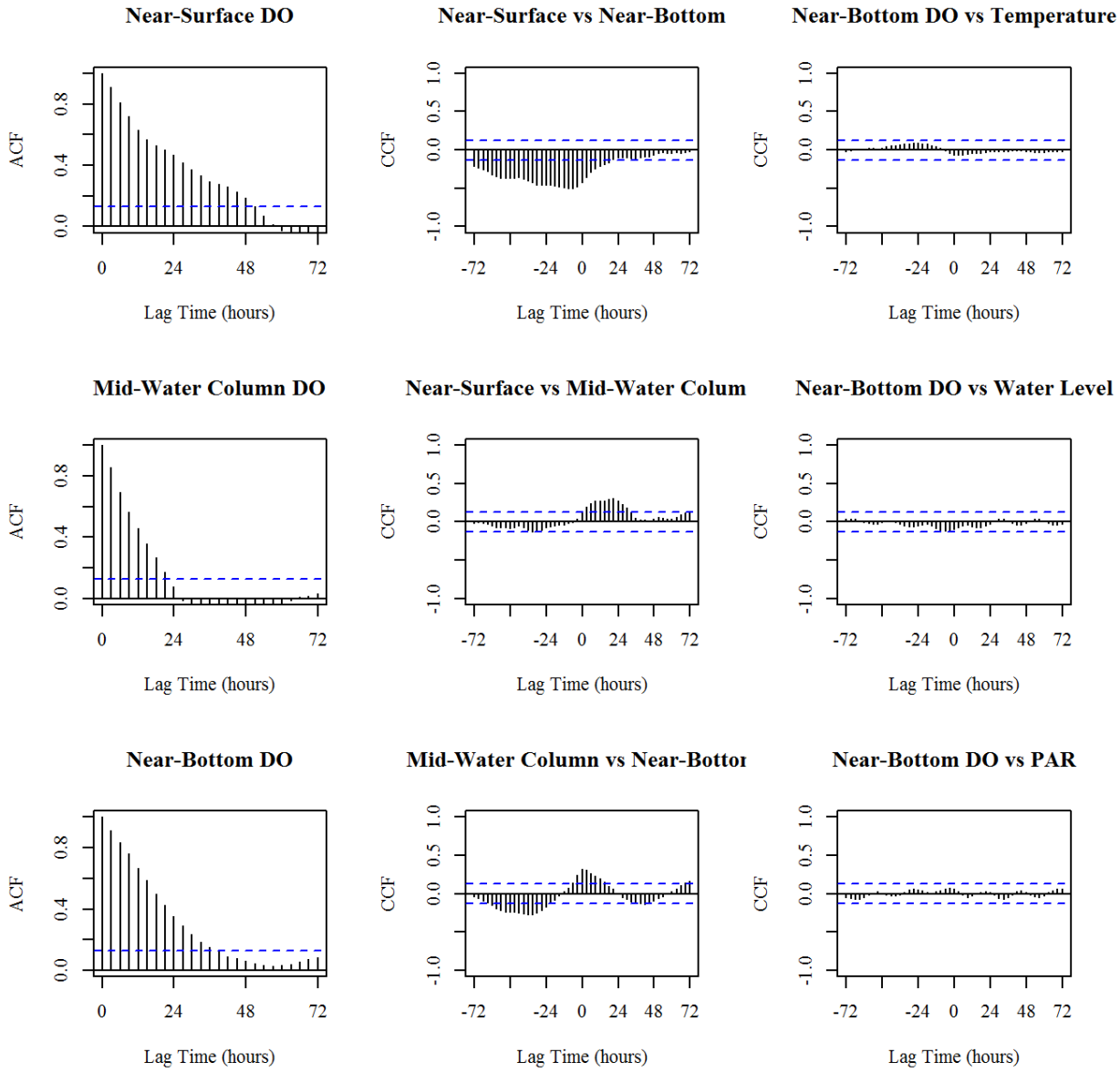

Figure B.24. Results for the month September 2003 (200309). Left Panel: Autocorrelation function (ACF) plots of DO concentrations from three depths, near surface (top), mid-water column (middle), and near-bottom (bottom); Middle Panel: Cross-correlation function (CCF) plots of DO concentrations between depths; Right Panel: Cross-correlation function (CCF) plots between near-bottom DO concentrations and the factors, temperature, water level, and PAR. Blue dotted lines represent 95% confidence limits. Further details are located on the first page of Appendix B.

October 2003 (200310)

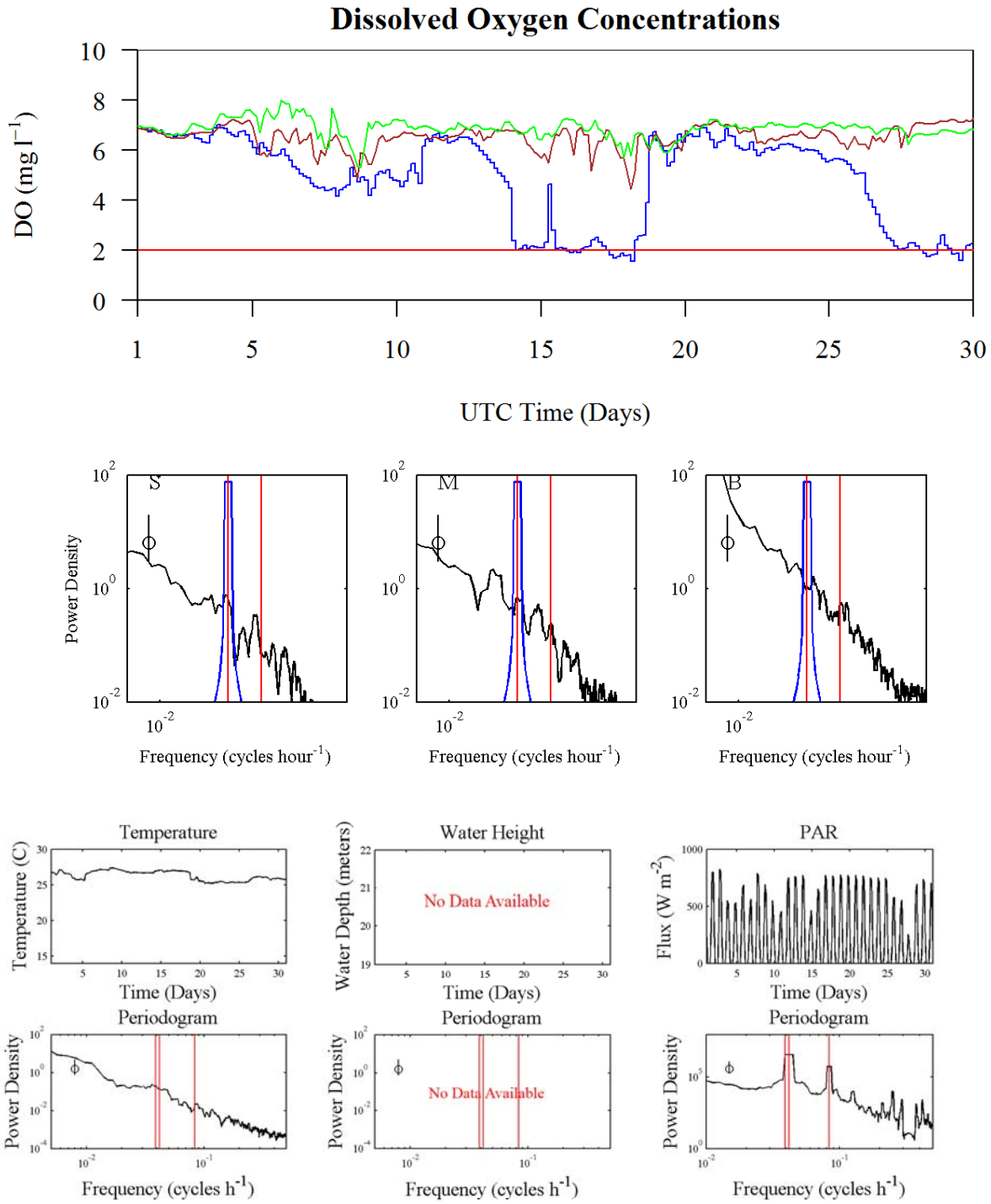

Figure B.24. Time-series plots and periodograms of dissolved oxygen (DO) concentrations and factors affecting DO concentrations for the month October 2003. Further details are located on the first page of Appendix B.

October 2003 (200310)

Autocorrelations and Cross Correlations

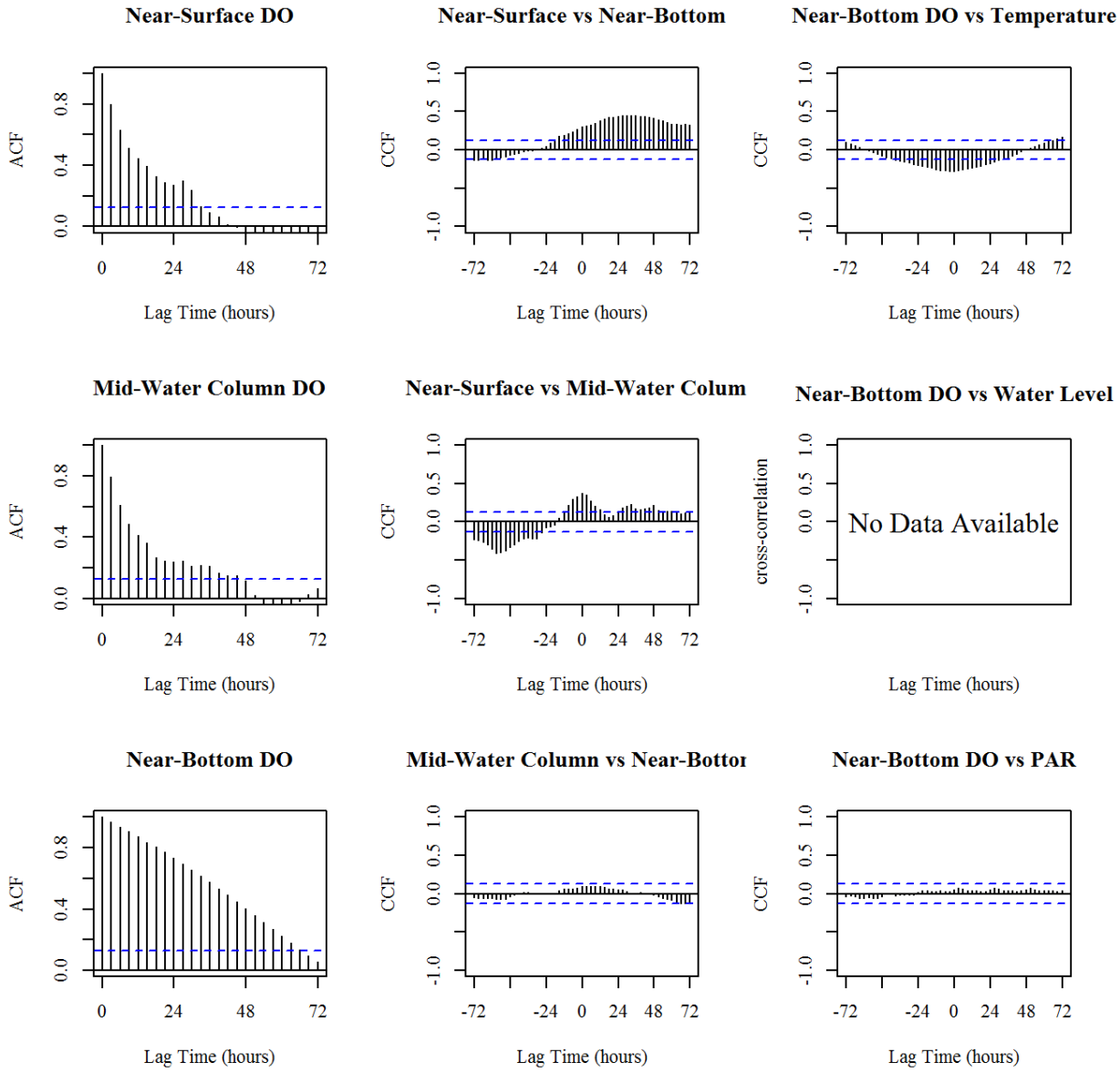

Figure B.25. Results for the month October 2003 (200310). Left Panel: Autocorrelation function (ACF) plots of DO concentrations from three depths, near surface (top), mid-water column (middle), and near-bottom (bottom); Middle Panel: Cross-correlation function (CCF) plots of DO concentrations between depths; Right Panel: Cross-correlation function (CCF) plots between near-bottom DO concentrations and the factors, temperature, water level, and PAR. Blue dotted lines represent 95% confidence limits. Further details are located on the first page of Appendix B.

January 2004 (200401)

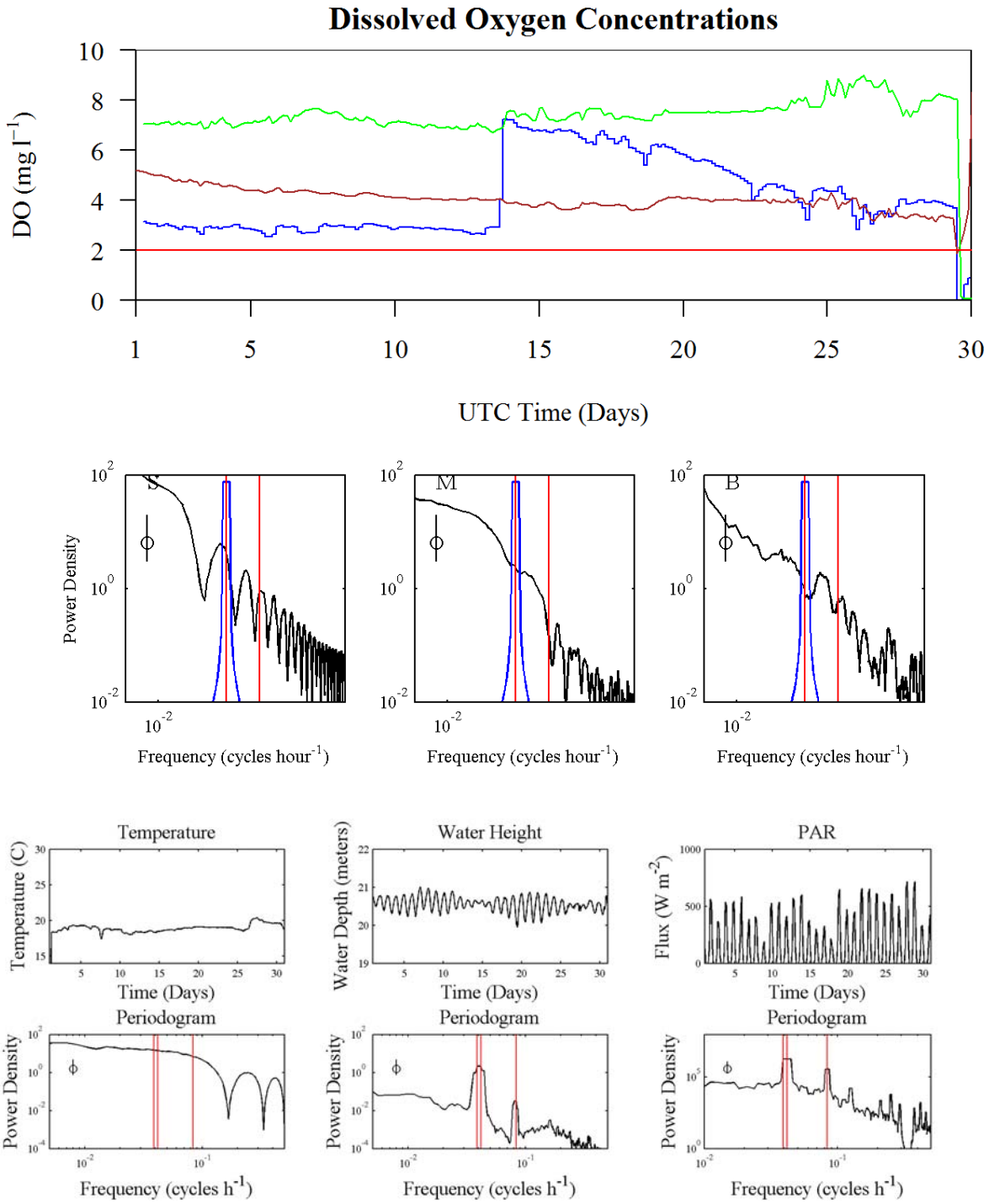

Figure B.25. Time-series plots and periodograms of dissolved oxygen (DO) concentrations and factors affecting DO concentrations for the month January 2004. Further details are located on the first page of Appendix B.

January 2004 (200401)

Autocorrelations and Cross Correlations

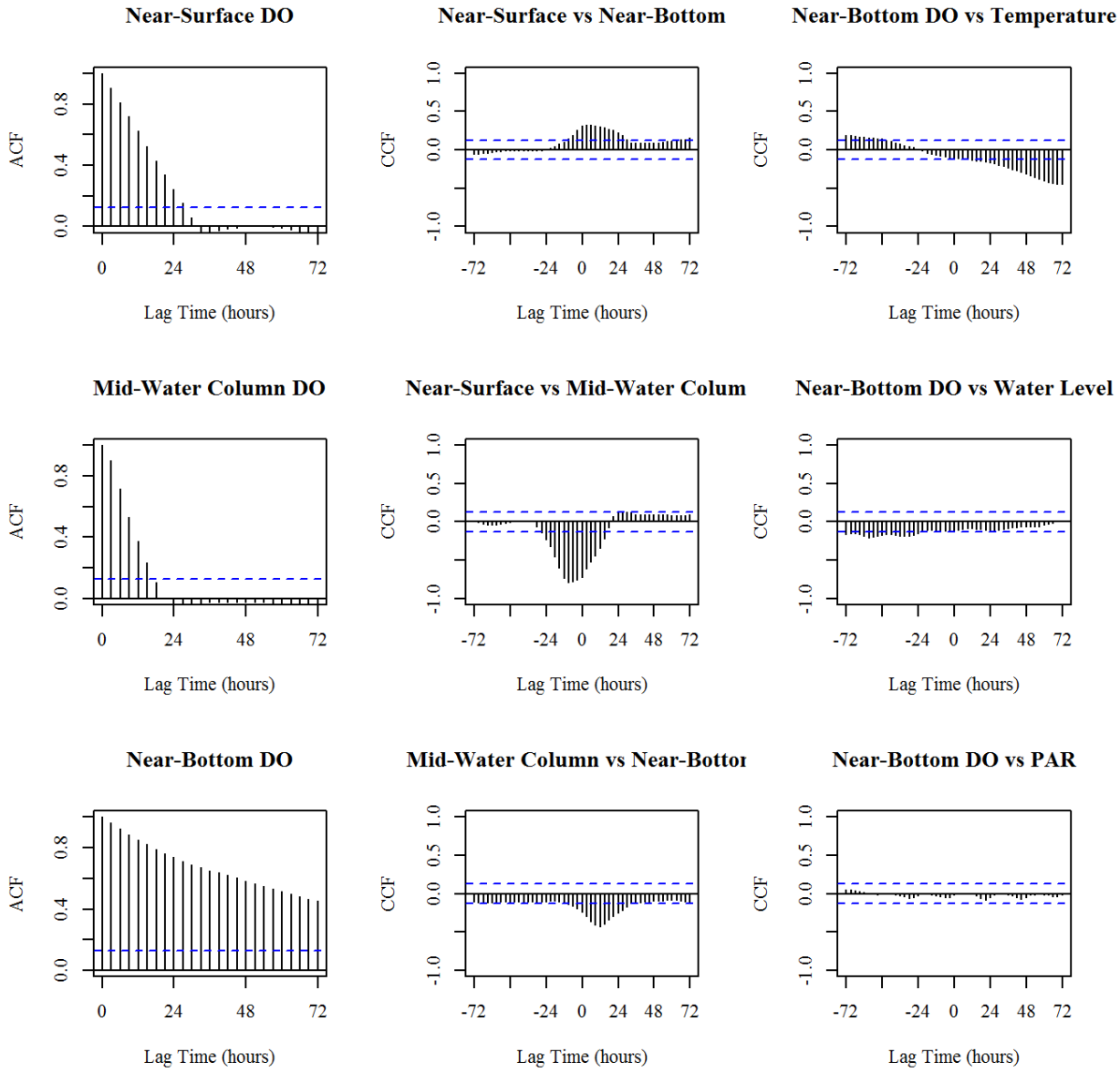

Figure B.26. Results for the month January 2004 (200401). Left Panel: Autocorrelation function (ACF) plots of DO concentrations from three depths, near surface (top), mid-water column (middle), and near-bottom (bottom); Middle Panel: Cross-correlation function (CCF) plots of DO concentrations between depths; Right Panel: Cross-correlation function (CCF) plots between near-bottom DO concentrations and the factors, temperature, water level, and PAR. Blue dotted lines represent 95% confidence limits. Further details are located on the first page of Appendix B.

February 2004 (200402)

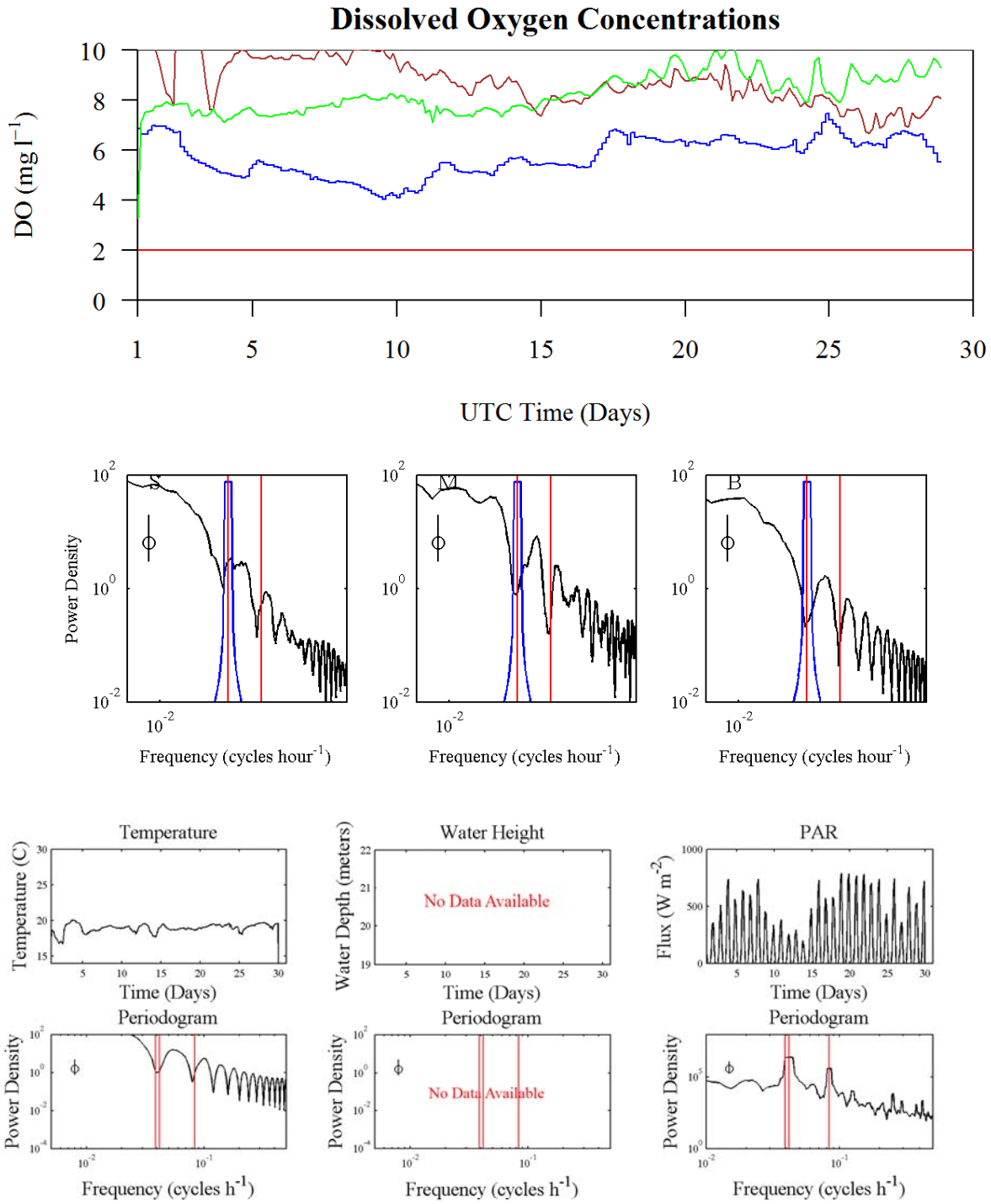

Figure B.26. Time-series plots and periodograms of dissolved oxygen (DO) concentrations and factors affecting DO concentrations for the month February 2004. Further details are located on the first page of Appendix B.

February 2004 (200402)

Autocorrelations and Cross Correlations

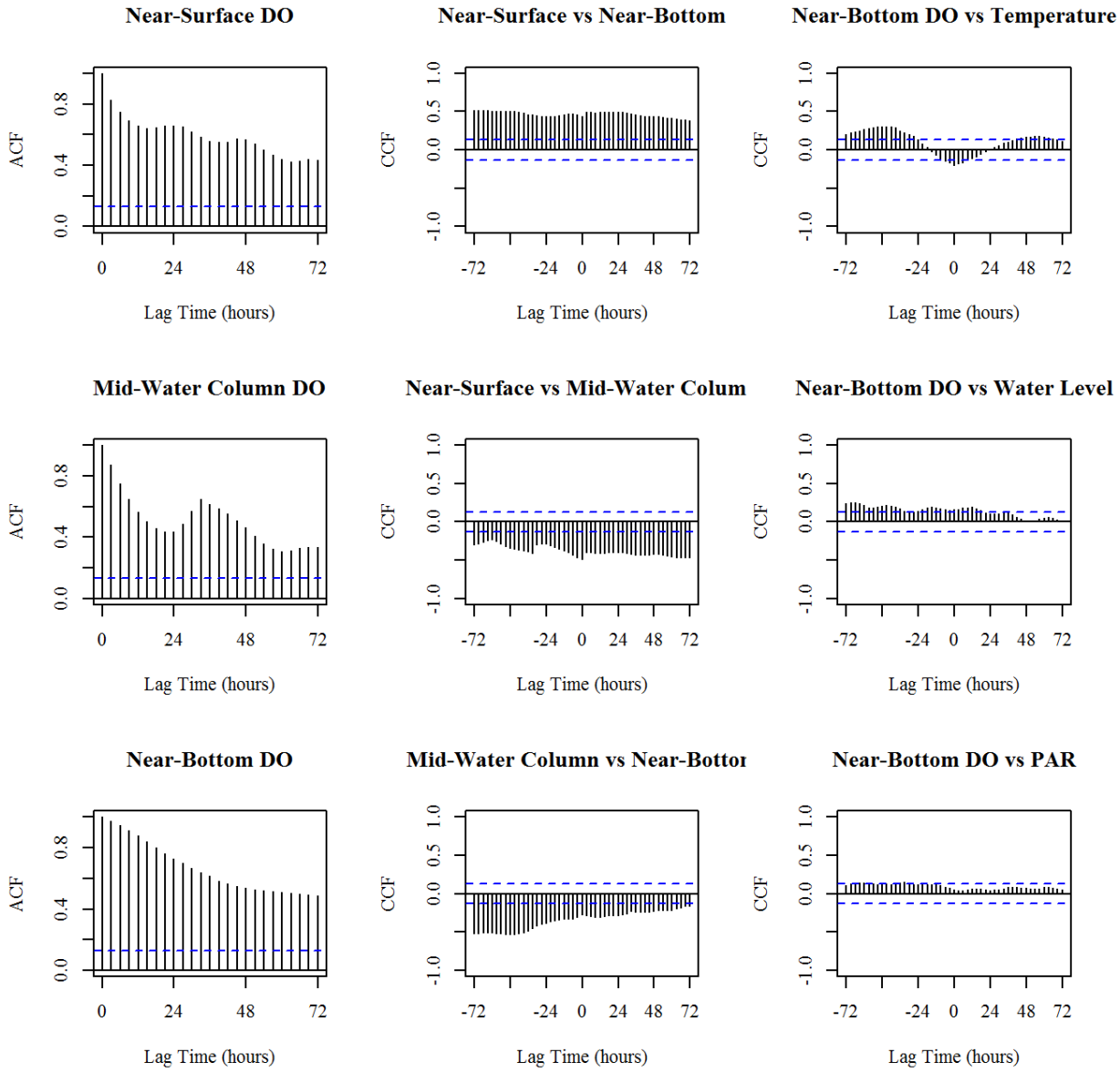

Figure B.27. Results for the month February 2004 (200402). Left Panel: Autocorrelation function (ACF) plots of DO concentrations from three depths, near surface (top), mid-water column (middle), and near-bottom (bottom); Middle Panel: Cross-correlation function (CCF) plots of DO concentrations between depths; Right Panel: Cross-correlation function (CCF) plots between near-bottom DO concentrations and the factors, temperature, water level, and PAR. Blue dotted lines represent 95% confidence limits. Further details are located on the first page of Appendix B.

March 2004 (200403)

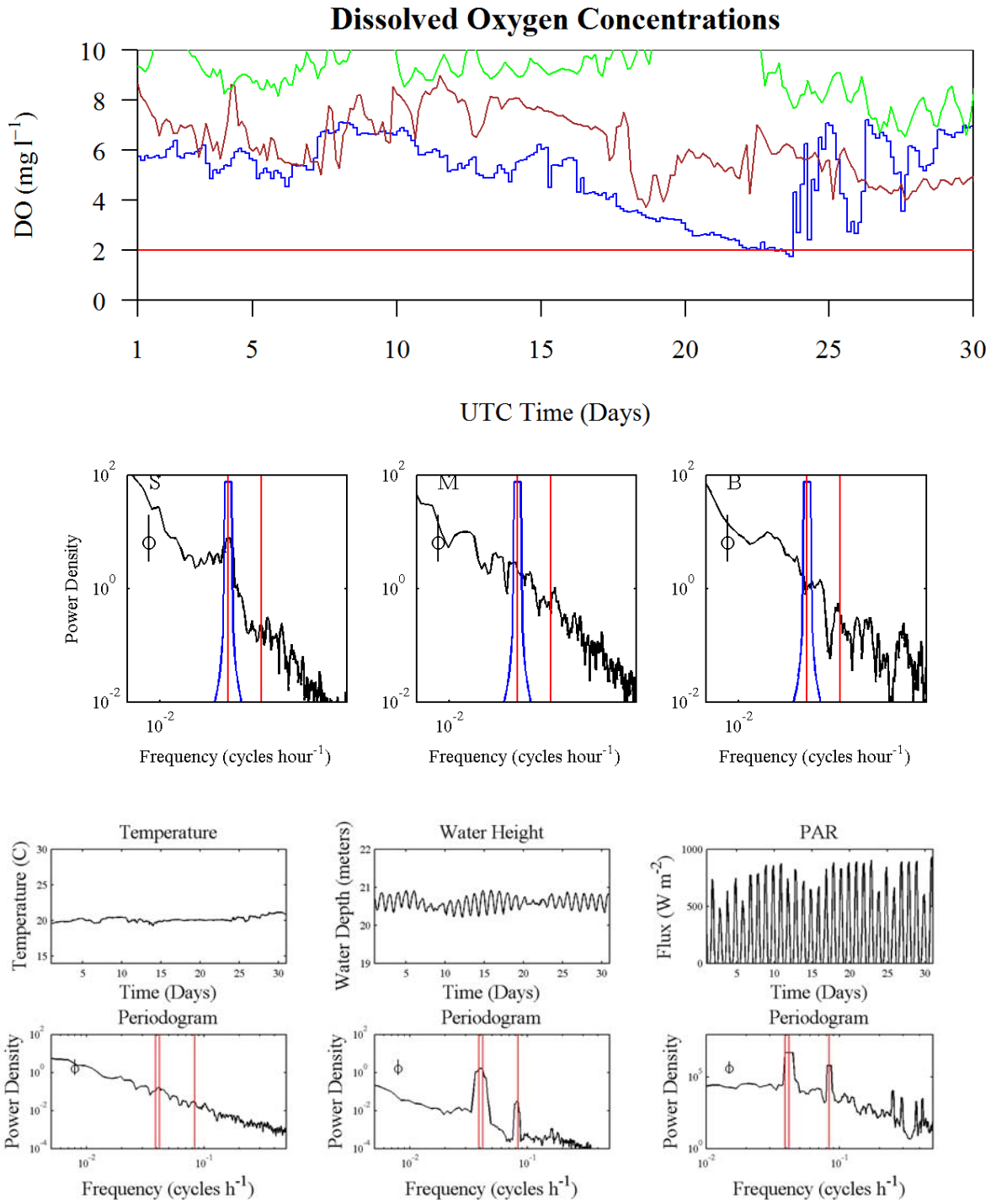

Figure B.27. Time-series plots and periodograms of dissolved oxygen (DO) concentrations and factors affecting DO concentrations for the month March 2004. Further details are located on the first page of Appendix B.

March 2004 (200403)

Autocorrelations and Cross Correlations

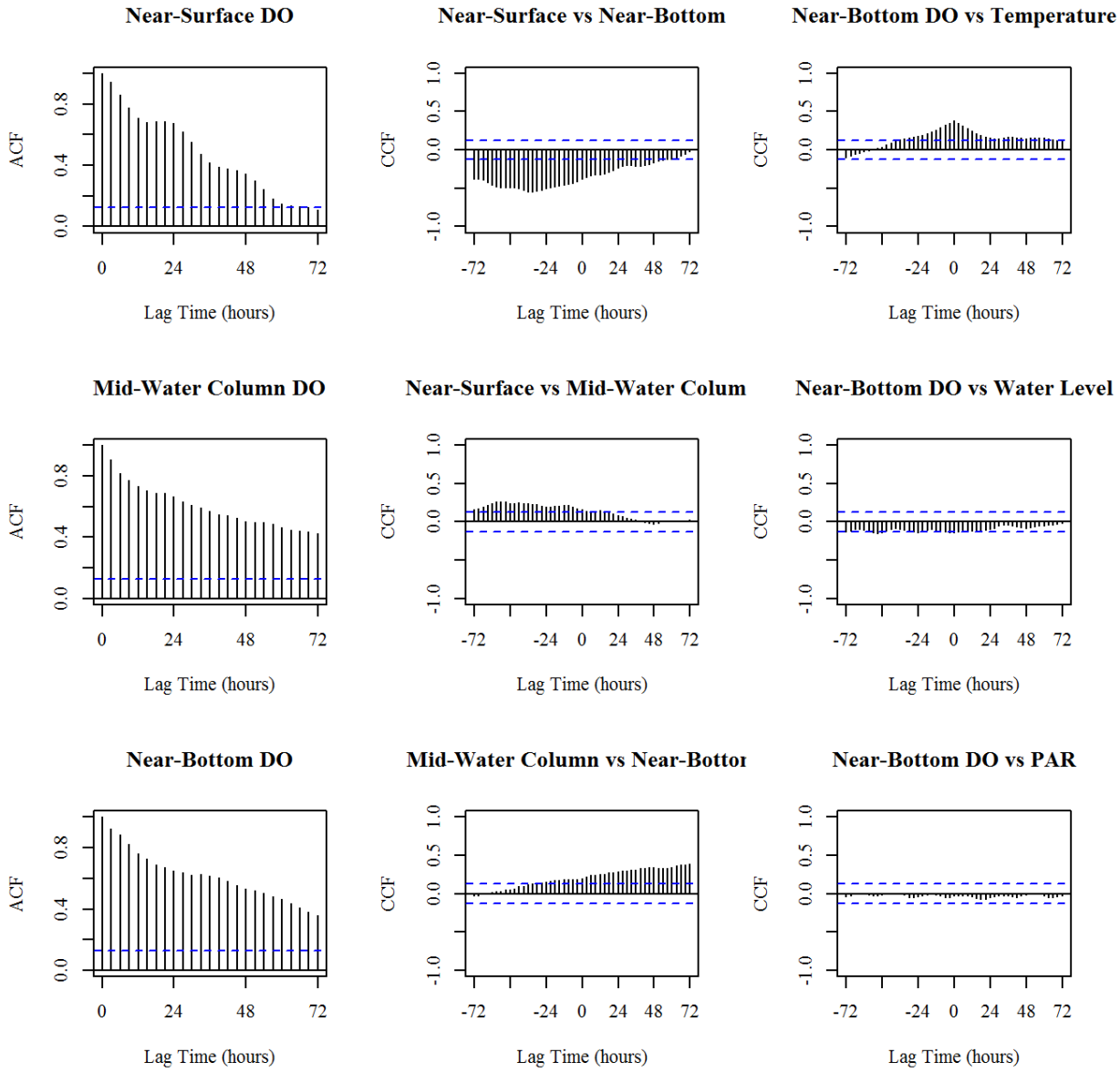

Figure B.28. Results for the month March 2004 (200403). Left Panel: Autocorrelation function (ACF) plots of DO concentrations from three depths, near surface (top), mid-water column (middle), and near-bottom (bottom); Middle Panel: Cross-correlation function (CCF) plots of DO concentrations between depths; Right Panel: Cross-correlation function (CCF) plots between near-bottom DO concentrations and the factors, temperature, water level, and PAR. Blue dotted lines represent 95% confidence limits. Further details are located on the first page of Appendix B.

April 2004 (200404)

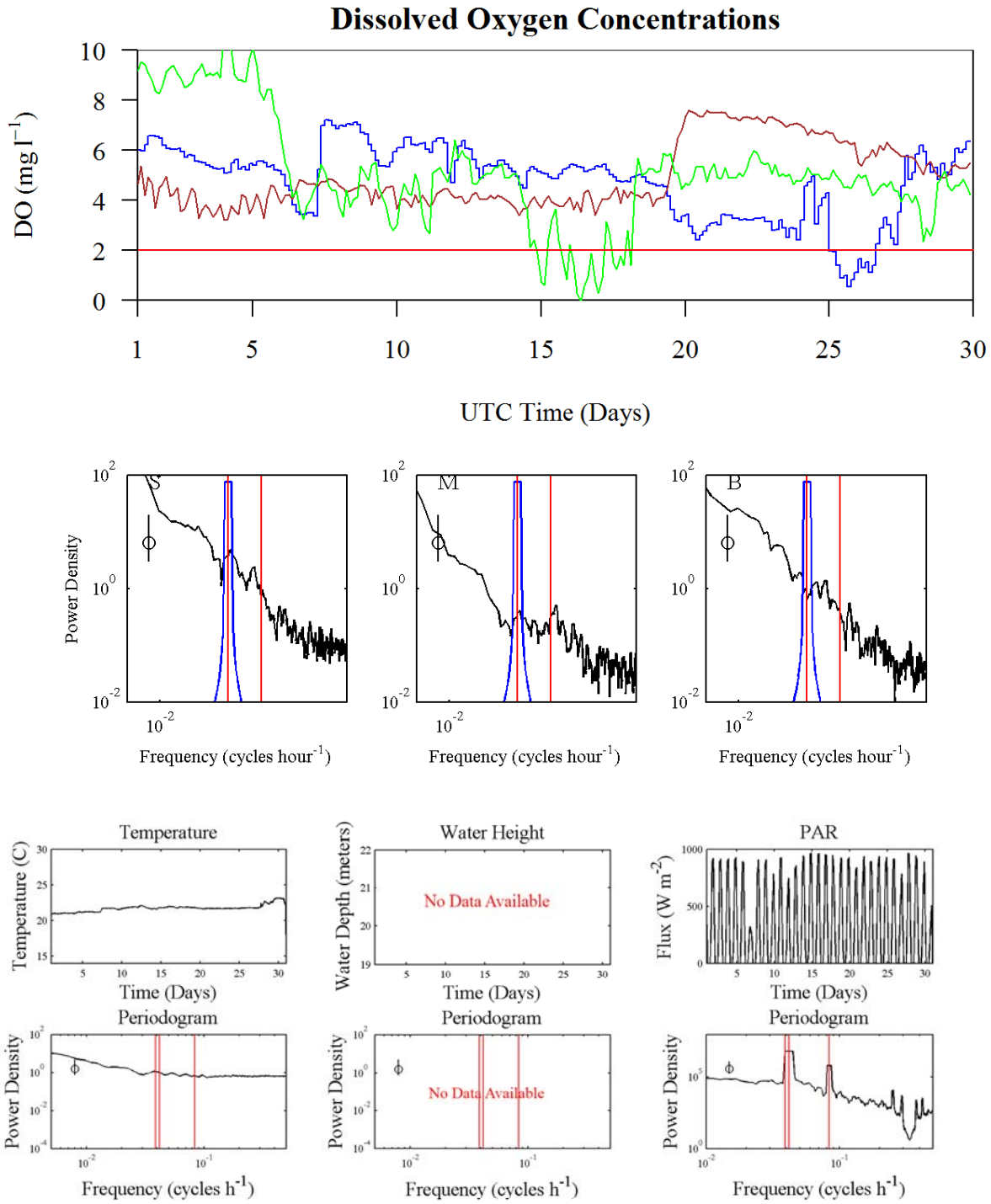

Figure B.28. Time-series plots and periodograms of dissolved oxygen (DO) concentrations and factors affecting DO concentrations for the month April 2004. Further details are located on the first page of Appendix B.

April 2004 (200404)

Autocorrelations and Cross Correlations

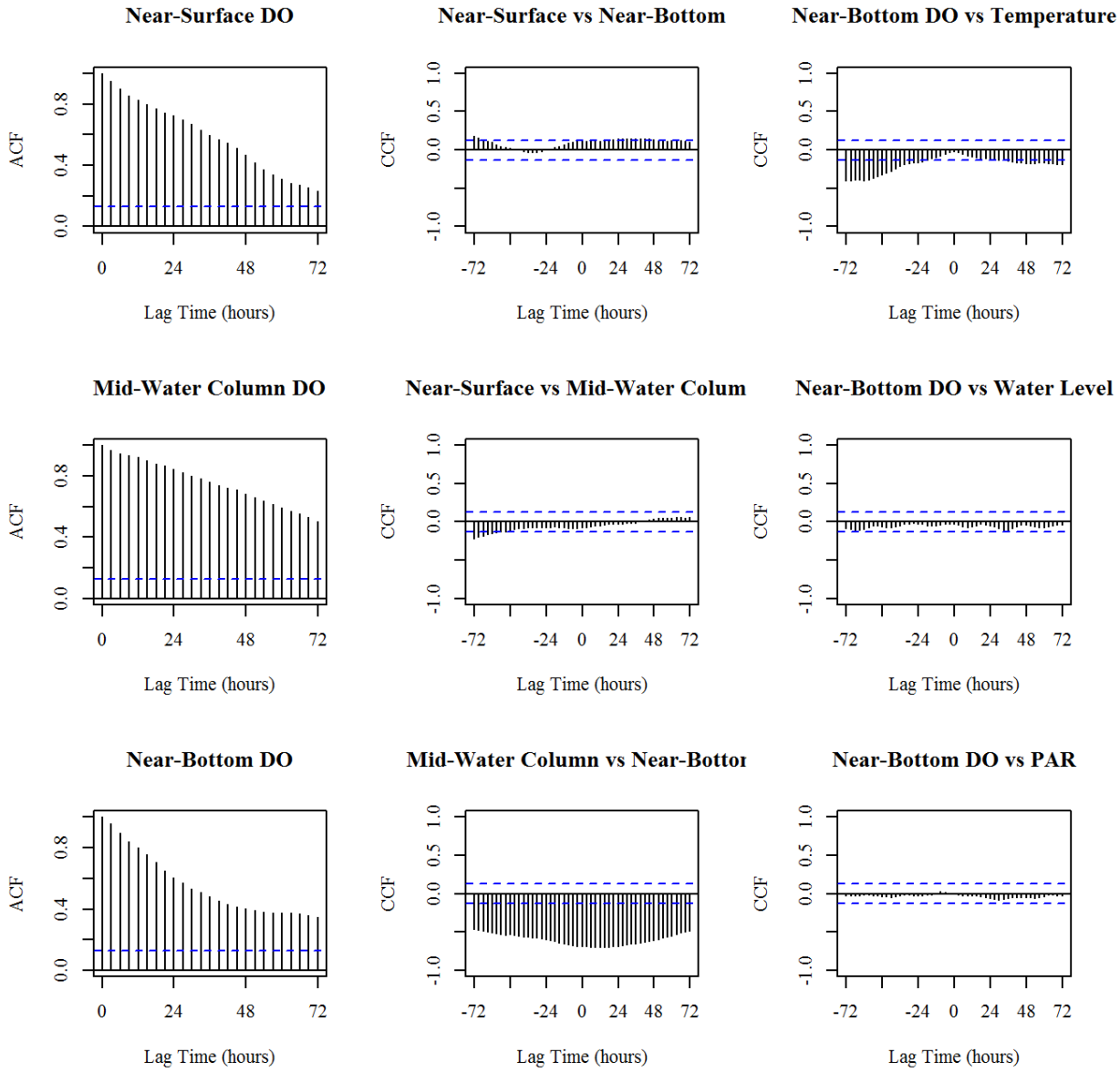

Figure B.29. Results for the month April 2004 (200404). Left Panel: Autocorrelation function (ACF) plots of DO concentrations from three depths, near surface (top), mid-water column (middle), and near-bottom (bottom); Middle Panel: Cross-correlation function (CCF) plots of DO concentrations between depths; Right Panel: Cross-correlation function (CCF) plots between near-bottom DO concentrations and the factors, temperature, water level, and PAR. Blue dotted lines represent 95% confidence limits. Further details are located on the first page of Appendix B.

May 2004 (200405)

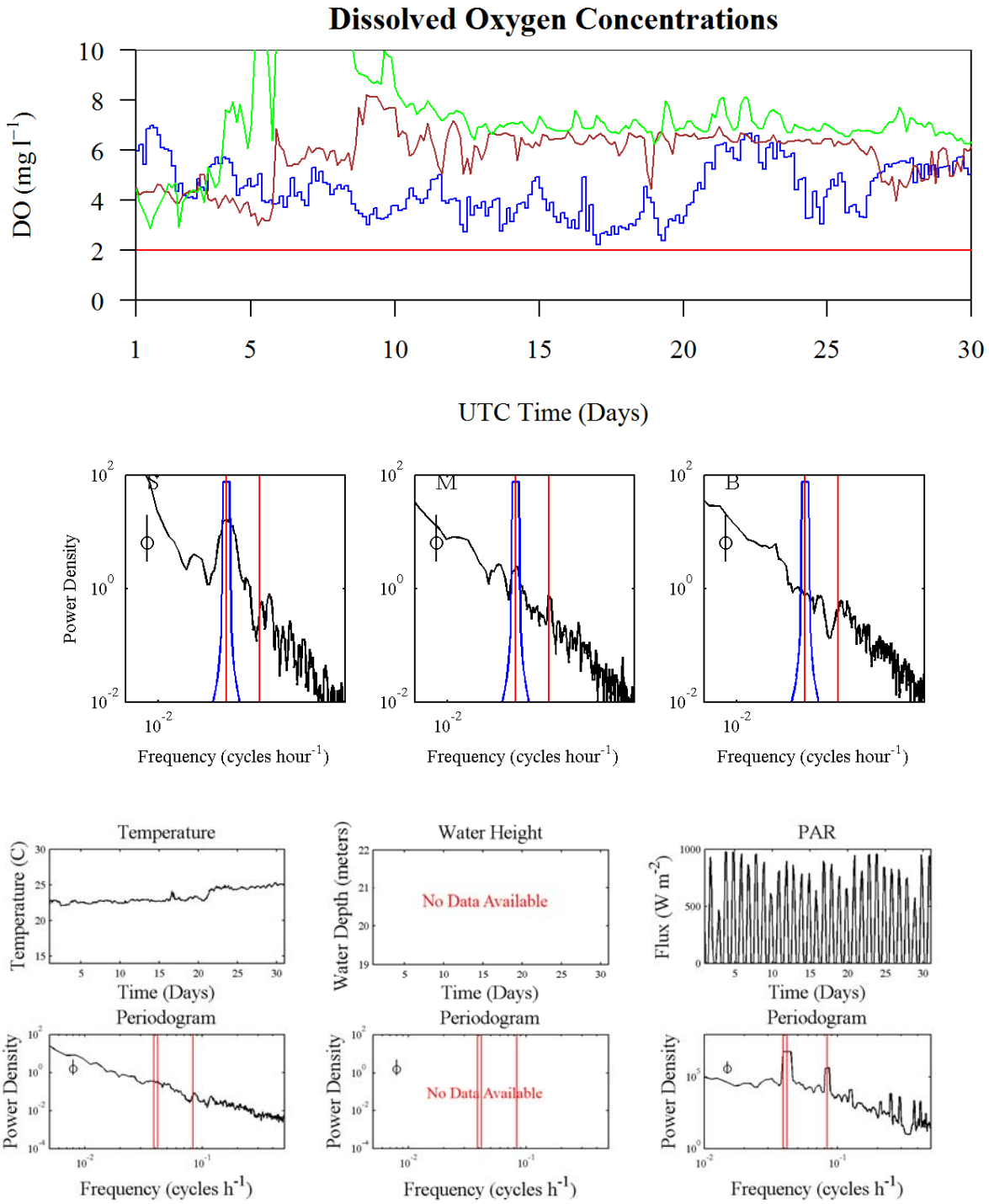

Figure B.29. Time-series plots and periodograms of dissolved oxygen (DO) concentrations and factors affecting DO concentrations for the month May 2004. Further details are located on the first page of Appendix B.

May 2004 (200405)

Autocorrelations and Cross Correlations

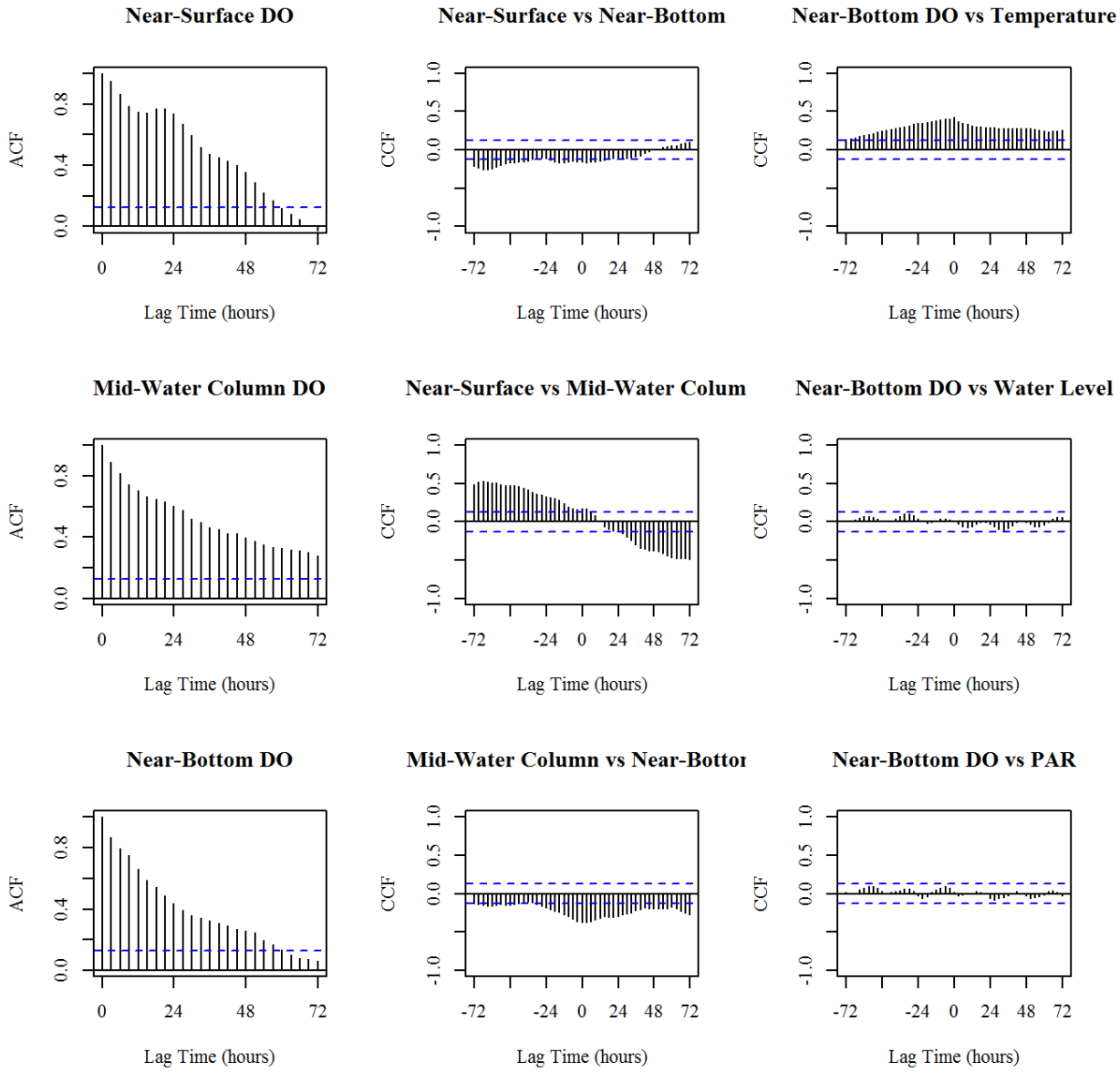

Figure B.30. Results for the month May 2004 (200405). Left Panel: Autocorrelation function (ACF) plots of DO concentrations from three depths, near surface (top), mid-water column (middle), and near-bottom (bottom); Middle Panel: Cross-correlation function (CCF) plots of DO concentrations between depths; Right Panel: Cross-correlation function (CCF) plots between near-bottom DO concentrations and the factors, temperature, water level, and PAR. Blue dotted lines represent 95% confidence limits. Further details are located on the first page of Appendix B.

June 2004 (200406)

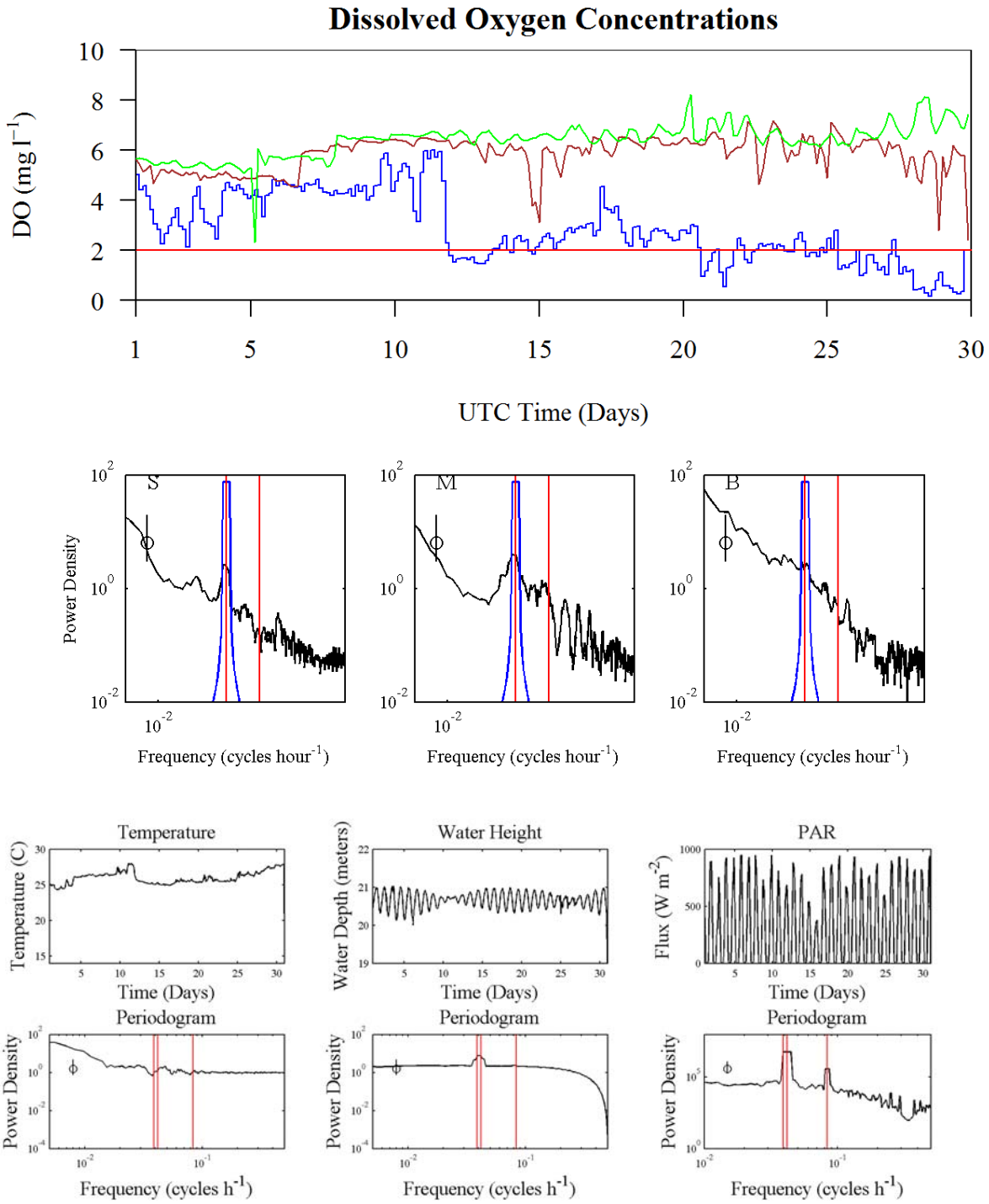

Figure B.30. Time-series plots and periodograms of dissolved oxygen (DO) concentrations and factors affecting DO concentrations for the month June 2004. Further details are located on the first page of Appendix B.

June 2004 (200406)

Autocorrelations and Cross Correlations

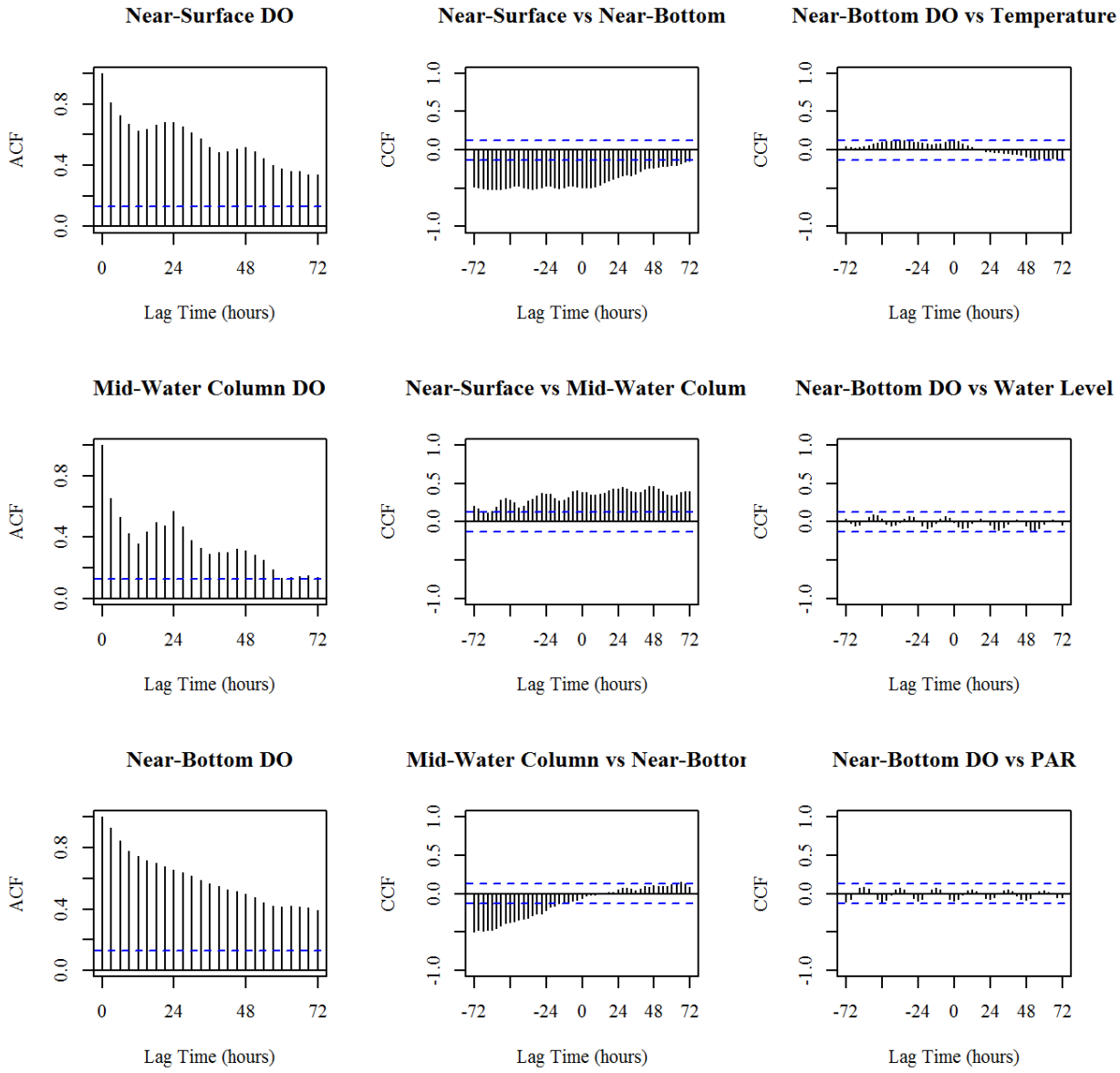

Figure B.31. Results for the month June 2004 (200406). Left Panel: Autocorrelation function (ACF) plots of DO concentrations from three depths, near surface (top), mid-water column (middle), and near-bottom (bottom); Middle Panel: Cross-correlation function (CCF) plots of DO concentrations between depths; Right Panel: Cross-correlation function (CCF) plots between near-bottom DO concentrations and the factors, temperature, water level, and PAR. Blue dotted lines represent 95% confidence limits. Further details are located on the first page of Appendix B.

July 2004 (200407)

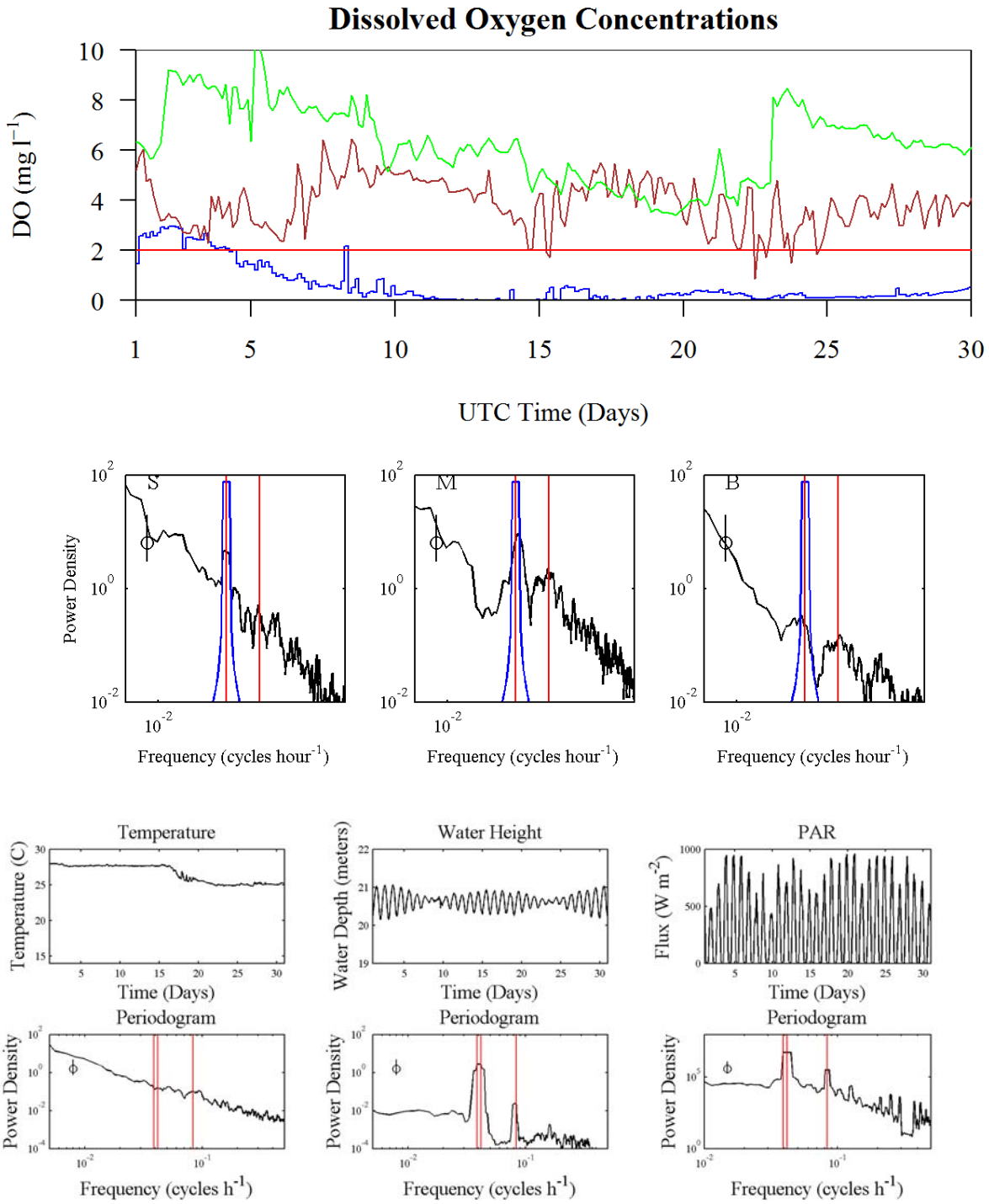

Figure B.31. Time-series plots and periodograms of dissolved oxygen (DO) concentrations and factors affecting DO concentrations for the month July 2004. Further details are located on the first page of Appendix B.

July 2004 (200407)

Autocorrelations and Cross Correlations

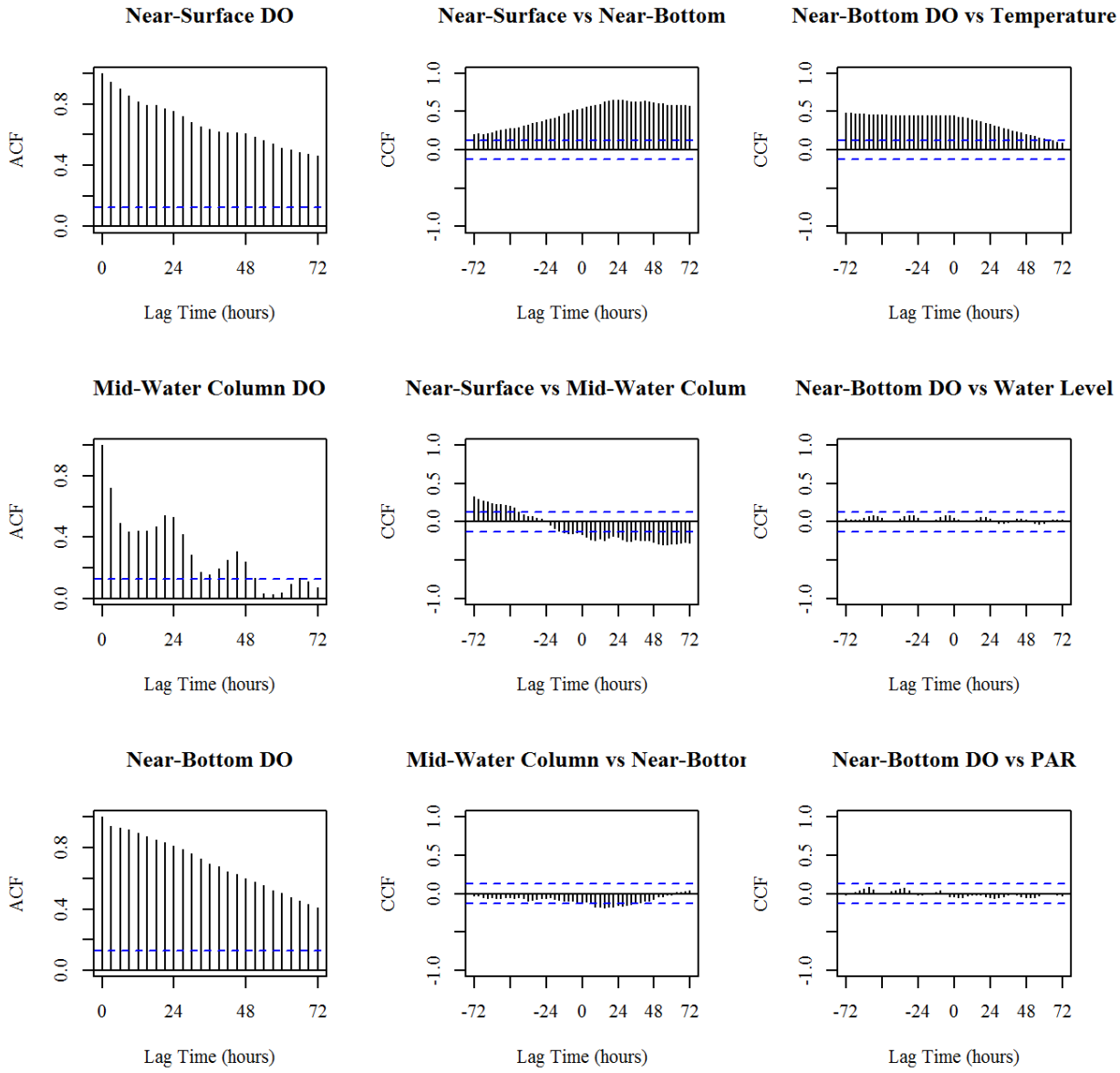

Figure B.32. Results for the month July 2004 (200407). Left Panel: Autocorrelation function (ACF) plots of DO concentrations from three depths, near surface (top), mid-water column (middle), and near-bottom (bottom); Middle Panel: Cross-correlation function (CCF) plots of DO concentrations between depths; Right Panel: Cross-correlation function (CCF) plots between near-bottom DO concentrations and the factors, temperature, water level, and PAR. Blue dotted lines represent 95% confidence limits. Further details are located on the first page of Appendix B.

August 2004 (200408)

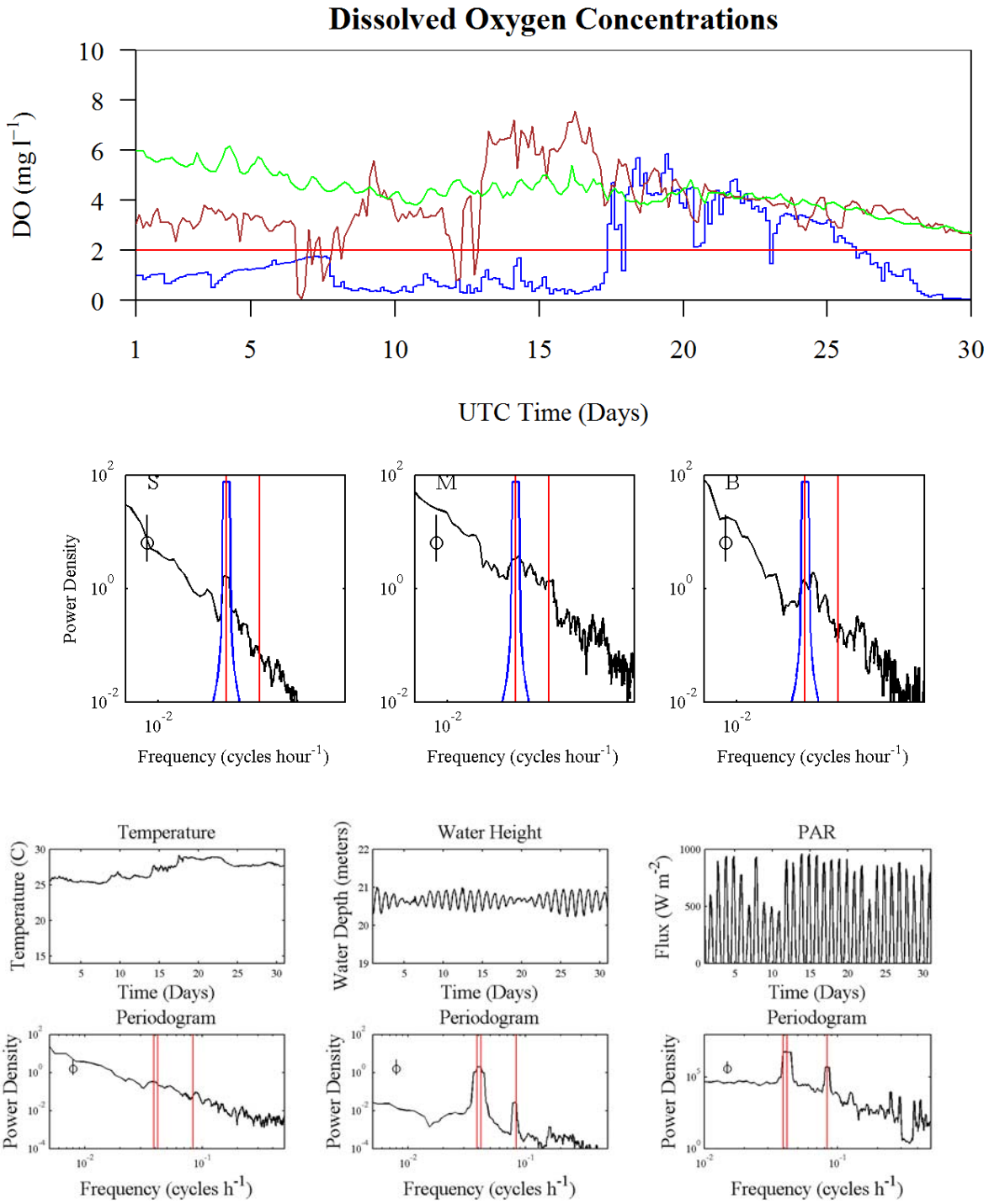

Figure B.32. Time-series plots and periodograms of dissolved oxygen (DO) concentrations and factors affecting DO concentrations for the month August 2004. Further details are located on the first page of Appendix B.

August 2004 (200408)

Autocorrelations and Cross Correlations

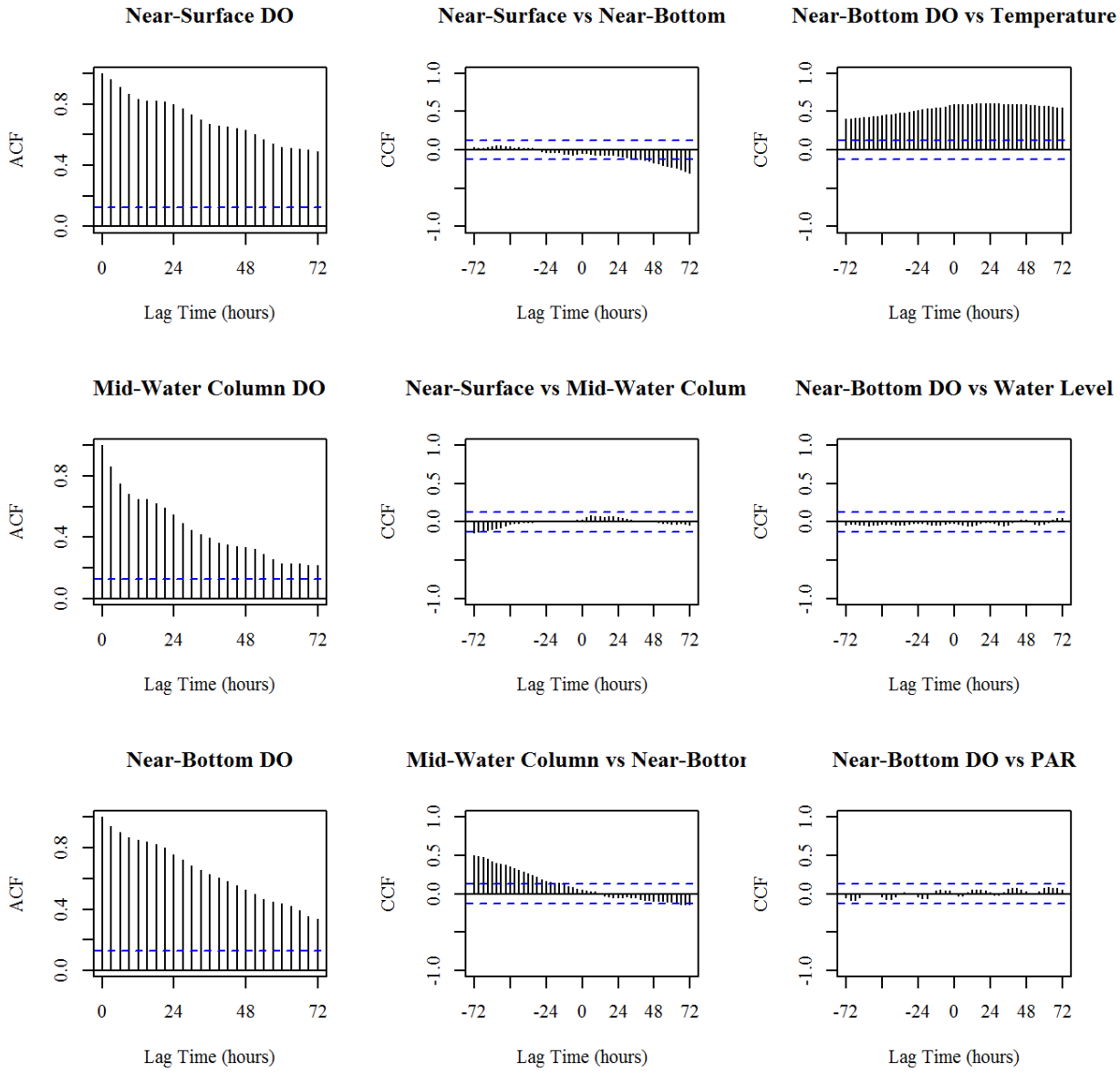

Figure B.33. Results for the month August 2004 (200408). Left Panel: Autocorrelation function (ACF) plots of DO concentrations from three depths, near surface (top), mid-water column (middle), and near-bottom (bottom); Middle Panel: Cross-correlation function (CCF) plots of DO concentrations between depths; Right Panel: Cross-correlation function (CCF) plots between near-bottom DO concentrations and the factors, temperature, water level, and PAR. Blue dotted lines represent 95% confidence limits. Further details are located on the first page of Appendix B.

September 2004 (200409)

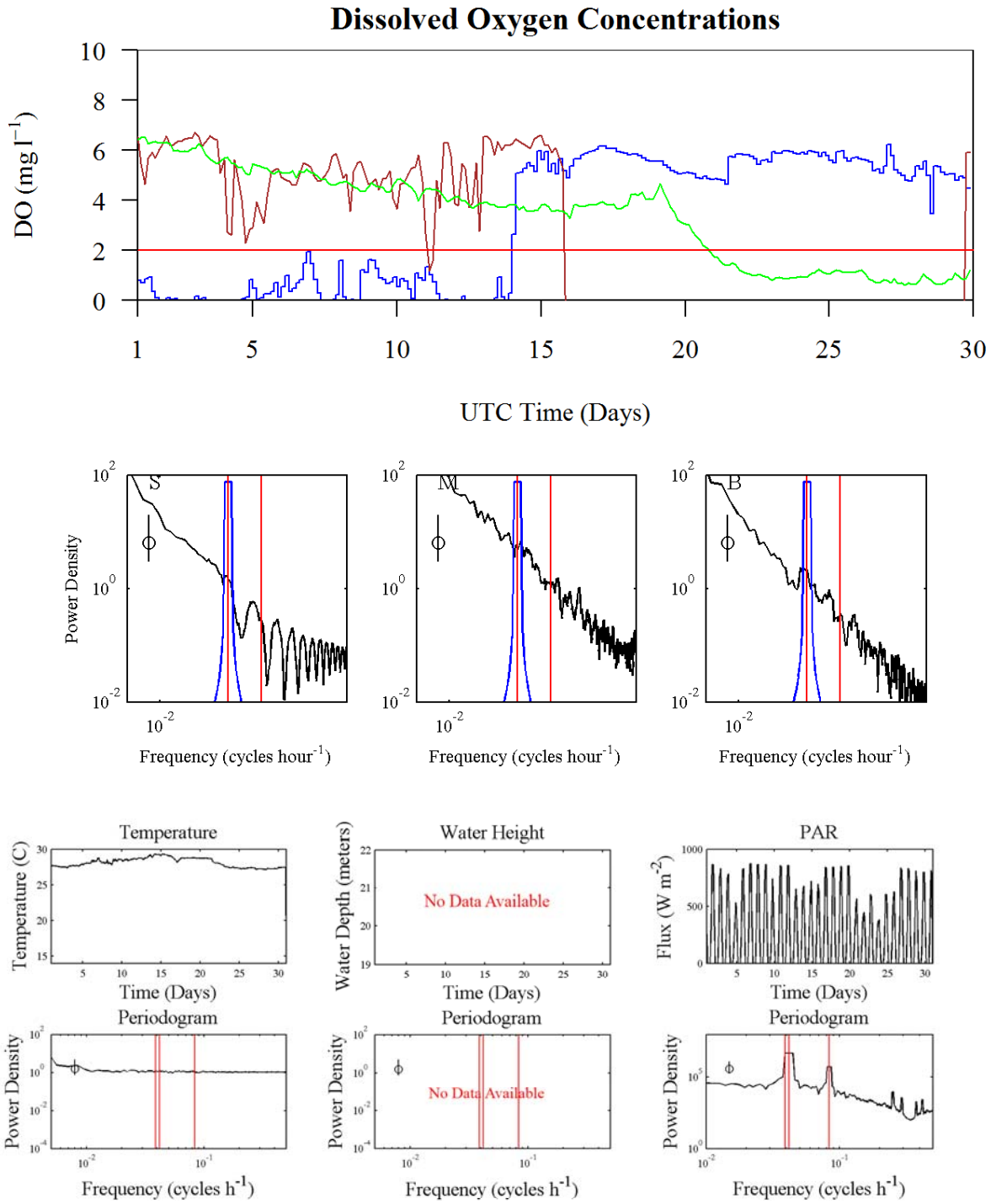

Figure B.33. Time-series plots and periodograms of dissolved oxygen (DO) concentrations and factors affecting DO concentrations for the month September 2004. Further details are located on the first page of Appendix B.

September 2004 (200409)

Autocorrelations and Cross Correlations

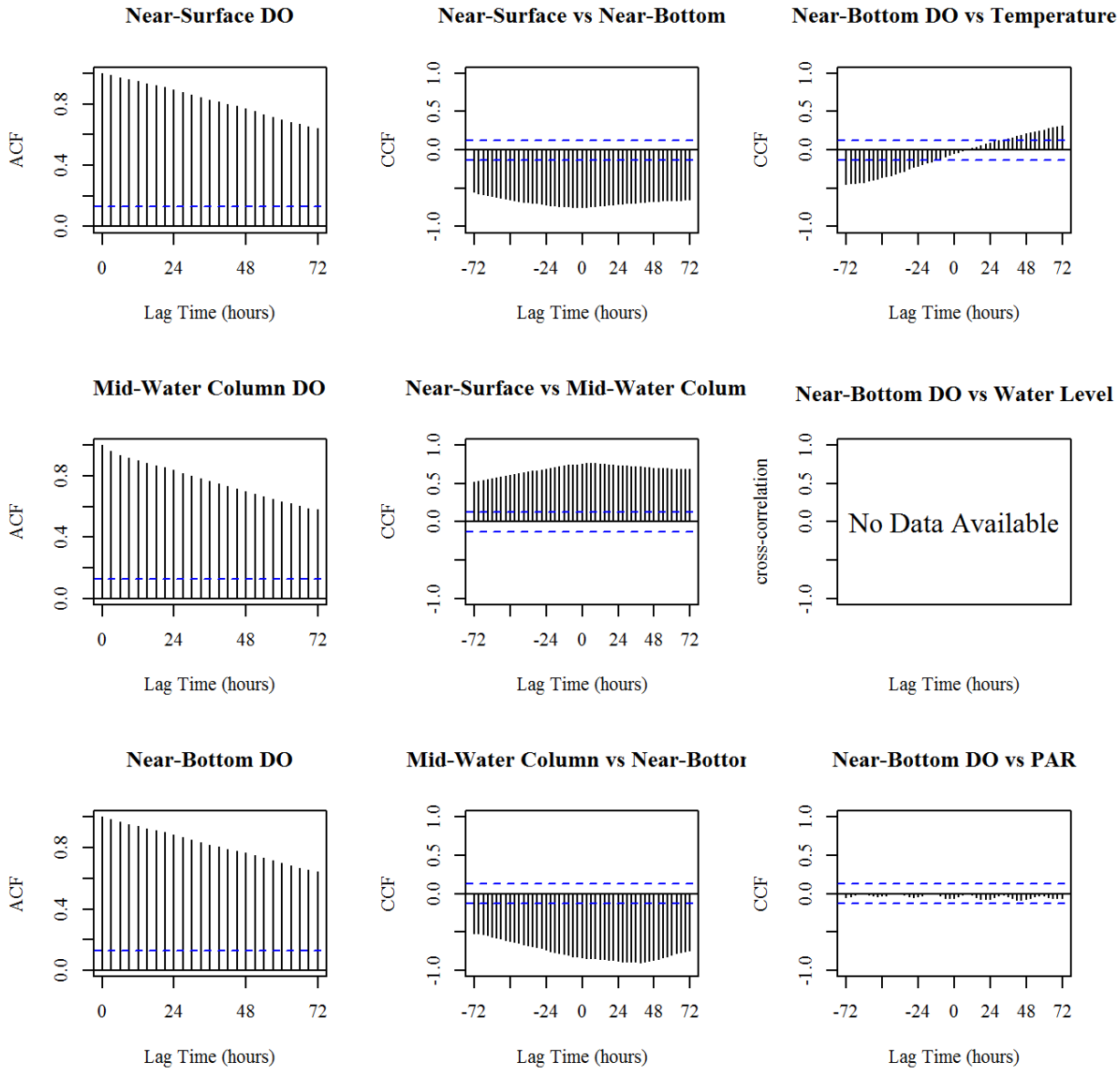

Figure B.34. Results for the month September 2004 (200409). Left Panel: Autocorrelation function (ACF) plots of DO concentrations from three depths, near surface (top), mid-water column (middle), and near-bottom (bottom); Middle Panel: Cross-correlation function (CCF) plots of DO concentrations between depths; Right Panel: Cross-correlation function (CCF) plots between near-bottom DO concentrations and the factors, temperature, water level, and PAR. Blue dotted lines represent 95% confidence limits. Further details are located on the first page of Appendix B.

April 2005 (200504)

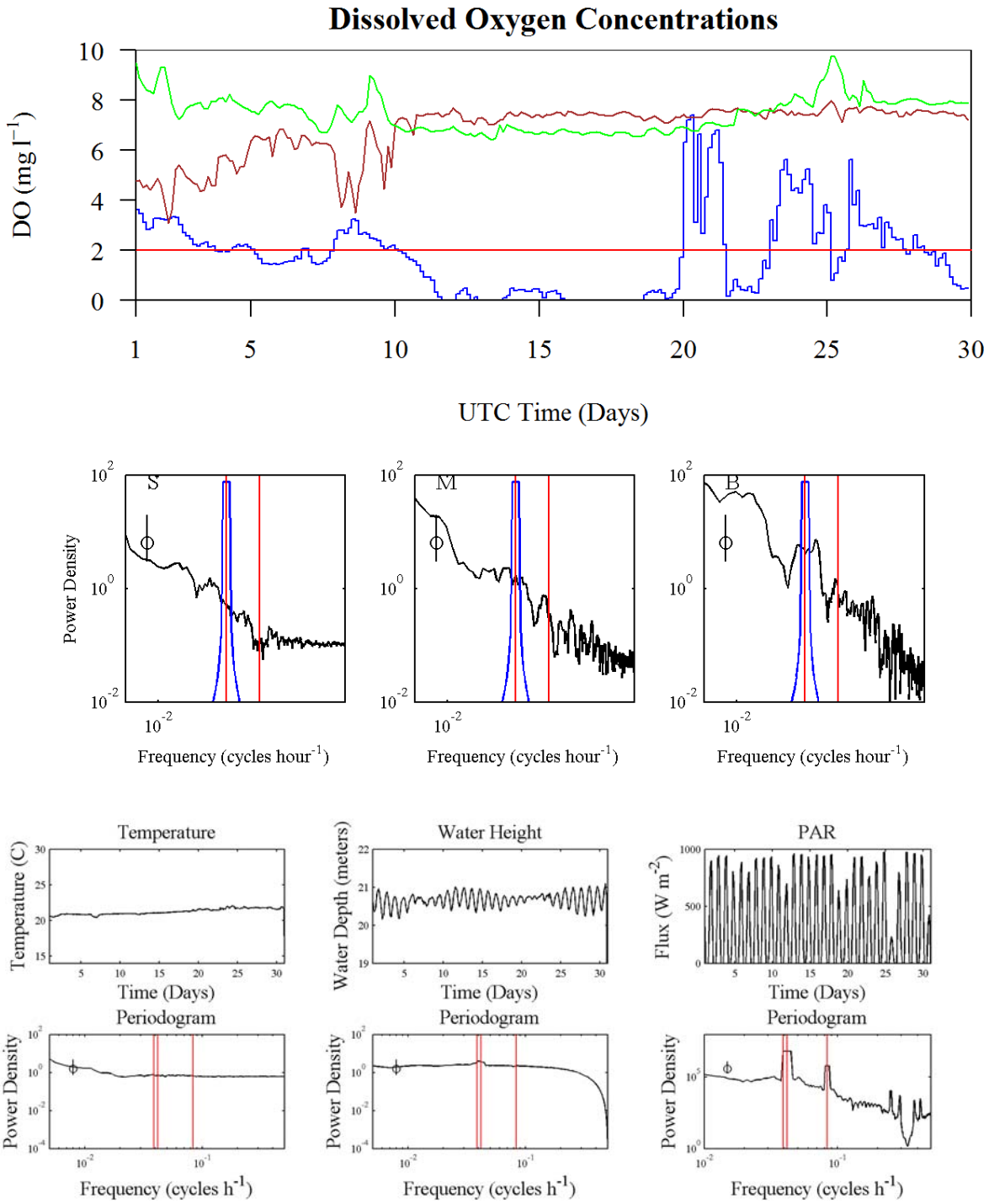

Figure B.34. Time-series plots and periodograms of dissolved oxygen (DO) concentrations and factors affecting DO concentrations for the month April 2005. Further details are located on the first page of Appendix B.

April 2005 (200504)

Autocorrelations and Cross Correlations

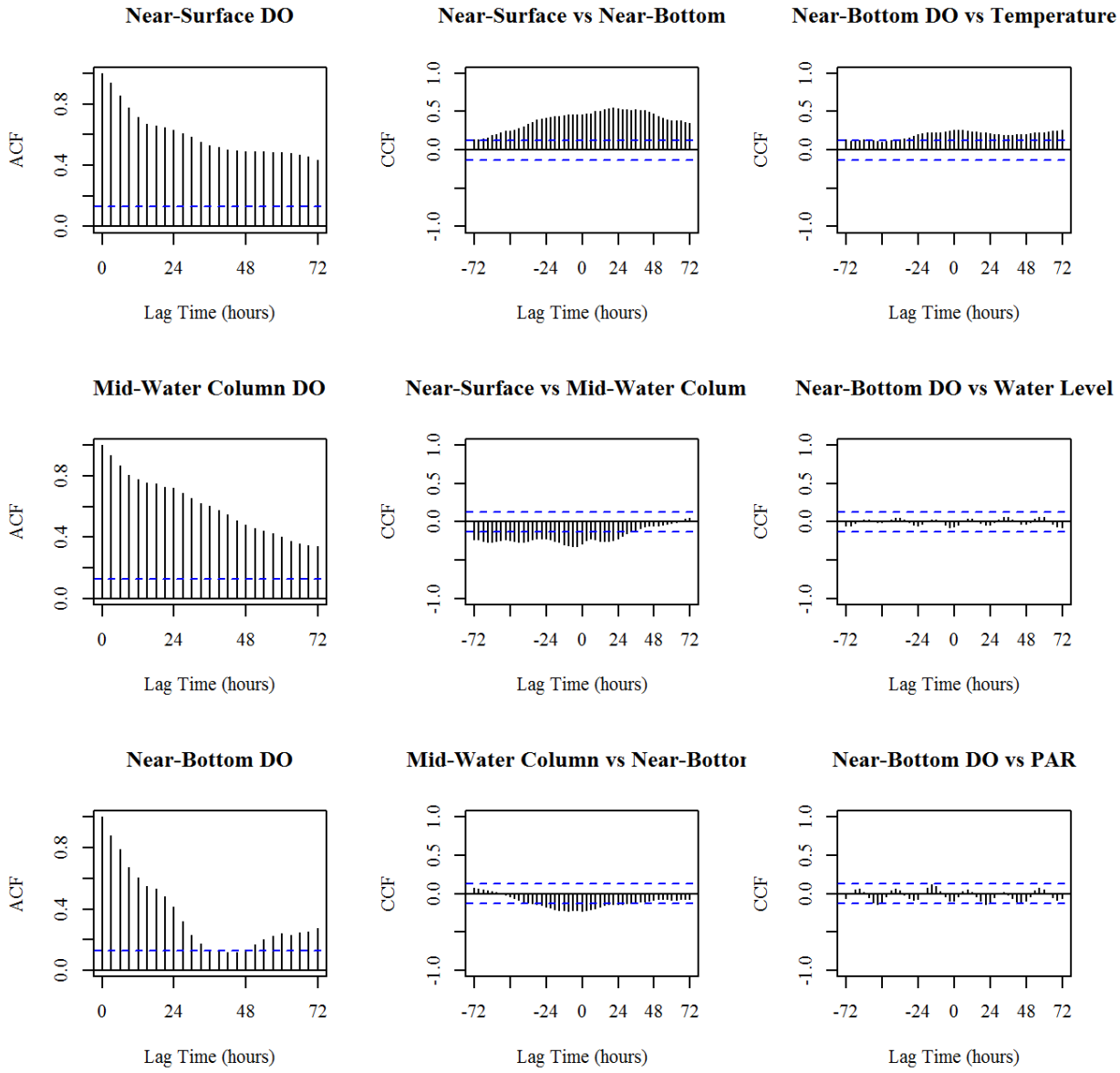

Figure B.35. Results for the month April 2005 (200504). Left Panel: Autocorrelation function (ACF) plots of DO concentrations from three depths, near surface (top), mid-water column (middle), and near-bottom (bottom); Middle Panel: Cross-correlation function (CCF) plots of DO concentrations between depths; Right Panel: Cross-correlation function (CCF) plots between near-bottom DO concentrations and the factors, temperature, water level, and PAR. Blue dotted lines represent 95% confidence limits. Further details are located on the first page of Appendix B.

July 2008 (200807)

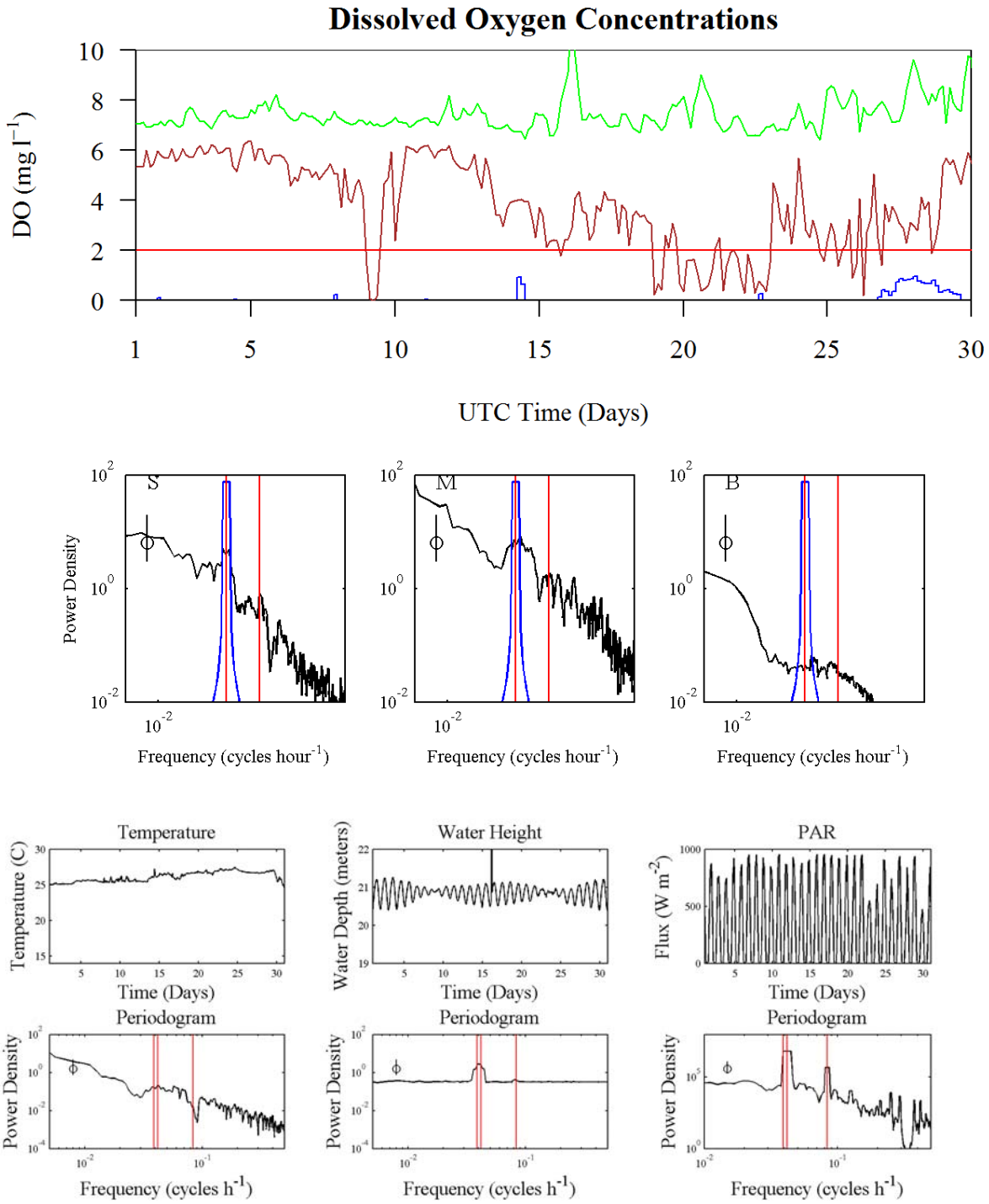

Figure B.35. Time-series plots and periodograms of dissolved oxygen (DO) concentrations and factors affecting DO concentrations for the month July 2008. Further details are located on the first page of Appendix B.

July 2008 (200807)

Autocorrelations and Cross Correlations

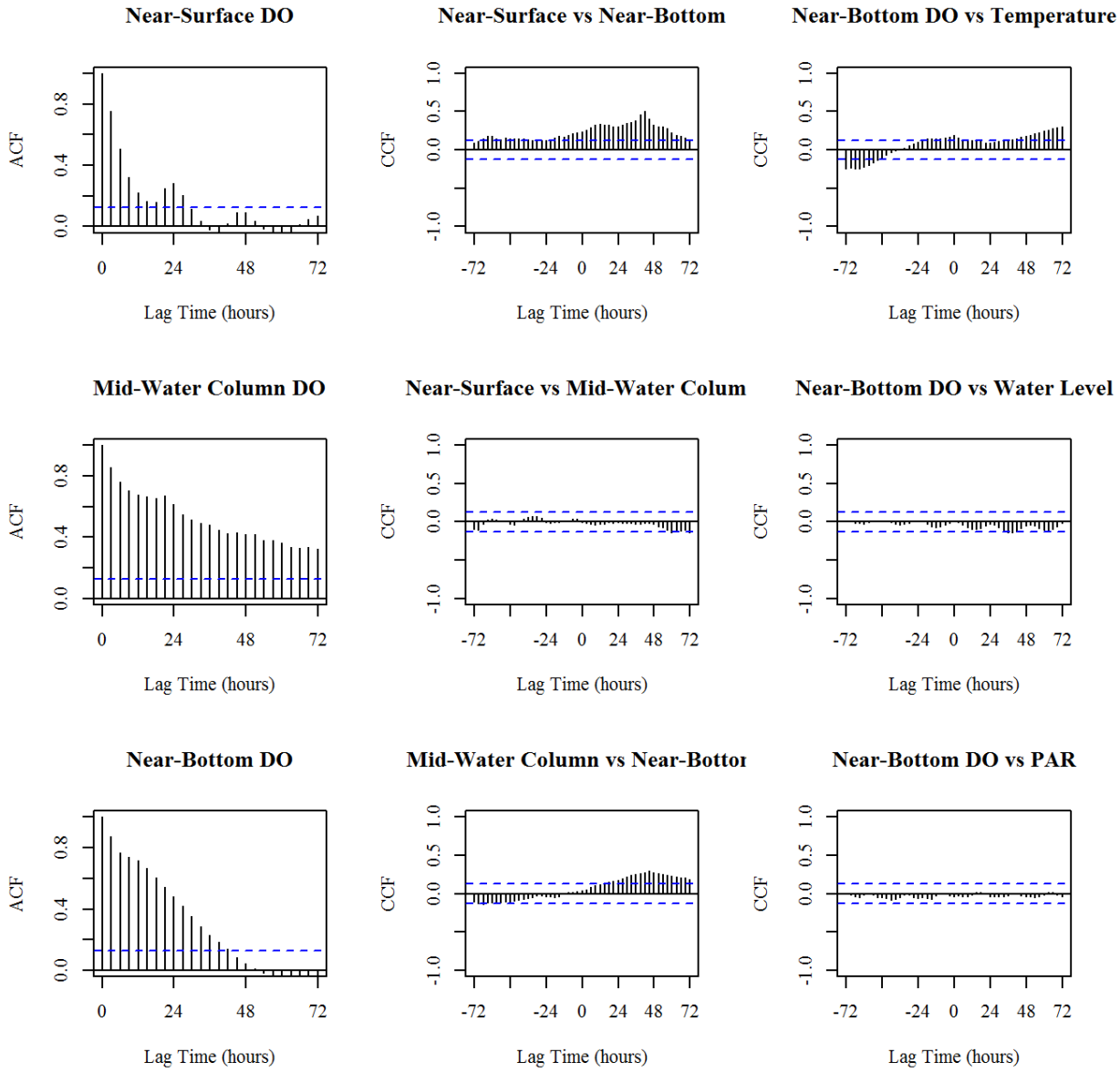

Figure B.36. Results for the month July 2008 (200807). Left Panel: Autocorrelation function (ACF) plots of DO concentrations from three depths, near surface (top), mid-water column (middle), and near-bottom (bottom); Middle Panel: Cross-correlation function (CCF) plots of DO concentrations between depths; Right Panel: Cross-correlation function (CCF) plots between near-bottom DO concentrations and the factors, temperature, water level, and PAR. Blue dotted lines represent 95% confidence limits. Further details are located on the first page of Appendix B.

APPENDIX C

TROPICAL CYCLONES STACKED PLOTS

Appendix C is a series of stacked plots of DO concentrations and other environmental conditions measured during the 31 tropical cyclones that passed within 200 nautical miles of station C6 over the 20 year period from 1989 to 2008. The plots span the time period from 5 days before the tropical cyclone's track first enters the 200 nautical mile radius until 5 days after. The brown shaded area shows days when the tropical cyclone's track was within the 200 nautical mile radius. The orange vertical lines indicate when a re-aeration event occurred. Panel A: DO concentrations in mg l^{-1}, blue line—near-bottom, brown line—mid-water column, green line—near-surface, red horizontal line represents the hypoxic threshold (2.0 mg l^{-1}), Panel B: sigma-t, blue line—near-bottom, brown line—mid-water column, green line—near-surface, red line represents delta sigma-t or the difference between near-surface sigma-t and near-bottom sigma-t, Panel C: blue line represents the u-wind component, or east-west winds, and green line represents the v-wind component, or north-south winds, in m s^{-1}, Panel D: tau, or wind stress, Panel E: wind vectors where the direction of the arrow represents wind direction and the length of the arrow represents wind speed. Where lines are missing no data were available for that time period. The small map on the bottom left of each page illustrates the tropical cyclone's track. The color bar indicates the intensity of the storm based on the Saffir-Simpson Scale. The maps were created using the web service available at http://www.csc.noaa.gov/hurricanes/.

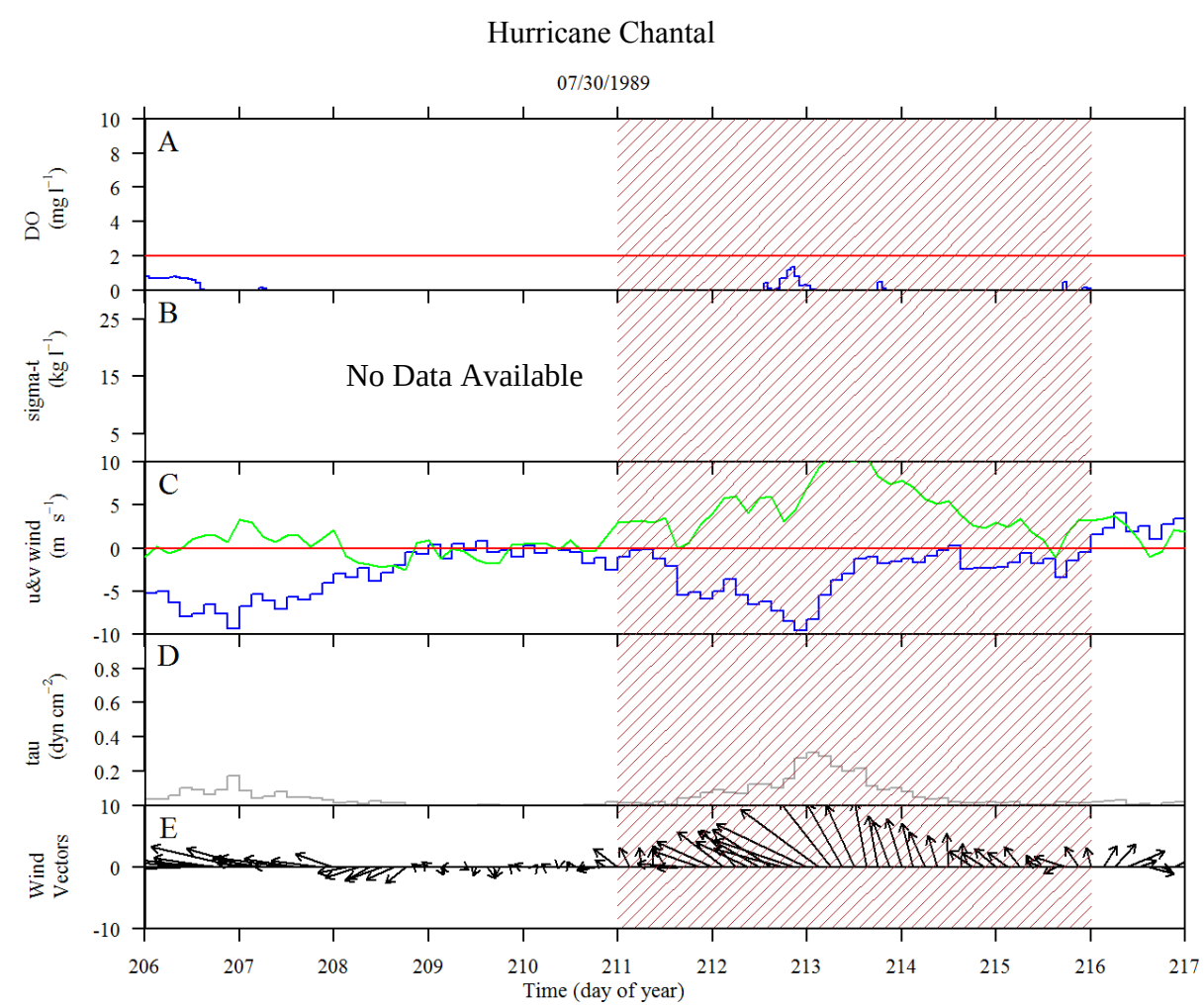

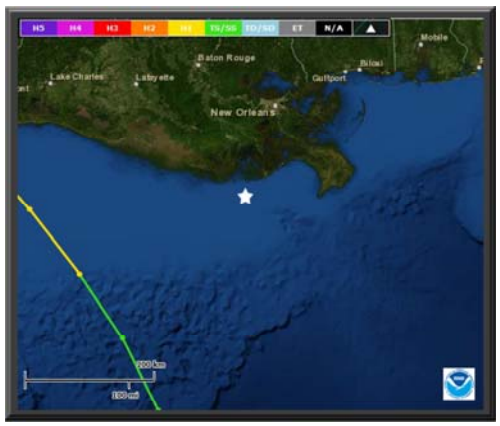

Figure A.1. Stacked plot of environmental data during Hurricane Chantal. Left is a map of Hurricane Chantal's track. White star on map represents station C6. Further details are located on the first page of Appendix C.

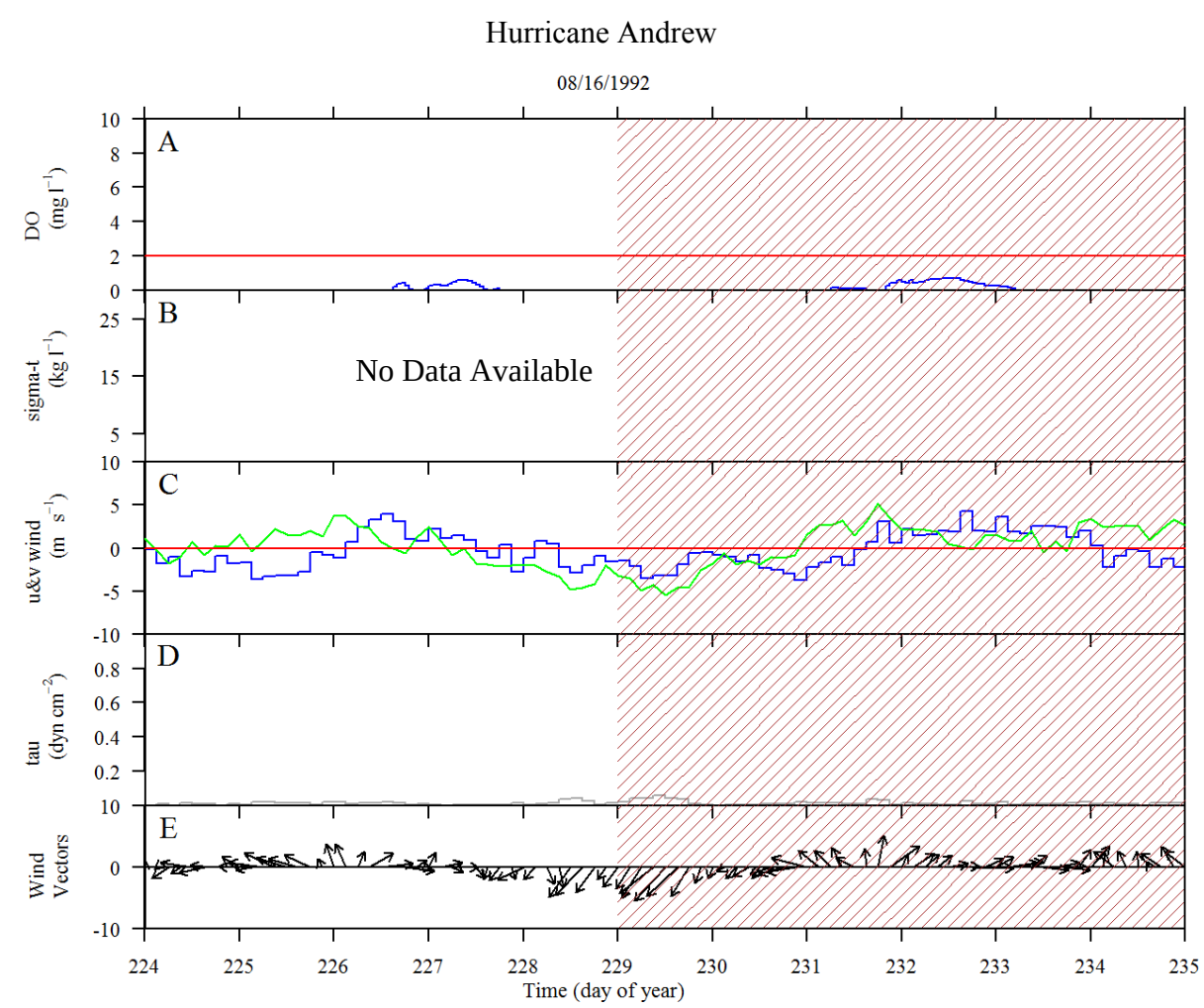

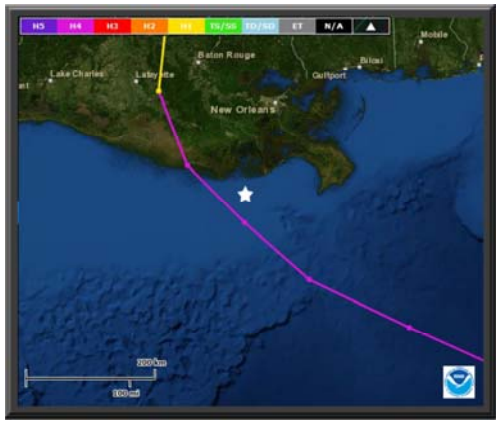

Figure A.2. Stacked plot of environmental data during Hurricane Andrew. Left is a map of Hurricane Andrew's track. White star on map represents station C6. Further details are located on the first page of Appendix C.

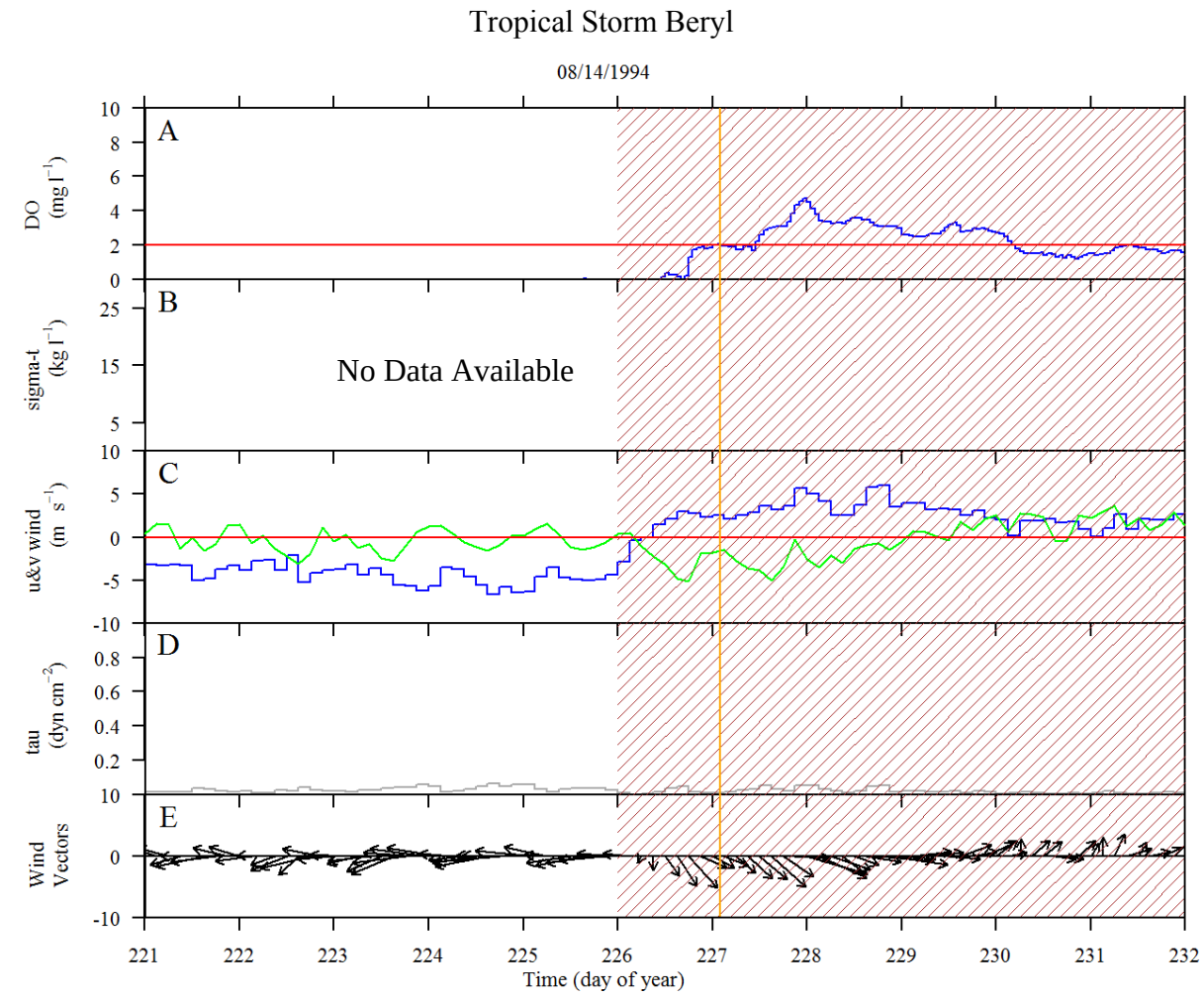

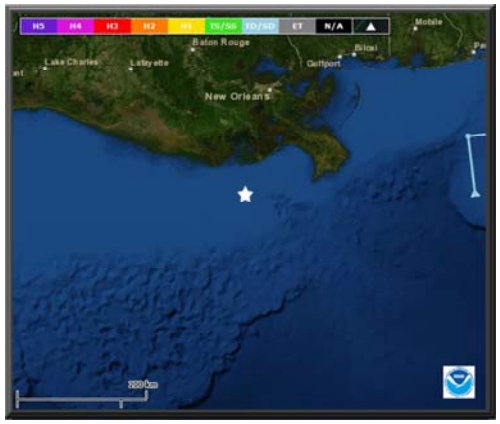

Figure A.3. Stacked plot of environmental data during Tropical Storm Beryl. Left is a map of Tropical Storm Beryl's track. White star on map represents station C6. Further details are located on the first page of Appendix C.

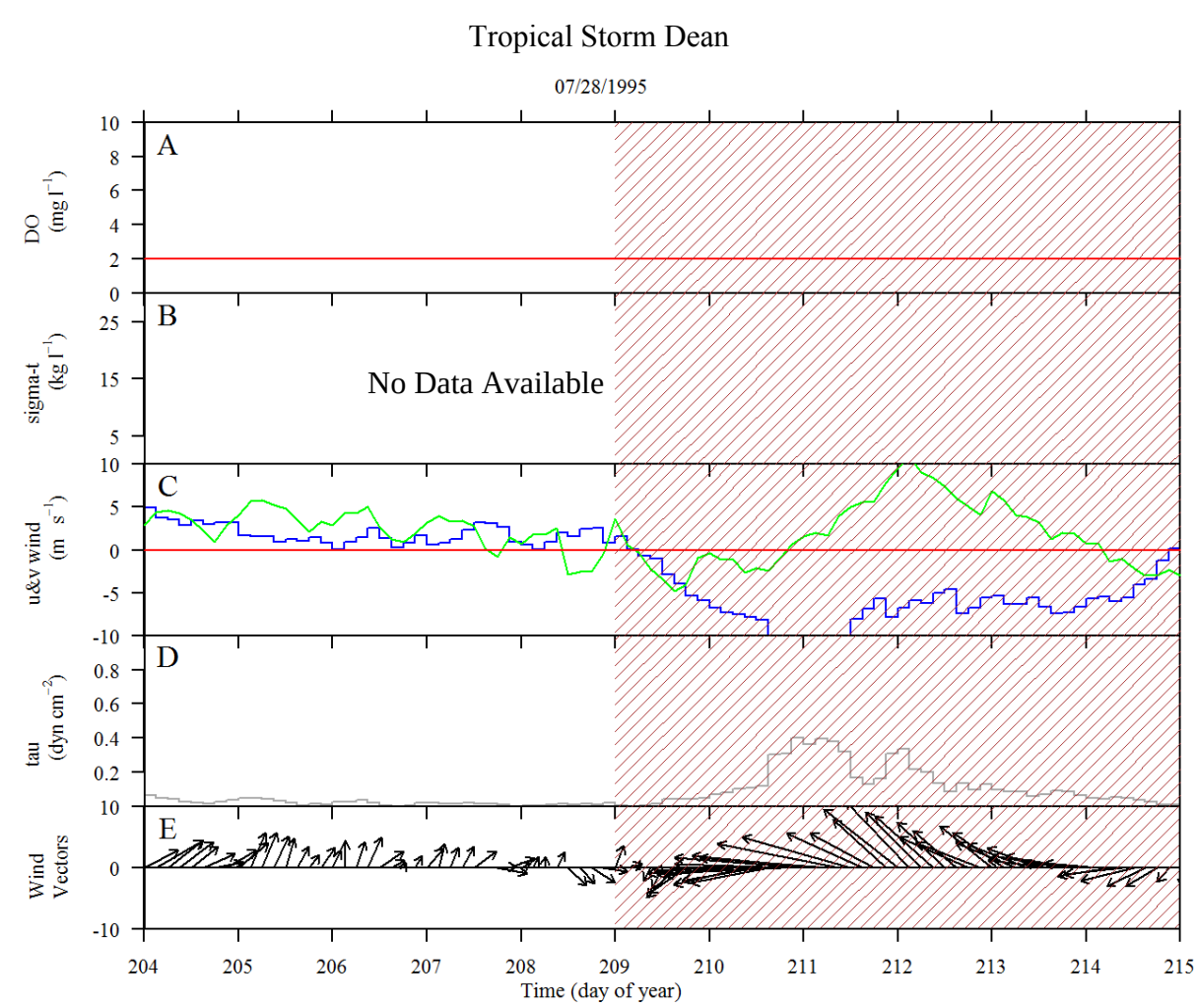

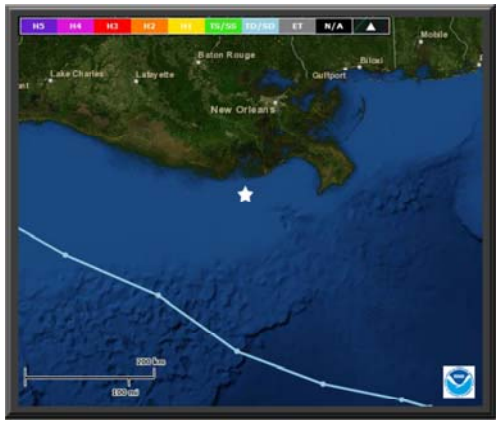

Figure A.4. Stacked plot of environmental data during Tropical Storm Dean. Left is a map of Tropical Storm Dean's track. White star on map represents station C6. Further details are located on the first page of Appendix C.

Hurricane Opal

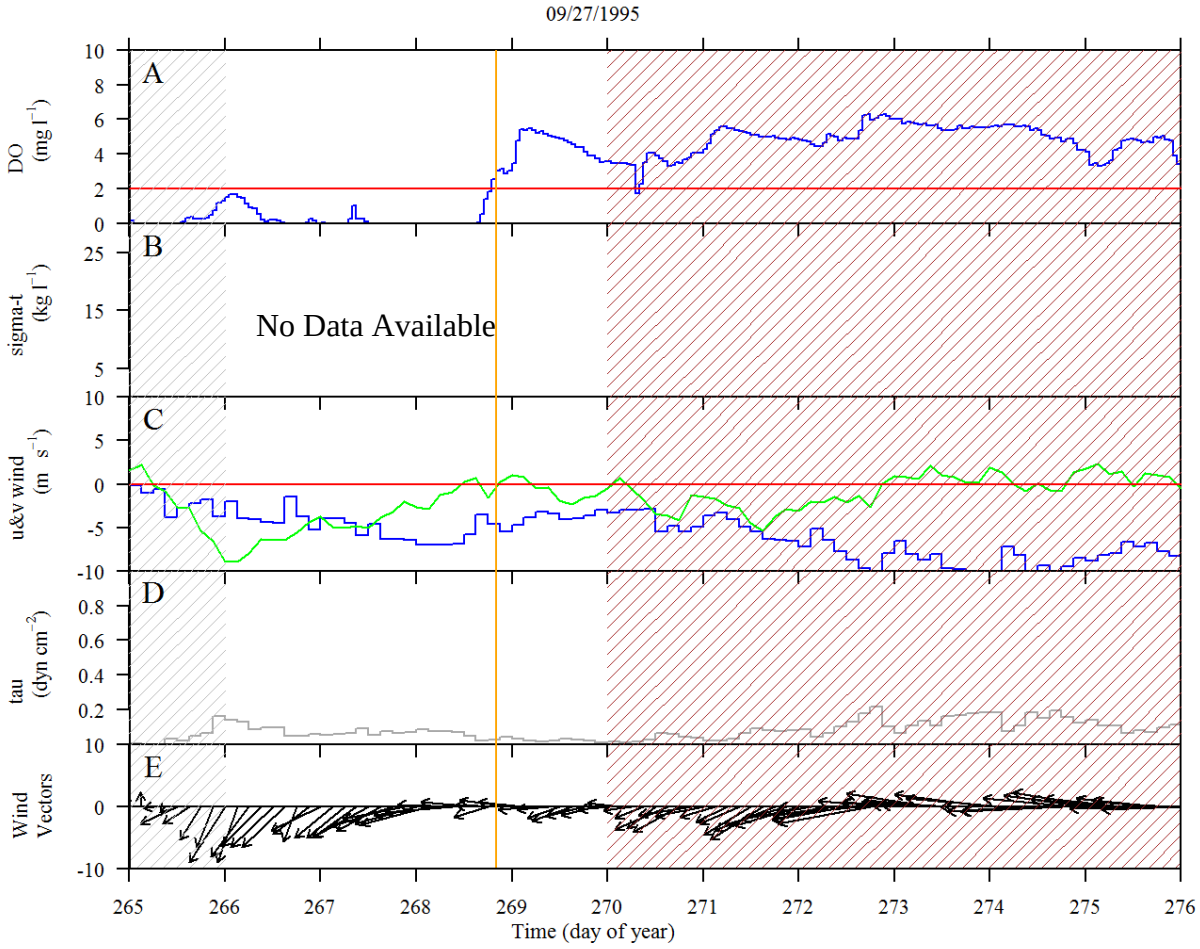

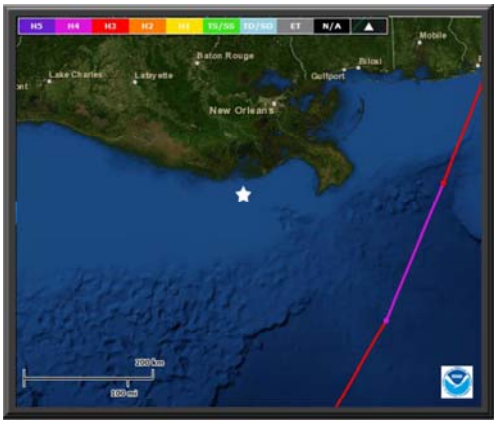

Figure A.5. Stacked plot of environmental data during Hurricane Opal. Left is a map of Hurricane Opal's track. White star on map represents station C6. Further details are located on the first page of Appendix C.

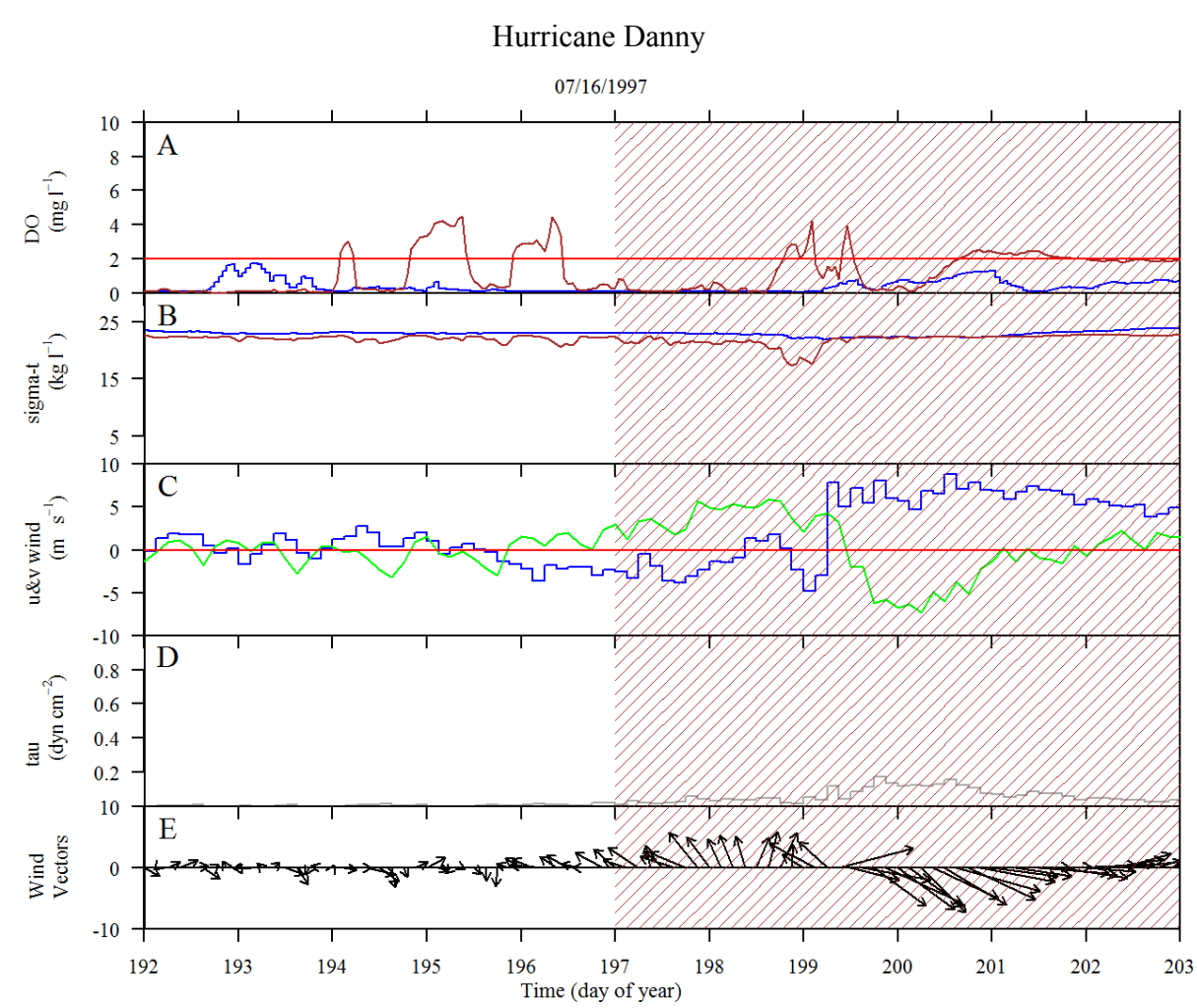

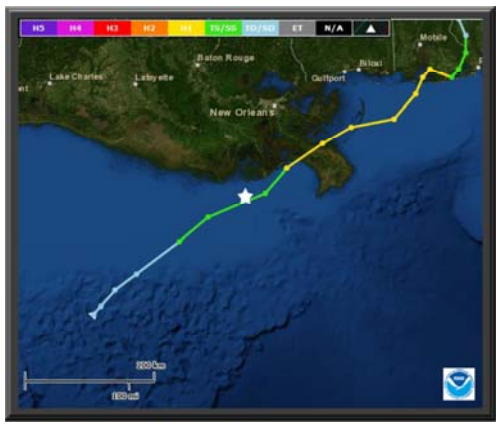

Figure A.6. Stacked plot of environmental data during Hurricane Danny. Left is a map of Hurricane Danny's track. White star on map represents station C6. Further details are located on the first page of Appendix C.

Hurricane Earl

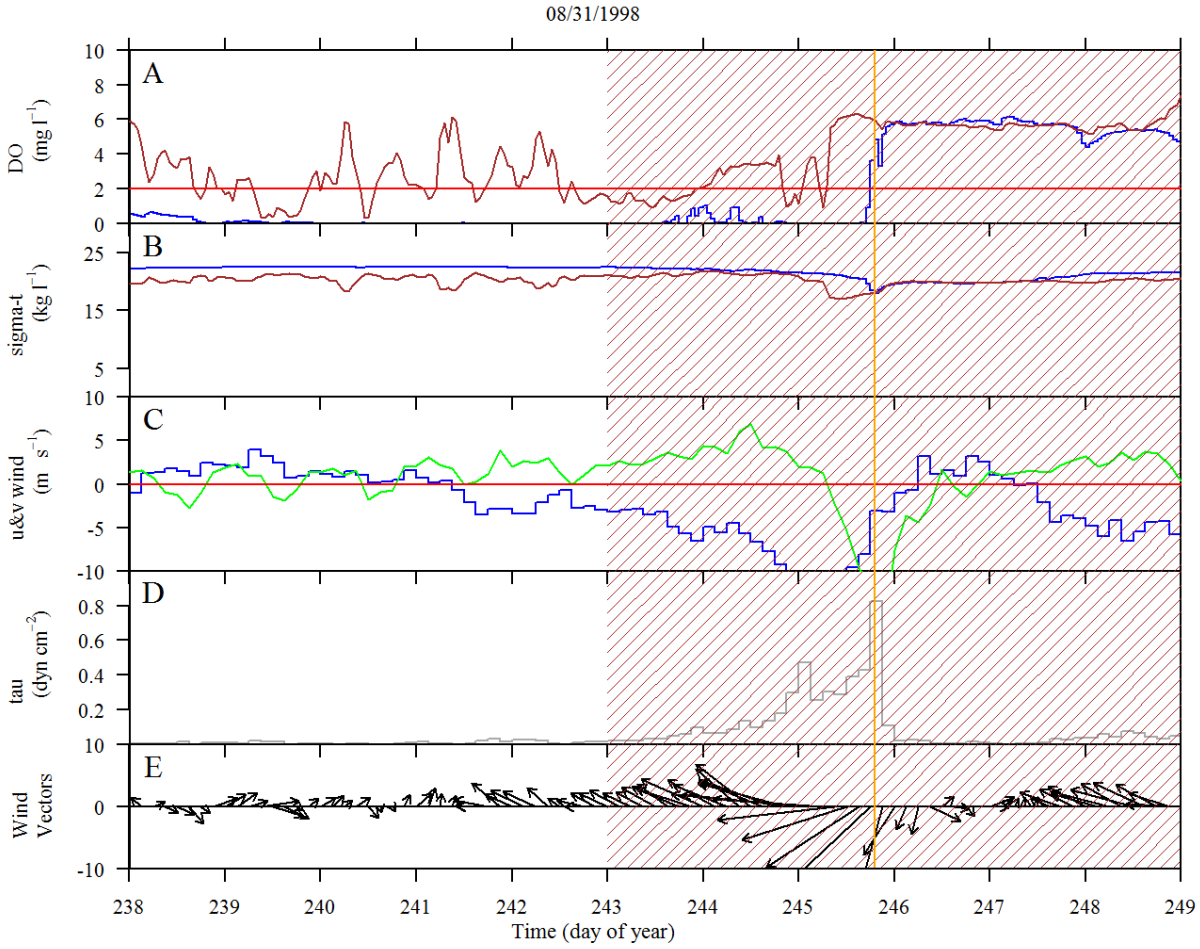

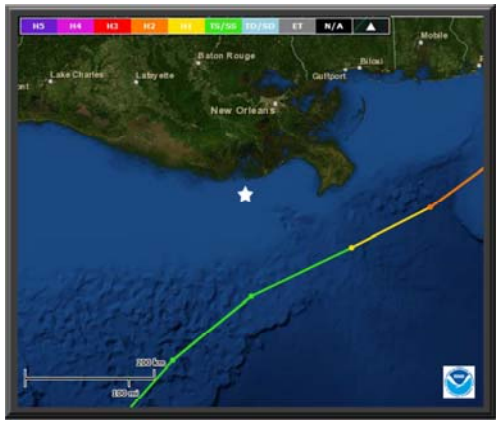

Figure A.7. Stacked plot of environmental data during Hurricane Earl. Left is a map of Hurricane Earl's track. White star on map represents station C6. Further details are located on the first page of Appendix C.

Hurricane Georges

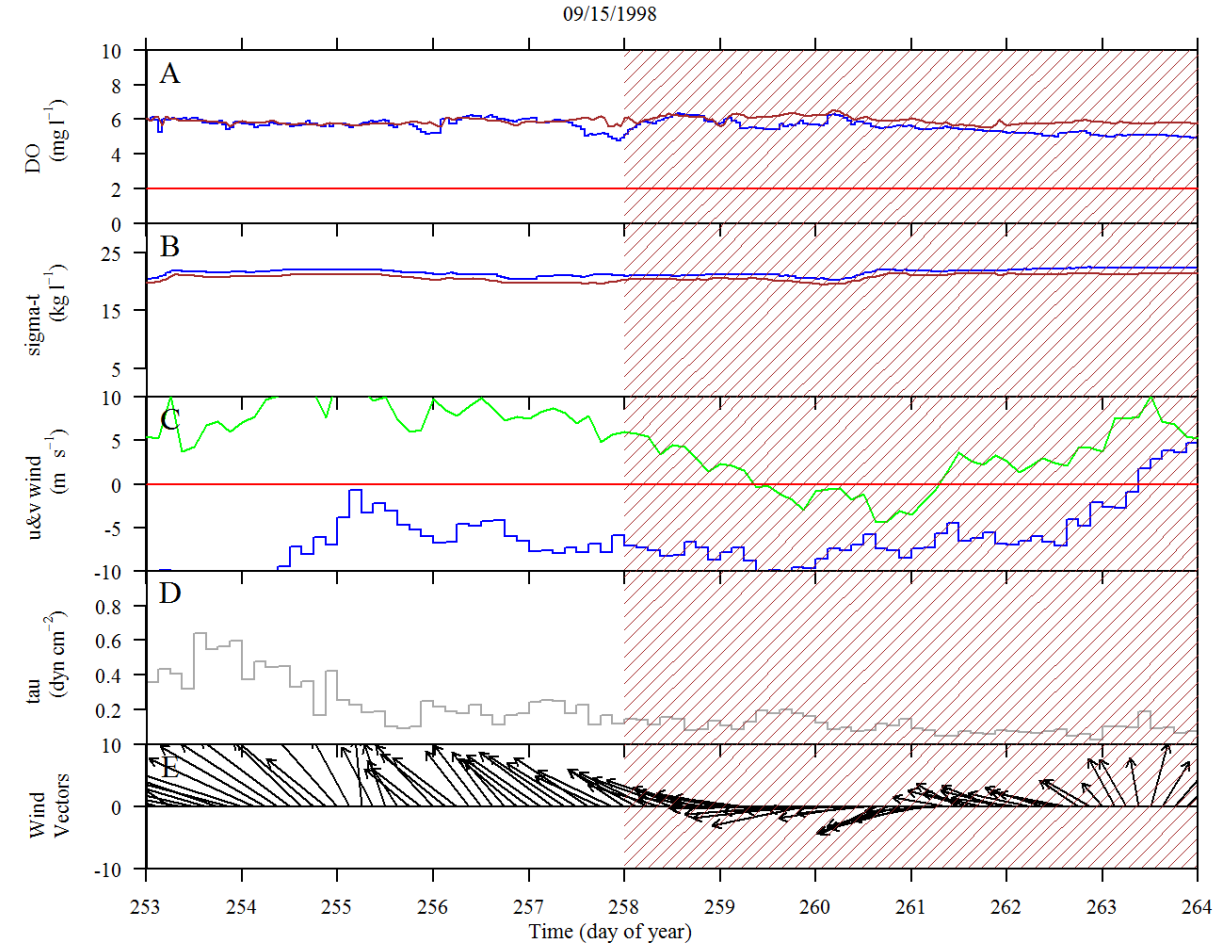

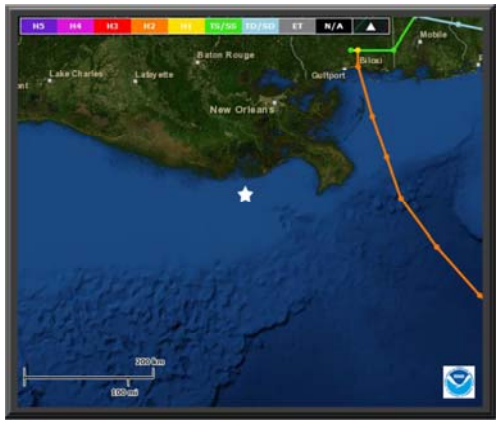

Figure A.8. Stacked plot of environmental data during Hurricane Georges. Left is a map of Hurricane Georges's track. White star on map represents station C6. Further details are located on the first page of Appendix C.

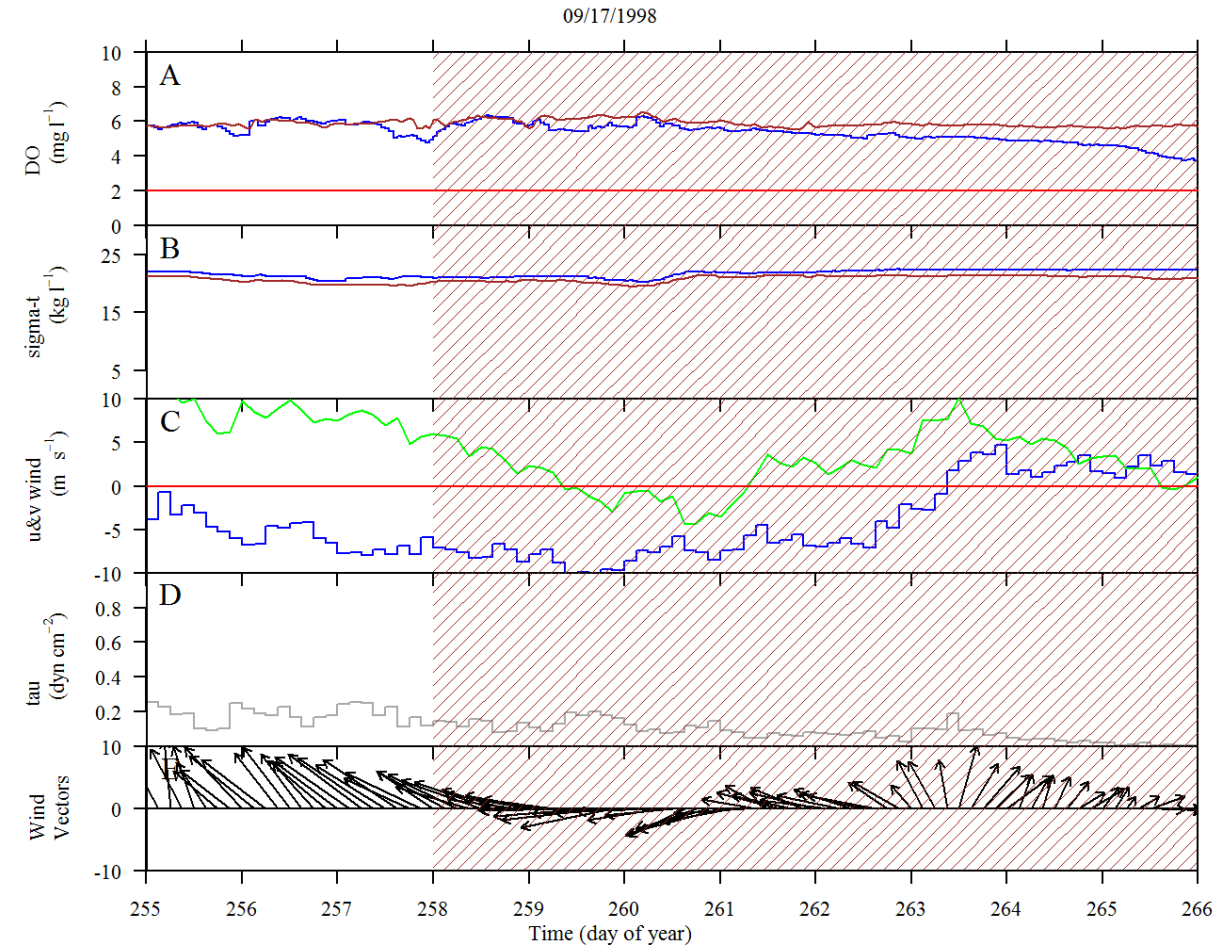

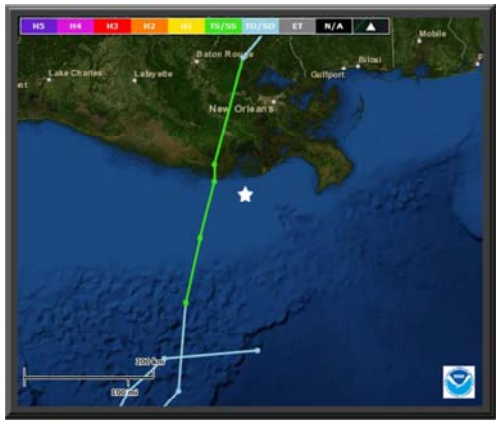

Figure A.9. Stacked plot of environmental data during Tropical Storm Hermine. Left is a map of Tropical Storm Hermine's track. White star on map represents station C6. Further details are located on the first page of Appendix C.

Not Named

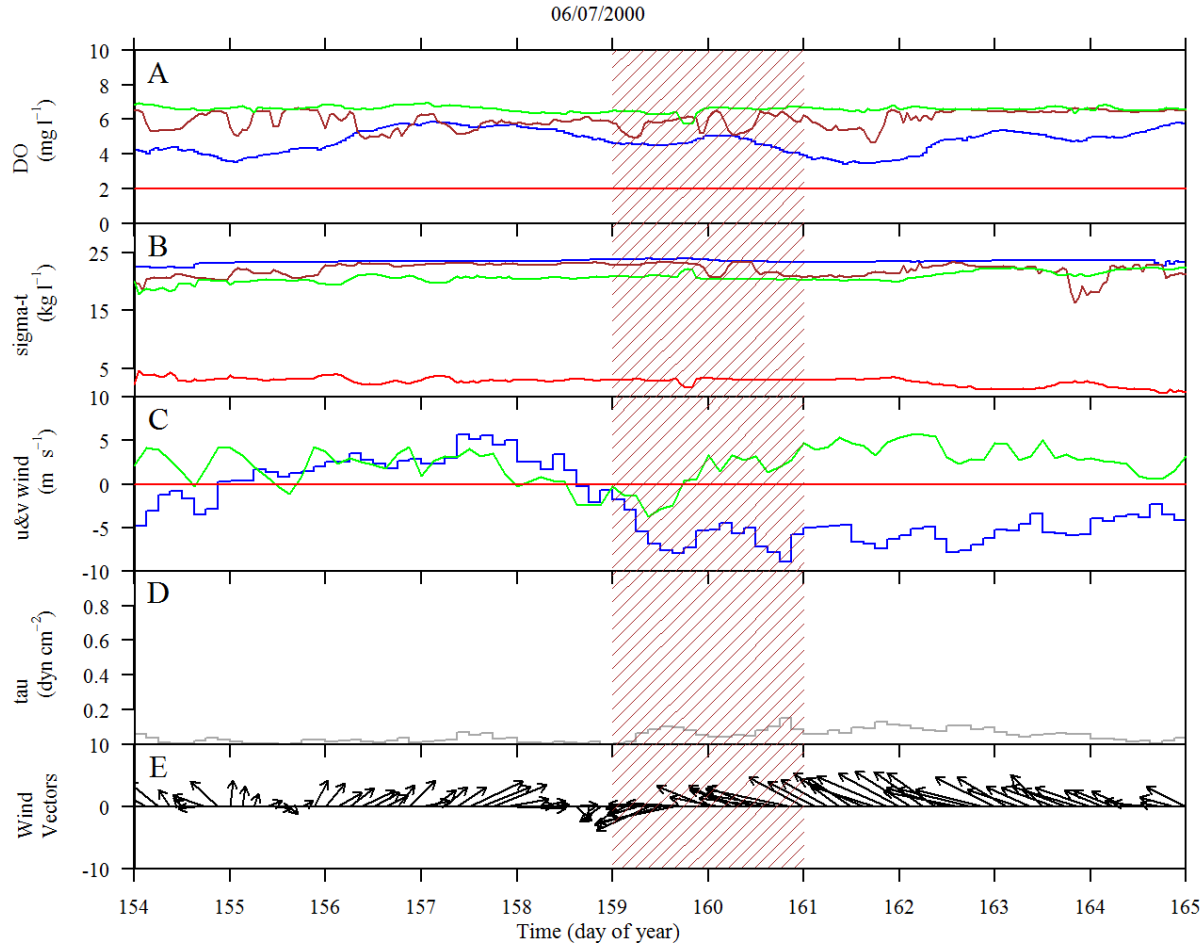

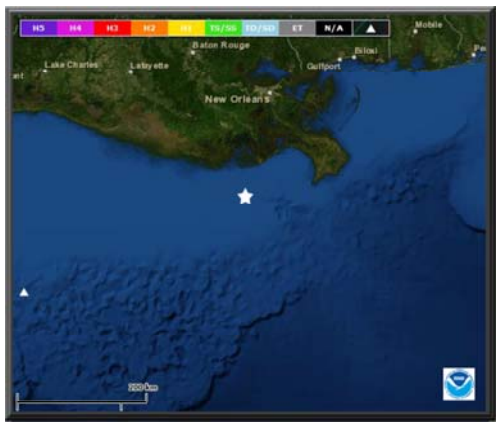

Figure A.10. Stacked plot of environmental data during Not Named. Left is a map of Not Named's track. White star on map represents station C6. Further details are located on the first page of Appendix C.

Tropical Storm Helene

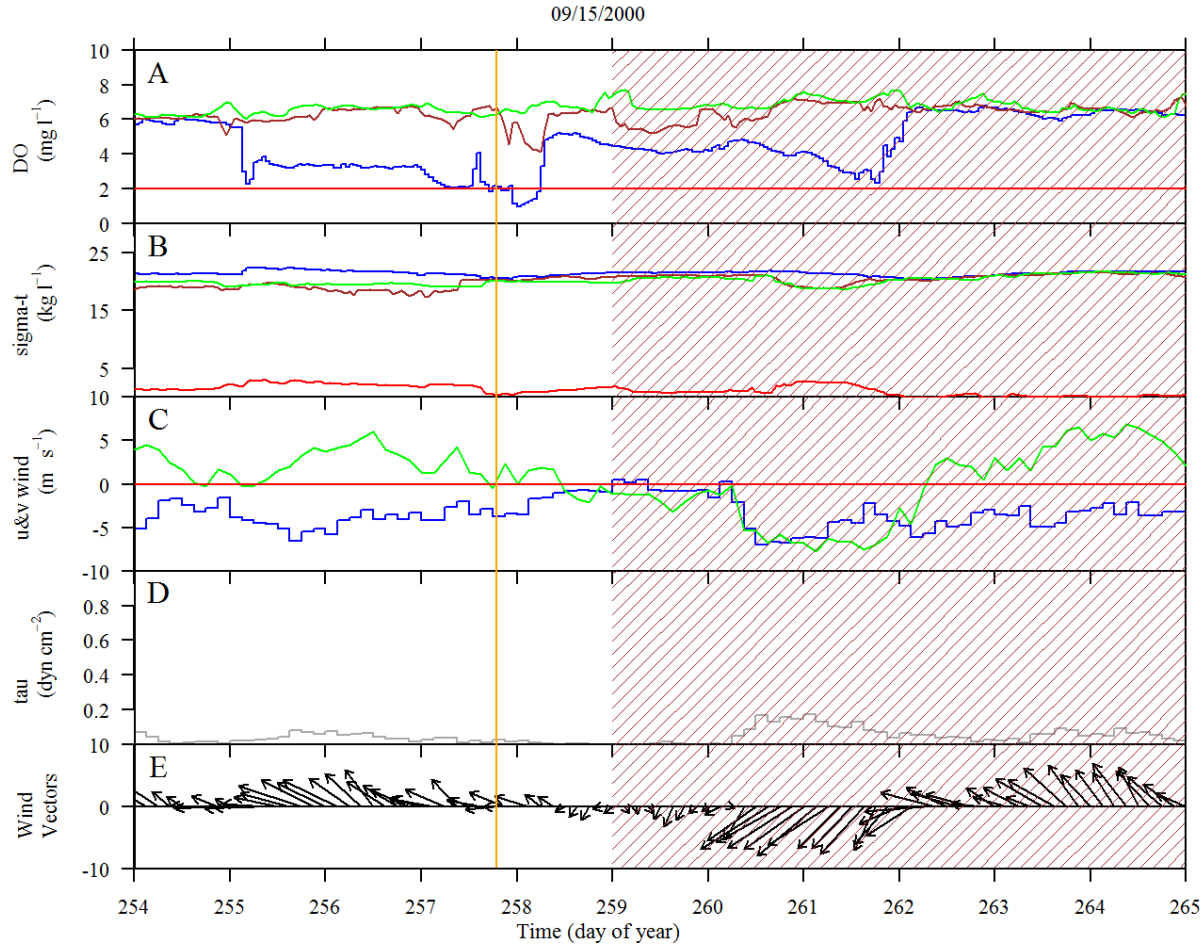

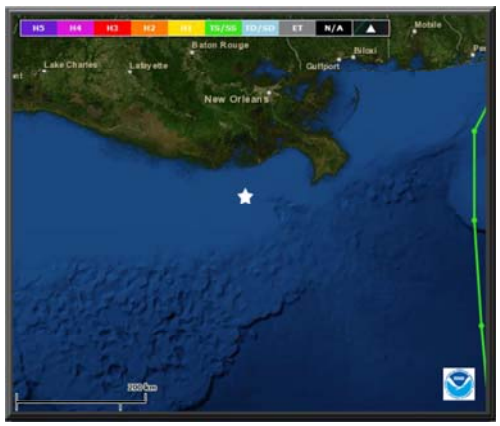

Figure A.11. Stacked plot of environmental data during Tropical Storm Helene. Left is a map of Tropical Storm Helene's track. White star on map represents station C6. Further details are located on the first page of Appendix C.

Tropical Storm Allison

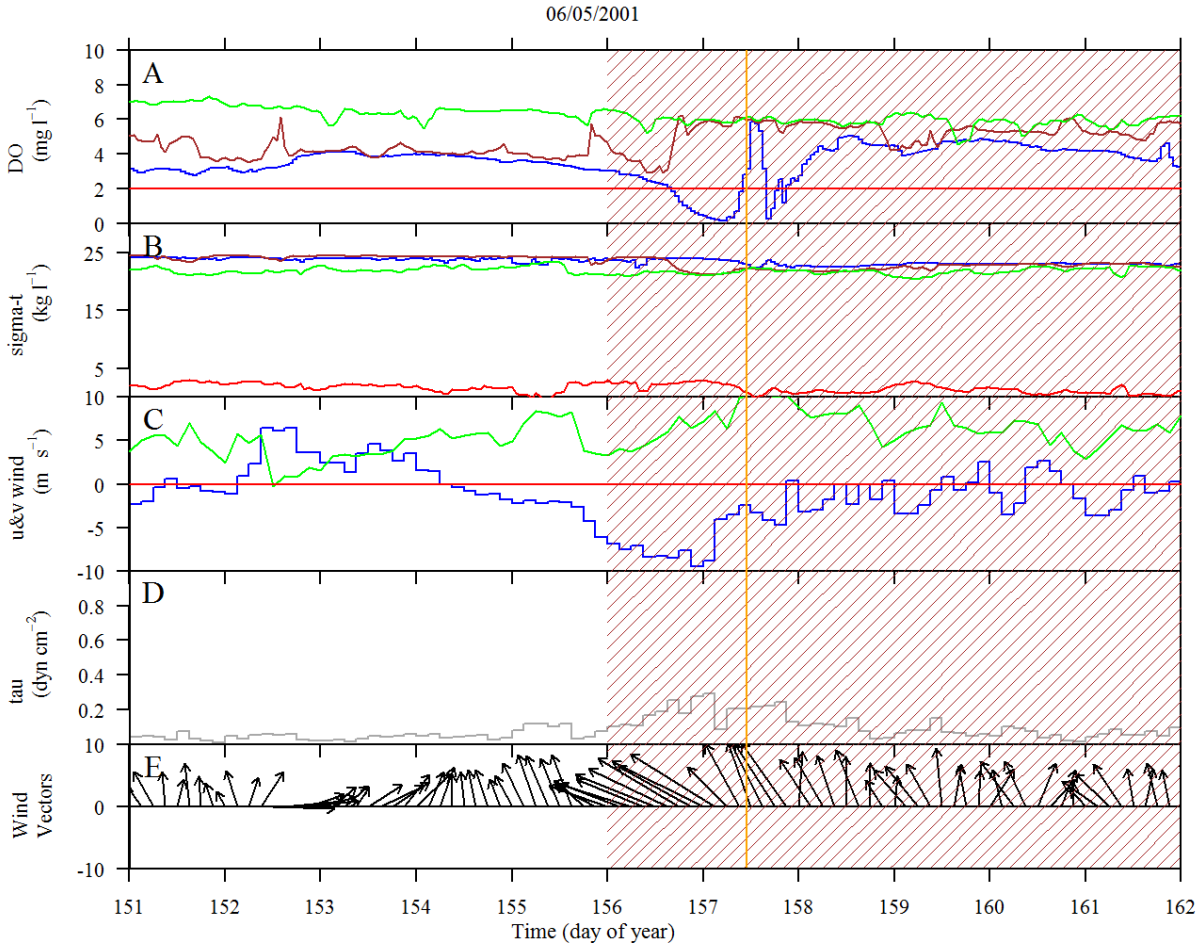

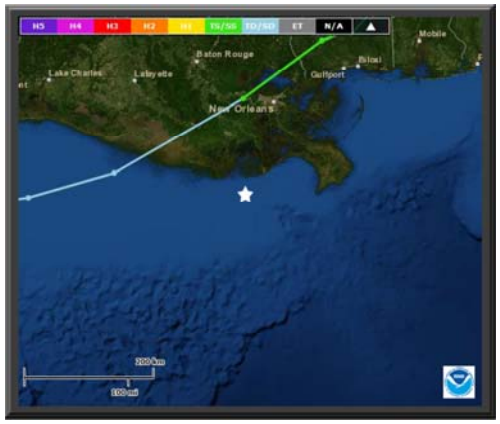

Figure A.12. Stacked plot of environmental data during Tropical Storm Allison. Left is a map of Tropical Storm Allison's track. White star on map represents station C6. Further details are located on the first page of Appendix C.

Tropical Storm Bertha

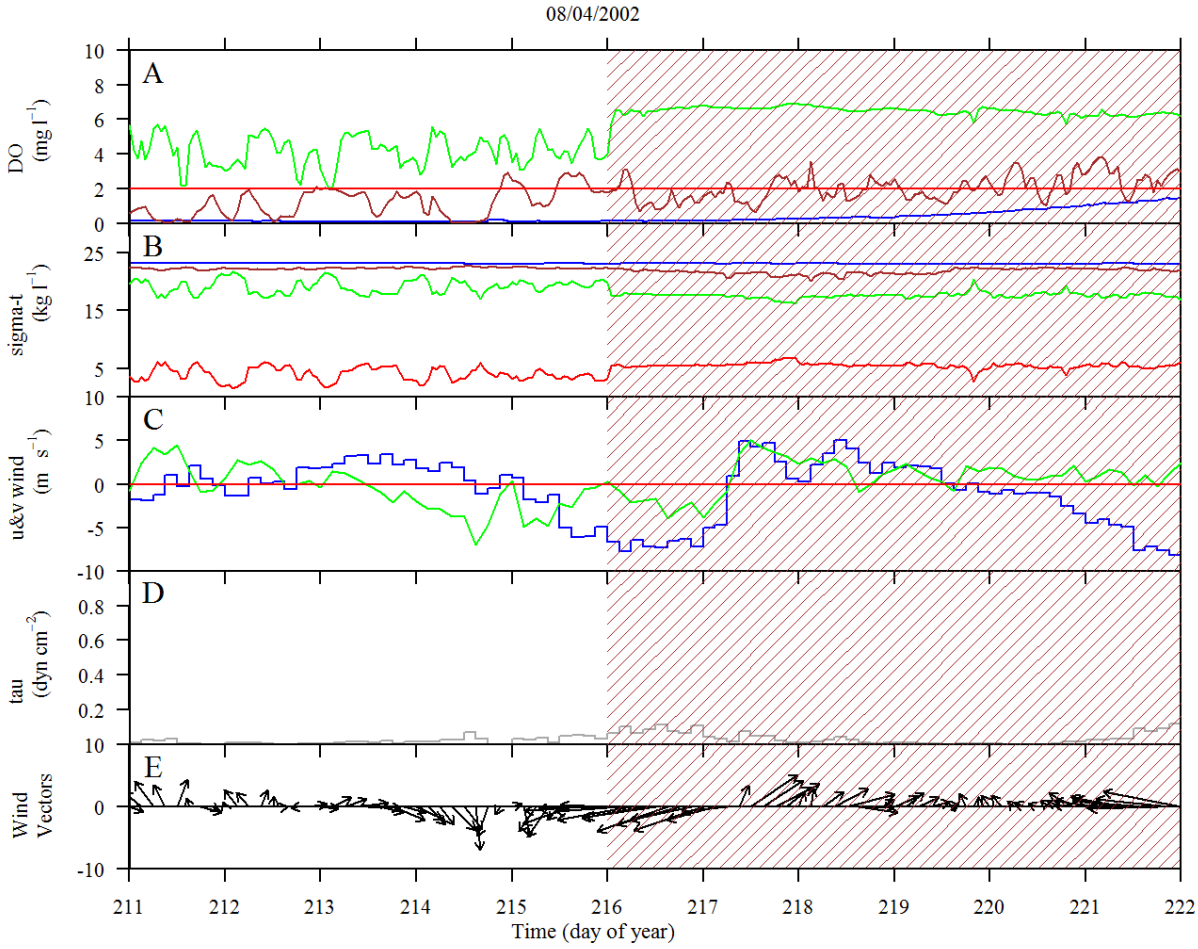

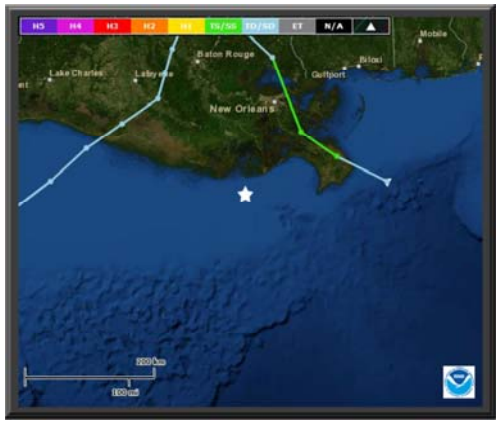

Figure A.13. Stacked plot of environmental data during Tropical Storm Bertha. Left is a map of Tropical Storm Bertha's track. White star on map represents station C6. Further details are located on the first page of Appendix C.

Tropical Storm Hanna

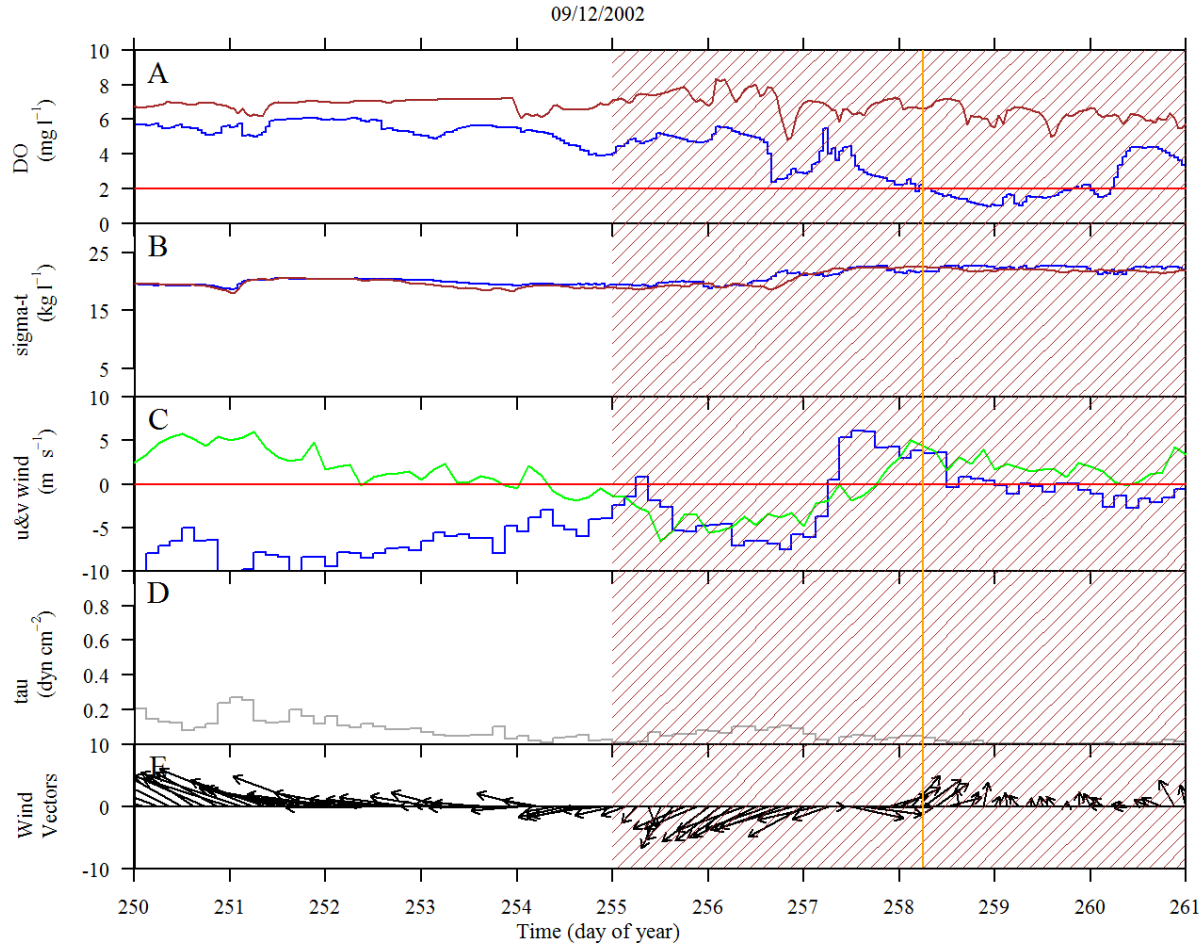

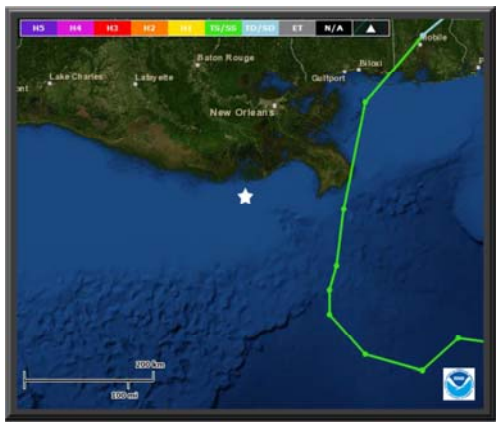

Figure A.14. Stacked plot of environmental data during Tropical Storm Hanna. Left is a map of Tropical Storm Hanna's track. White star on map represents station C6. Further details are located on the first page of Appendix C.

Hurricane Isidore

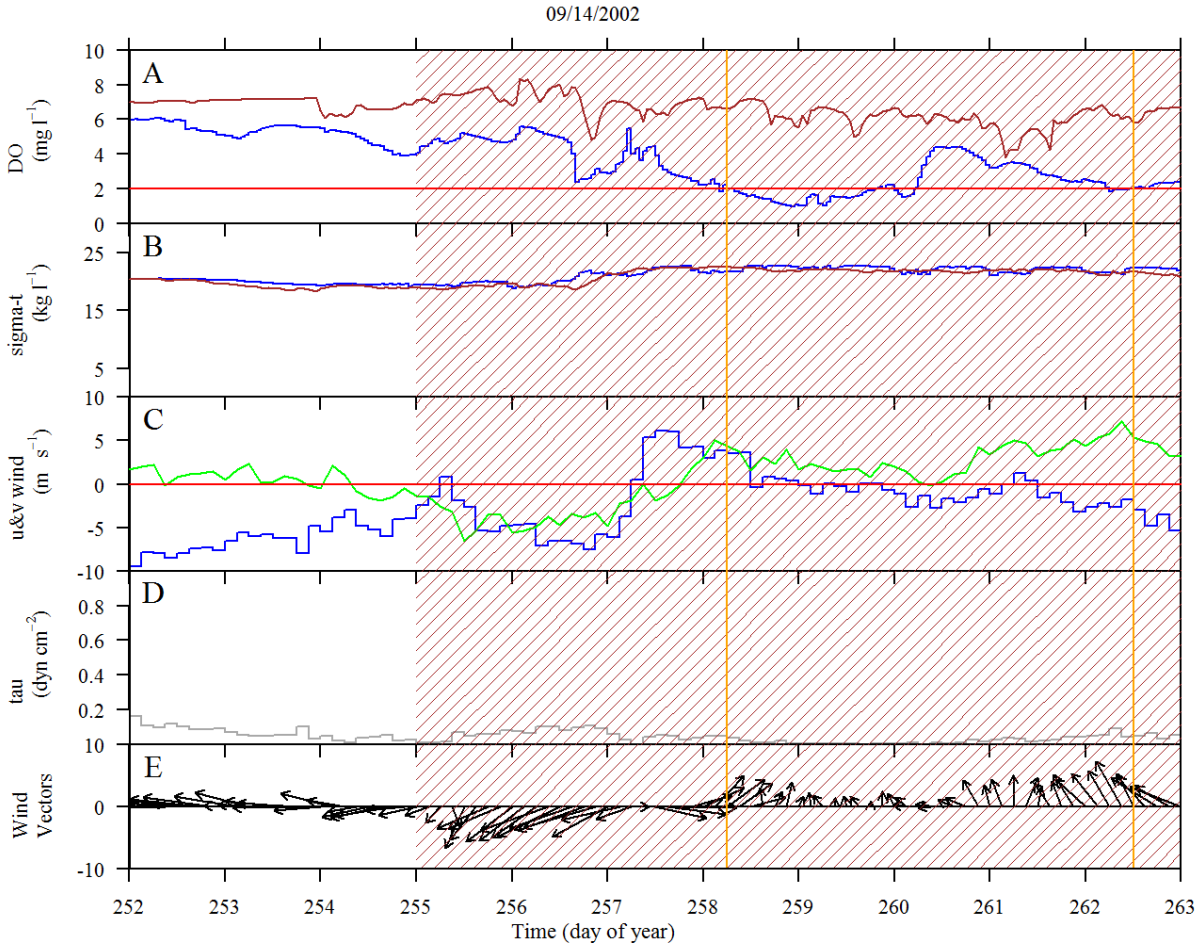

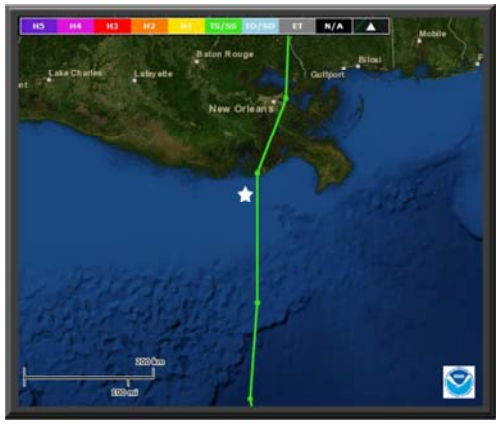

Figure A.15. Stacked plot of environmental data during Hurricane Isidore. Left is a map of Hurricane Isidore's track. White star on map represents station C6. Further details are located on the first page of Appendix C.

Hurricane Lili

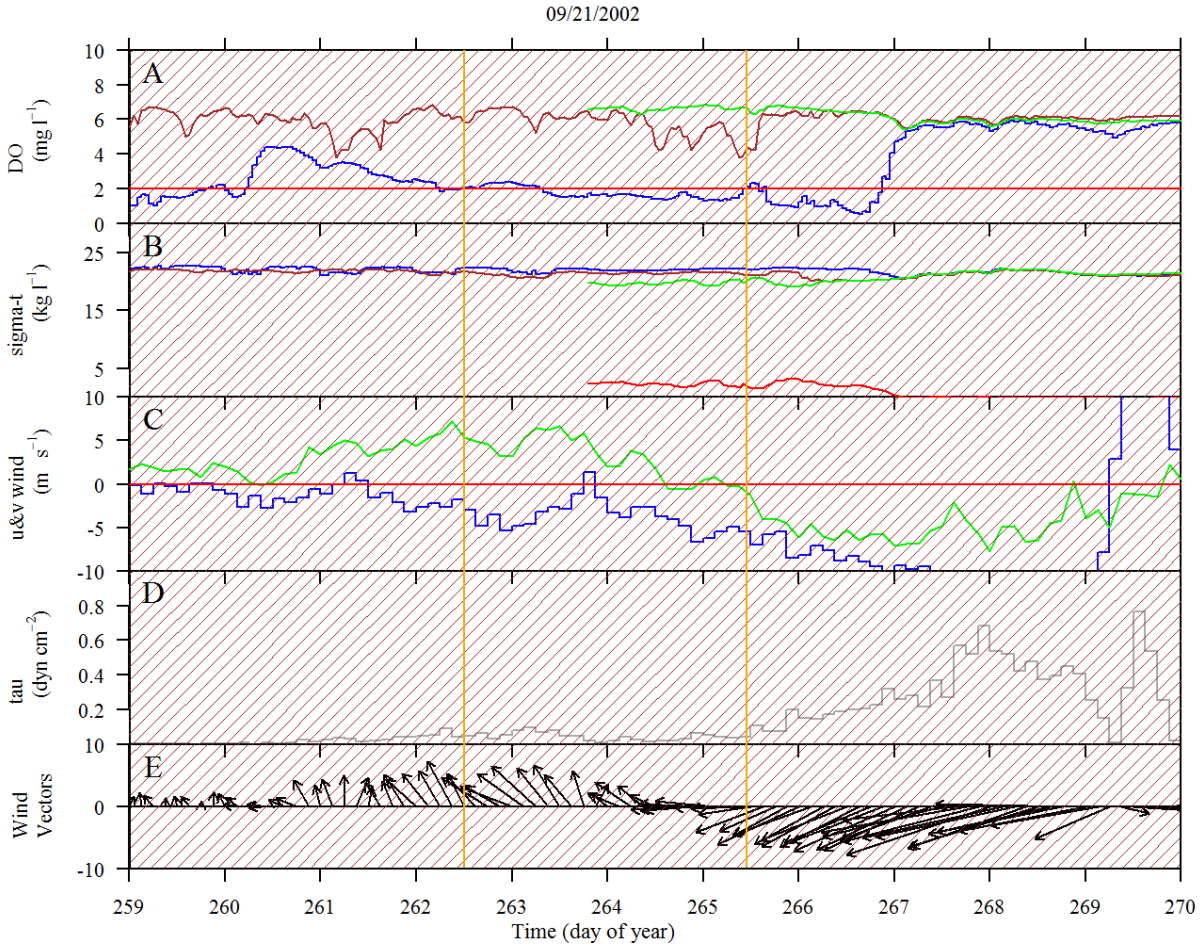

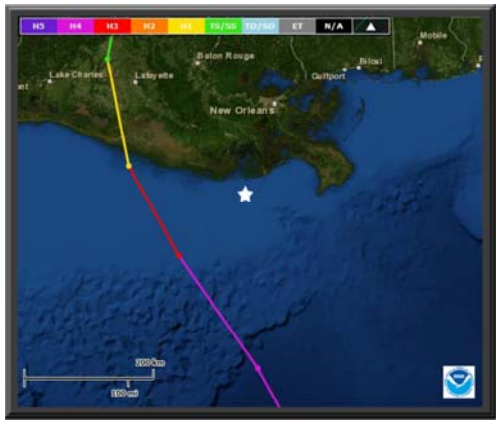

Figure A.16. Stacked plot of environmental data during Hurricane Lili. Left is a map of Hurricane Lili's track. White star on map represents station C6. Further details are located on the first page of Appendix C.

Tropical Storm Bill

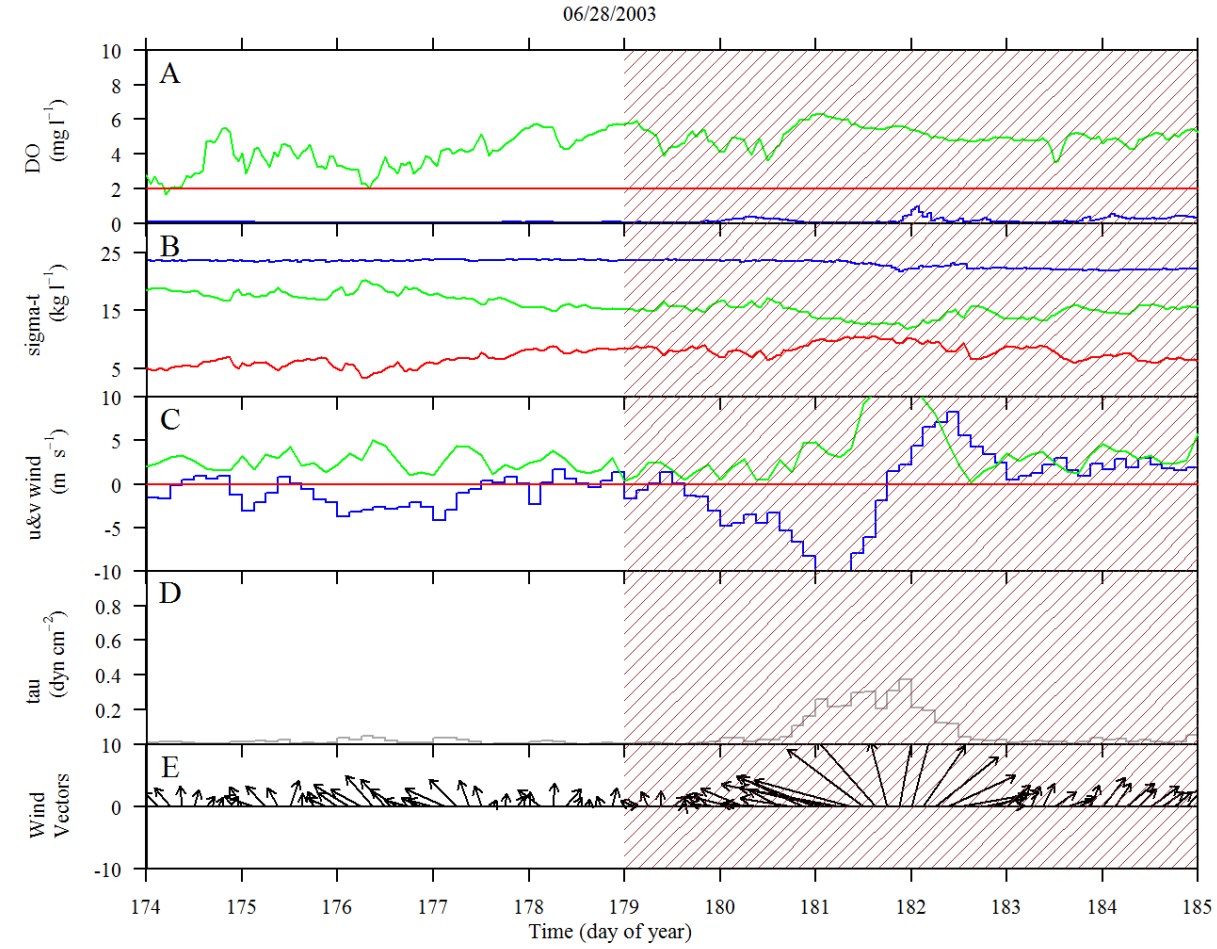

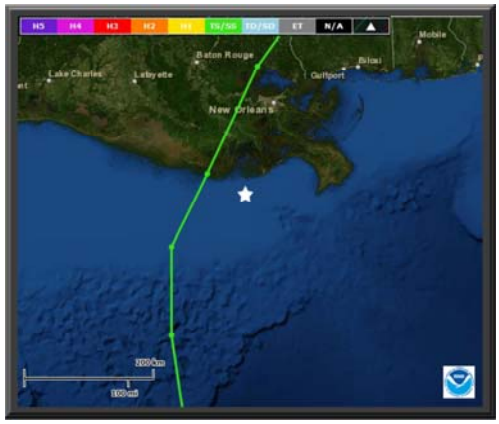

Figure A.17. Stacked plot of environmental data during Tropical Storm Bill. Left is a map of Tropical Storm Bill's track. White star on map represents station C6. Further details are located on the first page of Appendix C.

Hurricane Claudette

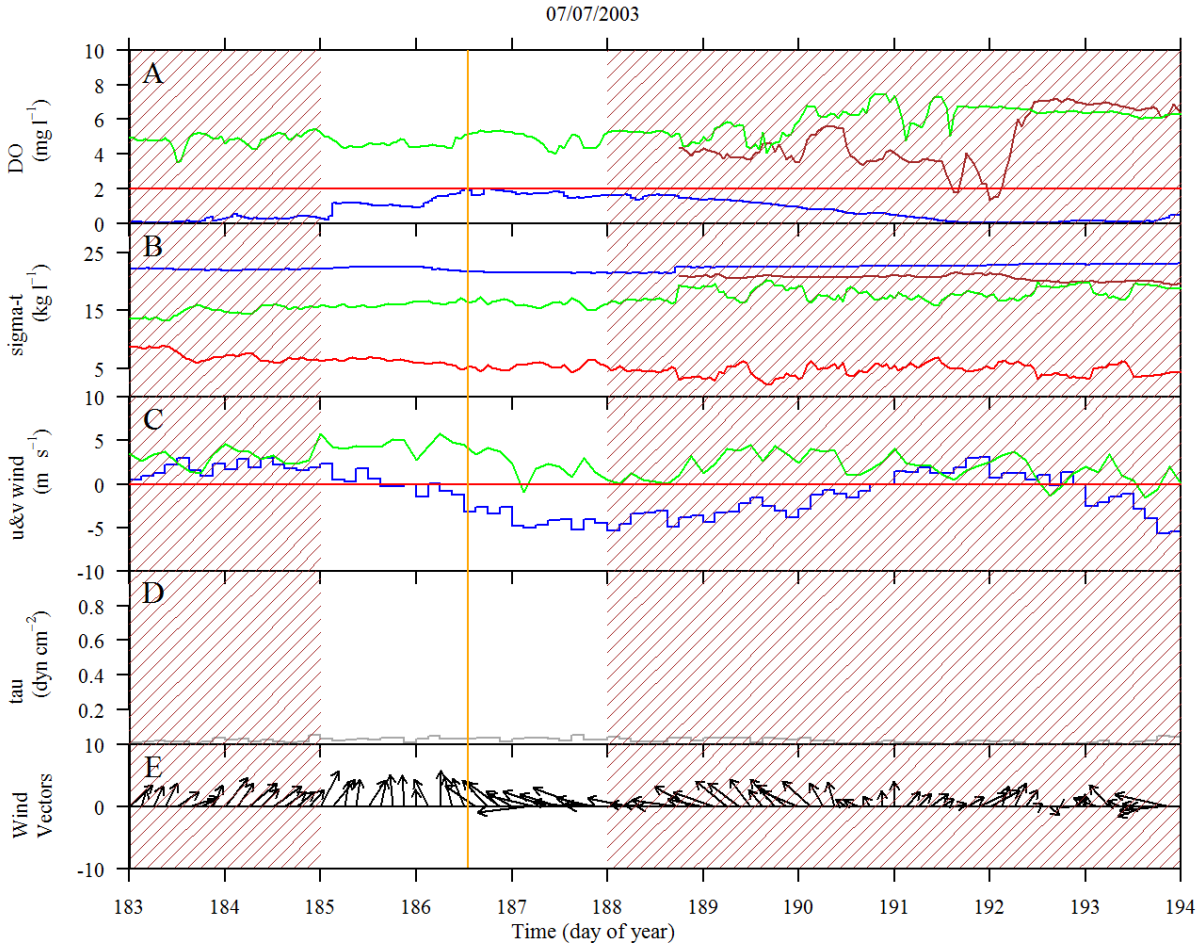

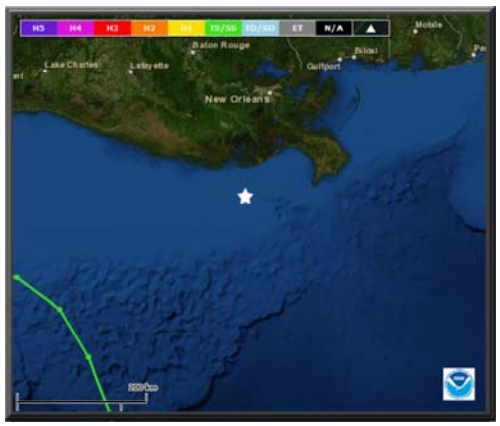

Figure A.18. Stacked plot of environmental data during Hurricane Claudette. Left is a map of Hurricane Claudette's track. White star on map represents station C6. Further details are located on the first page of Appendix C.

Hurricane Erika

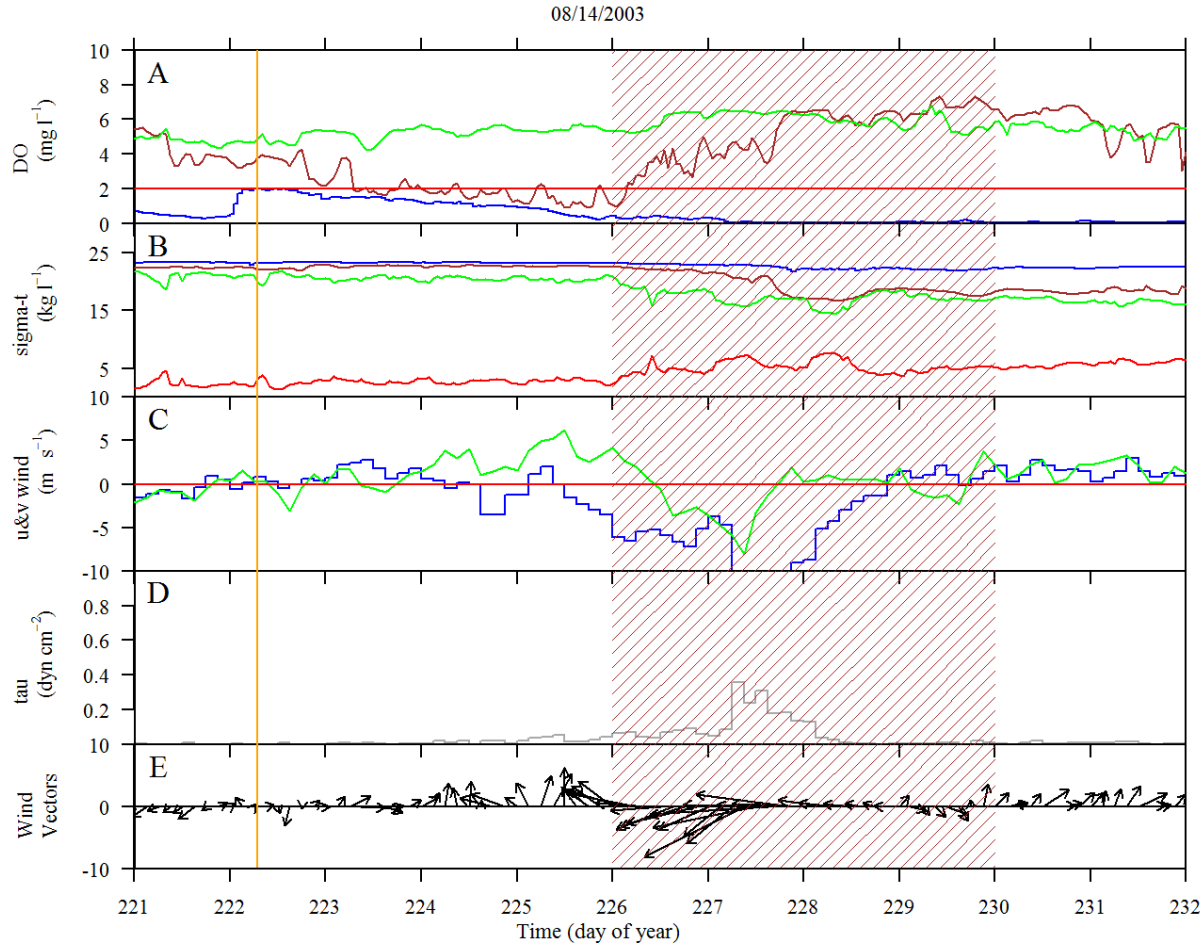

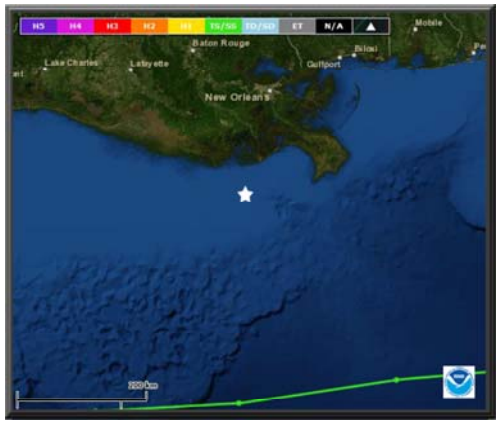

Figure A.19. Stacked plot of environmental data during Hurricane Erika. Left is a map of Hurricane Erika's track. White star on map represents station C6. Further details are located on the first page of Appendix C.

Tropical Storm Henri

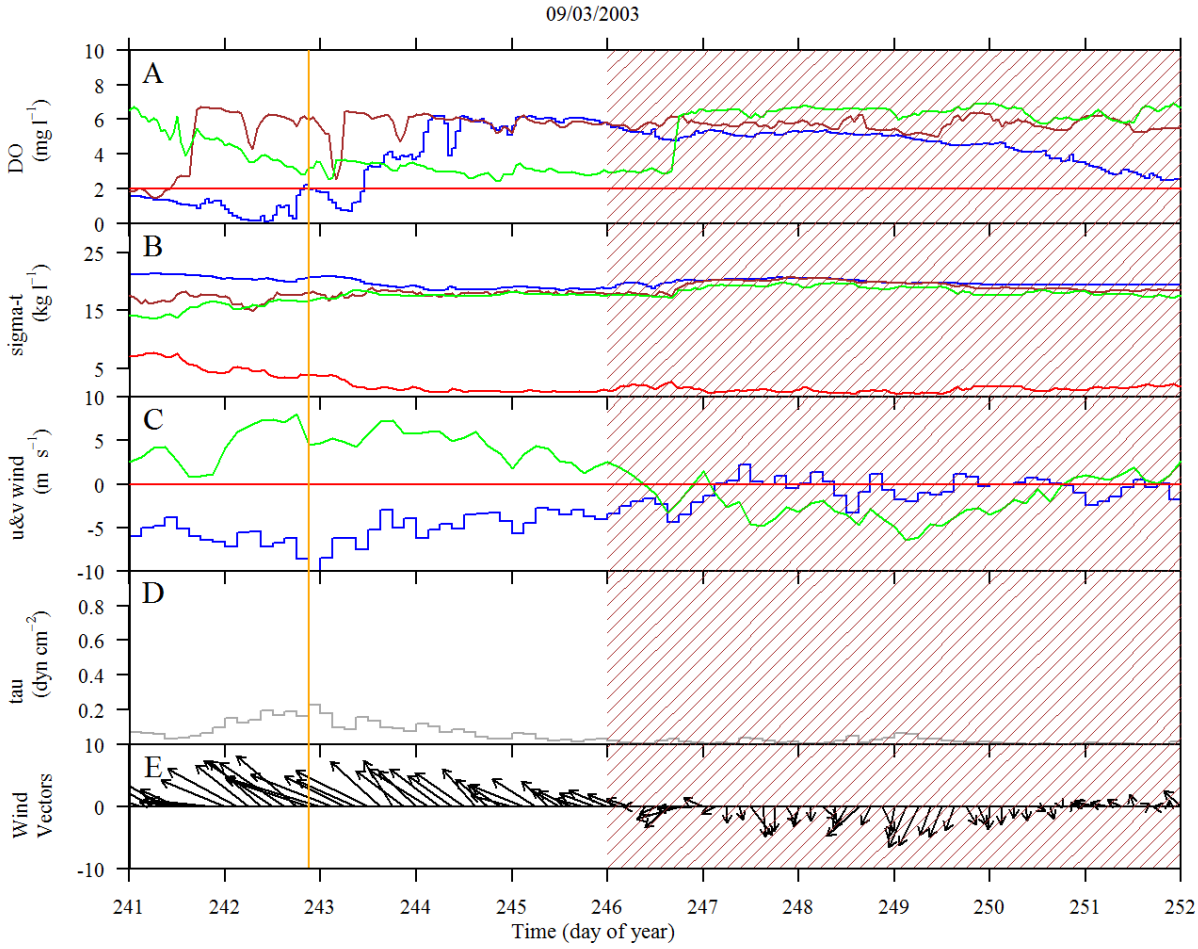

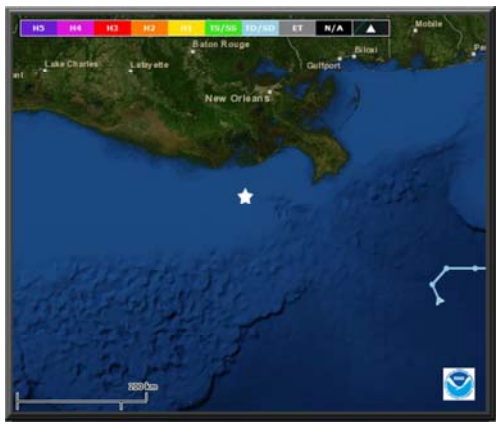

Figure A.20. Stacked plot of environmental data during Tropical Storm Henri. Left is a map of Tropical Storm Henri's track. White star on map represents station C6. Further details are located on the first page of Appendix C.

Tropical Storm Bonnie

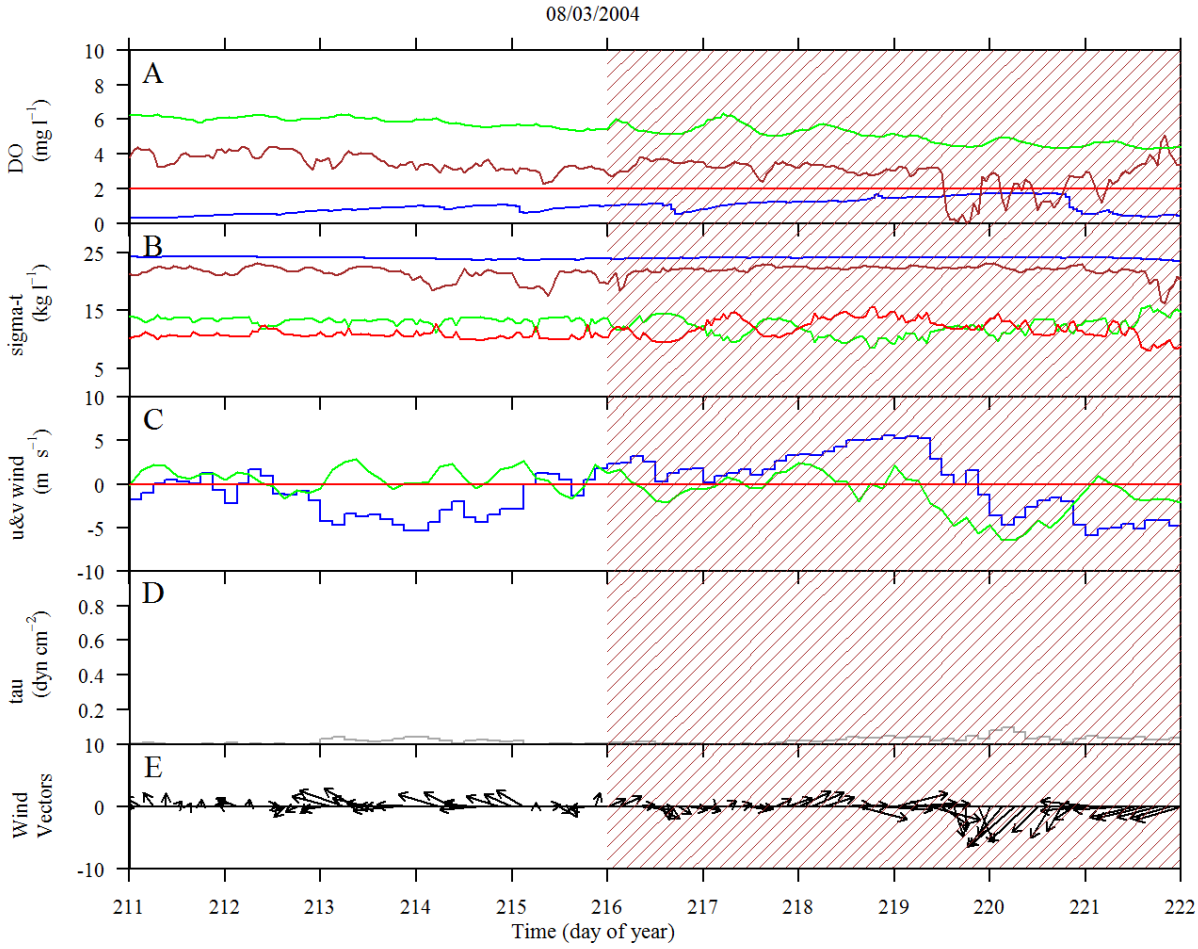

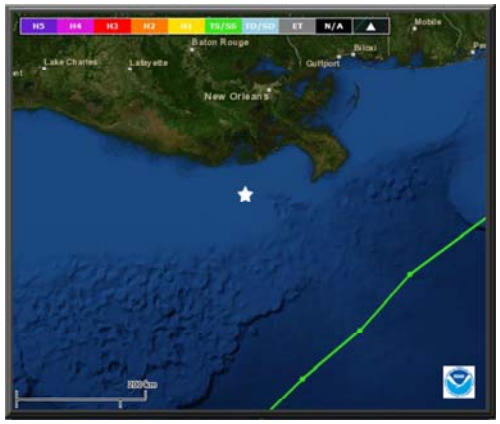

Figure A.21. Stacked plot of environmental data during Tropical Storm Bonnie. Left is a map of Tropical Storm Bonnie's track. White star on map represents station C6. Further details are located on the first page of Appendix C.

Hurricane Ivan

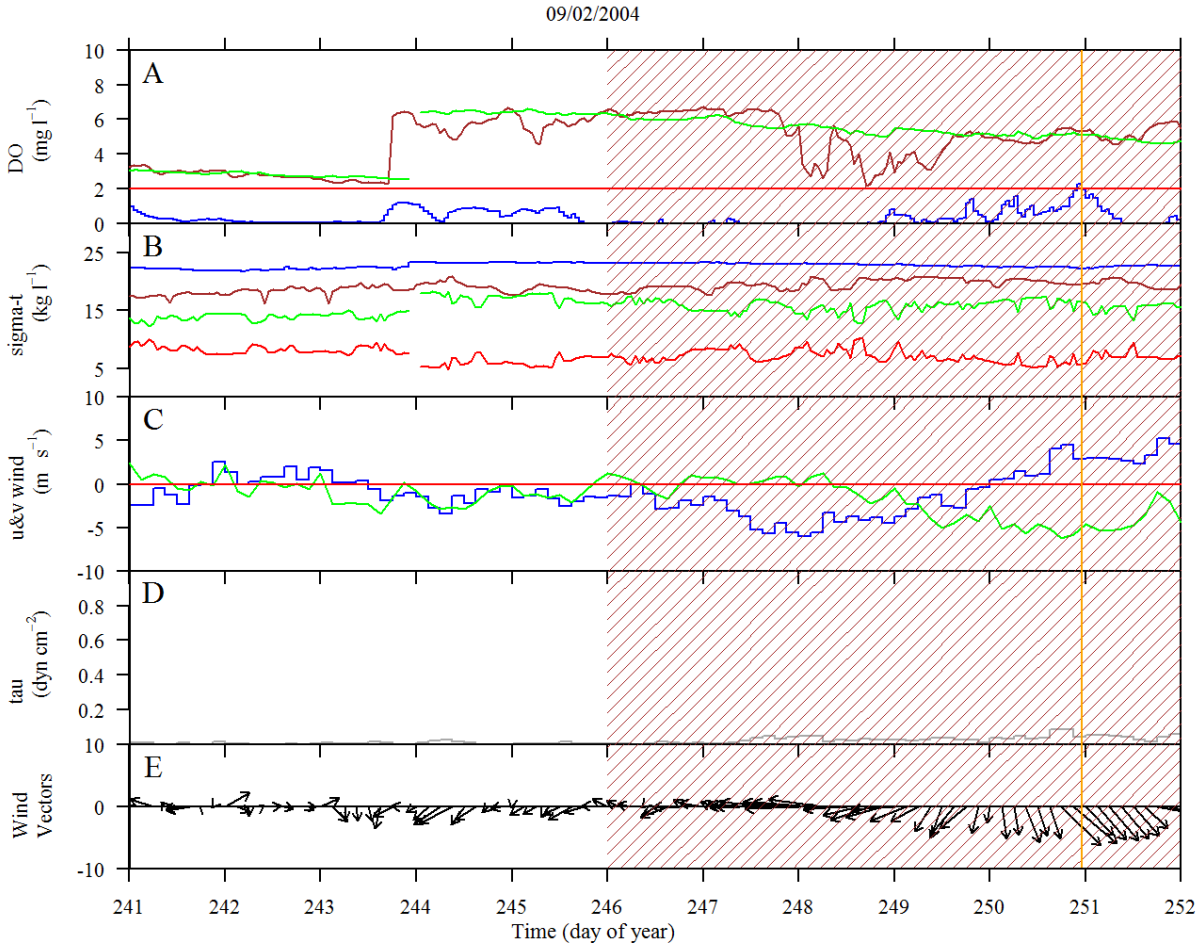

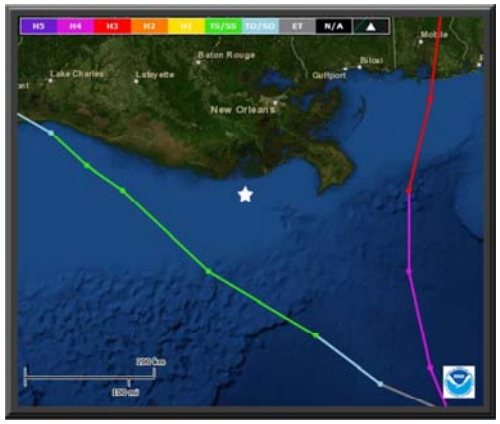

Figure A.22. Stacked plot of environmental data during Hurricane Ivan. Left is a map of Hurricane Ivan's track. White star on map represents station C6. Further details are located on the first page of Appendix C.

Tropical Storm Matthew

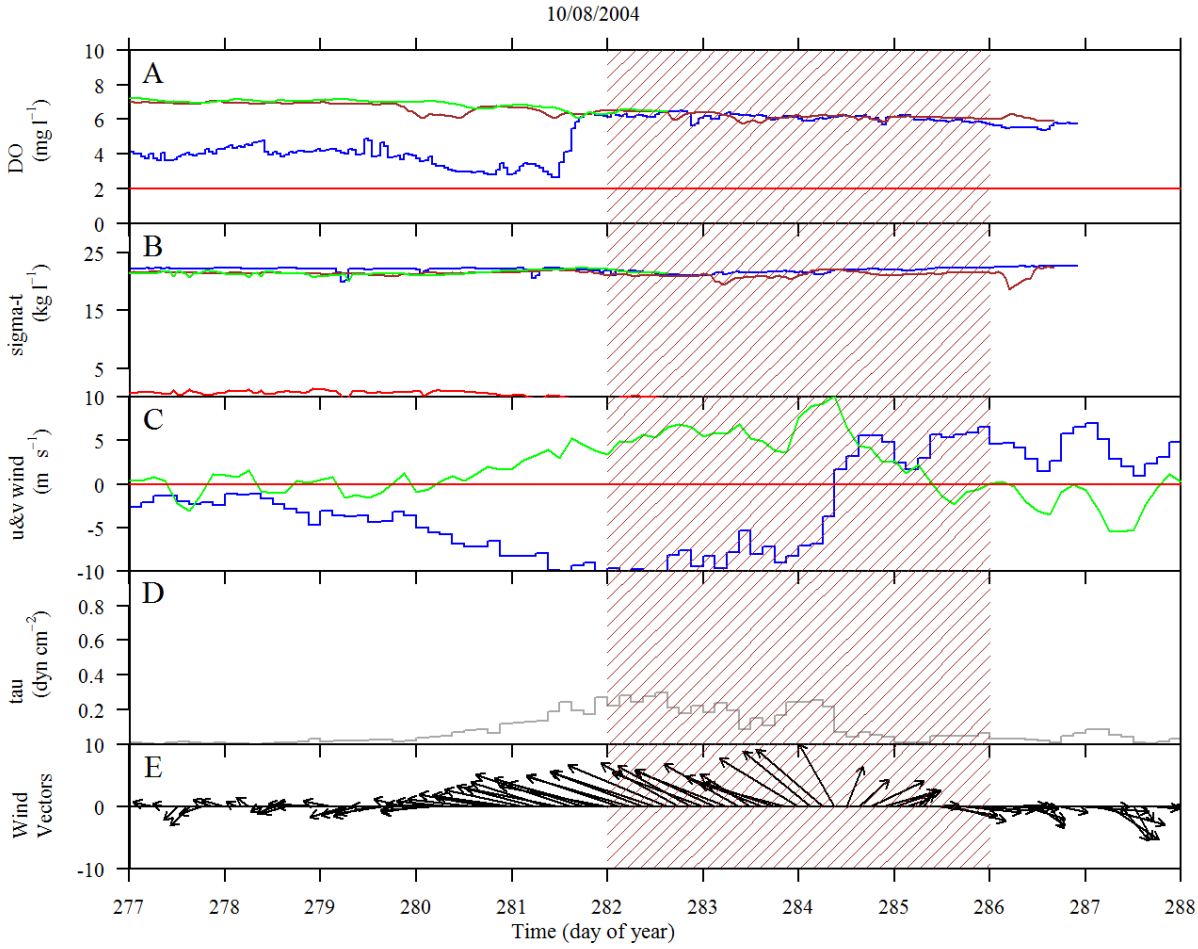

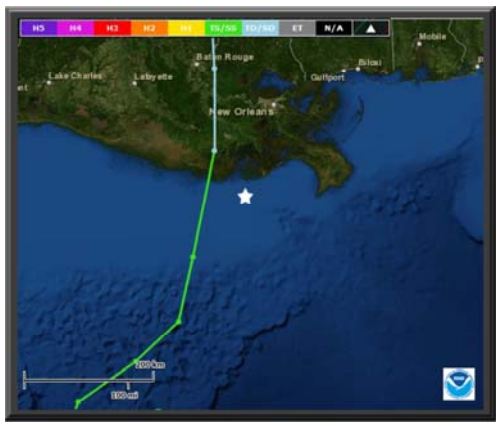

Figure A.23. Stacked plot of environmental data during Tropical Storm Matthew. Left is a map of Tropical Storm Matthew's track. White star on map represents station C6. Further details are located on the first page of Appendix C.

Tropical Storm Arlene

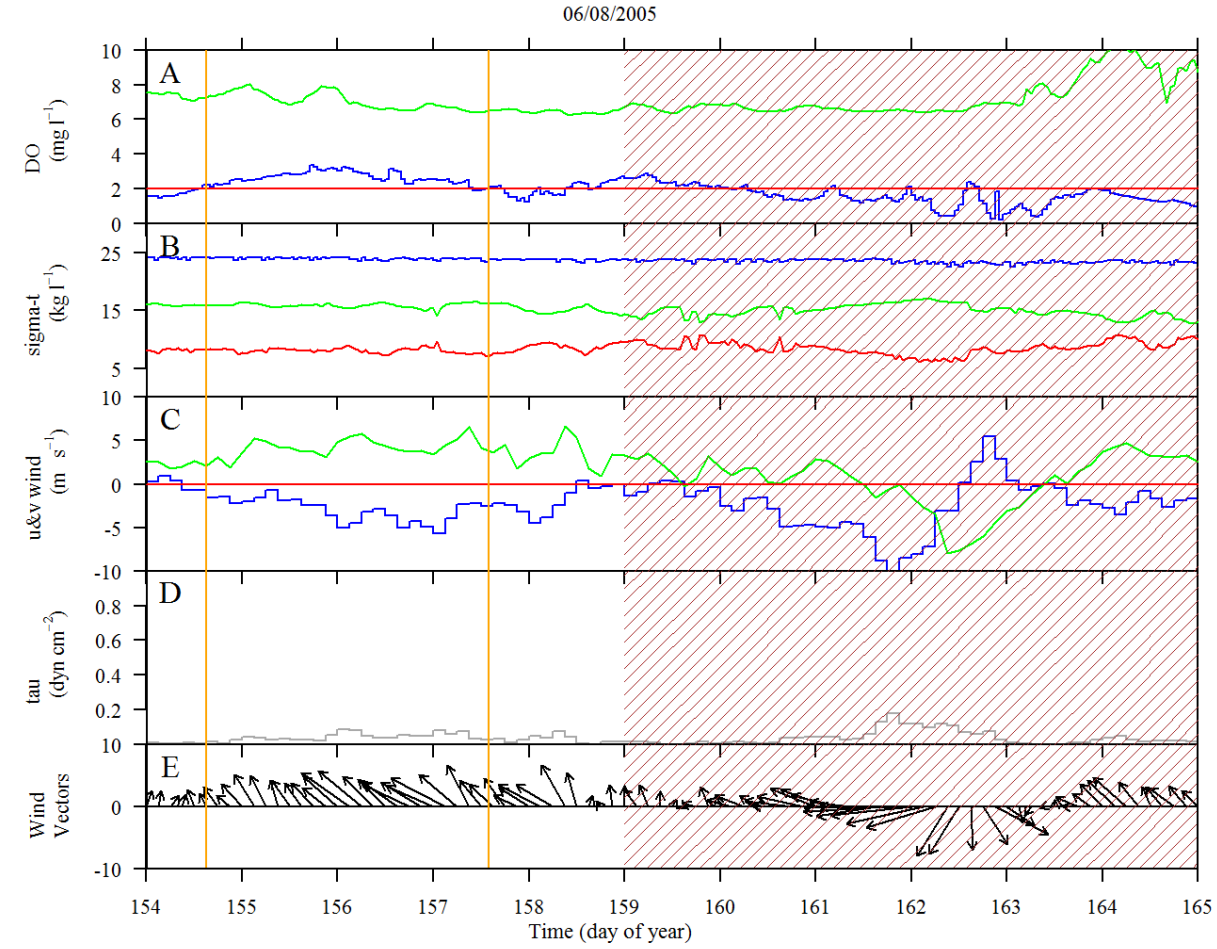

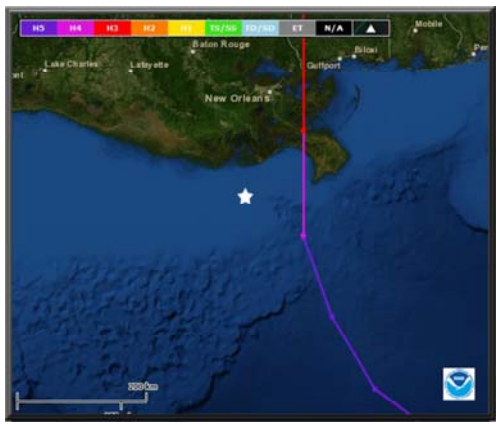

Figure A.24. Stacked plot of environmental data during Tropical Storm Arlene. Left is a map of Tropical Storm Arlene's track. White star on map represents station C6. Further details are located on the first page of Appendix C.

Hurricane Cindy

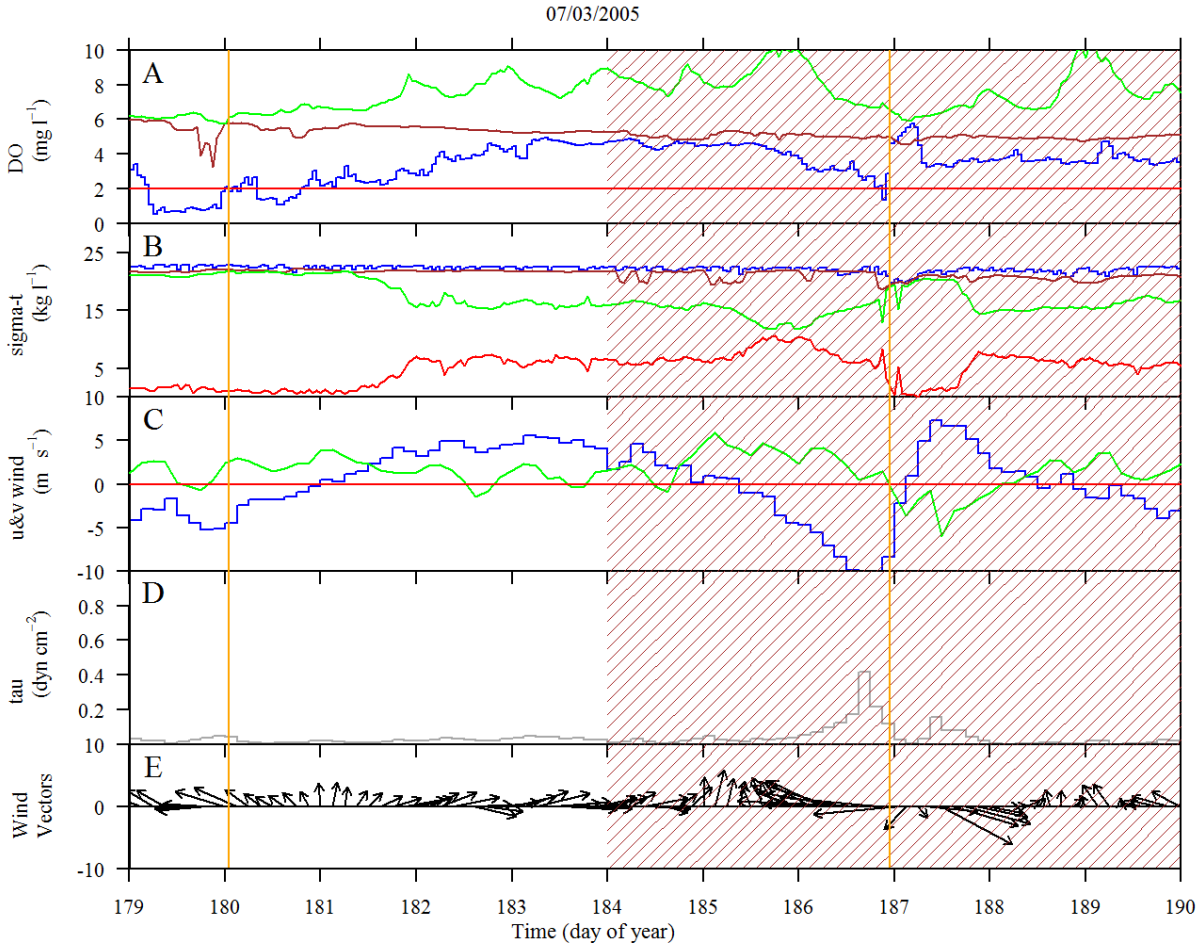

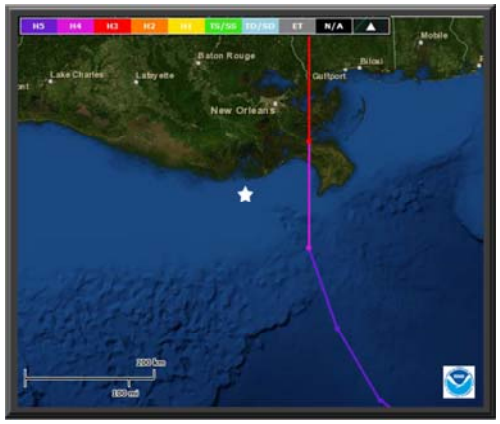

Figure A.25. Stacked plot of environmental data during Hurricane Cindy. Left is a map of Hurricane Cindy's track. White star on map represents station C6. Further details are located on the first page of Appendix C.

Hurricane Katrina

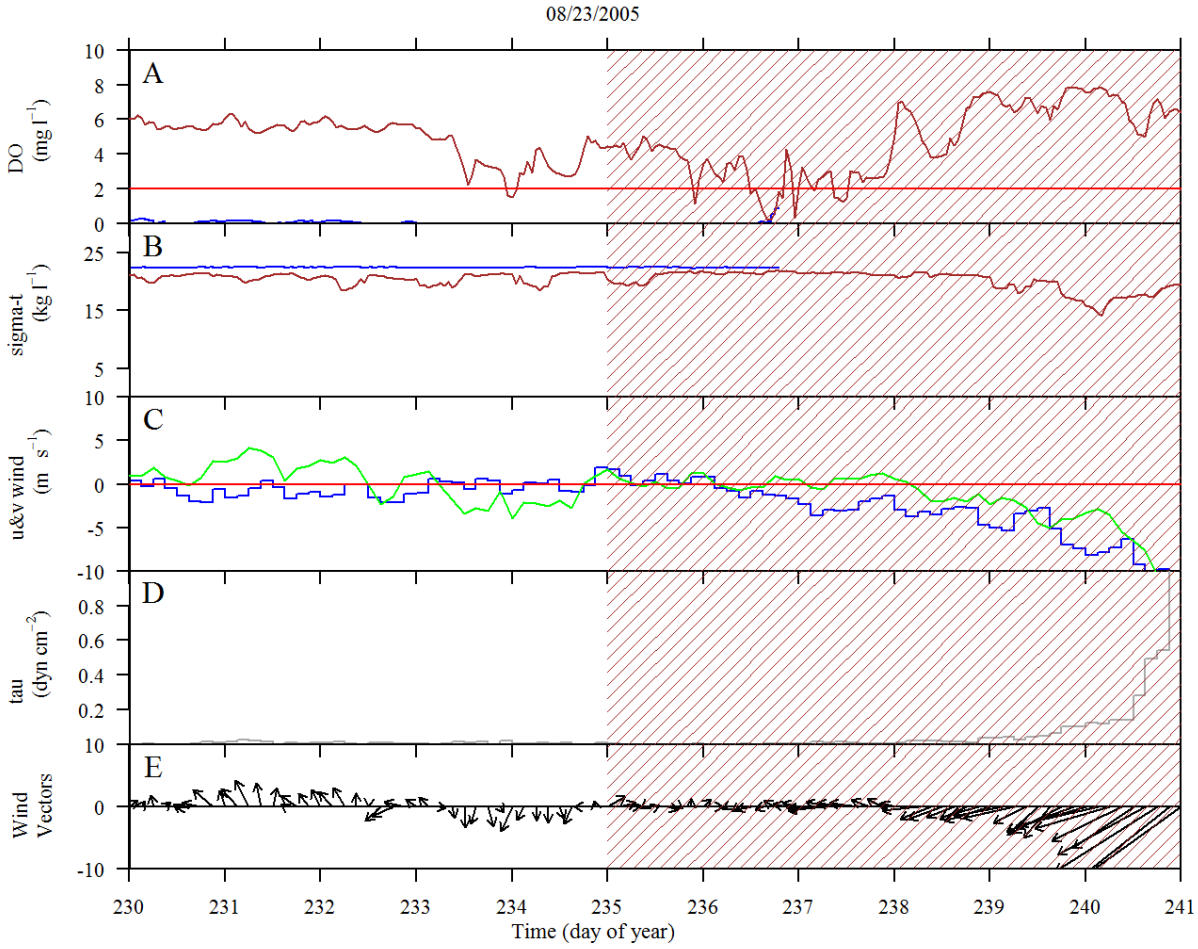

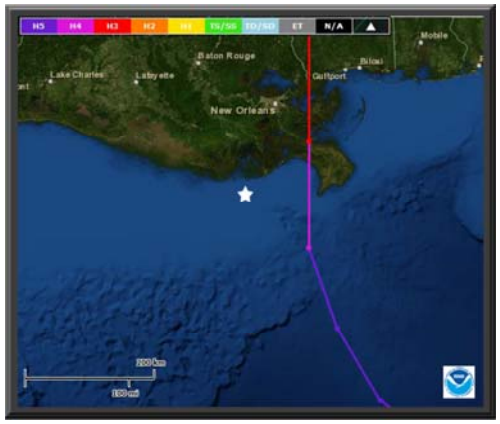

Figure A.26. Stacked plot of environmental data during Hurricane Katrina. Left is a map of Hurricane Katrina's track. White star on map represents station C6. Further details are located on the first page of Appendix C.

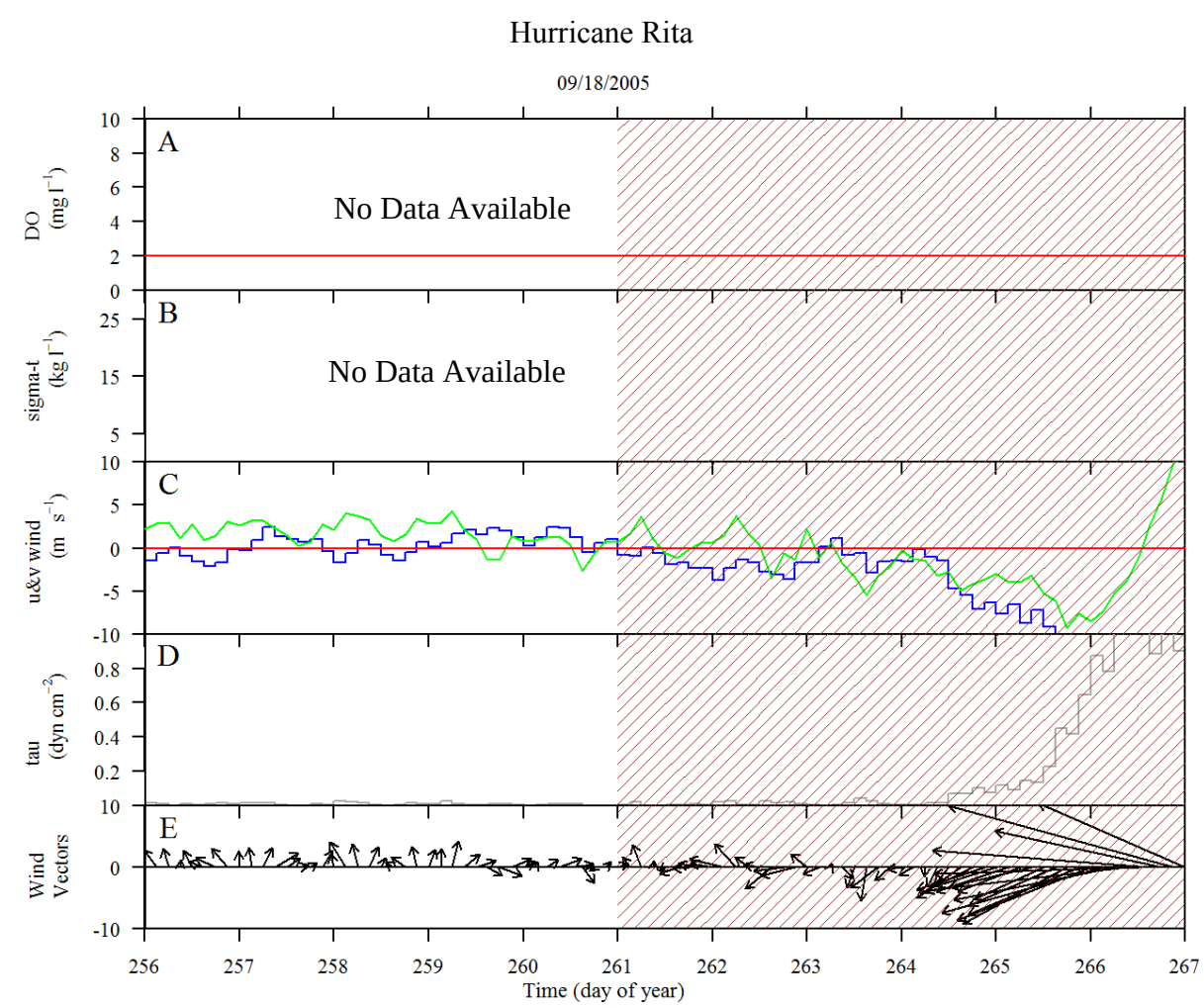

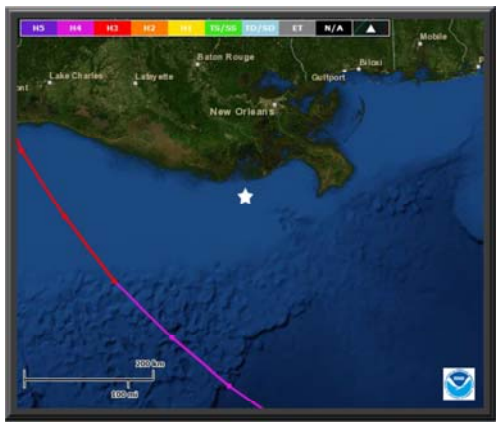

Figure A.27. Stacked plot of environmental data during Hurricane Rita. Left is a map of Hurricane Rita's track. White star on map represents station C6. Further details are located on the first page of Appendix C.

Tropical Storm Edouard

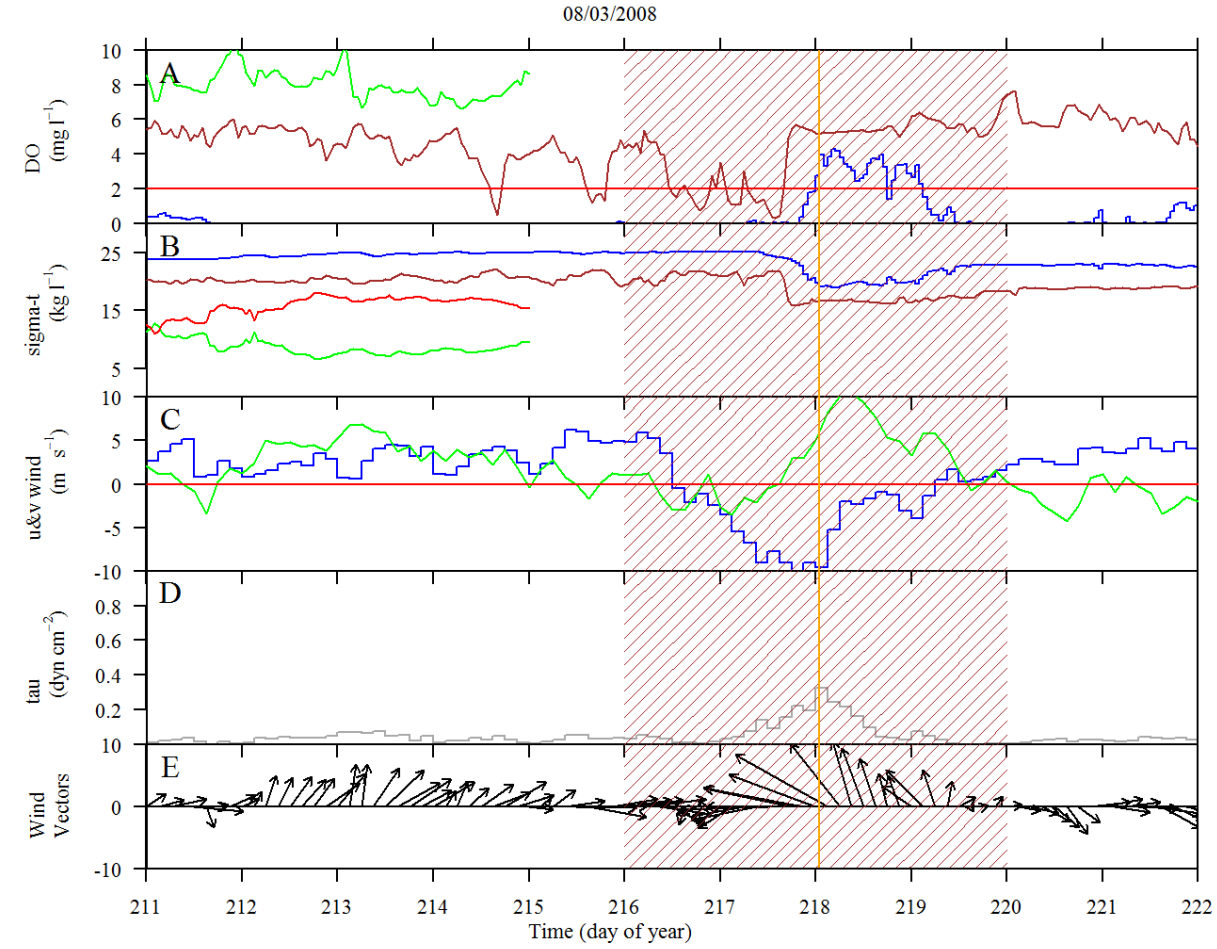

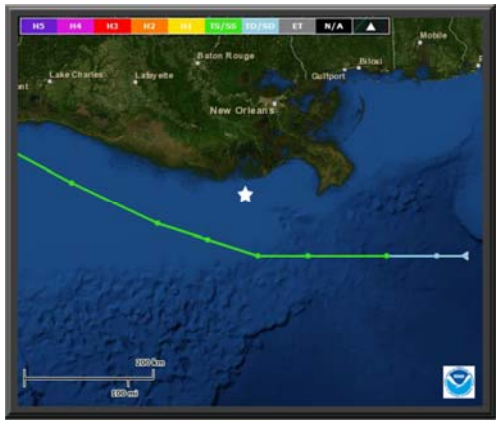

Figure A.28. Stacked plot of environmental data during Tropical Storm Edouard. Left is a map of Tropical Storm Edouard's track. White star on map represents station C6. Further details are located on the first page of Appendix C.

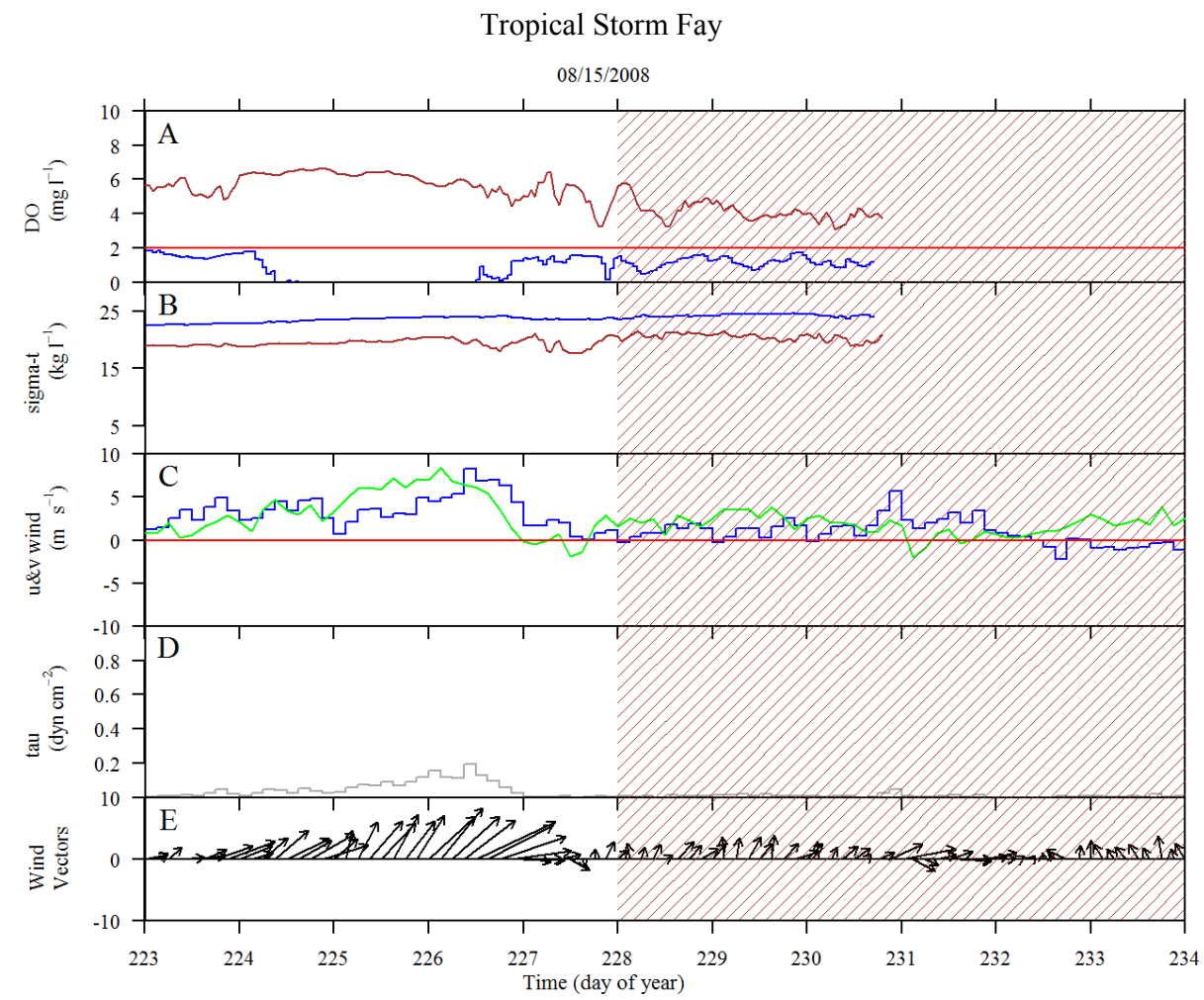

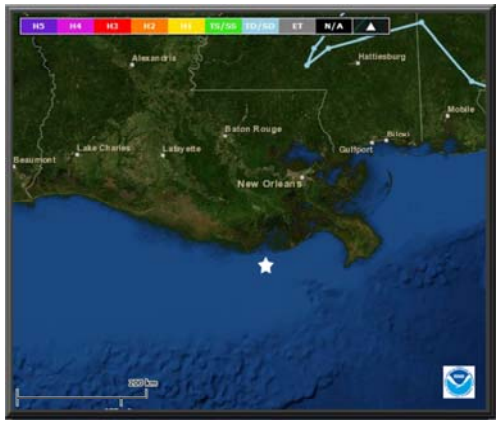

Figure A.29. Stacked plot of environmental data during Tropical Storm Fay. Left is a map of Tropical Storm Fay's track. White star on map represents station C6. Further details are located on the first page of Appendix C.

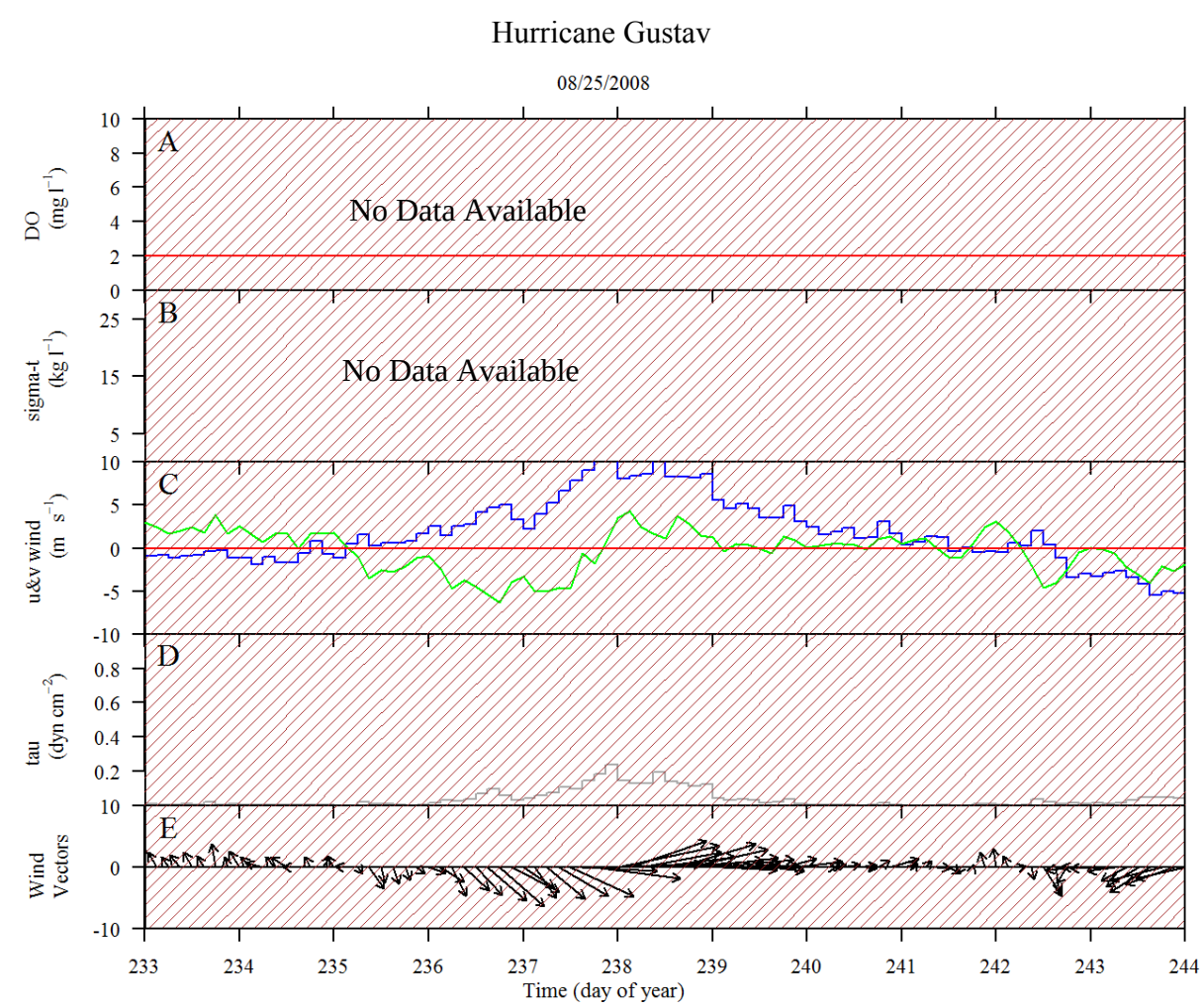

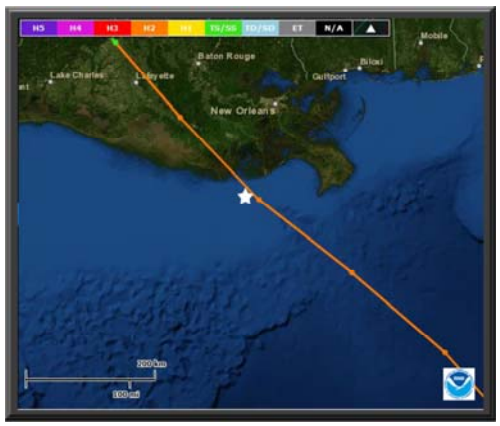

Figure A.30. Stacked plot of environmental data during Hurricane Gustav. Left is a map of Hurricane Gustav's track. White star on map represents station C6. Further details are located on the first page of Appendix C.

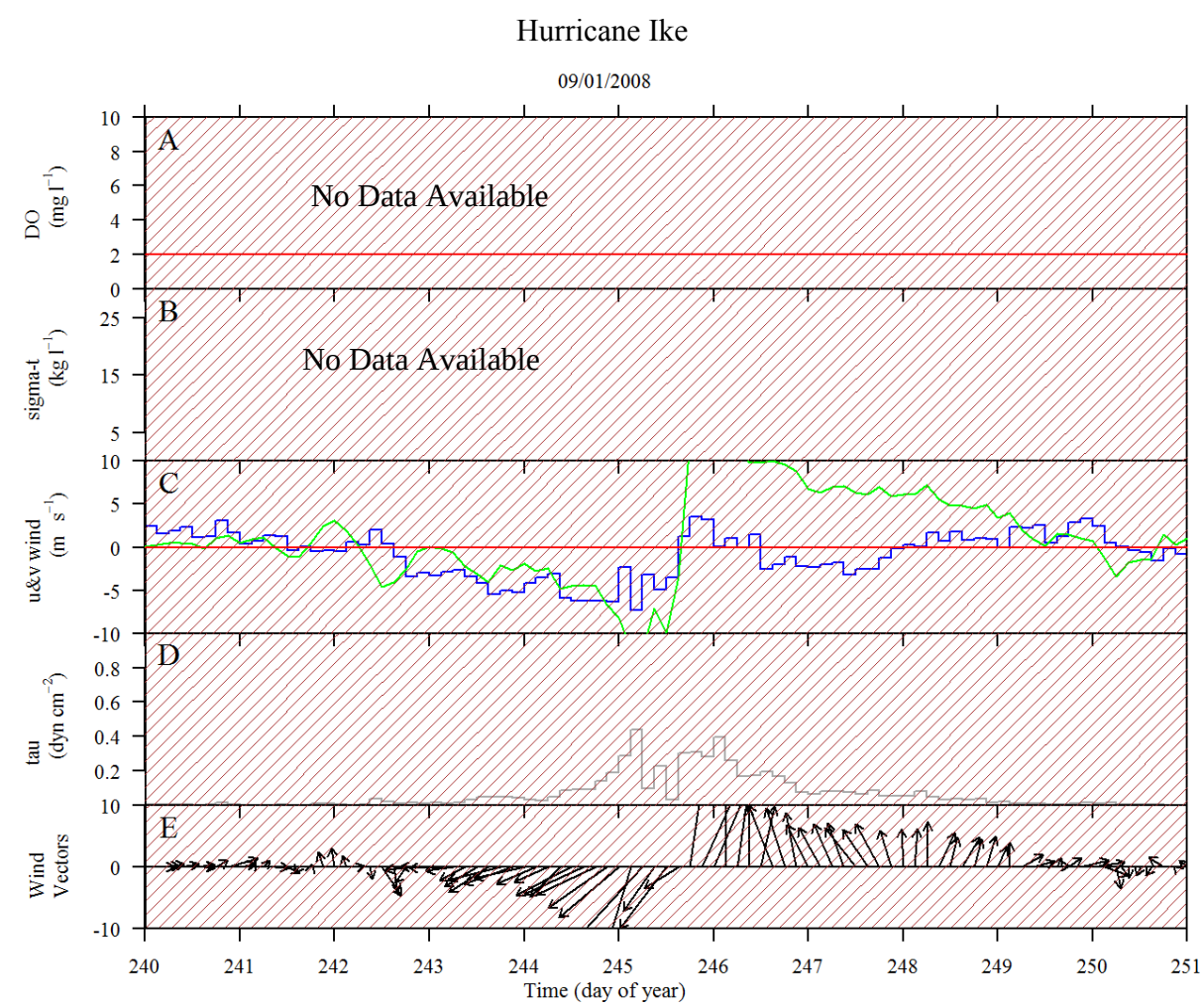

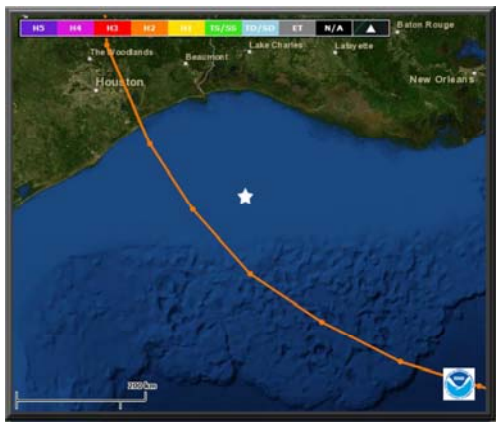

Figure A.31. Stacked plot of environmental data during Hurricane Ike. Left is a map of Hurricane Ike's track. White star on map represents station C6. Further details are located on the first page of Appendix C.

APPENDIX D

DEVELOPMENT OF A RELATIONAL DATABASE IN SUPPORT OF ECOSYSTEM RESEARCH

INTRODUCTION

Over the past 40 years scientists and agencies have been monitoring the environmental conditions in the northern Gulf of Mexico (NGOM) to better understand the dynamics of hypoxia. The dynamics of hypoxia in the NGOM are extremely complex and involve many environmental variables. Long-term monitoring data are a valuable resource to help disentangle the processes that interact to create hypoxia because they provide a set of natural experiments at the ecosystem scale (Stow et al., 2005). Coastal observing systems like the one located at C6 are the key to studying such a dynamic system (Stone, 2003). However, instrumentation of the observing system at C6 has not sampled all of the environmental variables necessary to explain the dynamics of the system or to explain the variability of short-term (hours to days) dissolved oxygen that determines whether or not the system is hypoxic.

Environmental monitoring of estuarine and coastal regions has dramatically increased over the past 30 years and will continue to do so in the future. Boyton and Kemp (2000) cite an increased awareness of natural resource deterioration in the environment due to human activities as a primary reason for this increase. Wilma Subra (2010) first discovered the hypoxia problem in the Gulf of Mexico while collecting data to determine the effects of oil exploration on the aquatic ecosystem. One of the parameters she collected in her research was dissolved oxygen concentrations and she began to notice that the bottom values of DO concentrations dropped below what was considered to be normal for the area during the summer sampling. Technological advances in the instrumentation to measure environmental variables have also increased coastal monitoring efforts. Prior to the 1970's, monitoring water quality required

manual sampling and subsequent lab analysis. In the case of dissolved oxygen this involved collecting a sample of the water and performing Winkler titrations on the samples in a lab setting to obtain a concentration value. With the development of electronic sensors that could be deployed in situ and can continuously sample unattended, it became more economically feasible to sample more frequently. Finally, the past decade has seen an increase in the number of collaboration efforts promoting environmental monitoring activities. In the late 90's efforts such as National Association of Marine Laboratories' (NAML) Labnet (Tenore, 1998) and later the Southeastern Universities Research Association's (SURA) Cast-net (Babin and Hu, 2008) demonstrated the value of having standard interface formats and data/interchange protocols by creating tools to share coastal ocean environmental monitoring data on the web. The National Data Buoy Center (NDBC) began adding partners to their network aggregating the partner data for dissemination on its website along with the NDBC data.

Even with this increase in environmental monitoring many scientific questions are still unanswered. One reason for this is that analysis and interpretations of these data sets have been limited (Boyton and Kemp 2000). For example, for the past 35 years a team of scientists from Louisiana Universities Marine Consortium annually sampled the NGOM shelf off the Louisiana-Texas coast to determine the areal extent of hypoxia in the northern Gulf of Mexico. Along with the dissolved oxygen concentrations, many other water quality parameters were collected. From these data the areal extent is published annually, but the other water quality parameters have only been analyzed in small subsets. The manner in which these data are stored is one of the problems that make data analysis on a large temporal scale time consuming and difficult. Also, data collection for scientific research often has little value at larger scales beyond individual scientists and programs to organization that might be relevant for resource management (Malone et al. 1993). For example, in 1989 LUMCON began collecting continuous 15 minute samples of

dissolved oxygen concentrations and temperature at a single site in the NGOM. Although these data have been presented in parts to support various research studies, the long-term analysis has not been possible due to the means of storage of the data. In order for these data to be useful they must be synthesized into something that focuses on time, space, and organizational scales appropriate to the questions being asked (Boyton and Kemp 2000).

Objectives

The primary goal of this project was to synthesize data sets collected by various sources over a 20 year period from 1989 to 2008 that might contribute to the study of short-term oxygen variability to more fully understand the dynamics of hypoxia in the northern Gulf of Mexico. The specific objectives are: (1) to identify datasets useful to the study of oxygen variability especially those that are publicly available, (2) to obtain these data sets, and (3) to design a relational database housing these data.

METHODS

Study Site and Data Domain

The temporal domain of this study consists of 20 years from 1989 to 2008. I primarily concentrated on a single site located in an area that experiences frequent hypoxia; however, the spatial domain of the data in this synthesis comprises the northern Gulf of Mexico along the Louisiana-Texas coast from the Mississippi bird-foot Delta to just past the Louisiana-Texas border and out to about the 60 meter isobaths (28,-89,30,-95). The synthesis also contains data collected along the Mississippi River. Figure 1.1 illustrates the spatial domain of this study and identifies the specific study site and other sites of data collection.

DATA SOURCES AND PROCESSING

Time-Series Sonde Data

The 20 year data set, 1989-2008, of continuously monitored sonde data was collected by Louisiana Universities Marine Consortium. The sondes were deployed 20 km offshore from Terrebonne Bay at 28° 52.12'N and 90° 29.42'W. These data were manually downloaded from the sondes after each deployment and stored in individual files in the manufacture's proprietary format. The data files from the first 12 years (1989-2000) were processed by combining the individual files into single year files. From 1989-1995, only temperature and dissolved oxygen data from ~1 m above the bottom were collected. In 1996, other parameters were added as well as a mid-water column (10.7 m) and near-surface (2 m) sonde. Data from 2001-2008 were stored in individual Microsoft Excel files for each approximately monthly sonde deployment. No naming conventions were used for the filenames or the worksheet names within each Microsoft Excel workbook. Also, each deployment had different a naming convention for individual measurements and each header row stored the observations were in a different order. This made programmatically combining the data into a single table for analysis impossible; therefore, each file had to be prepared by individually exporting the data worksheets as comma separated variable (CSV) files and mapping the observation header names to match the database data table before importing. As I imported these files into the database data table, I also added a Station ID field and a depth field. This allowed all of the data to be combined into a single data table for ease in querying and analysis and provided for geo-referencing of the data. I added a Universal Coordinated Time (UTC) offset field to the data table to correct for the fact that the data from years 1989-2004 were time-stamped in Central Standard Time (CST), while data from 2005-2008 were time-stamped in UTC. Adjustments are made when querying the data to standardize the data to UTC. When salinity was available, I calculated the water density anomly,

σ_T, (σ_T = water density-1000) values from temperature and salinity using the state of seawater equation (UNESCO, 1983).

Time-series Meteorological Data

I included data from two meteorological stations because these two are typically used by scientists for modeling and analyst of dissolved oxygen concentrations in the northern Gulf of Mexico. The Grand Isle, LA (GISL1 - 8761724) monitoring station is within 65 km of the station C6 at 29.263 N 89.957 W (29°15'48" N 89°57'24" W). This station is owned and operated by NOAA's National Ocean Service Water Level Observation Network. The height of the air temperature sensor is 2.4 m above the site elevation and the anemometer height 9.5 m above the site elevation. National Data Buoy Center owns and maintains the C-MAN Station at Southwest Pass, LA (BURL1). This station is located at 28.905 N 89.428 W (28°54'18" N 89°25'42" W) and is representative of offshore wind patterns (Walker and Rabalais, 2006). The site elevation is 0 m above mean sea level. The air temperature sensor height is 11.9 m above the site elevation. The anemometer height is 30.5 m above the site elevation. The barometer elevation is 12.5 m above mean sea level. The NDBC powered-down this station on August 30, 2007 through August 23, 2009. During this period they referred users to a nearby NOS station (PSTL1) providing reliable data in the vicinity of Southwest Pass. The Pilot's Station East, SW Pass, LA (PSTL1-8760922) is owned and maintained by NOAA's National Ocean Service Water Level Observation Network on the Pilot's station at the mouth of the Mississippi River at 28.932 N 89.407 W (28°55'55" N 89°24'25" W). The anemometer height is 24 m above the site elevation. These data sets were downloaded from the NDBC website as individual tab-delimited text files from http://www.ndbc.noaa.gov/. The header varied from year to year; therefore, I manually mapped each file as I uploaded these into a single database table adding a station

identification field to map each observation to the metadata table containing sensor height information needed when comparing wind information.

Water-Level Time Series

I downloaded water-level data from Louisiana State University's Coastal Studies Institute WavCIS program's website (www.wavcis.lsu.edu) for tide data. These data were collected at one hour intervals from the same location as the DO sonde data, station C6. These data were downloaded into a single CSV file and imported into a single table in the database.

Time-Series River Flow Data

I downloaded discharge data from the Mississippi River at Tarbert Landing, MS from the United States Army Corps of Engineers (USACE) website (http://www.mvn.usace.army.mil/cgi-bin/wcmanual.pl?01100). This site requires the user to complete a web-based form to subset the data with a 9 year maximum. I downloaded all of the river flow data from 1932 until 2008 to text files, stripped the header information from the file, and then imported these into a database table converting the text date time stamp to a SQL DateTime data type. Historic river stage data consists of daily 8:00am gauge readings. USACE has verified the data prior to January 1, 1998. A reading of -901.00 means the data point is missing. The gauge reading is recorded in cubic feet per second times 1000 (CFSX1000). The monitoring station at Tarbert Landing, MS, (USACE Gage ID 01100) is located at Mississippi River Mile 306.3, latitude 31° 00'30"N and longitude 91°37'23" W. The gage zero is NGVD. This site is 478 km upstream from the mouth of the MR and 13 km downstream from the Old River Control Structure where 1/3 of the flow is diverted down the Atchafalaya River. The discharge at the site accounts for 70% of the flow of the total MR and Atchafalaya River discharges.

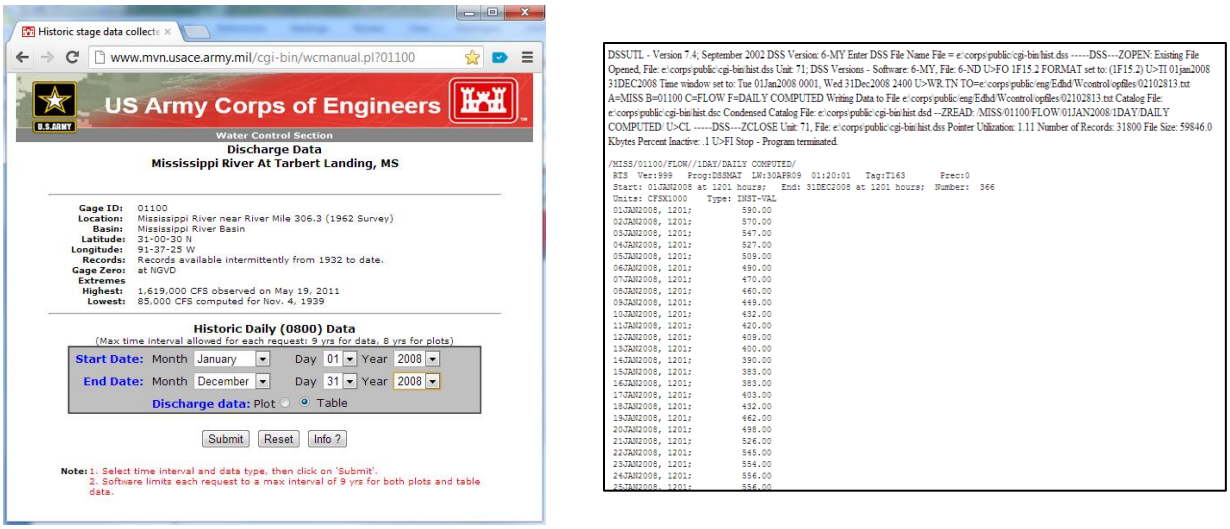

Figure D.1. Web interface and sample data output for Mississippi River at Tarbert Landing, MS from the United States Army Corps of Engineers (USACE) website (http://www.mvn.usace.army.mil/cgi-bin/wcmanual.pl?01100)

Time-Series Hurricane Data

I downloaded the Atlantic Hurricane track data from the NOAA's National Climatic Data Center (http://www.ncdc.noaa.gov/oa/ibtracs/index.php?name=wmo-data) to identify tropical cyclone events. International Best Track Archive for Climate Stewardship (IBTrACS-WMO) data consisted of tropical cyclone advisories issued every 6 hours by the National Hurricane Center from 1951 to 2010 on storms in the Atlantic Basin (Knapp et al., 2010). The data were contained in one CSV file; thus they were easily imported into the data base as a single file.

Time-Series NARR Data

NOAA National Centers for Environmental Prediction (NCEP) provides both climate and weather model data through the National Operational Model Archive and Distribution System (NOMADS). NOMADS provides a web-service that provides both real-time and retrospective format independent access to the data. I downloaded NCEP's North American Regional Reanalysis (NARR) from the NOMADS website (http://nomads.ncdc.noaa.gov/) (Figure D.2). NARR-A assimilates observational data with the model data through reanalysis. The THREDDS Data Server (TDS) is a web server that provides metadata and data access for scientific datasets,

using OPeNDAP, OGC WMS and WCS, HTTP, and other remote data access protocols. These data are stored as gridded NetCDF files. Gridded Datasets may be thought of as a collection of point data, with location at the center of each grid cell.

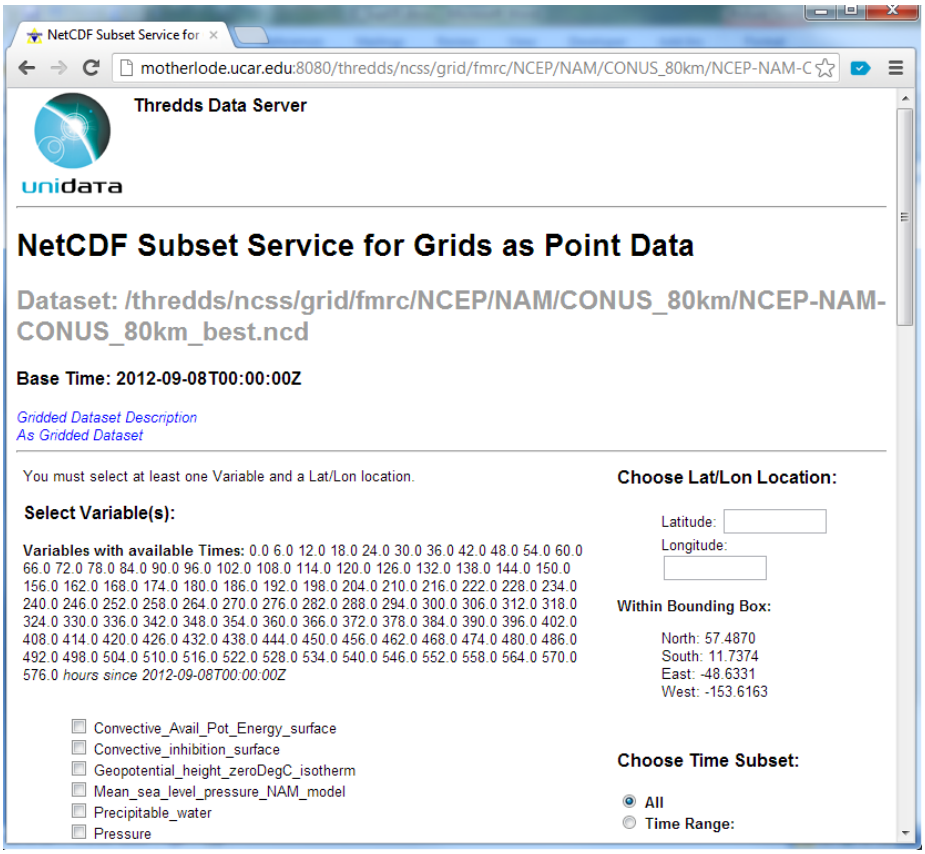

Figure D.2. The web interface for downloading the NCEP's North American Regional Reanalysis (NARR) from the NOMADS website (http://nomads.ncdc.noaa.gov/)

NOMADS provides the Grid as Point service through form-based web service to access the THREDDA server and subset the data temporally and spatially. This service requires selection of a single cell using latitude and longitude coordinates, then subsetting by Time, Variable, and vertical level. Either an XML, CSV (Comma Seperated Values in ASCII) document or a NetCDF files may be generated in Unidata Point Observation format. Because the observations had to be downloaded one observation at a time, I created a vbScript to automatically access the subsetting form and download the data for the single latitude and longitude location of the station of this study concatenating the observations into comma

separated files. I had to do this separately for both the FLUX data and the wind data because I could only access one vertical level of data at a time. The wind data is calculated for 10 meters above the surface and the flux data is for the surface. http://motherlode.ucar.edu:8080/thredds/ncss/grid/fmrc/NCEP/NAM/CONUS_80km/NCEP-NAM-CONUS_80km_best.ncd/pointDataset.html

Once these data were downloaded into comma separated value (CSV) files by year. I uploaded these files into a two tables in the database-one for flux data and one for wind data.

Cruise Data

I downloaded all cruise data from the National Oceanographic Data Center (NODC). The NGOMEX data from 1996-2008 were ingested into a SQL database. First, I identified a unique station identifier for each sampling station throughout the 10 years. The scheme for this unique identifier was the year of sampling followed by a 4-digit number indicating the station count of sampling within that year. This counting numbering scheme was already established in the datasets. A table containing a list of all sampling stations is linked to the various types of data collected through this unique identifier.

Mississippi River Nutrient Data

The USGS provides streamflow and nutrient delivery data to the Gulf of Mexico through water year 2009 (http://toxics.usgs.gov/hypoxia/mississippi/flux_ests/delivery/). These nutrient delivery estimates are based on approved data and extends the information provided by Aulenbach et al (2007). The website provides a Microsoft Excel spreadsheet of the data from October 1967 through September 2009 spanning water years 1968 through 2009. The nutrients measured each year varied slightly. The methods and other metadata are included in the spreadsheet with the data. Although this spreadsheet is easily understood by the human reader, it

is not easily machine readable to programmatically perform long-term analysis. Therefore, I modified the spreadsheet by stripping the metadata information and preparing machine readable field names for each of the data fields in the spreadsheet. Then, I imported the table in the database.

Relational Database

Using Microsoft Structured Query Language (SQL) database server, I created a database in Support of Ecosystem Research (SupER). SupER is a relational database synthesizing data from various sources (Figure D.3). The relational design of the database allows not only for maintaining referential integrity but also to maintain third normal form (Codd 1990). A station information table maintains information about each of the sites of data collection and links to the observations via a StationID.

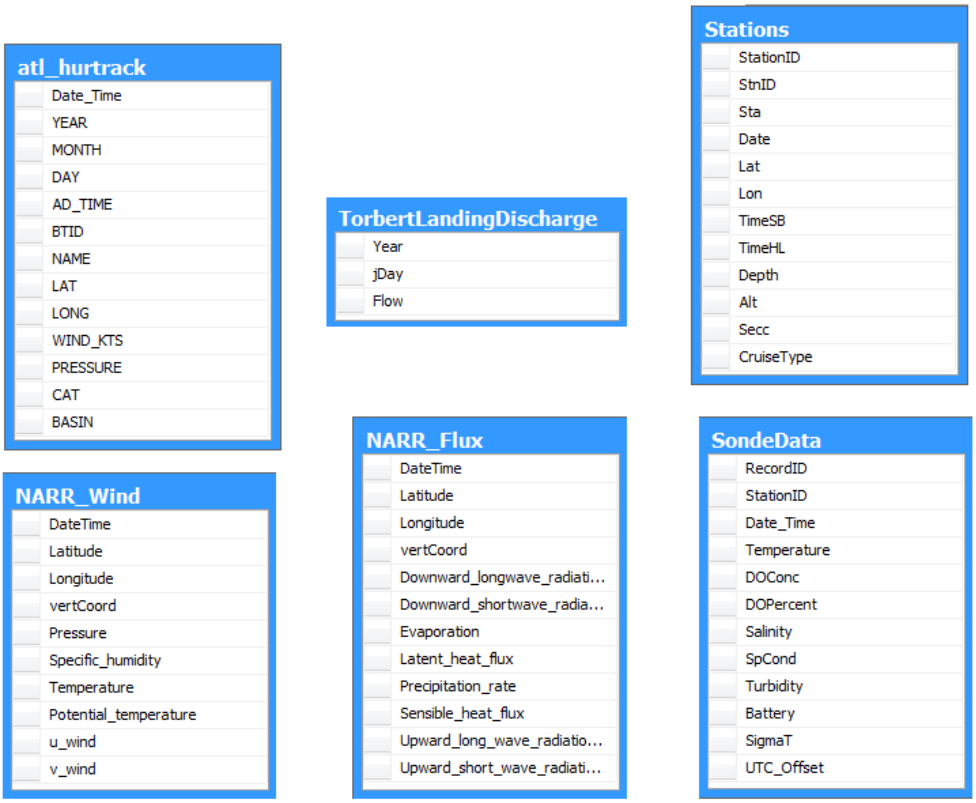

Figure D.3. Illustration of the tables in the Microsoft SQL database.

Graphical Analysis

These databases allowed for a variety of graphical analysis because I could easily subset the data and join the different datasets together. Appendices A, B, and C are all examples of this type of analysis

Climatological analysis

Climatologies are typically created with 30 years of data; however, I created climotogies for the study site with only 20 years of data so that they would match the temporal extent of the data of primary interest the dissolved oxygen data. I created a wind rose for the entire 20 years and for each year 1989-2008 from the u wind component and the v wind component of the NARR-A estimates by first converting the components to a wind speed variable and a wind direction variable using the "rosavent" algorithm in the "climatol" package for R Statistic Computing Software (R Development Core Team, 2011). I also created a climate diagram as designed by Walter (1963) for the study site using the NARR data using the "diagwl" algorithm in the "climatol" package for R Statistic Computing Software (R Development Core Team, 2011).

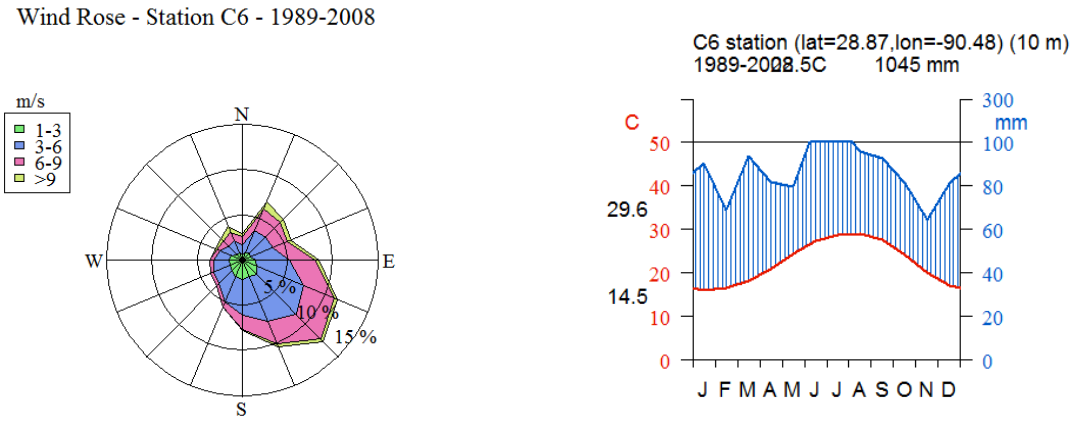

Figure D.4. Left side: Wind rose; Right side: climate diagram. Both were created with 20 years of NARR-A estimates

The wind rose indicated that the majority of the time the winds were from the southeast (~ 13 %). Annual wind rose plots indicated some variation in this pattern existed among the years. (See plots in Appendix A.) For example, although 2008 showed a similar pattern a greater percentage of the winds were from the southeast. In 2005, no direction prevailed more than 10% of the time.

The climate diagram indicated a typical seasonal variation in the air temperature and a typical rainfall for the area. The minimum monthly average air temperature was 14.5 C occurring in January and the maximum monthly average was 29.6 C occurring in August.

CONCLUSION

The database in Support of Ecosystem Research (SupER) has provided data to several research projects. The data from this data base has been used in several research projects including modeling projects. This database made the analysis of the time-series of DO concentrations in this dissertation possible. Adding a web interface to make the data available to other researchers will be the next addition to the SupER project.

REFERENCES

Aulenbach, B.T., Buxton, H.T., Battaglin, W.T., and Coupe R.H., 2007, Streamflow and nutrient fluxes of the Mississippi-Atchafalaya River Basin and subbasins for the period of record through 2005: U.S. Geological Survey Open-File Report 2007-1080.

Babin, B. L. and L. Hu. 2008. A Tale of Two observing systems: Data visualization of realtime coastal ocean data on the web. Proceedings of the Environmental Information Management Conference, 14-18.

Boynton, W.R. and W.M. Kemp. 2000 Influence of river flow and nutrient loads on selected ecosystem processes A synthesis of Chesapeake Bay Data pp 169-298 In: J E Hobble (Ed) Estuarine Science A Synthesis Approach to Research and Practice, Island Press Washington, D. C.

Codd, E.F. 1990. The Relational Model for Database Management: Version 2. Addison-Wesley, p. 271.

Knapp, K. R., M. C. Kruk, D. H. Levinson, H. J. Diamond, and C. J. Neumann, 2010: The International Best Track Archive for Climate Stewardship (IBTrACS): Unifying tropical cyclone best track data. Bulletin of the American Meteorology. Society, 91, 363-376.

Malone, T.C., Boynton, W., Horton, T., and Stevenson C. 1993. Nutrient loading to surface waters: Chesapeake case study, p 8-38. In M. F. Uman (ed.), Keeping pace with science and engineering. National Academy Press, Washington, DC.

R Development Core Team. 2011. R: A language and environment for statistical computing. R Foundation for Statistical Computing, Vienna, Austria

Stone, G.W., Zhang, X., Li, J., and Sheremet, A. 2003. Coastal observing systems: key to the future of coastal dynamics investigation. GCAGS/GCSSEPM Transactions 53, 783-799.

Stow, C.A., Qian, S. S., and Craig, J.K. 2005. Declining threshold for hypoxia in the Gulf of Mexico. Environmental Science & Technology 39(3), 716-723.

Subra, W. 2010. Reasons to worry about the dead zone. In Oceans: The threats to our seas and what you can do to turn the tide, ed. Jon Bowermaster. New York: Public Affairs, 131-136.

Tenore, K.R. 1998. LABNET: Networking environmental data bases of the coastal laboratories. University of Maryland Center for Environmental Science, Chesapeake Biological Laboratory

Turner, R.E., Rabalais, N.N., Swenson, E.M., Kasprzak, M., Romaire, T., 2005. Summer hypoxia in the northern Gulf of Mexico and its prediction from 1978 to 1995. Marine Environmental Research 59, 65-77.

UNESCO 1983. Algorithms for computation of fundamental properties of seawater, 1983. UNESCO Technical Papers in Marine Science, No. 44, 53 pp.

Walker, N.D. and Rabalais, N.N. 2006. Relationships among satellite chlorophyll a, river inputs and hypoxia on the Louisiana continental shelf, Gulf of Mexico. Estuaries and Coasts 29(6B), 1081-1093.

Walter, H. 1963. Climatic diagrams as a means to comprehend the various climatic types for ecological and agricultural purposes. In. Rutter, A. J., and F. H. Whitehead (eds.). The Water Relations of Plants, John Wiley and Sons, Inc., New York. p. 3-9.

VITA

In 1961, Brenda Leroux Babin began her love affair with water in coastal Louisiana in New Orleans, LA. When Babin was old enough to attend school her family moved down the bayou to Houma, LA where learned to swim at age six, to fish at age seven, and to water ski at sixteen. She swam on the Legion Park Swim team through high school and will someday swim across Lake Pontchartrain near the Causeway Bridge.

After graduating from South Terrebonne High School in 1979, Babin attended Nicholls State University where she graduated cum laude with a Bachelor of Arts degree in English Education and a Speech Education Minor. Babin continued on to graduate school graduating summa cum laude with her Master's in Curriculum and Instruction and a specialization in Reading Education focusing on the development of syntactic structures in the brain. After two years of teaching at Nicholls State University, she set out to mold young minds in the Louisiana State Public School System in the Terrebonne Parish School District teaching English and Speech. Later, Babin returned to school and completed the certification to teach Mathematics and Computer Science. While moving into these fields in her teaching, she felt called in her personal life to develop her intellectual spirituality. Her Master's degree in Pastoral Studies from Loyola University, New Orleans, focused on such things as organizational leadership, conflict resolution, and gender differences in the classroom.

In 2000, her career took her to Louisiana Universities Marine Consortium, LUMCON, where she was able to combine her passion for education and the marine environment. At LUMCON, Babin directed the Information and Technology Department which included the environmental monitoring program. LUMCON's Environmental Monitoring program received international recognition through Babin's efforts working with the Integrated Ocean Observing System and the Gulf Coast Ocean Observing System's (GCOOS) Regional Association. Babin

served as the dissolved oxygen lead expert on the Quality Assurance of Real Time Oceanographic Data (QARTOD) Project and she co-chaired the Data Management and Communications Committee (DMAC) for GCOOS. She also served on the Data Management committee for the Gulf of Mexico Hypoxia Monitoring Program. Babin's work on her doctoral dissertation grew out of this environmental monitoring work.

Currently, Babin is teaching Computer Science at Fletcher Technical Community College. Babin also serves on the Terrebonne Parish School Board and serves on the South Louisiana Wetlands Discovery Center State Commission. In the spring of 2012, she was inducted into the Louisiana State University chapter of Phi Kappa Phi. She will receive her Doctor of Philosophy degree from the Department of Oceanography and Coastal Sciences in December 2012.